DOCTORAL (PhD) DISSERTATION

NUR NADHIRAH SYAFIQAH BINTI SUHAIMI

Gödöllő

2026

HUNGARIAN UNIVERSITY OF AGRICULTURE AND LIFE SCIENCES

COMPARATIVE STUDIES OF MYXOZOAN PARASITES INFECTING FISHES AND ALTERNATE ANNELID HOSTS IN FRESHWATER ECOSYTSEMS OF HUNGARY AND MALAYSIA

DOCTORAL (PhD) DISSERTATION

NUR NADHIRAH SYAFIQAH BINTI SUHAIMI

Gödöllő

2026

The PhD School

Name: Doctoral School of Agricultural and Food Sciences

Discipline:
Animal Science

Head of the Doctoral School:
Prof. Dr. Melinda Kovács
University Professor, Full Member of the Hungarian Academy of Sciences

Supervisors:
Honorary Professor Dr. Csaba Székely
Scientific Advisor,
Fish Pathology and Parasitology Research Team Leader,
HUN-REN Veterinary Medical Research Institute,
Budapest, Hungary

Dr. Boglárka Sellyei
Senior Researcher,
Fish Pathology and Parasitology Research Team,
HUN-REN Veterinary Medical Research Institute,
Budapest, Hungary

....
Approval of the Supervisors

DECLARATION

Signed below, Nur Nadhirah Syafiqah Binti Suhaimi, a student of the Szent István Campus of the Hungarian University of Agriculture and Life Sciences, studying for a doctoral degree (PhD) in the Doctoral Program in Animal Science declares that the presented Dissertation is my own work and I have used the cited and quoted literature in accordance with the relevant legal and ethical rules. I understand that the four-page summary of my dissertation will be uploaded on the website of the Campus/Institute/Course, and my Dissertation will be available at the Host Department/Institute and in the repository of the University in following the relevant legal and ethical rules.

Confidential data are presented in the dissertation: yes **no***

Date: April / 2026

Nur Nadhirah Syafiqah Binti Suhaimi

Signature

DEDICATION

This dissertation is dedicated to:

My beloved parents,

Sharifah Suzana Binti Syed Sheh and Suhaimi Bin Ismail,

whose unwavering love, endless encouragement, and sacrifices have shaped who I am.

To my husband, the king of my heart,

Wan Muhammad Hazim Bin Wan Sajiri,

for his unshakeable support, patience, and devotion every step of this journey.

To my dearest parents-in-law,

Noriza Binti Othman and Wan Sajiri Bin Wan Hassan,

for their warmth, kindness, and continued blessings.

To my cherished siblings and in-laws,

whose unconditional love, support, and sacrifices have been the pillars of my success.

Your boundless love and belief in me have made this achievement possible.

For all that you have given and all that you are,

I am forever grateful.

CONTENTS

LIST OF TABLES

LIST OF FIGURES

CHAPTER 1

INTRODUCTION

1.1. Research background

Fish are highly susceptible to various diseases caused by infectious agents, including viruses, bacteria, fungi, and parasites. These pathogens can greatly affect fish health and aquaculture productivity, especially when environmental factors like water quality, temperature, and stocking density fluctuate, leading to stress and weakened immune responses. Viral infections such as cyprinid herpesvirus (CyHV-2) (Kurobe et al., 2024), and carp edema virus (CEV) (Palikova et al., 2025), as well as bacterial infections caused by *Francisella* spp. (Colquhoun & Duodu, 2011), *Streptococcus agalactiae*, *Aeromonas hydrophila*, *A. veronii*, and *A. jandae* and *Edwardsiella ictaluri* (Dong, 2018) are known for their significant impact on fish health and production. While fungal pathogens also play a role in fish diseases, their effects are generally less documented compared to viral and bacterial infections. Collectively, these infectious agents can lead to considerable morbidity and mortality in both wild and cultured fish populations.

Among these infectious agents, parasite infections are among the major threats to fish health, often compromising the overall fitness of the host by disrupting physiological, pathological, and immunological responses and making fish more susceptible to secondary infections. Despite their significant impact, the role of parasites in fish health is often underestimated in many fish health assessments. Fish parasites represent a diverse group, including monogeneans, trematode, cestodes, nematodes, acanthocephalans, crustaceans, microsporidians, flagellates and ciliates and myxozoans (Imran et al., 2021). One of the most noteworthy and widespread groups of fish parasites is the Myxozoa (Grasse, 1970). Myxozoans are spore-forming parasites within the phylum Cnidaria, recognized for their intricate life cycles and substantial influence on fish health. Their life cycle typically consists of alternation between a vertebrate host, where myxospores are produced, and an invertebrate host, where actinospores are generated. Myxozoans are capable of

infecting a broad spectrum of organisms and not restricted to fish, including amphibians, reptiles, mammals (Dyková et al., 2007; Prunescu et al., 2007) and birds (Bartholomew et al., 2008).

To date, over 3,000 species of myxozoans have been identified worldwide (Whipps et al., 2025a), many of which are known to cause serious diseases and pathogenic effects in fish of high economic importance. For example, *Tetracapsuloides bryosalmonae* is the causative agent of proliferative kidney disease in salmonids (Hedrick et al., 1993), while *Kudoa thyrsites* is known to cause post-mortem muscle myoliquification in salmons (Whitaker & Kent, 1991). In channel catfish, *Henneguya ictaluri* is associated with proliferative gill disease, often called "hamburger gill" (Pote et al., 2012). Other examples include *Hofferellus carassii*, which causes hofferellosis or polycystic kidney disease in goldfish (Ahmed, 1973), and *Sphaerospora renicola*, which has been linked to swimbladder inflammation in carp (Holzer et al., 2014). Additionally, *Thelohanellus kauri* induced intestinal giant cystic disease in carp (Akhmerov, 1960), while *Myxobolus cerebralis* is well known for causing whirling disease in salmonids (Hoffman, 1990). *Ceratomyxa shasta* is responsible for enteronecrosis in salmonid fish (Johnson et al., 1979), and *Myxobolus lentisuturalis* has been reported to cause body deformities specifically a characteristic dorsal hump in gibel carp and goldfish (Dyková et al., 2002; Caffara et al., 2009; Hepps Keeney et al., 2023). Likewise, *Thelohanellus nikolskii* has been associated with visible deformities in the fins and scales of common carp (Borzák et al., 2021).

The growing number of newly described species in scientific literature reflects a surge in research activity, suggesting that the true diversity of myxozoans is still significantly underexplored. This dissertation aims to contribute to that knowledge by focusing on myxozoan parasites in freshwater environments, with sampling efforts targeting aquaculture systems in Hungary and natural freshwater bodies in Malaysia. The study will also explore the potential discovery of previously undescribed species in these distinct ecological regions.

1.2. Problem statement and significance of study

Freshwater ecosystems harbour rich biodiversity and are vital to global aquaculture. However, these environments are threatened by parasitic infections, particularly those caused by myxozoan parasites. Despite their known impact, the diversity and biology of myxozoans remain poorly understood particularly in regions such as Southeast Asia, where aquaculture is rapidly expanding. In contrast, Europe countries such as Hungary have a longer history of parasitological research and well-established aquaculture practices. More than 100 myxozoan species have already been described in Hungary, yet numerous lakes and fish farms remain unexplored, suggesting that the actual diversity is still underestimated. Meanwhile, Malaysia, being a rapidly developing tropical aquaculture hub in the tropics, remains inadequately explored in terms of myxozoan biodiversity and ecological research. As of 2025, Malaysia is home of 629 species of freshwater fish (Froese & Pauly, 2025). However, only 23 myxozoan species have been described, and these are from just twelve fish species, highlighting a significant research gap (Shariff, 1982; Molnár et al., 2006a, b; Székely et al., 2009a, b, 2014; Borkhanuddin, 2013; Borkhanuddin et al., 2020a). This limited data suggests that a substantial portion of the myxozoan diversity in Malaysia freshwater ecosystems remains undocumented. To address this gap, the present study undertook a comprehensive survey of myxozoans, focusing on newly investigated fish farms in Hungary and diverse freshwater habitats and fish species in Malaysia. By targeting both cultured and wild fish populations, this research contributed to a deeper understanding of myxozoan diversity, distribution, and potential host associations in two ecologically and geographically distinct regions.

In both Hungary and Malaysia, the identification of actinosporean stages from oligochaetes remains limited, primarily due to the labor-intensive nature of the work involved. Collecting sediment samples containing oligochaetes, sorting individual worms, and conducting microscopic examinations require significant time and effort. To date, only 51 actinosporean types have been identified in Hungary (El-Mansy & Molnár, 1997a, b; El-Mansy et al., 1998a, b, c; Székely et al., 1998, 1999, 2002, 2009c, 2014; Molnár et al., 1999a, b; Eszterbauer et al., 2000, 2006; Rácz et al.,

2004, 2005; Marton & Eszterbauer, 2011; Borkhanuddin et al., 2014a; Zhao et al., 2016; Borzák et al., 2021), in contrast to over 100 myxosporean species that have been described from fish hosts. In Malaysia, no actinosporean stages have been reported so far, highlighting a major gap in the understanding of myxozoan life cycles in this region. Furthermore, their critical function in the transmission dynamics of these parasites and their connections to specific myxosporeans stages in fish are still largely unresolved. Traditionally, elucidating the complete life cycle of myxozoans relied on experimental infections, which are often time-consuming and frequently unsuccessful due to the complexity of host-parasite interactions. In recent years, however, molecular techniques such as DNA sequencing and phylogenetic analysis have increasingly been used to link actinospore and myxospores stages, offering more reliable and efficient approach to understanding myxozoan biodiversity and life cycles. This study will use molecular analysis to potentially elucidate the life cycles of both newly described and previously known myxosporean species in Hungary and Malaysia.

In the past, myxozoan species identification relied exclusively on spore morphology and morphometric measurements (Lom & Dyková 2006), before the integration of DNA technologies. However, the limitations of using only morphological characteristics became evident, as many myxozoan species exhibit high morphological similarity, overlapping traits, and plasticity depending on environmental or host-related factors. These issues have led to taxonomic ambiguities and potential misidentification of species. This gap highlights the need for an integrative taxonomy approach. By combining morphological, histopathological, and molecular techniques, this study improves species identification and helps resolve taxonomic uncertainties. Addressing this gap is particularly important in regions like Malaysia, where the myxozoan fauna remains poorly documented, and in Hungary, where new species continue to be discovered from unexplored fish farms and habitats.

1.3. Research aims and objectives

This thesis endeavors to enhance my understanding of myxozoan biodiversity in freshwater ecosystems, given the different composition of fish species in Hungary and Malaysia, and the existence of high fish diversity. The main goals of this study are to compile a comprehensive collection of myxozoans and to contribute novel insights into the diversity of myxozoans in freshwater biotopes. The central focus of this dissertation is on investigating myxospore infections in both wild (Malaysia) and cultured fishes (Hungary), and the infection of actinospores in oligochaete hosts, as well as to complete the life cycle. This involves conducting thorough morphological, morphometric, histopathological, molecular, and phylogenetic analyses for accurate species identification and taxonomy.

Considering the importance of myxosporeans in ecological and economic views in Hungary and Malaysia, this study specifically embarks on the following objectives:

1. To identify and document myxosporean species and actinosporean types infecting the fishes and oligochaetes from cultured ponds in Hungary.

2. To identify and document the detected myxosporean species and actinosporean types infecting wild fishes and oligochaetes in freshwater biotopes of Malaysia.

3. To characterize both myxosporean and actinosporean stages using an integrative approach combining morphological, morphometric, histopathological and molecular analyses.

4. To elucidate life cycles by matching DNA sequences of corresponding myxosporean and actinosporean stages.

5. To investigate phylogenetic relationships among myxozoans and reveal evolutionary patterns using Maximum Likelihood (ML) and Bayesian Inference (BI) methods.

CHAPTER 2

LITERATURE REVIEW

2.1. Historical overview of Myxozoan

Myxozoa is a group of metazoan parasites that play a significant role as pathogens affecting freshwater, brackish, and marine fishes in both wild and cultured stocks. This group has a long and complicated taxonomic classification history. The initial observation of a myxozoan parasite dates back to Jurine in 1825, who identified cysts (small pox on fish) in the musculature of the extinct whitefish species, *Coregonus fera*, within Lake Geneva. Later, first description of myxosporean is associated with *Henneguya zschokkei* (Gurley, 1893), which forms cysts in subcutaneous and superficial intermuscular tissue of salmonids. Subsequently, in the 1840s, Müller provided the first detailed insights into myxosporean spores, coining the term 'psorosperms' (Müller, 1841). Further advancements occurred when the German scientist Otto Bütschli established a systematic taxonomy for myxosporeans, assigning myxozoans to Sporozoa, as the subclass Myxosporidia (Bütschli, 1882).

The Sporozoa comprised a diverse group of parasitic spore-forming unicellular parasites, which also consisted of microsporidians and members of the protist phylum Apicomplexa Levine, 1970. The classification of myxozoans within the Metazoa rather than Protozoa was proposed by Štolc in 1899, supported by subsequent studies demonstrating metazoan-related structures, such as septate and adherens-type cell junctions (Emery, 1909; Ikeda, 1912; Weill, 1938). The study of Weill (1938) was particularly important, revealing the similarity between myxozoan polar capsules and cnidarian nematocysts (**Figure 1**). Although Weill first proposed that myxozoans might be cnidarians, this idea was not mostly accepted at the time. But later, molecular studies especially the discovery of cnidarian-specific minicollagen genes through DNA sequence analyses, provided strong evidence supporting their proposition as cnidarians, a classification that persists to the present day within the Phylum Cnidaria (Holland et al., 2010; Shpirer et al., 2014; Piriatinskiy et al., 2017). Although the features of polar capsules are similar to cnidarian nematocysts, but their

function differ significantly. The polar capsules of myxozoans possess a coiled polar filament that serves as an anchor to the host for their parasitic mechanism, while nematocyst cells in Cnidarians are responsible for prey acquisition and defense.

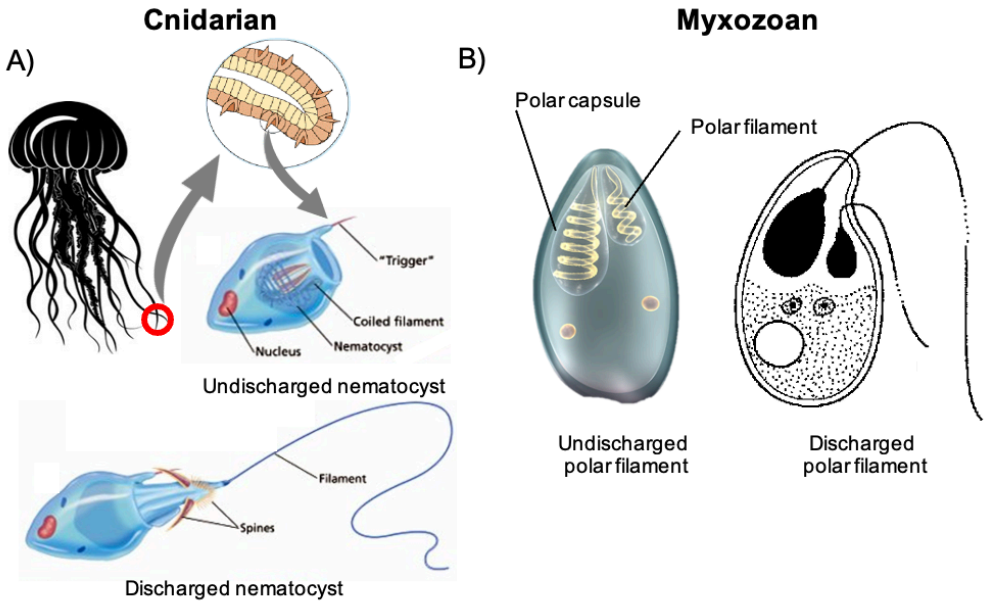

Figure 1. Structural features of (A) cnidarian nematocysts, containing a coiled harpoon-like thread for prey capture and defense, and (B) myxozoan polar capsules, which possess coiled polar filaments specialized for host attachment. Adapted from Jouiaei et al. (2015).

A taxonomic milestone was achieved with the discovery of the myxosporean two-host life cycle by Wolf & Markiw in 1984. Contrary to earlier beliefs in direct fish-to-fish transmission, this discovery highlighted the involvement of Actinosporea in the life cycle of Myxosporea. The previous understanding that myxospores needed to undergo a period of 'agieng' in mud for several months to attain infectivity has been rejected. Kent et al. (1994) subsequently suppressed the class

Actinosporea, consolidating it into a single class Myxosporea within the phylum Myxozoa. This led to a pivotal shift in the taxonomy, emphasizing the description of myxosporean species based on their myxosporean stages rather than actinosporean forms. The taxonomy of conventional myxosporeans has been persistently challenging, prompting numerous significant revisions. Among the first myxsoporean classifications was proposed by Kudo (1933) and Tripathi (1948). Later, Schulman (1966) presented a classification based on the spore shape. Mitchell (1977) described the major taxonomic schemes based on descriptive criteria. The last comprehensive

revision derived from Schulman's classification and conducted by Lom & Noble (1984) has been widely accepted. This classification not only provides a fundamental framework but also establishes a groundwork for forthcoming revisions in the taxonomy of myxosporeans.

Currently, the phylum Myxozoa comprises 60 genera and divided into two classes; Malacosporea and Myxosporea. The classification of malacosporea is poorly known, with only two genera described to date; *Tetracapsuloides* and *Buddenbrockia* (Canning & Okamura, 2004). However, the classification of the genus *Buddenbrockia* within Myxozoa has sparked debate due to conflicting morphological and evolutionary markers. *Buddenbrockia plumatellae* (Schröder, 1910) is a unique vermiform endoparasite found in freshwater bryozoans, initially placed in the class Malacosporea based on the similarities to *Tetracapsuloides bryosalmonae*, which possess 'nematocyst-like' polar capsules and a triploblastic organization. However, its worm-like body, which lacks a recognizable nervous system, gut and external sense organs, as well as the presence of four longitudinal muscle blocks, was more comparable to that of nematodes. These mixed features have led to suggestions that *B. plumatellae* represents a missing link in the evolution of myxozoans from a bilaterian ancestor (Canning et al., 2002; Okamura & Canning, 2003). Molecular studies have since confirmed the classification of *B. plumatellae* as a myxozoan within the Malacosporea subclass along with *Tetracapsuloides.* In the genus *Tetracapsuloides*, *Tetracapsuloides bryosalmonae* is widely studied species that infect salmonids, causing proliferative kidney disease (PKD) (McGurk et al., 2006; Skovgard & Buchmann, 2012). Today, the vast majority of myxozoan genera are classified within the class Myxosporea.

2.2. Life cycles and development

Initially, the life cycle of myxozoan was thought to be direct, requiring only fish as a host. However, a discovery by Wolf & Markiw (1984) revealed that myxozoan have a complex life cycle that requires two different hosts (indirect life cycle). Wolf & Markiw (1984) demonstrated that the transmission of the myxozoan *Myxobolus cerebralis*, which causes whirling disease, to rainbow trout (*Onchorynchus mykiss*) could only occur in sediment containing aquatic tubificid

oligochaetes, specifically *Tubifex tubifex*. Prior to this discovery, experimental transmission of myxozoans was rarely successful. Uspenskaya (1957) and Halliday (1976) reported that spores of *Myxobolus cerebralis* became infective after "ageing" in sediment for approximately four months. Molnár (1979) showed that transmission of *Myxobolus pavlovskii* from the gills of silver carp (*Hypophthalmichthys molitrix*) was successful only when muddy water was used. Although, these early findings showed a connection between muddy substrates and parasite infectivity, but the nature of the infectious agent was yet to be determined.

In freshwater environments, myxozoan species primarily use oligochaetes as invertebrate hosts and fish as vertebrate hosts (**Figure 2**). In contrast, marine myxozoan species primarily inhabit polychaetes, and rarely sipunculids as invertebrate hosts (Ikeda, 1912). Malacosporeans, however, use freshwater bryozoans as invertebrate hosts and fish as vertebrate hosts. Actinospores are formed within the invertebrate hosts, while myxospores are commonly found in vertebrate hosts, mostly teleost and cartilaginous fishes (Dyková & Lom, 1982), with fewer reports from amphibians, reptiles, birds and mammals (Eiras, 2005a; Dyková et al., 2007; Jirků et al., 2007; Prunescu et al., 2007; Bartholomew et al., 2008; Kawai et al., 2012; Ohnishi et al., 2013; Székely et al., 2015a). The initial stage of the myxozoan life cycle occurs in the oligochaetes host through sexual development. The short-lived actinospores are released into the water column, a process likely influences by warmer water temperatures due to seasonal fluctuations (Xiao et al., 1998a). These free actinospores then contact the epidermis of the fish host, triggering the extrusion of a polar filament that is responsible for attachment to the fish and injection of the sporoplasm (infective germ cells) into the host tissues (El-Matbouli et al., 1995; Kallert et al., 2010). Following invasion of the sporoplasm into the target tissue, an asexual phase of development occurs that leads to a second infective stage known as a myxospores. Myxospores are released from the fish either via urine, cyst rupture or upon the fish's death, and subsequently settle on the sediment where they are ingested by the invertebrate host. Development of actinospores typically occurs in the gut epithelium (Lom & Dyková, 2006) but has also been observed in the coelom (Hallett et al., 2001;

Bartholomew et al., 2006; Rangel et al., 2009, 2011), body wall (Bartholomew et al., 1997) and gonads (Køie et al., 2004) with mature spores being shed in faecal pellets or through pores in the body wall.

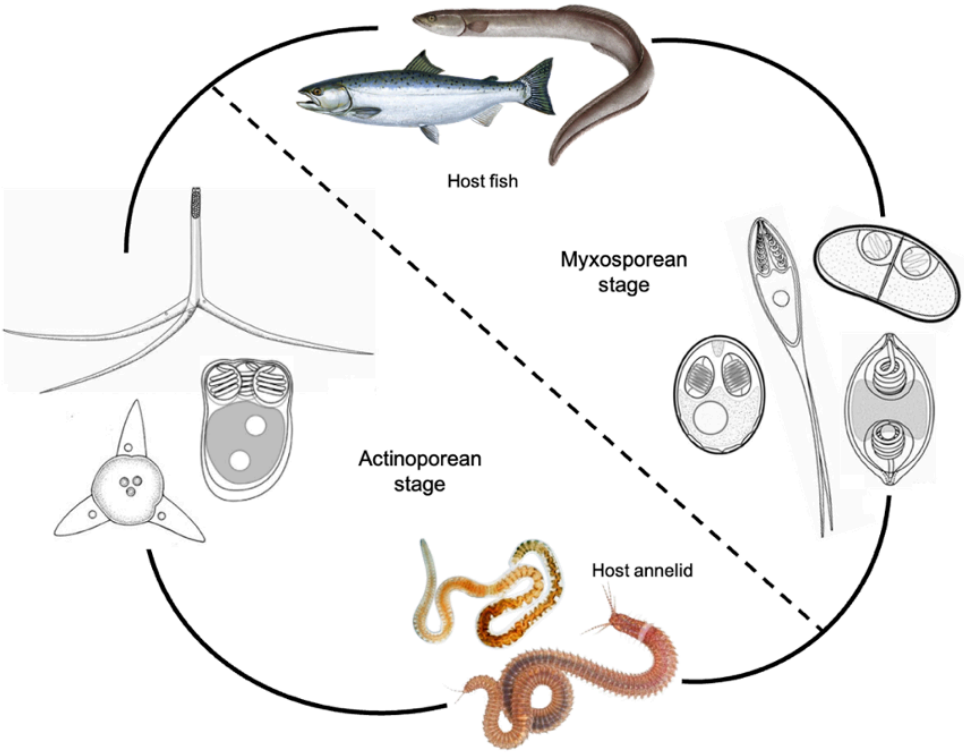

Figure 2. Indirect life cycle of myxozoans involving a fish host and an annelid host.

While the typical myxozoan life cycle involves two hosts, there are few exceptions, notably with the genus *Enteromyxum* exhibiting direct fish-to-fish transmission through vegetative stages (Diamant, 1997; Redondo et al., 2004; Yasuda et al., 2002). *Enteromyxum leei* develops within enterocytes of marine fish, and the dislodged developmental stages are orally ingested by other fish, establishing horizontal transmission, particularly in intensive culture systems where parasite spread is rapid (Sitjà-Bobadilla et al., 2007). Although *Enteromyxum* can infect naive fish through various routes, including effluent exposure, oral and anal intubation, spore injection, and cohabitation with infected fish, suggesting a broad host preference, there is no evidence of annelid host involvement (Diamant, 1997; Estensoro et al., 2010; Redondo et al., 2004; Sitjà-Bobadilla et al., 2007; Yanagida et al., 2006). However, the possibility of an alternative invertebrate host for *Enteromyxum* cannot be entirely dismissed. Other cases of successful direct transmission through

the transmission of extrasporogenic stages that caused renal sphaerosporosis in infection-free carp (Molnár & Kovács-Gayer, 1986), and through injection of blood stage of *Ceratomyxa shasta* (Johnson, 1980) and *Kudoa thyrsites* (Moran et al., 1999) into naive fish. However, there were also unsuccessful attempts to infect naive fish with *C. puntazzi* spores (Alama-Bermejo et al., 2013), *K. thyrsites* (Moran et al., 1999) and *C. shasta* (Johnson, 1980). Moreover, injection of extrasporogenic stages of *Sphaerospora* sp. from infected Atlantic salmon to naive Atlantic salmon and brown trout was successful, but not to rainbow trout (McGeorge et al., 1996). However, these examples of fish-to-fish transmission do not exclude the possibilities of vertical transmission in myxozoans. Furthermore, horizontal transmission has been observed in annelid hosts and bryozoan host via fragmentation or statoblasts in invertebrate hosts (Tops et al., 2005; Morris & Adams, 2006), providing that this might happen during the absence of vertebrate hosts.

Since 1984, significant progress has been made in elucidating myxosporean life cycles, with some revealed through experimental transmission studies or DNA sequence matching (18S rDNA gene) between myxosporean and actinosporean counterparts (Eszterbauer et al., 2015). However, transmission experiments are extremely laborious and time-consuming, due to challenges in obtaining and maintaining the correct hosts and the frequent failure to infect fish with actinospores. With the advent of molecular tools, the limitations of experimental infections have become more apparent, further reducing the reliability of this method (Holzer et al., 2004; Atkinson & Bartholomew, 2009; Marton & Eszterbauer, 2011; Székely et al., 2014). As a result, most life cycle studies rely on DNA matching, which has allowed 60 species to have their complete life cycles resolved, with 43 confirmed by molecular data from both hosts (**Table 1**). Most of the myxosporean life cycles are known from the freshwater environment, with 49 involve oligochaete intermediate hosts, only eight life cycles involve polychaetes and, three are known from bryozoans, leaving marine myxozoan life cycles remain poorly understood. Notably, certain actinospore morphotypes, such as hungactinomyxon and myxosporean genera like *Ceratomyxa*, have yet to be linked to specific counterparts through experimental transmission or DNA matching.

Table 1. List of complete myxozoan life cycles available to date. Abbreviations used in this table: Ecos. = Ecosystem, FW = Freshwater, MW = Marine, Exp = Experiment, Mol = Molecular data.

No	Myxospore species	Fish host	Actinospore type	Annelid host	Ecos.	Method	References
1	*Myxobolus cerebralis*	*Onchorhynchus mykiss*	Triactinomyxon	*Tubifex tubifex*	FW	Exp	Wolf & Markiw (1984)
2	*Myxobolus cotti*	*Cottus gobio*	Triactinomyxon	*Tubifex tubifex*	FW	Exp	El-Matbouli & Hoffmann (1989)
3	*Myxobolus pavlovskii*	*Hypothalmichtys molitrix*	Hexactinomyxon Echinactinomyxon	*Tubifex tubifex* *Limnodrilus* sp.	FW	Exp Mol	Ruidisch et al. (1991) Marton & Eszterbauer (2011)
4	*Hoferellus cyprini*	*Cyprinus carpio*	Aurantiactinomyxon	*Nais* sp.	FW	Exp	Grossheider & Körting, (1992)
5	*Myxobolus arcticus*	*Oncorhynchus nerka* *Oncorhynchus masou*	Triactinomyxon	*Stylodrilus heringianus* *Lumbriculus variegatus*	FW FW	Exp Mol	Kent et al. (1993) Urawa (1994); Urawa et al. (2011)
6	*Hoferellus carassii*	*Carassius auratus auratus*	Neoactinomyxum & Aurantiactinomyxon Aurantiactinomyxon	*Branchiura sowerbyi* *Nais* sp.	FW	Exp	Yokoyama et al. (1993a) Trouillier et al. (1996)
7	*Myxidium giardi*	*Anguilla anguilla*	Aurantiactinomyxon	*Tubifex* sp.	FW	Exp	Benajiba & Marquès (1993)
8	*Myxobolus carassii*	*Leuciscus idus*	Triactinomyxon	*Tubifex tubifex*	FW	Exp	El-Matbouli & Hoffmann (1993)
9	*Myxobolus cultus*	*Carassius auratus*	Raabeia	*Branchiura sowerbyi*	FW	Exp	Yokoyama et al. (1995) Xi et al. (2013)
10	*Zschokkella nova*	*Carassius carassius*	Siedleckiella	*Tubifex tubifex*	FW	Exp	Uspenskaya (1995)
11	*Ceratonova shasta*	*Oncorhynchus spp.*	Tetractinomyxon	*Manayunkia speciosa*	FW	Exp and Mol	Bartholomew et al. (1997)
12	*Myxobolus drjagini*	*Hypophthalmichthys molitrix*	Triactinomyxon	*Tubifex tubifex*	FW	Exp	El-Mansy & Molnár (1997a)
13	*Myxobolus hungaricus*	*Abramis brama*	Triactinomyxon	*Tubifex tubifex*	FW	Exp	El-Mansy & Molnár (1997b)
14	*Thelohanellus hovorkai*	*Cyprinus carpio*	Aurantiactinomyxon	*Branchiura sowerbyi*	FW	Exp and Mol	Yokoyama 1997 Székely et al. (1998) Anderson et al. (2000) Eszterbauer et al. (2006)
15	*Myxobolus portucalensis*	*Anguilla anguilla*	Triactinomyxon	*Tubifex tubifex*	FW	Exp	El-Mansy et al. (1998c)
16	*Thelohanellus nikolskii*	*Cyprinus carpio*	Aurantiactinomyxon	*Tubifex tubifex* *Nais* sp.	FW	Exp Mol	Székely et al. (1998) Borkhanuddin et al. (2013)
17	*Henneguya exilis*	*Ictalurus punctatus*	Aurantiactinomyxon	*Dero digitata*	FW	Mol	Lin et al. (1999)
18	*Myxobolus dispar*	*Cyprinus carpio*	Raabeia	*Tubifex tubifex*	FW	Exp	Molnár et al. (1999a)
19	*Sphaerospora dykovae*	*Cyprinus carpio*	Neoactinomyxum	*Branchiura sowerbyi*	FW	Exp	Molnár et al. (1999b)
20	*Myxobolus pseudodispar*	*Rutilus rutilus*	Triactinomyxon	*Limnodrilus hoffmeisteri* *Psammoryctides* spp. *Tubifex tubifex*	FW	Exp Mol Mol	Székely et al. (1999) Marton & Eszterbauer (2012)
21	*Henneguya ictaluri*	*Ictalurus punctatus*	Aurantiactinomyxon	*Dero digitata*	FW	Mol	Pote et al. (2000)
22	*Myxobolus bramae*	*Abramis brama*	Triactinomyxon	*Tubifex tubifex*	FW	Exp	Eszterbauer et al. (2000)
23	*Sphaerospora truttae*	*Salmo salar*	Echinactinomyxon	*Lumbriculus variegatus*	FW	Exp	Özer & Wootten (2000)
24	*Tetracapsuloides bryosalmonae*	*Oncorhynchus mykiss* *Salmo trutta*	Tetracapsuloides bryosalmonae	*Tubifex tubifex* *Fredericella sultana* *Plumatella repens*	FW	Exp and Mol	Feist et al. (2001) Morris & Adams (2006) Grabner & El-Matbouli (2008) Grabner & El-Matbouli (2010a)
25	*Myxobolus macrocapsularis*	*Abramis brama*	Triactinomyxon	*Tubifex tubifex*	FW	Exp	Székely et al. (2002)
26	*Chloromyxum truttae*	*Salmo salar* *Salmo trutta*	Aurantiactinomyxon	*Stylodrilus heringianus*	FW	Mol	Holzer et al. (2004)
27	*Myxidium truttae*	*Salmo trutta*	Raabeia	*Tubifex tubifex*	FW	Mol	Holzer et al. (2004)
28	*Ellipsomyxa gobii*	*Pomatoschistus microps*	Saccimyxon	*Nereis* sp.	M	Exp	Køie et al. (2004)
29	*Myxobolus intimus*	*Rutilus rutilus*	Triactinomyxon	*Tubifex tubifex*	FW	Exp	Rácz et al. (2004)
30	*Henneguya nuesslini*	*Salmo trutta* *Salvelinus fontinalis*	Triactinomyxon	*Tubifex tubifex*	FW	Exp and Mol	Kallert et al. (2005a)
31	*Myxobolus parviformis*	*Abramis brama*	Triactinomyxon	*Limnodrilus hoffmeisteri* *Tubifex tubifex*	FW	Exp and Mol	Kallert et al. (2005b)
32	*Chloromyxum schurovi*	*Salmo salar* *Salmo trutta*	Neoactinomyxum	*Eiseniella tetraedra*	FW	Mol	Holzer et al. (2006)
33	*Parvicapsula minibicornis*	*Oncorhynchus spp.*	Saccimyxon	*Manayunkia speciosa*	M	Mol	Bartholomew et al. (2006)
34	*Myxobolus woottenii*	*Rutilus rutilus*	Triactinomyxon	*Tubifex tubifex*	FW	Mol	Eszterbauer et al. (2006) Molnár et al. (2010)
35	*Chloromyxum auratum*	*Carassius auratus*	Antonactinomyxon	*Mix oligochaetes*	FW	Exp and Mol	Hallett et al. (2006); Atkinson et al. (2007)
36	*Gadimyxa atlantica*	*Gadus morhua*	Saccimyxon	*Spirorbis* spp.	M	Mol	Køie et al. (2007)
37	*Ceratomyxa auerbachi*	*Clupea harengus*	Saccimyxon	*Chone infundibuliformis*	M	Mol	Køie et al. (2008)
38	*Ellipsomyxa mugilis*	*Mugilidae spp.*	Saccimyxon	*Nereis diversicolor*	M	Mol	Rangel et al. (2009)
39	*Myxobilatus gasterostei*	*Gasterosteus aculeatus*	Triactinomyxon	*Nais communis* *Nais pseudobtusa*	FW	Mol	Atkinson & Bartholomew, (2009)
40	*Myxobolus lentisuturalis*	*Carassius auratus auratus*	Raabeia	*Branchiura sowerbyi*	FW	Mol	Caffara et al. (2009)
41	*Myxobolus rotundus*	*Abramis brama*	Triactinomyxon	*Tubifex tubifex*	FW	Exp and Mol	Székely et al. (2009c)
42	*Myxobolus diversicapsularis*	*Rutilus rutilus*	Triactinomyxon	*Tubifex tubifex*	FW	Mol	Molnár et al. (2010)
43	*Buddenbrockia plumatellae*	*Phoxinus phoxinus*	*Buddenbrockia* sp.	*Plumatella repens*	FW	Exp and Mol	Grabner & El-Matbouli, (2010b)
44	*Sigmomyxa sphaerica*	*Belone belone*	Saccimyxon	*Nereis pelagica*	M	Mol	Karlsbakk & Køie (2012)
45	*Myxobolus erythrophthalmi*	*Scardinius erythrophthalmus*	Triactinomyxon	*Isochaetides michaelseni*	FW	Mol	Székely et al. (2014)
46	*Myxobolus fundamentalis*	*Rutilus rutilus*	Triactinomyxon	*Isochaetides michaelseni*	FW	Mol	Székely et al. (2014)
47	*Myxobolus shaharomae*	*Alburnus alburnus*	Triactinomyxon	*Isochaetides michaelseni*	FW	Mol	Székely et al. (2014)
48	*Henneguya mississippiensis*	*Ictalurus punctatus*	Aurantiactinomyxon	*Dero digitata*	FW	Mol	Rosser et al. (2015)
49	*Ortholinea auratae*	*Sparus aurata*	Triactinomyxon	*Limnodriloides agnes*	M	Mol	Rangel et al. (2015)
50	*Thelohanellus wangi*	*Carassius auratus gibelio*	Neoactinomyxum	*Branchiura sowerbyi*	FW	Mol	Xi et al. (2015)
51	*Sphaerospora dicentrarchi*	*Dicentrarchus labrax*	Saccimyxon	*Capitella* sp.	M	Mol	Rangel et al. (2016a)
52	*Thelohanellus kitauei*	*Cyprinus carpio*	Aurantiactinomyxon	*Branchiura sowerbyi*	FW	Mol	Zhao et al. (2016)
53	*Ortholinea labracis*	*Dicentrarchus labrax*	Triactinomyxon	*Tectidrilus* sp.	M	Mol	Rangel et al. (2017)
54	*Buddenbrockia bryozoides*	*Cyprinus carpio*	Tetracapsuloides vermiformis	*Fredericella sultana*	FW	Exp and Mol	Patra et al. (2017)
55	*Thelohanellus testudineus*	*Carassius auratus gibelio*	Aurantiactinomyxon	*Branchiura sowerbyi*	FW	Mol	Zhao et al. (2017)
56	*Paramyxidium giardi*	*Anguilla anguilla*	Aurantiactinomyxon	*Tubificoides pseudogaster*	M	Mol	Rocha et al. (2019a)
57	*Myxobolus mugiliensis* *Myxobolus* sp. *Myxobolus labrosus*	*Mugil cephalus* *Chelon labrosus*	Sphaeractinomyxon Sphaeractinomyxon Sphaeractinomyxon	*Baltidrilus* sp.	M	Mol	Rocha et al. (2020a)
58	*Henneguya polarislonga*	*Astyanax lacustris*	Seisactinomyxon	Slavina evelinae	FW	Mol	Jorge et al. (2022)
59	*Myxobolus rasmusseni*	*Pimephales promelas*	Triactinomyxon	*Tubifex tubifex*	M	Mol	Tilley et al. (2024)
60	*Myxobolus* sp.	*Mugil cephalus*	Sphaeractinomyxon	–	FW	Mol	Salti et al. (2024)

2.3. Myxozoan diversity and morphotypes

The current understanding of myxozoan diversity encompasses 3,071 described species, accounting for approximately 15% of the known diversity within the Cnidarian phylum, which includes both Myxosporea and Malacosporea (Whipps et al., 2025a). Myxosporea comprises the majority of known species, with fewer than 20 known species identified in Malacosporea (Hartikainen et al., 2014; Bartošová-Sojková et al., 2014). During the 'discovery decade' of 1890 to 1900, ten genera of myxospreans were established. In the subsequent decades until 1980, the number of newly described genera varied between one and five per decade. However, there was a notable increase in the decade from 1980 to 1990, with 14 new genera being established, followed by nine more in the period from 1991 to 2000. By 2005, a total of 60 genera had been recorded (Lom & Dyková, 2006). From 2015 to the present, this number has increased to 64 genera, with 17 families of Myxosporea identified (Fiala et al., 2015a). These parasites predominantly use fish as hosts, with a smaller percentage infecting homeotherms such as reptiles, birds, and mammals host (Okamura et al., 2015).

The primary criteria for classifying myxozoan species rely on spore morphology (Andree et al., 1999; Lom & Dyková, 2006). Both myxospores and actinospores are multicellular, consisting of external shell valves that enclose sporoplasms and polar capsules. The polar capsules contain an extrudable polar tubule that upon release, can attach to the host's surface, facilitating the invasion of the host by the sporoplasms and initiating infection. Despite sharing key morphological features between myxospores and actinospores, they exhibit distinctive morphotypes (Lom & Dyková, 2006).

The guidelines for species descriptions were outlined by Lom & Arthur (1989), incorporating the host and vegetative stage as additional criteria for classifying and describing myxosporeans. While this system is well-suited for Myxosporea, it is less applicable to Malacosporea, which are rarely observed in fish hosts and lack sufficient diagnostic features for reliable classification. Malacosporean species differ from myxosporean species primarily in their hosts and spore

morphology. Specifically, malacospores of fish are spherical and consist of two unhardened valve cells that enclose two polar capsules, contrasting with the hard-shelled myxospores. Additionally, the vegetative stages of Malacosporea differ significantly from those of Myxosporea. While Myxosporea typically exhibit as spore-forming plasmodia, Malacosporea display vegetative stages that appear either as a primitive bilateral worm-like organism or a closed sac (Lom & Dykova, 2006; Jimenez-Guri et al., 2007).

2.3.1. Myxospore morphotypes

The morphology of the myxospores plays a crucial role in classification at the order and suborder levels, particularly in terms of the number of shell valves, and the number and position of polar capsules relative to the suture plane. For instances, the Class Myxosporea is divided into two distinct orders; Bivalvulida Schulman, 1959 characterized by two valves (Lom & Dyková, 2006) and Multivalvulida Schulman, 1959 characterized by three or more valves and polar capsules (Whipps et al., 2004). Within Bivalvulida, there are two suborders: Variisporina Lom et Noble, 1984 distinguished by polar capsules in various positions within the spore, and Platysporina Kudo, 1919 characterized by bilaterally symmetrical spores typically flattened parallel to the suture line.

Beyond these higher-level classifications, myxospore morphotypes are grouped into distinct genera based on specific morphological features such as the character of the polar filament, the presence or absence of caudal processes and the shape of the sutural line. The main myxospores morphotypes with high diversity comprise genera such as *Myxobolus, Henneguya*, *Thelohanellus*, *Ceratomyxa*, *Zschokkella, Myxidium, Sphaerospora, Chloromyxum*, *Kudoa* and *Sphaeromyxa* (Lom & Dyková, 2006). Among these, *Myxobolus* accounts for approximately 50% of all described myxosporean species (Liu et al., 2013) (**Figure 3**). Most of these species are histozoic in fish hosts, with a smaller proportion being coelozoic. Rare morphotypes make up only 10% of all described myxosporeans, yet many of these have undergone significant evolutionary adaptations. Finally, for the differential diagnosis of a species, several key characteristics are considered, including fish host, locality, site infection, plasmodium size, myxospores shape and

size, polar capsule(s) dimensions, shell valve symmetry and thickness, presence or absence of a triangular intercapsular appendix, structural markings on the shell valves, the number and arrangement of polar filament coils, the size of capsulogenic nuclei, shape and position of the sporoplasm, the size of the iodionophilous vacuole, number of striations and ridges, and presence or absence of a mucus envelope (Lom & Arthur, 1989; Lom & Dyková, 2006).

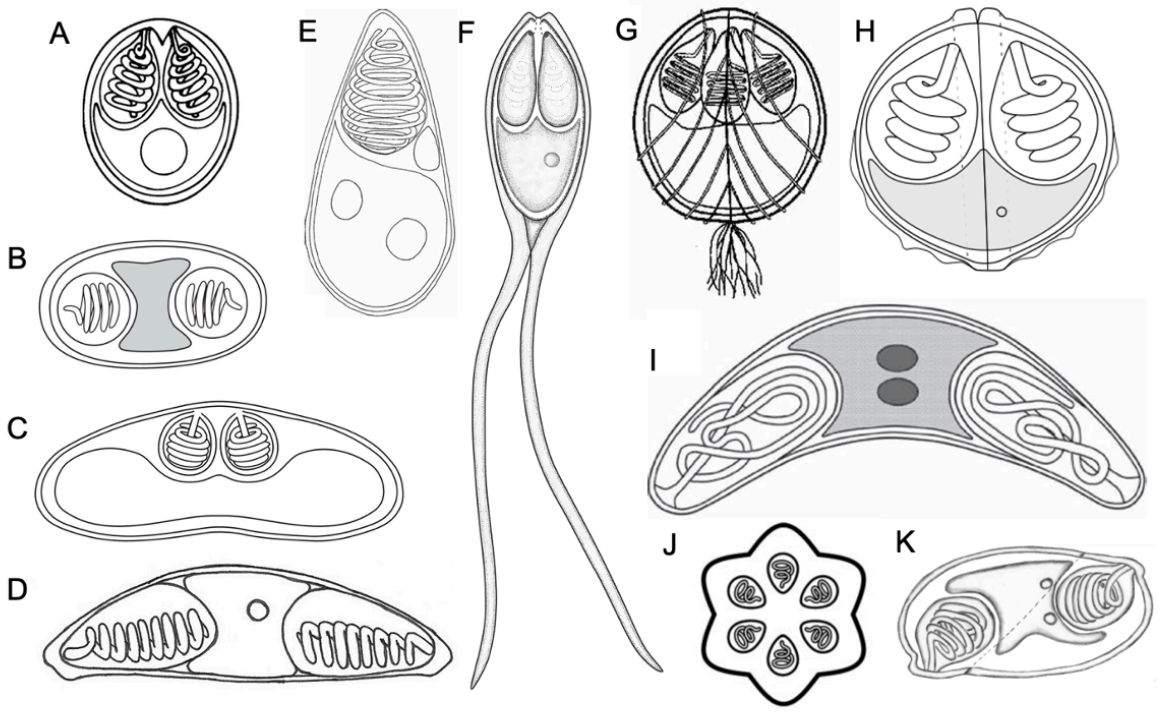

Figure 3. Schematic drawings representative of main myxospore morphotypes. (A) *Myxobolus*; (B) *Zschokkella*; (C) *Ceratomyxa*; (D) *Myxidium*; (E) *Thelohanellus*; (F) *Henneguya*; (G) *Choloromyxum*; (H) *Sphaerospora*; (I) *Sphaeromyxa*; (J) *Kudoa*; (K) *Ellipsomyxa*. Adapted from Fiala et al. (2015c).

2.3.2. Actinospore morphotypes

By 1984, when actinospores were still classified under the separate class Actinosporea, 13 taxonomic genera and 44 species had been described. Since then, approximately 136 new actinospore collective group types have been documented, though only two genera and four types remain recognized as independent taxonomic categories. Since actinospores represent sexual developmental stages in myxosporean life cycles (Wolf & Markiw, 1984), they cannot be classified as independent genera or species. Instead, should be referred as collective group names. For example, the actinospores could be designated as “Triactinomyxon type of Smith 1999 or Triactinomyxon type 2 of Smith 1999” (Kent et al., 1994, 2001; Lom et al., 1997; Kent & Lom,

1999). As of 2025, over 200 actinosporean types have been described (Lom & Dyková, 2006), but this number is expected to rise significantly. The discrepancy between the number of known actinospore types and myxosporeans suggests that many more remain to be discovered. Experimental infections and molecular data have linked 60 actinospore types to specific developmental stages of myxosporeans, while the remaining types await assignment to their corresponding myxosporean counterparts in fish hosts. The relatively low number of described actinospore types is largely attributed to the limited economic importance of their annelid hosts, which has led to under-sampling and moderately examination of oligochaetes (Milanin et al., 2017; Rocha, 2023).

Actinospores are typically characterized by their triradiate symmetry, numerous sporoplasms, and three polar capsules (Lom & Dyková, 2006). Upon release into the environment, the valves can inflate osmotically, producing valvular processes that diverge in different directions to reduce sinking. Differentiation between morphotypes primarily relies on the shape and size of the actinospore body and valvular processes, the shape and position of the polar capsules, and number of secondary cells in the sporoplasm (**Figure 4**). Based on these criteria, actinosporean morphotypes are grouped into 21 collective groups including triactinomyxon, raabeia, aurantiactinomyxon, neoactinomyxum, antonactinomyxon endocapsa, helioactinomyxon, hexactinomyxon, hungactinomyxon, ormieractinomyxon, pseudotriactinomyxon, synactinomyxon, seisactinomyxon, siedleckiella, guyenotia, echinactinomyxon, sphaeractinomyxon, saccimyxon, tetractinomyxon, tetraspora, and unicapsulactinomyxon. Freshwater environments globally report a high prevalence of aurantiactinomyxon, echinactinomyxon, neoactinomyxum, raabeia and triactinomyxon morphotypes (Lom & Dyková, 2006). In contrast, marine and brackish habitats are dominated by sphaeractinomyxon (in oligochaetes) and tetractinomyxon (in polychaetes) (Marques, 1984; Hallett et al., 1997, 1998, 1999; Køie, 2000; Køie et al., 2004, 2007, 2008, 2013; Bartholomew et al., 2006; Karlsbakk & Køie, 2012; Rangel et al., 2009, 2016a, 2016b; Rocha et al., 2019b, 2020a, 2020b; Araújo et al.,

2023). Historically, some groups such as hexactinomyxon, raabeia, sphaeractinomyxon and triactinomyxon were considered genera under the former class Actinosporea (Lom & Dyková, 2006). However, following taxonomic revisions that merged Actinospores into Myxosporea (Kent et al., 1994), these names are now used as vernacular terms for morphotypes.

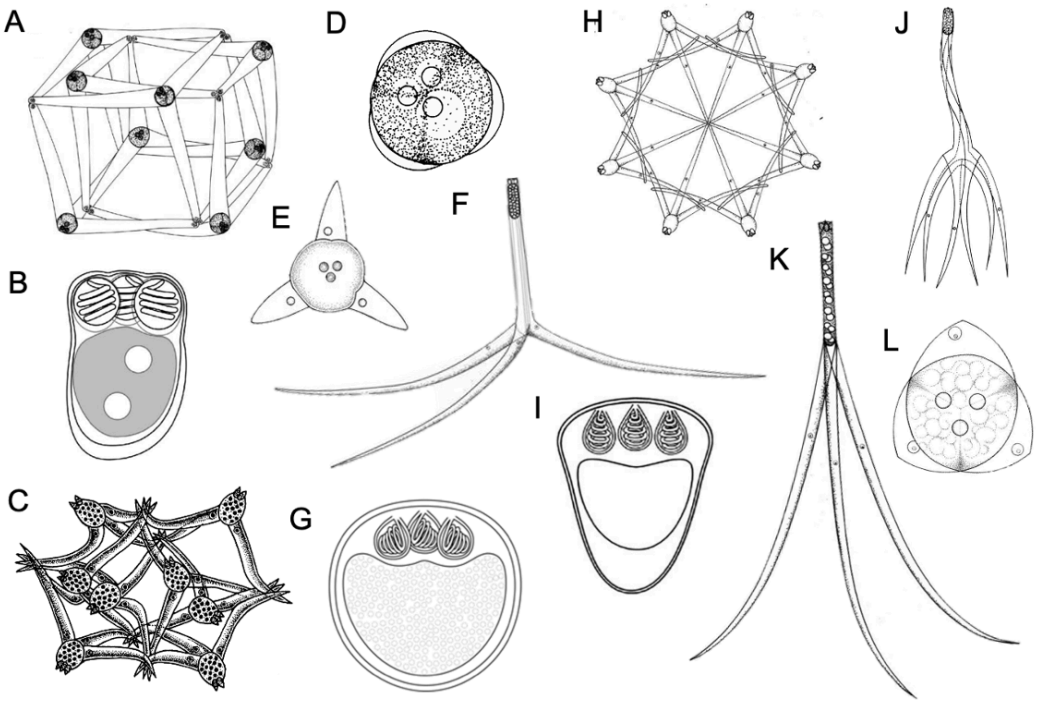

Figure 4. Schematic drawings representative of main actinospore morphotypes. (A) Hungactinomyxon; (B) Saccimyxon; (C) Antonactinomyxon; (D) Endocapsa; (E) Aurantiactinomyxon; (F) Triactinomyxon; (G) Sphaeractinomyxon, (H) Synactinomyxon; (I) Tetractinomyxon; (J) Hexactinomyxon; (K) Raabeia; (L) Neoactinomyxum. Adapted from Lom & Dyková (2006).

Recent taxonomic revisions have streamlined the classification of actinosporean collective groups. Rocha et al. (2019a) proposed invalidating echinactinomyxon types due to morphological overlap with raabeia collective group, while Rocha (2023) recommended merging the guyenotia collective group into aurantiactinomyxon collective group. These changes reduced the number of valid collective groups from 21 to 19. Newer collective groups, such as endocapsa, saccimyxon, seisactinomyxon, tetraspora and unicapsulactinomyxon were established to accommodate morphotypes described in recent decades (Hallett et al., 1999; Hallett & Lester, 1999; Rangel et al., 2011; Milanin et al., 2017; Atkinson et al., 2019). Despite sharing morphological similarities, sphaeractinomyxon and tetraspora are differentiated by the number of actinospores produced per

pansporocyst: tetraspora forms groups of four actinospores, whereas sphaeractinomyxon - groups of eight (Hallett & Lester, 1999). This distinction, debated by Rangel et al. (2016a), underscores the importance of molecular validation alongside morphology. To enhance buoyance and dispersal, some morphotypes, such as those in the antonactinomyxon, hungactinomyxon, ormieractinomyxon, siedleckiella and synactinomyxon collective groups, form spore nets. These actinospores exit the host not as isolated units but as interconnected networks of eight spores, linked by their valvular process tips (Lom & Dyková, 2006). Such adaptations are critical in benthic environments, for example, sphaeractinomyxon in marine oligochaetes lacks valvular processes, limiting buoyancy but aligning with the benthic-feeding behavior of hosts like mullets (Rocha et al., 2020a).

Although actinospores represent sexual developmental stages in myxosporean life cycles, there is no consistent correlation between myxospores and actinospore morphotypes. For example, multiple myxospores morphotypes share the same actinospore morphotype. The saccimyxon morphotype, developing in polychaete hosts is associated with diverse myxospores such as *Ceratomyxa auerbachi*, *Ellipsomyxa gobii*, *E. mugilis*, *Gadimyxa atlantica*, *Parvicapsula minibicornis*, *Sigmomyxa sphaerica* and *Sphaerospora dicentrarchi* (**Table 1**). Similarly, the aurantiactinomyxon morphotype linked to oligochaete hosts is shared by myxospores of *Chloromyxum*, *Henneguya*, *Hoferellus* and *Thelohanellus* species (**Table 1**). This lack of congruence suggests that myxospores have undergone greater morphological diversification than actinospores during evolution, likely as an adaptation to colonize diverse tissues and hosts across habitats. The production of distinct morphotypes (myxospores and actinospores) within the same life cycle evidences the considerable plasticity of myxosporean spore design and is hypothesized to correlate with optimizing transmission between vertebrate and invertebrate hosts (Fiala et al., 2015a). Molecular studies further reveal that a single actinosporean genotype may produce multiple phenotypes in invertebrate hosts, potentially designs for distinct fish hosts (Hallett et al., 2002; Holzer et al., 2004; Eszterbauer et al., 2006; Zhao et al., 2016).

2.4. Methods for identifying and classifying myxozoan species

2.4.1. Morphology features

For many years, the morphology, shape and size of spores were the primary criteria used to describe new species and differentiate existing species. A significant advancement in identification came with the consideration of host specificity and the organ and tissue tropism of specific species (Molnár, 1994; Hedrick et al., 2001; Urawa et al., 2011). However, classical zoological methods often struggle to distinguish morphologically similar myxosporean species that infect identical tissues in closely related host species (Molnár et al., 2002, 2009a). In some cases, species that appear identical based on morphology can be distinguished using molecular data. These are known as "cryptic species" (Pfenninger & Schwenk, 2007; Pérez-Ponce de León & Nadler, 2010), organisms that were once thought to be a single species but are later found to be multiple, distinct species through genetic analysis. In parasites, such distinctions are often supported by unique genetic markers or consistent variations in host specificity or tissue tropism (Nolan & Cribb, 2005; Martinsen et al., 2006). Modern diagnosis now requires the presentation of nucleotide sequences to support morphological data for a more robust classification of myxosporeans.

Discrepancies between molecular phylogenies and morphology-based taxonomy in myxozoans are often attributed to the plasticity of spore morphology. This plasticity is evident in studies showing that variations in spore morphology do not always correlate with significant genetic divergence. For instance, caudal appendages have traditionally been used to differentiate *Henneguya* from *Myxobolus*. However, molecular studies have shown that *Henneguya* species are scattered within the broader *Myxobolus* clade and do not form a monophyletic clade (Kent et al., 2001; Fiala, 2006; Liu et al., 2010a; Carriero et al., 2013). Phylogenetic evidence suggests that caudal appendages evolved independently in different lineages (Fiala & Bartošová, 2010; Liu et al., 2010a), indicating that this morphological feature provides limited phylogenetic insight into myxobolids' relationships. Moreover, atypical spore extensions have been observed in some *Myxobolus* species (Mitchell, 1989; Cone & Overstreet, 1997; Longshaw et al., 2003; Eiras et al.,

2005b; Bahri, 2008; Kaur & Singh, 2010; Liu et al., 2010a, b, 2013, 2014a, 2015; Velasco et al., 2024; de Sena et al., 2025), including recent findings in *Myxobolus lentisuturalis* (Hepps Keeney et al., 2023). Similar structures have also been documented in other genera such as *Unicauda*, *Dicauda*, *Hennegoides*, *Tetrauronema*, and *Laterocaudata*. Therefore, caudal appendages should be considered as species-specific characteristics rather than as diagnostic features at the genus level. Similarly, the separation of *Myxodavisia* from *Ceratomyxa* based on the presence of valve cell projections lacks support from molecular analyses (Fiala et al., 2015a). Genetic evidence also challenges the validity of separating *Polysporoplasma* from *Sphaerospora* solely on the basis of sporoplasm number (Bartošová et al., 2013). Furthermore, differentiating genera such as *Pentacapsula*, *Hexacapsula* and *Septemcapsula* based on the number of polar capsules have been rejected, as phylogenetic studies place them within the single genus *Kudoa*, prompting their reclassification under this genus (Whipps et al., 2004). In the line with these findings, taxonomic revisions have transferred *Zschokkella mugilis* to *Ellipsomyxa* (Koie & Karlsbakk, 2009), and species from the genus *Leptotheca* have been reassigned to *Ceratomyxa* and *Sphaerospora* (Gunter & Adlard, 2010). However, the number of polar capsules remains to serve as the key character for distinguishing *Thelohanellus* (with one polar capsule) and *Myxobolus* (with two polar capsules). The plasticity in spore morphology can result in convergent evolution of spore morphotypes (Fiala & Bartošová, 2010), where specific characters arise independently in different phylogenetic groups. Notable examples include the opposing placement of polar capsules in elongated spores of *Zschokkella* and *Myxidium*, the multiplication of polar capsules in *Chloromyxum* and *Kudoa*, and the presence of surface ridges on spores of *Myxidium*, *Zschokkella*, and *Chloromyxum*. The multiplication of polar capsules in *Chloromyxum* and *Kudoa* is believed to play a functional role in facilitating spore attachment to host tissues, thereby potentially enhancing transmission efficiency. These cases underscore the need for caution when using spore morphology alone in taxonomic assessments.

Beyond features such as caudal appendages, polar capsules orientation, polar capsule number, and surface ridges, others important biological characteristics should also be considered in distinguish cryptic species. These include the site of infection and host-related data such as host species, geographic locality, and infection prevalence. Scanning electron microscopy (SEM) is a valuable tool for resolving cryptic spore characteristics, especially in *Chloromyxum* species (Lom & Dyková, 1993). Additionally, principal component analysis (PCA) (Gunter & Adlard, 2008) has been employed to differentiate morphological and genetic traits within the genus *Ceratomyxa* (Heineger & Adlard, 2013). This analytical method has proven effective in distinguishing closely related species and had also been applied to other genera such as *Kudoa* (Burger & Adlard, 2010), *Coccomyxa*, *Aurbachia* (Heineger et al., 2011), and *Sphaerospora* (Holzer et al., 2013), highlighting its potential in taxonomic resolution.

2.4.2. Life cycles and development

Myxozoans exhibit a relatively broad range of both intermediate and definitive hosts, yet many demonstrate strict host specificity, often infecting only a single host species or family. Some species are highly host-specific, while others show more flexible host associations. For example, closely related fish species such as goldfish, gibel carp and common carp are parasitized by distinct *Sphaerospora* species (Holzer et al., 2013). *Ceratomyxa* species also tend to be highly host-specific, generally restricted to a single host species. In contrast, *Myxobolus cerebralis* is capable of infecting multiple salmonid species (Hoffman & Putz, 1969), and *Myxobolus pseudodispar*, although primarily infecting *Rutilus rutilus*, has also been reported in various other cyprinid hosts including *Abramis brama*, *Alburnus alburnus*, *Blicca bjoerkna*, *Pseudochondrostoma polylepis*, *Squalius squalus*, *Achondrostoma arcasii* and *Scardinius erythrophthalmus* (Gorbunova, 1936; Gonzalez-Lanza & Alvarez-Pellitero, 1985; Baska, 1987; Eszterbauer et al., 2001; Székely et al., 2001; Molnár et al., 2002). Similarly, *Kudoa thyrsites* has been identified in over 40 host species (Whipps & Kent, 2006), and *Enteromyxum leei* in more than 50 hosts across 20 families (Sekiya et al., 2016). However, the accuracy of these host records remains uncertain, as many earlier

identifications relied solely on morphological drawings and lacked original holotype specimens. In several cases, spores from different hosts may have been incorrectly attributed to similar species based on their morphology. Consequently, integrating host data with molecular and morphological analyses is essential for reliable species identification and descriptions.

Although vertebrate host specificity in myxozoans has been extensively studied, there is comparatively limited knowledge regarding their associations with invertebrate hosts. Recent research has revealed that the annelid *Baltidrilus* sp. can act as an intermediate host for four *Myxobolus* species infecting *Mugil* spp. (Rocha et al., 2020a), while *Tubifex tubifex* has been documented as a host for fourteen *Myxobolus* species (see **Table 1**). Moreover, *Myxobolus pseudodispar* has been identified in four different annelid species (Marton & Eszterbauer, 2012), and *Thelohanellus nikolskii* has been detected in both *Nais* sp. and *T. tubifex* (Borzák et al., 2021).

Myxosporean species exhibit not only high host specificity but also have high preference for particular tissues and organs. Their plasmodial development is often limited to specific anatomical sites such as fins, skin, muscles, gills, kidneys, spleen, heart, cartilage, bones, and liver. These parasites are broadly categorized into two groups based on the site of infection: coelozoic and histozoic species. Coelozoic myxosporeans typically inhabit cavities of organs, including the gallbladder, bile ducts, urinary tract and renal tubules. These infections usually have minimal pathological effects on the host and are often asymptomatic. Coelozoic plasmodia are most commonly disporic (producing two spores), while monosporic forms are rare (producing one spore), such as sphaerosporids (Lom & Dyková, 1992; Bartošová et al., 2013). In both freshwater and marine systems, polysporic plasmodia have also been observed, especially in genera like *Ceratomyxa*, *Chloromyxum* and *Parvicapsula*.

In contrast, histozoic myxosporeans develop within the tissues themselves, frequently targeting the gills due to their accessibility and high vascularity. This mode of infection is commonly seen in the genera *Myxobolus* and *Henneguya* (Molnár, 2002). Within the gills, plasmodia may form in

various locations; for example, *M. hungaricus* develops in the central and basal portions of the gill lamellae, whereas *M. bramae* and *M. macrocapsularis*, infecting the same host species, localize nearer the apical regions. *Myxobolus basilamellaris* forms beneath the epithelial layer of the gill filament, while *M. intrachondrealis* resides within the cartilage matrix of the gill arch. Determining the precise site of infection can assist in species identification and help differentiate closely related taxa. Histozoic infections typically manifest as small, localized white cysts that cause minimal tissue disruption. However, when cysts become abundant in vital organs such as the gills or heart, they can contribute to disease outbreaks, significantly impacting fish health and aquaculture productivity.

2.4.3. Molecular methods

Among the various molecular markers employed, the 18S ribosomal DNA (18S rDNA) has been the most widely used for phylogenetic analyses across metazoans (Hillis & Dixon, 1991) and has proven particularly informative in elucidating evolutionary relationships among myxozoan species (Kent et al., 2001). This marker provides a robust comparative dataset due to its combination of conserved and variable regions, which makes it suitable for resolving both deep and recent divergences.

The variability in 18S rDNA sequences, largely influences by nucleotide insertions or deletions results in noticeable differences in sequence length among the three major myxozoan lineage. Species in the marine clade typically possess 18S rDNA sequences of approximately 1800 base pairs (bp), those in the freshwater clade around 2000 bp, and species within *Sphaerospora* sensu stricto group can exhibit sequences up to 4000 bp in length (Fiala, 2006; Bartošová et al., 2013). In addition to 18S rDNA, the 28S ribosomal DNA gene (28S rDNA) has also been utilized as a molecular marker (Whipps et al., 2004), and in some cases, it provides even greater resolution for phylogenetic reconstruction than 18S rDNA (Bartošová et al., 2009). As a complementary marker, 28S rDNA enhances the robustness of phylogenetic inferences.

The growing number of 18S and 28S rDNA sequences in GenBank database has significantly improved the ability to compare and delineate species. Besides ribosomal markers, other genetic loci have been explored for their phylogenetic utility. These include protein-coding genes such as myosin heavy chain 2 (Fiala & Bartošová, 2010), heat shock protein 70 (HSP 70), and elongation factor 2 (EF2), which has been applied in studies of *Kudoa thyrsites*, *Kudoa dianae* and *Myxidium* spp. (Whipps & Kent, 2006; Bartošová, 2010; Fiala & Bartošová, 2010). Despite these efforts, the phylogenetic resolution offered by these protein-coding genes remain limited, and their broader applicability across myxozoans is still evaluation.

2.5. Myxozoan study in Hungary

Hungary has a well-documented record of myxozoan biodiversity, thanks to comprehensive research efforts that began in the 1980s and continue to the present day. Over the decades, researchers have described numerous new myxosporean species infecting fish, investigated actinospore stages in various annelid hosts, and elucidated life cycles through infection experiments. These studies have focused on both aquaculture systems and natural habitats, particularly in Lake Balaton and surrounding areas.

To date, over 100 myxosporean species have been identified in Hungary. Most of these identifications based on morphological characteristics, although some have been confirmed through a combination of morphological and molecular analyses. The recorded taxa span several genera, including *Henneguya*, *Hoferellus*, *Myxidium*, *Zschokkella*, *Myxobilatus*, *Myxobolus*, *Sphaerospora*, *Thelohanellus*, *Chloromyxum*, and *Ceratomyxa*. Of these, *Myxobolus* is the most abundant, with over 60 species reported primarily from cyprinid fish (Molnár & Székely, 1995, 1999; Székely & Molnár, 1997; Eiras et al., 2005b; Eiras et al., 2014; Eiras et al., 2021; Goswami, 2021; Goswami et al., 2021; Colunga-Ramírez et al., 2024). In contrast, only a single species of *Ceratomyxa*, *Ceratomyxa hungarica* has been described from a freshwater goby in Hungary. Among the fish hosts, *Cyrpinus carpio* harbors the greatest number of myxozoan species, followed

by *R. rutilus*, *A. alburnus*, and *B. bjoerkna* (Eiras et al., 2005b; Zhang et al., 2013; Eiras et al., 2014; Eiras et al., 2021).

Compared to myxosporean infections in fish, the actinosporean fauna in oligochaete hosts is relatively less documented. To date, 51 distinct actinospore types have been identified, classified into eight collective groups such as aurantiactinomyxon, guyenotia, neoactinomyxum, raabeia, triactinomyxon, hungactinomyxon, echinactinomyxon, and synactinomyxon (El-Mansy & Molnár, 1997a, b; El-Mansy et al., 1998a, b, c; Székely et al., 1998, 1999, 2002, 2009c, 2014; Molnár et al., 1999a, b; Eszterbauer et al., 2000, 2006; Rácz et al., 2004, 2005; Marton & Eszterbauer, 2011; Borkhanuddin et al., 2014a; Zhao et al., 2016; Borzák et al., 2021). Of these, 31 actinospore types were described by El-Mansy et al. (1998a, b), based solely on morphological characteristics, while an additional 14 types were identified by Eszterbauer et al. (2006) using a combination of morphological and molecular analyses. A significant contribution to actinosporean taxonomy was made by Rácz et al. (2005), who introduced a novel collective group named hungactinomyxon, distinguished by its unique morphological features that do not align with any previously known groups.

Field investigations have primarily targeted natural freshwater environments such as Lake Balaton (Keszthely, Tihany, Balatonvilágos, Balatonszemes, Siófok), Kis-Balaton Reservoir, and the River Zala, as well as the River Tisza. In contrast, research in aquaculture settings is limited and has so far been focused to the Warmwater Fish Hatchery (TEHAG) in Százhalombatta (El-Mansy et al., 1998b; Rácz et al., 2005; Eszterbauer et al., 2006; Marton & Eszterbauer, 2011). Interestingly, most actinospores described to date were actually discovered at this facility. Besides from natural and farm environments, experimental infection studies have further contributed to the understanding of myxozoan life cycles, resulting in the description of 12 additional actinospore types and the elucidation of their developmental pathways in Hungary (El-Mansy & Molnár, 1997a, b; El-Mansy et al., 1998c; Székely et al., 1998, 1999, 2002, 2009c; Molnár et al., 1999a, b; Eszterbauer et al., 2000; Rácz et al., 2004).

2.6. Myxozoan study in Malaysia

In contrast to Hungary, the biodiversity of myxozoans in Malaysia remains relatively underexplored, primarily due to limited research efforts and a lack of specialized expertise in this field. The first documented investigation into myxozoan infections in Malaysia was conducted by Shariff (1982), who provided a detailed morphological and pathological analyses of myxospores infecting *Oxyeleotris marmoratus* (Bleeker), and described a novel species, *Henneguya shaharini*. Subsequent studies examining myxozoan fauna in both wild and cultured freshwater fishes, particularly from biotopes in the Terengganu and Kelantan states, were carried out by Molnár et al. (2006a, b), Székely et al. (2009a, b, 2012), Borkhanuddin (2013) and Borkhanuddin et al. (2020a). These efforts collectively documented 23 myxosporean species belonging to genera such as *Myxobolus*, *Thelohanellus*, *Henneguya*, *Hennegoides*, and *Myxidium* (**Table 2**).

However, in marine biotopes specifically the Andaman Sea and the coastal waters of Terengganu have yielded descriptions of only 18 myxosporean species to date from genera such as *Latyspora*, *Gastromyxum*, *Ceratomyxa*, *Myxodavisia*, *Kudoa*, *Zschokkella*, *Henneguya,* and *Myxobolus* (**Table 2**). In freshwater habitats, *Myxobolus* species are the most frequently encountered, whereas in marine habitats, *Ceratomyxa* species appear to be more prevalent. Notably, most of the myxosporean-infected fishes from both freshwater and marine environments are of significant economic importance, serving either as food sources or for ornamental use.

Despite the limited scope of research, existing surveys have revealed a surprisingly rich diversity of myxozoans in Malaysian fish populations. However, the corresponding actinosporean stages and their oligochaete hosts remain entirely unstudied. To address this knowledge gap, this study focuses on freshwater fish and their associated oligochaetes to expand the inventory of Malaysian myxosporeans and actinospore types, and to elucidate their life cycles for the first time.

Table 2 Recorded myxosporean species infecting Malaysian fishes.

No.	Myxospore species	Site of infection	Fish host	Host Habitat	Locality	References
1.	*Henneguya shaharini* Shariff, 1982	Gills	*Oxyeleotris marmoratus*	Freshwater	Selangor and Tasik Kenyir, Terenganu	Shariff (1982); Székely et al. (2009a)
2.	*Henneguya shariffi* Molnár, Székely, Mohamed et Shaharom-Harrison, 2006	Gill filaments	*Pangasius hypophthalmus*	Freshwater	Terengganu River	Molnár et al. (2006a)
3.	*Hennegoides pangasii* Molnár, Székely, Mohamed et Shaharom-Harrison, 2006	Gill filaments	*Pangasius hypophthalmus*	Freshwater	Terengganu River	Molnár et al. (2006a)
4.	*Hennegoides malayensis* Molnár, Székely, Mohamed et Shaharom-Harrison, 2006	Gill rays	*Pangasius hypophthalmus*	Freshwater	Terengganu River	Molnár et al. (2006a)
5.	*Hennegoides berlandi* Molnár, Székely, Mohamed et Shaharom-Harrison, 2006	Gill filaments	*Pangasius hypophthalmus*	Freshwater	Terengganu River	Molnár et al. (2006a)
6.	*Myxobolus baskai* Molnár, Székely, Mohamed et Shaharom-Harrison, 2006	Gills	*Pangasius hypophthalmus*	Freshwater	Terengganu River	Molnár et al. (2006a)
7.	*Myxobolus pangasii* Molnár, Székely, Mohamed et Shaharom-Harrison, 2006	Spleen	*Pangasius hypophthalmus*	Freshwater	Terengganu River	Molnár et al. (2006a)
8.	*Henneguya mystusia* Sarkar, 1985	Gill filaments	*Hemibagrus nemurus*	Freshwater	Terengganu River	Molnár et al. (2006b)
9.	*Henneguya basifilamentalis* Molnár, Székely, Mohamed et Shaharom-Harrison, 2006	Basal crypts of hemibranchia	*Hemibagrus nemurus*	Freshwater	Terengganu River and Tasik Kenyir	Molnár et al. (2006b); Székely et al. (2009b)
10.	*Henneguya hemibagri* Tchang et Ma, 1993	Gill lamellae	*Hemibagrus nemurus*	Freshwater	Terengganu River and Tasik Kenyir	Molnár et al. (2006b); Székely et al. (2009a)
11.	*Myxobolus omari* Székely, Shaharom-Harrison, Cech, Mohamed et Molnár, 2009	Muscle cells	*Pangasius hypophthalmus*	Freshwater	Kuala Terengganu, Terengganu	Székely et al. (2009b)

12.	*Thelohanellus zahrahae* Székely, Shaharom-Harrison, Cech, Mohamed et Molnár, 2009	Gills	*Barbonymus gonionotus*	Freshwater	Macang, Kelantan	Székely et al. (2009b)
13.	*Myxobolus leptobarbi* Székely, Shaharom-Harrison, Cech, Mohamed et Molnár, 2009	Muscle cells	*Leptobarbus hoevenii*	Freshwater	Macang, Kelantan	Székely et al. (2009b)
14.	*Henneguya daoudi* Székely, Shaharom-Harrison, Cech, Mohamed et Molnár, 2009	Gills	*Trichopodus trichopterus*	Freshwater	Macang, Kelantan	Székely et al. (2009b)
15.	*Myxobolus terengganuensis* Székely, Shaharom-Harrison, Cech, Ostoros et Molnár, 2009	Muscle	*Osteochilus hasselti*	Freshwater	Tasik Kenyir, Terengganu	Székely et al. (2009a)
16.	*Myxobolus csabai* Székely, Shaharom-Harrison, Cech, Ostoros et Molnár, 2009	Kidney	*Osteochilus hasselti*	Freshwater	Tasik Kenyir, Terengganu	Székely et al. (2009a)
17.	*Myxobolus osteochii* Székely, Shaharom-Harrison, Cech, Ostoros et Molnár, 2009	Kidney	*Osteochilus hasselti*	Freshwater	Tasik Kenyir, Terengganu	Székely et al. (2009a)
18.	*Myxobolus tasikkenyirensis* Székely, Shaharom-Harrison, Cech, Ostoros et Molnár, 2009	Muscle	*Osteochilus vittatus*	Freshwater	Tasik Kenyir, Terengganu	Székely et al. (2009a)
19.	*Myxobolus dykovae* Székely, Shaharom-Harrison, Cech, Ostoros et Molnár, 2009	Gill lamellae	*Barbonymus schwanefeldii*	Freshwater	Tasik Kenyir, Terengganu	Székely et al. (2009a)
20.	*Latyspora scomberomori* Bartošová, Freeman, Yokoyama, Caffara et Fiala, 2011	Kidney tubules	*Scomberomosus guttatus*	Marine	Water off Peninsular Malaysia	Bartošová et al. (2011)
21.	*Myxobolus tambroides* Székely, Shaharom, Cech, Mohamed, Mohd Zin, Borkhanuddin, Ostoros et Molnár, 2012	Gill lamellae	*Tor tambroides*	Freshwater	Tasik Kenyir, Terengganu	Székely et al. (2012)
22.	*Myxobolus* sp.	Muscle	*Labiobarbus* sp.	Freshwater	Tasik Kenyir, Terengganu	Borkhanuddin (2013)
23.	*Myxidium* sp. II		*Tor tambroides*	Freshwater	Tasik Kenyir, Terengganu	Borkhanuddin (2013)

24.	*Myxbolus ophiocarae* Borkhanuddin, Cech, Mazelan, Shaharom-Harrison, Molnár et Székely, 2014	Gill lamellae	*Ophiocara porocephala*	Estuarine	Merang Estuary	Borkhanuddin et al. (2014b)
25.	*Gastromyxum rafii* Freeman and Kristmundsson, 2015	Stomach wall	*Elops machnata*	Marine	Langkawi Island	Freeman & Kristmundsson (2015)
26.	*Gastromyxum bulani* Freeman and Kristmundsson, 2015	Stomach wall	*Megalops cyprinoides*	Marine	Bachok, Kelantan	Freeman & Kristmundsson (2015)
27.	*Ceratomyxa leatherjacketi* Fiala, Hlavničková, Kodádková, Freeman, Bartošová-Sojková et Atkinson, 2015	Gall bladder	*Aluterus monoceros*	Marine	Andaman Sea	Fiala et al. (2015b)
28.	*Ceratomyxa ayami* Fiala Fiala, Hlavničková, Kodádková, Freeman, Bartošová-Sojková et Atkinson, 2015	Gallbladder	*Aluterus monoceros*	Marine	Pangkor Island	Fiala et al. (2015b)
29.	*Myxodavisia bulani* Fiala, Hlavničková, Kodádková, Freeman, Bartošová-Sojková et Atkinson, 2015	Gallbladder	*Megalops cyprinoides*	Marine	Langkawi Island	Fiala et al. (2015b)
30.	*Ceratomyxa* sp.	Gallbladder	*Epinephelus coioides*	Estuarine	Setiu Wetlands, Terengganu	Shahar et al. (2017)
31.	*Ceratomyxa* sp. 1	Gallbladder	*Nemipterus bathybius, N. tambuloides, N. nematophorus*	Marine	Terengganu waters	Samshuri (2018)
32.	*Ceratomyxa* sp. 2	Gallbladder	*Nemipterus furcosus, N. nemurus*	Marine	Tok Jembal and Terengganu waters	Samshuri (2018)
33.	*Ceratomyxa* sp. 3	Gallbladder	*Nemipterus marginatus*	Marine	Terengganu waters	Samshuri (2018)
34.	*Kudoa pagrusi* Al-Quraishy, Koura, Abdel-Baki, Bashtar, Deed, Al Rashied et Abdel-Ghaffar, 2008	Pericardium of heart	*Nemipterus tambuloides*	Marine	Terengganu waters	Samshuri (2018)
35.	*Zschokkella* sp. 1	Gallbladder	*Nemipterus aurora*	Marine	Terengganu waters	Samshuri (2018)

36.	*Myxidium cf. notopterum* Sarkar, 1996	Gallbladder	*Notopterus notopterus*	Freshwater	Tasik Kenyir, Terengganu	Borkhanuddin et al. (2020a)
37.	*Henneguya setiuensis* Borkhanuddin, Cech, Molnár, Shaharom-Harrison, Khoa, Samshuri, Mazelan, Atkinson et Székely, 2020	Gill lamellae	*Later calcarifer*	Estuarine	Setiu Wetlands, Terengganu	Borkhanuddin et al. (2020b)
38.	*Henneguya voronini* Borkhanuddin, Cech, Molnár, Shaharom-Harrison, Khoa, Samshuri, Mazelan, Atkinson et Székely, 2020	Gill filament	*Later calcarifer*	Estuarine	Setiu Wetlands, Terengganu	Borkhanuddin et al. (2020b)
39.	*Henneguya calcarifer* Borkhanuddin, Cech, Molnár, Shaharom-Harrison, Khoa, Samshuri, Mazelan, Atkinson et Székely, 2020	Skeletal muscle	*Later calcarifer*	Estuarine	Setiu Wetlands, Terengganu	Borkhanuddin et al. (2020b)
40.	*Myxobolus selari* Samshuri and Borkhanuddin, 2024	Brain	*Selar crumenophthalmus*	Marine	Terengganu waters	Samshuri & Borkhanuddin (2024)
41.	*Myxobolus acanthogobii* Hoshina, 1952	Brain	*Nemipterus flavimanus*	Marine	Terengganu waters	Samshuri & Borkhanuddin (2024)

CHAPTER 3

MATERIALS AND METHODS

3.1. Fish and oligochaete collections in Hungary

Fish were collected using gillnets from the earth ponds at two fish farms located at Ócsárd, near Pécs (45°55'53.544" N, 18°09'14.0472" E) and Dömsöd, Ráckeve Danube Arm Fishing Association (47°07'17.33" N, 19°01'34.23" E) between November 2023 to June 2024. The Ócsárd fish farm consists of 12 small ponds, covering a total area of 38 hectares. The primary fish species produced at the farm include pike perch (*Sander lucioperca*) and wels catfish (*Silurus glanis*), along with a smaller proportion of other species such as common carp (*Cyprinus carpio*), grass carp (*Ctenopharyngodon idella*), African catfish (*Clarias gariepinus*), tench (*Tinca tinca*), burbot (*Lota lota*), bream (*Abramis brama*), and gibel carp (*Carassius auratus gibelio*). For this study, fish were sampled from three of the twelve ponds (**Figure 5**).

The Dömsöd fish farm includes 13 ponds covering 1.3 hectares, producing primarily common carp (*Cyprinus carpio*), grass carp (*Ctenopharyngodon idella*), wels catfish (*Silurus glanis*), and pikeperch (*Sander lucioperca*), along with other cyprinids such as silver carp (*Hypophthalmichthys molitrix*) and bream (*Abramis brama*). Fish samples were collected from two of the thirteen ponds (**Figure 6**). Additionally, a small number of fish were provided by a fish farmer from a barrage pond in Szigetvár during autumn 2021 and 2022. Detailed information on the fish species, sizes, number of individuals sampled, and their respective sampling locations is presented in **Table 3**.

Table 3 Fish species, number of specimens collected or examined, and size range from each fish farm.

Species	Number of fish specimens examined	Fish size (length)	Locality
Carassius auratus gibelio	112	7–23 cm	Ócsárd, Szigetvár
Cyprinus carpio	27	4–21 cm	Ócsárd, Dömsöd
Rutilus rutilus	5	10–12.5 cm	Ócsárd
Total	**144**		

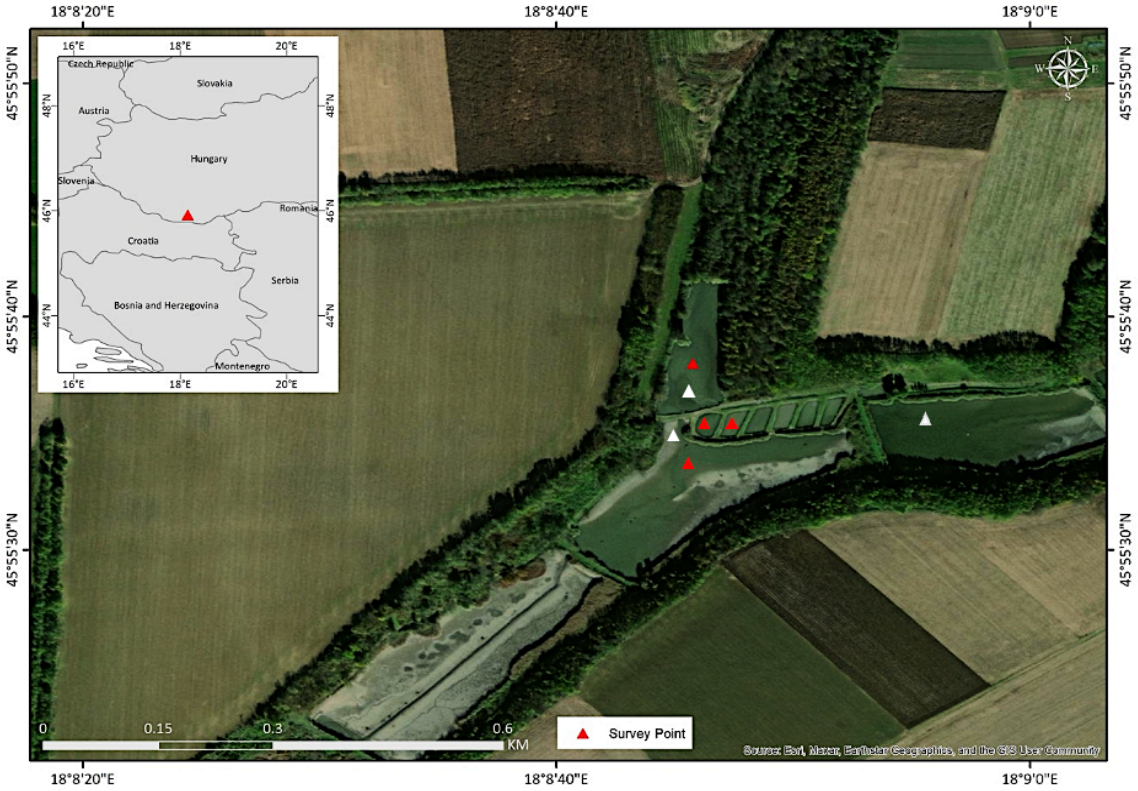

Figure 5. Map of Ócsárd fish farm near Pécs, showing the sampling sites. Fish were collected from three ponds (white arrowhead), and sediment samples for oligochaete collection were sampled from four ponds (red arrowhead).

Figure 6. Map of Dömsöd fish farm showing the sampling sites. Fish were collected from two ponds (white arrowhead).

For oligochaete collections, the sediment containing oligochaetes were collected using a shovel and a 1000 μm mesh net from low water levels earth ponds at Ócsárd, Szigetbecse, Makád, Dömsöd and Dinnyés between April 2023 to June 2024. In the Ócsárd fish farm, samples were taken from four ponds (**Figure 5**). The Szigetbecse, Makád and Dömsöd fish farms belong to the Ráckeve Danube Arm Fishing Association. The Szigetbecse (47°07'30.6" N, 18°57'48.7" E) facility consists of twelve small ponds with a total area of 1.9 ha, while the Makád fish farm (47°02'35.8" N, 18°57'57.9" E) consists of six fish ponds with 87.35 ha. These fish farms mainly produced common carp (*Cyprinus carpio*), but also a small proportion of herbivores and predatory fish such as pike (*Esox lucius*), asp (*Aspius aspius*), pikeperch (*Sander lucioperca*), tench (*Tinca tinca*), wels catfish (*Silurus glanis*), and grass carp (*Ctenopharyngodon idella*), yielding approximately 200–220 tons of fish annually. A large portion of this production is released into the Ráckeve Danube Branch to sustain fish populations. For this study, sediment samples were taken from four of the twelve ponds in Szigetbecse (**Figure 7**) and two ponds in Makád (**Figure 8**). Although sediment samples were also collected from ponds in Dömsöd and Dinnyés, no oligochaetes were found in those sediments; therefore, no further details on those sites are provided.

All live fish and sediment samples were transported to the Fish Pathology and Parasitology Laboratory at the HUN-REN Veterinary Medical Research Institute, Budapest, Hungary, where they were maintained in tanks or buckets with continuous aeration at a constant temperature of 23 °C. In the laboratory, the fish were dissected, and all organs were thoroughly examined for myxozoan infections under stereo and light microscopes. Oligochaetes were hand-sorted on a transparent tray placed over a light panel and individually transferred into the wells of 48-well microtiter plates filled with dechlorinated water. Large oligochaetes, such as *Branchiura sowerbyi* were placed into 12-well or 24-well microtiter plates. Each plate was examined daily for a period ranging from one week to two months to monitor the release of actinospores using a Zeiss Axiovert

25 inverted microscope (Zeiss, Jena, Germany). Oligochaete hosts were identified according to the key of Timm (1999) and by molecular analysis.

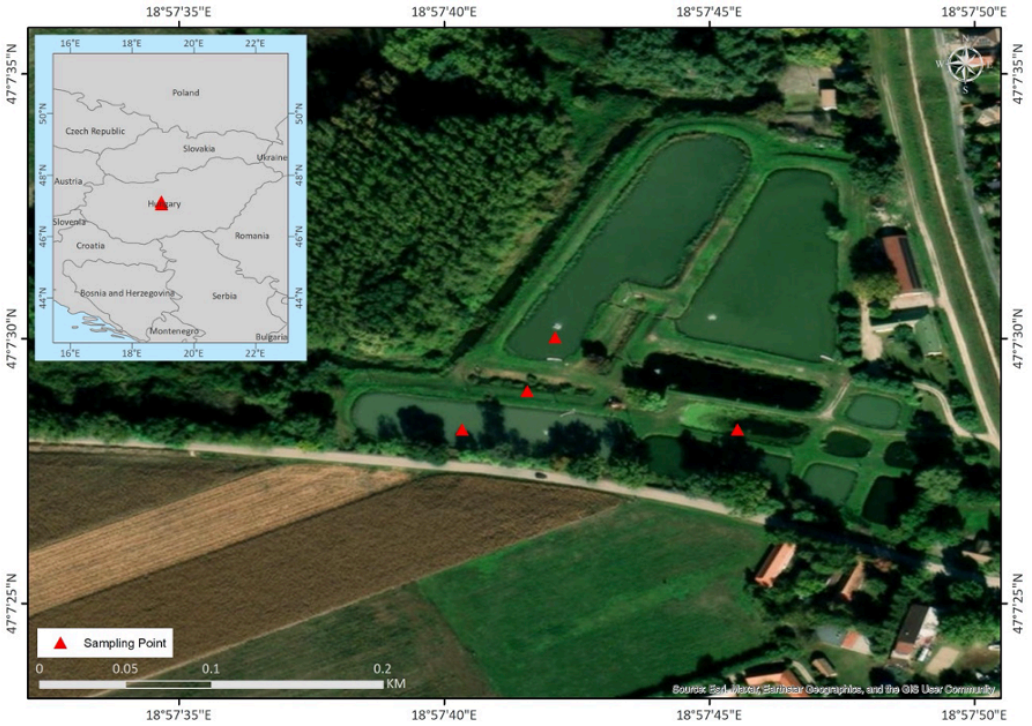

Figure 7. Map of Szigetbecse in Ráckeve, showing the sampling sites. Sediment samples for oligochaete collection were samples from four ponds (red arrowhead).

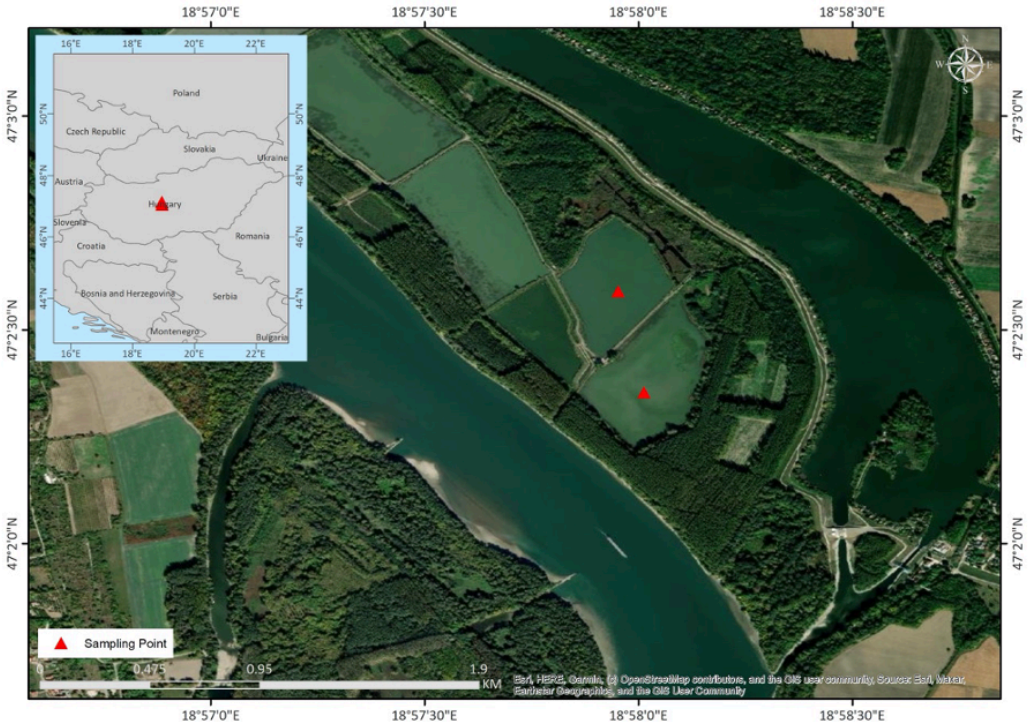

Figure 8. Map of Makád in Ráckeve, showing the sampling sites. Sediment samples for oligochaete collection were samples from two ponds (red arrowhead).

3.2. Fish and oligochaete collections in Malaysia

Fish originating from the rivers of Sungai Tong, Setiu; Sungai Nerus, Kuala Nerus and small channels across Kuala Terengganu, Terengganu were purchased from a local fish market in Kuala Terengganu, Terengganu, Malaysia (5°18′44.703″ N, 103°7′40.332″ E). The fish were procured at two-week intervals from July to August 2023 and September to November 2024. Detailed information on the fish species, sizes, number of individuals sampled, and their respective sampling locations is presented in **Table 4.**

Table 4 Fish species, number of specimens collected or examined, and size range from each locality in Terengganu.

Species	Number of fish specimens examined	Fish size (length)	Locality
Barbonymus gonionotus	6	15.5–30.0 cm	Sungai Tong
Barbonymus altus	16	9.5–14.5 cm	Sungai Nerus
Barbonymus schwanefeldii	6	13.0–25.0 cm	Sungai Tong
Leptobarbus rubripinna	5	9.5–16.0 cm	Sungai Nerus
Barbodes binotatus	13	8.0–11.5 cm	Sungai Nerus
Labiobarbus leptocheilus	15	7.0–13.0 cm	Sungai Nerus
Osteochilus waandersii	15	7.5–11.0 cm	Sungai Nerus
Trichopodus trichopterus	9	9.0–11.0 cm	Small channels
Trichopodus pectoralis	12	10.0–23.5 cm	Small channels
Channa gachua	12	7.5–15.5 cm	Small channels
Neolissochilus hexagonolepis	5	14.0–15.5 cm	Sungai Tong
Anabas testudineus	3	12.0–13.0 cm	Small channels
Notopterus notopterus	2	22.5–25.0 cm	Sungai Nerus
Total	**119**		

For oligochaete collections, the sediment containing oligochaetes were collected using a shovel from Tasik Telabak in July 2023, September 2024, and October 2024 (**Figure 9**). Tasik Telabak (5°37′58.22″ N, 102°28′44.52″ E) is located in the upstream region of Besut, Terengganu, and is recognized as a popular recreational area for fishing activities. Recently, the lake has been utilized by local communities for fish farming, including species such as *Oreochromis niloticus* (tilapia) and *Hemibagrus nemurus* (silver catfish). Additionally, various native and invasive fish species can also be found in the lake including peacock bass (*Cichla* sp.), tinfoil barb (*Barbonymus schwanenfeldii*), marble goby (*Oxyeleotris marmoratus*), bronze featherback (*Notopterus*

notopterus), silver shark minnow (*Osteochilus vittatus*), beardless barb (*Cyclocheilichthys apogon*), and common barb (*Labiobarbus* sp.). Tasik Telabak was chosen for this study due to the limited information available on fish parasites and the aquaculture activities are newly established, presenting opportunities for economic development and expansion in the region. Moreover, the lake is a crucial economic resource for local communities that depend on its ecosystem for their livelihoods. It serves as an excellent subject for studying biodiversity and the potential for sustainable aquaculture, including parasite surveys informing about pathogen-infection risk assessments of economically important cultured species.

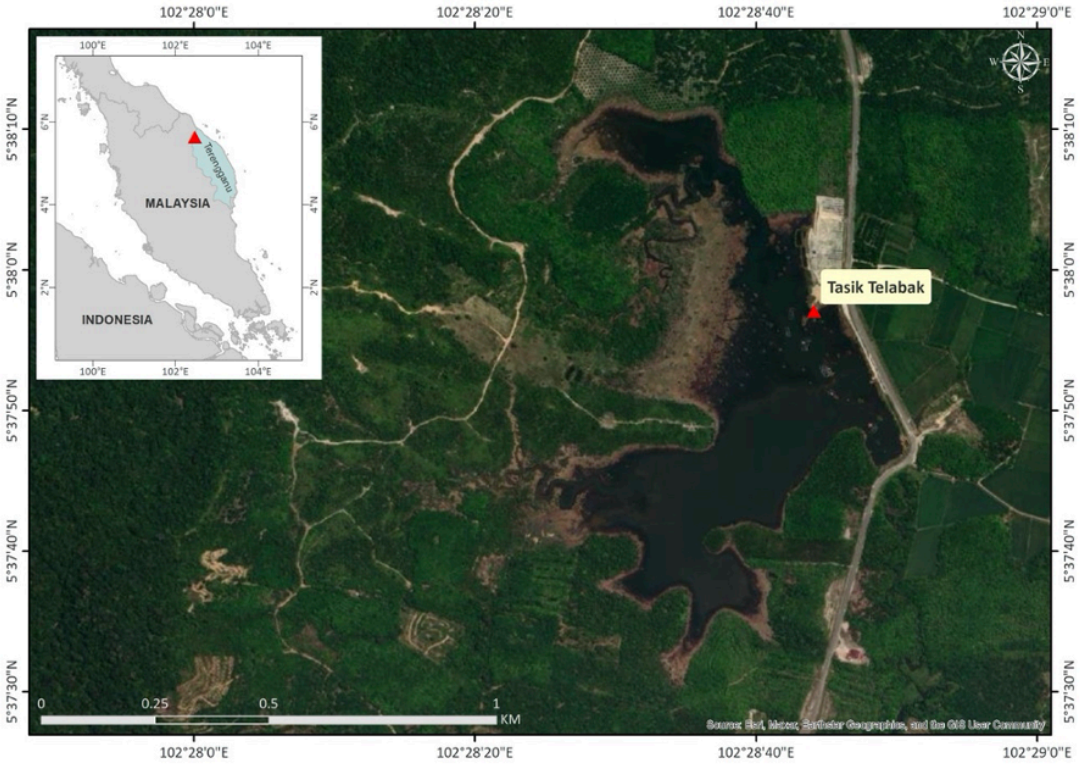

Figure 9. Map of Peninsular Malaysia showing studied area. Sediment samples with oligochaete were collected from the site at Tasik Telabak, Hulu Besut, Terengganu (arrowhead).

Live fish were transported in oxygenated plastic bags, while the sediment samples were placed in buckets with minimal lake water and transported to the Marine Science Biodiversity Laboratory of the Faculty of Science and Marine Environment at Universiti Malaysia Terengganu. Upon arrival, the fish were kept in a tank and the sediment was maintained in the buckets with continuous aeration system, regularly supplied with dechlorinated tap water, and kept at an ambient

temperature of 30 °C–35 °C. In the laboratory, fish were subjected to a comprehensive examination of the body surfaces, gills, and internal organs, including the kidney, heart, musculature, intestine, spleen, liver, gall bladder, urinary bladder, and gonads was conducted to detect plasmodia of myxosporean parasites by naked eye, which were then observed under stereo and light microscopes. Taxonomic identification of the fish specimens was based on their morphological characteristics. The oligochaetes were hand-sorted on a transparent tray placed over a light panel and individually placed into 48-well microtiter plates, while large oligochaetes such as *B. sowerbyi* and *Branchiodrilus* sp. were placed in 24-well plates containing dechlorinated water within 24 hours of collection. Each plate was examined daily for released actinospores using Leica DM IL LED inverted microscope (Leica, Wetzlar, Germany). Oligochaete hosts were identified according to the key of Timm (1999) and through molecular analysis.

3.3. Microscopic examination

Fresh myxospores and actinospores samples collected in Hungary were mounted on glass slide and examined under high magnification using an Olympus BX53 light microscope, equipped with an Olympus DP74 digital camera (Olympus Corporation, Japan). Following microscopic examination, the remaining spores were transferred to 1.5 mL Eppendorf tubes and preserved in 80% ethanol for molecular studies. For Malaysian samples, a portion of the myxospores and freshly released actinospores from infected oligochaetes were examined on a slide under an Olympus CX33 biological microscope (Olympus Corporation, Japan). The remaining spores and plasmodia were preserved in 90% ethanol for molecular studies and in 10% neutral buffered formalin for subsequent morphological analysis. All fixed samples were later transported to the Fish Pathology and Parasitology Laboratory at the HUN-REN Veterinary Medical Research Institute in Budapest, Hungary where further studies included high-magnification examinations (100× objective) and photographic documentation using an Olympus BX53 light microscope equipped with an Olympus DP74 digital camera (Olympus Corporation, Japan) were executed. In

certain cases, Lugol staining was employed to enhance the visibility of sporoplasm morphology and absence of iodinophilous vacuoles in spores.

Myxospore measurements were performed according to the guidelines of Lom & Arthur (1989), while actinospore measurements followed the guideline of Lom et al. (1997), using ImageJ software (http://imagej.nih.gov/ij). All measurements are presented as the mean and standard deviation (SD), with the range given in parentheses, in micrometers (μm). Spore measurements were compared with literature data for species-level identification. Line drawings of the new myxosporean species and actinospore types were prepared based on the photomicrographs taken during microscopic examination. Voucher specimens of the myxospores were deposited in the collection of the Zoological Department of the Hungarian Natural History Museum, Budapest, Hungary.

For histological analysis, infected organs and tissues were fixed in either 5% or 10% neutral buffered formalin (NBF) or Bouin's solution. In the case of infected oligochaetes, the anterior part was preserved in 90% ethanol for species identification through molecular techniques, while the posterior part was fixed in 10% NBF for histological examination. Tissues were then embedded in paraffin wax, sectioned at a thickness of 3–4 μm, and stained with hematoxylin and eosin (H&E). The prepared slides were examined and photographed using an Olympus DP74 digital camera.

3.4. Molecular analyses

3.4.1. DNA isolation, PCR and Sequencing

DNA was extracted from plasmodia and spores that had been preserved in 80% or 90% ethanol. Prior to extraction, the samples were centrifuged at 13,000 rpm for 15 min, and the ethanol was removed by pipetting. The pelleted spores were washed twice with 10mM Tris-HCL, pH 8.5 to remove residual ethanol. Genomic DNA was then isolated using the Geneaid Tissue Genomic DNA Mini Kit (Geneaid Biotech Ltd., Taiwan), according to the manufacturer's instructions for

animal tissue samples. Amplification of 18S rDNA and 28S rDNA genes was performed via direct, semi-nested or nested PCR (polymerase chain reaction) using various primer sets listed in **Table 5** and **Table S1**. For direct and semi-nested PCR, reactions were performed in 25 µL reaction volumes, containing 2 µL of template DNA, 1× DreamTaq buffer (10×; Thermo Scientific), 0.2 mM dNTP mix (10 mM; Thermo Scientific), 1.25 U DreamTaq polymerase (5 U; Thermo Scientific), 12.5 pmol of each primer, and molecular grade water. For nested PCR, reactions were performed in 50 µL volumes, containing 5 µL of template DNA, 1× DreamTaq buffer (10×; Thermo Scientific), 0.2 mM dNTP mix (10 mM; Thermo Scientific), 2.5 U DreamTaq polymerase (5 U; Thermo Scientific), 25 pmol of each primer, and molecular grade water.

Amplification of 18SrDNA and 28S rDNA was carried out using different primer pairs under various thermal cycling conditions. The MyxospecF-18R and 18E-MyxospecR primer sets were amplified following the protocol of Liu et al. (2016a), with a modified elongation time of 90 seconds. The ERIB1-ACT1R primer reactions followed the protocols from Úngari et al. (2021) and Atkinston & Bartholomew (2009). Amplifications using Mxygen4F-ERIB10, ACT1F-ACT1R and Myx1F-SphR primer combinations adhered to the conditions described by Colunga et al. (2024), while MC5-MC3 primers were amplified following Bittencourt et al. (2021). Semi-nested PCR, targeting *Ceratomyxa* species, was performed according to the protocol of Zatti et al. (2023).

Nested PCR amplification of the 18S rDNA gene involved two consecutive reactions, with ERIB1-ERIB10 primers in the first round following the protocols by Cech et al. (2015) and Eszterbauer et al. (2013), and Myx1F-SphR primers in the second round as per Cech et al. (2015). Amplification of the 28S rDNA gene utilized different primer pairs, including NLF184-NLR1270, NLF1050-NLR3284, Myxo28S1F-28S3R based on the protocols by Bartošová et al. (2009). For oligochaete samples, PCR targeting the 16S rRNA and ITS regions followed the conditions by Rocha et al. (2019a) and Erséus et al. (2017), respectively. Protocols specific to the Myx1F-

ERIB10, MyxospecF-ERIB10 and ERIB1-Myxgen4R primer sets used in this study, along with detailed conditions for each protocol, are provided in the appendices **(Table S2)**.

PCR products were visualized on agarose gels, and bands of the expected size were excised and purified using the DNA Fragment Purification Kit (InViTek GmbH, Berlin, Germany). Purified amplicons were sequenced in both directions using the BigDye Terminator v3.1 Cycle Sequencing Kit (Applied Biosystems, Foster City, CA, USA) on an ABI PRISM 3100 Genetic Analyzer, using the primers listed in **Table 5** and **Table S1**.

3.4.2. Phylogenetic analyses

The 18S rDNA and 28SrDNA sequences obtained in this study were examined, corrected and assembled using Geneious Prime v.11.1 (Kearse et al., 2012). Sequences alignment was conducted using the ClustalW algorithm (Thompson et al., 1994) in MEGA X (Kumar et al., 2018) and poorly aligned regions were eliminated using GBlocks v0.91b with less stringent selection parameters (Castresana, 2000; Talavera & Castresana, 2007). Phylogenetic trees were generated using both Maximum Likelihood (ML) in MEGA X with 1000 bootstrap replicates and the Bayesian Inference (BI) in MrBayes 3.2.4 (Ronquist et al., 2012). Alignment gaps were treated using partial deletion with a 75% site coverage cut-off. The analyses were performed using the GTR + G + I or GTR + G model based on the Akaike information criterion (AIC) and Bayesian Information Criterion (BIC) executed in jModelTest 2.1.10 v20160303 (Darriba et al., 2012). In the Bayesian analysis, Markov Chain Monte Carlo (MCMC) simulations were run for 1,000,000 generations, discarding the first 25% as burn-in before generating the consensus tree. Clades with ML bootstrap support values ≥ 70% for ML and BI posterior probabilities (PP) ≥ 0.90 were considered as well-supported. The resulting phylogenetic trees were visualized in MEGA X and FigTree v. 1.4.4 (Rambaut, 2018), and graphically edited with Inkscape (Free Software Foundation, Inc., MA, USA). Genetic distances were calculated using a *p*-distance model for transitions and transversions in MEGA X software package.

Table 5 Primers used for PCR amplification and sequencing of the 18S rDNA and 28S rDNA genes.

Primer	Sequence (5' to 3')	Reference
ERIB1	ACCTGGTTGATCCTGCCAG	Barta et al. (1997)
ERIB10	CTTCCGCAGGTTCACCTACGG	
SphR	GTTACCATTGTAGCGCGCGT	Eszterbauer & Székely (2004)
Myx1F	GTGAGACTGCGGACGGCTCAG	Hallett & Diamant (2001)
ACT1fr	TTGGGTAATTTGCGCGCCTGCTGCC	
ACT1R	AATTTCACCTCTCGCTGCCA	
ACT1F	GGCAGCAGGCGCGCAAATTACCCAA	
ACT3F	CATGGAACGAACAAT	
ACT3R	ATTGTTCGTTCCATG	
MC5	CCTGAGAAACGGCTACCACATCCA	Molnár et al. (2002)
MC3	GATTAGCCTGACAGATCACTCCACA	
Myxgen4F	GTGCCTTGAATAAATCAGAG	Diamant et al. (2004)
Myxgen4R	CTYTGATTTATTCAAGGCAC	Køie et al. (2008)
18E	CTGGTTGATCCTGCCAGT	Hillis & Dixon (1991)
18R	CTACGGAAACCTTGTTACG	Whipps et al. (2003)
MyxospecF	TTCTGCCCTATCAACTTGTTG	Fiala (2006)
MyxospecR	CAACAAGTTGATAGGGCAGAA	
CR1F	CGAAGACGATCAGATACCGTCCTAG	Székely et al. (2015)
CR1R	CTAGGACGGTATCTGATCGTCTTCG	
CerSAZ.1f	GTCCCTTCGATCGTAGTACCAC	Adriano et al. (2021)
CerSAZ.4f	GTTGGTTAGTTTCCACGCGAAA	
CerSAZ.3r	CTATCCCCACAGCCTGAAAACT	
My28SF	TTTACTGGCCCTGAAAATGG	Gupta & Kaur (2018)
NLF184	ACCCGCTGAAYTTAAGCATAT	Bartošová et al. (2009)
NLR1694	TCTYAGGAYCGACTNAC	
NLR1270	TTCATCCCGCATCGCCAGTTC	
Myxo28S1F	AGTAACTGCGAGTGAAGYG	
NLF1050	AATCGAACCATCTAGTAGCTGG	
NLR3284	TTCTGACTTAGAGGCGTTCAG	van der Auwera et al. (1994)
28S3R	GAGCACTGGGCAGAAATC	Whipps et al. (2004)
16sa-L	CGCCTGTTTATCAAAAACAT	Palumbi et al. (2002)
16sb-H	CCGGTCTGAACTCAGATCACGT	
ITS-5	TCCTCCGCTTATTGATATGC	White et al. (1990)
ITS-4	GGAAGTAAAAGTCGTAACAAGG	
5.8mussF	CGCAGCCAGCTGCGTGAATTAATGT	Källersjö et al. (2005)
5.8mussR	GATGTCGATGTTCAATGTGTCCTGC	

CHAPTER 4

RESULTS

4.1. Myxosporean species in Hungary

A total of 144 individuals from three fish species were collected in fish farms of Hungary for myxozoan examination (**Table 3**). Among them, *R. rutilus* showed the highest infection rate at 80.0% (4/5), while *C. auratus gibelio* had the lowest infection rate of 51.7% (58/112). *Cyprinus carpio* ranked the second, with an infection rate of 55.6% (15/27) (**Table 6**). In total, fifteen myxosporean species were identified from these fish, including eight *Myxobolus* spp., five *Thelohanellus* spp., one *Zschokkella* sp. and one *Sphaerospora* sp. Of these, eight species are newly described, while the remaining are previously known species. *Carassius auratus gibelio* harbored the greatest diversity of myxosporean parasites, with seven species comprising four *Myxobolus* spp., one *Thelohanellus* sp., one *Zschokkella* sp. and one *Sphaerospora* sp. (**Table 7**). Additionally, *C. carpio* hosted six myxosporean species, consisting of two *Myxobolus* spp. and four *Thelohanellus* spp., whereas *R. rutilus* was infected by only two *Myxobolus* spp. (**Table 7**). All fishes appeared to be in good condition without obvious scars or lesions, except for those infected with *Myxobolus lentisuturalis*.

Table 6 Infection prevalence rates for each fish species.

Species	Infected fish	Infection rate
Carassius auratus gibelio (Gibel carp)	58/112	51.7%
Cyprinus carpio (Common carp)	15/27	55.6%
Rutilus rutilus (Roach)	4/5	80.0%

4.1.1. Myxosporean parasites in Carassius auratus gibelio

4.1.1.1. Myxobolus lentisuturalis Dyková, Fiala et Nie, 2002

Eighteen gibel carp (15–20 cm in length) showed body deformities with bilateral crescent-shaped humps between the head and the dorsal fin (**Figure S1A**) caused by the highly pathogenic myxozoan, *M. lentisuturalis* infection. The dorsolateral (epaxial) musculature was severely

damaged by the expanded pseudocysts containing several plasmodia filled with developing spores, resulting in swollen tissue filled with creamy, viscous fluid containing muscle debris and a large mass of myxospores. Histopathological examination of tissue from various parts of the lesion revealed regressive degradation of the epaxial musculature. At the edges of the hump, muscle cells appeared relatively intact, though some *M. lentisuturalis* spores and cellular debris had infiltrated the intermuscular connective tissue (**Figure S1B**). In certain areas, muscle was definitely destroyed as myxosporean stages invaded the muscle fibrils (**Figure S1C**).

Spore: Ellipsoidal, symmetrical shell valves (**Figure S1D**); 11.8 (10.0–13.3) µm long, 7.6 (6.6–8.6) µm wide, 5.0 (4.1–5.6) µm thick (n = 14) (**Figure S1E**). Polar capsule: Two, equal, pyriform, anteriorly tapered, 4.3 (3.3–5.1) µm long, 2.7 (1.7–3.2) µm wide. Distance between the anterior ends of the polar capsules, 3.0 (1.7–3.8) µm from each other. Polar tubule: Coiled four to five times. Measurements from 90 fresh spores.

Locality: Fish farm in southern of Hungary.

Predilection site: Muscle.

Prevalence: 16.1% (18/112).

Molecular data: Partial 18S rDNA sequences of 1712 base pairs was deposited in GenBank under the accession numbers OR416132–34. The three 18S rDNA sequences showed ≥99.8% identity with *M. lentisuturalis* sequences from goldfish in Italy (AY278563), China (MF150547), and the USA (OP374272) (Caffara et al., 2009; Wang et al., 2019; Hepps Keeney et al., 2023), as well as ≥99.8% identity with *M. lentisuturalis* from gibel carp in Hubei, China (AY119688) (Dyková et al., 2002) (**Table 8**). Phylogenetic analysis of the 18S rDNA showed that *M. lentisuturalis* groups closely with *Myxobolus cultus*, *Myxobolus intrachondrealis* and *Myxobolus cultrati* (**Figure 10**).

Remarks: The morphology and morphometric data of *M. lentisuturalis* from Hungary were consistent with previously described *M. lentisuturalis* from goldfish and gibel carp reported in China, Italy, Croatia, and the USA **(Table S3)**.

Table 7 Myxosporean species detected in the investigated fish species.

Fish species	Myxosporean parasite	Predilection site
Carassius auratus gibelio	*Myxobolus lentisuturalis*	Muscle
	Myxobolus ocsardiensis n. sp.	Kidney, liver
	Myxobolus pecsensis n. sp.	Gill cartilage
	Myxobolus diversus	Fins
	Thelohanellus imrei n. sp.	Connective tissues of gill arch and pharynx
	Zschokkella chezhachei n. sp.	Bile duct
	Sphaerospora molnari	Gill lamellae
Cyprinus carpio	*Myxobolus intrachondrealis*	Gill cartilage
	Myxobolus basilamellaris	Base of gill filaments
	Thelohanellus serosae n. sp.	Serous membrane of kidney
	Thelohanellus paranikolskii n. sp.	Skin
	Thelohanellus nikolskii	Fin rays
	Thelohanellus hovorkai	Serous membrane of intestine
Rutilus rutilus	*Myxobolus* n. sp. 1	Connective tissue of gill arch
	Myxobolus n. sp. 2	Kidney

4.1.1.2. Myxobolus ocsardiensis n. sp.

Plasmodia: Found in kidney and liver, whitish, round or oval (**Figure S2A**), 0.23 ± 0.06 (0.16–0.35) mm diameter (n = 30). Spore: Round or ellipsoidal in frontal view (**Figure S2B** and **Figure S4A**), lemon-shaped in sutural view (**Figure S2C** and **Figure S4B**), 14.6 ± 0.8 (12.8–16.4) µm long, 11.7 ± 0.6 (10.6–13.0) µm wide, 7.3 ± 0.5 (6.2–8.6) µm thick. Polar capsule: Two, equal, pyriform, each reaching half the length of the spore, 7.1 ± 0.5 (6.1–8.3) µm in long, 3.9 ± 0.3 (3.2–4.7) µm wide. Distance between anterior ends of the polar capsules, 1.8 ± 0.2 (1.4–2.3) µm. Polar tubule: Coiled six to seven times, positioned perpendicularly to capsule axis (**Figure S2B**). Sutural ridge: Five to six sutural markings at the posterior end in some spores. Sporoplasm: Binucleate, iodinophilous vacuole absent, mucous envelope absent. Measurements from 50 fresh spores.

Locality: Ócsárd fish farm, county Baranya, Hungary.

Predilection site: Kidney and liver.

Prevalence: 15.2% (17/112).

Etymology: The species is named after the village of Ócsárd, where the fish hosts were collected.

Molecular data: Partial 18S rDNA sequence of *M. ocsardiensis* n. sp. of 1940 base pairs was deposited in GenBank under the accession number PV172147. The 18S rDNA sequence from the *M. ocsardiensis* n. sp. did not match any of the myxozoan sequences available in GenBank. Pairwise distance estimation of the newly obtained 18S rDNA sequence indicated the highest similarity of 97.7% to *Myxobolus hearti* (GU574808) reported from the cardiac muscles of *C. auratus gibelio* (**Table 8**). Both sequences from kidney and liver samples were identical; hence, only the sequence from the kidney was submitted to GenBank. Phylogenetic analyses of the 18S rDNA showed that *M. ocsardiensis* n. sp. formed a sister relationship with *M. hearti* and clustered within well-supported clade of *Myxobolus* spp., which infected the *C. auratus gibelio* (**Figure 10**). Remarks: The morphology and morphometrics of *M. ocsardiensis* n. sp. are compared with six *Myxobolus* spp. (**Table S4**), showing the closest similarity to *M. hearti* Chen, 1998. However, *M. ocsardiensis* n. sp. has longer spore and polar capsules than *M. hearti*. It differs from *Myxobolus pronini* Liu, Batueva, Zhao, Zhang, Zhang, Li et Li, 2016 from Russia by spore shape and size, while *M. pronini* from China has similar spore length (14.6 vs 14.7 µm). The polar capsule length of *M. ocsardiensis* n. sp. resembles *Myxobolus carassii* Klokachewa, 1914, while its polar filament coils are similar to those of *Myxobolus qiankiangensis* Chen et Ma, 1998 and *M. hearti*.

4.1.1.3. Myxobolus pecsensis n. sp.

Plasmodia: Found in cartilaginous gill arch, small and polymorphic (spherical to ovoid, elongated and irregularly shaped) (**Figure S2D**), 0.19 ± 0.09 (0.12–0.37) mm long, 0.11± 0.05 (0.07–0.19) mm wide (n = 6). Histology: Plasmodia were located within the hyaline cartilage of the gill arches, adjacent to and surrounded by chondrocytes (**Figure S2E**). Spore: Ellipsoidal in frontal view (**Figure S2F** and **Figure S4C**), biconvex in sutural view (**Figure S2H** and **Figure S4D**), 8.8 ± 0.5 (7.4–9.7) µm long, 5.5 ± 0.4 (4.9–6.4) µm wide, 4.4 ± 0.4 (3.8–5.1) µm thick (n = 11). Polar capsule: Two, equal, pyriform, 3.3 ± 0.1 (2.4–4.1) µm in long, 1.7 ± 0.1 (1.5–2.0) µm wide. Distance between anterior ends of the polar capsules, 1.5 ± 0.2 (1.2–1.8) µm. Polar tubule: Coiled

four times, positioned perpendicularly to capsule axis (**Figure S2G**). Sporoplasm: Binucleate, iodinophilous vacuole absent, mucous envelope absent. Measurement from 27 fresh spores.

Locality: Ócsárd fish farm, county Baranya, Hungary.

Predilection site: Gill cartilage.

Prevalence: 2.7% (3/112).

Etymology: The species is named after Pécs, the largest city of Baranya county, close to Ócsárd from which the fish hosts were collected.

Molecular data: Partial 18S rDNA sequence of *M. pecsensis* n. sp. of 1748 base pairs was deposited in GenBank under the accession number PV172146. The 18S rDNA sequence from the *M. pecsensis* n. sp. did not match any of the myxozoan sequences available in GenBank. Pairwise distance estimation of the newly obtained 18S rDNA sequence indicated the highest similarities of 98.4% and 98.3% to actinospores of Hungactinomyxon type (AY779062) and Hungactinomyxon type (KY784589), respectively, both reported from *B. sowerbyi* (**Table 8**). Phylogenetic analyses of the 18S rDNA showed that *M. pecsensis* n. sp. formed a sister relationship with three of Hungactinomyxon types, which were found in the intestine of *B. sowerbyi*, and clustered within *Myxobolus* spp., supported by high bootstrap values and posterior probabilities (**Figure 10**).

Remarks: The morphology and morphometrics of *M. pecsensis* n. sp. are distinct from all previously described *Myxobolus* spp. The closest morphological resemblance is with the *Myxobolus intrachondrealis* Molnár, 2000, but it is smaller and has a thicker spore wall (**Table S5**). Morphometrically, *M. pecsensis* n. sp. is most similar to *Myxobolus adlardi* Gupta et Kaur, 2016, particularly in polar capsule width, despite *M. adlardi* possesses smaller spores and longer polar capsules. The polar filament coils of *M. pecsensis* n. sp. closely match those of *Myxobolus cultus* Yokoyama, Ogawa et Wakabayashi, 1995, and *Myxobolus albi* Picon-camacho, Holzer, Freeman, Morris et Shinn, 2009, but differ distinctly from *M. intrachondrealis.*

Table 8 Genetic *p*-distance and sequence similarities (%) based on the 18S rDNA between *Myxobolus* spp., *Thelohanellus* spp. from Hungary and its most closely related species. Only identical or the closest-related sequences are presented.

Sequence	Genetic distance	Sequence similarities (%)
***Myxobolus lentisuturalis* OR416133**		
***Myxobolus lentisuturalis* OR416134**	**0.000**	**100.0**
***Myxobolus lentisuturalis* OR416132**	**0.002**	**99.8**
Myxobolus lentisuturalis MF150547	0.002	99.8
Myxobolus lentisuturalis AY278563	0.002	99.8
Myxobolus lentisuturalis AY119688	0.002	99.8
Myxobolus lentisuturalis OP374272	0.002	99.8
***Myxobolus ocsardiensis* n. sp. PV172147**		
***Myxobolus ocsardiensis* n. sp.**	**0.000**	**100.0**
Myxobolus hearti GU574808	0.023	97.7
Myxobolus pronini OM678576	0.036	96.4
Myxobolus nielii MN227344	0.038	96.2
Myxobolus oralis MF375468	0.045	95.5
***Myxobolus pecsensis* n. sp. PV172146**		
Hungactinomyxon type AY779062	0.016	98.4
Hungactinomyxon type KY784589	0.017	98.3
Hungactinomyxon type KY784588	0.018	98.2
***Myxobolus diversus* PV162749**		
Myxobolus elliptoides OQ725580	0.054	96.4
***Thelohanellus imrei* n. sp. PV172145**		
Neoactinomyxum type KY784596	0.011	98.9
Myxobolus intrachondrealis		
Myxobolus cultrati KU170935	0.000	100.0
Myxobolus cultus AB121146	0.024	97.6
Myxobolus basilamellaris		
Myxobolus basilamellaris OQ725581	0.002	99.8
Myxobolus tsangwuensis KJ561441	0.035	96.5
Myxobolus musseliusae FJ710801	0.040	96.0
Myxobolus elliptoides OQ725580	0.056	94.4
***Thelohanellus serosae* n. sp. PV172145**		
Aurantiactinomyxon type DQ231148	0.005	99.5
Thelohanellus macrovacuolaris KU160631	0.022	97.8
***Thelohanellus hovorkai* PV926536**		
Thelohanellus hovorkai DQ231155	0.000	100.0
***Thelohanellus paranikolskii* n. sp. PV942517**		
Thelohanellus nikolskii GU165832	0.055	94.5
***Thelohanellus nikoslkii* PV926531**	**0.062**	**93.8**
Thelohanellus pseudonikolskii OM801563	0.064	93.6
***Thelohanellus nikoslkii* PV926531**		
Thelohanellus nikolskii GU165832	0.003	99.7

Thelohanellus pseudonikolskii OM801563	0.037	96.3
***Myxobolus* n. sp. 2**		
Myxobolus erythrophthalmi EU567311	0.033	96.7
Myxobolus zaikae MT141124	0.051	94.9
Myxobolus rutili GU968201	0.052	94.8
***Myxobolus* n. sp. 1**	**0.056**	**94.4**
***Myxobolus* n. sp. 1**		
Myxobolus ellipsoides DQ439813	0.029	97.1
Myxobolus shaharomae KF515726	0.050	95.0
Myxobolus peleci KU170934	0.051	94.9
Myxobolus dogeili EU003977	0.078	92.2

4.1.1.4. Myxobolus diversus Nie et Li, 1973

Plasmodia: Found in cartilaginous fin rays, whitish to yellowish, polymorphic (spherical to ovoid and irregularly shaped) (**Figure S2I**), 0.50 ± 0.18 (0.14–0.80) mm long, 0.34 ± 0.11 (0.14–0.58) mm wide (n = 22). Spore: Ellipsoidal in frontal view (**Figure S2J**), lemon-shaped in sutural view (**Figure S2K**), 13.5 ± 0.5 (12.6–14.4) µm long, 9.3 ± 0.5 (8.4–10.6) µm wide, 7.8 ± 0.5 (6.8–8.9) µm thick (n = 30). Polar capsule: Two, pyriform, unequal size. Larger: 5.3 ± 0.3 (4.5–5.9) µm long, 3.4 ± 0.2 (2.9–4.0) µm wide. Smaller: 3.0 ± 0.3 (2.1–3.6) µm long, 1.9 ± 0.2 (1.4–2.4) µm wide. Small papilla-like intercapsular appendix present between the anterior ends. Polar tubule: Six coils in larger capsule, two to three in smaller capsule, positioned perpendicularly to capsule axis. Sporoplasm: Binucleate, iodinophilous vacuole absent, most spores surrounded by a mucus envelope (**Figure S2J**). Measurements from 50 fresh spores.

Locality: Ócsárd fish farm, county Baranya, Hungary.

Predilection site: Fins.

Prevalence: 5.4% (6/112).

Molecular data: Partial 18S rDNA sequence of *M. diversus* of 1946 base pairs was deposited in GenBank under the accession number PV162749. The 18S rDNA sequence from the *M. diversus* did not match any of the myxozoan sequences available in GenBank. Pairwise distance estimation of the newly obtained 18S rDNA sequence indicated the highest similarities of 94.6% to *M. elliptoides* (OQ725580) reported from the fin ray of *C. carpio* (**Table 8**). Phylogenetic analyses of

the 18S rDNA showed that *M. diversus* formed an independent branch and clustered within a clade comprising most gill-infecting *Myxobolus* spp. and a *Myxobolus* sp. infecting the fins (**Figure 10**). Remarks: The morphology and morphometric data of *M. diversus* are consistent with previously described *M. diversus* from goldfish in Hungary and China (**Table S6**). Minor differences in size are observed in all measurements, but these remained within the established range of variation. The remarkable discrepancy between the present *M. diversus* and the previously described *M. diversus* is the presence of a mucus envelope.

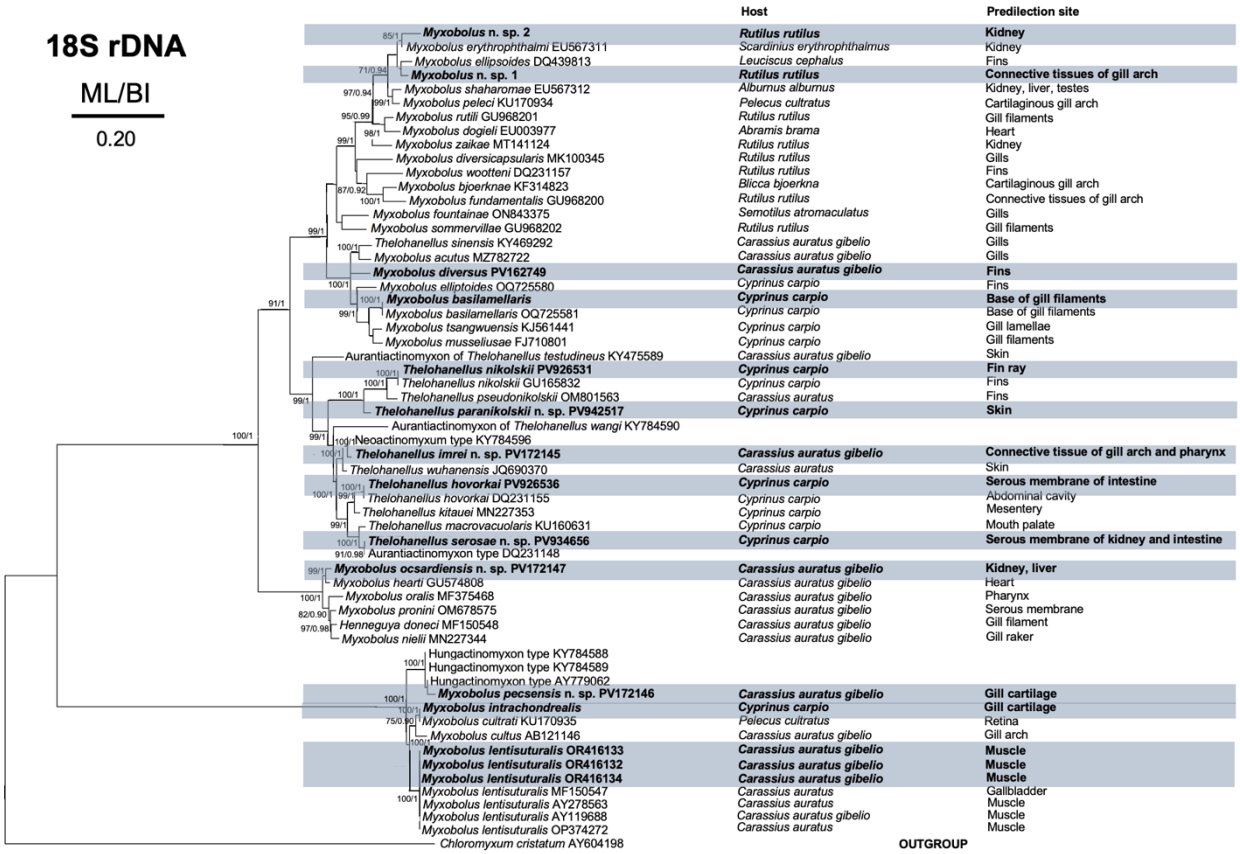

Figure 10. Maximum likelihood (ML) phylogenetic tree of 18S rDNA sequences of *Myxobolus* spp., *Thelohanellus* spp., and related species. *Chloromyxum cristatum* was used as outgroup. Nodal supports are indicated for ML at 1000 replicates and Bayesian Inference (BI). Only values with ≥ 70% bootstrap (BS) and ≥ 0.90 posterior probabilities (PP) support are presented. The names of the parasite species are presented before GenBank accession numbers, following the host species and predilection site. Sequences obtained in the present study are shown in bold within colored boxes. The scale bar indicates the expected number of substitutions per site.

4.1.1.5. Thelohanellus imrei n. sp.

Plasmodia: Found in connective tissue of the gill arch and pharynx, yellowish to brownish, oval in shape (**Figure S3A**), 0.18 ± 0.10 (0.11–0.37) mm long, 0.16 ± 0.09 (0.08–0.31) mm wide (n =

5). Spore: Pyriform in frontal view, with a papilla near the anterior end (**Figure S3B** and **Figure S4E**), lemon-shaped in lateral view (**Figure 3SC** and **Figure S4F**), 20.9 ± 1.2 (18.2–22.9) µm long, 10.1 ± 0.7 (8.5–11.1) µm wide, 4.4 ± 0.4 (3.8–5.1) µm thick (n = 11). Polar capsule: Single, round with a slightly protrusion at the anterior end, 8.1 ± 0.5 (6.9–9.3) µm long, 6.4 ± 0.4 (5.2–line: Straight, distinct, joining two unequal valves. Sporoplasm; Binucleate, iodinophilous vacuole absent, most spores surrounded by a mucus envelope. Measurements from 30 fresh spores.

Locality: Ócsárd fish farm, county Baranya, Hungary.

Predilection site: Connective tissues of gill arch and pharynx.

Prevalence: 2.7% (3/112).

Etymology: The species is named after the son of Hungarian Fish Pathology expert, Assoc. Prof. Dr. Ferenc Baska.

Molecular data: Partial 18S rDNA sequence of *T. imrei* n. sp. of 1816 base pairs was deposited in GenBank under the accession number PV172145. 18S rDNA sequence from the *T. imrei* n. sp. did not match any of the myxozoan sequences available in GenBank, but it showed the closest similarity (98.9%) to Neoactinomyxum type (KY784596) based on pairwise distance estimation (**Table 8**). In a BLAST search, the sequence showed the highest similarity (99.3%) to Neoactinomyxum type CZ-2 (KP642139); however, this sequence was excluded from the phylogenetic tree due to it shorten length and low query coverage (50%). These findings suggest that Neoactinomyxum type CZ-2 may represent the actinospore stage of *T. imrei* n. sp., based on their genetic similarity. Phylogenetic analyses of the 18S rDNA showed that *T. imrei* n. sp. formed a sister relationship with the Neoactinomyxum type and *T. wuhanensis*, which infected the skin of *C. auratus gibelio* (**Figure 10**).

Remarks: The morphology and morphometrics of *T. imrei* n. sp. are compared with all described *Thelohanellus* spp., revealing close similarities to eight of them (**Table S7**). It most closely resembles *T. macrovacuolaris* Liu, Zhai et Gu, 2016, as both possess a mucus envelope around half of the spore body; however, *T. imrei* n. sp. uniquely has a papilla near the anterior end, which

is rare among *Thelohanellus* species (Zhang et al., 2013). Except for *T. wuhanensis*, that also possesses this papilla/pit near the anterior end (Liu et al., 2014b), but it has a thinner mucus envelope. Morphometrically, *T. imrei* n. sp. is similar to *T. wangi* Yuan et Zhang, 2014 and *T. nanhaiensis* Chen in Chen et Ma, 1998, but differs by having wider spores and smaller, narrower polar capsules. The spore length is closely resembling to *T. hovorkai* Akhmerov, 1960, though with smaller polar capsule. The number of polar filament coils in *T. imrei* n. sp. almost identical to *T. wangi*, *T. nanhaiensis*, *T. parasagittarius* Chen et Ma, 1998, and *T. hovorkai* but differs from *T. sagittarius* Chen et Ma, 1998, *T. testudineus* Liu et Gu, 2014, *T. macrovacuolaris*, and *T. wuhanensis* Xiao et Chen, 1993.

4.1.1.6. Sphaerospora molnari Lom, Dyková, Pavlásková et Grupcheva, 1983

Plasmodia: Located dispersed among epithelial cells of gill filaments (**Figure S3G**). Monosporous young stages in pseudoplasmodia were not found. At some parts of the gills, spores were agglomerated into whitish to yellowish and oval shaped spore masses surrounding a thin transparent membrane (**Figure S3D** and **S3H**); 87.4 ± 17.0 (48.2–65.9) µm diameter. Spore: Subspherical in frontal (**Figure S3E**) and sutural views (**Figure S3F)**, 9.9 ± 0.3 (9.1–10.4) µm long, 10.4 ± 0.4 (9.6–11.2) µm wide, 8.6 ± 0.3 (8.1–8.4) µm thick (n = 11). Polar capsule: Two, equal, subspherical, 5.2 ± 0.4 (4.4–5.9) µm long, 4.1 ± 0.3 (3.5–4.7) µm wide. Polar tubule: Coiled five times, positioned parallel to capsule axis. Sutural line: Straight, prominently visible at the anterior end. Sutural ridge: Present between the thickened borders of the shell valves. Measurements from 30 fresh spores.

Locality: Ócsárd fish farm, county Baranya, Hungary.

Predilection site: Gill lamellae.

Prevalence: 1.8% (2/112).

Molecular data: Partial 18S rDNA sequence of *S. molnari* of 3537 base pairs was deposited in GenBank under the accession number PV172148. Two nearly identical 18S rDNA sequences (99.8%) from the present *Sphaerospora* samples matched with the sequences of *S. molnari* from

Hungary and the Czech Republic. Pairwise distance estimation of the newly obtained SSU rDNA sequence indicated the highest similarities of 99.6% and 99.5% to *S. molnari* (JX431510) and *S. molnari* (JX431511), respectively, both reported from the gills of *C. carpio* (Table 8). The low divergence in 18S rDNA sequences (0.40–0.50%) amongst the isolates of *S. molnari* (JX431510 and JX431511) confirms that these isolates are conspecific. The sequence of *S. molnari* (AF378345) from Kent et al. (2001) was excluded from the phylogenetic tree analysis because of its shorter DNA length of 1876 base pairs and its significantly high divergence (48.5%), which suggests that AF378345 was misidentified as *S. molnari* (**Table 9**). Phylogenetic analyses of the 18S rDNA showed that *S. molnari* clustered with others *S. molnari* from Hungary (HU) and the Czech Republic (CZ) (**Figure 11**).

Remarks: Most *Sphaerospora* species infect fish kidney, but only two species, *S. molnari* and *S. carassii* Kudo, 1920, are known to infect the gills of fish. *Sphaerospora carassii* was first described in *Carassius carassius* in Japan (Kudo, 1920), but later found in *C. carpio* (Schulman, 1966). Following this latter observation, Molnár (1980) described a *Sphaerospora* gill infection in the common carp caused by *S. carassii*. It was Lom et al. (1983) who discriminated the species infecting common carp from that infecting the original host *Carassius cuvieri*, thereby establishing a new species named *S. molnari*, which infects common carp, while leaving the name *S. carassii* for parasite from *Carassius* spp. Finding *Sphaerospora* invasion in the gill filaments of two separate gibel carp from a pond farm in Hungary suggests that this pathogenic agent is *S. molnari*. The morphology and morphometrics of present *S. molnari* are consistent with previously described *S. molnari* from common carp in Hungary and the Czech Republic. Minor differences in polar capsule size were observed, but remained within the established range of variation (**Table S8**).

Table 9 Genetic *p*-distance and sequence similarities (%) based on the 18S rDNA between *Sphaerospora molnari* and its most closely related species. Only identical or the closest-related sequences are presented.

Sequence	Genetic distance	Sequence similarities (%)
***Sphaerospora molnari* PV172148**		
Sphaerospora molnari JX431510 (Hungary)	0.004	99.6
Sphaerospora molnari JX431511 (Czech Republic)	0.005	99.5
Sphaerospora diversa KY851774	0.286	71.4
Sphaerospora dentata MG214666	0.286	71.4
Sphaerospora rutili MF347687	0.292	70.8
Sphaerospora sp. KY851765	0.295	70.5
Sphaerospora squalii KY851780	0.305	69.5
Sphaerospora molnari AF378345 (Japan)	0.485	51.5

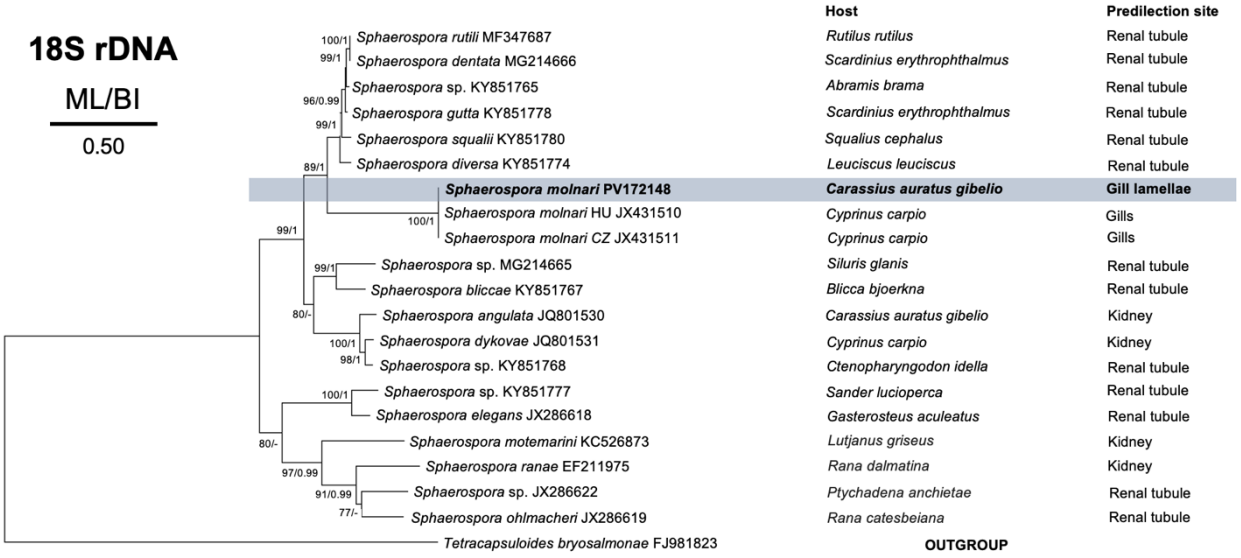

Figure 11. Maximum likelihood (ML) phylogenetic tree of 18S rDNA sequences of *Sphaerospora molnari* and other *Sphaerospora* species. *Tetracapsuloides bryosalmonae* was used as outgroup. Nodal supports are indicated for ML at 1000 replicates and Bayesian Inference (BI). Only values with ≥ 70% bootstrap (BS) and ≥ 0.90 posterior probabilities (PP) support are presented. The names of the parasite species are presented before GenBank accession numbers, following the host species and predilection site. Sequence obtained in the present study is shown in bold within colored box. The scale bar indicates the expected number of substitutions per site.

4.1.1.7. Zschokkella chezhachei n. sp.

Plasmodia: Coelozoic, found in the bile duct, whitish, polymorphic (long, slender and irregularly shaped) (**Figure S3I**). Disporic pansporoblast, 1.11 ± 0.96 (0.16–4.53) mm long, 0.32 ± 0.14 (0.04–0.62) mm wide. Spore: Sub-ovoid in valvular view (**Figure S3J**), elliptical in sutural view with rounded ends (**Figure S3K**), 17.4 ± 0.3 (16.7–17.9) µm long, 10.1 ± 0.3 (9.5–10.6) µm wide,

8.9 ± 0.4 (8.0–9.5) µm thick. Polar capsule: Two, equal, spherical, 6.4 ± 0.6 (5.4–7.3) µm diameter. Polar tubule: Coiled five times, positioned perpendicularly to capsule axis. Sutural line: Curved, valves exhibiting nine to ten longitudinal striations (**Figure S3K**). Sporoplasm: Filling the spore cavity between the two polar capsules. Measurements from 30 fresh spores.

Locality: Ócsárd fish farm, county Baranya, Hungary.

Predilection site: Bile duct.

Prevalence: 30.4% (34/112).

Etymology: The species is named after the combination of the three authors (Chen, W., Zhao, Y. and Chen, H.) who deposited the sequences of an undescribed *Zschokkella* species in GenBank.

Molecular data: Partial 18S rDNA sequence of *Z. chezhachei* n. sp. of 1840 base pairs was deposited in GenBank under the accession number PV172149. Pairwise distance estimation of the newly obtained 18S rDNA sequence indicated the highest similarities of 100.0% to "*Z. chongqingense*" (MT112714) and aurantiactinomyxon type of "*Z. chongqingense*" (KY475591) (**Table 10**). Phylogenetic analyses of the 18S rDNA showed that *Z. chezhachei* n. sp. clustered with other *Z. chongqingense* in the same branch, which infected the gallbladder of *C. auratus auratus*, as well as the actinospore stage of *Z. chongqingense*, belonging to the aurantiactinomyxon type. Furthermore, *Z. chezhachei* n. sp. formed a sister relationship with the aurantiactinomyxon types, with maximum bootstrap support and posterior probabilities (**Figure 12**).

Remarks: Based on spore morphology, this species is classified as a new member of the genus *Zschokkella*. The morphology and morphometrics of *Z. chezhachei* n. sp. are inconsistent with any previously described *Zschokkella* spp. (**Table S9**). However, we found sequences from goldfish deposited in GenBank by Chen, W., Zhao, Y. and Chen, H. under the name *Zschokkella chongqingense* (an invalid name at publication time), with deposit numbers MT112713 and MT112714, with similarities of 99.9% and 100.0%, respectively. Unfortunately, the morphology and morphometric measurements of these spores have not been published. Morphologically, *Z.*

chezhachei most closely resembles *Z. nilei* Abdel-Ghaffar et Bashtar, 2008, while its spore size is similar to *Z. scomberosis* Sarkar, 2012 in terms of spore length and width.

Table 10 Genetic *p*-distance and sequence similarities (%) based on the 18S rDNA between *Zschokkela chezhachei* n. sp. and its most closely related species. Only identical or the closest-related sequences are presented.

Sequence	Genetic distance	Sequence similarities (%)
***Zschokkella chezhachei* n. sp. PV172149**		
Zschokkella chongqingense MT112714	0.000	100.0
Aurantiactinomyxon type of *Z. chongqingense* KY475591	0.000	100.0
Aurantiactinomyxon type KY784583	0.016	98.4
Aurantiactinomyxon type KY784582	0.017	98.3
Myxidium sp. PP693376	0.019	98.1
Zschokkella ophiocephali PP693379	0.029	97.1

4.1.2. Myxosporean parasites in Cyprinus carpio

4.1.2.1. Thelohanellus serosae n. sp.

Plasmodium: Found in the serous membrane of the kidney, yellowish to brownish, oval in shape (**Figure S5A**); 0.24 mm long, 0.19 mm wide (n = 1). Spore: Pyriform in frontal and sutural views (**Figure S5B–S5C**). Size 22.6 ± 1.1 (20.0–25.1) µm long, 12.6 ± 0.6 (11.3–13.6) µm wide, 12.1 ± 0.5 (10.8–12.9) µm thick (n = 20). Polar capsule: Single, large, pyriform, 13.3 ± 0.8 (11.7–14.6) µm long, 10.5 ± 0.5 (9.5–11.5) µm wide, occupying more than half of the spore body cavity. Polar tubule: Coiled seven times. Sutural line: Straight, smooth, thick in the middle of spore body. Sporoplasm: Binucleate, iodinophilous vacuole absent, surrounded by a thin, narrow mucous envelope. Measurements from 30 fresh spores.

Locality: Ócsárd fish farm, county Baranya, Hungary.

Predilection site: Serous membrane of the kidney.

Prevalence: 3.7% (1/27).

Etymology: The species is named after the predilection site of the plasmodia, which were found on the serous membranes of the host's internal organs.

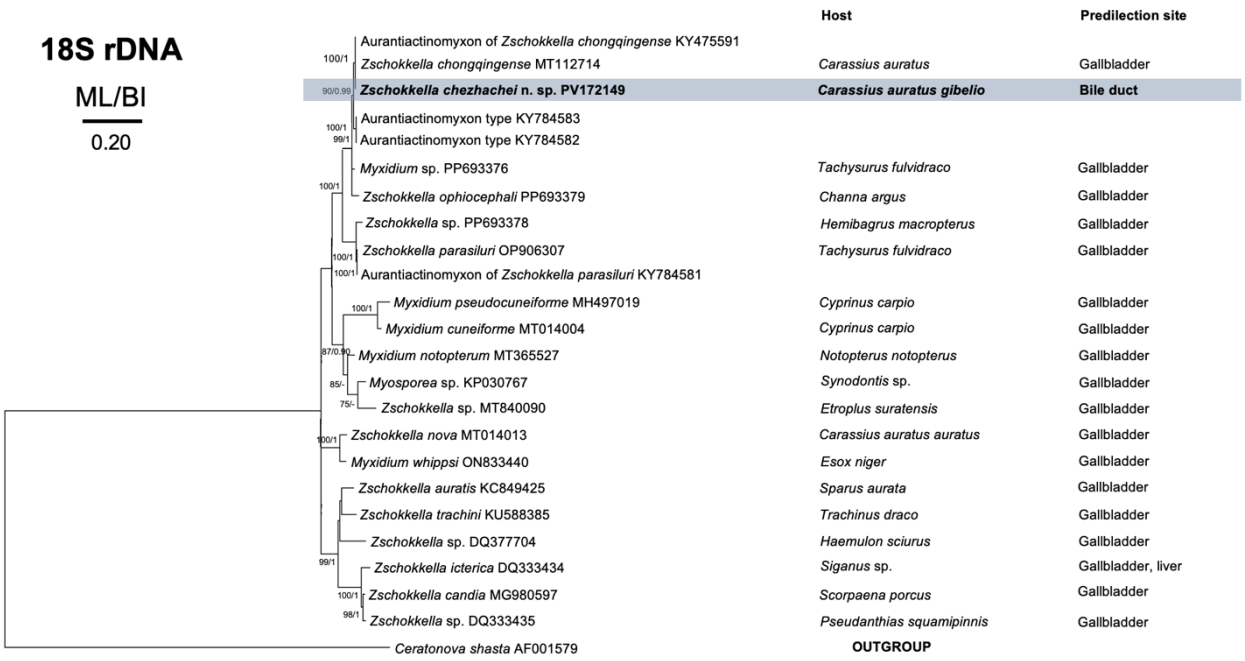

Figure 12. Maximum likelihood (ML) phylogenetic tree of 18S rDNA sequences of *Zschokkella chezhachei* n. sp. and related species. *Ceratonova shasta* was used as outgroup. Nodal supports are indicated for ML at 1000 replicates and Bayesian Inference (BI). Only values with ≥ 70% bootstrap (BS) and ≥ 0.90 posterior probabilities (PP) support are presented. The names of the parasite species are presented before GenBank accession numbers, following the host species and predilection site. Sequence obtained in the present study is shown in bold within colored box. The scale bar indicates the expected number of substitutions per site.

Molecular data: Partial 18S rDNA sequence of *T. serosae* n. sp. of 1890 base pairs was deposited in GenBank under the accession number PV934656. Pairwise distance estimation of the newly obtained 18S rDNA sequence indicated the highest similarity of 99.5% to the aurantiactinomyxon B2 (DQ231148) (**Table 8**) from the river Tisza. Phylogenetic analyses showed that *T. serosae* n. sp. clustered in the same branch with aurantiactinomyxon B2, which is the actinospore stage of *T. serosae* n. sp., with maximum bootstrap values and posterior probabilities. Additionally, *T. serosae* n. sp. formed a close relationship with *T. macrovacuolaris* (**Figure 10**).

Remarks: The morphology and morphometrics of *T. serosae* n. sp. are compared with all known *Thelohanellus* spp., showing remarkable similarities to those *Thelohanellus* spp. from *C. carpio* (**Table S10**). It most closely resembles *T. hovorkai* Akhmerov, 1960, but differs by having thinner, slim fitting mucous envelope compared to the thin, loose fitting mucous envelope of *T. hovorkai*. Morphometrically, *T. serosae* n. sp. is nearly identical to *Thelohanellus hokiangensis* Ma, Dong

et Wang, 1999 and *T. macrovacuolaris* Liu, Zhai et Gu, 2016, but generally larger in most dimensions, except that *T. hokiangensis* has a longer spore body.

4.1.2.2. Thelohanellus paranikolskii n. sp.

Plasmodium: Found in the skin located within the stratum spongiosum of the dermis (**Figure S5D** and **Figure S5H**). Yellowish to brownish, elongated (**Figure S5D**); 3.5 mm long, 1.5 mm wide (n = 1). Spore: Subspherical in frontal view (**Figure S5E**), pyriform in sutural view (**Figure S5F**); 17.0 ± 0.7 (15.4–18.9) µm long, 9.9 ± 0.6 (8.5–10.8) µm in wide, 7.7 ± 0.4 (7.0–8.3) µm thick (n = 13). Polar capsule: Single, large, subspherical, 6.8 ± 0.4 (5.8–7.6) µm long, 5.8 ± 0.3 (4.8–6.7) µm wide, occupying ¼ of the spore body cavity. Polar tubule: Coiled seven to eight times (**Figure S5G**). Sutural line: Straight, smooth, thick in the middle of spore body. Sporoplasm: Binucleate, iodinophilous vacuole absent. Measurements from 30 fresh spores.

Locality: Dömsöd, Hungary (Ráckeve Danube Arm Fishing Association).

Predilection site: Skin.

Prevalence: 3.7% (1/27).

Etymology: The species is named for its spore morphology, which closely resembles that of *Thelohanellus nikolskii* Akhmerov, 1955.

Molecular data: Partial 18S rDNA sequence of *T. paranikolskii* n. sp. of 1923 base pairs was deposited in GenBank under the accession number PV942517. The newly obtained 18S rDNA sequence did not match any of myxozoan sequences available in GenBank. Pairwise distance estimation indicated the highest similarities of 94.5% to *Thelohanellus nikolskii* (GU165833) and 93.6% to 93.8% similarity to the newly obtained *T. nikolskii* (PV926531) and *Thelohanellus pseudonikolskii* (OM801563), respectively (**Table 8**). Phylogenetic analyses showed that *T. paranikolskii* n. sp. is closely related to *T. pseudonikolskii* and to *T. nikolskii* (PV926531, GU165832), with high bootstrap values and posterior probabilities (**Figure 10**).

Remarks: The morphology and morphometrics of *T. paranikolskii* n. sp. are closely resemble to *T. nikolskii*, as observed both in the present and previous studies (**Table S11**). The main

distinguishing features include a smaller spore thickness in *T. paranikolskii* n. sp. compared to *T. nikolskii* described in this study and the *T. nikolskii* from fin rays reported by Borzák et al. (2021), but greater than that of *T. nikolskii* from scales, also described by Borzák et al. (2021). Additionally, *T. paranikolskii* n. sp. has 7 to 8 number of polar tubule coils, while *T. nikolskii* has 6 to 7 polar tubule coils. Morphologically, they can also be differentiated by the absence of slightly narrowed, flattened anterior ends in *T. paranikolskii* n. sp., a feature present in *T. nikolskii*.

4.1.2.3. Redescription of *Thelohanellus nikolskii* Akhmerov, 1955

Plasmodia of *T. nikolskii* were observed in the cartilage of the fin rays (**Figure S6A** and **Figure S6D**) in a single specimen out of twenty-seven common carp (3.7%) collected from the Ócsárd fish farm. The plasmodia were brownish and rounded in shape (**Figure S6A**), measuring 0.8 ± 0.1 (0.7–0.9) mm in length and 0.9 ± 0.2 (0.7–1.0) mm in width (n = 3). Fresh myxospores appearing subspherical in the frontal view, with slightly narrowed and flattened anterior ends, and pyriform in the sutural view (**Figure S6B–S6C**). The spores measured 17.3 ± 0.7 (15.9–18.6) µm in length, 9.8 ± 0.5 (8.7–10.7) µm in width and 8.4 ± 0.3 (8.0–8.9) µm in thickness. Each spore containing a single large, subspherical polar capsule, measuring 7.3 ± 0.3 (6.6–8.0) µm in length and 6.0 ± 0.3 (5.5–6.5) µm in width occupying $^{1}/_{3}$ of the spore body cavity. The polar tubule coiled six to seven times. The sutural line straight, smooth and thickened at the middle of the spore body. The sporoplasm binucleated, and no iodinophilous vacuole observed. Measurements from 30 fresh spores.

The morphology and morphometric data of *T. nikolskii* are consistent with the recently described *T. nikolskii* from the fin rays of common carp in Hungary (**Table S11**). Minor size differences are observed in all measurements, but these remained within the established range of variation. In contrast, compared with *T. nikolskii* from the scales (Borzák et al., 2021), the present specimens of *T. nikolskii* are distinctly smaller in all measured features.

A partial 18S rDNA sequence of *T. nikolskii*, consisting of 1626 base pairs was deposited in GenBank under the accession number PV926531. Pairwise distance estimation of the newly

obtained sequence indicated the highest similarity of 99.7% to previously published *T. nikolskii* sequences (GU165832) (**Table 8**). Phylogenetic analyses demonstrated that the present *T. nikolskii* clustered in the same branch as the previously published sequences of *T. nikolskii* (GU165832), with high bootstrap values and posterior probabilities (**Figure 10**).

4.1.2.4. Redescription of *Thelohanellus hovorkai* Akhmerov, 1960

Plasmodia of *T. hovorkai* were observed on the serous membranes of the intestine, with disperse spores also detected in the kidney and gallbladder of nine out of twenty-seven common carp (33.3%) collected from both fish farms. The plasmodia were whitish, rounded or polymorphic in shape (**Figure S7A–S7B**), measuring 0.69 ± 0.37 (0.34–1.21) mm in length and 0.55 ± 0.40 (0.21–1.14) mm in width (n = 4). Fresh myxospores appeared elongated, pyriform with tapered anterior ending in the frontal and sutural views (**Figure S7C–S7D**). The spores measured 20.0 ± 0.8 (18.6–21.4) µm in length, 9.9 ± 0.7 (8.9–11.6) µm in width and 8.0 ± 0.5 (7.1–8.9) µm in thickness. Each spore containing a single, large, round polar capsule with a prominent protrusion at the anterior end, measuring 10.4 ± 0.5 (9.5–11.9) µm in length and 7.5 ± 0.4 (6.4–8.6) µm in width, occupying ½ of the spore body cavity. The polar tubule coiled eight to ten times (**Figure S7E**). The sutural line straight, smooth and thickened at the middle of the spore body. The sporoplasm binucleated and an iodinophilous vacuole visible (**Figure S7E**). The spores surrounded by a thin, elongated mucous envelope. The spores with mucous envelope measured 24.9 ± 0.7 (23.6–26.5) µm in length and 13.8 ± 0.8 (12.1–15.8) µm in width.

The morphology of *T. hovorkai* in present study is consistent with that reported in previous studies (**Table S10**). Morphometrically, *T. hovorkai* from this study was larger in size compared to those described by Akhmerov (1960) and Molnár & Kovács-Gayer (1982).

Partial 18S rDNA sequence of *T. hovorkai*, consisting of 1938 base pairs was deposited in GenBank under the accession number PV926536. Pairwise distance estimation of the newly obtained sequence revealed the highest similarity of 100.0% to *T. hovorkai* (DQ231155) (**Table 8**). Phylogenetic analyses demonstrated that the present *T. hovorkai* clustered within the same

branch as the previously published *T. hovorkai* sequence (DQ231155) with high bootstrap values and posterior probabilities (**Figure 10**). The sequence of *T. hovorkai* (AJ133419) from Japan was excluded from the phylogenetic tree analysis due to its shorter DNA length of 710 base pairs and only 95.6% similarity.

4.1.2.5. Redescription of *Myxobolus intrachondrealis* Molnár, 2000

Plasmodia were found in the cartilaginous gill arch (**Figure S8A)** in five out of twenty-seven common carp (18.5%) collected from the Dömsöd fish farm. Histology: Plasmodia located within the hyaline cartilage of the gill arches (**Figure S8D–S8E**). The plasmodia were whitish and oval to elongated in shape (**Figure S8A**), measuring 0.6 ± 0.4 (0.1–1.3) mm in length and 0.3 ± 0.3 (0.1–0.9) mm in width (n = 6). Fresh myxospores ellipsoidal in frontal view (**Figure S8B**) and biconvex in sutural view (**Figure S8C**). The spores measured 10.1 ± 0.4 (9.4–11.0) µm in length, 6.6 ± 0.2 (5.9–7.1) µm in width and 4.6 ± 0.3 (4.1–5.4) µm in thickness (n = 16). Two polar capsules elongated pyriform and equal in size, measuring 4.3 ± 0.3 (3.8–5.1) µm in length and 2.4 ± 0.2 (2.1–2.8) µm in width. The polar tubules were coiled six to seven times. An indistinct, triangular intercapsular appendix located between the polar capsules at the anterior end of the spore. The sporoplasm binucleated, and no iodinophilous vacuole observed. Measurements from 30 fresh spores.

The morphology of *M. intrachondrealis* in the present study is consistent with descriptions from previous reports (**Table S5**). The only difference observed concerns the number of polar filament coils, which in the present study, spores have 6–7 coils, whereas Molnár (2000) reported 9–11 coils. This discrepancy may be due to the lower magnification used in earlier observations, which could have led to misinterpretation.

Pairwise distance estimation of the newly obtained 18S rDNA sequence (1990 bp) revealed 100.0% similarity to *Myxobolus cultrati* (KU170935), previously reported from the retina of *Pelecus cultratus* (**Table 8**). Phylogenetic analyses placed the present *M. intrachondrealis* in the same branch as *M. cultrati*, supported by high bootstrap and posterior probabilities (**Figure 10**).

The observed similarity may be explained by the absence of an available sequence of *M. intrachondrealis* in GenBank, as well as differences in host species, since *M. cultrati* was described from *P. cultratus*. Additionally**,** *M. intrachondrealis* formed a close relationship with *M. cultus*.

4.1.2.6. Redescription of *Myxobolus basilamellaris* Lom et Molnár, 1983

Plasmodia found at the base of gill filaments in one out of twenty-seven common carp (3.7%) collected from the Dömsöd fish farm. Histology: Plasmodia were located within the cartilaginous branchial arch and developed between the two neighbouring gill filaments (**Figure S8F**). The plasmodia whitish and oval, measuring 0.57 x 0.19 mm (n = 1). Fresh myxospores broadly ellipsoidal in frontal view (**Figure S8G**) and lemon-shaped in sutural view (**Figure S8H**). Spores measured 10.2 ± 0.7 (9.0–12.2) µm in length, 8.3 ± 0.4 (7.5–9.1) µm in width and 6.2 ± 0.3 (5.7–6.7) µm in thickness (n = 15). Two pyriform polar capsules unequal in size. The large polar capsule measured 4.5 ± 0.4 (3.7–5.4) µm in length and 2.9 ± 0.3 (2.4–3.5) µm in width, and the small one 3.2 ± 0.3 (2.7–3.9) × 2.1 ± 0.2 (1.8–2.5) µm. The polar filaments spirally arranged, perpendicular to the longitude axis, with five to six coils in the large polar capsules and four to five coils in the smaller ones. The sporoplasm binucleated, and no iodinophilous vacuole observed. Measurements from 30 fresh spores.

The morphology of *M. basilamellaris* in the present study is consistent with descriptions from previous reports (**Table S6**). However, *M. basilamellaris* described by Lom & Molnár (1983) was smaller in size and were reported to possess ten sutural markings and a mucous envelope. In contrast, neither sutural markings nor a mucous envelope were observed in the present study, which is consistent with the findings of Zhang et al. (2023a).

Pairwise distance estimation of the newly obtained 18S rDNA sequence (1983 bp) revealed 99.8% similarity to *M. basilamellaris* (OQ725580) (**Table 8**). Phylogenetic analyses placed the present *M. basilamellaris* in the same branch as *M. basilamellaris* from koi carp in China,

supported by high bootstrap and posterior probabilities. Additionally, *M. basilamellaris* formed a close relationship with *M. tsangwuensis, M. musseliusae,* and *M. elliptoides* (**Figure 10**).

4.1.3. Myxosporean parasites in Rutilus rutilus

4.1.3.1. Myxobolus n. sp. 1

Plasmodium: Found in the connective tissue of gill arch, round (**Figure S9A**); 0.25 mm diameter (n = 1). Spore: Round or ellipsoidal in frontal view (**Figure S9B**); 13.0 ± 0.6 (11.9–14.4) µm long, 10.4 ± 0.5 (8.7–11.0) µm wide, 7.5 ± 0.4 (7.0–8.1) µm thick (n = 6). Polar capsule: Two, pyriform, equal size, 5.7 ± 0.4 (4.9–6.4) µm long, 3.4 ± 0.3 (2.8–4.0) µm wide. Polar tubule: Coiled six times, positioned perpendicularly to capsule axis. Sutural ridge: Eight to ten sutural markings, symmetrically distributed. Triangular intercapsular appendix present. Sporoplasm: Binucleate, iodinophilous vacuole absent, mucous envelope absent. Measurements from 30 fresh spores.

Locality: Ócsárd fish farm, county Baranya, Hungary.

Predilection site: Connective tissue of gill arch.

Prevalence: 40.0% (2/5).

Molecular data: Partial 18S rDNA sequence of *Myxobolus* n. sp. 1 of 1689 base pairs did not match any of the myxozoan sequences available in GenBank. Pairwise distance estimation indicated the highest similarity of 97.1% to *Myxobolus ellipsoides* (DQ439813), reported from the fins of *Leuciscus cephalus* (**Table 8**). Phylogenetic analyses placed *Myxobolus* n. sp. 1 as closely related to *M. ellipsoides* and forming a sister relationship with *Myxobolus* n. sp. 2 and *Myxobolus erythrophthalmi*, supported by high bootstrap values and posterior probabilities (**Figure 10**).

Remarks: The morphology and morphometrics of *Myxobolus* n. sp. 1 are distinct from all previously described *Myxobolus* spp. The closest morphological resemblance is to *Myxobolus fundamentalis* Molnár, Marton, Szekely et Eszterbauer, 2010, *Myxobolus rutili* Donec et Tozyyakova, 1984 and *Myxobolus* n. sp. 2; however, *M. fundamentalis* is larger in size. Morphometrically, *Myxobolus* n. sp. 1 is most similar to *Myxobolus* n. sp. 2 and *Myxobolus rutili*

in all measurements, except that *M. rutili* has different number of sutural markings (8–10 vs 4–6) (**Table S12**).

4.1.3.2. Myxobolus n. sp. 2

Plasmodia: Found in kidney, whitish to yellowish, oval in shape (**Figure S9C**), 0.2 (0.1–0.3) mm diameter (n = 23). Histology: Plasmodium located in renal interstitium (**Figure S9D**). Spore: Round or ellipsoidal in frontal view, lemon-shaped in sutural view (**Figure S9E–S9F**). Size 12.6 ± 0.4 (11.7–13.2) µm long, 10.5 ± 0.4 (9.6–11.4) µm wide, 7.4 ± 0.3 (6.7–8.1) µm thick (n = 19). Polar capsule: Two, pyriform, slightly unequal. Larger: 5.6 ± 0.2 (5.3–6.3) µm long, 3.4 ± 0.1 (3.2–3.8) µm wide. Smaller: 4.9 ± 0.4 (4.1–5.6) × 3.2 ± 0.2 (2.7–3.5) µm. Polar tubule: Coiled five to six times, positioned perpendicularly to capsule axis. Sutural ridge: Six to seven sutural markings, symmetrically distributed. Sporoplasm: Binucleate, iodinophilous vacuole absent, mucous envelope absent. Measurements from 30 fresh spores.

Locality: Ócsárd fish farm, county Baranya, Hungary.

Predilection site: Kidney.

Prevalence: 60.0% (3/5).

Molecular data: Partial 18S rDNA sequence of *Myxobolus* n. sp. 2 of 1626 base pairs did not match any of the myxozoan sequences available in GenBank. Pairwise distance estimation of the newly obtained 18S rDNA sequence indicated the highest similarity of 96.7% to *M. erythrophthalmi* (EU567311), reported from the kidney of *S. erythrophthalmus* (**Table 8**). Phylogenetic analyses placed *Myxobolus* n. sp. 2 as closely related to *M. erythrophthalmi* and forming a sister relationship with *Myxobolus* n. sp. 1 and *M. ellipsoides*, supported by high bootstrap values and posterior probabilities (**Figure 10**).

Remarks: The morphology and morphometrics of *Myxobolus* n. sp. 2 are distinct from all previously described *Myxobolus* spp. The closest morphological resemblance is to *Myxobolus zaikae* Batueva, 2020 infecting the connective tissue near kidney and liver blood vessels of *R. rutilus* and to *Myxobolus* n. sp. 1 from the same host. Morphometrically, *M. zaikae* slightly smaller

than *Myxobolus* n. sp. 2 in all measurements, except both species share a similar number of filament coils and sutural markings, while *Myxobolus* n. sp. 1 is identical in all measured features. Genetically, *Myxobolus* n. sp. 2 is more closely related to *M. erythrophthalmi* than to *M. zaikae*; however, *M. erythrophthalmi* is considerably smaller than both *Myxobolus* n. sp. 2 and *M. zaikae,* and differs remarkably in the number of sutural markings (6–7 vs 7–9) (**Table S12**).

4.2. Actinosporeans in Hungary

A total of 5,976 oligochaetes isolated from sediment collected at a fish farm in Ráckeve and Ócsárd fish farms. Myxozoan infection was detected in the intestinal epithelium of 71 oligochaetes, resulting in an overall prevalence of 1.18% (71 out of 5,976 oligochaetes examined). The comprehensive survey of oligochaetes in the sediment samples revealed the presence of at least eight morphologically distinct species such as *Branchiura sowerbyi*, *Tubifex tubifex*, *Limnodrilus hoffmeisteri*, *Dero* sp., *Stylaria* sp., *Potamothrix* sp., *Branchiodrilus hortensis*, and *Ophidonais serpentina.* However, myxozoan infections were detected in only four species, namely *B. sowerbyi*, *Tubifex tubifex*, *Ophidonais serpentina*, and *Limnodrilus hoffmeisteri*. Among these, B. *sowerbyi* exhibited the highest prevalence of myxozoan infection, with 12.1%; 38 out of 315 oligochaetes testing positive. In contrast, *L. hoffmeisteri* exhibited a much lower infection rate of 1.2% (21 out of 1,721), *O. serpentina* had 0.9% (1 out of 110), and *T. tubifex* had the lowest prevalence at 0.3% (3 out of 986). This study identified ten different actinospore types, including one triactinomyxon type, two raabeia types, six aurantiactinomyxon types, and one neoactinomyxum type. Of these, the triactinomyxon type, five aurantiactinomyxon types and one raabeia type were identified as novel, while the others had been previously described. Furthermore, four of the actinospore types were matched with their myxosporean counterparts: one belongs to the new *Z. chezhachei*, thus completing its life cycle, and four involved in the life cycles of previously known *Thelohanellus wangi*, *T. hovorkai* and *M. cultus*.

4.2.1. Collective group Triactinomyxon Štolc (1899)

The spores possess an elongated spore body with three protruding tips of polar capsules and plasmodial sporoplasm containing numerous secondary cells, ranging from 8 to 256. Spores have a style and three anchor-shaped caudal processes with sharp points. The spores typically found in freshwater and marine oligochaetes. The key features of this collective group include the presence of a style and the variability in the number of secondary cells. The original type of the collective group is Triactinomyxon ignotum Štolc, 1899 described from *Tubifex* sp. collected from the Vltava River in Prague, Czech Republic.

4.2.1.1. Triactinomyxon type 1 (Figure S10A–S10B)

Spore body: Cylindrical, elongated, 37.6 ± 4.9 (29.1–48.8) µm long, 13.6 ± 1.4 (11.5–15.8) µm wide. Style: Long, 131.2 ± 13.9 (103.6–154.4) µm long, 16.4 ± 1.1 (14.7–19.6) µm wide. Total length: 172.4 ± 10.6 (153.3–192.4) µm. Caudal process: Upward, tapering to pointed ends, equal length, 274.89 ± 15.3 (257.8–298.9) µm long, 21.2 ± 1.9 (17.2–24.4) µm wide at base. Largest span: 486.2 ± 76.3 (311.2–560.3) µm. Valve cell nuclei: Located at base of caudal processes, 4.9 ± 0.7 (4.1–6.1) µm diameter (n = 5). Polar capsule: Pyriform, equal size, protruding from anterior end, 6.0 ± 0.9 (4.3–7.7) µm long, 4.0 ± 0.6 (3.2–5.0) µm wide. Polar tubule: Coiled four to five times. Sporoplasm: 32 secondary cells. Measurements from 15 fresh actinospores.

Host: *Limnodrilus hoffmeisteri* Claparède, 1862.

Predilection site: The intestinal epithelium.

Prevalence: 0.06% (1 out of 1,721 infected host species).

Locality: Szigetbecse, Csepel Island, Hungary.

Molecular data: Partial 18S rDNA sequence of triactinomyxon type 1 of 1648 base pairs was deposited in GenBank under the accession number PQ164813. The newly obtained 18S rDNA sequence did not match any of myxozoan sequences available in GenBank. Pairwise distance estimation indicated the highest similarities of 98.3% to *Myxobolus diversicapsularis* (GU968199) reported from the gills of *R. rutilus* and 98.0% to triactinomyxon type (AY495706) (**Table 11**).

Phylogenetic analyses showed that triactinomyxon type 1 formed a sister relationship with *M. diversicapsularis* (GU968199) and triactinomyxon type (AY495706), with maximum bootstrap values and posterior probabilities (**Figure 13**).

Remarks. The morphology and morphometrics of the present triactinomyxon type are distinct from those described in the literature. It is morphologically similar to triactinomyxon type 2 (Székely et al., 2014) but differs morphometrically. Spore body length closely resembles triactinomyxon type 3 (Lowers & Bartholomew, 2003) and triactinomyxon type 5 (El-Mansy et al., 1998a). It also greatly resembles triactinomyxon type 4 described by El-Mansy et al. (1998a), though with slightly smaller polar capsules (6.0 × 4.0 vs 5.9 × 3.5). Additionally, the length of the style of the triactinomyxon type 1 is also slightly smaller compared to triactinomyxon type 4 of El-Mansy et al. (1998b). Notably, the length and width of the caudal processes of the triactinomyxon type 1 differed from those described in the literature (**Table S13**).

4.2.2. Collective group Raabeia Janiszewska (1955)

The spores possess an ellipsoidal spore body with three protruding tips of polar capsules and plasmodial sporoplasm. Caudal projections are divergent with three elongated, sharp pointed and curved or straight caudal process emerging from the spore body without a style. However, several described types exhibited branches at the tip of the caudal processes, which serves as another characteristic feature for the collective group. The spores typically found in freshwater oligochaetes. The original type of the collective group is Raabeia gorlicensis Janiszewska, 1955 described from *Tubifex tubifex* collected from Carpathian rivers in Poland.

4.2.2.1. Raabeia type 1 (Figure S10C–S10F)

Spore body: Elongated, cylindrical in side view, 51.8 ± 2.7 (47.7–50.2) µm long, 5.5 ± 0.9 (4.1–6.0) µm wide. Caudal process: Equal length, long, curved upwards, tapering to sharp point, 153.0 ± 16.5 (123.9–136.0) µm long, 7.0 ± 0.9 (5.5–8.7) µm wide at base. Valve cell nuclei: Located at spore body base, 3.2 ± 0.6 (2.2–4.6) µm diameter (n = 19). Polar capsule: Spherical in apical view, pyriform in side view, protruding from anterior end, 5.0 ± 0.8 (3.9–4.7) µm long, 2.8 ± 0.4 (1.9–

2.7) µm wide, each with four coils polar tubule. Sporoplasm: 16 secondary cells, arranged in 2 columns. Measurements from 30 fresh actinospores. Measurements above are from spores in oligochaetes from Ráckeve fish farm; those from Ócsárd fish farm are presented in **Table S14.**

Host: *Limnodrilus hoffmeisteri* Claparède, 1862.

Predilection site: The intestinal epithelium. Pansporocyst of the raabeia type 1 is visible in the intestinal epithelium of the infected oligochaete (**Figure S10G**).

Prevalence: 0.92% (16 out of 1,721 infected host species).

Locality: Szigetbecse, Csepel Island and Ócsárd fish farm, county Baranya, Hungary.

Molecular data: Partial 18S rDNA sequences of raabeia type 1 of 2019 and 1939 base pairs were deposited in GenBank under the accession numbers PQ217959 and PV818391, respectively. Two nearly identical 18S rDNA sequences (99.5%) did not match any of myxozoan sequences available in GenBank. Pairwise distance estimation indicated the highest similarity of 99.3% to "triactinomyxon 'F'" (AF378351) (**Table 11**). Phylogenetic analyses showed that raabeia type 1 clustered with "triactinomyxon 'F'" (AF378351), with maximum bootstrap values and posterior probabilities and formed a sister relationship with raabeia type 1 (KJ152184), and *Myxobolus dechtiari* (MW588908) (**Figure 13**).

Remarks. Morphology of raabeia type 1 resembles raabeia type 2 (Borkhanuddin et al., 2014a) and "triactinomyxon 'F'" (Xiao & Desser, 1998b), with both having cylindrical spore body and 16 secondary cells arranged in 2 columns. This morphology does not resemble any of the raabeia types described so far. In terms of morphometric measurements, raabeia type 1 shows closest similarity to "triactinomyxon 'F'" in polar capsule length, although "triactinomyxon 'F'" has larger caudal processes and a slightly smaller spore body (**Table S14**). Compared with raabeia type of Borkhanuddin et al. (2014a), it has slightly larger caudal processes but a smaller spore body. Spore body length closely resembles Raabeia magna (Janiszewska, 1957), width resembles raabeia type 2 (Borkhanuddin et al., 2014a), while polar capsule length is similar to Raabeia furciligera (Marques, 1984) and raabeia type 2 of Oumouna et al. (2003).

4.2.2.2. Raabeia type 2 (Figure S11A–S11C)

Spore body: Barrel-shaped in side view, 22.6 ± 1.5 (20.0–25.3) μm long, 9.5 ± 0.7 (8.0–11.0) μm wide. Caudal process: Equal length, curved upwards, and taper to a sharp point, 204.1 ± 17.0 (177.7–233.5) μm long, 6.4 ± 0.7 (5.1–5.9) μm wide at the base. Six short branches visible at the end of caudal processes (**Figure S11B**). Valve cell nuclei: Located at the base of caudal processes, 3.7 ± 0.5 (2.9–3.6) μm diameter. Polar capsule: Pyriform in sutural view, equal size, protruding from anterior end, 5.5 ± 0.3 (4.9–5.6) μm long, 2.8 ± 0.3 (2.0–3.0) μm wide. Polar tubule: Coiled four to five times (**Figure S11C**). Sporoplasm: 16 secondary cells. Measurements from 30 fresh actinospores.

Host: *Branchiura sowerbyi* Beddard, 1892.

Predilection site: The intestinal epithelium. Several pansporocysts were clearly observed in the intestinal epithelium of *B. sowerbyi* after the worm was treated with lactic acid (**Figure S11D–S11E**).

Prevalence: 1.90% (6 infected in 315 oligochaetes examined).

Locality: Ócsárd fish farm, county Baranya, Hungary.

Molecular data: Partial 18S rDNA sequence of raabeia type 2 of 1648 base pairs was deposited in GenBank under the accession number PV818390. The 18S rDNA sequence from the raabeia type 2 matched with the sequences of raabeia type (HQ613407) and *M. cultus* (HQ613409). Pairwise distance estimation indicated the highest similarities of 99.8% to raabeia type (HQ613407) and 99.6% to *M. cultus* (HQ613409) (**Table 11**). Phylogenetic analyses showed that raabeia type 2 clustered in the same branch with *M. cultus*, as well as the actinospore stage of *M. cultus*, which belongs to the raabeia type. Additionally, raabeia type 2 formed a close relationship with *M. cultrati*, with high bootstrap values and posterior probabilities (**Figure 13**).

Remarks: The morphology and morphometric data of raabeia type 2 are consistent with those of previously described raabeia types by Yokoyama et al. (1995), Eszterbauer et al. (2006) and Xi et al. (2013), although minor size differences are observed (**Table S14**). However, raabeia type 2

exhibited a shorter polar capsule length compared to raabeia types mentioned above (2.7 vs 4.0 and 4.1 μm). A remarkable difference between the present raabeia type 2 and previously described raabeia types of *M. cultus* is the presence of short branches at the ends of the caudal processes, which have not previously been reported in raabeia types of *M. cultus*. A few raabeia and echinactinomyxon types have shown similar features. For instance, raabeia type 1 of Özer et al. (2002) had four branches at the ends of caudal processes, but the processes were shorter than those of the present raabeia type 2 (94.5 vs 204.1 μm). Raabeia type 2 of the same study also had four branches arranged in two pairs at the ends of the caudal processes. Similarly, echinactinomyxon types reported by Marcucci et al. (2009) and Xi et al. (2015) displayed comparable morphological traits but possessed shorter caudal processes than the present raabeia type 2. This study is the first to report the presence of caudal process branches in a raabeia type of *M. cultus*.

4.2.3. Collective group Aurantiactinomyxon Janiszewska (1952)

The spores possess spherical, subspherical, cylindrical and triangular spore body without a style. Three polar capsules protruding from the apex of the spore body and three caudal processes equal in length, curving downwards, and taper to a rounded or pointed end. The processes can be leaf-like, propeller-like, digitiform or triangular that arise from the spore body (Rocha, 2023). The spores typically found in freshwater oligochaetes. The original type of the collective group is Aurantiactinomyxon raabeiiunioris Janiszewska, 1952 described from *L. hoffmeisteri* collected from the southern Carpathians, Poland. Currently, 64 types of this collective group have been identified (Rocha, 2023; Rocha et al., 2024).

4.2.3.1. Aurantiactinomyxon type 1 (Figure S12A–S12E)

Spore body: Triangular apical view, 13.6 ± 1.9 (8.2–17.3) μm diameter, subspherical in side view. Caudal process: Three leaf-like, equal size, 25.7 ± 2.9 (21.3–31.6) μm long, 7.4 ± 1.3 (4.2–10.1) μm wide at base, slightly curved downwards in side view. Valve cell nuclei: Located randomly in each caudal process, 2.1 ± 0.3 (1.5–2.6) (n = 15). Polar capsule: Positioned at apex of spore body, globular in apical view, 2.4 ± 0.3 (1.9–3.3) μm diameter, pyriform in side view. Polar tubule: Not

visible. Sporoplasm: Approximately 32 secondary cells. Measurements from 20 fresh actinospores.

Host: *Ophidonais serpentina* Müller, 2015.

Predilection site: The intestinal epithelium.

Prevalence: 0.90% (1 out of 110 infected host species).

Locality: Makád, Csepel Island, Hungary.

Molecular data: Partial 18S rDNA sequence of aurantiactinomyxon type 1 of 1917 bp was deposited in GenBank under the accession number PQ189140. The 18S rDNA sequence from aurantiactinomyxon type 1 did not match any of the myxozoan sequences available in GenBank. Pairwise distance estimation indicated the highest similarity of 97.0% to *Henneguya* sp. (EU732601) reported from the gills of *Esox lucius* (**Table 11**). Phylogenetic analyses showed that aurantiactinomyxon type 1 clustered with *Henneguya* sp. (EU732601), with maximum bootstrap values and posterior probabilities. Additionally, the aurantiactinomyxon type 1 formed a sister relationship with *Henneguya lobosa* (EU732600) and *Henneguya michiganensis* (MT711164). This aurantiactinomyxon type 1 was also positioned within a *Henneguya* clade comprising seven other species (**Figure 13**).

Remarks: The morphology and morphometrics of aurantiactinomyxon type 1 differ from all previously described types. It most closely resembles the aurantiactinomyxon type of Zhao et al. (2017), but has longer caudal processes and a smaller spore body, with a similar number of secondary cells. In addition, the morphometric measurements of aurantiactinomyxon type 1 are close to those of McGeorge et al. (1997), though with slightly longer caudal processes, smaller spore body, and smaller polar capsules. Spore body diameter resembles that of aurantiactinomyxon type 1 (Székely et al., 2003). Polar capsules are slightly larger than aurantiactinomyxon type 1 (El-Mansy et al., 1998a) and aurantiactinomyxon type 9 (El-Mansy et al., 1998b) collected from *B. sowerbyi*, but slightly smaller than aurantiactinomyxon type 4 (Özer et al., 2002) from *T. tubifex* (**Table S15**).

Table 11 Genetic *p*-distance and sequence similarities (%) based on the 18S rDNA between triactinomyxon type 1, raabeia types, aurantiactinomyxon types, neoactinomyxum type 1 and its most closely related species. Only identical or the closest-related sequences are presented.

Sequence	Genetic distance	Sequence similarities (%)
Triactinomyxon type 1 PQ164813		
Myxobolus diversicapsularis GU968199	0.017	98.3
Triactinomyxon type AY495706	0.020	98.0
Raabeia type 1 PV818391		
Raabeia type 1 PQ217959	**0.005**	**99.5**
"Triactinomyxon type 'F'" AF378351	0.007	99.3
Raabeia type 1 KJ152184	0.075	92.5
Myxobolus dechtiari MW588908	0.080	92.0
Aurantiactinomyxon type 2 PV818388		
Aurantiactinomyxon type 2 PQ189141	**0.002**	**99.8**
Raabeia type 1 PV818391	**0.099**	**90.1**
Raabeia type 1 PQ217959	**0.101**	**89.9**
"Triactinomyxon type 'F'" AF378351	0.102	89.8
Raabeia type 1 KJ152184	0.102	89.8
Raabeia type 2 PV818390		
Raabeia type HQ613407	0.002	99.8
Myxobolus cultus HQ613409	0.004	99.6
Aurantiactinomyxon type 1 PQ189140		
Henneguya sp. EU732601	0.030	97.0
Henneguya lobosa EU732600	0.069	93.1
Henneguya michiganensis MT711164	0.080	92.0
Aurantiactinomyxon type 3 PV818389		
Aurantiactinomyxon type KY784585	0.030	97.0
Thelohanellus wuhanensis MH329614	0.048	95.2
Neoactinomyxum type KY784596	0.083	91.7
Aurantiactinomyxon type 4 PV818387		
Aurantiactinomyxon type KY475591	0.000	100.0
Zschokkella chongqingense MT112714	0.000	100.0
Zschokkella chezhachei n. sp. PV172149	0.000	100.0
Aurantiactinomyxon type 5 PV942516		
Aurantiactinomyxon type 6 PV942515	**0.001**	**99.9**
***Thelohanellus hovorkai* PV926536**	**0.001**	**99.9**
Aurantiactinomyxon type DQ231154	0.001	99.9
Thelohanellus hovorkai DQ231155	0.000	100.0
Aurantiactinomyxon type DQ231153	0.000	100.00
Neoactinomyxum type 1 PV818389		
Thelohanellus wangi JX458816	0.000	100.0
Neoactinomyxum type KY784590	0.005	99.5

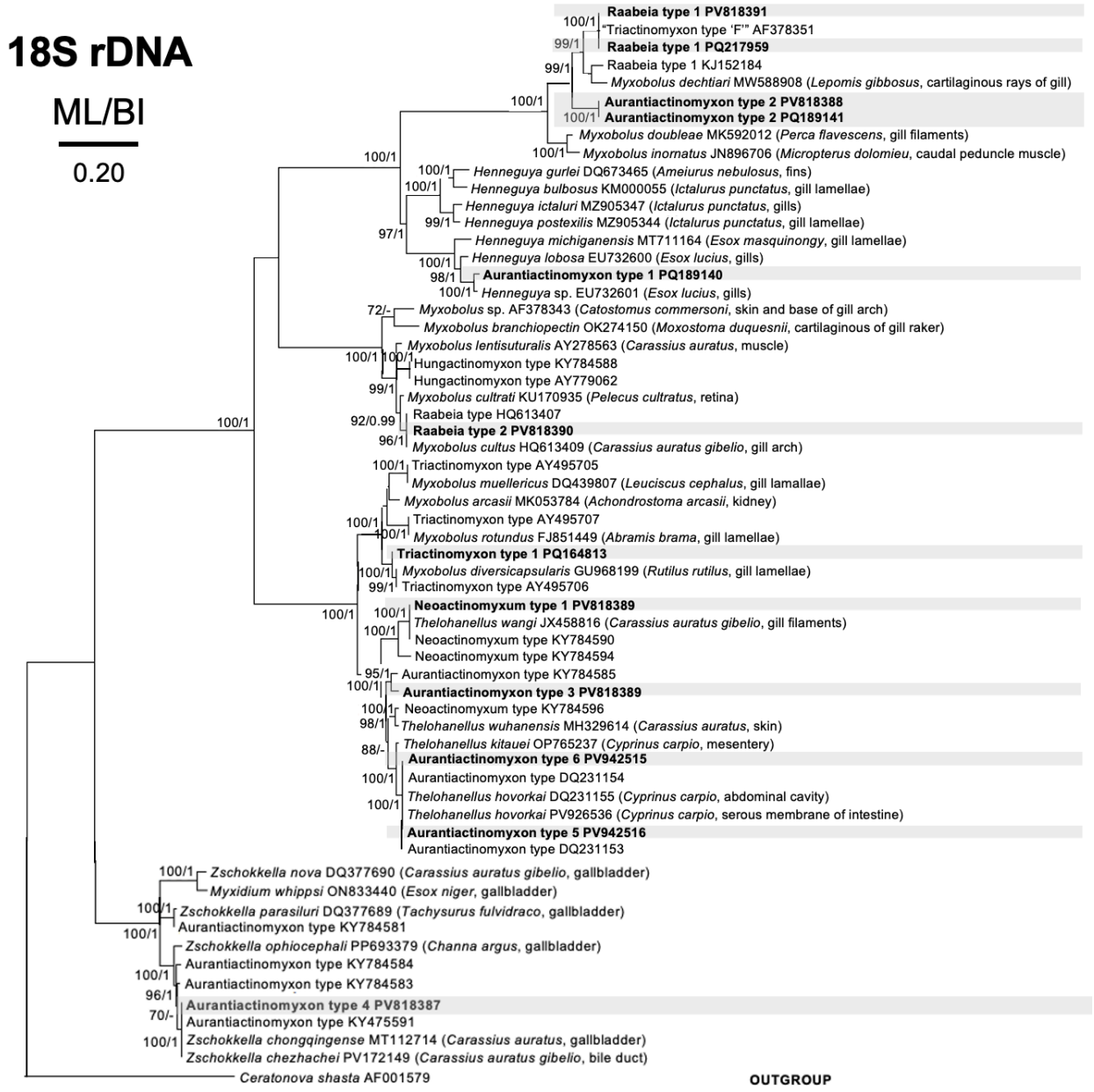

Figure 13. Maximum likelihood (ML) phylogenetic tree of 18S rDNA sequences of triactinomyxon type, raabeia types, aurantiactinomyxon types, neoactinomyxum type and related species. *Ceratonova shasta* was used as outgroup. Nodal supports are indicated for ML at 1000 replicates and Bayesian Inference (BI). Only values with ≥ 70% bootstrap (BS) and ≥ 0.90 posterior probabilities (PP) support are presented. The names of the parasite species are presented before GenBank accession numbers, following the host species and predilection site. Sequences obtained in the present study is shown in bold within colored boxes. The scale bar indicates the expected number of substitutions per site.

4.2.3.2. Aurantiactinomyxon type 2 (Figure S13A–S13E)

Spore body: Spherical in apical view, 10.5 ± 0.9 (8.8–13.3) µm diameter, bulbous in side view. Caudal process: Long, straight, sharp point, equal length, 64.5 ± 4.2 (55.8–71.6) µm long, 4.7 ± 0.6 (3.7–5.7) µm wide at base, slightly curved downwards in side view. Valve cell nuclei: Located

randomly in each caudal process. Polar capsule: Positioned at apex of spore body, globular in apical view, 2.6 ± 0.3 (2.0–3.2) μm diameter, pyriform in side view. Polar tubule: Not visible. Sporoplasm: Approximately 16 secondary cells. Measurements from 30 fresh actinospores. Measurements above are from spores in oligochaetes from Ráckeve fish farm; those from Ócsárd fish farm are presented in **Table S16**.

Host: *Tubifex tubifex* Müller, 2015.

Predilection site: The intestinal epithelium. Histological analysis and microscopic examination showed that the pansporocysts located in the intestinal epithelium of the infected oligochaetes (**Figure S13F**). In the semithin sections, matured spores could be observed within the pansporocyst (**Figure S13G**).

Prevalence: 0.29% (5 out of 1,677 infected host species).

Locality: Szigetbecse, Csepel Island and Ócsárd fish farm, county Baranya, Hungary.

18S rDNA sequence: Partial 18S rDNA sequences of aurantiactinomyxon type 2 of 1559 and 1922 base pairs were deposited in GenBank under the accession numbers PQ189138 and PV818388, respectively. Two nearly identical 18S rDNA sequences (99.8%) did not match any of myxozoan sequences available in GenBank. Pairwise distance estimation indicated the highest similarities of 90.1% and 89.9% to raabeia type 1 (PV818391, PQ217959) identified in this study (**Table 11**). Phylogenetic analyses showed that aurantiactinomyxon type 2 formed a well-supported sister relationship with the *Myxobolus* spp. clade, including *Myxobolus inornatus* (JN896706), *Myxobolus doubleae* (MK592012), and *Myxobolus dechtiari* (MW588908), as well as triactinomyxon F (AF378351), raabeia type 1 (KJ152184) and raabeia type 1 (PV818391, PQ217959) identified in the present study (**Figure 13**).

Remarks: The morphology and morphometrics of aurantiactinomyxon type 2 differ from all previously described types. Its spore body diameter closely resembles those described by Borkhanuddin (2013), and Borzák et al. (2021), but the aurantiactinomyxon type 2 have a larger spore body (**Table S16**). The caudal processes are longer and wider than most described in the

literature, though smaller than those of El-Mansy et al. (1998b). The polar capsules diameter closely similar that of aurantiactinomyxon type 1 (Özer et al., 2002), aurantiactinomyxon type B (Eszterbauer et al., 2006) and aurantiactinomyxon types described by Borkhanuddin (2013), Rocha et al. (2019a), and Borzák et al. (2021).

4.2.3.3. Aurantiactinomyxon type 3 (Figure S14A–S14E; Figure S17A–S17B)

Spore body: Spherical in both apical and side views, 18.9 ± 1.0 (16.5–20.8) μm diameter. Caudal process: Equal in size, leaf-like in apical view, curved downward in side view, 16.2 ± 1.6 (14.0–19.1) μm long, 8.4 ± 1.2 (6.7–10.5) μm wide at the base. Largest span between the ends of two caudal processes, 37.7 ± 2.0 (33.6–40.3) μm long (n = 19). Valve cell nuclei: Ovoid, visible, located randomly within each caudal process but mostly found at the ends, 3.1 ± 0.4 (2.2–4.4) μm diameter (**Figure S14E**). Polar capsule: Positioned at the apex of spore body, globular in apical view, 3.4 ± 0.3 (2.9–4.2) μm diameter, pyriform in side view. Polar tubule: Not visible. Sporoplasm: 32 secondary cells (**Figure S14E**). Measurements from 50 fresh actinospores.

Host: *Branchiura sowerbyi* Beddard, 1892.

Predilection site: The intestinal epithelium.

Prevalence: 1.58% (5 infected in 315 oligochaetes examined).

Locality: Ócsárd fish farm, county Baranya, Hungary.

Molecular data: Partial 18S rDNA sequence of aurantiactinomyxon type 3 of 1990 base pairs was deposited in GenBank under the accession number PV818386. The 18S rDNA sequence from aurantiactinomyxon type 3 did not match any of the myxozoan sequences available in GenBank. Pairwise distance estimation indicated the highest similarity of 97.0% to aurantiactinomyxon type (KY784585) previously reported from *B. sowerbyi* (**Table 11**). Phylogenetic analyses revealed that aurantiactinomyxon type 3 formed a close relationship with aurantiactinomyxon type (KY784585) and clustered within a well-supported clade of *Thelohanellus*, with maximum bootstrap values and posterior probabilities (**Figure 13**).

Remarks: The morphology and morphometrics of aurantiactinomyxon type 3 differ from all previously described types. It most closely resembles the aurantiactinomyxon type of *Thelohanellus testudineus* (Zhao et al., 2017), but larger in all measurements. In terms of morphometric measurements, the spore body of aurantiactinomyxon type 3 matches aurantiactinomyxon type 7 of El-Mansy et al. (1998b) (**Table S17**). The length of the caudal processes closely resembles aurantiactinomyxon type 1 (El-Mansy et al., 1998b), while caudal process length and width resemble those of aurantiactinomyxon type of *Thelohanellus kitauei* (Zhao et al., 2016). The polar capsule diameter is identical to the polar capsule length of the aurantiactinomyxon type of *Thelohanellus kitauei* (Zhao et al., 2016), both having 32 secondary cells (**Table S17**).

4.2.3.4. Aurantiactinomyxon type 4 (Figure S15A–S15B; Figure S17C–S17D)

Spore body: Spherical in both apical and side views, 10.9 ± 0.9 (8.9–12.6) μm diameter. Caudal process: Equal in size, leaf-like with rounded ends in apical view, curved downward in side view, 18.9 ± 1.7 (15.7–23.1) μm long, 4.5 ± 0.4 (4.0–5.4) μm wide at the base. Valve cell nuclei: Ovoid, visible, located at the end of caudal processes, 1.7 ± 0.2 (1.3–2.2) μm diameter. Polar capsule: Positioned at apex of spore body, globular in apical view, 2.0 ± 0.2 (1.7–2.5) μm diameter, pyriform in side view. Polar tubule: Coiled three times. Sporoplasm: Not determined. Measurements from 30 fresh actinospores.

Host: *Branchiura sowerbyi* Beddard, 1892.

Predilection site: The intestinal epithelium. Histopathological sections of the intestinal epithelium of *B. sowerbyi* revealed heavy infection with pansporocysts (**Figure S15D**), where mature spores are visible (**Figure 15E**). Additionally, released pansporocysts could be observed in the water surrounding from dead *B. sowerbyi* (**Figure 15C**).

Prevalence: 5.71% (18 infected in 315 oligochaetes examined).

Locality: Ócsárd fish farm, county Baranya, Hungary.

Molecular data: Partial 18S rDNA sequence of aurantiactinomyxon type 4 of 1995 base pairs was deposited in GenBank under the accession number PV818387. The 18S rDNA sequence of aurantiactinomyxon type 4 matched those of *Zschokkella chezhachei* (PV172149), *Zschokkella chongqingense* (MT112714) and aurantiactinomyxon type (KY475591). Pairwise distance estimation indicated 100.0% similarity to both *Z. chezhachei* and *Z. chongqingense* (invalid name), and 99.9% similarity to the aurantiactinomyxon type (KY475591) (**Table 11**). Phylogenetic analyses revealed that aurantiactinomyxon type 4 clustered with *Z. chezhachei*, *Z. chongqingense* in the same branch, as well as the actinospore stage of *Z. chongqingense*, which belongs to the aurantiactinomyxon type. Additionally, aurantiactinomyxon type 4 formed a close relationship with other aurantiactinomyxon types (KY784583, KY784584) and *Zschokkella ophiocephali* (PP693379), with maximum bootstrap values and posterior probabilities (**Figure 13**).

Remarks: The morphology and morphometrics of aurantiactinomyxon type 4 closely resemble the guyenotia type described by Xi et al. (2013), except that the guyenotia type has wider caudal processes (**Table S17**). The caudal process width of aurantiactinomyxon type 4 is similar to the guyenotia type reported by Eszterbauer et al. (2006). Additionally, we identified a sequence of aurantiactinomxon type 4 with the name *Zschokkella* sp. AUM-9 under the accession number KY475591 deposited in GenBank by Zhao, D.D., Zhai, Y.H., Liu, Y., Wang, S.J. and Gu, Z.M., which showed 99.9% similarity to our sequence. Unfortunately, the morphology and morphometric measurements of these spores have not been published. Based on these findings, we hypothesize that our aurantiactinomyxon type 4 may correspond to *Zschokkella* sp. AUM-9 in GenBank, and we are confident in identifying it as a novel type due to the lack of morphological data for comparison.

4.2.3.5. Aurantiactinomyxon type 5 (Figure S16A–S16B; Figure S17E)

Spore body: Spherical in both apical and side views, 20.7 ± 1.3 (18.7–24.1) μm diameter. Caudal process: Equal in size, straight with pointed tips, 51.5 ± 4.0 (43.4–56.3) μm long, 9.9 ± 0.9 (8.3–11.3) μm wide at the base. Valve cell nuclei: Ovoid, visible, located at the base of caudal processes,

3.7 ± 0.4 (3.0–4.2) µm diameter. Polar capsule: Positioned at the apex of spore body, globular in apical view, 3.5 ± 0.3 (3.1–4.1) µm diameter, tear-drop shaped in side view. Polar tubule: Coiled three times. Sporoplasm: 32 secondary cells (**Figure S16B**). Measurements from 16 fresh actinospores.

Host: *Branchiura sowerbyi* Beddard, 1892.

Predilection site: The intestinal epithelium.

Prevalence: 1.26% (4 infected in 315 oligochaetes examined)

Locality: Ócsárd fish farm, county Baranya, Hungary.

Molecular data: Partial 18S rDNA sequence of aurantiactinomyxon type 5 of 1931 base pairs was deposited in GenBank under the accession number PV942516. Pairwise distance estimation indicated the highest similarity of 99.9% to 100.0% with newly generated sequences of *T. hovorkai* (PV926536) and aurantiactinomyxon type 6 (PV942515), as well as with previously published sequences of *T. hovorkai* (DQ231155) and aurantiactinomyxon types (DQ231153, DQ231154) (**Table 11**). Phylogenetic analyses revealed that aurantiactinomyxon type 5 clustered in the same branch as other aurantiactinomyxon types (DQ231153, DQ231154), newly obtained aurantiactinomyxon type 6 (PV942515) and their corresponding myxospore stage, including the newly obtained sequence of *T. hovorkai* (PV926536), and a previously published sequence (DQ231155), with maximum bootstrap values and posterior probabilities (**Figure 13**).

Remarks: The morphology of aurantiactinomyxon type 5 closely resemble aurantiactinomyxon type ‘A’ described by Eszterbauer et al. (2006). In terms of morphometric measurements, aurantiactinomyxon type 5 is consistent with previous studies (**Table S18**), with only minor differences observed in all measurements. However, significant differences are noted in the length of the caudal processes and polar capsules.

4.2.3.6. Aurantiactinomyxon type 6 (Figure S16C–S16D; Figure S17F–S17G)

Spore body: Spherical in both apical and side views, 19.7 ± 1.0 (17.4–21.6) µm diameter. Caudal process: Equal in size, straight, long, slightly rounded with almost pointed tips, 72.1 ± 6.1 (61.0–

86.9) µm long, 9.0 ± 0.6 (7.8–10.1) µm wide at the base. Valve cell nuclei: Ovoid, visible, located randomly within each caudal process, 3.9 ± 0.4 (3.0–4.6) µm diameter. Polar capsule: Positioned at the apex of spore body, globular in apical view, tear-drop shaped in side view, 4.6 ± 0.4 (3.8–5.6) µm long, 3.3 ± 0.3 (2.7–3.9) µm wide. Polar tubule: Coiled three times. Sporoplasm: 32 secondary cells. Measurements from 30 fresh actinospores.

Host: *Branchiura sowerbyi* Beddard, 1892.

Predilection site: The intestinal epithelium.

Prevalence: 0.32% (1 infected in 315 oligochaetes examined)

Locality: Ócsárd fish farm, county Baranya, Hungary.

Molecular data: Partial 18S rDNA sequence of aurantiactinomyxon type 2 of 1986 base was deposited in GenBank under the accession number PV942515. Pairwise distance estimation indicated the highest similarity of 99.9% to 100.0% with newly generated sequences of *T. hovorkai* (PV926536), and aurantiactinomyxon type 5 (PV942516), as well as with previously published sequences of *T. hovorkai* (DQ231155) and aurantiactinomyxon types (DQ231153, DQ231154) (**Table 11**). Phylogenetic analyses revealed that aurantiactinomyxon type 6 clustered in the same branch as other aurantiactinomyxon types (DQ231153, DQ231154) newly obtained aurantiactinomyxon type 5 (PV942516) and their corresponding myxospore stage, including the newly obtained sequence of *T. hovorkai* (PV926536), and a previously published sequence (DQ231155), with maximum bootstrap values and posterior probabilities (**Figure 13**).

Remarks: The morphology of aurantiactinomyxon type 6 does not match any previously described aurantiactinomyxon types. Morphometrically, aurantiactinomyxon type 6 is consistent with previous studies (**Table S18**), with only minor differences observed in all measurements. However, the lengths of the caudal processes and polar capsules differ significantly. Notably, aurantiactinomyxon type 6 exhibits the longest caudal processes and polar capsule among all aurantiactinomyxon types of *T. hovorkai*.

4.2.4. Collective group Neoactinomyxum Granata, 1922

The spores spherical and do not connect to each other with prominent apex. Three polar capsules protruding from the apex of the spore body. Caudal processes are reduced to disc-like, bulging swellings of equal size, with their bases enclosing the epispore body. Spore valves extend into rounded triangular flaps, giving the spore a rounded-triangular appearance in apical view. The plasmodial sporoplasm contains numerous infectious cells. The original type of the collective group is Neoactinomyxum globosum Granata, 1992, that was described from the freshwater oligochaete *Limnodrilus udekemianus* collected from the Mugove River, Florence, Italy.

4.2.4.1. Neoactinomyxum type 1 (Figure S18A–S18B)

Spore: Elliptical in side view, triangular in apical view. Spore body: Globular in apical view, 21.6 ± 1.0 (20.2–23.8) µm diameter. Caudal process: Equal in size, wide, short, crescent-shaped, 9.4 ± 0.7 (8.1–10.4) µm long, 22.0 ± 1.0 (20.2–24.0) µm wide at the base. Valve cell nuclei: Ovoid, visible, located at the base of caudal processes, 3.2 ± 0.2 (2.9–3.8) µm diameter (n = 12). Polar capsule: Positioned at apex of spore body, globular in apical view, 2.7 ± 0.3 (2.1–3.2) µm diameter, tear-drop shaped in side view. Polar tubule: Not visible. Sporoplasm: 32 secondary cells (**Figure S18B**). Measurements from 32 fresh actinospores.

Host: *Branchiura sowerbyi* Beddard, 1892.

Predilection site: The intestinal epithelium. Histopathological sections of *B. sowerbyi* showed several pansporocysts in the intestinal epithelium, containing mature spores with visible secondary cells (**Figure S18C**).

Prevalence: 1.27% (4 infected in 315 oligochaetes examined).

Locality: Ócsárd fish farm, county Baranya, Hungary.

Molecular data: Partial 18S rDNA sequence of neoactinomyxum type 1 of 1894 base pairs was deposited in GenBank under the accession number PV818389. The 18S rDNA sequence from the neoactinomyxum type 1 matched with the sequences of neoactinomyxum type of *Thelohanellus wangi* (KY784590) and *T. wangi* (JX458816). Pairwise distance estimation indicated the highest

similarities of 100.0% to *T. wangi* (JX458816) and 99.5% to neoactinomyxum type (KY784590) (**Table 11**). Phylogenetic analyses revelead that the neoactinomyxum type 1 clustered in the same branch with *T. wangi*, as well as the actinospore stage of *T. wangi*, which belongs to the neoactinomyxum type, with maximum bootstrap values and posterior probabilities (**Figure 13**).

Remarks: The morphology and morphometric data of neoactinomyxum type 1 are consistent with previously described neoactinomyxum type JD by Xi et al. (2015), with only minor size differences. The present spores are slightly larger in size, except for the caudal process width, which is smaller (**Table S19**). A key difference is the present of 32 secondary cells, reported here for the first time in this actinospore type. Neoactinomyxum type 1 also resembles neoactinomyxum type A1 (Eszterbauer et al., 2006), though the spores are slightly larger, contain 32 rather than 16 secondary cells.

4.3. Myxosporean species in Malaysia

A total of 119 individuals from thirteen fish species were collected from rivers and small channels in Terengganu for myxozoan examination (**Table 4**). Among them, *Barbonymus gonionotus, Osteochilus waandersii,* and *Channa gachua* showed 100.0% infection rates. *Trichopodus pectoralis* ranked second, with an infection rate of 66.7% (6/9), followed by *Labiobarbus leptocheilus* with 60.0% (9/15). The remaining species exhibited infection rates at or below 50.0% (**Table 12**). In total, thirty-five myxosporean species were identified, including fifteen *Myxobolus* spp., eleven *Henneguya* spp., five *Thelohanellus* spp., three *Myxidium* spp. and one *Ceratomyxa* sp. Of these, thirty-three are newly described species, while two are previously known. *Channa gachua* and *L. leptocheilus* harbored the highest diversity of myxosporean parasites, with seven species comprising six *Henneguya* spp. and one *Myxidium* sp. in *C. gachua*, and five *Myxobolus* spp., one *Thelohanellus* sp. and one *Myxidium* sp. in *L. leptocheilus* (**Table 13**). Additionally, *O. waandersii* and *T. pectoralis* each hosted five species, while *B. gonionotus* was infected by four species, comprising only two *Myxobolus* spp. and two *Thelohanellus* spp. (**Table 13**). The

remaining fish species harbored one or two myxosporean species each. All fishes appeared to be in good condition without obvious scars or lesions.

Table 12 Infection prevalence rates for each fish species.

Species	Infected fish	Infection rate
Barbonymus gonionotus (Java barb)	6/6	100.0%
Barbonymus altus (Red-tailed tinfoil barb)	7/16	43.7%
Barbonymus schwanefeldii (Tinfoil barb)	3/6	50.0%
Leptobarbus rubripinna (Red-finned cigar barb)	2/5	40.0%
Barbodes binotatus (Spotted barb)	1/13	7.7%
Labiobarbus leptocheilus (Thin-lips barb)	9/15	60.0%
Osteochilus waandersii (Waanders's hard-lipped barb)	15/15	100.0%
Trichopodus trichopterus (Three spot gourami)	6/9	66.7%
Trichopodus pectoralis (Snakeskin gourami)	10/12	83.3%
Channa gachua (Dwarf snakehead)	12/12	100.0%
Neolissochilus soroides (Copper mahseer)	0/5	0.0%
Anabas testudineus (Climbing perch)	0/3	0.0%
Notopterus notopterus (Bronze featherback)	0/2	0.0%

4.3.1. Myxosporean parasites in Barbonymus gonionotus

4.3.1.1. Myxobolus gonionoti **n. sp.**

Plasmodia: Found on the gill filaments, histozoic, big, round in shape (**Figure S19A**), 0.3 mm long, 0.2 mm wide (n = 2). Spore: Oval in both frontal and sutural views, tapering at the anterior ends, 9.3 ± 0.3 (8.2–9.8) µm long, 6.1 ± 0.3 (5.4–6.6) µm wide, 4.7 ± 0.3 (4.4–5.1) µm thick (n = 9) (**Figure S19B–S19C, Figure S22A**). Polar capsule: Two, pyriform, closely equal size, occupying half of the spore body cavity. Larger: 5.2 ± 0.3 (4.3–6.0) µm long, 2.1 ± 0.2 (1.6–2.4) µm wide. Smaller: 4.9 ± 0.3 (3.9–5.4) µm long, 1.9 ± 0.2 (1.6–2.3) µm wide. No intercapsular appendix. Polar tubule: Seven coils in larger capsule, six in smaller capsule, positioned perpendicularly to capsule axis. Sporoplasm: Binucleate, iodinophilous vacuole present, mucous envelope absent. Measurements from 30 formalin-fixed spores.

Locality: Sungai Tong, Setiu, Terengganu, Malaysia.

Predilection site: Gill filaments.

Prevalence: 16.6% (1/6).

Etymology: The name *Myxobolus gonionoti* n. sp. was derived from the name of the fish host, *Barbonymus gonionotus*.

Molecular data: Partial 18S rDNA sequence of *M. gonionoti* n. sp. of 1917 base pairs was deposited in GenBank under the accession number PV665937. The 18S rDNA sequence from the *M. gonionoti* n. sp. did not match any of the myxozoan sequences available in GenBank. Pairwise distance estimation indicated the highest similarity of 91.0% to *Myxobolus barbonymi* n. sp. (PV665939) (**Table 14**). Phylogenetic analyses revealed that *M. gonionoti* n. sp. clustered within a clade of muscle-infecting *Myxobolus* spp. that primarily infect cyprinids, with maximum bootstrap values and posterior probabilities. However, its position is basal and separated from the rest of the clade (**Figure 14–15**).

Remarks: The morphology of *M. gonionoti* n. sp. most closely resembles *M. dykovae* Székely et Molnár, 2009, though distinct morphometric differences are present (**Table S20**). The spore of *M. gonionoti* n. sp. are smaller and have unequal polar capsules, unlike *M. dykovae*, which has equal polar capsule sizes. Morphometrically, *M. gonionoti* n. sp. shows greatest similarity to *Myxobolus sange*i Fomena, Lekeufack Folefack et Tang, 2007 in spore width and small polar capsule dimensions, but it has shorter spores and polar capsules. The number of filament turns in the larger polar capsule is similar to *M. sangei*, but differs in the smaller capsule. Spore and polar capsule widths also resemble those of *Myxobolus carlhubbsi* McAllister, Cloutman, Leis, Camus et Robinson, 2023. Notably, Ky & Te (2007) in Chinh et al. (2023) reported *Myxobolus macrocapsularis* Reuss, 1849 from the gills of *B. gonionotus*, is a common parasite of the common bream (*A. brama*) and white bream (*B. bjoerkna*) in Europe. The reports likely represent a misidentification as *M. macrocapsularis* has equal-sized polar capsules and slightly convergent anterior ends, whereas *M. gonionoti* n. sp. possesses slightly unequal polar capsules and tapered anterior ends. Comparison with other *M. macrocapularis* descriptions in the literature (Molnár et al., 2011) shows morphological and morphometric similarities to *M. macrocapularis* described by Donec & Shulman. However, the schematic drawing by Donec & Shulman (1984) indicates

unequal capsule sizes, while their description provides measurements for only one capsule size, suggesting they may be similar.

Table 13 Myxosporean species detected in the investigated fish species.

Fish species	Myxosporean parasite	Predilection site
Barbonymus gonionotus	*Myxobolus gonionoti* n. sp.	Gill filaments
	Myxobolus barbonymi n. sp.	Muscle
	Thelohanellus gonionoti n. sp.	Caudal fin
	Thelohanellus zahrahae	Gill filaments
Barbonymus altus	*Myxobolus faizahae* n. sp.	Muscle
	Thelohanellus barbonymi n. sp.	Gill arch
Barbonymus schwanefeldii	*Myxobolus dykovae*	Gill lamellae
	Ceratomyxa schwanefeldii n. sp.	Gallbladder
Leptobarbus rubripinna	*Myxobolus* n. sp. 3	Muscle
Barbodes binotatus	*Myxobolus* n. sp. 4	Ovaries
Labiobarbus leptocheilus	*Myxobolus* n. sp. 5	Connective tissue of gill arch
	Myxobolus n. sp. 6	Gill filaments
	Myxobolus n. sp. 7	Fin rays
	Myxobolus n. sp. 8	Ovaries
	Myxobolus n. sp. 9	Muscle
	Thelohanellus n. sp. 1	Skin
	Myxidium n. sp. 1	Gallbladder
Osteochilus waandersii	*Myxobolus* n. sp. 10	Cartilage of gill arch, bulbus arteriosus of heart
	Myxobolus n. sp. 11	Gill cartilage
	Myxobolus n. sp. 12	Muscle
	Myxobolus n. sp. 13	Muscle
	Thelohanellus n. sp. 2	Fin rays
Trichopodus trichopterus	*Henneguya* n. sp. 1	Gill lamellae
Trichopodus pectoralis	*Henneguya* n. sp. 2	Gill lamellae
	Henneguya n. sp. 3	Cartilaginous tissue of gill arch
	Henneguya n. sp. 4	Gill arch
	Henneguya n. sp. 5	Pharynx
	Myxidium n. sp. 2	Gallbladder
Channa gachua	*Henneguya* n. sp. 6	Serous membrane of internal organs
	Henneguya n. sp. 7	Ovaries
	Henneguya n. sp. 8	Vertebral column
	Henneguya n. sp. 9	Gills
	Henneguya n. sp. 10	Muscle
	Henneguya n. sp. 11	Muscle near caudal peduncle
	Myxidium n. sp. 3	Gallbladder

Table 14 Genetic *p*-distance and sequence similarities (%) based on the 18S rDNA between *Myxobolus* spp., *Thelohanellus* spp. from Malaysia and its most closely related species. Only identical or the closest-related sequences are presented.

Sequence	Genetic distance	Sequence similarities (%)
***Myxobolus gonionoti* n. sp. PV665937**		
***Myxobolus barbonymi* n. sp. PV665939**	**0.090**	**91.0**
Myxobolus macrocapsularis AF507969	0.230	77.0
***Myxobolus barbonymi* n. sp. PV665939**		
Myxobolus pseudodispar KU340979	0.073	92.7
Myxobolus musculi JQ388891	0.077	92.3
Myxobolus bhadrensis KX832046	0.077	92.3
Myxobolus klamathellus KX261616	0.079	92.1
Myxobolus sp. AY591531	0.079	92.1
***Myxobolus faizahae* n. sp. PV665938**		
Myxobolus terengganuensis EU643629	0.052	94.8
Myxobolus bhadrensis KX832046	0.058	94.2
Myxobolus kingchowensis MH521302	0.062	93.8
***Thelohanellus gonionoti* n. sp. PV665940**		
***Thelohanellus barbonymi* n. sp. PV665941**	**0.011**	**98.9**
Thelohanellus sp. MK332024	0.014	98.6
***Thelohanellus zahrahae* PV647347**	**0.016**	**98.4**
Thelohanellus zahrahae EU643622	0.017	98.3
***Thelohanellus zahrahae* PV647347**		
Thelohanellus zahrahae EU643622	0.003	99.7
***Myxobolus dykovae* PV647344**		
Myxobolus dykovae EU643627	0.006	99.4
***Myxobolus* n. sp. 3**		
***Myxobolus* n. sp. 3**	**0.001**	**99.9**
Myxobolus leptobarbi EU643623	0.069	93.1
Myxobolus koi FJ841887	0.147	85.3
***Myxobolus* n. sp. 4**		
Myxobolus huasaensis OQ848597	0.122	87.8
Myxobolus acutus MZ782721	0.126	87.4
Myxobolus basilamellaris MZ343303	0.126	87.4
Myxobolus tsangwuensis KJ561441	0.126	87.4
Myxobolus elliptoides OQ725580	0.127	87.3
***Myxobolus* n. sp. 5**		
***Myxobolus* n. sp. 13**	**0.047**	**95.3**
***Myxobolus* n. sp. 9**	**0.049**	**95.1**
Myxobolus csabai EU643628	0.055	94.5
Myxobolus tasikkenyirensis EU643626	0.056	94.4
***Myxobolus* n. sp. 6**		
***Myxobolus* n. sp. 8**	**0.090**	**91.0**
***Myxobolus* n. sp. 8**	**0.090**	**91.0**
***Myxobolus* n. sp. 7**	**0.109**	**89.1**

***Myxobolus* n. sp. 7**		
***Myxobolus* n. sp. 8**	**0.104**	**89.6**
***Myxobolus* n. sp. 8**	**0.105**	**89.5**
***Myxobolus* n. sp. 6**	**0.109**	**89.1**
***Myxobolus* n. sp. 9**		
***Myxobolus* n. sp. 13**	**0.026**	97.4
Myxobolus tasikkenyirensis EU643626	0.038	96.2
***Myxobolus* n. sp. 5**	**0.049**	95.1
Myxobolus csabai EU643628	0.053	94.7
***Myxobolus* n. sp. 10**		
***Myxobolus* n. sp. 10**	**0.001**	**99.9**
***Myxobolus* n. sp. 12**	**0.163**	**83.7**
Myxobolus mucosus KP751909	0.164	83.6
Myxobolus huasaensis OQ848597	0.164	83.6
***Thelohanellus* n. sp. 1**	**0.167**	**83.3**
***Thelohanellus* n. sp. 2**	**0.175**	82.5
***Myxobolus* n. sp. 11**		
Raabeia type PP856689	0.090	91.0
***Myxobolus* n. sp. 12**		
***Thelohanellus* n. sp. 1**	**0.101**	**89.9**
***Thelohanellus* n. sp. 2**	**0.122**	**87.8**

4.3.1.2. Myxobolus barbonymi n. sp.

Plasmodia: Found in the muscle, histozoic, elongated in shape (**Figure S19D**), 0.8 mm long and 0.2 mm wide (n = 2). Histology: Plasmodium developed intracellularly within muscle cells (**Figure S19E**). Spore: Ellipsoidal, asymmetrical in frontal view, with flattened anterior end, lemon-shaped in sutural view, 8.4 ± 0.5 (7.4–9.9) µm long, 6.9 ± 0.5 (6.1–7.8) µm wide, 5.2 ± 0.2 (4.9–5.4) µm thick (n = 5) (**Figure S19F–S19H, Figure S22E**). Polar capsule: Two, pyriform, unequal. Larger: 4.9 ± 0.3 (4.2–5.5) µm long, 2.9 ± 0.3 (2.4–3.4) µm wide. Smaller: 3.8 ± 0.4 (3.0–4.7) µm long, 2.4 ± 0.2 (2.0–2.8) µm wide. Intercapsular appendix: Strong, 'U'-shaped between the anterior ends of the polar capsules. Polar tubule: Coiled five to six times in larger capsule, three to four times in smaller capsule, positioned perpendicularly to capsule axis. Sporoplasm: Binucleate, iodinophilous vacuole absent, mucous envelope absent. Measurements from 30 formalin-fixed spores.

Locality: Sungai Tong, Setiu, Terengganu, Malaysia.

Predilection site: Intracelullarly in the muscle cell.

Etymology: The name *Myxobolus barbonymi* n. sp. was derived from the genus name of the fish host, *Barbonymus gonionotus*.

Molecular data: Partial 18S rDNA sequence of *M. barbonymi* n. sp. of 1849 base pairs was deposited in GenBank under the accession number PV665939. The 18S rDNA sequence from the *M. barbonymi* n. sp. did not match any of the myxozoan sequences available in GenBank. Pairwise distance estimation indicated the highest similarity of 92.7% to *Myxobolus pseudodispar* (KU340979) (**Table 14**). Phylogenetic analyses revealed that *M. barbonymi* n. sp. was positioned in a monophyletic clade basally to other muscle-infecting *Myxobolus* spp., with high bootstrap values and posterior probabilities (**Figure 14–15).**

Remarks: The morphology and morphometrics of *M. barbonymi* n. sp. differ from all previously described *Myxobolus* spp. with unequal polar capsules. It most resembles *Myxobolus tauricus* Miroshnichenko, 1979 and *Myxobolus hakyi* Landsberg et Lom, 1991. *Myxobolus barbonymi* n. sp. can be distinguished by its flattened anterior end, a feature not previously reported in any *Myxobolus* spp. nor any muscle-infecting *Myxobolus* species. Morphometrically, *M. barbonymi* n. sp. is similar to *Myxobolus faizahae* n. sp., but larger, with wider and shorter polar capsules resembling those of *M. pseudodispar* (Molnar et al., 2002, 2010) (**Table S21**).

4.3.1.3. Thelohanellus gonionoti n. sp.

Plasmodia: Ellipsoidal, found under the dermis covering the interlepidotrichial ligament and the fin rays (**Figure S20A–S20B**). Spore: Elongate-pyriform, with tapered and truncated anterior ends in both frontal and sutural views, 18.4 ± 1.0 (16.3–18.3) µm long, 8.9 ± 0.8 (7.2–9.2) µm wide, 6.9 ± 0.4 (6.4–6.9) µm thick (n = 5) (**Figure S20C–S20D, Figure S22C**). Polar capsule: Single, pyriform, 9.2 ± 1.0 (7.3–10.3) µm long, 4.8 ± 0.5 (3.8–5.6) µm wide, occupying more than half of the spore body cavity. Polar tubule: Coiled eight to nine times, positioned perpendicularly to capsule axis. Sutural line: Straight, smooth, thick in the middle of spore body. Sporoplasm:

Binucleate, 1.1 ± 0.2 (0.7–0.9) µm diameter, iodinophilous vacuole present, 3.8 ± 0.5 (2.8–3.9) µm diameter. Mucous envelope absent. Measurements from 30 formalin-fixed spores.

Locality: Sungai Tong, Setiu, Terengganu, Malaysia.

Predilection site: Under the dermis and above the interlepidotrichial ligament.

Prevalence: 50.0% (3/6).

Etymology: The name *Thelohanellus gonionoti* n. sp. was derived from the name of the fish host, *Barbonymus gonionotus*.

Molecular data: Partial 18S rDNA sequence of *T. gonionoti* n. sp. of 1897 base pairs was deposited in GenBank under the accession number PV665940. The 18S rDNA sequence from the *T. gonionoti* n. sp. did not match any of the myxozoan sequences available in GenBank. Pairwise distance estimation indicated the highest similarity of 98.9% to *T. barbonymi* n. sp. (PV665941) (**Table 14**). Phylogenetic analyses revealed that *T. gonionoti* n. sp. was clustered within a monophyletic clade together with other gill-infecting *Thelohanellus* spp., that parasitize cyprinids such as *B. altus*, *B. gonionotus*, and *Mystacoleucus marginatus* Valenciennes, 1842 (**Figure 14–15)**.

Remarks: The morphology and morphometrics of *T. gonionoti* n. sp. differ from all previously described *Thelohanellus* spp., characterized by truncated anterior ends (**Table S22**). It most closely resembles *T. zahrahae* (both from previous and present studies) and the newly described *T. barbonymi* n. sp., though notable morphometric differences are present. *Thelohanellus gonionoti* n. sp. is distinguished from both species by the polar capsule position, which leans towards the side of the spore body. Morphometrically, it differs significantly from other *Thelohanellus* spp., sharing similarity only with *T. barbonymi* n. sp. in polar capsule length and the number of filament coils.

4.3.1.4. Redescription *Thelohanellus zahrahae* Székely et Molnár, 2009

Plasmodia: Found in the gill filaments, histozoic, elongated in shape (**Figure S20E**), 1.27 ± 7.2 (1.26–1.28) mm long, 0.29 ± 7.8 (0.28–0.29) mm wide (n = 2). Spore: Elongate-pyriform, with

tapered and truncated anterior ends in both frontal and sutural views, 20.5 ± 0.5 (19.4–21.6) µm long, 9.1 ± 0.6 (8.1–10.6) µm wide (**Figure S20F)**, 7.6 ± 0.2 (7.3–7.8) µm thick (n = 7) (**Figure S20G**). Polar capsule: Single, pyriform, 8.8 ± 0.8 (6.6–10.2) µm long, 5.5 ± 0.5 (4.7–6.8) µm long, occupied half of the spore body cavity. Polar tubule: Coiled seven times, positioned perpendicularly to capsule axis. Sutural line: Straight, smooth, thick in the middle of spore body. Sporoplasm: Binucleate, 1.0 ± 0.3 (0.6–1.7) µm diameter (n = 12), iodinophilous vacuole present, 3.9 ± 0.5 (3.1–4.8) µm diameter, mucous envelope absent. Measurements from 30 formalin-fixed spores.

Locality: Sungai Tong, Setiu, Terengganu, Malaysia.

Predilection site: Gill filaments.

Prevalence: 33.3% (2/6).

18S rDNA sequence: Partial 18S rDNA sequence of *T. zahrahae* of 1901 base pairs was deposited in GenBank under the accession number PV647345. The 18S rDNA sequence from the present *T. zahrahae* matches with the sequence of *T. zahrahae* (EU643622) available in GenBank showing 99.7% (**Table 14**). Phylogenetic analysis revealed that *T. zahrahae* sequences is closely related to an undescribed *Thelohanellus* species (MK332024) infecting *M. marginatus* (**Figure 14–15**).

Remarks: The morphology and morphometrics of *T. zahrahae* are consistent with previously described *T. zahrahae* from Java barb in a fish farm at Machang, Kelantan (**Table S22**). Minor size differences are observed, with *T. zahrahae* from the previous study are larger. Notably, *T. catlae* was reported by Ky & Te (2007) in Chinh et al. (2023), a common parasite of the common carp from the gills and skin of *B. gonionotus*. However, significant morphological and morphometric differences are observed, with *T. catlae* being larger in size and possesses pear-shaped spores and spherical polar capsules, whereas *T. zahrahae* has elongated-pyriform spores with truncated anterior ends and a pyriform polar capsule.

4.3.2. Myxosporean parasites in Barbonymus altus

4.3.2.1. Myxobolus faizahae **n. sp.**

Plasmodia: Found between muscle cells, histozoic, elongated and oval in shape (**Figure S21A**), 92.9 ± 62.7 µm long, 59.3 ± 29.9 µm wide (n = 4). Histology: Plasmodium is encapsulated by a thin layer of connective tissue and associated with the intramuscular connective tissue among muscle cells (**Figure S21B**). Spore: Ellipsoidal, asymmetrical in frontal view, lemon-shaped in sutural view, 9.3 ± 0.3 (8.7–9.9) µm long, 5.8 ± 0.2 (5.4–6.1) µm wide, 4.4 ± 0.3 (3.5–4.8) µm thick (**Figure S21C–S21D, S22B**). Polar capsule: Two, pyriform, unequal. Larger: 4.4 ± 0.3 (3.8–5.0) µm long, 2.8 ± 0.3 (2.3–3.3) µm wide. Smaller: 3.3 ± 0.2 (2.9–3.9) µm long, 1.9 ± 0.1 (1.6–2.2) µm wide. Intercapsular appendix: Absent. Polar tubule: Coiled four to five times in larger polar capsule, three to four times in smaller capsule, positioned perpendicularly to capsule axis. Sporoplasm: Binucleate, iodinophilous vacuole absent, mucous envelope absent. Measurements from 30 formalin-fixed spores.

Locality: Sungai Tong, Setiu and Sungai Nerus, Kuala Nerus, Terengganu, Malaysia.

Predilection site: Associated with intramuscular connective tissues.

Prevalence: 66.6% (4/6).

Etymology: The name *Myxobolus faizahae* n. sp. is dedicated to Professor Emeritus Dr. Faizah Shaharom, a renowned fish parasitologist from Malaysia.

Molecular data: Partial 18S rDNA sequence of *M. faizahae* n. sp. of 1783 base pairs was deposited in GenBank under the accession number PV665938. The 18S rDNA sequence from the *M. faizahae* n. sp. did not match any of the myxozoan sequences available in GenBank. Pairwise distance estimation indicated the highest similarities of 94.8% to *Myxobolus terengganuensis* (EU643629) and 94.2% to *Myxobolus bhadrensis* (KX832046) (**Table 14**). Phylogenetic analyses revealed that *M. faizahae* n. sp. formed a close relationship with *M. terengganuensis* and clustered within well-supported clade of muscle-infecting *Myxobolus* spp. (**Figure 14–15).**

Remarks: The morphology of *M. faizahae* n. sp. most closely resembles *M. pseudodispar* (Molnar et al., 2002; 2010), although it is smaller and differs morphometrically. Morphometrically, it also resembles *M. bhadrensis* Székely, Cech, Chaudhary, Borzák Singh et Molnár, 2015 in spore thickness, smaller polar capsule width, and number of filament coils but remains smaller overall (**Table S21**).

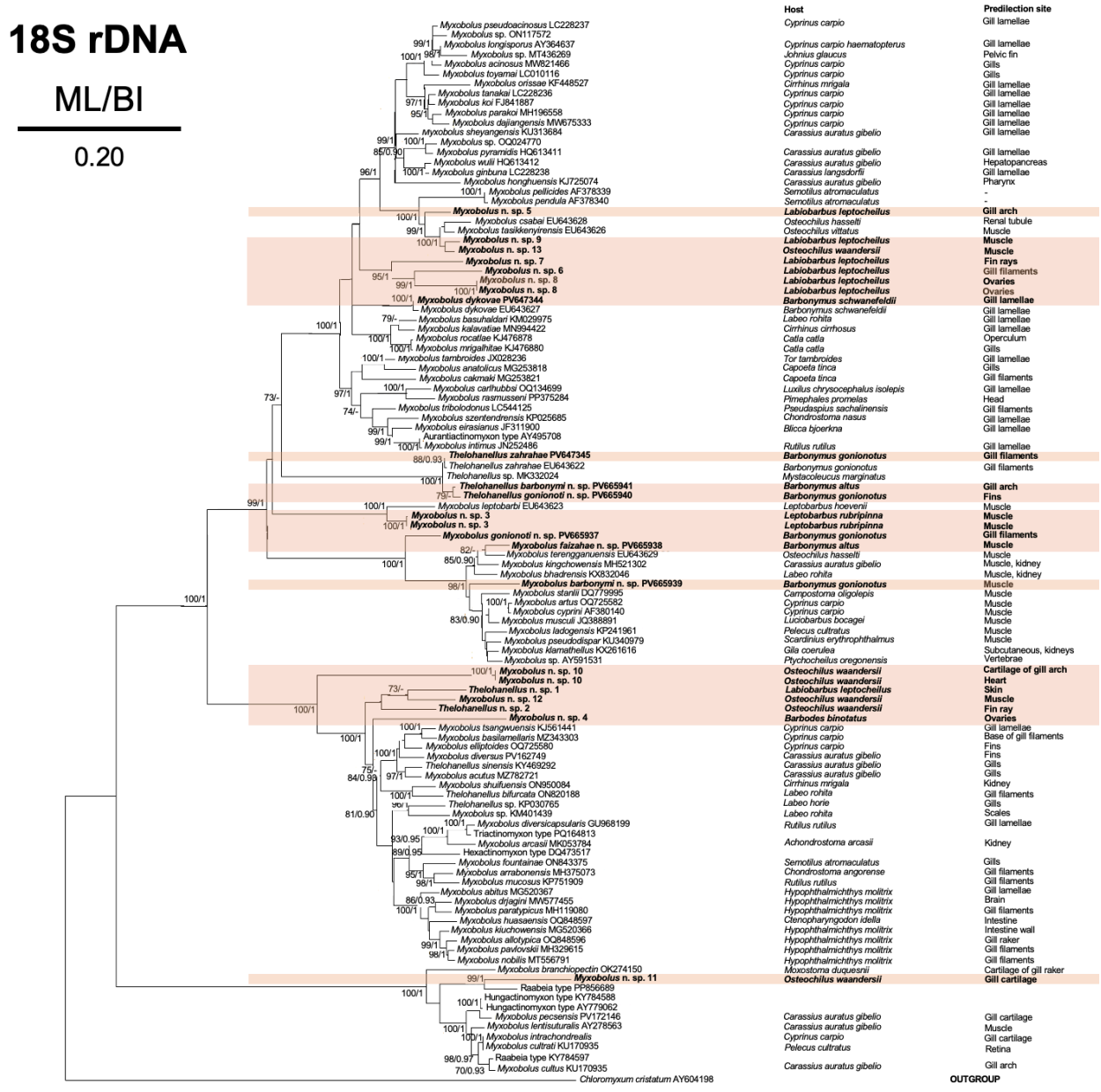

Figure 14. Detailed maximum likelihood (ML) phylogenetic tree of 18S rDNA sequences of *Myxobolus* spp., *Thelohanellus* spp., and related species. *Chloromyxum cristatum* was used as outgroup. Nodal supports are indicated for ML at 1000 replicates and Bayesian Inference (BI). Only values with ≥ 70% bootstrap (BS) and ≥ 0.90 posterior probabilities (PP) support are presented. The names of the parasite species are presented before GenBank accession numbers, following the host species and predilection site. Sequences obtained in the present study are shown in bold within colored boxes. The scale bar indicates the expected number of substitutions per site.

4.3.2.2. Thelohanellus barbonymi n. sp.

Plasmodia: Found in the gill arch, histozoic, round to oval in shape (**Figure S21E**), 0.22 mm diameter (n = 1). Spore: Elongate-pyriform, with tapered and truncated anterior ends in both frontal and sutural views, 22.0 ± 0.7 (20.3–23.2) µm long, 9.9 ± 0.6 (8.1–10.8) µm wide, 7.7 ± 0.5 (6.7–8.3) µm thick (n = 15) (**Figure S21F–S21G**, **S22D**). Polar capsule: Single, pyriform, 9.1± 0.5 (8.2–10.1) µm long, 5.4 ± 0.3 (4.9–5.9) µm wide, occupying ¼ of the spore body cavity. Polar tubule: Coiled eight times, positioned perpendicularly to capsule axis. Sutural line: Straight, smooth, thin in the middle of spore body. Sporoplasm: Binucleate, iodinophilous vacuole present, 4.4 ± 0.4 (3.4–4.9) µm diameter, mucous envelope absent. Measurements from 30 formalin-fixed spores.

Locality: Sungai Tong, Setiu and Sungai Nerus, Kuala Nerus, Terengganu, Malaysia.

Predilection site: Gill arch.

Prevalence: 12.5% (2/16).

Etymology: The name *Thelohanellus barbonymi* n. sp. was derived from the genus name of the fish host, *Barbonymus altus*.

Molecular data: Partial 18S rDNA sequence of *T. barbonymi* n. sp. of 1907 base pairs was deposited in GenBank under the accession number PV665941. The 18S rDNA sequence of *T. barbonymi* n. sp. did not match any other myxozoan sequences available in GenBank. Pairwise distance estimation indicated the highest similarity of 98.9% to *T. gonionoti* n. sp. (PV665940) (**Table 14**). Phylogenetic analyses revealed that *T. barbonymi* n. sp. was positioned in a monophyletic clade together with other gill-infecting *Thelohanellus* spp., along with *T. gonionoti* n. sp. that parasitize cyprinids such as *B. altus*, *B. gonionotus*, and *M. marginatus* (**Figure 14–15).**

Remarks: The morphology and morphometrics of *T. barbonymi* n. sp. are distinct from any previously described *Thelohanellus* spp. characterized by truncated anterior ends (**Table S22**). It most closely resembles *T. zahrahae*, both in previous and present study. *Thelohanellus barbonymi* n. sp. is smaller than *T. zahrahae* from previous study by Székely et al. (2009b) but larger than *T.*

zahrahae from the present study. However, *T. barbonymi* n. sp. is wider than both *T. zahrahae* from previous study and the present study, and having a different number of coils (8 vs 7). Regarding the spore width, *T. barbonymi* n. sp. shows the greatest similarity to *T. catlae*, Chakravarty et Basu, 1948. When comparing the newly described *T. gonionoti* n. sp. and *T. zahrahae* from the present study, *T. barbonymi* n. sp. is the largest in size among these species.

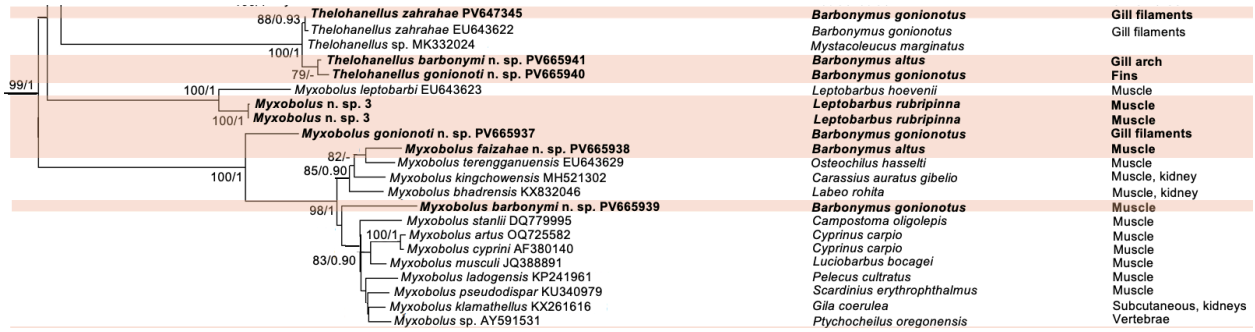

Figure 15. Partial phylogenetic tree showing *Myxobolus gonionoti* n. sp., *Myxobolus barbonymi* n. sp., *Thelohanellus gonionoti* n. sp., *Thelohanellus zahrahae*, *Myxobolus faizahae* n. sp., *Thelohanellus barbonymi* n. sp. and related species.

4.3.3. Myxosporean parasites in Barbonymus schwanefeldii

4.3.3.1. Ceratomyxa schwanefeldii **n. sp.**

Plasmodia: Exhibited a vermiform shape (**Figure S23A**) with worm-like undulations. Formalin-fixed mature plasmodia (filled with mature myxospores) elongate, 151.6 ± 86.0 (43.0–271.0) µm long, 15.1 ± 4.8 (9.3–22.7) µm wide (n = 11), with blunt poles at both ends (**Figure S23B**). Mature plasmodia displayed slow undulatory motility. Spore: Crescent-shaped, strongly arched in frontal view, with a sutural line between the two valve cells, 3.0 ± 0.4 (2.4–3.9) µm long, 12.6 ± 1.2 (10.8–15.4) µm thick (**Figure S23C–S23E**). Valve cell: Approximately equal-size, smooth surface, tapering to blunt ends. Posterior angle: Concave, 104.8° ± 10.2° (73.4–123.8)°. Polar capsule: Spheroid, equal, located on either side of sutural line, 1.5 ± 0.2 (1.2–1.8) µm long, 1.3 ± 0.2 (0.9–1.7) µm wide. Polar filament: Not visible. Sporoplasm: Binucleate, occupies nearly half of each valve.

Predilection site: Bile in gall bladder.

Type locality: Sungai Tong, Setiu, Terengganu, Malaysia.

Prevalence: 2 of 6 (33.3%).

Molecular data: Partial 18 rDNA and 28 rDNA sequences of *C. schwanefeldii* n. sp. of 1580 base pairs and 1354 base pairs were deposited in GenBank under the accession number PQ778208 and PQ778207, respectively. The 18S rDNA sequence of *C. schwanefeldii* n. sp. did not match any other myxozoan sequences available in GenBank. Pairwise distance estimation of the 18S rDNA indicated the highest similarities (93.4% and 93.3%) to *Ceratomyxa vermiformis* (KX278420) reported from the gall bladder of *Colossoma macropomum*, and to *Ceratomyxa barbata* (MZ504286), reported from the gallbladder of *Rhaphiodon vulpines*, respectively (**Table 15**). Additionally, pairwise distance estimation for the 28S rDNA sequence revealed the highest similarities to *Ceratomyxa synaphobranchi* (82.2%; KM392425) and *Ceratomyxa leatherjacketi* (74.8%; KM392427) (**Table 16**). Phylogenetic analysis of 18S rDNA revealed two main distinct lineages: A and B (**Figure 16**). Clade A consisted of *Myxidium* spp., while the Clade B was split into two subclades B1 and B2. Subclade B1 harboured mostly freshwater *Ceratomyxa* species from South American, except *Unicapsulocaudum mugilum* Yang, Zhou, Zhao, Huang and Huang, 2017, which infected the gall bladder of brackish/marine fish. Subclade B2 included only *Ceratomyxa* spp. that parasitized marine fish. *Ceratomyxa schwanefeldii* n. sp. formed a sister relationship with *U. mugilum* and clustered within the clade of freshwater *Ceratomyxa* species, supported by high bootstrap values and posterior probabilities. The 28S rDNA phylogeny revealed that the *C. schwanefeldii* n. sp. within the marine *Ceratomyxa* clade as a sister to *C. leatherjacketi* (**Figure 17**). *Ceratomyxa schwanefeldii* n. sp. did not cluster with the freshwater *Ceratomyxa* species, as there was only one available 28S rDNA sequence for freshwater *Ceratomyxa* species in GenBank, *Ceratomyxa ranunculiformis* Zatti, Araújo, Adriano et Maia, 2023.

Etymology: The name *Ceratomyxa schwanefeldii* n. sp. was derived from the name of the fish host, *Barbonymus schwanefeldii*.

Remarks: *Ceratomyxa schwanefeldii* n. sp. differs morphologically and morphometrically from all known freshwater *Ceratomyxa* species (**Table S23**). It resembles *C. amazonensis*,

morphologically but is larger in all measurements. Morphometrically, it shows similarities to *C. huangheensis* and *C. hongtzensis* from China. The spore thickness is closely resembling to *C. hongtzensis* (12.6 vs 13.7 µm), while the spore length is most similar to *C. huangheensis* (3.0 vs 4.6 µm). The polar capsule dimensions are close to those of *C. barbata* (1.5 × 1.3 µm vs 1.6 × 1.4 µm) from Brazil. The polar capsule width is also similar to that of *C. anomala* (1.3 vs 1.3 µm) and nearly identical to *C. deformis* (1.3 vs 1.4 µm).

Table 15 Genetic *p*-distance and sequence similarities (%) based on the 18S rDNA between *Ceratomyxa schwanefeldii* n. sp. from Malaysia and its most closely related species. Only identical or the closest-related sequences are presented.

Sequence	Genetic distance	Sequence similarities (%)
***Ceratomyxa schwanefeldii* n. sp. PQ778208**		
Ceratomyxa vermiformis KX278420	0.000	93.4
Ceratomyxa barbata MZ504286	0.066	93.3

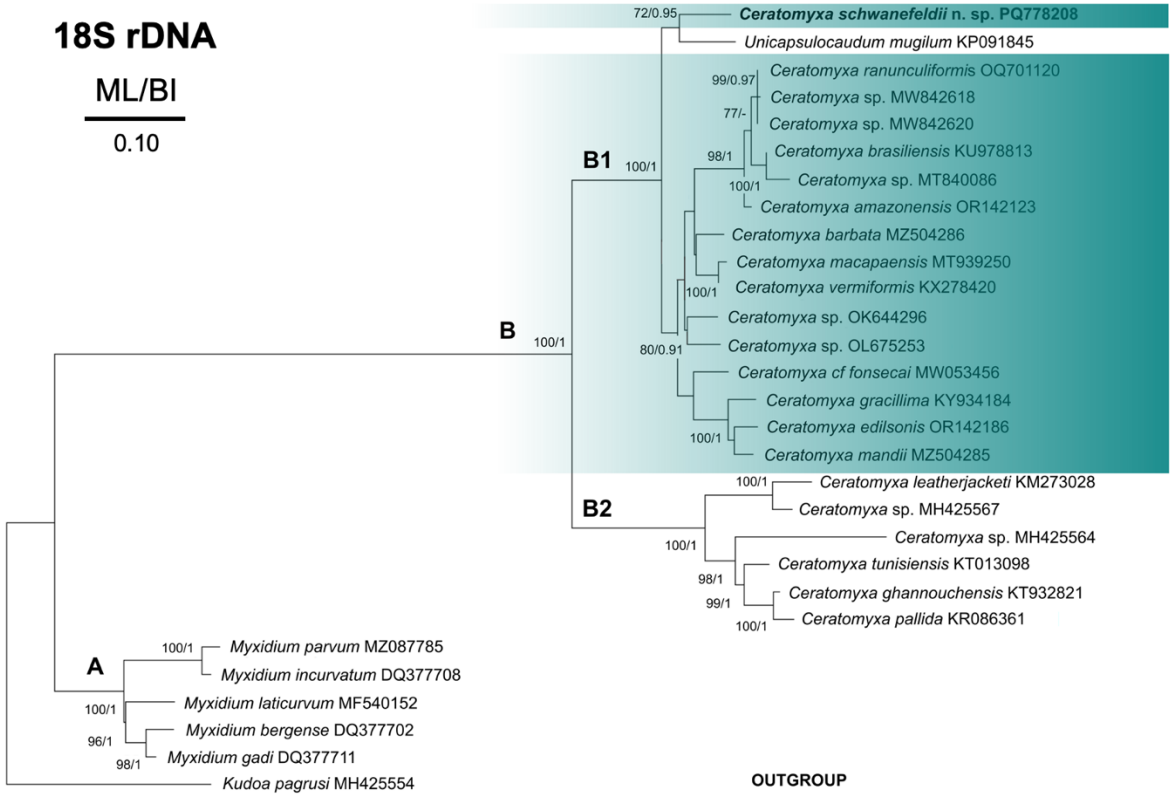

Figure 16. Maximum likelihood phylogenetic tree based of 18S rDNA sequences of *Ceratomyxa schwanefeldii* n. sp. and related species. *Kudoa pagrusi* was used as outgroup. Nodal supports are indicated for MLat 1000 replicates and Bayesian Inference (BI). Only values with ≥70% bootstrap (BS) and ≥ 0.90 posterior probabilities (PP) support are presented. The names of the parasite species are presented before GenBank accession numbers. *Ceratomyxa schwanefeldii* n. sp. examined in the present study is in bold. The scale bar indicates the expected number of substitutions per site.

Table 16 Genetic *p*-distance and sequence similarity (%) of 28S rDNA between *Ceratomyxa schwanefeldii* n. sp. from Malaysia and its most closely related species. Only identical or the closest-related sequences are presented.

Sequence	Genetic distance	Sequence similarities (%)
***Ceratomyxa schwanefeldii* n. sp. PQ778207**		
Ceratomyxa synaphobranchi KM392425	0.178	82.2
Ceratomyxa leatherjacketi KM392427	0.252	74.8
Ceratomyxa sp. FJ417050	0.300	70.0

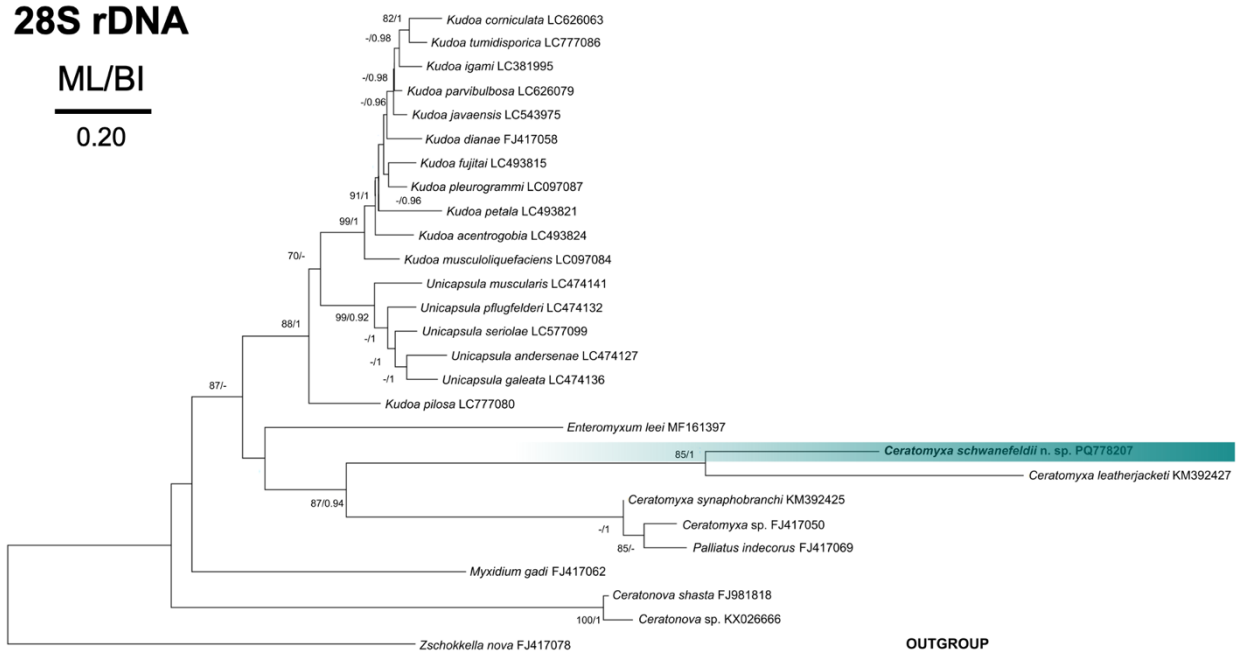

Figure 17. Maximum likelihood phylogenetic tree based of 28S rDNA sequences of *Ceratomyxa schwanefeldii* n. sp. and related species. *Zschokkella nova* was used as outgroup. Nodal supports are indicated for ML at 1000 replicates and Bayesian Inference (BI). Only values with ≥70% bootstrap (BS) and ≥ 0.90 posterior probabilities (PP) support are presented. The names of the parasite species are presented before GenBank accession numbers. Sequence obtained in the present study is shown in bold within colored box. The scale bar indicates the expected number of substitutions per site.

4.3.3.2. Redescription of *Myxobolus dykovae* Székely et Molnár, 2009

Plasmodia: Found in the gill lamellae, histozoic, small and oval in shape (**Figure S23F**), 0.1 (0.1–0.2) mm long and wide (n = 10). Histology: Plasmodia filled with mature spores were found intralamellarly within the gills (**Figure S23H**). Spore: Oval in both frontal and sutural views, tapering at the anterior ends (**Figure S23G**), 11.7 ± 0.6 (10.3–12.8) µm long, 6.8 ± 0.4 (5.9–7.7) µm wide, 5.4 ± 0.3 (5.1–5.7) µm thick (n = 4). Polar capsule: Two, equal, pyriform, 5.8 ± 0.5 (4.7–

7.0) µm long, 2.2 ± 0.2 (1.8–2.6) µm wide, occupied half of the spore body cavity. Intercapsular appendix: Absent. Polar tubule: Coiled six to seven times, positioned perpendicularly to capsule axis. Sporoplasm: Binucleate, iodinophilous vacuole absent, mucous envelope absent. Measurements from 30 formalin-fixed spores.

Locality: Sungai Tong, Setiu, Terengganu, Malaysia.

Predilection site: Gill lamellae.

Prevalence: 16.6% (1/6).

Molecular data: Partial 18S rDNA sequence of *M. dykovae* of 1643 base pairs was deposited in GenBank under the accession number PV647344. The 18S rDNA sequence of present *M. dykovae* matched with the sequence of *M. dykovae* available in GenBank. Pairwise distance estimation indicated the highest similarity of 99.4% to *M. dykovae* (EU643627) (**Table 14**). Phylogenetic analyses revealed that *M. dykovae* sequences were positioned in a clade comprising many gill-infecting *Myxobolus* spp. and various *Myxobolus* spp. that infect others organs besides gills (**Figure 14** and **Figure 18)**.

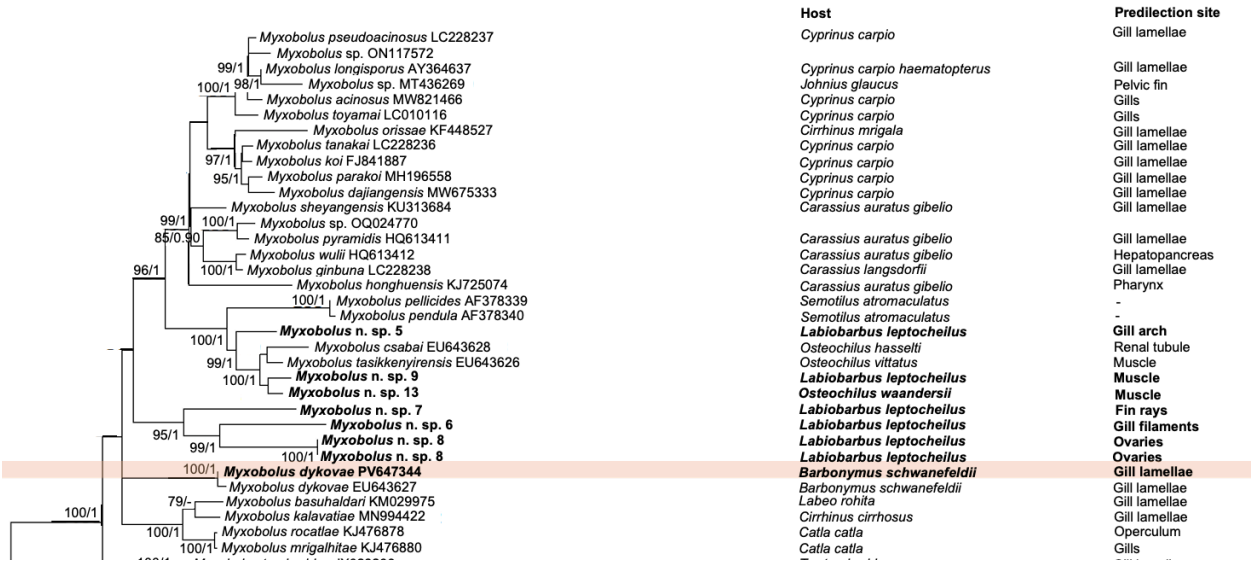

Figure 18. Partial phylogenetic tree showing *Myxobolus dykovae* in a clade comprising many gill-infecting *Myxobolus* spp. and various *Myxobolus* spp. that infect others organs besides gills.

Remarks: The morphology and morphometrics of *M. dykovae* match those previously described *M. dykovae* from tinfoil barb in Tasik Kenyir (**Table S20**). Minor size differences are observed in

all characters, but remain within the established range of variation. The present *M. dykovae* most closely resembles *Myxobolus alvarezae* Cech, Molnár et Székely, 2012 in all measurements except spore thickness and polar capsule length.

4.3.4. Myxosporean parasites in Leptobarbus rubripinna

4.3.4.1. Myxobolus n. sp. 3

Plasmodia: Found in the muscle, histozoic, elongated (**Figure S24A**), 0.58 mm long, 0.14 mm wide (n = 1). Histology: Plasmodium of *Myxobolus* n. sp. 3 developed intracellularly within muscle cells (**Figure S24B**). Spore: Oval in frontal view (**Figure S24C**), fusiform in sutural view (**Figure S24E**), truncate or tapering at the anterior ends, 16.2 ± 0.5 (15.1–17.2) µm long, 8.9 ± 0.3 (8.5–9.7) µm wide, 5.5 ± 0.4 (5.0–5.9) µm thick (n = 4). Polar capsule: Two, pyriform, unequal. Larger: 10.6 ± 0.4 (10.0–11.4) µm long, 3.0 ± 0.2 (2.7–3.6) µm wide. Smaller: 10.0 ± 0.4 (9.1–10.7) µm long, 2.9 ± 0.2 (2.4–3.4) µm wide, occupying more than half of the spore body cavity. Intercapsular appendix: Absent. Polar tubule: Coiled thirteen to fourteen times in larger capsule, eleven to twelve times in smaller capsule, positioned perpendicularly to capsule axis (**Figure S24D**). Sporoplasm: Binucleate, iodinophilous vacuole absent, mucous envelope present. Measurements from 30 formalin-fixed spores.

Locality: Sungai Tong, Setiu, and Sungai Nerus, Terengganu, Malaysia.

Predilection site: Intracelullarly in the muscle cell.

Prevalence: 40.0% (2/5)

Molecular data: Two nearly identical 18S rDNA sequences of *Myxobolus* n. sp. 3 (99.8%; 1821, 1647bp) did not match any of myxozoan sequences available in GenBank. Pairwise distance estimation indicated the highest similarity of 93.1% to *Myxobolus leptobarbi* (EU643623) (**Table 14**). Phylogenetic analyses placed *Myxobolus* n. sp. 3 as closely related to *M. leptobarbi* supported by high bootstrap values and posterior probabilities (**Figure 14** and **Figure 19**).

Remarks: The morphology and morphometrics of *Myxobolus* n. sp. 3 closely resemble *Myxobolus leptobarbi* Székely, Shaharom-Harrison, Cech, Mohamed et Molnár, 2009 (**Table S24**), which

infects the muscle of *Leptobarbus hoevenii*, another species of the same genus. They differ only in the number of polar filament coils in the smaller polar capsule (11–12 vs 13 –15) and the presence of a mucus envelope. However, genetic analyses confirm that the two are distinct species.

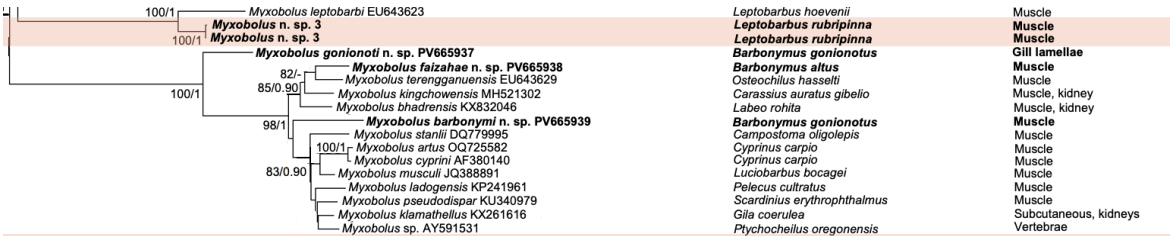

Figure 19. Partial phylogenetic tree showing *Myxobolus* n. sp. 3 formed a sister group with *Myxobolus leptobarbi*.

4.3.5. Myxosporean parasites in Barbodes binotatus

4.3.5.1. Myxobolus n. sp. 4

Plasmodia: Found in the ovaries, oval in shape (**Figure S24F**). Spore: Oval in both frontal (**Figure S24G)**, lemon-shaped in sutural view (**Figure S24I**), 10.7 ± 0.4 (10.0–11.4) µm long, 8.3 ± 0.3 (7.8–8.9) µm wide, 6.2 ± 0.3 (5.9–6.8) µm thick (n = 10). Polar capsule: Two, pyriform, unequal. Larger: 4.8 ± 0.4 (4.0–5.8) µm long, 2.8 ± 0.2 (2.4–3.4) µm wide. Smaller: 2.7 ± 0.3 (2.1–3.1) µm long, 1.6 ± 0.2 (1.3–1.9) µm wide, occupying more than half of the spore body cavity. Intercapsular appendix: Absent. Polar tubule: Coiled six to seven times in larger capsule, four times in smaller capsule, positioned perpendicularly to capsule axis. Sutural ridge: Eight to ten sutural markings, unsymmetrically distributed (**Figure S24H)**. Sporoplasm: Binucleate, iodinophilous vacuole absent, mucous envelope absent. Measurements from 30 formalin-fixed spores.

Locality: Sungai Tong, Setiu, and Sungai Nerus, Terengganu, Malaysia.

Predilection site: Ovaries.

Prevalence: 7.69% (1/13)

Molecular data: Partial 18S rDNA sequence of *Myxobolus* n. sp. 4 (1591bp) did not match any of myxozoan sequences available in GenBank. Pairwise distance estimation indicated the highest similarity of 87.8% to *Myxobolus huasaensis* (OQ848597) (**Table 14**). Phylogenetic analyses

placed *Myxobolus* n. sp. 4 close to gill-infecting *Myxobolus-Thelohanellus* spp., and several species with unequal polar capsules, although it formed a distinct basal branch within the clade (**Figure 14** and **Figure 20**).

Remarks: The morphology and morphometrics of *Myxobolus* n. sp. 4 are distinct from any previously described *Myxobolus* species. It closely resembles *Myxobolus csabai* Székely, Shaharom-Harrison, Cech, Ostoros et Molnár, 2009 and *Myxobolus nekrasovae* Batueva, Vlasenko, Solovyev et Abasheev, 2023 (**Table S25)**, but both are larger and lack sutural markings. Morphometrically, *Myxobolus* n. sp. 4 is most similar to the newly identified *Myxobolus* n. sp. 12 from the muscle of *Osteochilus waandersii*, differing mainly in the number of sutural markings (8–10 vs 6–8). Both species possess unequal polar capsules.

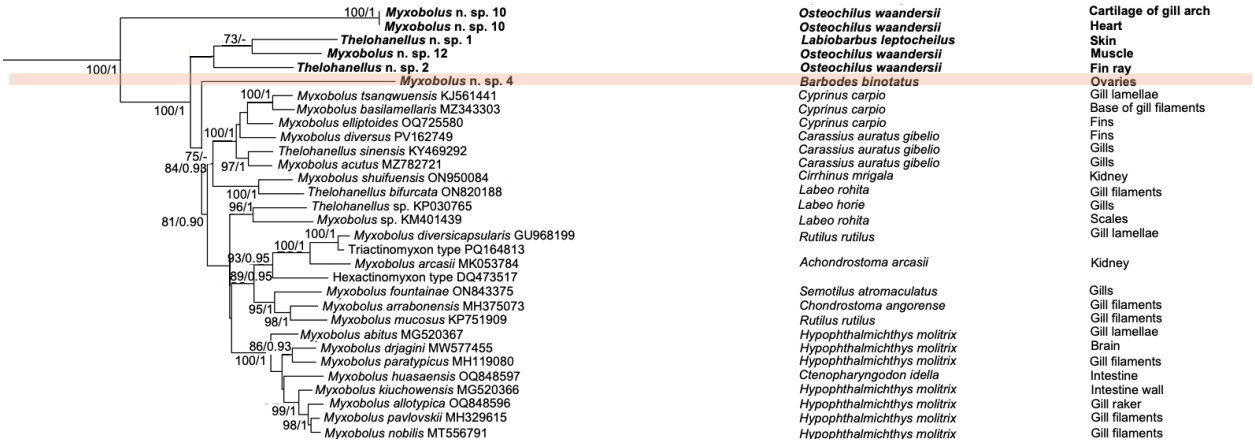

Figure 20. Partial phylogenetic tree showing *Myxobolus* n. sp. 4 positioned basally within the *Myxobolus* and *Thelohanellus* clade.

4.3.6. Myxosporean parasites in Labiobarbus leptocheilus

4.3.6.1. Myxobolus n. sp. 5

Plasmodia: Found in the gill arch membrane, elongated (**Figure S25A**), 0.28 mm long, 0.11 mm wide (n = 1). Spore: Oval to pyriform in frontal (**Figure S25B)**, pyriform in sutural view (**Figure S25C**), 12.0 ± 0.3 (11.4–12.5) µm long, 7.8 ± 0.3 (7.4–8.4) µm wide, 5.6 ± 0.3 (5.1–6.0) µm thick (n = 19). Polar capsule: Two, pyriform, equal, 6.0 ± 0.3 (5.3–6.7) µm long, 2.7 ± 0.2 (2.2–3.1) µm wide, occupying half of the spore body cavity. Intercapsular appendix: Absent. Polar tubule:

Coiled seven times, positioned perpendicularly to capsule axis. Sporoplasm: Binucleate, iodinophilous vacuole present, mucous envelope absent. Measurements from 26 formalin-fixed spores.

Locality: Sungai Nerus, Terengganu, Malaysia.

Predilection site: Connective tissue of gill arch.

Prevalence: 6.67% (1/15)

Molecular data: Partial 18S rDNA sequence of *Myxobolus* n. sp. 5 (1752bp) did not match any of myxozoan sequences available in GenBank. Pairwise distance estimation indicated the highest similarities of 95.3% to *Myxobolus* n. sp. 13 and 95.1% to *Myxobolus* n. sp. 9 (**Table 14**), both described in this study. Phylogenetic analyses placed *Myxobolus* n. sp. 5 basally within the *Myxobolus* clade and formed a sister group with *Myxobolus* n. sp. 9, *Myxobolus* n. sp. 13, *M. csabai* and *Myxobolus tasikkenyirensis* (**Figure 14** and **Figure 21**).

Remarks: The morphology and morphometrics of *Myxobolus* n. sp. 5 are distinct from any previously described *Myxobolus* species. It closely resembles *Myxobolus tribolodonus* Sekiya, Sakai, Li, Rosyadi, Yunus et Sato, 2024, which infects the gill filaments of *Pseudaspius sachalinensis* (**Table S26)**, but differs morphometrically, with *Myxobolus* n. sp. 5 being larger. Morphometrically, it is most similar to *Myxobolus paludinosus* Reed, Basson et Van As, 2002 from the gill lamellae of *Barbus paludinosus*, showing only minor size differences. The main differences is found in spore width. The polar capsule width closely resembles *Myxobolus aureus* Carriero, Adriano, Silva, Ceccarelli et Maia, 2013 and *Myxobolus curimatae* Zatti, Naldoni, Silva, Maia et Adriano, 2015, while the polar capsule length is similar to *Myxobolus iecoris* Naldoni, Zatti, da Silva, Maia et Adriano, 2019 and *Myxobolus pyramidis* Chen, 1958.

Figure 21. Partial phylogenetic tree showing the positions of *Myxobolus* n. sp. 5*, Myxobolus* n. sp. 9 and *Myxobolus* n. sp. 13 within the *Myxobolus* clade.

4.3.6.2. Myxobolus n. sp. 6

Plasmodia: Found in the gill filaments, oval (**Figure S25D**), 0.34 mm long, 0.15 mm wide (n = 1). Spore: Pyriform in both frontal and sutural views (**Figure S25E– S25F**), 8.8 ± 0.3 (8.3–9.5) µm long, 5.0 ± 0.3 (4.5–5.4) µm wide, 3.9 ± 0.2 (3.6–4.2) µm thick (n = 7). Polar capsule: Two, pyriform, unequal. Larger: 4.6 ± 0.2 (4.0–5.2) µm long, 1.7 ± 0.2 (1.3–2.0) µm wide. Smaller: 4.3 ± 0.3 (3.5–4.8) µm long, 1.5 ± 0.2 (1.1–1.9) µm wide, occupying more than half of the spore body cavity. Intercapsular appendix: Absent. Polar tubule: Coiled six to seven times in larger capsule, five to six times in smaller capsule, positioned perpendicularly to capsule axis. Sporoplasm: Binucleate, iodinophilous vacuole present, mucous envelope absent. Measurements from 30 formalin-fixed spores.

Locality: Sungai Nerus, Terengganu, Malaysia.

Predilection site: Gill filaments.

Prevalence: 26.6% (4/15).

Molecular data: Partial 18S rDNA sequence of *Myxobolus* n. sp. 6 (1852bp) did not match any of myxozoan sequences available in GenBank. Pairwise distance estimation indicated the highest similarities of 91.0% to *Myxobolus* n. sp. 8 and 89.1% to *Myxobolus* n. sp. 7 (**Table 14**), both described in this study. Phylogenetic analyses revealed that *Myxobolus* n. sp. 6 is closely related

to *Myxobolus* n. sp. 8 and *Myxobolus* n. sp. 7, with high bootstrap values and posterior probabilities (**Figure 14** and **Figure 22**).

Remarks: The morphology and morphometrics of *Myxobolus* n. sp. 6 are distinct from any previously described *Myxobolus* species. It closely resembles *Myxobolus carlhubbsi* McAllister et Robison, 2023, which infects the gills of *Luxilus chrysocephalus isolepis* (**Table S27)**, but differs morphometrically, with *M. carlhubbsi* being larger. Morphometrically, *Myxobolus* n. sp. 6 is most similar to *Myxobolus imparfinis* Vieira, Tagliavini, Abdallah et de Azevedo, 2018 from the gill filament of *Imparfinis mirini* showing only minor size differences. The main differences are observed in spore and polar capsule lengths. Notably, only *M. carlhubbsi, M. imparfinis* and *Myxobolus bilobus* Cone, Yang, Sun et Easy, 2005 possesses unequal polar capsule, whereas all other species listed in **Table S27** have equal polar capsules.

4.3.6.3. Myxobolus n. sp. 7

Plasmodia: Found in the fin rays, oval in shape (**Figure S25G**), 0.16 ± 0.2 (0.1–0.2) mm long, 0.13 ± 0.2 (0.12–0.16) µm wide (n = 4). Histology: Plasmodium located in the interlepidotrichial region of the fin rays (**Figure S25H**). Spore: Pyriform in both frontal and sutural views (**Figure S25I–S25K**), 14.2 ± 0.4 (13.5–14.9) µm long, 5.8 ± 0.2 (5.5–6.4) µm wide, 4.6 ± 0.4 (4.0–5.3) µm thick (n = 11). Polar capsule: Two, pyriform, unequal. Larger: 9.1 ± 0.3 (8.6–9.9) µm long, 2.7 ± 0.2 (2.2–3.6) µm wide. Smaller: 8.0 ± 0.5 (7.1–9.0) µm long, 1.7 ± 0.1 (1.4–1.9) µm wide, occupying $^{3}/_{4}$ of the spore body cavity. Intercapsular appendix: Absent. Polar tubule: Coiled eight to ten times in larger capsule, six times in smaller capsule, positioned perpendicularly to capsule axis (**Figure S25J**). Sporoplasm: Binucleate, iodinophilous vacuole present, mucous envelope absent. Measurements from 30 formalin-fixed spores.

Locality: Sungai Nerus, Terengganu, Malaysia.

Predilection site: Fin rays.

Prevalence: 80.0% (12/15).

Molecular data: Partial 18S rDNA sequence of *Myxobolus* n. sp. (1850bp) did not match any of myxozoan sequences available in GenBank. Pairwise distance estimation indicated the highest similarities of 89.5% to 89.6% to *Myxobolus* n. sp. 8 and 89.1% to *Myxobolus* n. sp. 6 (**Table 14**), both described in this study. Phylogenetic analyses placed *Myxobolus* n. sp. 7 basally within the *Myxobolus* clade and formed a sister group with *Myxobolus* n. sp. 6 and *Myxobolus* n. sp. 8, with high bootstrap values and posterior probabilities (**Figure 14** and **Figure 22**).

Remarks: The morphology and morphometrics of *Myxobolus* n. sp. 7 are distinct from any previously described *Myxobolus* species. No morphology similarities can be observed when comparing *Myxobolus* n. sp. 7 with other *Myxobolus* spp., which possesses a pyriform spore body characterized unequal polar capsules, which one being notably wide and the other very narrow. Notably, most species exhibiting somewhat similar morphology to *Myxobolus* n. sp. 7 as listed in **Table S28**, are reported from the gills, whereas none are found in the fin rays. Morphometrically, *Myxobolus* n. sp. 7 shows the greatest resemblance to *Myxobolus zoohuri* Majumder, Panda, Ghosh et Bandyopadhyay, 2013 described from the gill lamellae of *Cirrhinus mrigala*. However, distinct differences are evident in the length of the large polar capsule, as well as in the length, width and number of polar tubule coils of both small and large polar capsules (**Table S28)**.

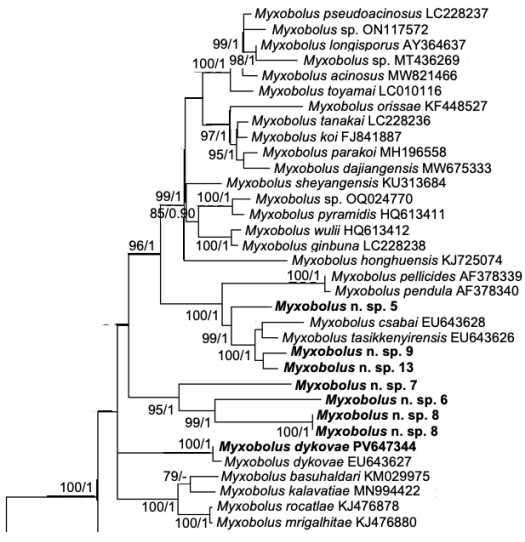

Host	Predilection site
Cyprinus carpio	Gill lamellae
Cyprinus carpio haematopterus	Gill lamellae
Johnius glaucus	Pelvic fin
Cyprinus carpio	Gills
Cyprinus carpio	Gills
Cirrhinus mrigala	Gill lamellae
Cyprinus carpio	Gill lamellae
Cyprinus carpio	Gill lamellae
Cyprinus carpio	Gill lamellae
Cyprinus carpio	Gill lamellae
Carassius auratus gibelio	Gill lamellae
Carassius auratus gibelio	Gill lamellae
Carassius auratus gibelio	Hepatopancreas
Carassius langsdorfii	Gill lamellae
Carassius auratus gibelio	Pharynx
Semotilus atromaculatus	-
Semotilus atromaculatus	-
Labiobarbus leptocheilus	**Gill arch**
Osteochilus hasselti	Renal tubule
Osteochilus vittatus	Muscle
Labiobarbus leptocheilus	**Muscle**
Osteochilus waandersii	**Muscle**
Labiobarbus leptocheilus	**Fin rays**
Labiobarbus leptocheilus	**Gill filaments**
Labiobarbus leptocheilus	**Ovaries**
Labiobarbus leptocheilus	**Ovaries**
Barbonymus schwanefeldii	**Gill lamellae**
Barbonymus schwanefeldii	Gill lamellae
Labeo rohita	Gill lamellae
Cirrhinus cirrhosus	Gill lamellae
Catla catla	Operculum
Catla catla	Gills

Figure 22. Partial phylogenetic tree showing the positions of *Myxobolus* n. sp. 6*, Myxobolus* n. sp. 7, *Myxobolus* n. sp. 8, *Myxobolus* n. sp. 9 and *Myxobolus* n. sp. 13 within the *Myxobolus* clade.

4.3.6.4. Myxobolus n. sp. 8

Plasmodia: Found in the ovaries, round in shape (**Figure S26A**), 0.3 ± 0.2 (0.1–0.9) mm long, 0.2 ± 0.1 (0.1–0.5) mm wide (n = 8). Spore: Pyriform in both frontal and sutural views (**Figure S26B–S26C**), 11.3 ± 0.5 (10.4–12.5) µm long, 6.2 ± 0.5 (5.2–6.9) µm wide, 4.7 ± 0.3 (4.1–5.2) µm thick (n = 23). Polar capsule: Two, pyriform, equal, 4.6 ± 0.4 (3.7–5.3) µm long, 1.6 ± 0.2 (1.4–2.1) µm wide, occupying half of the spore body cavity. Intercapsular appendix: Absent. Polar tubule: Coiled six times, positioned perpendicularly to capsule axis. Sporoplasm: Binucleate, iodinophilous vacuole absent, mucous envelope absent. Measurements from 30 formalin-fixed spores.

Locality: Sungai Nerus, Terengganu, Malaysia.

Predilection site: Ovaries.

Prevalence: 6.67% (1/15).

Molecular data: Two nearly identical 18S rDNA sequences of *Myxobolus* n. sp. 8 (99.9%; 1613bp, 1616bp) did not match any of myxozoan sequences available in GenBank. Pairwise distance estimation indicated the highest similarity of 91.0% to *Myxobolus* n. sp. 6 described in this study (**Table 14**). Phylogenetic analyses revealed that *Myxobolus* n. sp. 8 is closely related to *Myxobolus* n. sp. 6, with high bootstrap values and posterior probabilities (**Figure 14** and **Figure 22**).

Remarks: The morphology and morphometrics of *Myxobolus* n. sp. 8 are distinct from any previously described *Myxobolus* species. It most closely resembles *Myxobolus marajoensis* Abrunhosa, Sindeaux-Neto, Santos, Hamoy et Matos, 2017, which infects the intestine of *Rhamdia quelen*, and *Myxobolus pharyngeus* Parker, Spall et Warner, 1971, which infects the branchial cavity epithelium of *Gambusia affinis* (**Table S29)**, but differs from both in several morphometrics characteristics. *Myxobolus marajoensis* is smaller, whereas *M. pharyngeus* is larger than *Myxobolus* n. sp. 8. The spore width and polar capsule length of *Myxobolus* n. sp. 8 closely resembles those of *Myxobolus aculeatus* Xu, Zhao, Huang, Xin et Zhang, 2025, while its spore thickness almost similar to *Myxobolus miyarii* Kudo, 1919. In addition, *Myxobolus ompok*

Chaudhary, Goswami, Gupta, Cech, Singh, Molnár, Székely et Sharma, 2018, and *Myxobolus batalhensis* Vieira, Alama-Bermejo, Bartholomew, Abdallah et de Azevedo, 2017, exhibit similar number of polar tubule coils.

4.3.6.5. Myxobolus n. sp. 9

Plasmodia: Found in the muscle, elongated (**Figure S26D**), 0.8 ± 0.3 (0.6–1.1) mm long, 0.15 (0.1–0.2) mm wide (n = 3). Histology: Plasmodium located within the muscle cells (**Figure S26E**). Spore: globular to oval in frontal view (**Figure S26F**) and oval to lemon-shaped in sutural view (**Figure S26H**), 10.1 ± 0.4 (9.4–10.8) µm long, 7.9 ± 0.5 (6.8–8.7) µm wide, 5.7 ± 0.3 (6.0–6.3) µm thick (n = 8). Polar capsule: Two, pyriform, equal, 5.2 ± 0.3 (4.7–5.7) µm long, 2.6 ± 0.2 (2.1–3.1) µm wide, occupying half of the spore body cavity (**Figure S26G**). Intercapsular appendix: Absent. Polar tubule: Coiled six to seven times, positioned perpendicularly to capsule axis. Sporoplasm: Binucleate, iodinophilous vacuole present, mucous envelope absent. Measurements from 40 formalin-fixed spores.

Locality: Sungai Nerus, Terengganu, Malaysia.

Predilection site: Intracelullarly in the muscle cell.

Prevalence: 20.0% (3/15).

Molecular data: Partial 18S rDNA sequence of *Myxobolus* n. sp. 9 (1981bp) did not match any of myxozoan sequences available in GenBank. Pairwise distance estimation indicated the highest similarities of 97.4% to *Myxobolus* n. sp. 13 and 96.2% to *M. tasikkenyirensis* (EU643626) (**Table 14**). Phylogenetic analyses revealed that *Myxobolus* n. sp. 9 is closely related to *Myxobolus* n. sp. 13, and formed a sister group with *M. csabai* and *M. tasikkenyirensis*, with maximum bootstrap values and posterior probabilities (**Figure 14** and **Figure 22**).

Remarks: The morphology and morphometrics of *Myxobolus* n. sp. 9 are distinct from any previously described *Myxobolus* species. It most closely resembles *Myxobolus talievi* Dogiel, 1957, which infects the muscle of *Cyphocottus eurystomus*, and *Myxobolus tasikkenyirensis* Székely, Shaharom-Harrison, Cech, Ostoros et Molnár, 2009, which infects the muscle of

Osteochilus vittatus, but differs from both species in most measurements. Morphometrically, *Myxobolus* n. sp. 9 is most similar to *M. talievi,* though notable differences occur in spore width and the number of polar filament coils (**Table S30)**. Furthermore, while several species listed in **Table S30** exhibit a somewhat similar morphology, they display significant morphometric differences from *Myxobolus* n. sp. 9.

4.3.6.6. Thelohanellus n. sp. 1

Plasmodia: Found in the skin, oval in shape (**Figure S27A**), 1.0 mm diameter (n = 1). Spore: Elongate-pyriform, tapering anteriorly in both frontal and sutural views (**Figure S27B–S27C**), 16.0 ± 0.8 (14.1–17.8) µm long, 8.4 ± 0.5 (7.1–9.2) µm wide, 6.7 ± 0.2 (6.4–7.0) µm thick (n = 5). Polar capsule: Single, pyriform, 6.2 ± 0.6 (5.1–7.6) µm long, 4.1 ± 0.4 (3.3–4.6) µm wide, occupying ¼ of the spore body cavity. Polar tubule: Coiled six times, positioned perpendicularly to capsule axis. Sutural line: Straight, smooth, thin in the middle of spore body. Sporoplasm: Binucleate, iodinophilous vacuole present, 4.1 ± 0.4 (3.3–4.5) µm diameter, mucous envelope absent. Measurements from 30 formalin-fixed spores.

Locality: Sungai Nerus, Kuala Nerus, Terengganu, Malaysia.

Predilection site: Skin.

Prevalence: 6.67% (1/15).

Molecular data: Partial 18S rDNA sequence of *Thelohanellus* n. sp. 1 (1984 bp) did not match any of myxozoan sequences available in GenBank. Pairwise distance estimation indicated the highest similarity with 89.9% to *Myxobolus* n. sp. 12 (**Table 14**), described in this study. Phylogenetic analyses revealed that *Thelohanellus* n. sp. 1 is closely related to *Myxobolus* n. sp. 12, and formed a sister group with *Thelohanellus* n. sp. 2 (**Figure 14** and **Figure 23**).

Remarks: The morphology and morphometrics of *Thelohanellus* n. sp. 1 are distinct from any previously described *Thelohanellus* spp. (**Table S31**). It most closely resembles *Thelohanellus liaohoensis* Chen et Ma, 1998, which infects the mucosal membranes and gallbladder of *C. carpio.* Morphometrically, *Thelohanellus* n. sp. 1 is most similar to *Thelohanellus leshanensis* Zhao et

Ma, 1992, sharing comparable measurements in most dimensions, except for the number of polar filament coils (6 vs 2–3). *Thelohanellus indiana* also exhibits a similar polar capsule width. Furthermore, although several species listed in **Table S31** display somewhat similar morphological characteristics, they display significant morphometric differences from *Thelohanellus* n. sp. 1.

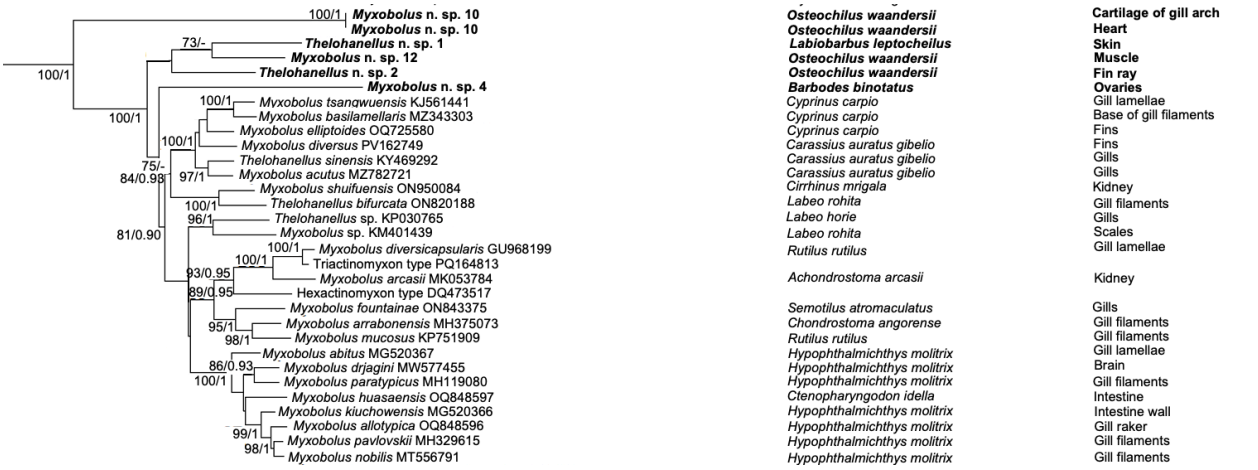

Figure 23. Partial phylogenetic tree showing the positions of *Thelohanellus* n. sp. 1, *Thelohanellus* n. sp. 2, *Myxobolus* n. sp. 10 and *Myxobolus* n. sp. 12 within the intermixed clade of *Myxobolus* and *Thelohanellus* species.

4.3.6.7. Myxidium n. sp. 1

Spore: Dispersal spores, coelozoic, elongate and fusiform in both frontal and sutural views, with tapered ends (**Figure S27D–S27E**), 12.5 ± 0.6 (11.4–14.1) µm long, 5.1 ± 0.4 (4.4–5.8) µm wide, 4.3 ± 0.4 (3.4–4.7) µm thick (n = 16). Polar capsule: Two, equal, slightly pyriform polar capsules, 3.3 ± 0.3 (2.6–3.7) µm long, 2.7 ± 0.2 (2.3–3.1) µm wide. Distance between two polar capsules, 5.0 ± 0.5 (4.1–6.3) µm in distance. Polar tubule: Coiled four to five times, positioned perpendicularly to capsule axis. Sutural line: Straight. Valvular striation: Six to seven longitudinal striations. Sporoplasm: Binucleate, filling the spore body cavity between the two polar capsules. Measurements from 30 formalin-fixed spores.

Locality: Sungai Nerus, Kuala Nerus, Terengganu, Malaysia.

Predilection site: Gallbladder.

Prevalence: 6.67% (1/15).

Molecular data: Pairwise distance estimation of *Myxidium* n. sp. 1 (1862 bp) indicated the highest similarity of 99.4% to *Zschokkella* sp. (KM401441) (**Table 17**). Phylogenetic analyses revealed that *Myxidium* n. sp. 1 clustered with *Zschokkella* sp. (KM401441), which infects the gallbladder of *Labeo rohita* and formed a sister group with *Myxidium* sp. (PP693377), *Myxidium spinibarba* (MN922568) and *Myxidium hoabinhense* (MK913426) (**Figure 24**).

Remarks: Based on spore morphology, this species is classified as a new member of the genus *Myxidium*. The morphology and morphometrics of *Myxidium* n. sp. 1 did not match any previously described *Myxidium* spp. (**Table S32**). However, we found a sequence of *Zschokkella* sp. (KM401441; 2057 base pairs) deposited in GenBank sharing 99.4% similarity to *Myxidium* n. sp. 1. Unfortunately, the morphology and morphometric measurements of these spores have not been published. However, the host species differs, infecting *L. leptocheilus* and *Labeo rohita* from Myanmar. The closest morphological and morphometric similarities are observed with *Myxidium spinibarba* Chen, Yang et Zhao, 2020, which infects the gallbladder of *Myxocyprinus asiaticus*, diverging only in the number of valvular striations (6–7 vs 8–10). Morphometrically, *Myxidium* n. sp. 1 is also similar to *Myxidium horatioense* McAllister, Cloutman, Leis et Robinson, 2025 from the gallbladder of *Ameiurus natalis*, differing mainly in the number of polar filament coils.

Table 17 Genetic *p*-distance and sequence similarities (%) based on the 18S rDNA between *Myxidium* n. sp. 1, *Myxidium* n. sp. 2, *Myxidium* n. sp. 3 and its most closely related species. Only identical or the closest-related sequences are presented.

Sequence	Genetic distance	Sequence similarities (%)
***Myxidium* n. sp. 1**		
Zschokkella sp. KM401441	0.006	99.4
Myxidium sp. PP693377	0.023	97.7
Myxidium spinibarba MN922568	0.026	97.4
Myxidium hoabinhense MK913426	0.026	97.4
***Myxidium* n. sp. 2**		
Zschokkella sp. MT840090	0.054	94.6
Myxosporea KP030767	0.055	94.5
***Myxidium* n. sp. 3**		
Myxidium chuatsi PQ869811	0.090	91.0
Myxidium sp. KP030766	0.103	89.7

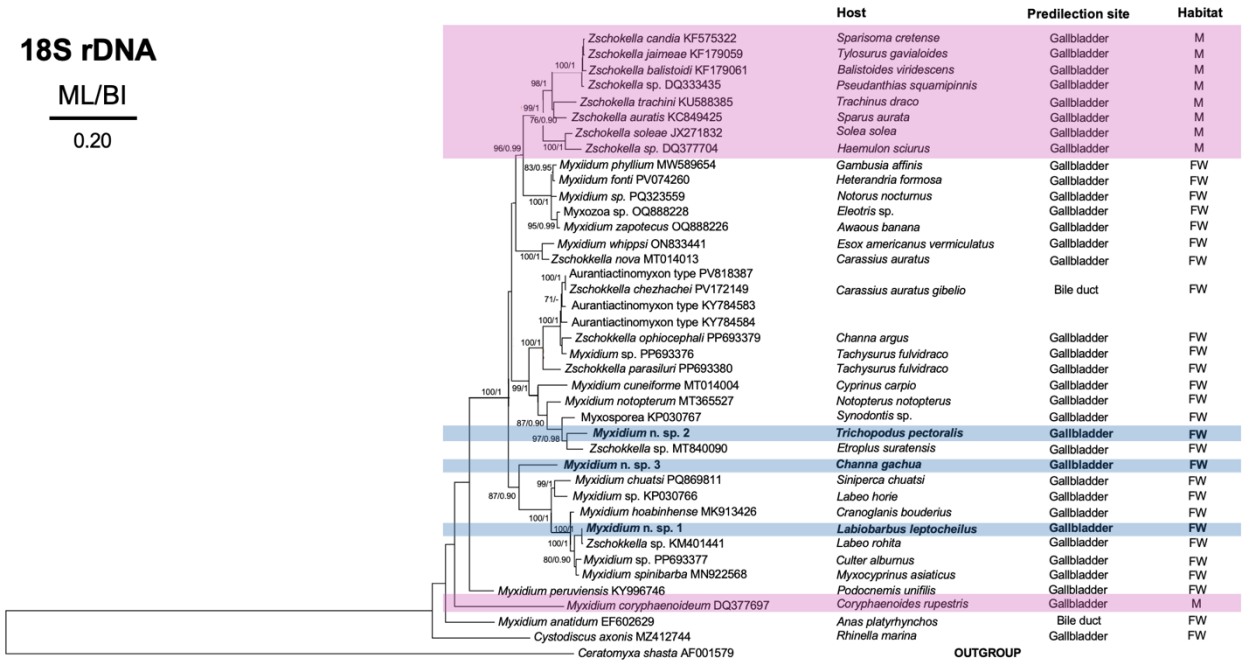

Figure 24. Maximum likelihood (ML) phylogenetic tree of 18S rDNA sequences of *Myxidium* n. sp. 1, *Myxidium* n. sp. 2, *Myxidium* n. sp. 3 and related species. *Ceratomyxa shasta* was used as outgroup. Nodal supports are indicated for ML at 1000 replicates and Bayesian Inference (BI). Only values with ≥ 70% bootstrap (BS) and ≥ 0.90 posterior probabilities (PP) support are presented. The names of the parasite species are presented before GenBank accession numbers, following the host species, predilection site and habitat. Sequences obtained in the present study are shown in bold within colored boxes. The scale bar indicates the expected number of substitutions per site. M = Marine, FW = Freshwater.

4.3.7. Myxosporean parasites in Osteochilus waandersii

4.3.7.1. Myxobolus n. sp. 10

Plasmodia: Found in the cartilage of gill arch and in the bulbus arteriosus of heart, elongated and oval in shape (**Figure S28A–S28B**), 0.18 (0.17–1.19) mm long, 0.09 (0.09–0.1) mm wide (n = 4). Spore: ellipsoidal in frontal view (**Figure S28C**) and lemon-shaped in sutural view (**Figure S28D**), 10.5 ± 0.6 (9.4–11.8) µm long, 8.3 ± 0.3 (7.4–8.9) µm wide, 5.6 ± 0.4 (4.8–6.2) µm thick (n = 17). Polar capsule: Two, pyriform, equal, 5.3 ± 0.3 (4.6–5.8) µm long, 2.7 ± 0.2 (2.1–3.0) µm wide, occupying half of the spore body cavity. Intercapsular appendix: Absent. Polar tubule: Coiled seven to eight times, 49.0 µm long, positioned perpendicularly to capsule axis (**Figure S28E**). Sporoplasm: Binucleate, iodinophilous vacuole absent, mucous envelope absent. Measurements from 40 formalin-fixed spores.

Locality: Sungai Nerus, Terengganu, Malaysia.

Predilection site: Cartilage of gill arch and in the bulbus arteriosus of heart.

Prevalence: 33.3% (5/15).

Molecular data: Two nearly identical 18S rDNA sequences of *Myxobolus* n. sp. 10 (99.9%; 2055, 2010 bp) did not match any of myxozoan sequences available in GenBank. Pairwise distance estimation indicated the highest similarity of 83.7% to *Myxobolus* n. sp. 12, described in this study (**Table 14**). Phylogenetic analyses placed *Myxobolus* n. sp. 10 basally within the large mixed *Myxobolus* and *Thelohanellus* clade, with maximum bootstrap values and posterior probabilities (**Figure 14** and **Figure 23**).

Remarks: The morphology and morphometrics of *Myxobolus* n. sp. 10 are distinct from any previously described *Myxobolus* species. It most closely resembles *Myxobolus branchiofilum* Ksepka et Bullard, 2021, which infects the gill lamellae of *Moxostoma duquesnei*, but differs in all measurements except for the polar capsule length and width. Morphometrically, *Myxobolus* n. sp. 10 shows the greatest similarity to *M. intrachondrealis* and *Myxobolus lamellobasis*, which infects the gills of *C. carpio* and *B. bjoerkna*, respectively, although notable

differences are observed in several measurements (**Table S33)**. *Myxobolus intrachondrealis* is comparable in spore length and polar capsule width, whereas *M. lamellobasis* is similar in spore length, thickness and polar capsule length. Furthermore, while several species listed in **Table S33** exhibit a somewhat similar morphology, they display significant morphometric differences from *Myxobolus* n. sp. 10.

4.3.7.2. Myxobolus n. sp. 11

Plasmodia: Found in the gill cartilage, oval in shape (**Figure S28F**), 0.32 (0.31–0.33) mm long, 0.19 (0.18–0.20) mm wide (n = 2). Spore: round to oval in frontal view (**Figure S28G**), 7.9 ± 0.3 (7.2–8.4) µm long, 6.7 ± 0.3 (6.2–7.3) µm wide. Polar capsule: Two, pyriform, equal, 3.7 ± 0.2 (3.4–4.1) µm long, 2.1 ± 0.2 (1.7–2.6) µm wide, occupying half of the spore body cavity. Intercapsular appendix: Absent. Polar tubule: Not visible. Sporoplasm: Binucleate, iodinophilous vacuole absent, mucous envelope absent. Measurements from 30 formalin-fixed spores.

Locality: Sungai Nerus, Terengganu, Malaysia.

Predilection site: Gill cartilage.

Prevalence: 13.3% (2/15).

Molecular data: Partial 18S rDNA sequences of *Myxobolus* n. sp. 11 (1922 bp) did not match any of myxozoan sequences available in GenBank. Pairwise distance estimation indicated the highest similarity of 91.0% to raabeia type (PP856689) (**Table 14**). Phylogenetic analyses revealed that *Myxobolus* n. sp. 11 is closely related to raabeia type collected from *Aulodrilus acutus* in Malaysia and formed a sister group with other *Myxobolus* spp. (PV172146, AY278563, KU170935, KU170935), raabeia type (KY784597) and Hungactinomyxon types (KY784588, AY779062), with high bootstrap values and posterior probabilities (**Figure 14** and **Figure 25**).

Remarks: The morphology and morphometrics of *Myxobolus* n. sp. 11 are distinct from any previously described *Myxobolus* species. It most closely resembles *Myxobolus gallaicus* Iglesias, Paramá, Alvarez, Leiro et Sanmartín, 2001, which infects the gill filaments of *Chondrostoma polylepis,* but differs by the presence of sutural markings in *M. gallaicus* and thicker spore valves

in *Myxobolus* n. sp. 11. In terms of spore length, *Myxobolus* n. sp. 11 does not show close similarity to any *Myxobolus* spp. listed in **Table S5**, but it most comparable to *M. pecsensis*. The spore and polar capsule widths show the greatest similarity to *M. intrachondrealis* and *M. cultrati,* whereas the polar capsule length is similar to *Myxobolus albi* and *Myxobolus sharpeyi*.

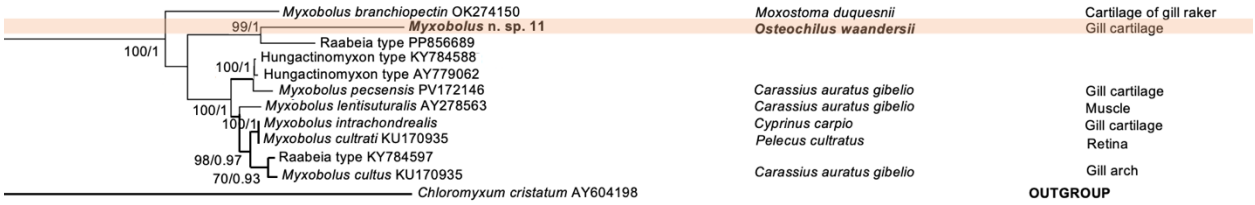

Figure 25. Partial phylogenetic tree showing the positions of *Myxobolus* n. sp. 11 within the *Myxobolus* clade including raabeia types and hungactinomyxon types.

4.3.7.3. Thelohanellus n. sp. 2

Plasmodia: Found in the fin rays, oval in shape (**Figure S28H**), 0.15 (0.13–0.18) mm long, 0.12 (0.08–0.13) mm wide (n = 3). Spore: Elongate-oval, tapering anteriorly in frontal view (**Figure S28I)** and lemon-shaped in sutural view (**Figure S28K)**, 9.4 ± 0.4 (8.8–10.4) µm long, 6.4 ± 0.3 (5.7–7.1) µm wide, 5.3 ± 0.3 (4.5–5.8) µm thick (n = 29). Polar capsule: Single, pyriform, 4.5 ± 0.2 (4.2–5.0) µm long, 2.8 ± 0.2 (2.5–3.2) µm wide, occupying half of the spore body cavity. Polar tubule: Coiled seven times, positioned perpendicularly to capsule axis (**Figure S28J**). Sutural line: Straight, smooth, thick in the middle of spore body. Sporoplasm: Binucleate, iodinophilous vacuole present, 3.1 ± 0.3 (2.3–3.9) µm long, 2.1 ± 0.3 (1.5–2.6) µm wide, mucous envelope absent. Measurements from 40 formalin-fixed spores.

Locality: Sungai Nerus, Kuala Nerus, Terengganu, Malaysia.

Predilection site: Connective tissue between fin rays.

Prevalence: 86.7% (13/15).

Molecular data: Partial 18S rDNA sequence of *Thelohanellus* n. sp. 2 (2007 bp) did not match any of myxozoan sequences available in GenBank. Pairwise distance estimation indicated the highest similarity of 87.8% to *Myxobolus* n. sp. 12 (**Table 14**), described in this study. Phylogenetic

analyses revealed that *Thelohanellus* n. sp. 2 formed a sister group with *Myxobolus* n. sp. 12 and *Thelohanellus* n. sp. 1 (**Figure 14** and **Figure 23**).

Remarks: The morphology and morphometrics of *Thelohanellus* n. sp. 2 are distinct from any previously described *Thelohanellus* spp. (**Table S34**). It most closely resembles *Thelohanellus cf. sinensis* (Zhang et al., 2018), which infects the gills of *C. auratus gibelio.* Morphometrically, *Thelohanellus* n. sp. 2 is most similar to *Thelohanellus goldi* Saha et Bandyopadhyay, 2018, sharing comparable measurements in most dimensions, except for the polar capsule length. Several *Thelohanellus* species infecting fin rays listed in **Table S34** display somewhat similar morphological characteristics, but still differ significantly from *Thelohanellus* n. sp. 2. Notably, *Thelohanellus* n. sp. 2 can be distinguished by having petite, oval spores with polar capsule leans towards the side of the spore body.

4.3.7.4. Myxobolus n. sp. 12

Plasmodia: Found in the muscle, oval in shape (**Figure S29A**), 0.7 ± 0.2 (0.4–0.9) mm long, 0.4 ± 0.2 (0.1–0.6) mm wide (n = 3). Histology: Plasmodium located within the muscle cells (**Figure S29B**). Spore: Ellipsoidal in frontal view (**Figure S29C)** and lemon-shaped in sutural view (**Figure S29E)**, 10.0 ± 0.3 (9.5–10.5) µm long, 7.7 ± 0.2 (7.2–8.3) µm wide, 5.6 ± 0.2 (5.3–5.9) µm thick. Polar capsule: Two, pyriform, unequal. Larger: 4.5 ± 0.3 (3.7–5.2) µm long, 2.6 ± 0.2 (2.2–3.1) µm wide. Smaller: 2.5 ± 0.3 (1.8–3.0) µm long, 1.5 ± 0.1 (1.2–1.8) µm wide. Intercapsular appendix: Absent. Polar tubule: Coiled six times in larger capsule, three to four times in smaller capsule, positioned perpendicularly to capsule axis. Sutural ridge: Six to eight sutural markings, symmetrically distributed (**Figure S29D)**. Sporoplasm: Binucleate, iodinophilous vacuole present; 3.5 ± 0.4 (2.7–4.3) µm long, 2.4 ± 0.3 (1.9–3.0) µm wide, mucous envelope absent. Measurements from 30 formalin-fixed spores.

Locality: Sungai Nerus, Terengganu, Malaysia.

Predilection site: Intracelullarly in the muscle cell.

Prevalence: 33.3% (5/15).

Molecular data: Partial 18S rDNA sequences of *Myxobolus* n. sp. 12 (1913 bp) did not match any of myxozoan sequences available in GenBank. Pairwise distance estimation indicated the highest similarities of 89.9% to *Thelohanellus* n. sp. 1 and 87.8% to *Thelohanellus* n. sp. 2 (**Table 14**), described in this study. Phylogenetic analyses revealed that *Myxobolus* n. sp. 12 is closely related to *Thelohanellus* n. sp. 1 and formed a sister group with *Thelohanellus* n. sp. 2 from the same host (**Figure 14** and **Figure 23**).

Remarks: The morphology and morphometrics of *Myxobolus* n. sp. 12 are distinct from any previously described *Myxobolus* species. It most closely resembles *Myxobolus* n. sp. 4 from this study, which was described from the ovary of *B. binotatus* (**Table S25)**, differing mainly in the number of sutural markings (6–8 vs 8–10). Overall, *Myxobolus* n. sp. 4 is larger in all measured characteristics. In terms of spore width, *Myxobolus* n. sp. 12 shows close similarity to *Myxobolus pavlovskii* Akhmerov, 1954 and *M. csabai*. The polar capsule length and width are most similar to those of *Myxobolus acutus* Wu et Chen, 1987, *Myxobolus calbasui* Chakravarty, 1939, *M. nekrasovae* and *Myxobolus paratypicus* Xi, Zhao, Li et Xie, 2019.

4.3.7.5. Myxobolus n. sp. 13

Plasmodia: Found in the muscle, elongate-oval in shape (**Figure S29F**), 0.6 mm long, 0.2 mm wide (n = 1). Histology: Plasmodium located among the muscle cells (**Figure S29G**). Spore: Ellipsoidal in frontal view and biconvex in sutural view (**Figure S29H–S29I)**, 12.9 ± 0.4 (12.1–13.8) µm long, 9.1 ± 0.4 (8.0–9.9) µm wide, 6.4 ± 0.5 (5.8–6.6) µm thick (n = 3). Polar capsule: Two, pyriform, equal, 6.5 ± 0.5 (5.3–7.6) µm long, 3.0 ± 0.2 (2.5–3.5) µm wide. Intercapsular appendix: Absent. Polar tubule: Coiled ten times, positioned perpendicularly to capsule axis. Sporoplasm: Binucleate, iodinophilous vacuole absent, mucous envelope absent. Measurements from 30 formalin-fixed spores.

Locality: Sungai Nerus, Terengganu, Malaysia.

Predilection site: Muscle.

Prevalence: 13.3% (2/15).

Molecular data: Partial 18S rDNA sequences of *Myxobolus* n. sp. 13 (1910 bp) did not match any of myxozoan sequences available in GenBank. Pairwise distance estimation indicated the highest similarity of 97.4% to *Myxobolus* n. sp. 9 (**Table 14**), described in this study. Phylogenetic analyses revealed that *Myxobolus* n. sp. 13 is closely related to *Myxobolus* n. sp. 9, and formed a sister group with *M. csabai* and *M. tasikkenyirensis*, with maximum bootstrap values and posterior probabilities (**Figure 14** and **Figure 22**).

Remarks: The morphology and morphometrics of *Myxobolus* n. sp. 13 are distinct from any previously described *Myxobolus* species. Morphologically and morphometrically, it shows the closest resemblance to *M. tasikkenyirensis* from the muscle of *O. vittatus* and *Myxobolus osteochili* Székely, Shaharom-Harrison, Cech, Ostoros et Molnár, 2009 from the kidney of *Osteochilus hasselti*. Notably, these species differ significantly in the number of polar filament coils (10 vs 5–6 vs 8–10) (**Table S30**). Although *Myxobolus* n. sp. 13 is closely related to *Myxobolus* n. sp. 9, both infecting muscle tissue, they differ in spore morphology, where *Myxobolus* n. sp. 13 possesses ellipsoidal spores, whereas *Myxobolus* n. sp. 9 has globular to oval-shaped spores.

4.3.8. Myxosporean parasites in Trichopodus trichopterus

4.3.8.1. Henneguya n. sp. 1

Plasmodia: Found in the gill lamellae, brownish, obovate in shape (**Figure S30A**), 0.25 (0.2–0.3) mm long, 0.2 mm wide (n = 3). Histology: Plasmodium located between gill lamellae (**Figure S30B**). Spore: Ovoid, rounded or blunt anterior end in frontal view (**Figure S30C)**, biconvex in sutural view (**Figure S30D**), 11.8 ± 0.5 (10.3–12.9) µm long, 6.8 ± 0.3 (6.3–7.5) µm wide, 5.2 ± 0.2 (4.9–5.5) µm thick (n = 9). Total length: 48.5 ± 1.9 (44.2–51.7) µm. Caudal appendage: Two, equal, 36.7 ± 1.8 (33.1–39.5) µm long. Polar capsule: Two, pyriform, equal, 5.1 ± 0.3 (4.4–5.6) µm long, 2.6 ± 0.2 (2.2–3.1) µm wide, occupying half of the spore body cavity. Polar tubule: Coiled six to seven times, positioned perpendicularly to capsule axis. Sporoplasm: Binucleate, iodinophilous vacuole absent. Measurements from 30 formalin-fixed spores.

Locality: Small channels across Kuala Terengganu, Terengganu, Malaysia.

Predilection site: Gill lamellae.

Prevalence: 66.7% (6/9).

Molecular data: Two identical 18S rDNA sequences of *Henneguya* n. sp. 1 (100.0%; 1965 bp) did not match any of myxozoan sequences available in GenBank. Pairwise distance estimation indicated the highest similarity of 98.7% to *Henneguya daoudi* (EU643635) (**Table 18**). In the phylogenetic tree, *Henneguya* n. sp. 1 formed a sister group with *H. daoudi* and *Henneguya* n. sp. 2, clustering within freshwater gill-infecting *Henneguya* species, with maximum bootstrap values and posterior probabilities (**Figure 26**).

Remarks: The morphology and morphometrics of *Henneguya* n. sp. 1 are distinct from any previously described *Henneguya* species with blunt anterior ends (**Table S35**). It most closely resembles *H. daoudi* from the same host species and *Henneguya voronini* Borkhanuddin, Cech, Molnár, Shaharom-Harrison, Khoa, Samshuri, Mazelan, Atkinson et Székely, 2020, which infects the base of gill filaments of *Lates calcarifer*. Both species differ significantly in the length of their caudal appendages, whereas *H. voronini* deviates in all other morphometric characteristics. Besides from *H. daoudi, H. schizura* Gurley, 1893, has also been reported from the gills of the same host species, but differs significantly in all measured parameters (**Table S35**).

4.3.9. Myxosporean parasites in Trichopodus pectoralis

4.3.9.1. Henneguya n. sp. 2

Plasmodia: Found in the gill lamellae, brownish, oval in shape (**Figure S31A**), 0.1–0.2 mm diameter (n = 6). Spore: Ellipsoidal in frontal view (**Figure S31B)**, biconvex in sutural view (**Figure S31C**), 19.4 ± 0.9 (17.5–20.9) µm long, 7.9 ± 0.5 (6.8–8.6) µm wide, 5.3 ± 0.3 (4.7–5.8) µm thick (n = 9). Total length: 62.2 ± 2.3 (57.7–66.3) µm. Caudal appendage: Two, equal, 42.9 ± 2.2 (39.9–47.4) µm long. Polar capsule: Two, pyriform, equal, 7.7 ± 0.5 (6.5–8.6) µm long, 2.8 ± 0.2 (2.3–3.2) µm wide, occupying half of the spore body cavity. Polar tubule: Coiled ten to twelve times, positioned perpendicularly to capsule axis. Sporoplasm: Binucleate, iodinophilous vacuole present. Measurements from 30 formalin-fixed spores.

Locality: Small channels across Kuala Terengganu, Terengganu, Malaysia.

Predilection site: Gill lamellae.

Prevalence: 50.0% (6/12).

Molecular data: Partial 18S rDNA sequences of *Henneguya* n. sp. 2 (1965 bp) did not match any of myxozoan sequences available in GenBank. Pairwise distance estimation indicated the highest similarities of 96.9% to *Henneguya daoudi* (EU643635) and 96.6% to *Henneguya* n. sp. 1 (**Table 18**). Phylogenetic analyses revealed that *Henneguya* n. sp. 2 formed a sister group with *H. daoudi* and *Henneguya* n. sp. 1, clustering within freshwater gill-infecting *Henneguya* species, with maximum bootstrap values and posterior probabilities (**Figure 26**).

Remarks: The morphology and morphometrics of *Henneguya* n. sp. 2 are distinct from any previously described *Henneguya* species (**Table S36**). It most closely resembles *Henneguya suprabranchiae* Landsberg, 1987, which infects the gill cartilage of *Clarias gariepinus*. However, *Henneguya* n. sp. 2 is notably larger in all dimensions than *H. suprabranchiae*. Several *Henneguya* species infecting gills listed in **Table S36** display somewhat similar morphological characteristics, they display still significantly differ from *Henneguya* n. sp. 2.

4.3.9.2. Henneguya n. sp. 3

Plasmodia: Found in the cartilaginous tissue of gill arch, brownish, round in shape (**Figure S31D**), 0.16 (0.1–0.2) mm long, 0.12 (0.07–0.17) mm wide (n = 6). Spore: Ellipsoidal in frontal view (**Figure S31E)**, biconvex in sutural view (**Figure S31F**), 11.9 ± 0.6 (10.0–13.8) µm long, 4.7 ± 0.3 (4.0–5.2) µm wide, 3.7 ± 0.2 (3.4–4.1) µm thick (n = 15). Total length: 31.0 ± 1.5 (27.5–34.5) µm. Caudal appendage: Two, equal, 19.1 ± 1.4 (16.9–22.3) µm long. Polar capsule: Two, pyriform, unequal. Larger: 5.3 ± 0.4 (4.3–6.2) µm long, 2.0 ± 0.2 (1.6–2.2) µm wide. Smaller: 3.9 ± 0.4 (3.1–4.5) µm long, 1.6 ± 0.1 (1.3–1.8) µm wide. Polar tubule: Not visible. Sporoplasm: Binucleate, iodinophilous vacuole absent. Measurements from 30 formalin-fixed spores.

Locality: Small channels across Kuala Terengganu, Terengganu, Malaysia.

Predilection site: Cartilaginous tissue of gill arch.

Prevalence: 25.0% (3/12).

Molecular data: Partial 18S rDNA sequences of *Henneguya* n. sp. 3 (1988 bp) did not match any of myxozoan sequences available in GenBank. Pairwise distance estimation indicated the highest similarities of 89.7% to *Henneguya* n. sp. 4 and 88.5% to *Henneguya* n. sp. 5 (**Table 18**). Phylogenetic analyses revealed that *Henneguya* n. sp. 3 formed a sister group with *Henneguya* n. sp. 4 and *Henneguya* n. sp. 5, clustering within freshwater gill-infecting *Henneguya* species, with maximum bootstrap values and posterior probabilities (**Figure 26**).

Remarks: The morphology and morphometrics of *Henneguya* n. sp. 3 are distinct from any previously described *Henneguya* species with unequal polar capsules (**Table S37**). Remarkably, no previously recorded species exhibits a morphology that similar to *Henneguya* n. sp. 3, in which plane of spore body and polar capsules deviate from the median. In contrast, all known *Henneguya* species have centrally positioned spore bodies and polar capsules. Morphometrically, it most closely resembles *Henneguya gilbert* Casal, Sao Clemente, Lopes, Rocha, Felizardo, Oliveira, Al-Quraishy et Azevedo, 2017, *Henneguya* sp., and *Henneguya nagelli* de Azevedo, Abdallah, Paes, da Silva, Matos, Velasco et Matos, 2013. *Henneguya gilbert* and *H. nagelli* infect the gills of *Cyphocharax* gilbert and *Cyphocharax nagelli*, respectively, while *Henneguya* sp. infects the liver and spleen of *Channa aurantimaculata*. However, these species differ from *Henneguya* n. sp. 3 in several morphometric characteristics. Furthermore, several *Henneguya* species listed in **Table S37** exhibit morphometric similarities to *Henneguya* n. sp. 3 in some characteristics.

4.3.9.3. Henneguya n. sp. 4

Plasmodia: Found in the gill arches, brownish, round in shape (**Figure S31G**), 0.16 (0.14–0.18) mm long, 0.11 (0.10–0.12) mm wide (n = 2). Spore: Fusiform in frontal view (**Figure S31H)**, biconvex in sutural view (**Figure S31I**), 10.9 ± 0.4 (10.3–11.7) µm long, 4.9 ± 0.3 (4.3–5.5) µm wide, 4.0 ± 0.3 (3.7–4.7) µm thick (n = 12). Total length: 28.0 ± 1.1 (25.9–29.7) µm. Caudal appendage: Two, equal, 17.0 ± 1.1 (15.2–18.9) µm long. Polar capsule: Two, pyriform, equal, 5.0

± 0.2 (4.6–5.4) µm long, 1.6 ± 0.1 (1.4–1.9) µm wide. Polar tubule: Not visible. Sporoplasm: Binucleate, iodinophilous vacuole absent. Measurements from 16 formalin-fixed spores.

Locality: Small channels across Kuala Terengganu, Terengganu, Malaysia.

Predilection site: Gill arch.

Prevalence: 25.0% (3/12).

Molecular data: Partial 18S rDNA sequences of *Henneguya* n. sp. 4 (1985 bp) did not match any of myxozoan sequences available in GenBank. Pairwise distance estimation indicated the highest similarity of 92.0% to *Henneguya* n. sp. 5 (**Table 18**). Phylogenetic analyses revealed that *Henneguya* n. sp. 4 is closely related to *Henneguya* n. sp. 5 and formed a sister group with *Henneguya* n. sp. 3, clustering with freshwater gill-infecting *Henneguya* species, with maximum bootstrap values and posterior probabilities (**Figure 26**).

Remarks: The morphology and morphometrics of *Henneguya* n. sp. 4 are distinct from any previously described *Henneguya* species (**Table S38**). It most closely resembles *Henneguya corruscans* Eiras, Takemoto et Pavanelli, 2009, which infects the gill lamellae of *Pseudoplatystoma corruscans* and *Henneguya multiplasmodialis* Adriano, Carriero, maia, Silva, Naldoni, Ceccarelli et Arana, 2012, which infects the gill arches of the same host species. Morphometrically, *Henneguya* n. sp. 4 is greatly similar to *Henneguya* n. sp. 5 in most measurements, differing mainly in spore length and caudal appendage length. They also differ in their infection sites, despite sharing the same host species. Furthermore, several *Henneguya* species listed in **Table S38** exhibit partial morphometric similarities to *Henneguya* n. sp. 4.

4.3.9.4. Henneguya n. sp. 5

Plasmodia: Found in the pharynx, brownish, round in shape (**Figure S32A**), 0.2 ± 0.1 (0.1–0.2) mm long, 0.1 ± 0.1 (0.1–0.2) mm wide (n = 2). Histology: Plasmodium located within the stratified epithelia (**Figure S32B**). Spore: Fusiform in both frontal and sutural views (**Figure S32C– S32D)**, 11.8 ± 0.5 (10.9–12.7) µm long, 4.9 ± 0.3 (4.3–5.5) µm wide, 4.0 ± 0.3 (3.6–4.5) µm thick (n = 10). Total length: 27.1 ± 1.1 (25.2–29.2) µm. Caudal appendage: Two, equal, 15.4 ± 0.9 (14.0–

17.0) µm long. Polar capsule: Two, pyriform, equal, 5.9 ± 0.3 (5.5–6.5) µm long, 1.8 ± 0.2 (1.4–2.2) µm wide. Polar tubule: Coiled four times. Sporoplasm: Binucleate, iodinophilous vacuole absent. Measurements from 30 formalin-fixed spores.

Locality: Small channels across Kuala Terengganu, Terengganu, Malaysia.

Predilection site: Pharynx.

Prevalence: 25.0% (3/12).

Molecular data: Partial 18S rDNA sequences of *Henneguya* n. sp. 5 (1935 bp) did not match any of myxozoan sequences available in GenBank. Pairwise distance estimation indicated the highest similarity of 92.0% to *Henneguya* n. sp. 4 (**Table 18**). Phylogenetic analyses revealed that *Henneguya* n. sp. 5 is closely related to *Henneguya* n. sp. 4 and formed a sister group with *Henneguya* n. sp. 3, clustering within freshwater gill-infecting *Henneguya* species, with maximum bootstrap values and posterior probabilities (**Figure 26**).

Remarks: The morphology and morphometrics of *Henneguya* n. sp. 5 are distinct from any previously described *Henneguya* species (**Table S38**). It most closely resembles *H. corruscans*. Morphometrically, *Henneguya* n. sp. 5 is greatly similar to *Henneguya* n. sp. 4 in most measurements, differing mainly in spore length and caudal appendage length. Remarkably, differences are observed in the shape of the spore body, where *Henneguya* n. sp. 4 possesses an ellipsoidal shape, while *Henneguya* n. sp. 5 exhibits a fusiform spore body. In addition to spore morphology, they also differ in their infection sites, despite sharing the same host species. Furthermore, several *Henneguya* species listed in **Table S38** exhibit partial morphometric similarities to *Henneguya* n. sp. 5.

4.3.9.5. Myxidium n. sp. 2

Spore: Dispersal spores, coelozoic, elongate and fusiform in both frontal and sutural views, with truncated ends (**Figure S32E–S32G**), 11.7 ± 0.6 (10.8–12.5) µm long, 4.4 ± 0.3 (3.9–4.8) µm wide, 3.8 ± 0.3 (3.1–4.3) µm thick. Polar capsule: Two, equal, pyriform polar capsules, 3.8 ± 0.3 (2.7–4.5) µm long, 2.7 ± 0.2 (2.3–3.0) µm wide. Distance between two polar capsules, 2.5 ± 0.3

(2.0–3.0) µm in distance. Polar tubule: Coiled four times, positioned perpendicularly to capsule axis. Sutural line: Straight. Valvular striation: Five longitudinal striations. Sporoplasm: Binucleate, filling the spore body cavity between the two polar capsules. Measurements from 30 formalin-fixed spores.

Locality: Sungai Nerus, Kuala Nerus, Terengganu, Malaysia.

Predilection site: Gallbladder.

Prevalence: 66.7% (8/15).

Molecular data: Pairwise distance estimation of *Myxidium* n. sp. 2 (1930 bp) indicated the highest similarities of 94.6% to *Zschokkella* sp. (MT840090) and 94.5% to Myxsosporea (KP030767) (**Table 17**). Phylogenetic analyses revealed that *Myxidium* n. sp. 2 is closely related to *Zschokkella* sp. (MT840090), which infects the gallbladder of *Etroplus suratensis* from India, and formed a sister group with Myxosporea (KP030767) from the gallbladder of *Synodontis* sp. (**Figure 24**).

Remarks: Based on spore morphology, this species is classified as a new member of the genus *Myxidium*. The morphology and morphometrics of *Myxidium* n. sp. 2 do not match any previously described *Myxidium* spp. (**Table S39**). It most closely resembles *Myxidium djolonensis* Benoít, Vanessa et Abraham, 2020, which infects the gallbladder and urinary bladder of *Paramormyrops kingsleyae*. Notable, both species possess truncated ends, a feature rarely observed among other *Myxidium* spp., but they differ in their morphometric characteristics. Morphometrically, *Myxidium* n. sp. 2 shows the greatest similarity to *Myxidium macrocheilia* Mitchell, 1967 and *Myxidium phyllium* Davis, 1917 in terms of spore and polar capsule lengths and polar capsule width, while other features differ significantly.

4.3.10. Myxosporean parasites in Channa gachua

4.3.10.1. Henneguya n. sp. 6

Plasmodia: Found in the serous membrane of internal organs, yellowish to brownish, oval in shape (**Figure S33A–S33B**), 0.2 ± 0.1 (0.1–0.3) mm long, 0.1 (0.1–0.2) mm wide (n = 4). Histology: Plasmodium located within the serosa membrane (**Figure S33C**). Spore: Oval in frontal view

(**Figure S33D–S33E**) and biconvex in sutural view (**Figure S33F)**, 10.6 ± 0.5 (9.6–11.4) µm long, 5.2 ± 0.3 (4.5–6.0) µm wide, 4.0 ± 0.1 (3.9–4.1) µm thick (n = 3). Total length: 24.5 ± 1.6 (21.5–27.2) µm. Caudal appendage: Two, equal, 14.0 ± 1.6 (10.3–16.7) µm long. Polar capsule: Two, pyriform, equal, 3.4 ± 0.3 (2.6–3.9) µm long, 1.3 ± 0.1 (1.2–1.7) µm wide. Polar tubule: Not visible. Sporoplasm: Binucleate, iodinophilous vacuole absent. Measurements from 30 formalin-fixed spores.

Locality: Small channels across Kuala Terengganu, Terengganu, Malaysia.

Predilection site: Serous membrane of internal organs.

Prevalence: 66.7% (8/12).

Molecular data: Two nearly identical 18S rDNA sequences of *Henneguya* n. sp. 6 (99.9%; 1986, 1614 bp) did not match any of myxozoan sequences available in GenBank. Pairwise distance estimation indicated the highest similarity of 97.1% to *Henneguya* n. sp. 10 (**Table 18**). Phylogenetic analyses revealed that *Henneguya* n. sp. 6 formed a sister group with *Henneguya* n. sp. 10 and *Henneguya* n. sp. 8, within the clade comprising *Henneguya* species infecting *C. gachua* (**Figure 26**).

Remarks: The morphology and morphometrics of *Henneguya* n. sp. 6 are distinct from any previously described *Henneguya* species with oval-shaped spore body (**Table S40**). It most closely resembles *Henneguya caquetaia* Figueredo, Müller, Arana, Long et Adriano, 2023, *Henneguya guanduensis* Abdallah, Azevedo, Luque et Do Bomfim, 2007 and *Henneguya* n. sp. 10 from this study. However, both *H. caquetaia* and *H. guanduensis* are larger in overall size. Morphometrically, *Henneguya* n. sp. 6 is most similar to *Henneguya lacustris* Vieira, Rangel, Tagliavini, Abdallah, Santos et Azevedo, 2020, which infects the gill lamellae of *Astyanax lacustris* and to *Hennguya* n. sp. 10 from the muscle of *C. gachua*, the same host species. *Henneguya lacustris* is smaller in all morphometrics except for polar capsule length, whereas *Henneguya* n. sp. 10 is larger in all measurements except for caudal appendage and polar capsule

lengths, though these remain within the established range of variation. Other *Henneguya* species listed in **Table S40** differ significantly in their morphometric measurements.

Table 18 Genetic *p*-distance and sequence similarities (%) based on the 18S rDNA between *Henneguya* spp. and its most closely related species. Only identical or the closest-related sequences are presented.

Sequence	Genetic distance	Sequence similarities (%)
***Henneguya* n. sp. 1**		
***Henneguya* n. sp. 1**	**0.000**	**100.0**
Henneguya daoudi EU643635	0.013	98.7
***Henneguya* n. sp. 2**	**0.034**	**96.6**
***Henneguya* n. sp. 2**		
Henneguya daoudi EU643635	0.031	96.9
***Henneguya* n. sp. 1**	**0.034**	**96.6**
***Henneguya* n. sp. 1**	**0.034**	**96.6**
***Henneguya* n. sp. 3**		
***Henneguya* n. sp. 4**	**0.103**	**89.7**
***Henneguya* n. sp. 5**	**0.115**	**88.5**
***Henneguya* n. sp. 4**		
***Henneguya* n. sp. 5**	**0.080**	**92.0**
***Henneguya* n. sp. 6**		
***Henneguya* n. sp. 6**	**0.001**	**99.9**
***Henneguya* n. sp. 10**	**0.029**	**97.1**
***Henneguya* n. sp. 8**	**0.041**	**95.9**
***Henneguya* n. sp. 7**		
***Henneguya* n. sp. 9**	**0.053**	**94.7**
***Henneguya* n. sp. 11**	**0.077**	**92.3**
***Henneguya* n. sp. 8**		
***Henneguya* n. sp. 10**	**0.015**	**98.5**
***Henneguya* n. sp. 6**	**0.040**	**96.0**
***Henneguya* n. sp. 6**	**0.041**	**95.9**
***Henneguya* n. sp. 9**		
***Henneguya* n. sp. 10**	**0.048**	**95.2**
***Henneguya* n. sp. 7**	**0.050**	**95.0**
***Henneguya* n. sp. 8**	**0.055**	**94.5**
***Henneguya* n. sp. 10**		
***Henneguya* n. sp. 8**	**0.015**	**98.5**
***Henneguya* n. sp. 6**	**0.025**	**97.5**
***Henneguya* n. sp. 6**	**0.029**	**97.1**
***Henneguya* n. sp. 11**		
***Henneguya* n. sp. 10**	**0.055**	**94.5**
***Henneguya* n. sp. 6**	**0.058**	**94.2**

***Henneguya* n. sp. 8**	**0.059**	**94.1**
***Henneguya* n. sp. 6**	**0.060**	**94.0**

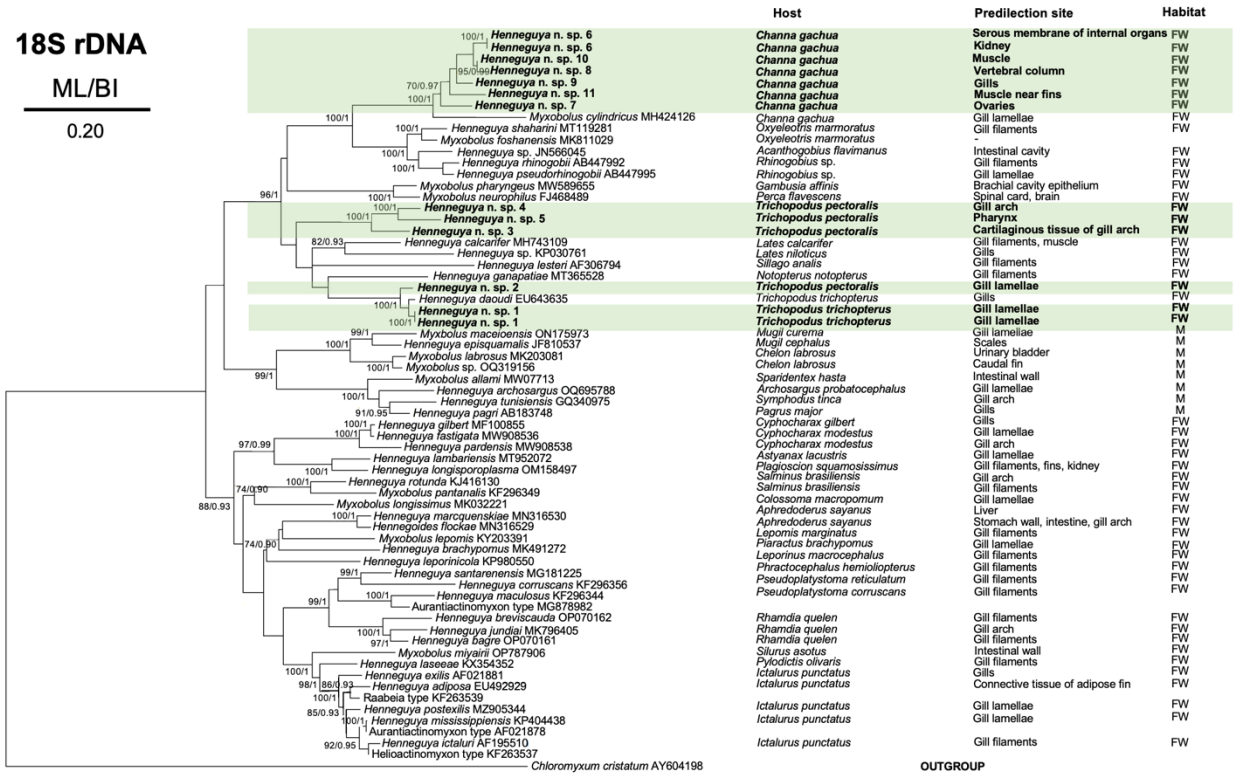

Figure 26. Maximum likelihood (ML) phylogenetic tree of 18S rDNA sequences of *Henneguya* spp. described in this study and related species. *Chloromyxum cristatum* was used as outgroup. Nodal supports are indicated for ML at 1000 replicates and Bayesian Inference (BI). Only values with ≥ 70% bootstrap (BS) and ≥ 0.90 posterior probabilities (PP) support are presented. The names of the parasite species are presented before GenBank accession numbers, following the host species, predilection site and habitat. Sequences obtained in the present study are shown in bold within colored boxes. The scale bar indicates the expected number of substitutions per site. M = Marine, FW = Freshwater.

4.3.10.2. Henneguya n. sp. 7

Plasmodia: Found in the ovarian tissue, brownish, oval in shape (**Figure S33G–S33H**), 0.2 ± 0.3 (0.1–0.8) mm long, 0.3 ± 0.3 (0.1–0.9) mm wide (n = 7). Histology: Plasmodium located in the fibrous connective tissue of the tunica albuginea (**Figure S33I**). Spore: Elongate to lanceolate in frontal view with slightly pointed ends (**Figure S33J**) and fusiform in sutural view (**Figure S33K)**, 12.7 ± 0.5 (11.4–13.3) µm long, 4.8 ± 0.5 (3.9–5.8) µm wide, 3.6 ± 0.3 (3.0–4.2) µm thick. Total length: 35.5 ± 2.2 (31.0–39.2) µm. Caudal appendage: Two, equal, 22.5 ± 2.2 (17.9–26.5) µm long. Polar capsule: Two, pyriform, equal, 4.7 ± 0.3 (4.1–5.3) µm long, 1.4 ± 0.2 (1.2–1.9) µm

wide. Polar tubule: Coiled five to six times, approximately. Sporoplasm: Binucleate, iodinophilous vacuole absent. Measurements from 30 formalin-fixed spores.

Locality: Small channels across Kuala Terengganu, Terengganu, Malaysia.

Predilection site: Ovaries.

Prevalence: 8.3% (1/12).

Molecular data: Partial 18S rDNA sequences of *Henneguya* n. sp. 7 (1924 bp) did not match any of myxozoan sequences available in GenBank. Pairwise distance estimation indicated the highest similarity of 94.7% to *Henneguya* n. sp. 9 (**Table 18**). Phylogenetic analyses revealed that *Henneguya* n. sp. 7 positioned basally within the clade comprising *Henneguya* species infecting *C. gachua* (**Figure 26**).

Remarks: The morphology and morphometrics of *Henneguya* n. sp. 7 are distinct from any previously described *Henneguya* species with lanceolate-shaped spore (**Table S41**). It most closely resembles *Henneguya* n. sp. 9 from this study, which infects the gills of the same host species, sharing in both morphology and morphometrics. Despite these similarities in spore shape, measurements, and host species, their infection sites are different, and molecular data confirmed they are distinct species. *Henneguya paraensis* Velasco, Videira, Nascimento, Matos, Gonçalves et Matos, 2016, which infect the gill filament of *Cichla temensis* shows similarity only in spore length, while other characteristics differ significantly to those of *Henneguya* n. sp. 7. Furthermore, several *Henneguya* species listed in **Table S41** exhibit partial morphometric similarities to *Henneguya* n. sp. 7.

4.3.10.3. Henneguya n. sp. 8

Plasmodia: Found in the vertebrae, brownish, oval in shape (**Figure S34A**), 1.7 mm long, 1.9 mm wide (n = 1). Spore: Ellipsoidal in frontal view with slightly pointed ends (**Figure S34B**) and fusiform in sutural view (**Figure S34C)**, 12.6 ± 0.4 (11.5–13.5) µm long, 5.2 ± 0.5 (4.3–6.7) µm wide, 4.1 ± 0.4 (3.7–4.8) µm thick (n = 19). Total length: 36.5 ± 2.8 (30.1–41.4) µm. Caudal appendage: Two, equal, 23.8 ± 2.8 (17.7–28.9) µm long. Polar capsule: Two, pyriform, equal, 5.4

± 0.5 (4.7–6.4) µm long, 1.5 ± 0.1 (1.2–1.8) µm wide. Polar tubule: Coiled eight to ten times. Sporoplasm: Binucleate, iodinophilous vacuole absent. Measurements from 30 formalin-fixed spores.

Locality: Small channels across Kuala Terengganu, Terengganu, Malaysia.

Predilection site: Vertebral column.

Prevalence: 8.3% (1/12).

Molecular data: Partial 18S rDNA sequences of *Henneguya* n. sp. 8 (1596 bp) did not match any of myxozoan sequences available in GenBank. Pairwise distance estimation indicated the highest similarity of 98.5% to *Henneguya* n. sp. 10 (**Table 18**). Phylogenetic analyses revealed that *Henneguya* n. sp. 8 is closely related to *Henneguya* n. sp. 10 and formed a sister group with *Henneguya* n. sp. 6 within the clade comprising *Henneguya* species infecting *C. gachua* (**Figure 26**).

Remarks: The morphology and morphometrics of *Henneguya* n. sp. 8 are distinct from any previously described *Henneguya* species with an ellipsoidal spore body (**Table S42**). It most closely resembles *Henneguya* n. sp. 11 from this study, which infects the muscle tissue near caudal peduncle, differing only slightly in size. However, *Henneguya* n. sp. 11 is generally larger in all measured characteristics than *Henneguya* n. sp. 8. Morphometrically, *Henneguya mystasi* Haldar, Samal et Mukhopadhyay, 1997 and *Henneguya psorospermica* Thélohan, 1895 share similarities in several features, including spore length, polar capsule length and width. In contrast, *Henneguya jaczoi* Székely, Borzák et Molnár, 2018, *Henneguya quelen* Abrunhosa, Sindeaux-Neto, Hamoy et Matos, 2018, and *Henneguya multiradiatus* Mathews, Mertins, Espinoza, Milanin, Alama-Bermejo, Audebert et Morandini, 2020 resemble *Henneguya* n. sp. 8 mainly in polar capsule length and width. Furthermore, other *Henneguya* species listed in **Table S42** exhibit significant morphometric differences from *Henneguya* n. sp. 8.

4.3.10.4. Henneguya n. sp. 9

Plasmodia: Found in the gills, exact location of the plasmodia could not be determined. Spore: Elongate to lanceolate in frontal view with blunt anterior ends (**Figure S34D**–**S34E**) and fusiform in sutural view (**Figure S34F)**, 12.5 ± 0.5 (11.3–13.3) µm long, 4.6 ± 0.4 (3.6–5.3) µm wide, 3.8 ± 0.1 (3.7–3.9) µm thick (n = 3). Total length: 37.6 ± 2.7 (32.2–43.0) µm. Caudal appendage: Two, equal, 25.3 ± 1.9 (22.1–28.8) µm long. Polar capsule: Two, pyriform, equal, 4.3 ± 0.5 (2.9–5.2) µm long, 1.4 ± 0.2 (1.0–1.7) µm wide. Polar tubule: Coiled five to six times. Sporoplasm: Binucleate, iodinophilous vacuole absent. Measurements from 30 formalin-fixed spores.

Locality: Small channels across Kuala Terengganu, Terengganu, Malaysia.

Predilection site: Gills.

Prevalence: 16.7% (2/12).

Molecular data: Partial 18S rDNA sequences of *Henneguya* n. sp. 9 (1507 bp) did not match any of myxozoan sequences available in GenBank. Pairwise distance estimation indicated the highest similarity of 95.2% to *Henneguya* n. sp. 10 (**Table 18**). Phylogenetic analyses revealed that *Henneguya* n. sp. 9 formed a sister group with *Henneguya* n. sp. 6, *Henneguya* n. sp. 8 and *Henneguya* n. sp. 10, within the clade comprising *Henneguya* species infecting *C. gachua* (**Figure 26**).

Remarks: The morphology and morphometrics of *Henneguya* n. sp. 9 are distinct from any previously described *Henneguya* species with an ellipsoidal spore body (**Table S41**). It most closely resembles *Henneguya* n. sp. 7 from this study, which infects the ovary of the same host species, sharing similarities in both morphology and morphometric characteristics. Despite these similarities in spore shape, size and host species, their infection sites differ, and molecular data have confirmed they are distinct species. *Henneguya paraensis,* which infect the gill filament of *C. temensis* shows similarity only in spore length, while other characteristics differ significantly to those of *Henneguya* n. sp. 9. Furthermore, several *Henneguya* species listed in **Table S41** exhibit partial morphometric similarities to *Henneguya* n. sp. 9.

4.3.10.5. Myxidium n. sp. 3

Plasmodia: Found in the gallbladder, orbicular in shape (**Figure S34G)**. Spore: Dispersal spores, ellipsoidal, slightly concave with slightly truncated ends in both frontal and sutural views (**Figure S34H–S34I**), 13.4 ± 0.4 (12.5–14.4) µm long, 6.5 ± 0.4 (5.7–7.3) µm wide, 5.5 ± 0.3 (4.8–6.4) µm thick. Polar capsule: Two, equal, rounded with papilla-like tips, positioned at opposite ends of the spore and oriented outward in opposite directions, 4.1 ± 0.3 (3.5–4.8) µm long, 3.3 ± 0.2 (2.9–3.7) µm wide. Distance between two polar capsules, 3.9 ± 0.6 (2.8–4.6) µm in distance. Polar tubule: Coiled four times, positioned perpendicularly to capsule axis. Sutural line: Straight. Valvular striation: Seven longitudinal striations. Sporoplasm: Binucleate, filling the spore body cavity between the two polar capsules. Measurements from 30 formalin-fixed spores.

Locality: Small channels across Kuala Terengganu, Terengganu, Malaysia.

Predilection site: Gallbladder.

Prevalence: 16.7% (2/12).

Molecular data: Pairwise distance estimation of *Myxidium* n. sp. 3 (2017 bp) indicated the highest similarity of 91.0% to *Myxidium chuatsi* (PQ869811) (**Table 17**). Phylogenetic analyses revealed that *Myxidium* n. sp. 3 is positioned basally within a clade of *Myxidium* species infecting the gallbladder of *Siniperca chuatsi*, *L. horie*, *Cranoglanis bouderius*, *L. leptocheilus*, *L. rohita*, *Culter alburnus*, and *Myxocyprinus asiaticus* (**Figure 24**).

Remarks: Based on spore morphology, this species is classified as a new member of the genus *Myxidium*. The morphology and morphometrics of *Myxidium* n. sp. 3 do not match any previously described *Myxidium* spp. (**Table S32**). Remarkably, no previously recorded species exhibits a morphology that similar to *Myxidium* n. sp. 3 characterized by a moderately concave body with slightly truncated ends, a feature rarely observed, though a few *Myxidium* spp. possess fusiform spores with truncated ends. Morphometrically, *Myxidium* n. sp. 3 shows the greatest similarity to *Myxidium shilba* Ali, Sakran et Abdel-Baki, 1999 that infects the gallbladder of *Schilbe mystus* and *Myxidium onyhosionmatis* Chen et Ma, 1998, which infects the gallbladder of *Varicorhinus*

simus, sharing comparable measurements. However, *Myxidium asiaticum* is larger in most features except for the polar capsule dimensions.

4.3.10.6. Henneguya n. sp. 10

Plasmodia: Found in the skeletal muscle, brownish, oval in shape (**Figure S35A**), 0.12 (0.10–0.14) mm long, 0.11 (0.08–0.13) mm wide (n = 2). Histology: Plasmodium located among muscle cells, surrounding connective tissue (**Figure S35B**). Spore: Oval in frontal view (**Figure S33C**) and biconvex in sutural view (**Figure S33D)**, 11.1 ± 0.6 (10.2–12.9) µm long, 5.8 ± 0.5 (4.7–6.6) µm wide, 4.1 ± 0.5 (3.2–5.4) µm thick. Total length: 23.9 ± 1.9 (19.8–27.0) µm. Caudal appendage: Two, equal, 12.8 ± 2.0 (8.6–16.7) µm long. Polar capsule: Two, pyriform, equal, 4.0 ± 0.4 (3.3–4.6) µm long, 1.2 ± 0.2 (0.9–1.6) µm wide. Polar tubule: Not visible. Sporoplasm: Binucleate, iodinophilous vacuole absent. Measurements from 30 formalin-fixed spores.

Locality: Small channels across Kuala Terengganu, Terengganu, Malaysia.

Predilection site: Skeletal muscle.

Prevalence: 100.0% (12/12).

Molecular data: Two nearly identical 18S rDNA sequences of *Henneguya* n. sp. 10 (1879 bp) did not match any of myxozoan sequences available in GenBank. Pairwise distance estimation indicated the highest similarity of 98.5% to *Henneguya* n. sp. 8 (**Table 18**). Phylogenetic analyses revealed that *Henneguya* n. sp. 10 is closely related to *Henneguya* n. sp. 8 and formed a sister group with *Henneguya* n. sp. 6, within the clade comprising *Henneguya* species infecting *C. gachua* in Clade A (**Figure 26**).

Remarks: The morphology and morphometrics of *Henneguya* n. sp. 10 are distinct from any previously described *Henneguya* species with oval-shaped spore body (**Table S40**). It most closely resembles *H. caquetaia*, *H. guanduensis* and *Henneguya* n. sp. 6 from this study. However, both *H. caquetaia* and *H. guanduensis* are larger in overall size. Morphometrically, *Henneguya* n. sp. 10 is most similar to *H. lacustris*, which infects the gill lamellae of *A. lacustris* and to *Hennguya* n. sp. 6 from the serous membrane of *C. gachua*, the same host species. *Henneguya lacustris* is

smaller in all morphometrics except for polar capsule length and width, whereas *Henneguya* n. sp. 6 is slightly smaller in all measurements except for caudal appendage length and polar capsule width, though these remain within the established range of variation. Other *Henneguya* species listed in **Table S40** differ significantly in their morphometric measurements.

4.3.10.7. Henneguya n. sp. 11

Plasmodia: Found in the skeletal muscle near caudal peduncle, brownish, elongate-oval in shape (**Figure S35E**), 0.5 (0.2–0.7) mm long, 0.1 (0.1–0.2) mm wide (n = 6). Histology: Plasmodium located among skeletal muscle cells, along with the hypural plate and the caudal fin rays (**Figure S35F**). Spore: Ellipsoidal in frontal view with slightly pointed ends (**Figure S35G**) and fusiform in sutural view (**Figure S35H)**, 13.0 ± 0.5 (11.9–14.1) µm long, 5.6 ± 0.4 (4.9–6.1) µm wide, 4.3 ± 0.4 (4.0–4.6) µm thick (n = 2). Total length: 40.1 ± 1.5 (35.9–42.0) µm. Caudal appendage: Two, equal, 27.1 ± 1.6 (23.0–29.6) µm long. Polar capsule: Two, pyriform, equal, 5.5 ± 0.3 (4.9–6.1) µm long, 1.7 ± 0.2 (1.3–2.0) µm wide. Polar tubule: Coiled eight to nine times. Sporoplasm: Binucleate, iodinophilous vacuole absent. Measurements from 30 formalin-fixed spores.

Locality: Small channels across Kuala Terengganu, Terengganu, Malaysia.

Predilection site: Skeletal muscle near caudal peduncle.

Prevalence: 25.0% (3/12).

Molecular data: Partial 18S rDNA sequences of *Henneguya* n. sp. 11 (1986 bp) did not match any of myxozoan sequences available in GenBank. Pairwise distance estimation indicated the highest similarity of 94.5% to *Henneguya* n. sp. 10 (**Table 18**). Phylogenetic analyses revealed that *Henneguya* n. sp. 11 positioned basally within the clade comprising *Henneguya* species infecting *Channa gachua* (**Figure 26**).

Remarks: The morphology and morphometrics of *Henneguya* n. sp. 11 are distinct from any previously described *Henneguya* species with an ellipsoidal spore body (**Table S42**). It most closely resembles *Henneguya* n. sp. 8 from this study, which infects the vertebrae, differing only slightly in size. However, *Henneguya* n. sp. 11 is generally larger in all measured characteristics

than *Henneguya* n. sp. 8. Morphometrically, *H. mystasi* and *H. psorospermica* share similarities in several features, including spore length, polar capsule length and width, whereas *Henneguya* n. sp. 8 share similarities in all measurements. In contrast, *H. quelen* shows resemblance *Henneguya* n. sp. 11 in spore length, and polar capsule dimensions, while, *H. jaczoi*, and *H. multiradiatus* are similar to *Henneguya* n. sp. 11 mainly in polar capsule length and width. Furthermore, other *Henneguya* species listed in **Table S42** exhibit significant morphometric differences from *Henneguya* n. sp. 8.

4.4. Actinosporeans in Malaysia

A total of 2,666 oligochaetes were isolated from sediment collected at Tasik Telabak. The comprehensive survey of oligochaetes in the sediment samples revealed the presence of at least eight morphologically distinct species, with the genera *Branchiodrilus* and *Aulophorus* being the most dominant. Myxozoan infection was detected in the intestinal epithelium of 24 oligochaetes, resulting in an overall prevalence of 0.90% (24 out of 2,666 oligochaetes examined). Infected worms were detected in only four species, namely *Bothrioneurum* sp., *Branchiodrilus* sp., *Aulodrilus acutus* and *Aulophorus* sp. Among these, *Aulodrilus acutus* exhibited the highest prevalence of myxozoan infection, with 3.37%; 3 out of 89 oligochaetes testing positive. In contrast, *Aulophorus* sp. exhibited a much lower infection rate of 1.90% (15 out of 788), *Bothrioneurum* sp. had 1.30% (2 out of 150), and *Branchiodrilus* sp. had the lowest prevalence at 0.37% (4 out of 1,067). This study identified six different actinospore types, including one triactinomyxon type, one raabeia type, and four aurantiactinomyxon types, all of which were novel. Moreover, none of the obtained sequences from these actinospore types matched any known myxosporean sequences in GenBank, and therefore their corresponding life cycles could not be elucidated.

4.4.1. Raabeia type 1 (Figure S36A–S36C)

Spore body: Elongated oval in side view, 29.7 ± 2.1 (25.4–30.2) µm long, 11.1 ± 0.6 (10.1–10.9) µm wide. Caudal processes: Equal size, curved upwards, tapering to a ‘pencil point’, 271.2 ± 8.6

(252.0–276.2) µm long, 9.7 ± 0.8 (8.0–10.9) µm wide at the base. Valve cell nuclei: Located at base of spore body, 3.7 ± 0.6 (2.2–3.8) µm diameter. Polar capsules: Three, equal size, tear-shaped in side view, protruding from the anterior end, 5.3 ± 0.6 (4.3–6.4) µm long, 3.6 ± 0.2 (3.2–3.8) µm wide. Polar tubule: Coiled four times, total length, 27.8 ± 3.6 (25.6–25.9) µm (n = 3). Sporoplasm: Not determined. Measurements from 20 fresh actinospores.

Host: *Aulodrilus acutus* Ohtaka and Usman (1997).

Predilection site: The intestinal epithelium. Histological analyses have proved that the pansporocysts located in the intestinal epithelium of the infected oligochaetes (**Figure S36D**). Prevalence: 3.37% (3 infected in 89 oligochaetes examined).

Locality: Tasik Telabak, Hulu Besut, Terengganu.

Molecular data: Two identical sequences from different individuals (100.0%; 1768, 1523 bp) were deposited in GenBank under the accession numbers PP856689 and PP856690, respectively. The 18S rDNA sequences of raabeia type 1 did not match any of the myxozoan sequences available in GenBank. Pairwise distance estimation indicated the highest similarity of 90.3% to *Myxobolus* n. sp. 11 from this study (**Table 19**). Phylogenetic analyses revealed that raabeia type 1 are closely related to *Myxobolus* n. sp. 11 from this study in Clade B, with maximum bootstrap values and posterior probabilities (**Figure 27**).

Remarks: The morphology of raabeia type 1 does not match any previously described raabeia types. It is morphologically similar to raabeia type 1 (Oumouna et al., 2003) and raabeia type (Eszterbauer et al., 2006), but differs morphometrically (**Table S43**). Its spore body length resembles raabeia type 4 and raabeia type 6 (Özer et al., 2002), while the width is closest to raabeia type E (Xiao & Desser, 1998b) and raabeia of *M. lentisuturalis* (Caffara et al., 2009). The caudal processes length differs from all reported types, and the polar capsule dimensions most closely match to raabeia type 1 (Oumouna et al., 2003) and raabeia type 2 (Hallett et al., 2004).

Table 19 Genetic *p*-distance and sequence similarities (%) based on the 18S rDNA between raabeia type 1, aurantiactinomyxon type 1, aurantiactinomyxon type 2, aurantiactinomyxon type 3, and its most closely related species. Only identical or the closest-related sequences are presented.

Sequence	Genetic distance	Sequence similarities (%)
Raabeia type 1		
Raabeia type 1	**0.000**	**100.0**
Myxobolus n. sp. 11	0.097	90.3
Aurantiactinomyxon type 1		
Henneguya sp. PP852214	0.141	85.9
Henneguya quelen MH230064	0.142	85.8
Henneguya sutherlandi MZ905346	0.146	85.4
Henneguya pellis FJ468488	0.149	85.1
Myxobolus miyairii KT001495	0.157	84.3
Aurantiactinomyxon type 3		
Aurantiactinomyxon type 3	**0.001**	**99.9**
Aurantiactinomyxon type 2	**0.059**	**94.1**
Henneguya sp. PP852214	0.098	90.2

4.4.2. Aurantiactinomyxon type 1 (Figure S37A)

Spore body: Spherical, 10.3 ± 0.5 (9.4–11.0) µm diameter. Caudal processes: Equal size, elongated, tapering to pencil ends, 39.7 ± 2.2 (34.4–43.4) µm long, 6.8 ± 0.4 (6.0–7.5) µm wide at the base. Valve cell nuclei: Not visible. Polar capsule: Equal size, pyriform, protrude from the apex of spore body in both side and apical views, 2.6 (2.6–2.7) µm long, 1.6 ± 0.1 (1.5–1.8) µm wide (n = 3). Polar filament: Not visible. Sporoplasm: 32 secondary cells. Measurements from 26 formalin-fixed actinospores.

Host: Species of the genus *Aulophorus* Schmarda, 1861.

Predilection site: The intestinal epithelium.

Prevalence: 0.13% (1 infected in 788 oligochaetes examined).

Locality: Tasik Telabak, Hulu Besut, Terengganu.

Molecular data: Partial 18S rDNA sequence of aurantiactinomyxon type 1 of 1447 bp did not match any of the myxozoan sequences available in GenBank. Pairwise distance estimation indicated the highest similarities of 85.9% to *Henneguya* sp. (PP852214) and 85.8% to *Henneguya quelen* (MH230064) (**Table 19**). Phylogenetic analyses revealed that aurantiactinomyxon type 1

is closely related to *Myxobolus miyairii* and formed a sister group with others aurantiactinomyxon types described in this study, raabeia type and *Henneguya* spp. in Clade A, with high bootstrap values and posterior probabilities (**Figure 27**).

Remarks: The morphology of aurantiactinomyxon type 1 does not match any previously described aurantiactinomyxon types. It is morphologically similar to aurantiactinomyxon type 5 of *Thelohanellus hovorkai* described in this study, although the present aurantiactinomyxon type 1 was smaller in all measurements. The only shared feature is the presence of 32 secondary cells. Morphometrically, it most closely resembles auratiactinomyxon type 2 of Milanin et al. (2018), with similar polar capsule width. However, the spore body and polar capsule width of auantiactinomyxon type 1 are smaller, while the caudal processes and polar capsule lengths are larger than those reported for aurantiactinomyxon type 2 (Milanan et al., 2018) (**Table S44**).

4.4.3. Aurantiactinomyxon type 2 (Figure S37B–S37C)

Spore body: Subspherical in both apical and side views, 16.4 ± 1.3 (14.3–19.7) μm diameter. Caudal processes: Equal in size, elongated, tapering to pointed ends, 153.6 ± 7.2 (144.2–171.0) μm long, 8.4 ± 0.7 (7.1–9.9) μm wide at the base. Valve cell nuclei: Not visible. Polar capsule: Pyriform, protrude from the apex of spore body in both side and apical views, 5.1 ± 0.5 (4.1–6.4) μm long, 2.6 ± 0.4 (2.0–3.3) in wide (n = 25). Polar tubule: Coiled three times. Sporoplasm: Not determined. Measurements from 33 formalin-fixed actinospores.

Host: Species of the genus *Aulophorus* Schmarda, 1861.

Site of infection: The intestinal epithelium.

Prevalence: 0.25% (2 infected in 788 oligochaetes examined).

Locality: Tasik Telabak, Hulu Besut, Terengganu.

Molecular data: Partial 18S rDNA sequence of aurantiactinomyxon type 2 (1780 bp) did not match any of the myxozoan sequences available in GenBank. Pairwise distance estimation indicated the highest similarity of 94.1% to aurantiactinomyxon types 3 described in this study (**Table 19**). Phylogenetic analyses revealed that aurantiactinomyxon type 2 is closely related to

aurantiactinomyxon type 3 of this study in Clade A, with maximum bootstrap values and posterior probabilities (**Figure 27**).

Remarks: The morphology of aurantiactinomyxon type 2 does not match any previously described aurantiactinomyxon types. According to the literature, only the aurantiactinomyxon types reported by Xi et al. (2013) and Özer et al. (2002) exhibit caudal processes lengths exceeding 100 µm (**Table S44**). However, the present aurantiactinomyxon type 2 differs from these in all measurements and infects a different host species. Based on caudal process length, width and polar capsule width, aurantiactinomyxon type 2 ranks the second largest among the types mentioned above. In contrast, it possesses the longest polar capsule length and the smallest spore body compared to the aurantiactinomyxon type of Xi et al. (2013) and aurantiactinomyxon type 3 of Özer et al. (2002).

4.4.4. Aurantiactinomyxon type 3 (Figure S37D–S37F)

Spore body: Triangle in both apical and side views, 11.7 ± 0.7 (10.5–13.2) µm diameter. Caudal processes: Equal size, elongated, tapering to pointed ends, 44.3 ± 2.9 (40.4–49.3) µm long, 6.3 ± 0.5 (5.5–7.6) µm wide at the base. Valve cell nuclei: Not visible. Polar capsule: Pyriform, protrude from the apex of spore body in both side and apical views, 3.2 ± 0.2 (2.7–3.5) µm long, 2.0 ± 0.2 (1.5–2.4) µm wide (n = 25). Polar tubule: Coiled three times. Sporoplasm: Not determined. Measurements from 30 formalin-fixed actinospores.

Host: Species of the genus *Aulophorus* Schmarda, 1861.

Predilection site: The intestinal epithelium.

Prevalence: 1.52% (12 infected in 788 oligochaetes examined).

Locality: Tasik Telabak, Hulu Besut, Terengganu.

Molecular data: The two nearly identical 18S rDNA sequences of aurantiactinomyxon type 3 (99.9%; 1838, 1939bp) did not match any of the myxozoan sequences available in GenBank. Pairwise distance estimation indicated the highest similarity of 94.1% to aurantiactinomyxon type 2 described in this study (**Table 19**). Phylogenetic analyses revealed that aurantiactinomyxon type

3 are closely related to aurantiactinomyxon type 2 of this study in Clade A, with maximum bootstrap values and posterior probabilities (**Figure 27**).

Remarks: The morphology of aurantiactinomyxon type 3 does not match any previously described aurantiactinomyxon types. Its morphology closely resembles of the aurantiactinomyxon type 4 described in this study. However, significant differences are observed in morphometric measurements, with the present aurantiactinomyxon type 3 being larger in most dimen';/sions. Morphometrically, aurantiactinomyxon type 3 shows the closest resemblance to the aurantiactinomyxon type of *Henneguya exilis* (Rosser et al., 2014) (**Table S44**).

4.4.5. Aurantiactinomyxon type 4 (Figure S38A–S38E)

Spore body: Subspherical, 8.8 ± 0.7 (7.6–10.1) µm diameter. Caudal processes: Equal size, elongated, tapering to pointed ends in apical view and extending in a downward curve from spore body in side view, 36.7 ± 2.7 (30.7–43.8) µm long, 4.9 ± 0.6 (3.9–6.2) µm wide at the base. Valve cell nuclei: Not visible. Polar capsule: Elongated pyriform, prominently protrude from the apex of spore body in both side view and apical view (**Figure S38E*)***. Side view, 3.6 ± 0.3 (3.0–4.3) µm long, 1.3 ± 0.2 (1.1–1.9) µm wide. Apical view, 2.0 ± 0.3 (1.5–2.5) µm diameter. Polar tubule: Not visible. Sporoplasm: Not determined. Measurements from 25 ethanol-fixed actinospores.

Host: Species of the genus *Bothrioneurum* Štolc, 1886.

Predilection site: The intestinal epithelium. The oligochaete displayed a severe infection, with pansporocysts at different developmental stages observed in the intestinal epithelium (**Figure S38F**). In some parts of the oligochaete, six to seven out of eight actinospores can be seen in the pansporocysts (**Figure S38G**).

Prevalence: 1.30% (2 infected in 150 oligochaetes examined).

Locality: Tasik Telabak, Hulu Besut, Terengganu.

Remarks: The morphology of aurantiactinomyxon type 4 does not match any previously described aurantiactinomyxon types. The closest resemblance with aurantiactinomyxon type 11 (El-Mansy et al., 1998b) but aurantiactinomyxon type 4 of this study has larger spore body and longer caudal

processes, while type 11 has shorter polar capsules (**Table S44**). The spore body resembles that of aurantiactinomyxon type 1 (Milanin et al., 2018), and the polar capsule diameter is similar to aurantiactinomyxon type 1 (Hallett et al., 1997), while other morphological features do not resemble to any known aurantiactinomyxon types. The prominently elongated pyriform polar capsules, appear to be a distinguishing feature, suggesting that this aurantiactinomyxon type is novel. During this study, several attempts were made using various primers to obtain a specific sequence, but they were unsuccessful. This failure is probably due to errors in sample fixation that impeded the extraction of high-quality genomic DNA.

4.4.6. Triactinomyxon type 1 (Figure S39A–S39D)

Spore body: Cylindrical, elongated, 27.9 ± 3.1 (21.7–33.0) µm long, 8.9 ± 0.7 (7.4–10.5) µm wide. Style: Short, 29.8 ± 3.9 (22.4–38.6) µm long, 9.5 ± 1.1 (8.0–12.1) µm wide. Total length: 57.6 ± 4.1 (51.2–67.8) µm. Caudal processes: Short, with blunt tips and equal in length, 29.9 ± 3.2 (24.6–35.1) µm long, 9.7 ± 0.9 (8.2–11.0) µm wide at the base. Largest span of caudal processes, 59.3 ± 3.6 (52.3–66.7) µm. Valve cell nuclei: Located at the base of caudal processes. Polar capsule: Three, pyriform, equal size, protruding from the anterior end, 3.4 ± 0.4 (2.8–4.0) µm long, 2.2 ± 0.2 (1.7–2.6) µm wide. Polar tubule: Not visible. Sporoplasm: 8 secondary cells (**Figure 39D**). Measurements from 25 ethanol-fixed actinospores.

Host: Species of the genus *Branchiodrilus* Michaelsen, 1900.

Predilection site: The intestinal epithelium. The oligochaete showed a massive infection, with pansporocysts at various stages of development observed in the intestinal epithelium (**Figure S39E–S39F**).

Prevalence: 0.37% (4 infected in 1,067 oligochaetes examined).

Locality: Tasik Telabak, Hulu Besut, Terengganu.

Remarks: Morphometric comparisons with 10 previously described triactinomyxon types possessing 8 secondary cells (**Table S45**) show that the triactinomyxon type 1 does not match any known actinospores. The spores have short caudal processes and a distinctive style length, features

that differentiate them from previously described types. Therefore, this triactinomyxon type 1 appears to be novel. Throughout this study, several attempts were conducted - unsuccessfully - to obtain a specific secqence from triactinomyxon type 1, using several primer combinations. This is probably due to inadequate fixation that hindered the extraction of high-quality genomic DNA.

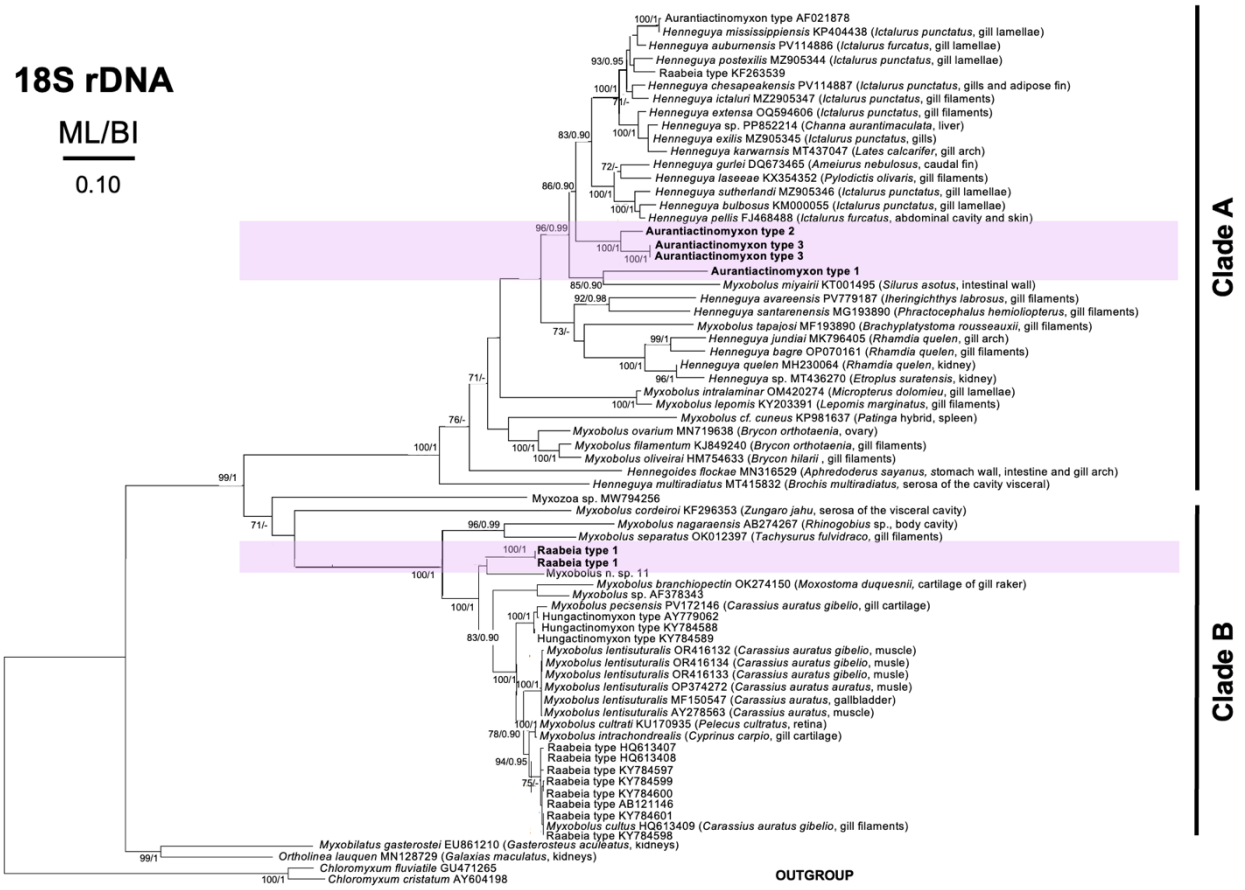

Figure 27. Maximum likelihood (ML) phylogenetic tree of 18S rDNA sequences of raabeia type 1, aurantiactinomyxon type 1, aurantiactinomyxon type 2, aurantiactinomyxon type 3 described in this study and related species. *Chloromyxum cristatum* was used as outgroup. Nodal supports are indicated for ML at 1000 replicates and Bayesian Inference (BI). Only values with ≥ 70% bootstrap (BS) and ≥ 0.90 posterior probabilities (PP) support are presented. The names of the parasite species are presented before GenBank accession numbers, following the host species, predilection site and habitat. Sequences obtained in the present study are shown in bold within colored boxes. The scale bar indicates the expected number of substitutions per site.

CHAPTER 5

DISCUSSION

The intensive research of myxosporea began in the late nineteenth century, when Bütschli (1882), Thélohan (1892), and Gurley (1893) established the taxonomic categories for myxosporeans that remain valid today. For many years, the morphology, dimension of spores were the primary criteria used to describe new species and differentiate existing species. A significant advancement in identification came with the consideration of host specificity and the organ and tissue tropism of specific species (Molnár, 1994; Hedrick et al., 2001; Urawa et al., 2011). However, modern diagnosis now relies on combining morphological data with nucleotide sequence information to achieve more robust classifications. In this study, comprehensive surveys of myxozoans were conducted in fish farms in Hungary and freshwater ecosystems in Malaysia. Morphological, morphometric, histological and molecular analyses revealed 15 myxosporean parasites and 10 actinosporeans in Hungary, as well as 35 myxosporean parasites and 6 actinosporeans in Malaysia.

5.1. Myxosporean species in Hungary

Carassius auratus gibelio is a native and economically important freshwater species in China. Conversely, it is considered a highly invasive species in Europe, where it has caused significant declines in native fish populations, such as the crucian carp (Molnár et al., 2018). This species was accidentally introduced to Europe along with other cyprinids from Amur Basin for aquaculture activities and accidental introduction through common carp stock (Hensel, 1971; Kalous et al., 2012). Today, *C. auratus gibelio* can be found in most of European waters and fish farm ponds. Although fish farmers in Hungary generally do not favor this species, it remains popular among anglers. In contrast, in Hungary, *C. carpio* is the main fish species produced (FAO, 2018). Given the economic importance of *C. carpio* and the invasive status of *C. auratus gibelio* in Hungary, parasite surveys are crucial to assess the risk of pathogen infections among these species. In this study, *C. auratus gibelio* hosted the largest number of myxosporean parasites, comprising four new species along with three species that were redescribed; *C. carpio* harbored two new species

and four redescribed species, while *R. rutilus* contained two new species. *Rutilus rutilus* is common in Europe. This a small fish prefers the slow or stagnant waters, explaining their abundance in fish farms.

Myxobolus lentisuturalis has been reported in China, Italy, Croatia and the USA as a highly pathogenic myxozoan infecting the dorsal epaxial musculature of *C. auratus gibelio* and *C. auratus*. The present findings from Hungary are consistent with previous observations, showing dorsolateral body deformation caused by muscle infection. The spore morphology closely matches descriptions by Dyková et al. (2002), Caffara et al. (2009), Wang et al. (2019) and Huskanović (2021), except for slightly smaller spores reported by Caffara et al. (2009) (**Table S3**). The measured spore dimensions (11.8 μm and 7.6 μm) are nearly to those from Hubei, China (Dyková et al., 2002), likely due to infection of the same host species, *C. auratus gibelio*. The muscle infection caused by *M. lentisuturalis* is an unusual form of myxosporean parasitism but it can be easily diagnosed by visible body deformities. Similar deformities in Hungarian cyprinids were previously associated with *Sphaerospora dykovae* Dyková et Lom, 1982 and *Myxobolus pfeifferi* Thélohan, 1895, although *M. pfeifferi* develops in intermuscular connective tissue, whereas *M. lentisuturalis* occurs intracellularly within the muscle cells. It is assumed that the spores, which are located in the intermuscular connective tissue and may indicate intermuscular development, derive from damaged muscle cells. The detection of *M. lentisuturalis* in the Hungarian gibel carp population confirms its establishment in Europe and provides new data on the spread of myxozoans from the Far East to Europe.

Myxobolus ocsardiensis n. sp. is morphologically and morphometrically most similar to *M. hearti*. Phylogenetic analyses placed *M. ocsardiensis* n. sp. in a well-supported clade with *M. hearti*, *M. pronini*, *Myxobolus oralis* Liu, Whipps, Nie et Gu, 2014, *Myxobolus nielli* Landsberg et Lom, 1991 and *Henneguya doneci* Schulman, 1962. All of them share oval to ellipsoidal spore shapes and the identical host species, except for *H. doneci*. *Myxobolus ocsardiensis* n. sp. was compared with other kidney-infecting *Myxobolus* spp. documented in the literature both in *C. auratus gibelio*

and *C. auratus* (*Myxobolus artus* Akhmerov, 1960; *Myxobolus gibelio* Yukhimenko, 1986; *Myxobolus platyrostris* Akhmerov, 1960; *Myxobolus sacchalinensis* Landsberg et Lom, 1991; *Myxobolus sphaericus* Landsberg et Lom, 1991; *Myxobolus echengensis* Chen, 1998, *Myxobolus egregious* Li et Nie, 1973; *Myxobolus pekingensis* Chen, 1998; *Myxbolus tunghuensis* Chen, 1998; *Myxobolus valatus* Li et Nie, 1973; *Myxobolus wuhanensis* Chen, 1998 and *Myxobolus wushingensis* Chen, 1998). However, these species differed morphologically and morphometrically; unfortunately, molecular data of those species are currently unavailable for comparison. The majority of them can parasitize similar organs or tissues in closely related fish hosts, but *M. ocsardiensis* n. sp. is recognized as a new species considering its distinctive morphological and morphometric characteristics, as well as its placement in the phylogenetic tree.

Tissue tropism is an important criterion beside spore characteristics for separating myxozoans, including *Thelohanellus* species that infect the same or closely related fish hosts. Although *T. imrei* n. sp. shows morphometric similarity to *T. wangi* and *T. nanhaiensis* (**Table S7**), their tissue tropism are different. Plasmodia of *T. imrei* n. sp. were found in the connective tissues of the gill arch and pharynx of *C. auratus gibelio*, while *T. wangi* forms intrafilamental-chondroidal plasmodia of the same host (Yuan et al., 2015). *Thelohanellus nanhaiensis* infects the gills of *C. auratus*, although the exact location of plasmodia within the gills was not specified. However, the latter can be differentiated by the S-shaped sutural line of the spore, as *T. imrei* n. sp. has a straight sutural line. This finding was corroborated by BLAST search showed that *T. wangi* shared 91.1% similarity with *T. imrei* n. sp. Regrettably, it must be excluded from the phylogenetic tree because of low query coverage (80%), as only sequences with >90% coverage were included. Comparisons with other gill-infecting *Thelohanellus* species from *C. auratus gibelio* and *C. auratus,* including *Thelohanellus carassi* Akhmerov, 1960, *Thelohanellus membranicaudata* Sun, 2006, and *Thelohanellus relortus* Chen et Ma, 1998, showed that none of them shared the exact predilection sites as *T. imrei* n. sp. Unfortunately, no molecular data were available for the above mentioned species to determine their phylogenetic relationship. Interestingly, a BLAST search revealed that

Neoactinomyxum type CZ-2 (KP642139) from *B. sowerbyi* showed 99.3% similarity to *T. imrei* n. sp., although it was excluded from the phylogenetic analysis due to short sequence length which caused low query coverage (50%). This high similarity suggested that Neoactinomyxum type CZ-2 might represent the actinospore stage of *T. imrei* n. sp. Hence, further sampling of oligochaetes, especially *B. sowerbyi*, or resequencing of the original Chinese sample was recommended to clarify the life cycle of *T. imrei* n. sp. The previous molecular studies confirmed that host affinity is a crucial criterion for differentiation of myxobolids, including those in the genus *Thelohanellus* (Carriero et al., 2013; Moreira et al., 2013). *Thelohanellus imrei* n. sp. clustered with other *Thelohanellus* species infecting *C. auratus gibelio* or *C. carpio* from the order Cypriniformes, suggesting that host specificity is as significant as spore morphology and predilection site for classification.

Among the myxosporean species collected from *C. auratus gibelio*, *Zschokkella* species, whose spores were found in the bile duct, exhibited the highest infection rate. Based on BLAST analysis, the *Zschokkella* samples from this study exhibited 100.0% similarity to previously submitted sequences of an undescribed species called "*Z. chongqingense*" found in the gallbladder of *C. auratus*. However, morphological and morphometric data for this species were unavailable due to the lack of a valid species description under this name at the time of publication, therefore it was not possible to verify the validity of this species. It is important to note that there is a species with a different generic identity but a similar specific name in its binomen, *Myxidium chongqingense* reported from the gallbladder of common carp (Eiras et al., 2011). The morphological differences between spores of *M. chongqingense* and this *Zschokkella* were significant enough to rule out any possibility of synonymy, leading to the classification of *Zschokkella chezhachei* n. sp. as a new species. Phylogenetic analysis revealed that *Z. chezhachei* n. sp. clustered together with "*Z. chongqingense*" and forms a well-supported monophyletic group with other *Zschokkella* species. Notably, the sequence identity with the aurantiactinomyxon type (KY475591) suggested that this actinospore stage corresponded to *Z. chezhachei* n. sp. Histopathological analysis unveiled that Z.

chezhachei n. sp. developed within the bile duct, as evidenced by the presence of polymorphic plasmodia in this area; however, very few dispersal spores were found in the gallbladder. According to Su & White (1995), fish with gallbladder infections often also harbor liver infections, suggesting that the gallbladder may serve as a secondary infection site. However, since no plasmodia or dispersal spores were found in the liver, it was to conclude that *Z. chezhachei* n. sp. developed primarily in the bile duct or gallbladder.

The spore morphology revealed that *M. pecsensis* n. sp. was similar to *M. intrachondrealis*, which infects the cartilage of the gill arches of *C. carpio*. Both species share identical predilection sites and tissue tropism, which crucial for differentiating gill-infecting myxosporean parasites (Molnar, 2002). *Myxobolus pecsensis* n. sp. also showed high similarities to *M. adlardi*; however, the two differ in infection site, as *M. adlardi* forms intrafilamental-epithelial plasmodia (Gupta & Kaur, 2016). There are relatively few cartilage-infecting *Myxobolus* spp., including *Myxobolus cerebralis* (Hoffman, 1990); *Myxobolus cartilaginis* (Hoffman et al., 1965); *M. cultus* (Yokoyama et al., 1995); *Myxobolus sharpeyi* (Molnár et al., 1996); *Myxobolus buckei* (Longshaw et al., 2003); *Myxobolus groenlandicus* (Buchmann et al., 2012); *Myxobolus albi* (Cavin et al., 2012); *Myxobolus aeglefini* (Karlsbakk et al., 2017); and *M. intrachondrealis* (Molnár, 2000; present study). Among these, three gills cartilage-infecting *Myxobolus* species (*M. cartilaginis*, *M. sharpeyi*, *M. intrachondrealis*) but only *M. intrachondrealis* and *M. pecsensis* n. sp. share the same predilection sites, precisely in islets surrounded by chondrocytes. However, molecular data and morphometric comparisons confirm that these are two distinct species, infecting different fish host. Phylogenetically, *M. pecsensis* n. sp. was closely related to Hungactinomyxon types from Hungary and China, suggesting that the actinospore stage of *M. pecsensis* n. sp. may correspond to the Hungactinomyxon type released from *B. sowerbyi*. To date, no myxozoan species have been associated definitively with Hungactinomyxon types. Therefore, future work should aim to collect more oligochaetes from this farm to clarify the life cycle. Additionally, *M. pecsensis* n. sp. placed in a well-supported clade with *M. lentisuturalis*, *M. cultus*, *M. lentisuturalis* and *M. cultrati*, all

having ellipsoidal spore shape and infecting similar host species, except for *M. cultrati* infecting the retina of *Pelecus cultratus*.

Identifying myxosporean species can be challenging due to incomplete descriptions that often lack important information on the spore and plasmodial characteristics, host specificity, tissue tropism or molecular data. For *M. diversus*, *S. molnari* and *M. intrachondrealis*, redescription was essential because of the diverse fish host specificity, the lack of spore morphometrics, and molecular data. *Myxobolus diversus* was first described from the fins of *C. auratus* in China, and later it was reported in Hungary from the same host and predilection site. Initially, spores collected from Hungary (Molnár & Székely, 2003) were thought to be *T. nikolskii*, which also develops in the cartilaginous fin rays of *C. carpio*. However, the spore characteristics were consistent with those of the genera *Myxobolus* than *Thelohanellus*. Comparative analysis by Molnár & Székely (2003) confirmed that the Hungarian specimens were morphologically identical to *M. diversus* from China (Chen & Ma, 1998). The present spores also shared same morphology but are slightly larger and possess a mucus envelope that was not included in the original description. Given the close relationship between *C. auratus gibelio* and *C. auratus*, *M. diversus* likely infects both fishes, similar to *M. hearti*, *M. lentisuturalis* and *Myxobolus turpisrotundus* Zhang, 2009 (Liu et al., 2010a, b; Ye et al., 2014). Histopathological analysis in the present study also corroborated findings of Molnár & Székely (2003) showing that plasmodia developed in the intrasegmental region between the two cartilaginous hemisegments of the fin rays, filling the intrasegmental space. Although no sequence data for the earlier *M. diversus* description exist in GenBank, phylogenetic analysis showed that *M. diversus* formed an independent branch and clustered within a clade comprising most gill-infecting *Myxobolus* spp. and a *Myxobolus* sp. infecting the fins. Based on its host, predilection site, and spore morphology, the myxozoan found in the fin rays of *C. auratus gibelio* is identified as *M. diversus*.

To date, there are only two gill-infecting *Sphaerospora* species, *S. molnari* and *S. carassii*. The spores observed in this study from *C. auratus gibelio* showed significant morphological and

morphometric similarity to *S. molnari*, previously described from the gills of *C. carpio* in Hungary and the Czech Republic (Eszterbauer et al., 2013), although they slightly differed in size. Distance matrix analysis revealed < 1% divergence between the *Sphaerospora* sequences from this study and previously published *S. molnari* sequences. According to established 18S rDNA divergence criteria for myxozoans, where < 1% divergence indicates conspecificity (Whipps & Kent, 2006; Bartošová & Fiala, 2011; Patra et al., 2017). The low divergence (0.40–0.50%) among the *S. molnari* isolates (JX431510 and JX431511) confirmed their conspecific status, supporting the high diversification of sphaerosporids within cyprinids hosts. Initially, *S. molnari* was considered specific to the gills of *C. carpio* (Molnár, 1980), but later Kent et al. (2001) also found it from the gills of *C. auratus*. Molecular analysis by Kent et al. (2001) showed that *S. molnari* did not cluster within the *Sphaerospora* clade, but it was instead closely related to *M. hearti*. This discrepancy likely resulted from the shorter DNA fragments used for analysis. Holzer et al. (2013) and Eszterbauer et al. (2013) only later recognized that *Sphaerospora* species often possess unusually long 18S rDNA inserts, exceeding 3000 base pairs. The validity of sequence AF378345 is also questionable due to its high divergence (48.5%), suggesting misidentification. Phylogenetic analysis in this study revealed that the *Sphaerospora* sequence from *C. auratus gibelio* was identical to *S. molnari* samples from Hungary and the Czech Republic. These results indicate that *S. molnari* is not limited to *C. carpio* but also infects *C. auratus gibelio*. Further research involving a broader sampling of *Sphaerospora*-infected gibel carp is recommended to confirm its host range.

Six *Myxobolus* species such as *M. cyprini*, *M. cyprinicola*, *M. dispar*, *M. encephalicus*, *M. intrachondrealis*, and *M. basilamellari*s were reported from *C. carpio* in Hungary (Molnár et al., 2025). Among them, *M. intrachondrealis*, which infects the gill cartilage, was also found in this study which is the second record of *M. intrachondrealis* infecting *C. carpio* in Hungary and worldwide**.** The spore morphology and measurements were consistent with *M. intrachondrealis* described by Molnár (2000), with only differences being the number of polar filament coils. This variation may be due to the limitations of resolution power of earlier microscopies, which might

have prevented accurate observation of the actual number of coils. Histological analysis also corroborated previous findings, showing plasmodia developing within the hyaline cartilage of the gill arches. Interestingly, molecular data revealed that *M. intrachondrealis* in this study shared 100.0% sequence identity to *M. cultrati,* although they were described as different species. Morphometric comparisons showed they are nearly identical, except that the host species and predilection site were different. *Myxobolus cultrati* was described by Borzák et al. (2016) from the retina of *P. cultratus*, but the description was based solely on dispersed spores and sequence data without confirmed plasmodial localization. At that time, there was no available sequence from *M. intrachondrealis* to compare with *M. cultrati*, therefore the identity of the two species was not foreseeable because of the difference in host specificity and predilection sites. The newly obtained sequences of *M. intrachondrealis* suggests that *M. cultrati* should likely be regarded as a synonym of *M. intrachondrealis.*

Besides *M. intrachondrealis*, *M. basilamellari*s were also detected in *C. carpio* collected from the Dömsöd fish farm. *Myxobolus basilamellaris* was first published in Europe (Kovacs & Molnár, 1983; Lom & Molnár, 1983; Eszterbauer, 2004), and later reported from the same host in Syria (Dayoub et al., 2007) and China (Wang et al., 2021), its occurrence in koi carp was documented by Zhang et al. (2023a). The spore morphology and measurements in this study were consistent with those described by Zhang et al. (2023a), although spores reported by Lom & Molnár (1983) were smaller and exhibited ten sutural markings and a mucous envelope; these features were not detected in the present study and Zhang et al. (2023a). In addition to *M. basilamellaris*, *M. dispar* and *M. intrachondrealis* also infected the gills of common carp, but their predilection sites were different. While *M. basilamellaris* formed plasmodia at the base of the gill filaments, *M. intrachondrealis* developed inside the cartilage of the gill arch, and *M. dispar* occurred in the arteries of the gill filaments. The observed predilection site of *M. basilamellaris* agreed with the histological analysis and previous findings by Lom & Molnár (1983). Moreover, the phylogenetic analysis confirmed that the sequence obtained from the base of gill filaments of *C. carpio* clustered

with other sequences of *M. basilamellaris*, clearly separating them from *M. intrachondrealis* and *M. dispar*.

Thelohanellus dogieli was the first species of *Thelohanellus* described from Hungary; however, it was later reclassified as *T. hovorkai* due to their close morphological similarity. According to the schematic drawing by Akhmerov (1955), the polar capsule of *T. dogieli* was pyriform and elongated. In comparison with illustrations by Chen & Ma (1998), the morphology of *T. dogieli* appeared similar to that of *T. serosae* n. sp., which possessed large and wide polar capsules. However, differences in predilection sites (*T. dogieli* parasitizes skin and gills, while *T. serosae* n. sp. parasitizes the serous membrane of kidney), spore thickness, spore width and polar capsule width, confirm these as distinct species. Apart from morphometric measurements, comparisons between *T. serosae* n. sp. and *T. dogieli* rely solely on schematic drawings, as actual spores' micrographs are unavailable in the literature. Akhmerov (1960) described *T. hovorkai* as having a large polar capsule occupying half of the spore body, a characteristic also observed in *T. serosae* n. sp. However, the two species can be differentiated by their mucous envelope: *T. hovorkai* exhibits a thin, loose-fitting mucous envelope, while *T. serosae* n. sp. has an ultra-thin and slim-fitting mucous envelope. Furthermore, *T. serosae* n. sp. and *T. hovorkai* in this study were found in similar predilection sites, such as the serous membranes. Although these species share similar predilection site and spore morphology, their plasmodia differ in size. The plasmodia of *T. hovorkai* were larger than those of *T. serosae* n. sp. Nonetheless, molecular data provided strong evidence for separating these taxa as distinct species. Remarkably, the actinospore stage of *T. serosae* n. sp. was confirmed through molecular analysis. Pairwise distance estimations revealed that sequences of *T. serosae* n. sp. from the fish farm (Ócsárd) shared 100.0% identity with the previous sequence of aurantiactinomyxon type B2 (DQ231148) from *B. sowerbyi* described by Eszterbauer et al. (2006).

Molecular techniques also promoted the separation of *T. paranikolskii* n. sp. and *T. nikolskii*, two closely related species that exhibit overlapping morphological features and have the same host

specificity. *Thelohanellus nikolskii* is a well-documented myxozoan parasite commonly infecting the fins and scales of common carp. In this study, we identified *T. nikolskii* from the fins of common carp as well as a closely related species that was previously undescribed, *T. paranikolskii* n. sp., from the skin of the same host. Morphologically and morphometrically, these two species are barely indistinguishable, displaying highly similar spore shape and morphometrics. The subtle morphological differences observed were only in spore thickness, the number of polar tubule coils, and the absence of a narrowed, flattened anterior end in *T. paranikolskii* n. sp. Based solely on these minor morphological variations, species differentiation was not possible; however, molecular analyses revealed a clear separation. Pairwise distance estimations showed that the sequence of *T. paranikolskii* n. sp. shared only 94.5% identity with newly obtained *T. nikolskii* (PV926531) and 93.8% with *T. pseudonikolskii* (OM801563), indicating that *T. paranikolskii* n. sp. is a genetically distinct species. Phylogenetic analysis supported this finding, placing *T. paranikolskii* n. sp. in a clade closely related to *T. nikolskii* and *T. pseudonikolskii*, all of which exhibit the characteristic '*nikolskii*-type' spore morphology. Furthermore, differences in tissue tropism provide additional argument for their differentiation. Histological examination revealed that the plasmodium of *T. paranikolskii* n. sp. was located beneath the skin, specifically within the stratum spongiosum of the dermis. In contrast, plasmodia of *T. nikolskii* developed within the cartilage of the fin rays and on the edge of the scales. This suggests that these two species are closely related yet distinct species.

Seventeen *Myxobolus* species have been reported from the *R. rutilus* to date (Eiras, 2005b, 2014, 2021; Batueva, 2020), although most were described solely based on morphology without molecular data. The present study demonstrates two additional novel *Myxobolus* species infecting the gills and kidneys of *R. rutilus*. Both *Myxobolus* n. sp. 1 and *Myxobolus* n. sp. 2 shared similar morphological features, differing only in the number of sutural markings. Their predilection sites also differed; while plasmodia of *Myxobolus* n. sp. 1 was found in the connective tissues of the gill arch, *Myxobolus* n. sp. 2 occurred in the kidneys. *Myxobolus* n. sp. 1 was compared with ten gill-

infecting *Myxobolus* spp. (Eiras, 2005b, 2014, 2021; Liu et al., 2016b), and showed the highest similarity to *M. fundamentalis*. Uniquely, *Myxobolus* n. sp. 1 exhibited a 'muelleri-like' morphology resembling *Myxobolus muelleri* Buetschli, 1882, the first *Myxobolus* species described from cyprinids. Phylogenetic analysis placed *Myxobolus* n. sp. 1 within the 'muelleri-type' clade alongside *M. erythrophthalmi*, *M. ellipsoides*, *M. shaharomae*, *M. peleci, M. rutili, M. dogieli*, and *M. zaikae*. But it was clearly distinct from these species and occupied a different gill predilection site. In contrast, *Myxobolus* n. sp. 2 was morphologically compared with *M. zaikae*, infecting the kidneys and liver of *R. rutilus*, but *M. zaikae* was smaller in size (Batueva, 2020). Additionally, it was also compared to other kidney-infecting *Myxobolus* spp. from cyprinids, including *M. shaharomae* from *A. alburnus* and *M. erythrophthalmi* from *S. erythrophthalmus* (Molnár et al., 2009b). While *M. erythrophthalmi* was slightly smaller, *M. shaharomae* showed close morphologically similarity. Genetic analysis revealed that *Myxobolus* n. sp. 2 clustered with *M. erythrophthalmi*, but was clearly separated from *M. shaharomae* and especially from *M. zaikae* despite sharing the same host and predilection site. These findings support that *Myxobolus* n. sp. 1 and *Myxobolus* n. sp. 2 are novel species based on their distinct molecular characteristics and predilection sites, despite their nearly identical spore morphology.

5.2. Actinosporeans in Hungary

Previous surveys of myxozoan infections in oligochaetes from aquaculture settings in Hungary were limited to a single spot, the TEHAG fish farm, where more than 30 actinospore types were identified, belonging to six collective groups: triactinomyxon, raabeia, neoactinomyxum, aurantiactinomyxon, hungactinomyxon, and echinactinomyxon, (El-Mansy et al., 1998b; Rácz et al., 2005; Eszterbauer et al., 2006; Marton & Eszterbauer, 2011). In this study, other fish farm locations in Hungary were investigated to survey myxozoan diversity and identify new actinospore stages of myxozoans and their alternate annelid hosts. Out of 5,976 examined oligochaetes, ten actinospore types were identified across four collective groups (triactinomyxon,

aurantiactinomyxon, neoactinomyxum, raabeia). Remarkably, seven of these actinospore types represented novel forms, and four of them were matched with myxosporean counterparts.

The prevalence of actinospores in oligochaetes collected from fish farms is expected to be higher than in natural waters (Özer et al., 2002). As the high density of host populations (fish and oligochaete) present in confined pond environments is more likely to facilitate the completion of the complex life cycle of myxozoans. In contrast, in natural habitats, infected fish can migrate to other areas, resulting in the reduction of the frequency of infection. Overall, the prevalence of infected worm in this study was low at 1.18%, which is lower than the prevalence rates reported by El-Mansy et al. (1998b) and Özer et al. (2002), who observed oligochaetes collected from fish farms in Hungary and an Atlantic salmon fish farm in Scotland. In contrast, the prevalence observed here is higher than those typically reported in natural freshwater environments, which generally range from 0.01% to 1.5% (Xiao & Desser, 1998b, c; Székely et al., 2004; Rosser et al., 2014; Xi et al., 2013, 2015; Borkhanuddin et al., 2014a; Zhao et al., 2016; Milanin et al., 2017; Rocha et al., 2019a, 2019c, 2024; Rocha, 2023). It can be attributed to low sampling collections that were conducted once a year or seasonally, and oligochaetes were studied in a short-term follow-up period. However, in this study, sampling was conducted twice over two years, the incidence was still low. This may be associated with the low infection rates of myxospores occurring in the fish ponds of Ócsárd and Ráckeve.

The calculated prevalence among the examined invertebrate host species showed that the *B. sowerbyi* population was mainly infected (12.1%). This correlated with studies by Yokoyama et al. (1993a, 1993b), who observed oligochaete species in a goldfish pond. In contrast, Rosser et al. (2014) reported 4.4% infection prevalence of *Dero digitata* in catfish ponds, while El-Mansy et al. (1998b) published a high prevalence (33–43%) in *T. tubifex*. These variations may reflect differences in host susceptibility. The myxozoan species from Ócsárd fish farm prefer *B. sowerbyi* as intermediate host than other host species such as *T. tubifex*, *L. hoffmesiteri* and *O. serpentina*.

The triactinomyxon type described in this study was morphologically similar to triactinomyxon type 2 (Székely et al., 2014), but differed morphometrically. Remarkably, the length and width of the caudal processes were distinct from all known triactinomyxon types, hence represented as a novel type (**Table S13**). The actinospore morphotypes involved in the life cycles show a consistent relationship with myxosporean genera in both marine and freshwater environments. In marine environment, the tetractinomyxon morphotype has been associated to the life cycles of species such as *Ellipsomyxa* (Køie et al., 2004; Rangel et al., 2009), *Gadimyxa* (Køie et al., 2007), *Parvicapsula* (Køie et al., 2013), *Sigmomyxa* (Karlsbakk & Køie, 2012), and *Ceratomyxa* (Køie et al., 2008). Similarly, in freshwater environments, the triactinomyxon morphotype is mainly associated with the life cycles of *Myxobolus* species (Yokoyama, 2003), exception for *M. cultus* (Yokoyama et al., 1995), *M. dispar* (Molnár et al., 1999a; Holzer et al., 2004) and *M. lentisuturalis* (Caffara et al., 2009), which possess raabeia type actinospore stages. Phylogenetic tree and genetic distance analyses supported this observation, as the triactinomyxon type 1 identified in this study clustered closely with a clade primarily contained of a gill-infecting *Myxobolus* spp. from cyprinid hosts. The triactinomyxon type 1 shared the highest genetic similarity with *M. diversicapsularis*, which parasitizes the gill lamellae of *R. rutilus*. The life cycle of *M. diversicapsularis* involves triactinomyxon actinospores (Eszterbauer et al., 2015), which highlights the possibility that the triactinomyxon type 1 could also complete its life cycle in cyprinid hosts by developing into a *Myxobolus* species in the gills of fish. To date, life cycles with triactinomyxon-type actinospores have been described for *M. drjagini* (El-Mansy & Molnár, 1997a), *M. hungaricus* (El-Mansy & Molnár, 1997b), *M. portucalensis* (El-Mansy et al., 1998c), *M. bramae* (Eszterbauer et al., 2000), *M. pseudodispar* (Székely et al., 1999, 2001), *M. macrocapsularis* (Székely et al., 2002), *M. intimus* (Rácz et al., 2004), *M. rotundus* (Székely et al., 2009c), *M. wootteni*, *M. diversicapsularis* (Molnár et al., 2010), *M. erythrophthalmi*, *M. fundamentalis* and *M. shaharomae* (Székely et al., 2014) in Hungary. Future studies should include sampling of cyprinid fish from the same ponds to

identify the corresponding myxospore stage and confirm the complete life cycle of the triactinomyxon type 1.

The raabeia type 1 exhibited morphology similar to raabeia type 2 (Borkhanuddin et al., 2014a) and showed minimal morphometric differences from “triactinomyxon ’F’” reported by Xiao & Desser, 1998b infecting *L. hoffmeisteri*. In contrast, raabeia type 2 described by Borkhanuddin et al. (2014a) displayed distinct morphometric variations due to its development in *Isochaetides michaelseni*. Both raabeia type 1 and “triactinomyxon ’F’” shared key features of the raabeia collective group, which is characterized by an elongated spore body without a style and caudal processes that curve upwards. However, Xiao & Desser (1998b) classified “triactinomyxon ’F’” within the triactinomyxon collective group rather than the raabeia collective group, possibly due to confusion or challenges in accurately assigning spore types to these groups in earlier studies. Given its morphological similarity to the raabeia collective group (lacking a style) and distinct differences from triactinomyxon types, raabeia type 1 was classified within the raabeia collective group. Phylogenetic analysis supported this classification, as raabeia type 1 clustered with “triactinomyxon ’F’” and was closely related to raabeia type 1 (KJ152184) and *Myxobolus dechtiari*, which is found in the gill filaments of *Lepomis gibbosus*. This relationship suggests that the corresponding myxospore stages may develop in the gills of centrarchid fish and share close affinities with the genus *Myxobolus*. Therefore, future research should focus on collecting *Lepomis gibbosus* and other centrarchid species from waters surrounding fish farms, particularly channels exchanging water with the ponds, and thoroughly examining their gills to identify *Myxobolus* species, which is a potential myxospore stage of the raabeia type 1.

Actinospores belonging to the aurantiactinomyxon collective group often presented challenges in comparison of morphological characteristics (Hallett et al., 2002; Eszterbauer et al., 2006; Zhao et al., 2016). In this study, all aurantiactinomyxon types were described using morphological, morphometric, and molecular analyses. Notable differences were observed between them in all morphological features, including the length and width of the caudal processes, spore body

diameters, and the number of secondary cells (**Table S15–S18**). Four aurantiactinomyxon types have been previously reported from species of the genus *Nais*, such as *Nais bretscheri* (Bartholomew et al., 1992), *Nais elinguis* (Trouillier et al., 1996), and *Nais* spp. (Grossheider & Korting, 1992; Borkhanuddin et al., 2014a; Borzák et al., 2021). However, no myxosporean infections have been reported from *O. serpentina*. It is possible that some aurantiactinomyxon types previously described from *Nais* spp. by Grossheider & Korting (1992), Borkhanuddin et al. (2014a), and Borzák et al. (2021), may originated from *O. serpentina*; the host morphology was not detailed in these studies, excluding the definitive identification. The present finding thus represented the first record of *O. serpentina* as an annelid host within the family Naididae for these parasites in freshwater environments, suggesting that this species may harbor greater myxozoan diversity than previously recognized. Additionally, ten aurantiactinomyxon types have been reported from *T. tubifex* (El-Matbouli et al., 1992; El-Mansy et al., 1998b; Székely et al., 1998, 2003; Hallett et al., 2002; Özer et al., 2002; Morris & Freeman, 2010). All of them exhibited distinct morphological and morphometric characteristics compared to aurantiatinomyxon type 2 identified in this study.

The aurantiactinomyxon type 3 and aurantiactinomyxon type 4 exhibited distinguish morphological features. Aurantiactinomyxon type 3 was characterized by leaf-like caudal processes, typical of the aurantiactinomyxon group, whereas type 4 displayed traits resembling the guyenotia type, with rounded caudal process ends. In contrast, aurantiatinomyxon type 2 resembled the echinactinomyxon type, which can be identified by its straight caudal processes that taper to sharp tips. However, recent taxonomic revisions refined the classification of actinospore collective groups. Rocha et al. (2019c) proposed invalidating the echinactinomyxon type due to its morphological overlaps with raabeia group, then recommended merging the guyenotia group into the aurantiactinomyxon collective group (Rocha, 2023). Given the close morphological resemblance of aurantiactinomyxon type 2 to typical aurantiactinomyxon features, along with auratiactinomyxon type 4, both were classified within the aurantiactinomyxon group. Furthermore,

phylogenetic tree reconstruction and genetic distance analyses revealed that these aurantiactinomyxon types clustered in a clade with other members of the aurantiactinomyxon group, supporting their classification within this collective group.

Molecular analyses were conducted on the aurantiactinomyxon types in this study to help clarify their transient stages of the life cycles. Among the six aurantiactinomyxon types identified, only three had known myxosporean counterparts. This study described a new species, *Z. chezhachei*, from the bile duct of *C. auratus gibelio*. The 18S rDNA sequence of aurantiactinomyxon type 4 showed 100.0% identity with *Z. chezhachei* and 99.9% similarity to a previously reported aurantiactinomyxon type (KY475591). Although, aurantiactinomyxon type 4 exhibited close genetic similarity to the previously described sequences, the lack of corresponding morphological and morphometric data prevented direct comparison. Therefore, aurantiactinomyxon type 4 was described as a novel actinospore and confirmed as the actinospore stage of *Z. chezhachei*. This finding was further validated through experimental transmission, in which twenty naïve *B. sowerbyi* were placed in a plastic container and exposed to *Z. chezhachei* spores collected from *C. auratus gibelio*, successfully confirming their participation in the same life cycle. Notably, the morphology and measurements of aurantiactinomyxon type 4 closely resembled the guyenotia type of Xi et al. (2013). It is possible that the actinospore reported by Xi et al. (2013) and aurantiactinomyxon type 4 are the same, as both were found developing in the same oligochaete host species collected from ponds with *C. auratus gibelio*. Given that the myxospore stage was found in the *C. auratus gibelio*, it can be assumed that the actinospore described by Xi et al. (2013) corresponds to aurantiactinomyxon type 4; however, further examinations, such as sequencing, are needed to prove this postulate.

Thelohanellus hovorkai plasmodium was identified in common carp from the fish farms of Dömsöd and Ócsárd, along with its actinospore stage at the Ócsárd fish farm. Pairwise distance estimations revealed that the newly obtained sequences of *T. hovorkai* (PV926536), aurantiactinomyxon type 5 (PV942516) and aurantiactinomyxon type 6 (PV942515), shared

99.9% to 100.0% identity with previously reported sequences of *T. hovorkai* (DQ231155) and aurantiactinomyxon types (DQ231153, DQ231154). Despite the existing genetic identity, aurantiactinomyxon type 6 exhibited distinct morphometric differences, especially in the length of its caudal processes and polar capsules, compared to previously described aurantiactinomyxon types (Yokoyama, 1997; Székely et al., 1998; Eszterbauer et al., 2006). In contrast, aurantiactinomyxon type 5 showed only minor variations from aurantiactinomyxon type 'A' (Eszterbauer et al., 2006). With the inclusion of these findings, *T. hovorkai* is now associated with three different aurantiactinomyxon morphotypes, all of which have been collected from individuals of *B. sowerbyi*. Interestingly, the morphometric characteristics of *T. hovorkai* reported by Yokoyama (1997) and Székely et al. (1998) were similar to each other. Remarkably, Hallett et al. (2004) detected eleven triactinomyxon types with different morphometrics but identical genotypes, all released from *T. tubifex*. Similarly, Marquès (1984) documented two forms of *Aurantiactinomyxon pavinsis*, a 'grande forme' and a 'petite forme', which differed in the size of their caudal processes. These findings suggested that actinospores can exhibit significant intraspecific morphometric variations. The phenomenon can also be observed among myxospores. For example, Hallett et al. (1998) reported morphometric variability in *Sphaeractinomyxon ersei*, while Lom & Hoffman (1972) demonstrated that size and shape in *Myxobolus cerebralis* varied significantly within rainbow trout fingerlings. Similarly, mature spores of *Myxobolus encephalicus* (Mulsow, 1911; Dyková et al., 1986) and *Myxobolus* species studies by Mitchell (1989) showed great intraspecific variations depending on the tissues of origin and host species.

The neoactinomyxum type 1 identified in this study showed morphological and molecular matches with neoactinomyxum type JD (KY784590; Xi et al., 2015), which is known as the actinospore stage of *T. wangi*. Phylogenetic tree reconstruction and genetic distance analyses supported this finding, as the neoactinomyxum type 1 clustered together with *T. wangi* found in the gill filaments of *C. auratus gibelio*, and its corresponding actinospore stage. Similarly, raabeia type 2, which morphologically resembled the raabeia types reported by Yokoyama et al. (1995), Eszterbauer et

al. (2006) and Xi et al. (2013), are known to represent the actinospore stage of *M. cultus*. In the phylogenetic tree, raabeia type 2 clustered with *M. cultus* infecting the gill filaments of *C. auratus* and *C. auratus gibelio*, along with its actinospore stage (HQ613407). Despite these matches, examination of 112 *C. auratus gibelio* individuals (7.0–23.0 cm) from the Ócsárd and Szigetvár fish farms revealed no infections by *T. wangi* or *M. cultus*. This was likely due to both *T. wangi* and *M. cultus* developed in young fish, from fry to fingerling stages (Yokoyama et al., 1995; Yuan et al., 2015), while this study primarily focused on mature *C. auratus gibelio* (7.0–23.0 cm). Remarkably, this is the first report of the actinospore stage of *T. wangi* in Hungary, and the second report of the actinospore stage of *M. cultus*. The first report of *M. cultus* was published by Eszterbauer et al. (2006) from a fish farm, although they were also unable to find infected *C. auratus gibelio* or *C. auratus*. Therefore, future studies should focus on examining fry and fingerling stages of *C. auratus gibelio* to complete the life cycle of these species in Hungary.

5.3. Myxosporean species in Malaysia

Myxozoan research in Malaysia remained limited, covering only four states (Terengganu, Kelantan, Kedah and Selangor), which have focused on cultured ponds and natural waters, including freshwater, brackish, and marine environments (Molnár et al., 2006a, b; Székely et al., 2009a, b; Bartošová et al., 2011; Székely et al., 2012; Borkhanuddin, 2013; Borkhanuddin et al., 2014b, 2020a, b; Fiala et al., 2015b; Freeman & Krismundsson, 2015; Shahar, et al., 2017; Samshuri, 2018; Samshuri & Borkhanuddin et al., 2024). In Terengganu, studies on myxozoan fauna were conducted in Tasik Kenyir, the Terengganu River, Setiu Wetlands, the Merang Estuary, and the South China sea. This study aimed to expand the survey to additional river systems, including Sungai Tong, Setiu, Sungai Nerus, Kuala Nerus and small channels across Kuala Terengganu, Terengganu, as well as to widen the range of studied fish species.

The genus *Barbonymus* comprises ten species that are widely distributed across Southeast Asia (Kottelat, 2001; Cheng et al., 2004; Batubara et al., 2018; Garcia et al., 2020; Kenthao et al., 2020). In Malaysia, three species including *B. schwanefeldii*, *B. gonionotus*, and *B. altus* are particularly

common in freshwater ecosystems. These species are not only ecologically important but also hold significant commercial value, both as ornamental fish and as food, due to their high market price and consumer preference (Mansour et al., 2017; Zakaria et al., 2018). During the examination of myxozoan infection in these fishes, six novel myxozoan species (three *Myxobolus* spp., two *Thelohanellus* spp., one *Ceratomyxa* sp.), and two previously described species (*M. dykovae*, and *T. zahrahae*) were identified from *Barbonymus* spp., based on analyses of the 18S rDNA gene sequences and morphological characteristics. These species exhibited distinct tissue preferences, with two *Myxobolus* spp. infecting the muscle cells, two *Myxobolus* and two *Thelohanellus* spp. infecting the gills, one *Thelohanellus* sp. infecting the fins and one *Ceratomyxa* sp. occurring in the gallbladder.

Organ and tissue specificity are key features for identification of myxosporean species (Molnár et al., 2002). Besides the gills, muscle cells were also common infection sites for various myxosporean parasites in fish (Molnár & Eszterbauer, 2015). As of 2021, approximately 75 of 979 *Myxobolus* spp. had been described from muscle tissue (Eiras et al., 2005b, 2014, 2021). The majority of these muscle-dwelling species, such as *M. cyprini*, *M. musculi* and *M. pseudodispar*, belonged to the 'pseudodispar' morphological type and formed intracellular plasmodia. The *Myxobolus* spp. (*M. barbonymi* n. sp. and *M. faizahae* n. sp.) identified in this study also exhibited 'pseudodispar'-like morphology. Notably, *M. barbonymi* n. sp. developed intracellular plasmodia, resembling those of *M. pseudodispar*, *gt*whereas *M. faizahae* n. sp., formed intramuscular plasmodia. Phylogenetic analyses and pairwise distance estimations confirmed the validity of *M. barbonymi* n. sp. and *M. faizahae* n. sp. as new species. These results indicated that the phylogenetic relationships among *Myxobolus* spp. in this study showed some correlation with their predilection sites in the host. Specifically, the newly identified *Myxobolus* spp. that infect muscle tend to cluster together within one clade. This finding was consistent with previous studies that highlighted the importance of tissue tropism (Fiala, 2006; Carriero et al., 2013; Shin et al., 2014). Notably, the two unequal polar capsules also appear to be relevant for the phylogenetic

relationships of *Myxobolus* species in this study. The newly identified *M. barbonymi* n. sp. and *M. faizahae* n. sp., along with other muscle-infecting *Myxobolus* species have two unequal polar capsules (except for *Myxobolus stanlii* Iwanowicz, Iwanowicz, Howerth, Schill, Blazer et Johnson, 2013, which has equal polar capsule sizes) (**Figure 15**).

The gills are the most commonly affected organs by myxosporean parasites (Ahmad & Kaur, 2018). In this study, two newly described gill-infecting myxosporeans: *M. gonionoti* n. sp. and *T. barbonymi* n. sp., were identified along with two previously described species *M. dykovae* and *T. zahrahae*. *Myxobolus gonionoti* n. sp. was compared with all known gill-infecting *Myxobolus* species from the literature, and exhibited the closest morphological resemblance to *M. dykovae*. Additional comparisons with related species, including *M. sangei* and *M. carlhubbsi*, revealed distinguishing features that supported the designation of *M. gonionoti* n. sp. as a new species. Interestingly, *M. gonionoti* n. sp. may be confused with *M. macrocapsularis*, a species previously reported from *B. gonionotus* by Ky & Te (2007) in Chinh et al. (2023). However, a BLAST search revealed only 77% sequence similarity to *M. macrocapsularis*, which strongly supported that it is a distinct species. The sequence was excluded from the phylogenetic analysis since only those showing >88.0% similarity with that were included in the phylogenetic tree. It is important to note that earlier identifications of *M. macrocapsularis* were based solely on morphological features, as molecular data were not widely used at the time. Therefore, the spores reported by Ky & Te (2007) may have been misidentified, and it is plausible that they were actually observing *M. gonionoti* n. sp.

Plasmodia of *T. barbonymi* n. sp. were situated in the gill arches, an unusual location for *Thelohanellus* species. Most of them typically develop in gill lamellae and gill filaments. There are only a few species whose predilection site is different, such as *Thelohanellus valeti* Fomena et Bouix, 1987 that have been reported from both stomach and gill arches of *Barbus jae* and *Barbus aspilus* from Cameroon, correlating with *T. barbonymi* n. sp. These findings highlighted the diversity of tissue tropism among *Thelohanellus* species and supported the acceptance of *T.*

barbonymi n. sp. as a novel taxon. Although *T. barbonymi* n. sp. shared morphological similarities with *T. zahrahae* infected the gills of different hosts within the same genus; it represented a distinct taxon based on its genetic characteristics and host species.

This study also detected two previously described gill-infecting myxozoan species, T. *zahrahae* and *M. dykovae*. Both species were identified based on morphological characteristics consistent with earlier descriptions and were validated by molecular analyses. *T. zahrahae* differed notably from previously reported *Thelohanellus* species from *B. gonionotus* (such as *T. catlae*) in several key features. The most significant difference was in the shape of the plasmodia; *T. zahrahae* exhibited elongated plasmodia, while *T. catlae* had spherical-shaped plasmodia. The molecular analysis of 18S rDNA sequences confirmed the identification of these samples as *T. zahrahae* and *M. dykovae*, supporting their classification despite the minor morphological differences.

The phylogenetic relationships among *Myxobolus* spp. and *Thelohanellus* spp. observed in this study mostly showed a correlation with their predilection sites in the host. *M. dykovae* clustered with predominantly gill-infecting *Myxobolus* spp., but also with some *Myxobolus* spp. that infect other organs (**Figure 14** and **Figure 18**). However, *M. gonionoti* n. sp. (a gill infecting sepcies) was clustered exclusively with muscle-infecting *Myxobolus* spp. (**Figure 14–15**). Its unique position can be explained by the absence of closely related species that also infect gills in current genetic databases, suggesting that such species are still undiscovered. It is also plausible that these parasites evolved in parallel with muscle parasites but later adapted to infect gills (Eszterbauer, 2004). Regarding the *Thelohanellus* lineage, *T. barbonymi* n. sp. and *T. zahrahae* clustered with other gill-infecting *Thelohanellus* spp. (**Figure 14–15**). *Thelohanellus barbonymi* n. sp. formed a close relationship with *T. gonionoti* n. sp., which infected the fins of *B. barbonymus*, while, *T. zahrahae* formed a sister group with *Thelohanellus* sp. (MK332024) from *M. marginatus*. This pattern highlighted the complex phylogenetic connections within the genus *Thelohanellus*, which often exhibit polyphyly and intermix with *Myxobolus* clades.

The morphometrics of *T. gonionoti* n. sp. were distinct from those of any previously described *Thelohanellus* spp., including those characterized by truncated anterior ends. *Thelohanellus gonionoti* n. sp. possessed a unique feature in which the polar capsule position leans towards the side of the spore body, in contrast to *T. barbonymi* n. sp. and *T. zahrahae*. Relatively abundant the number of *Thelohanellus* spp. have been reported to infect fins, including *Thelohanellus assambai* Fomena, Marqués, Bouix et Njine, 1994; *Thelohanellus avijiti* Basu et Haldar, 2003; *Thelohanellus caudatus* Pagarkar et das, 1993; *Thelohanellus disporomorphus* Basu, Modak et Haldar, 2006; *Thelohanellus globulosa* Singh et Kaur, 2012; *Thelohanellus habibpuri* Acharya et Dutta, 2007; *Thelohanellus kalavatae* Singh et Kaur, 2013; *Thelohanellus leshanensis* Zhao et Ma, 1992; *Thelohanellus nikolskii* Akhmerov, 1955; *Thelohanellus potaili* Lalitha Kumari, 1969; *Thelohanellus sanagaensis* Fomena, Marqués, Bouix et Njine, 1994; *Thelohanellus shaochingensis* Chen in Chen et Ma, 1998; *Thelohanellus shortii* Qadri, 1967; *Thelohanellus wusihensis* Chen in Chen et Ma, 1998; *Thelohanellus deri* Singh et Kaur, 2012; *Thelohanellus haldari* Singh et Kaur, 2012; *Thelohanellus rohi* Singh et Kaur, 2015. Among these, *T. assambai* from *Labeo* sp., was only species that exhibited truncated anterior ends. Unfortunately, no nucleotide sequence of *T. assambai* was available for comparison with *T. gonionoti* n. sp. to clarify their phylogenetical relationship. Furthermore, 18S rDNA sequence and pairwise distance analyses have confirmed that *T. gonionoti* n. sp. represented a valid new species (**Table 14**). Phylogenetic analyses have revealed that *T. gonionoti* n. sp. clustered within the gill-infecting *Thelohanellus* spp. clade consisted *T. barbonymi* n. sp., *Thelohanellus* sp., and T. *zahrahae* (**Figure 14–15**).

Geographical origin can also serve as an important criterion for phylogenetic relationships. Notably, all *Thelohanellus* species in this study, which were collected from Southeast Asia, formed a cohesive cluster. Specifically, *T. gonionoti* n sp., *T. barbonymi* n. sp., *T. zahrahae* were identified in Malaysia, while *Thelohanellus* sp. was found in Thailand.

Ceratomyxa parasites are primarily known as marine species, making the presence of *Ceratomyxa* in the freshwater ecosystem quite uncommon. To date, nineteen *Ceratomyxa* species have been documented in the gall bladders of freshwater fish from South America, Europe and Asia (**Table S23**). Eleven of these species possessed worm-like plasmodia with active motility, a feature that primarily associated with freshwater *Ceratomyxa* species from South America (Zatti et al., 2017; Zatti et al., 2018a; da Silva et al., 2020; Adriano & Okamura, 2021; Araújo et al., 2022; Bittencourt et al., 2022; Franzolin et al., 2022; Zatti et al., 2023). The plasmodia of *C. schwanefeldii* n. sp. also exhibited this motility feature, indicating that this feature was not exclusive to South American *Ceratomyxa* species. The plasmodial morphology of *C. schwanefeldii* n. sp. closely resembled that of *Ceratomyxa* sp. 7 (Adriano et al., 2021), as both were elongated with blunt poles. However, *Ceratomyxa* sp. 7 was observed to exhibit fast undulatory locomotion, while the plasmodia of *Ceratomyxa ranunculiformis* demonstrated slow undulatory motility similar to that of *C. schwanefeldii* n. sp. The variability in motility may be attributed to cytoskeletal elements, different size of internal vacuoles, and a rigid glycocalyx that facilitate movement in accordance with their hydrostatic skeleton (Adriano et al., 2021). This structure was considered to prevent the premature release of immature plasmodia into the bile (Adriano & Okamura, 2017) or to aid in nutrient acquisition (Adriano et al., 2021). In terms of morphometrics, the plasmodia of *C. schwanefeldii* n. sp. were similar to those of *C. gracillima*, being slightly shorter in length (151.6 vs 181.0 μm) but somewhat wider (15.1 vs 11.4 μm).

Morphological and morphometric data of the novel *C. schwanefeldii* n. sp. were compared with other freshwater *Ceratomyxa* species that parasitized the gall bladders of various hosts from different geographical regions (**Table S23**). The spores of *C. schwanefeldii* n. sp. exhibited a distinctly strong arched shape resembling *C. amazonensis*, but differed from all known freshwater *Ceratomyxa* species. Among Asian ceratomyxidae, *C. huangheensis* and *C. hongtzensis* shared some morphometric similarities; however, *C. hongtzensis* can be distinguished via its slightly thicker spore wall, while *C. huangheensis* had larger spores. In comparison to known marine

species, the morphology of *C. schwanefeldii* n. sp. was similar to *Ceratomyxa protopsettae* Fujita, 1923, *Ceratomyxa flexa* Meglitsch 1960, *Ceratomyxa hokarari* Meglitsch 1960, *Ceratomyxa uncinata* Meglitsch 1960, *Ceratomyxa torquate* Meglitsch 1960, *Ceratomyxa trachinocephali* Kpatcha, Diebakate, Faye et Toguebaye, 1996, *Ceratomyxa trichiuri* Kpatcha, Diebakate, Faye et Toguebaye, 1996, and *Ceratomyxa costata* Aseeva, 2001 (Eiras, 2006).

Phylogenetic analysis of 18S rDNA showed that the *Ceratomyxa* species formed two main subclades: a larger subclade B1, comprising species infecting freshwater fish from South America, and a smaller subclade B2, containing *Ceratomyxa* species that parasitize marine fish. In this study, *C. schwanefeldii* n. sp. formed a distinct lineage closely related to *Unicapsulocaudum mugilum*. Despite their phylogenetic proximity, the sequence similarity between the two was only 92.8%, that substantial genetic divergence. Both are clustered within the freshwater *Ceratomyxa* clade, with a possible shared ancestor origin. Morphologically, *C. schwanefeldii* n. sp. clearly differed from *U. mugilum*; *C. schwanefeldii* n. sp. exhibited the typical crescent-shaped morphology with a sutural line visible between the shell valves and two polar capsules, while *U. mugilum* possessed an ophidian shape with a horn-like protuberance, long tapering tail, and a single pyriform polar capsule. The close phylogenetic association may reflect an evolutionary transition within ceratomyxids, as proposed by Yang et al. (2017). Notably, this was the first *Ceratomyxa* species recorded from *Barbonymus*. The absence of closely related *Ceratomyxa* species from similar hosts might have been the reason of *C. schwanefeldii* n. sp. formed a separate lineage, appearing more closely related to *U. mugilum*. The reason for the close genetic relationship between *C. schwanefeldii* n. sp. and *U. mugilum* remained unclear, as *U. mugilum* differs remarkably in morphology. Hence, further sampling especially in Malaysia, is required to clarify the molecular relationship between *Ceratomyxa*, and *Unicapsulocaudum*.

Additionally, *C. schwanefeldii* n. sp. was phylogenetically distinct from the sensu stricto Amazonian freshwater *Ceratomyxa* lineage, likely due to its Asian origin. Its clustering with the brackish-water *U. mugilum*, from China, may reflect ecological influences, particularly host

migration between freshwater and brackish environments. *Barbonymus schwanefeldii* is a potamodramous species (Bakar et al., 2023) that migrates between upstream and downstream habitats as juveniles to mature into adults, where saltwater incursion occurs seasonally.

The 28S rDNA analysis also placed *C. schwanefeldii* n. sp. within a clade of marine *Ceratomyxa* species. The availability of 28S rDNA sequences in GenBank is limited, so the phylogenetic analysis provided only limited information. This study represented the second 28S rDNA sequence for a *Ceratomyxa* that infects a freshwater host, following *C. ranunculiformis*.

There are two species from genus *Leptobarbus* in Malaysia such as *L. hoevenii* and *L. rubripinna*. *Leptobarbus hoevenii* is a native cyprinid found in rivers and lakes in Malaysia, Cambodia, Indonesia, Laos, Thailand, and Vietnam (Mohsin & Ambak, 1983; Roberts, 1989; Rainboth, 1993; Vidthayanon et al., 1997; Kottelat, 2001). In contrast, *L. rubripinna* is a native of the Mekong River in Thailand, and occurs also in Laos, Cambodia and Vietnam, but was considered an introduced species in Malaysia. Previous studies in Malaysia had investigated myxozoan parasites in *L. hoevenii* and described *M. leptobarbi* from the muscle tissue (Székely et al., 2009a), while in Thailand, *M. koi*, a common parasite of *C. carpio* found in gill lamellae, had been reported from the gallbladder and kidneys of *L. rubripinna* (Thumvittayakul et al., 2018). In this study, *Myxobolus* n. sp. 3 was described from the muscle tissue of *L. rubripinna*. Morphometrically, *Myxobolus* n. sp. 3 closely resembled *M. leptobarbi* in most measurements, except for the different number of polar filament coils in the smaller polar capsule and the presence of a mucus envelope. Meanwhile, *Myxobolus* n. sp. 3 showed similarities to *M. koi*, differing mainly in spore length and had similar polar capsule sizes. Molecular analyses confirmed that *Myxobolus* n. sp. 3 represented a distinct species to *M. leptobarbi*, suggesting host specificity despite similar predilection sites. However, the sequence of *M. koi* from Thumvittayakul et al. (2018) was unavailable in GenBank for comparison, as their identification was based solely on morphological characteristics. The available *M. koi* sequence from *C. carpio* was compared with *Myxobolus* n. sp. 3, which strongly supported its recognition as a distinct species. Since *Myxobolus* n. sp. 3 shared the same host

species as *M. koi* described by Thumvittayakul et al. (2018), and only dispersed spores were observed in the gallbladder and kidneys, it was plausible that the spores reported by Thumvittayakul et al. (2018) were misidentified and actually represented *Myxobolus* n. sp. 3.

Myxobolus n. sp. 4 represented the first myxozoan parasite described from female specimens of *B. binotatus* and notably, the first species to be reported from ovarian tissue in Malaysia. Morphologically, it closely resembled *M. csabai* and *M. nekrasovae*, while its morphometrics were most similar to *Myxobolus* n. sp. 12 described in this study from the muscle of *O. waandersi*, differing only in the number of sutural markings. Molecular analysis confirmed that *Myxobolus* n. sp. 4 was distinct from *M. csabai* and formed a distinct basal branch within a gill-infecting *Myxobolus–Thelohanellus* clade comprising species with unequal polar capsules (**Figure 20**). Its unique placement likely reflected the absence of closely related ovarian-infecting species in current databases. In contrast, *Myxobolus* n. sp. 12 clustered within the *Myxobolus–Thelohanellus* clade containing species from similar host taxa in Malaysia, highlighting the role of host specificity and geographic distribution in shaping phylogenetic relationships.

The genus *Labiobarbus* is widely distributed in Southeast Asia, with five species reported in Peninsular Malaysia such as *L. leptocheilus*, *L. fasciatus*, *L. festivus*, *L. sabanus* and *L. ocellatus* (Ismail, 1989; Roberts, 1993). In this study, only *L. leptocheilus* was collected, from which seven novel species were identified from different predilection sites. The first species described was *Myxobolus* n. sp. 5 that found in the connective tissue of the gill arch. Morphologically and morphometrically, *Myxobolus* n. sp. 5 closely resembled *M. tribolodonus* and *M. paludinosus* reported from the gills, suggesting that parasites found in similar predilection sites may share similar morphotypes such as oval-ellipsoidal shape. This pattern parallels muscle-infecting species like *M. pseudodispar*, *M. cyprini*, and *M. musculi*, which share the characteristic 'pseudodispar-like' morphology. However, molecular analyses revealed that *Myxobolus* n. sp. 5 clusters not with gill-infecting *Myxobolus* spp. but with newly described *Myxobolus* species; *Myxobolus* n. sp. 9 from the same host (*L. leptocheilus*) and similar spore morphotypes (*Myxobolus* n. sp. 9,

Myxobolus n. sp. 13, *M. csabai*, *M. tasikkenyirensis*), highlighting the influence of host specificity and spore characteristics on phylogenetic relationships. Furthermore, *Myxobolus* n. sp. 5 formed a distinct basal branch, likely reflecting the absence of closely related gill-arch–infecting taxa in current databases.

In addition to *Myxobolus* n. sp. 5, *Myxobolus* n. sp. 6, *Myxobolus* n. sp. 7 and *Myxobolus* n. sp. 8 were also identified from *L. leptocheilus*. Interestingly, these species exhibited different predilection sites (gill arches, gill filaments, fins and ovarian tissue, respectively), but shared similarly pyriform spores. Among them, only *Myxobolus* n. sp. 8 possessed equal polar capsules, while *Myxobolus* n. sp. 6 and *Myxobolus* n. sp. 7 exhibited unequal polar capsules. While *Myxobolus* n. sp. 6 and *Myxobolus* n. sp. 8 shared typical *Myxobolus* features consistent with their phylogenetic position, *Myxobolus* n. sp. 7 was distinguished by a unique polar capsule structure; one prominent and one rudimentary ('toyamai-like'). Although species such as *Myxobolus toyamai* (Kudo, 1917), *Myxobolus paratoyamai* (Kato et al., 2017) and *Myxobolus stellatus* (Stilwell et al., 2020) share a superficially similar 'toyamai-like' morphology, their polar capsules occupy half of the spore body, whereas in *Myxobolus* n. sp. 7 they extend over three-quarters of it. Moreover, most 'toyamai-like' species have been reported from gills, while *Myxobolus* n. sp. 7 was found in the fins, which may explain its basal position in the phylogenetic tree. This unique position suggests that additional 'toyamai-like' *Myxobolus* morphotypes infecting fins may yet be undiscovered in Malaysia. Notably, all three species clustered within a clade comprising parasites from the same host species, reinforcing the influence of host specificity in shaping phylogenetic relationships.

Previous studies reported two *Myxobolus* species with morphotypes similar to *Myxobolus* n. sp. 9 and *Myxobolus* n. sp. 13, namely *M. tasikkenyirensis* from *O. vittatus* and *M. osteochili* from *Osteochilus hasselti*. The phylogenetic analyses corroborated that *Myxobolus* n. sp. 9 and *Myxobolus* n. sp. 13 formed a sister relationship with *M. tasikkenyirensis* and *M. csabai*. This

relationship may be attributed to tissue tropism, as all species were reported from muscle tissue except *M. csabai*, which was described from the kidneys of *O. hasselti*. However, *M. osteochili* was excluded from the phylogenetic tree reconstruction due to low sequence similarity (<88%). Pairwise distance analysis showed that *Myxobolus* n. sp. 9 exhibited the highest similarity to *Myxobolus* n. sp. 13 (97.4%) and 96.2% similarity to *M. tasikkenyirensis*. Although *M. csabai* displayed distinct morphological traits, such as unequal polar capsules and a different predilection site, its placement within the same clade likely reflected the close phylogenetic relationship among their fish hosts and their shared geographical distribution. Although they shared similar morphotypes and predilection sites, their occurrence in different host species (*L. leptocheilus* and *O. waandersii*) and difference in the 18S rDNA supported their recognition as distinct novel species.

In Hungary, two gill-cartilage-infecting *Myxobolus* spp., *M. pecsensis* n. sp. and *M. intrachondrealis* were described in this study from *C. auratus gibelio* and *C. carpio*. Notable, two additional novel gill-cartilage-infecting species**,** *Myxobolus* n. sp. 10 and *Myxobolus* n. sp. 11, were identified from *O. waandersii* in Malaysia for the first time. Morphologically and morphometrically, all four species differed significantly. Spores of *Myxobolus* n. sp. 11 were the smallest, whereas those of *Myxobolus* n. sp. 10 were the largest. *Myxobolus* n. sp. 11 was distinguished by its definitely thicker shell valves compared to other gill-cartilage *Myxobolus* spp. supported its designation as a novel species. In terms of predilection sites, *Myxobolus* n. sp. 11, *M. pecsensis* n. sp. and *M. intrachondrealis* all developed in the gill cartilage, consistent with their close clustering within the same phylogenetic clade (**Figure 14** and **Figure 25**). Interestingly, phylogenetic and pairwise distance analyses revealed that *Myxobolus* n. sp. 11 was closely related to the raabeia-type actinospores described in this study, suggesting a possible link between their life stages. However, *Myxobolus* n. sp. 10 was positioned distinctly from this clade, forming a basal branch within a larger group that included predominantly *Myxobolus* and *Thelohanellus* species infect gill and other organs (**Figure 23**). This divergence may be explained by its unusual

infection site, the plasmodia located under the gill filament base attached to the gill arch cartilage and bulbus arteriosus of heart (**Figure S28A**), for which no data are currently available for species with a similar location. The distinct phylogenetic placements confirmed *Myxobolus* n. sp. 10 and *Myxobolus* n. sp. 11 as separate, novel species.

Two novel *Myxobolus* species, *Myxobolus* n. sp. 12 and *Myxobolus* n. sp. 13, were found from the muscle of *O. waandersii*. Microscopic examination revealed clear morphological differences, *Myxobolus* n. sp. 12 exhibited unequal polar capsules, larger and oval-shaped plasmodia, whereas *Myxobolus* n. sp. 13 possessed equal polar capsules, smaller and elongate-oval plasmodia. In addition to molecular data, histological analyses provided critical evidence for species differentiation. Histologically, *Myxobolus* n. sp. 12 developed intracellularly within muscle fibers, while *Myxobolus* n. sp. 13 developed intercellularly among muscle cells. These findings collectively confirmed that the two species are distinct, supported by molecular, morphological, and histological characteristics.

Most previously described *Thelohanellus* species have been reported from the gills rather than other organs such as the skin, scales, fins, or abdominal cavity (Basu et al., 2006; Zhang et al., 2013). In this study, in addition to *T. gonionoti* n. sp., *T. barbonymi* n. sp. and *T. zahrahae*, two further novel species, *Thelohanellus* n. sp. 1 and *Thelohanellus* n. sp. 2, were described from *L. leptocheilus* and *O. waandersii*, respectively. Large, whitish, oval-shaped plasmodia of *Thelohanellus* n. sp. 1 were found in the skin of *L. leptocheilus*. *Thelohanellus* n. sp. 1 were compared with all skin-infecting *Thelohanellus* species from the literature and showed closely resembled to *T. leshanensis*. Subsequent comparisons with other *Thelohanellus* spp. from different organs displayed close resembled to *T. liaohoensis* reported in the mucosal membranes and gallbladder of *C. carpio*. Molecular analysis supported its novelty, revealing a close phylogenetic relationship with *Myxobolus* n. sp. 12. Notably, *Thelohanellus* n. sp. 1 represents the first *Thelohanellus* species described from *L. leptocheilus* and the first skin-infecting *Thelohanellus*

reported in Malaysia. In contrast, *Thelohanellus* n. sp. 2 formed large, whitish, oval plasmodia within connective tissue between the fin rays of *O. waandersii*. Comparisons with fin-infecting *Thelohanellus* spp. from previous studies revealed distinct morphological differences. *Thelohanellus* n. sp. 2 exhibited small, oval spores with polar capsule leans towards the side of the spore body, features resembling Indian *Thelohanellus* species. Although it resembled to *T. goldi*, it differed in the number of polar tubules coils, parallel to the long axis of the spore polar capsule, and host species. Further confirmation was provided by the phylogenetic analysis, which showed that *Thelohanellus* n. sp. 2 positioned basally within a clade composed primarily of myxozoan parasites from the same host species. The placement can be explained by the fact that there are currently no comparable sequences in GenBank for the Malaysian fin-infecting *Thelohanellus* species, thereby confirming its status as a new species.

Based on BLASTn analysis, the *Myxidium* sample collected from gallbladder of *L. leptocheilus* in this study showed 99.4% sequence similarity to *Zschokkella* sp. (KM401441; 2057 base pairs) previously reported from the gallbladder of *Labeo rohita*. However, no morphological and morphometric data are available currently for that species, due to the lack of a published valid description. The spores of *Myxidium* n. sp. 1 exhibited typical *Myxidium* morphology such as fusiform or sigmoid shape with pointed ends and pyriform polar capsules located at each pole (Lom & Dyková, 2006), in which clearly differed from the characteristics of *Zschokkella* spp. These morphological distinctions ruled out synonymy, supporting its classification as a new species. Phylogenetic analysis further showed that *Myxidium* n. sp. 1 clustered with *Zschokkella* sp. (KM401441) within a well-supported monophyletic clade of *Myxidium* species, suggesting that *Zschokkella* sp. (KM401441) likely represents a member of the *Myxidium* genus. The previous misidentification of *Myxidium* as *Zschokkella* may have resulted from limited microscope resolution or insufficient taxonomic expertise. Therefore, additional sampling of *L. rohita* in Myanmar to obtain specimens for morphological and morphometric comparison, as well as resequencing of the existing sample, is necessary to confirm this assumption.

The genus *Trichopodus* comprises six valid species namely *Trichopodus trichopterus*, *Trichopodus leerii*, *Trichopodus pectoralis*, *Trichopodus microlepis*, *Trichopodus cantoris*, and *Trichopodus poptae* (Low et al., 2014). Among them, four species can be found in Malaysia; *T. trichopterus, T. pectoralis*, *T. leerii* and *T. cantoris* (Froese & Pauly, 2025). Owing to their colourful bodies, these species are valued as ornamental aquarium fish and commonly used as bait. Previous studies by Székely et al. (2009a) described *H. daoudi* from the gills of *T. trichopterus*, while Ky & Te (2007) described *H. schizura* (common parasite of *Esox lucius* infecting the connective tissue of eye muscles) from the gills of *T. trichopterus*, though their exact location was not specified. In this study, *Henneguya* n. sp. 1 was identified from the gill filaments of the same host. Morphologically, it closely resembles *H. daoudi* exhibiting blunt anterior ends but differed slightly in morphometrics, particularly in caudal appendage length (**Table S35**). In contrast, *H. schizura* differed significantly, being larger in size and distinct host and tissue specificity (*E. lucius* in connective tissue of eye muscles vs *T. trichopterus* in the gills). Molecular analysis supported the novelty of *Henneguya* n. sp. 1 showing 98.7% (969 bp) similarity to *H. daoudi*; the sequence of *H. schizura* was unavailable in GenBank for comparison. Phylogenetic analysis confirmed that *Henneguya* n. sp. 1 was closely related to *H. daoudi*, with both species forming a sister group to *Henneguya* n. sp. 2, a parasite identified from the genetically related fish host, *T. pectoralis*. Therefore, longer sequences of *H. daoudi* and molecular data for *H. schizura* are needed to confirm their taxonomic identities and enable more comprehensive phylogenetic comparisons with *Henneguya* n. sp. 1.

Trichopodus pectoralis is widely distributed across Southeast Asia, covering countries especially in Thailand, Vietnam, Malaysia, Indonesia and Myanmar (Paepke, 2009) and is naturally found in the Mekong Basin of Thailand, Cambodia and Vietnam (Rainboth, 1996; Kottelat, 2001). In Malaysia, this species was intentionally introduced to support subsistence fisheries in paddy-growing areas (Chong et al., 2010) but is not considered invasive as there is no evidence that indicates it dominates natural habitats. The present study represents the first investigation of

myxozoan parasites in *T. pectoralis*, leading to the identification of five novel species. The first species found was *Myxidium* n. sp. 2 identified in the gallbladder. Morphological and morphometric comparisons with previously described *Myxidium* spp. revealed significant differences. Its morphology was most similar to *M. djolonensis* from Cameroon, sharing the rare feature of a fusiform body with truncated ends, in contrast to the most *Myxidium* spp. possessing pointed ends. Despite their resemblance, they differed in spore dimensions, geographical location, and host specificity. Phylogenetic tree reconstruction and pairwise distance analyses showed that *Myxidium* n. sp. 2 was closely related to *Zschokkella* sp. (MT840090) from *E. suratensis* and Myxosporea (KP030767) from *Synodontis* sp. However, due to the lack of available morphological and morphometric data for these species, direct comparison was not possible. Since *Myxidium* n. sp. 2 exhibited typical *Myxidium* morphology and clustered in the *Myxidium* clade (**Figure 24**), it was confirmed to belong to genus *Myxidium*. Furthermore, this clade consisted *Myxidium* spp. infecting diverse fish hosts across Malaysia, Kenya, India and China, highlighting its broad geographic and host diversity. Further sampling of *E. suratensis* and *Synodontis* sp. is recommended to enable full species descriptions of *Zschokkella* sp. and Myxosporea and clarify their taxonomic relationships.

In addition to *Myxidium* n. sp. 2, four novel *Henneguya* species were identified in various organs and tissues of *T. pectoralis.* Specifically, *Henneguya* n. sp. 2 was found in the gill lamellae, *Henneguya* n. sp. 3 occurred in the cartilaginous tissue of the gills, *Henneguya* n. sp. 4 developed in the gill arches, and *Henneguya* n. sp. 5 was found in the pharynx. Each of these newly described *Henneguya* spp. exhibited distinct morphological and morphometric characteristics. For example, *Henneguya* n. sp. 2 and *Henneguya* n. sp. 3 possessed ellipsoidal spores, while *Henneguya* n. sp. 4 and Henneguya n. sp. 5 exhibited fusiform spores. Notably, *Henneguya* n. sp. 2 was distinguished from the others by possessing the longest caudal appendages. Noteworthy finding was observed in *Henneguya* n. sp. 3, which displayed a unique polar capsule arrangement not previously reported from this genus. This species possessed unequal polar capsules, and the plane of spore body and

polar capsules deviate from the median, providing strong evidence that *Henneguya* n. sp. 3 represented a novel species. Asides from unique morphological traits and predilection sites, phylogenetic analyses also supported the novelty of all four *Henneguya* spp. Genetic identity and phylogenetic positioning consistently differentiated each species within the *Henneguya* clade. *Henneguya* n. sp. 2 clustered was grouped with *H. daoudi* and *Henneguya* n. sp. 1, all infecting *T. trichopterus* from Malaysia, suggesting a close evolutionary relationship link to their hosts. In contrast, *Henneguya* n. sp. 3, *Henneguya* n. sp. 4, and *Henneguya* n. sp. 5 formed a distinct clade from *Henneguya* n. sp. 2, possibly due to different infection sites. Furthermore, *Henneguya* n. sp. 4 and *Henneguya* n. sp. 5 were closely related characterized with fusiform spores and demonstrated a sister-group relationship to *Henneguya* n. sp. 3, which had ellipsoidal spore. Hence, the *Henneguya* species from *T. pectoralis* in this study were described as novel species based on their unique predilection sites, distinctive morphological and morphometric features, and corroborating molecular evidence.

Only few studies have investigated myxozoan parasites infecting the genus *Channa*. To date, most records originate from India and China. In India, ten species have been described, including *Myxobolus cylindricus* Sarkar, Mazumdar et Pramanik, 1985 from *C. gachua*; *Myxobolus maruliensis* Sarkar, Mazumdar, Pramanik et 1985 from *Channa marulius*; *Myxobolus noblei* Sarkar, 1982 from *Channa striata*; *Myxobolus aligarhensis* Bhatt et Siddiqui, 1964, *Myxobolus andhrae* Kumari, 1969, *Myxobolus channai* Kalavati, Sandeep et Narasimhamurti, 1981 and *Henneguya chaudhuryi* Bajpai et Haldar, 1982 from *Channa punctatus*; *Henneguya renalis,* and *Myxidium islampurium* Sarkar, Mazumber et Pramanik, 1985 from *Channa marulius*. Additionally, more than thirty myxozoan parasites have been reported from *Channa* in China by Chen & Ma (1998) and Zhang et al. (2023b). This study conducted an extended survey of myxozoan parasites particularly in *C. gachua*, as it previously known to host only a single species, and revealed seven novel species from its different organs and tissues, including one *Myxidium* sp. and six *Henneguya* spp.

Plasmodia and dispersed spores of *Myxidium* n. sp. 3 were found in the gallbladder of *C. gachua*. This species exhibited a unique morphological feature, as it possessed a concave body with slightly truncated ends that had not been previously reported in other *Myxidium* species. In comparison, *M. islampurium* from *C. marulis* displays a fusiform spore body with tapered ends (Eiras et al., 2011), distinguishing the two species. Unfortunately, the absence of *M. islampurium* sequences in GenBank prevented molecular comparison. Molecular analyses revealed that *Myxidium* n. sp. 3 shared highest similarity (91.0%) to *M. chuatsi*, which also exhibits a concave body but with tapered ends. Phylogenetic analysis confirmed that *Myxidium* n. sp. 3 as a distinct species, as it formed a basal position within *Myxidium* clade, comprising *Myxidium* spp. infecting diverse hosts (*S. chuatsi*, *Labeo horie*, *Cranoglanis bouderius*, *Culter alburnus*, *L. leptocheilus*, *L. rohita*, *Myxocyprinus asiaticus* from Order Centrarchiformes, Cypriniformes and Siluriformes) from China, Kenya, Malaysia and Myanmar. The basal placement of *Myxidium* n. sp. 3 reflects the absence of available *Myxidium* sequences from *Channa* species in current databases. It is plausible that inclusion of *M. islampurium* sequence data would position both species in close proximity on the phylogenetic tree, given their shared host genus. Notably, this represents the first record of a *Myxidium* species infecting *C. gachua*. Further surveys of *Channa* species across Southeast Asia could help clarify host-parasite coevolution, reveal the diversity of myxozoans in this genus, and better characterize the morphological features of Malaysian *Myxidium*.

Previous studies have reported twelve *Henneguya* spp. from five *Channa* spp., including *C. argus*, *C. maculatus*, *C. striata*, *C. punctatus* and *C. marulius* (Sarkar et al., 1985; Chen & Ma, 1998; Chaudhary et al., 2017). However, no *Henneguya* parasites had been described in *C. gachua* before this study. Here, six *Henneguya* spp., namely *Henneguya* n. sp. 6, *Henneguya* n. sp. 7, *Henneguya* n. sp. 8, *Henneguya* n. sp. 9, *Henneguya* n. sp. 10 and *Henneguya* n. sp. 11 were identified from different predilection sites, including serous membrane of internal organs, ovarian tissue, vertebral column, gills, muscle tissues, and muscle near the caudal peduncle. *Henneguya* n. sp. 6 and *Henneguya* n. sp. 10 exhibited oval spores resembling *H. caquetaia* from *Caquetaia spectabilis*,

H. guanduensis from *Hoplosternum litoralle* in Brazil, *Henneguya disparis* and *Henneguya ovaliformis* infects *C. striata* from China. Spores of *H. caquetaia* and *H. guanduensis* were larger that those of *Henneguya* n. sp. 6 and 10. For detailed comparison no morphometric data about *H. disparis* and *H. ovaliformis* were available (Chen & Ma, 1998). Despite their morphological similarity, *Henneguya* n. sp. 6 and *Henneguya* n. sp. 10 differed in caudal appendage and polar capsule lengths, confirming their distinct identities.

Although, both *Henneguya* n. sp. 10 and *Henneguya* n. sp. 11 were found in the skeletal muscle, the exact location of plasmodia were differed. Histological slides revealed that *Henneguya* n. sp. 10 developed among skeletal muscle cells in the body while *Henneguya* n. sp. 11 developed among the skeletal muscle cells of caudal peduncle. Morphologically, both species differed significantly, *Henneguya* n. sp. 10 having oval spores and *Henneguya* n. sp. 11 showing ellipsoidal spores. Morphology of *Henneguya* n. sp. 11 was compared to other *Henneguya* spp. infecting *Channa* spp. and resembled *Henneguya sinensis* from *C. argus* in overall shape, but their morphometric data were missing (Chen & Ma, 1998). The closest morphological similarity was observed between *Henneguya* n. sp. 11 and *Henneguya* n. sp. 8 found in the vertebral column both possessed ellipsoidal spores but differed slightly in size. Similarly, *Henneguya* n. sp. 7 and *Henneguya* n. sp. 9 exhibited comparable elongated to lanceolate spores but differed in predilection sites, being localized in ovarian tissue and gills, respectively. Comparisons with previously described *Henneguya* species revealed no identical forms. Only two ovarian-infecting species, *Henneguya oviperda* (Sokolov et al., 2019) and *Henneguya amazonica* (Rocha et al., 1992) have been reported to date, both possessed considerably larger spores. Given the strong organ and tissue tropisms characteristic of myxozoans, the six *Henneguya* species described here are recognized as novel taxa, distinguished primarily by their unique predilection sites and morphological characteristics.

Beyond the morphological differences mentioned above, the six *Henneguya* species possessed different genetic attributes. The six *Henneguya* species exclusively from *C. gachua* formed a well-supported monophyletic group, indicating their high level of host specificity. Such specificity is a

recurring feature in myxozoan phylogeny, where host-parasite associations often reflect the evolutionary lineages (Okamura et al., 2015). The clustering of *Henneguya* from the same host suggested possible coevolutionary processes between the parasites and *C. gachua*, which was also supported by their distinct group apart from *Henneguya* species of other hosts. Although all species infected *C. gachua*, they displayed variation in their predilection sites: serous membrane or kidney, muscle, vertebral column, gills, and ovaries. This ecological diversity within a single host species could indicate adaptive radiation of these parasites to exploit different microenvironments or tissues within the fish (Fiala et al., 2015c). These findings highlighted not only genetic but also ecological differentiation, supporting the recognition as separate species. The exclusive Malaysian origin of these *Henneguya* spp. might have reflected regional diversification, possibly driven by the biogeographic history of *C. gachua* populations in Southeast Asia. The phylogenetic tree structure showed that these species formed their own clade, separate from other *Henneguya* parasites of different hosts or geographic regions, suggesting a unique evolutionary lineage within the Malaysian biota. This pattern was consistent with previous studies that reported the strongest evolutionary signals, represented in myxozoan phylogenetic trees, were host affiliation and geographic clustering (Carriero et al., 2013; Zatti et al., 2018b; Velasco et al., 2025). The inclusion of the novel six *Henneguya* spp. in the phylogeny expanded the understanding of myxozoan biodiversity in freshwater fish, especially in Southeast Asia. Their distinct clustering highlights the unrecognized diversity within the *Henneguya* group and underscores the importance of molecular phylogenetics in identifying cryptic species.

5.4. Actinosporeans in Malaysia

During this study, six actinospore types belonging to three collective groups namely raabeia, triactinomyxon, and aurantiactinomyxon were described from 2,666 examined oligochaetes collected from Tasik Telabak were described. In the past, several attempts to survey actinospores in Malaysia had been conducted in various locations such as Tasik Kenyir, the Terengganu River, and fish farms in Terengganu and Kelantan; however, these efforts were unsuccessful in detecting

any actinospore stages (Székely C., personal communication). Nevertheless, about 23 myxospore species had been described from fishes inhabiting those areas (Molnár et al., 2006a, 2006b; Székely et al., 2009b, 2009c, 2012; Borkhanuddin, 2013). Therefore, this study represented the first successful report describing actinospore stages of myxozoans in Malaysia.

The prevalence rate of infected worms in this study was low (0.90%), consistent with previous studies reporting generally low infection levels in wild environments (Xiao & Desser, 1998b, c; Xi et al., 2013, 2015; Zhao et al., 2016; Milanin et al., 2017; Rocha et al., 2019a, 2019c, 2024). Conversely, El-Mansy et al. (1998a) and Székely et al. (2003) reported a high prevalence of actinospores in wild oligochaete populations from Lake Balaton and Japan. The low prevalence could be explained by limited samplings, as oligochaete collection was conducted twice (over a two to three month period) rather than year-round and seasonally (McGeorge et al., 1997; Oumouna et al., 2003; Eszterbauer et al., 2006). Additionally, some worms died after one week of separation in the cell-well plates without releasing actinospores during the observation period. Moreover, sampling was conducted out between in July to August and September to November, coinciding with the dry and intermonsoon periods in Malaysia. According to Patra (2023), a high abundance of oligochaetes is recorded in the rainy/monsoon season. High rainfall favours dense macrophyte growth due to increased food resources, shelter and suitable breeding areas. Similarly, fish populations tend to increase in rivers during the rainy/monsoon season from November to March (Radhi et al., 2017) as a result of greater water flow and nutrient availability (Saifullah et al., 2014), which often coincides with spawning activity. Some fish species also migrate to breeding grounds during this period. The higher presence of fish and oligochaetes during the monsoon season provides optimal conditions for actinospores proliferation as more potential hosts are available, leading to higher infection rates. Therefore, seasonal sampling during pre-monsoon (July–October), monsoon (November–March) and post-monsoon (March–June) periods is crucial to acquire more accurate data on the occurrence of actinospores in Malaysia.

The raabeia type 1 described in this study showed minimal morphometric differences from other raabeia types reported in the literature, with only some overlapping features (**Table S43**). Morphologically, the spores closely resembled raabeia type 1 of Oumouna et al. (2003) and the raabeia type described by Eszterbauer et al. (2006), but they possessed at least one different character. Comparison of 18S rDNA sequences indicated that the present raabeia type 1 did not correspond to any myxozoan sequences available in GenBank, although 23 freshwater myxozoan species had been identified in Malaysia. Notably, despite the presence of the same fish species in Malaysia and neighbouring countries like Vietnam, Thailand and Myanmar, the current sequences of actinospores also did not match any of the myxozoan species identified in those adjacent countries (U-taynapun et al., 2011; Chinh et al., 2023; Thu et al., 2023). Genetic distances among the raabeia type 1 and other closely related species were no greater than 90% (**Table 19**), indicating a clear genetic distinction. This divergence was likely due to geographical isolation among Malaysia, China, Hungary, the USA, and Japan. Phylogenetic analyses revealed that raabeia type 1 was grouped within a clade exclusively consisted of *Myxobolus* spp. parasitizing fish of the Order Cypriniformes, and was closely related to one of the new *Myxobolus* species described in this study from the gill cartilage of *O. waandersii* in Clade B. This finding suggested that the corresponding myxospore stage of raabeia type 1 might develop in Cypriniformes hosts. Future studies should aim to collect additional cyprinid hosts to elucidate the complete life cycle and confirm the myxospore counterpart of this raabeia type.

According to current knowledge, the aurantiactinomyxon group represented one of the most diverse collective groups, comprising approximately 64 known types (Rocha, 2023; Rocha et al., 2024). In this study, four additional novel aurantiactinomyxon types were identified from two different oligochaete hosts. None of the aurantiactinomyxon types described here exhibited morphological or morphometric resemblance to any previously reported aurantiactinomyxon types (**Table S44**). When compared to each other, all four types showed significant differences across all morphometric measurements. Although, aurantiactinomyxon type 1, aurantiactinomyxon type

2 and aurantiactinomyxon type 3 were found in the same oligochaete host (*Aulophorus* sp.), clear distinctions were observed in the length of their caudal processes. For example, aurantiactinomyxon type 2 exhibited the longest caudal processes among the three and ranked as the second largest when compared to all aurantiactinomyxon types reported in the literature, following only the aurantiactinomyxon type of Xi et al. (2013) from *B. sowerbyi*. In contrast, aurantiactinomyxon type 1 possessed the shortest caudal processes, and its spore morphology closely resembled that of the aurantiactinomyxon type of *T. hovorkai* described in this study, sharing a similar number of secondary cells, but being overall smaller in size. Furthermore, aurantiactinomyxon type 2 was compared with aurantiactinomyxon type 4, which originated from a different host; although they shared morphological similarities, they differed substantially in morphometric measurements. Notably, aurantiactinomyxon type 4 exhibited a unique feature, having prominent, elongated pyriform polar capsules protruding from the anterior of the spore body, distinguishing it from any known aurantiactinomyxon types.

Traditionally, spore morphology was used as the sole criterion for myxozoan identification before the advent of molecular techniques. However, subsequent research has shown that relying on morphology alone can be problematic, especially in cases where actinospores display overlapping or similar morphological features. For instance, studies by Hallett et al. (2002), Eszterbauer et al. (2006), Zhao et al. (2016), and Rocha et al. (2019b) have reported instances where genetically identical aurantiactinomyxon type, neoactinomyxum type, and sphaeractinomyxon type actinospores exhibited phenotypic variations in spore shape. In the present study, genetic analyses confirmed that all analyzed aurantiactinomyxon types represented distinct species. However, aurantiactinomyxon type 4 could not be amplified, and thus, no genetic data are available for this type. Phylogenetic analyses revealed that all three aurantiactinomyxon types are positioned within *Henneguya-Myxobolus* mixed Clade A (**Figure 27**). Aurantiactinomyxon type 2 and aurantiactinomyxon type 3 clustered closely with several species of *Henneguya*, particularly those infecting *Ictalurus punctatus* and related catfish. This close relationship suggested a possible life

cycle of both aurantiactinomyxon types from *Henneguya* species that develop in Malaysian catfish or related catfish hosts. In contrast, aurantiactinomyxon type 1 formed a sub-cluster with *Myxobolus miyairii* from *Silurus asotus* within *Henneguya* cluster of clade A. This may indicated that the myxospore counterpart of aurantiactinomyxon type 1 could belong to the *Myxobolus* genus infecting *Silurus* species. However, there are currently no known aurantiactinomyxon life cycles that correspond to *Myxobolus* genus (**Table 1**). The observed clustering of aurantiactinomyxon type 1 with *Myxobolus* may also result from the limited *Henneguya* sequence data available in GenBank for *Silurus* spp. and Malaysian species, thus restricting direct life cycle comparisons.

According to the currently available data, the second most diverse actinospore collective group after aurantiactinomyxon is triactinomyxon, with 59 types described in the literature (Borkhanuddin et al., 2014a; Székely et al., 2014; Xi et al., 2015; Rangel et al., 2015, 2016b). Triactinomyxon is the most common actinospore stage representing the genus *Myxobolus*. The triactinomyxon type 1 identified in this study differed from all known triactinomyxon types possessing 8 secondary cells, in terms of their spore shape and dimensions. Key morphological traits used for triactinomyxon identification include caudal processes, spore body, and style (Xiao & Desser, 1998b; Özer et al., 2002; Hallett et al., 2004, 2005; Xi et al., 2017). The unique features distinguishing this spore from all known triactinomyxon types were the much shorter style and caudal processes found in triactinomyxon type 1. The ratio of caudal processes to spore body reached 1.07 (29.9/27.9), whereas for most triactinomyxon types the ratio ranged between 2.72 and 16 (**Table S45**). Moreover, this spore lacked the typical anchor-shaped caudal process characteristics of triactinomyxons, further supporting their classification as a novel type.

In this study, due to preservation error and the low probability of resampling, 18S rDNA sequences could not be obtained for the aurantiatinomyxon type 4 and triactinomyxon type 1. Therefore, classification relied solely on morphological and morphometric data. Despite this limitation, these types were confidently classified as novel types based on their unique features, host specificity and geographical location. However, further specimens from the same sampling site are

recommended for molecular analysis to confirm their status as novel types and to identify their myxosporean stage and fish host. Therefore, based on these distinctive morphological and morphometric characters, the aurantiactinomyxon type 4 and triactinomyxon type 1 described herein were considered novel until additional molecular data become available.

CHAPTER 6

CONCLUSION AND RECOMMENDATIONS

Earlier studies on myxozoan parasites were largely limited to descriptions of their morphology, biology and ecology, while knowledge on their phylogeny and evolution remained unclear. With the introduction of molecular tools, more questions have emerged about the evolutionary history, functional roles, life cycle and cryptic diversity of myxosporeans in aquatic and terrestrial ecosystems. In this study, morphological, histological and molecular analyses were conducted for each species to better understand their taxonomy, evolutionary relationships, host-parasite interaction, as well as their life cycles.

Overall, the extensive number of myxosporean species and actinosporean stages reported in this study demonstrated that the biodiversity of myxozoans in Malaysian and Hungarian freshwater ecosystems has still many species to be discovered. From the Hungarian collection of this study, fifteen myxosporean parasites from three fish hosts and ten actinosporean were identified across three fish farms. Among them, eight were described as novel myxosporean species and seven as novel actinosporean types. Hungary harbors numerous fish species (Froese & Pauly, 2025), fewer than Malaysia, due to its geographical status as a landlocked country, with only natural rivers and lakes. To meet domestic demands for food and support sport fishing, numerous fish farms have been established to facilitate fish production, import, and export. Previous myxozoan research on Hungarian fish farms has been scarce; however, this study expanded the surveys to three additional fish farms. Therefore, further investigations should include more fish farms throughout the country to better understand parasite distribution. Moreover, only a small proportion of Hungarian fish species have been reported to host myxozoans to date (Molnár et al., 2025). Further studies should focus on examining additional fish species to reveal the full extent of myxozoan diversity within Hungarian ichthyofauna.

Among the fifteen species described in this study, most of them was found in *C. auratus gibelio*. This species is considered invasive in Hungary and has therefore received limited research attention. In contrast, in China *C. auratus gibelio* is an important cultured fish species valued for consumption, and consequently, it has been extensively studied for myxozoan parasites, with more than 40 species described. In Hungary, only few parasitology surveys had previously been conducted, reporting only three species, *M. diversus*, *Hoferellus carassii* and *Sphaerospora carassii*. In this study, a comprehensive parasitology survey on *C. auratus gibelio* revealed seven myxosporean species, including four that were newly described. Notably, the muscle-infecting pathogenic species *M. lentisuturalis*, previously reported from China, was recorded for the first in Hungary. These results highlight that even invasive fish species can host different myxozoan assemblages in new environments, likely due to the presence of the same oligochaete hosts and environmental conditions that influence parasite adaptation. Therefore, it is recommended that other invasive fish species in Hungary be examined to identify potentially overlooked myxozoan parasites associated with these hosts.

Thelohanellus imrei n. sp. was described from the connective tissues of gill arch and pharynx of *C. auratus gibelio*, while *Thelohanellus hovorkai* and *T. nikolskii* are well-established parasites of *C. carpio* in Hungary to date. Another species, *T. kitauei*, has been detected only in its actinospore stage, suggesting that *T. kitauei* may also occur in Hungary. In this study, in addition to *T. hovorkai* and *T. nikolskii*, two new *Thelohanellus* species were identified: *T. serosae* n. sp., which developed in the serous membrane of the kidney and intestine, and *T. paranikolskii* n. sp., which was found in the skin. *Thelohanellus serosae* n. sp. exhibited morphological and predilection site similarities with *T. hovorkai*, while *T. paranikolskii* n. sp. shared similar features but different predilection site with *T. nikolskii*. However, molecular analyses clearly distinguished these as separate species whose differences could not be resolved through morphology data. This finding suggests that *T. serosae* n. sp. and *T. paranikolskii* n. sp. may have been previously encountered in Hungary but were misidentified as *T. hovorkai* and *T. nikolskii* due to their similar morphological features and

infection sites. Therefore, it is strongly recommended that molecular analyses be incorporated into future species descriptions, especially when dealing with cryptic species that cannot be reliably distinguished based on morphology alone.

The present study successfully validated three life cycles: *Zschokkella chezhachei* n. sp., *Thelohanellus serosae* n. sp., and *Thelohanellus imrei* n. sp. Although a large number of myxozoan parasites have been described in Hungary, information on their corresponding actinosporean stages remains limited. Therefore, further investigations should focus on identifying these missing life-cycle counterparts. The life cycle of *Z. chezhachei* n. sp. was confirmed through molecular analysis and experimental infection, whereas the life cycles of *T. serosae* n. sp. and *T. imrei* n. sp. were inferred using molecular data. These results demonstrate that molecular analysis provides a rapid and reliable means of linking actinospore and myxospore stages; however, complementary experimental infection studies are necessary to confirm these molecular findings.

Notably, the 35 species described from Malaysia originated solely from fish collected in two rivers in Terengganu and small channels across Kuala Terengganu, along with six actinosporean types from Tasik Telabak. Previous studies on Malaysian myxozoans have been limited to only a few states and islands in Malaysia, including Terengganu, Kelantan, Selangor, Langkawi Island, Pangkor Island and the Andaman Sea, producing a total of 41 species (**Table 2**). Combined with the findings of this study, a total of 76 species are now known from Malaysia. Remarkably, this study provided the first successful report and description of actinosporean stages of myxosporeans in Malaysia, a goal that had not been achieved in earlier surveys. However, only six actinosporean types were identified, and none could be linked to the 76 myxospores species described, thus preventing the completion of their life cycles. This limitation may be attributed to the short sampling period duration and the low number of oligochates available during the examination, which reduced the likelihood of detecting infected worms. Given that Malaysia comprises 13 states with numerous rivers, lakes, and islands, continued and expanded efforts are essential to explore

the country's myxozoan diversity further. Future surveys should include broader geographical regions such as rivers, lakes, estuaries and coastal waters.

Two actinospore types, aurantiactinomyxon type 4 and triactinomyxon type 1 from Malaysia were described solely based on morphological and morphometric analyses, as molecular data could not be obtained. This limitation resulted from preservation issues that occurred during sample storage and transportation. Therefore, future research should focus on obtaining molecular data for these actinospore types to confirm their status as novel forms, clarify their phylogenetic relationships, and identify their corresponding myxosporean stages and fish hosts.

The fish examined in this study comprised both native and introduced species; however, endemic species were not included. In Malaysia, 49 endemic fish species have been documented, most of which occur in the states of Sabah and Sarawak (Froese & Pauly, 2025). Since 35 myxosporean species were recorded from both native and introduced hosts, it is likely that Malaysian endemic fish also harbor a hidden diversity of myxosporeans. Therefore, future myxozoan research in these regions should be expanded to include a wider range of endemic fish species, as they may represent unexplored reservoirs of myxozoan biodiversity.

The 28S rDNA marker has been widely utilized alongside 18S rDNA in myxozoan phylogenetic studies due to several key benefits. It provides greater sequence length and incorporates both conserved and variable regions, allowing enhanced resolution of relationships, especially among closely related species. In this study, all amplifications were performed using 18S rDNA, except for *C. schwanefeldii* n. sp., which was also amplified using 28S rDNA. Future studies should include amplification using 28S rDNA to better understand phylogenetic relationships, as this gene is more conserved and provides additional informative sites for analysis. This approach could enhance resolution and confidence in evolutionary inferences compared to relying solely on 18S rDNA sequences, thereby improving the accuracy of myxozoan taxonomy and phylogeny.

NEW SCIENTIFIC RESULTS

1. Documentation of eight novel myxosporean species from three fish hosts collected from three fish farms in Hungary. These records were supported by morphological, morphometric, histological, and molecular analyses. The newly identified species belonged to three genera: *Myxobolu*s, *Thelohanellus*, and *Zschokkella.* Additionally, *Myxobolus diversus* and *Myxobolus intrachondrealis* were provided with molecular data for the first time. Of these, 6 species were scientifically described.

2. Description of seven novel actinosporean types from two fish farms in Hungary. These actinosporeans belonged to three collective groups: Raabeia, Aurantiactinomyxon, and Triactinomyxon.

3. Documentation of 33 novel myxosporean species from native and introduced fish species collected from two rivers and small channels across Kuala Terengganu, Terengganu, Malaysia. These records were supported by morphological, morphometric, histological, and molecular analyses. The newly identified species belonged to five genera: *Myxobolu*s, *Thelohanellus*, *Henneguya*, *Myxidium*, and *Ceratomyxa*. Of these, 6 species were scientifically described.

4. First report and description of actinosporean stages in Malaysia, specifically from Tasik Telabak, Terengganu. Six novel actinosporean types were identified belonging to three collective groups: Raabeia, Aurantiactinomyxon, and Triactinomyxon.

5. Elucidation of three new myxosporean life cycle from fish farms in Hungary, as listed below:

- *Zschokkella chezhachei* n. sp.
- *Thelohanellus imrei* n. sp.
- *Thelohanellus serosae* n. sp.

LIST OF PUBLICATIONS

Peer-reviewed journal articles

1. **Suhaimi, N.S.**, Colunga-Ramírez, G., Sellyei, B., Cech, G., Molnár, K., & Székely, C. (2023). The first detection of *Myxobolus lentisuturalis* Dyková, Fiala et Nie, 2002, a highly pathogenic muscle-infecting parasite of gibel carp (*Carassius auratus gibelio* Berg, 1932) in Hungary. *Journal Fish Diseases*, 46 (12), 1367–1376. https://doi.org/10.1111/jfd.13855.
2. Colunga-Ramírez, G., **Suhaimi, N.S.**, Cech, G., Molnár, K., Székely, C., & Sellyei, B. (2024). Morphological and molecular characterisation of two closely related species: *Myxobolus tihanyensis* n. sp. and *Myxobolus sandrae* Reuss, 1906. *International Journal of Parasitolology: Parasites and Wildlife,* 23, 100909. https://doi.org/10.1016/j.ijppaw.2024.100909.
3. **Suhaimi, N.S.**, Sellyei, B., Cech, G., Székely, C., & Borkhanuddin, M.H. (2024). First record and description of actinospore stages (raabeia, triactinomyxon, and aurantiactinomyxon types) of fish parasitic myxozoans from Malaysia. *International Journal of Parasitolology: Parasites and Wildlife,* 24, 100964. https://doi.org/10.1016/j.ijppaw.2024.100964.
4. **Suhaimi, N.S.**, Sellyei, B., Udvari, Z., Székely, C., & Cech, G. (2024). Characterization of four novel actinospore types of fish parasitic myxozoans and the occurrence of *Branchiodrilus hortensis* and *Ophidonais serpentina* from fish farms of Hungary. *International Journal of Parasitolology: Parasites and Wildlife,* 25, 100994. https://doi.org/10.1016/j.ijppaw.2024.100994.
5. **Suhaimi, N.S.**, Székely, C., Cech, G., Sellyei, B., & Borkhanuddin, M.H. (2025). New freshwater *Ceratomyxa* species, *Ceratomyxa schwanefeldii* n. sp. (Myxozoa: Ceratomyxidae) from the gall bladder of tinfoil barb, *Barbonymus schwanefeldii* (Cyprinidae, Cypriniformes) in Malaysia. *Parasitology International*, 108, 103073. https://doi.org/10.1016/j.parint.2025.103073.

6. **Suhaimi, N.S.**, Cech, G., Molnár, K., Székely, C., & Sellyei, B. (2025). Infection of the gibel carp (*Carassius auratus gibelio* Berg, 1932) with myxozoan parasites in a pond farm of Hungary. *Aquaculture Reports*, 42, 102833. https://doi.org/10.1016/j.aqrep.2025.102833.
7. **Suhaimi, N.S.**, Székely, C., Sellyei, B., & Cech, G. (2025). Actinosporean diversity in a Hungarian fish farm and description of the life cycle of *Zschokkella chezhachei*. *International Journal of Parasitolology: Parasites and Wildlife*, 101124. https://doi.org/10.1016/j.ijppaw.2025.101124.
8. **Suhaimi, N.S.**, Székely, C., Molnár, K., Cech, G., Sellyei, B., & Borkhanuddin, M.H. (2025). Biodiversity and five novel species of myxozoan parasites in *Barbonymus* spp. (Cyprinidae, Cypriniformes) from Malaysia. *Scientific Reports*, 15(1), 29134. https://doi.org/10.1038/s41598-025-14254-y.
9. **Suhaimi, N.S.**, Sellyei, B., Mosonyi-Borzák, R., Cech, G., Molnár, K., & Székely, C. (2026). *Thelohanellus* species in common carp (*Cyprinus carpio*) and their life cycles from fish farms and Lake Balaton in Hungary. *Aquaculture Reports.* 46, 103380. https://doi.org/10.1016/j.aqrep.2026.103380.

Publications in progress

1. **Suhaimi, N.S.**, Székely, C., Cech, G., Sellyei, B., & Borkhanuddin, M.H. (2026). Description of three new types of aurantiactinomyxon actinospore (Myxozoa: Myxosporea) from the oligochaete *Aulophorus* sp. in Tasik Telabak, Malaysia. *Pasitology Research*. (Submitted)
2. **Suhaimi, N.S.**, Székely, C., Cech, G., Sellyei, B., & Borkhanuddin, M.H. (2026). Three novel *Myxidium* species (Myxozoa: Myxosporea) from fishes in river and small channels across Terengganu, Malaysia. *Acta Tropica*. (Writing process)

Conference abstracts/ papers/ oral and poster presentations

1. **Suhaimi N.S.,** Colunga-Ramírez, G., Sellyei B., Cech G., Molnár K. & Székely C. (2023). The first occurrence of *Myxobolus lentisuturalis* Dyková, Fiala et Nie, 2002, a pathogenic muscle-infecting parasite of gibel carp (*Carassius auratus gibelio* Berg, 1932) in Hungary.

[Oral presentation]. In: Proceeding of Academical Days/ Parasitology-Zoology-Fish Pathology Session, Budapest, Hungary, January 20–23, 2023.

2. **Suhaimi N.S.,** Colunga-Ramírez*,* G., Sellyei B., Cech G., Molnár K. *&* Székely C. (2023). The first occurrence of *Myxobolus lentisuturalis* Dyková, Fiala et Nie, 2002, a pathogenic muscle-infecting parasite of gibel carp (*Carassius auratus gibelio* Berg, 1932) in Hungary. [Oral presentation]. In: Proceedings of the 47th Hungarian Scientific Conference on Fisheries & Aquaculture (A XLVII. Halászati Tudományos Tanácskozás), Szarvas, Hungary, June 7–8, 2023.
3. **Suhaimi N.S.,** Colunga-Ramírez*, G.*, Sellyei B., Cech G., Molnár K. *&* Székely C. (2023). The first diagnosis of *Myxobolus lentisuturalis* a highly pathogenic muscle-infecting parasite of gibel carp (*Carassius auratus gibelio*) in Hungary [Poster presentation]. In: Proceedings of the 21st International EAFP Conference on Diseases of Fish and Shellfish, Aberdeen, Scotland, September 11–14, 2023.
4. **Suhaimi N.S.,** Borkhanuddin, M.H., Sellyei, B., Cech, G., & Székely, C. (2024). Exploration of actinospores and myxospores (myxozoa) in the freshwater ecosystems of Terengganu, Malaysia: a preliminary study [Oral presentation]. In: Proceeding of Academical Days / Parasitology-Zoology-Fish Pathology Session, Budapest, Hungary, January 30–31, 2024.
5. **Suhaimi N.S.** (2024). A journey from marine biologist to fish parasitologist [Oral presentation]. The Society of Hungarian Parasitologists/ The Situation of Domestic Fish Parasitology, Budapest, Hungary, April, 10, 2024.
6. **Suhaimi N.S.,** Borkhanuddin, M.H., Sellyei, B., Cech, G., & Székely, C. (2024). Survey on actinospores and myxospores (Myxozoa) in the freshwater ecosystems of Terengganu, Malaysia: A preliminary study. [Oral presentation]. In: Proceedings of the 48th Hungarian Scientific Conference on Fisheries & Aquaculture (A XLVII. Halászati Tudományos Tanácskozás), Szarvas, Hungary, June 5–6, 2024.

7. Colunga-Ramírez, G., **Suhaimi, N.S.**, Cech, G., Molnár, K., Székely, C., & Sellyei, B. (2024). Differentiation of the closely related *Myxobolus tihanyensis* n. sp. and *Myxobolus sandrae* Reuss, 1906 [Poster presentation]. 1st Joint Meeting of the Central and Eastern European Branches of the European Association of Fish Pathologists (EAFP), Brno, Czech Republic, December 4–6, 2024.
8. **Suhaimi, N.S.**, Cech, G., Molnár, K., Székely, C., & Sellyei, B. (2025). Infection of the gibel carp (*carassius auratus gibelio* berg, 1932) with myxozoan parasites in a pond farm of Hungary [Oral presentation]. In: Proceedings of the 49th Hungarian Scientific Conference on Fisheries & Aquaculture (A XLVII. Halászati Tudományos Tanácskozás), Szarvas, Hungary, June 3–4, 2025.
9. **Suhaimi, N.S.**, Cech, G., Molnár, K., Székely, C., & Sellyei, B. (2025). Infection of the gibel carp (*carassius auratus gibelio* berg, 1932) with myxozoan parasites in a pond farm of Hungary [Poster presentation]. In: Proceedings of the 22st International EAFP Conference on Diseases of Fish and Shellfish, Heraklion, Greece, September 1–4, 2025.

SUMMARY

Myxozoan parasites have attracted considerable attention from parasitology researchers due to their ability to cause significant diseases in commercially important fish species such as salmonids and carps. This is evident from the large number of myxozoan species described worldwide. Despite the growing research interest in myxozoans globally, Malaysia remains one of the countries where the diversity of myxozoan parasites is still understudied. In contrast, Hungary is recognized as one of the pioneering countries in myxozoan research, and still novel species continue to be reported to this day. This study aimed to further expand the knowledge by investigating (mainly actinosporean stages of) myxozoan parasites in freshwater environments, focusing on aquaculture systems in Hungary and natural freshwater bodies in Malaysia. Additionally, this study sought to uncover previously undescribed species within these ecologically distinct regions.

During a two-year survey of myxozoan parasites in Hungarian fish farms, new collections of myxosporean species and actinosporean types were identified. A total of fifteen myxosporean species and ten actinosporean types were analysed using morphological, morphometric, histological and molecular (18S rDNA) approaches for accurate species identification. Based on these analyses, eight novel myxosporean species and seven actinosporean types were documented. Among the examined hosts (*C. auratus gibelio, C. carpio, R. rutilus*), *C. auratus gibelio* harbored the greatest prevalence of myxozoan parasites, totaling seven species. Of these, four were identified as new species: *M. ocsardiensis* n. sp. infecting the kidney and liver, *M. pecsensis* n. sp. occurring in the gill cartilage, *T. imrei* n. sp. developing in the connective tissue of the gill arch and pharynx, and *Z. chezhachei* n. sp. found in the bile duct. Additionally, *M. lentisuturalis* was reported for the first time in Hungary. Remarkably, *S. molnari*, a common parasite of *C. carpio* was also detected in *C. auratus gibelio*, suggesting that *S. molnari* has a broader host range than previously known. Furthermore, *M. diversus* was found to infecting the fins, and this study provides the first molecular data for this species.

In *C. carpio*, two new species were described namely *T. serosae* n. sp. developing in the serous membrane of the kidney, and *T. paranikolskii* n. sp. occurring in the skin. Both of them exhibit close morphological resemblance and share predilection sites with *T. hovorkai*, and *T. nikolskii* described in this study. However, molecular and phylogenetic analyses confirmed that all four represent distinct species. Moreover, *M. basilamellaris* was reported from the base of gill filaments, while *M. intrachondrealis* was recorded for the second time in Hungary, with this study providing its first molecular data. Two additional *Myxobolus* spp. were identified from *R. rutilus*, each infecting different tissues, *Myxobolus* n. sp. 1 was found in the connective tissues of the gill arch resembling *M. fundamentalis*, whereas *Myxobolus* n. sp. 2 in the kidney, showing similarity to *M. shaharomae*. Genetic analyses clearly separated them as distinct species.

From a total of 5,976 oligochaetes examined, ten actinosporean types were identified belonging to four collective groups such as triactinomyxon, raabeia, aurantiactinomyxon and neoactinomyxum. These actinosporeans were found infecting *B. sowerbyi*, *T. tubifex*, *L. hoffmeisteri* and *O. serpentina*. Remarkably, seven of them were described as novel types, including triactinomyxon type 1, raabeia type 1, aurantiactinomyxon type 1, aurantiactinomyxon type 2, aurantiactinomyxon type 3, aurantiactinomyxon type 4, and aurantiactinomyxon type 6. The remaining three types, which are raabeia type 2, aurantiactinomyxon type 5 and neoactinomyxum type 1 were previously known, and had established life cycles. Molecular analyses confirmed that raabeia type 2 corresponded to the actinospore stage of *M. cultus*, aurantiactinomyxon type 5 represented the actinospore stage of *T. hovorkai*, and neoactinomyxum type 1 was linked to *T. wangi*. Interestingly, although aurantiactinomyxon type 5 and aurantiactinomyxon type 6 represented the actinospore stage of *T. hovorkai*, they exhibited morphological differences and thus were classified as separate types.

The complete life cycles of three myxosporean species were elucidated during this study. The life cycle of *Z. chezhachei* was confirmed through molecular analysis and in experimental infection trials, too. Molecular data verified that the aurantiactinomyxon type 4 described in this study

corresponded to the actinospore stage of *Z. chezhachei*. Infection experiments performed on 20 naïve *B. sowerbyi* oligochaetes using myxospores collected from *C. auratus gibelio* resulted in the production of aurantiactinomyxon type 4. In addition, the life cycle of *T. serosae* n. sp. was inferred based on molecular analyses, which showed 100.0% sequence similarity to aurantiactinomyxon type B2 (DQ231148) described in a previous study. Furthermore, BLAST analysis revealed that Neoactinomyxum type CZ-2 (KP642139) from *B. sowerbyi* shared 99.3% sequence similarity to *T. imrei* n. sp. This high similarity suggests that Neoactinomyxum type CZ-2 likely represents the actinospore stage of *T. imrei* n. sp., although this conclusion is tentative due to the short sequence length available for Neoactinomyxum type CZ-2.

A total of 119 individuals representing thirteen fish species were collected from two rivers and small channels in Terengganu for myxozoan examination in 2023 and 2024. All fish were obtained from local fishermen and purchased at a fish market in Kuala Terengganu, Terengganu, Malaysia. In total, 35 myxosporean species were identified, including fifteen *Myxobolus* spp., eleven *Henneguya* spp., five *Thelohanellus* spp., three *Myxidium* spp. and one *Ceratomyxa* sp. Species identification was based on morphological, morphometric, histological and molecular (18S rDNA, 28S rDNA for *Ceratomyxa* sp.) analyses. Of these, 33 were newly described species, while two are previously known. Among the examined hosts, *C. gachua* and *L. leptocheilus* harbored the highest myxosporean diversity, both of them seven species. *Channa gachua* was infected by six *Henneguya* spp., and one *Myxidium* sp., whereas *L. leptocheilus* hosted five *Myxobolus* spp., one *Thelohanellus* sp., and one *Myxidium* sp. Additionally, *O. waandersii* and *T. pectoralis* each harbored five species consisted four *Myxobolus* spp. and one *Thelohanellus* sp. in *O. waandersii*, while four *Henneguya* spp. and one *Myxidium* sp. in *T. pectoralis*. *Barbonymus gonionotus* was infected by four species, comprising two *Myxobolus* spp. and two *Thelohanellus* spp. The remaining fish species hosted one or two myxosporean species each. For example, *B. altus* was infected by one *Myxobolus* sp. and one *Thelohanellus* sp., while *B. schwanefeldii* by one *Myxobolus* sp. and one *Ceratomyxa* sp. Both *L. rubripinna* and *Barbodes binotatus* were infected

by a single *Myxobolus* sp., and *T. trichopterus* hosted one *Henneguya* sp. Morphological, morphometric and histology examinations, supported by molecular analyses, confirmed that all species represented distinct taxa.

A two-to-three-month survey of actinosporeans was conducted over two consecutive years (2023 and 2024) in Tasik Telabak. A total of 2,666 oligochaetes were successfully isolated of which 24 individuals tested positive for actinosporean infections after one day of observation in cell-well plates. In this study, six actinospore types were identified from the 24 infected oligochaetes, which belonged to four species namely *Bothrioneurum* sp., *Branchiodrilus* sp., *A. acutus* and *Aulophorus* sp. These six actinosporean types represented three collective groups comprising one raabeia, four aurantiactinomyxon and one triactinomyxon. Two of the actinosporean types, aurantiactinomyxon type 4 and triactinomyxon type 1 were documented solely based on morphological and morphometric analyses, as molecular data could not be obtained due to preservation errors during sampling. Nevertheless, their distinct morphological features, which differed from previously described types, indicated that they represented novel actinosporean types. The remaining types such as raabeia type 1, aurantiactinomxon type 1, aurantiactinomyxon type 2, and aurantiactinomyxon type 3 were thoroughly characterized using morphological, morphometric, and molecular analyses, which confirmed them as novel types. Unfortunately, none of the actinosporean sequences matched any known myxosporean sequences in GenBank; therefore, their corresponding myxosporean stages and life cycles could not be elucidated.

ÖSSZEFOGLALÁS

A különböző kereskedelmi szempontból fontos halfajokat, mint például lazac- és pontyféléket, megbetegítő nyálkaspórásokat különös figyelem övezi a parazitológusok körében. Ezt bizonyítja a világon leírt myxozoa fajok nagy száma. Annak ellenére, hogy ezen paraziták iránti érdeklődés világszerte növekszik, Malajzia még mindig azon országok közé tartozik, ahol a nyálkaspórások vizsgálata elhanyagolt területe a parazitológiának. Ezzel szemben Magyarországon, ami a nyálkaspórás kutatások egyik úttörő országa, napjainkban is kerülnek új fajok leírásra.

Jelen tanulmány célja a meglévő tudás bővítése volt, amelynek a keretén belül édesvízi környezetben vizsgáltuk a nyálkaspórás parazitákat különböző ökológiailag régiókban, különös tekintettel a magyarországi tógazdasági rendszerekre és a malajziai természetes édesvízi élőhelyekre.

A kétéves felmérés során több új myxospóra faj és actinospóra típus kimutatása történt meg magyarországi halgazdaságokban. Összesen tizenöt myxospóra faj és tíz aktinospóra típus került elemzésre morfológiai, morfometriai, szövettani és molekuláris (18S rDNS) módszerekkel a pontos fajazonosítás érdekében. Ennek során, nyolc új myxospóra faj és hét új aktinospóra típus került leírásra. A vizsgált halfajok közül (*C. auratus gibelio* - ezüstkárász, *C. carpio* - ponty, *R. rutilus* - bodorka) a legváltozatosabb nyálkaspórás faunával az ezüstkárász rendelkezett. E halban összesen hét fajt találtak, melyek közül négyet új fajként azonosítottak: a *M. ocsardiensis* n. sp., amely vese és máj fertőzését okozta; a *M. pecsensis* n. sp., amely a kopoltyúporcban fordult elő; a *T. imrei* n. sp., amely a kopoltyúív kötőszövetében és garatban fejlődött; valamint az epevezetékből a *Z. chezhachei* n. sp. Szükséges kiemelni, hogy első ízben került kimutatásra Magyarországon a *M. lentisuturalis*.

A *S. molnari*, ami a ponty gyakori parazitája, szintén jelen volt az ezüstkárászban arra utalva, hogy e faj gazdaspektruma szélesebb, mint azt korábban feltételezték. Továbbá kimutatható voltaz

aranyhal uszonyáról ismert *M. diversus* fertőzése a pikkelyeken, amihez jelen tanulmány szolgáltatta az első molekuláris adatokat.

Pontyban két új faj került leírásra: a *T. serosae* n. sp., amely a vesék és a belek savós hártyájában fejlődött, valamint a *T. paranikolskii* n. sp., mely a bőrt fertőzi. Mindkettő morfológiailag nagyban hasonlít a korábbi tanulmányokban már leírt *T. hovorkai* és *T. nikolskii* fajokhoz, predilekciós helyeik megegyeznek, mégis a molekuláris és filogenetikai elemzések alapján négy különálló fajról van szó.

A kopoltyúredők tövéből kimutatásra került a *M. basilamellaris*, valamint a *M. intrachondrealis* (második alkalommal Magyarországon), melyhez e tanulmány szolgáltatta az első molekuláris adatokat.

Két további *Myxobolus* faj azonosítása történt meg bodorkából különböző szöveti elhelyezkedésben. Az egyik a kopoltyúív kötőszöveteiben volt megtalálható és morfológiai hasonlóságot mutatott a *M. fundamentalis*-hoz, míg a másik a vesében hozott létre plazmódiumokat és a *M. shaharomae* fajhoz hasonlatos. A genetikai elemzések azonban egyértelműen új fajként különítették el őket.

A magyarországi mintákból megvizsgált 5,976 kevéssertéjű féregben tíz aktinospóra típus azonosítása történt meg, melyek négy gyűjtőcsoportba tartoztak: triactinomyxon, raabeia, aurantiactinomyxon és neoactinomyxum. Az actinospórák a *B. sowerbyi*, *T. tubifex*, *L. hoffmeisteri* és *O. serpentina* fajú férgekből kerültek kimutatásra. Figyelemre méltó, hogy közülük hét bizonyult új típusnak: triactinomyxon típus 1, raabeia típus 1, aurantiactinomyxon típus 1, 2, 3, 4 és 6. A fennmaradó három típus (raabeia típus 2, aurantiactinomyxon típus 5 és neoactinomyxum típus 1) már korábban ismert volt és feltérképezett életciklussal is rendelkezett. A molekuláris elemzések megerősítették, hogy a raabeia típus 2 megfelel a *M. cultus* aktinospóra szakaszának, az aurantiactinomyxon típus 5 a *T. hovorkai* aktinospórájának, míg a neoactinomyxum típus 1 a *T. wangi* fajhoz köthető. Bár az aurantiactinomyxon típus 5 és 6 egyaránt a *T. hovorkai* aktinospóra

szakaszát képviseli, a mutatott morfológiai különbségek alapján külön típusokként kerültek osztályozásra.

Érdemes megemlíteni, hogy ebben a tanulmányban három myxospóra faj teljes életciklusát is tisztázták. A *Z. chezhachei* életciklusát molekuláris vizsgálatok és kísérleti fertőzési során igazolták. A molekuláris adatokkal megerősítették, hogy az aurantiactinomyxon típus 4 megfelel a *Z. chezhachei* aktinospóra szakaszának. Az ezüstkárászból gyűjtött myxospórák felhasználásával 20 *B. sowerbyi* férgen végzett fertőzéses kísérletek aurantiactinomyxon 4 típusú aktinospórák termelődését eredményezte.

A *T. serosae* n. sp. életciklusára a molekuláris elemzések engednek következtetni, mivel a nyert szekvenciák 100%-os hasonlóságot mutattak egy korábbi tanulmányban leírt aurantiactinomyxon típus B2-vel (DQ231148). Illetve, a filogeneikai elemzés kimutatta, hogy a *B. sowerbyi* fajból származó Neoactinomyxum típus CZ-2 (KP642139) szekvencciája 99,3%-os hasonlóságot mutat a *T. imrei* n. sp.-hez, ami alapján feltételezhető, hogy a Neoactinomyxum típus CZ-2 a *T. imrei* n. sp. aktinospóra stádiumát képviseli, bár ez a következtetés fenntartással kezelendő, mivel a rendelkezésre álló nukleotid szakasz rövid.

Malajziában, 2023 és 2024 év folyamán tizenhárom halfaj összesen 119 példányát gyűjtötték be két folyóból és kisebb csatornákból Terengganu tartományban, hogy nyálkaspórás vizsgálatokat végezzenek rajtuk. A halakat helyi halászoktól vásárolták Kuala Terengganu halpiacán. Összesen 35 myxospóra fajt: 15 *Myxobolus* sp., 11 *Henneguya* sp., 5 *Thelohanellus* sp., 3 *Myxidium* sp. és 1 *Ceratomyxa* sp. mutattak ki belőlük. A fajok azonosítása morfológiai, morfometriai, szövettani és molekuláris (18S rDNS) vizsgálatokon alapult. Közülük 33 új fajnak bizonyult, míg kettő már korábban is ismert volt. A vizsgált halfajok közül a *C. gachua* és a *L. leptocheilus* hordozta a legtöbb myxospóra fajt, hét-hét fajt. A *C. gachua* hat *Henneguya* spp. és egy *Myxidium* sp. hordozott, míg az *L. leptocheilus* öt *Myxobolus* spp., egy *Thelohanellus* spp. és egy *Myxidium* sp. fajt. Az *O. waandersii* és a *T. pectoralis* egyenként öt fajjal volt fertőzött: az *O. waandersii*-ben

négy *Myxobolus* és egy *Thelohanellus* sp., míg a *T. pectoralis*-ban négy *Henneguya* spp. és egy *Myxidium* sp. került kimutatásra. A *B. gonionotus* négy nyálkaspórás faj gazdája volt, két *Myxobolus* spp. és két *Thelohanellus* spp. A többi halfajt egy-két myxospóra faj fertőzte, így például a *B. altus* egy *Myxobolus* sp. és egy *Thelohanellus* sp., a *B. schwanefeldii* egy *Myxobolus* sp. és egy *Ceratomyxa* sp.; a *L. rubripinna* és a *B. binotatus* egy-egy *Myxobolus* sp., míg a *T. trichopterus* egy *Henneguya* sp. Morfológiai, morfometriai és szövettani vizsgálatok, melyeket molekuláris elemzések is alátámasztottak, megerősítették, hogy ezek mindegyike különálló parazita fajt képvisel.

Két egymást követő évben (2023 és 2024) 2-3 hónapos aktinospóra felmérést végezték Tasik Telabakban. Ennek során összesen 2666 kevéssertéjű férget gyűjtöttek, amelyek közül 24 bizonyult nyálkaspóra fertőzöttnek és termelt aktinospórát a mikrotiter platen végzett egy napos megfigyelés után. Hat aktinospóra típust azonosítottak a 24 fertőzött féregből, amelyek négy fajhoz tartoztak, úgy mint *Bothrioneurum* sp., *Branchiodrilus* sp., *A. acutus* és *Aulophorus* sp. A hat aktinospóra típus három gyűjtőcsoportba tartozott, nevezetesen egy raabeia, négy aurantiactinomyxon és egy triactinomyxon. Közülük két aktinospóra típust, az aurantiactinomyxon típus 4-et és a triactinomyxon típus 1-et, kizárólag morfológiai és morfometriai elemzések alapján került leírásra, mivel tisztázatlan mintavételi hibák miatt, molekuláris adatokat nem sikerült nyerni a mintákból. Ennek ellenére, biztosan állítható, hogy ezek a típusok egyedi morfológiai jellemzőkkel bírtak, amelyek eltértek a korábbról ismert típusoktól, és ezért új típusoknak tekinthetők.

A fennmaradó aktinospóra típusok, úgy mint a raabeia típus 1, aurantiactinomyxon típus 1, 2 és 3, részletes morfológiai, morfometriai és molekuláris elemzések során kerültek jellemzésre. Mivel egyik nyert aktinospóra szekvencia sem egyezett a már ismert myxospóra szekvenciával a GenBank-ban, így ezek myxospóra stádiumai és életciklusai nem kerültek tisztázásra.

ACKNOWLEDGEMENTS

Alhamdulillah, all praise and deepest gratitude to Allah, the Almighty.

First and foremost, I sincerely thank the Hungarian government for awarding me the Stipendium Hungaricum scholarship, which provided invaluable support for my studies and living expenses.

My heartfelt appreciation goes to my supervisors, Prof. Dr. Csaba Székely and Dr. Boglárka Sellyei, whose expert mentorship, unwavering patience, and generous support have been pillars throughout my academic endeavor. I am also grateful to Prof. Dr. Kálmán Molnár and Dr. Gábor Cech for their insightful guidance and encouragement throughout this research.

My deepest appreciation goes to the HUN-REN Veterinary Medical Research Institute in Budapest for providing excellent research infrastructure and conducive environment for my work.

I am eternally thankful to my husband, dear parents, and family for their boundless love, support, and encouragement. Your steady strength has been my anchor, empowering me to persevere and reach this milestone.

Special thanks are owed to my colleagues in the Fish Pathology and Parasitology laboratory, Hazim Sajiri (my support system), Virág Marek, Graciela Colunga Ramírez, and Gergely Lajos Zöldi for their continuous support and assistance. I am also deeply grateful to Dr. Zoltán Horváth and his family for their warm hospitality and for embracing my husband and me as members of their family during our stay.

To myself, for enduring years of relentless study, discovery, and perseverance; this journey has been nothing short of extraordinary. As the next chapter unfolds, remember to breathe, stay grounded, and embrace the title that’s soon to come: Doctor.

APPENDICES

Appendix A: Bibliography

Abdallah, V.D., De Azevedo, R.K., Luque, J.L., & Do Bomfim, T.C. (2007). Two new species of *Henneguya* Thélohan, 1892 (Myxozoa, Myxobolidae), parasitic on the gills of *Hoplosternum littorale* (Callichthyidae) and *Cyphocharax gilbert* (Curimatidae) from the Guandu River, State of Rio de Janeiro, Brazil. Parasitol. Latinoam. 62(1-2), 35–41.

Abdel-Ghaffar, F., El-Toukhy, A., Al-Quraishy, S., Al-Rasheid, K., Abdel-Baki, A., Hegazy, A., & Bashtar, A.R. (2008). Five new myxosporean species (Myxozoa: Myxosporea) infecting the Nile tilapia *Oreochromis niloticus* in Bahr Shebin, Nile Tributary, Nile Delta, Egypt. Parasitol. Res. 103, 1197–1205. https://doi.org/10.1007/s00436-008-1116-z.

Abraham, T.J., Banerjee, S., Patra, A., Sarkar, A., Adikesavalu, H., & Dash, G. (2015). Molecular phylogeny of *Myxobolus orissae* (Myxosporea: Myxobolidae) infecting the gill lamellae of mrigal carp *Cirrhinus mrigala* (Actinopterygii: Cyprinidae). Mol. Biol. Res. Comm. 4(1), 15.

Abrunhosa, J., Sindeaux-Neto, J.L., Santos, Â.K.D., Hamoy, I., & Matos, E. (2017). *Myxobolus marajoensis* sp. n. (Myxosporea: Myxobolidae), parasite of the freshwater catfish *Rhamdia quelen* from the Brazilian Amazon region. Rev. Bras. Parasitol. Vet. 26(4), 465–471. https://doi.org/10.1590/S1984-29612017067.

Abrunhosa, J., Sindeaux-Neto, J.L., Hamoy, I. Matos, E.R. (2018). A new species of Myxosporea, *Henneguya quelen*, from silver catfish *Rhamdia quelen* (Siluriforme: Pimelodidae) in the Amazonian region. Parasitol. Res. 117, 3809–3820. https://doi.org/10.1007/s00436-018-6086-1.

Acharya, S., & Dutta, T. (2007). *Thelohanellus habibpuri* sp. n. (Myxozoa: Bivalvulida) from the tropical freshwater fish rohu, *Labeo rohita* (Hamilton-Buchanan, 1882) in West Bengal, India: Light and electron microscope observations. Anim. Biol. 57(3), 293–300.

Adriano, E.A., Carriero, M.M., Maia, A.A.M., Silva, M.R.M.D., Naldoni, J., Ceccarelli, P.S., & Arana, S. (2012). Phylogenetic and host–parasite relationship analysis of *Henneguya multiplasmodialis* n. sp. infecting *Pseudoplatystoma* spp. in Brazilian Pantanal wetland. Vet. Parasitol. 185, 110–120.

Adriano, E.A., & Okamura, B. (2017). Motility, morphology and phylogeny of the plasmodial worm, *Ceratomyxa vermiformis* n. sp. (Cnidaria: Myxozoa: Myxosporea). Parasitol. 144(2), 158–168. https://doi.org/10.1017/S0031182016001852.

Adriano, E.A., Zatti, S.A., & Okamura, B. (2021). How to build single-celled cnidarians with worm-like motility: lessons from Myxozoa. J. Anat. 240, 475–488.

Ahmed, A.T.A. (1973). Morphology and life history of *Mitraspora cyprini* Fujita, parasitic in the kidney of goldfish. Jpn. J. Med. Sci. Biol. 26, 87–101. https://doi.org/10.7883/yoken1952.26.87.

Ahmad, I. & Kaur, H. (2018). Prevalence, site and tissue preference of myxozoan parasites infecting gills of cultured fingerlings of Indian major carps in District Fatehgarh Sahib, Punjab (India). J. Parasit. Dis. 42, 559–569.

Akhmerov, A. Kh. (1955). Ways of the origin of Myxosporidia species of the genus *Thelohanellus* Kudo from Amur wild carp. Dokl. Akad. Nauk SSSR, 105, 1129–1132. (in Russian).

Akhmerov, A. Kh. (1960). Myxosporidia of fish in the basin of River Amur. Rybnoe Khozyaistvo vnutrennikh vodoemov Latviiskoi SSR, 5, 239–308. (in Russian).

Ali, M.A. (1999). *Henneguya ghaffari* sp. n. (Myxozoa: Myxosporea), infecting the Nile perch *Lates niloticus* (Teleostei: Centropomidae). Dis. Aquat. Org. 28, 225–230.

Alama-Bermejo, G., Šíma, R., Raga, J.A., & Holzer, A.S. (2013). Understanding myxozoan infection dynamics in the sea: Seasonality and transmission of *Ceratomyxa puntazzi*. Int. J. Parasitol. 43(9), 771–780. http://doi.org/10.1016/j.ijpara.2013.05.003.

Andree, K.B, Székely, C., Molnár, K., Gresoviac, S.J., & Hedrick, R.P. (1999). Relationships among members of the genus *Myxobolus* (Myxozoa: Bilvalvulidae) based on small subunit ribosomal DNA sequences. J. Parasitol 85, 68–74.

Anderson, C.L., Canning, E.U., Schafer, S.M., Yokoyama, H. Okamura, B. (2000). Molecular confirmation of the life cycle of *Thelohanellus hovorkai* Achmerov, 1960 (Myxozoa: Myxosporea). Bull. Eur. Assoc. Fish Pathol. 20, 111–115.

Araújo, B.L., Adriano, E.A., Franzolin, G.N., Zatti, S.A., & Naldoni, J. (2022). A novel *Ceratomyxa* species (Myxozoa: Cnidaria) infecting an Amazonian catfish. Parasitol. Int. 89, 102582. https://doi.org/10.1016/j.parint.2022.102582.

Araújo, C., Rangel, L. F., Casal, G., Araújo, D. C., & Rocha, S. (2023). Description of sphaeractinomyxon types (Cnidaria: Myxosporea) from marine oligochaetes in the Minho River estuary and nearby coastal area. Sci. Lett. J. 1. https://doi.org/10.48797/sl.2023.69.

Atkinson, S.D., Hallett, S.L., & Bartholomew, J.L. (2007). The life cycle of *Chloromyxum auratum* (Myxozoa) from goldfish, *Carassius auratus* (L.), involves an antonactinomyxon actinospore. J. Fish Dis. 30, 149–156.

Atkinson, S.D, & Bartholomew, J.L. (2009). Alternate spore stages of *Myxobilatus gasterostei*, a myxosporean parasite of three-spined sticklebacks (*Gasterosteus aculeatus*) and oligochaetes (*Nais communis*). Parasitol. Res. 104, 1173–1181. https://doi.org/10.1007/s00436-008-1308-6.

Atkinson, S.D., Hallett, S.L., Diaz-Morales, D., Bartholomew, J.L. & de Buron, I. (2019). First myxozoan infection (Cnidaria: Myxosporea) in a marine polychaete from North America and erection of actinospore collective group Saccimyxon. J. Parasitol. 111(5), 252–262.

Azevedo, C., Ribeiro, M., Clemente, S. C., Casal, G., Lopes, L., Matos, P., Al-Quraishy, S.A. & Matos, E. (2011). Light and ultrastructural description of *Meglitschia mylei* n. sp. (Myxozoa) from *Myleus rubripinnis* (Teleostei: Serrasalmidae) in the Amazon River system. J. Eukaryot. Microbiol. 58(6), 525–528. https://doi.org/10.1111/j.1550-7408.2011.00583.x.

Azevedo, C., São Clemente, S.C., Casal, G., Matos, P., Alves, Â., Al-Quraishy, S., & Matos, E. (2012). *Myxobolus myleus* n. sp. infecting the bile of the Amazonian freshwater fish *Myleus rubripinnis* (Teleostei: Serrasalmidae): morphology and pathology. Syst. Parasitol. 82(3), 241–247. https://doi.org/10.1007/s11230-012-9360-0.

Azevedo, C., Rocha, S., Casal, G., Clemente, S.C.S., Matos, P., Al-Quraishy, S., & Matos, E. (2013). Ultrastructural description of *Ceratomyxa microlepis* sp. nov. (Phylum Myxozoa): a parasite infecting the gall bladder of *Hemiodus microlepis*, a freshwater teleost from the Amazon River. Mem. Inst. Oswaldo Cruz 108, 150–154. https://doi.org/10.1590/0074-0276108022013004.

Bahri, S. (2008). Abnormal forms of *Myxobolus bizerti* and *Myxobolus mulleri* (Myxosporea: Bivalvulida) spores with caudal appendages. Bull. Eur. Assoc. Fish Pathol. 28, 252–255.

Baiko, D., Lisnerová, M., Bartošová-Sojková, P., Holzer, A.S., Blabolil, P., Schabuss, M., & Fiala, I. (2024). Solving the *Myxidium rhodei* (Myxozoa) puzzle: insights into its phylogeny and host specificity in Cypriniformes. Parasite 31, 35.

Bakar, S.D.S.A., Farinordin, F.A., Izam, N.A.M., Ismail, N.A., Abidin, M.K.Z., Sharir, S., Mohamad, A., Razali, N.B., & Zulkipli, N. (2023). Preliminary Checklist of Fish Species of Sungai Rengai, Kuala Lipis, Pahang, Malaysia. Bioresources Environ. 1(1), 9–21. https://doi.org/10.24191/bioenv.v1i1.15.

Banerjee, S., Patra, A., Adikesavalu, H., Mondal, A., & Abraham, T.J. (2015). The phylogenetic position of *Myxobolus carnaticus* (Myxozoa, Myxosporea, Bivalvulida) infecting gill lamellae of *Cirrhinus mrigala* (Hamilton, 1822) based on 18S rRNA sequence analysis. Mol. Biol. Res. Comm. 4(3), 125.

Barassa, B., Adriano, E.A., Cordeiro, N.S., Arana, S., & Ceccarelli, P.S. (2012). Morphology and host–parasite interaction of *Henneguya azevedoi* n. sp., parasite of gills of *Leporinus*

obtusidens from Mogi-Guaçu River, Brazil. Parasitol. Res. 110(2), 887–894. https://doi.org/10.1007/s00436-011-2571-5.

Barta, J.R., Martin, D.S., Liberator, P.A., Dashkevicz, M., Anderson, J.W., Feighner, S.D., Elbrecht, A., Perkins-Barrow, A., Jenkins, M.C., Danforth, H.D., Ruff, M.D., & Profous-Juchelka, H. (1997). Phylogenetic relationships among eight *Eimeria* species infecting domestic fowl inferred using complete small subunit ribosomal DNA sequences. J. Parasitol. 83, 262–271. https://doi.org/10.2307/3284453.

Bartholomew, J.L., Atkinson, S.D., & Hallett, S.L. (2006). Involvement of *Manayunkia speciosa* (Annelida; Polychaeta: Sabellidae) in the life cycle of *Parvicapsula minibicornis*, a myxozoan parasite of Pacific salmon. J. Parasitol. 92, 742–748.

Bartholomew, J.L., Atkinson, S.D., Hallett, S.L., Lowenstine, L.J., Garner, M.M., Gardiner, C.H., Rideout, B.A., Keel, M.K., & Brown, J.D. (2008). Myxozoan parasitism in waterfowl. Int. J. Parasitol. 38,1199–1207.

Bartholomew, J.L., Fryer, J.L., & Rohovec, J.S. (1992). *Ceratomyxa shasta* infections of salmonid fish. In: Proceedings OJI International Symposium Salmonid Diseases. Hokkaido University Press, Sapporo, pp. 267–275.

Bartholomew, J.L., Whipple, M.J., Stevens, D.G., & Fryer, J.L. (1997) The life cycle of *Ceratomyxa shasta*, a myxosporean parasite of salmonids, requires a freshwater polychaete as an alternate host. J. Parasitol. 83, 859–868.

Bartošova, P., Fiala, I., & Hypša, V. (2009). Concatenated SSU and LSU rDNA data confirm the main evolutionary trends within myxosporeans (Myxozoa: Myxosporea) and provide an effective tool for their molecular phylogenetics. Mol. Phylogenet. Evol. 53(1), 81–93. https://doi.org/10.1016/j.ympev.2009.05.018.

Bartošová, P. (2010). Phylogenetic analyses of myxosporeans based on the molecular data (Doctoral dissertation, PhD thesis, University of South Bohemia).

Bartošová, P., & Fiala, I. (2011). Molecular evidence for the existence of cryptic species assemblages of several myxosporeans (Myxozoa). Parasitol. Res. 108, 573–583. https://doi.org/10.1007/s00436-010-2100-y.

Bartošová, P., Freeman, M.A., Yokoyama, H., Caffara, M., & Fiala, I. (2011). Phylogenetic position of *Sphaerospora testicularis* and *Latyspora scomberomori* n. gen. n. sp. (Myxozoa) within the marine urinary clade. Parasitol. 138, 381–393.

Bartošová, P., Fiala, I., Jirků, M., Cinková, M., Caffara, M., Fioravanti, M.L., Atkinson, S.D., Bartholomew, J.L., & Holzer, A.S. (2013) *Sphaerospora sensu* stricto: Taxonomy, diversity and evolution of a unique lineage of myxosporeans (Myxozoa). Mol. Phylogenet. Evol. 68(1), 93–105. https://doi.org/10.1016/j.ympev.2013.02.026.

Bartošová-Sojková, P., Hrabcová, M., Pecková, H., Patra, S., Kodádková, A., Jurajda, P., Tyml, T., & Holzer, A.S. (2014) Hidden diversity and evolutionary trends in malacosporean parasites (Cnidaria: Myxozoa) identified using molecular phylogenetics. Int. J. Parasitol. 44(8), 565–577. https://doi.org/10.1016/j.ijpara.2014.04.005.

Baska, F. (1987). Histological studies on the development of *Myxobolus pseudodispar* Gorbunova, 1936 in the roach (*Rutilus rutilus*). Acta Vet. Hung. 35: 251–257.

Basu, S., Kumar, B., & Haldar, D.P. (2006). Synopsis of the indian species of the genus *Thelohanellus* kudo, 1933 along with description of *Thelohanellus disporomorphus* sp. n. J. Parasit. Appl. Anim. Biol. 15, 81–94.

Batubara, A.S., Muchlisin, Z.A., Efizon, D., Elvyra, R., Fadli, N., & Irham, M. (2018). Morphometric variations of the genus *Barbonymus* (Pisces, Cyprinidae) harvested from Aceh waters, Indonesia. Fish. Aquat. Life 26(4), 231–237.

Batueva, M.D.D. (2020). Morphological, histological, and molecular aspects of *Myxobolus zaikae* n. sp., a parasite of the roach *Rutilus rutilus*, in Lake Baikal. Dis. Aquat. Org. 142, 75–82. https://doi.org/10.3354/dao03534.

Batueva, M.D.D., & Burdukovskaya, T.G. (2022). Supplementary studies on *Myxobolus talievi* Dogiel, 1957 (Cnidaria, Myxozoa) from the skeletal muscle of the cottoid fish *Cyphocottus*

eurystomus in Lake Baikal: Morphological, histological and molecular characterisations. Acta Vet. Hung. 70(1), 35–43. https://doi.org/10.1556/004.2021.00054.
Batueva, M.D., Vlasenko, P., Solovyev, M.M., & Abasheev, R.Y. (2023b). *Myxobolus nekrasovae* n. sp. (Cnidaria, Myxozoa) is a new species parasitizing the gills of the gibel carp, *Carassius auratus gibelio*. Microb. Pathog, 185, 106454. https://doi.org/10.1016/j.micpath.2023.106454.
Bellerud, B.L. (1993). Etiological and epidemiological factors affecting outbreaks of proliferative gill disease on Mississippi channel catfish farms. Mississippi State University.
Benajiba, M.H., & Marques, A. (1993). The alternation of actinomyxidian and myxosporidian sporal forms in the development of *Myxidium giardia* (parasite of *Anguilla Anguilla*) through oligochaetes. Bull. Eur. Ass. Fish Pathol. 13(1), 100.
Benoît, L.F.G., Vanessa, F.T.C., & Abraham, F. (2020). Description of three new species of Myxosporidia (Cnidaria: Myxobolidae) parasites of *Paramormyrops kingsleyae* Gunther, 1896 (Mormyridae) in the Nyong Basin in Cameroon. Fish. Aquac. J. 11(2), 1–9.
Bittencourt, L.S., Ferreira, R.L.D.S., Videira, M.N., Silva, M.F.D., Silva, D.T.D., Hamoy, I., Carvalho, J.C.T., & Matos, E. (2021). *Sphaerospora festivus* n. sp., a parasite of the flag cichlid, *Mesonauta festivus* (Teleostei: Cichlidae) from eastern Amazon, Brazil. Rev. Bras. Parasitol. Vet. 30, e004621. https://doi.org/10.1590/S1984-29612021056.
Bittencourt, L.S., da Silva, D.T., Hamoy, I., de Carvalho, A.A., da Silva, M.F., Videira, M., Carvalho, J.C.T., & Matos, E. (2022). Morphological and phylogenetic features of *Ceratomyxa macapaensis* n. sp. (Myxozoa: Ceratomyxidae) in *Mesonauta festivus* Heckel, 1840 (Cichliformes: Cichlidae) from the eastern Amazon region. Acta Parasitol. 67(1), 322–329. https://doi.org/10.1007/s11686-021-00460-x.
Bonetto A., & Pignalberi C. (1965). *Myxobolus paranensis* (Protozoa, Myxosporidea), una nueva especie parasita del BDoradô (*Salminus maxillosus*). Physis 25, 3–2.
Borkhanuddin, M.H. (2013). Studies on fish parasitic myxozoans in Lake Balaton, Hungary and in freshwater and marine biotopes in Malaysia. The Hungarian University of Agriculture and Life Sciences, pp. 107.
Borkhanuddin, M.H., Cech, G., Mazelan, S., Shaharom-Harrison, F., Molnár, K., & Székely, C. (2014b). *Myxobolus ophiocarae* sp. n. (Myxozoa: Myxosporea: Bivalvulida) infecting the gill of wild goby, *Ophiocara porocephala* (Perciformes: Gobioidei) in Malaysia. Parasitol. Res. 113(1), 29–37. https://doi.org/10.1007/s00436-013-3622-x.
Borkhanuddin, M.H., Cech, G., Molnár, K., Németh, S., & Székely, C. (2014a). Description of raabeia, synactinomyxon and neoactinomyxum developing stages of myxosporeans (Myxozoa) infecting Isochaetides michaelseni Lastočkin (Tubificidae) in Lake Balaton and Kis-Balaton Water Reservoir, Hungary. Syst. Parasitol. 88, 245–259. https://doi.org/10.1007/s11230-014-9496-1.
Borkhanuddin, M.H., Cech, G., Molnár, K., Shaharom-Harrison, F., Khoa, T.N.D., Samshuri, M.A., Mazelan, S. Atkinson, S.D., & Székely, C. (2020b). *Henneguya* (Cnidaria: Myxosporea: Myxobolidae) infections of cultured barramundi, *Lates calcarifer* (Perciformes: Latidae) in an estuarine wetlands system of Malaysia: description of *Henneguya setiuensis* n. sp., *Henneguya voronini* n. sp. and *Henneguya calcarifer* n. sp. Parasitol. Res. 119(1), 85–96. https://doi.org/10.1007/s00436-019-06541-1.
Borkhanuddin, M.H., Goswami, U., Cech, G., Molnár, K., Atkinson, S.D., & Székely, C. (2020a). Description of myxosporeans (Cnidaria: Myxozoa) infecting the popular food fish *Notopterus notopterus* (Pisces: Notopteridae) in Malaysia and India. Food Waterborne Parasitol 20, e00092. https://doi.org/10.1007/s00436-019-06541-1.
Borzák, R., Borkhanuddin, M.H., Cech, G., Molnár, K., Hallett, S.L., & Székely, C. (2021). New data on *Thelohanellus nikolskii* Achmerov, 1955 (Myxosporea, Myxobolidae) a parasite of the common carp (*Cyprinus carpio*, L.): The actinospore stage, intrapiscine tissue preference and molecular sequence. Int. J. Parasitol. Parasites Wildl. 15, 112–119. https://doi.org/10.1016/j.ijppaw.2021.04.004.

Borzák, R., Molnár, K., Cech, G., Papp, M., Deák-Paulus, P., & Székely, C. (2016). Description of two new species of *Myxobolus* Bütschli, 1892, *M. peleci* n. sp. and *M. cultrati* n. sp., detected during an intensive mortality of the sichel, *Pelecus cultratus* (L.) (Cyprinidae), in Lake Balaton, Hungary. Syst. Parasitol. 93, 667–677. https://doi.org/10.1007/s11230-016-9651-y.

Buchmann, K., Skovgaard, A., & Kania, P.W. (2012). *Myxobolus groenlandicus* n. sp. (Myxozoa) distorting skeletal structures and musculature of Greenland halibut *Reinhardtius hippoglossoides* (Teleostei: Pleuronectidae). Dis. Aquat. Org. 98, 133–141. https://doi.org/10.3354/dao02437.

Burger, M.A.A., & Adlard, R.D. (2010). Four new species of *Kudoa* Meglitsch, 1947 (Myxosporea: Multivalvulida) from Australia with recommendations for species descriptions in the Kudoidae. Parasitology 1947, 793–814. http://doi.org/10.1017/S0031182009991557.

Bütchli, O. (1882). Myxosporidia. In: Winter CF (ed) Bronn‘s Klassen und Ordnungen des Tierreichs 1 Protozoa, Leipzig, 590–603.

Caffara, M., Raimondi, E., Florio, D., Marcer, F., Quaglio, F., & Fioravanti, M.L. (2009). The life cycle of *Myxobolus lentisuturalis* (Myxozoa: myxobolidae), from goldfish (*Carassius auratus auratus*), involves a raabeia-type actinospore. Folia Parasitol. 56(1), 6–12.

Camus A.C, & Griffin M.J. (2010). Molecular characterization and histopathology of *Myxobolus koi* infecting the gills of a koi. *Cyprinus carpio*, with an amended morphological description of the agent. J. Parasitol. 96(1), 116–124.

Camus, A.C., Dill, J.A., Rosser, T.G. Pote, L.M. & Griffin, M.J. (2017). *Myxobolus axelrodi* n. sp. (Myxosporea: Myxobolidae) a parasite infecting the brain and retinas of the cardinal tetra *Paracheirodon axelrodi* (Teleostei: Characidae). Parasitol Res 116, 387–397. https://doi.org/10.1007/s00436-016-5301-1.

Canning, E.U., Tops, S., Curry, A., Wood, T.S., & Okamura, B. (2002). Ecology, development and pathogenicity of *Buddenbrockia plumatellae* Schröder, 1910 (Myxozoa, Malacosporea) (syn. *Tetracapsula bryozoides*) and establishment of *Tetracapsuloides* n. gen. for *Tetracapsula bryosalmonae*. J. Eukaryot. Microbiol. 49, 280–295.

Canning, E.U., & Okamura, B. (2004). Biodiversity and evolution of the myxozoa. Adv. Parasitol. 56, 43–131.

Carriero, M.M., Adriano, E.A., Silva, M.R., Ceccarelli, P.S., & Maia, A.A. (2013). Molecular phylogeny of the *Myxobolus* and *Henneguya* genera with several new South American species. PLoS One 8, e73713. https://doi.org/10.1371/journal.pone.0073713.

Casal, G., Matos, E., & Azevedo, C. (2002). Ultrastructural data on the spore of *Myxobolus maculatus* n. sp. (phylum Myxozoa), parasite from the Amazonian fish *Metynnis maculatus* (Teleostei). Dis. Aquat. Org. 51(2), 107–112. https://doi.org/10.3354/dao.

Casal, G., Sao Clemente, S.C., Lopes, L., Rocha, S., Felizardo, N., Oliveira, E., Al-Quraishy, S., & Azevedo, C. (2017). Ultrastructural morphology and phylogeny of *Henneguya gilbert* n. sp. (Myxozoa) infecting the teleostean *Cyphocharax gilbert* (Characiformes: Curimatidae) from Brazil. Parasitol. Res. 116(10), 2747–2756. https://doi.org/10.1007/s00436-017-5585-9.

Castresana, J. (2000). Selection of conserved blocks from multiple alignments for their use in phylogenetic analysis. Mol. Biol. Evol. 17, 540–552.

Cavin, J.M., Donahoe, S.L., Frasca Jr, S., Innis, C.J., Kinsel, M.J., Kurobe, T., Naples, L. M., Nyaoke, A., Poll, C.P., & Weber III, E.S. (2012). *Myxobolus albi* infection in cartilage of captive lumpfish (*Cyclopterus lumpus*). J. Vet. Diagn. Invest. 24, 516–524. https://doi.org/10.1177/10406387124409.

Cech, G., Molnár, K. & Székely, C. (2012). Molecular genetic studies on morphologically indistinguishable *Myxobolus* spp. infecting cyprinid fishes, with the description of three new species, *M. alvarezae* sp. nov., *M. sitjae* sp. nov. and *M. eirasianus* sp. nov. Acta. Parasitol. 57, 354–366. https://doi.org/10.2478/s11686-012-0045-2.

Cech, G., Borzák, R., Molnár, K., & Székely, C. (2015). Three new species of *Myxobolus* Bütschli, 1882 (Myxozoa: Myxobolidae) infecting the common nase *Chondrostoma nasus* (L.) in the river Danube. Syst. Parasitol. 92(2), 101–111. https://doi.org/10.1007/s11230-015-9589-5.

Cellere, E.F., Cordeiro, N.S., & Adriano, E.A. (2002). *Myxobolus absonus* sp. n. (Myxozoa: Myxosporea) parasitizing *Pimelodus maculatus* (Siluriformes: Pimelodidae), a South American freshwater fish. Mem. Inst. Oswaldo Cruz 97, 79–80. https://doi.org/10.1590/S0074-02762002000100012.

Chaudhary, A., Molnár, K., Gupta, A., Cech, G., Singh, H.S., & Székely, C. (2017). Redescription of *Henneguya chaudhuryi* (Bajpai & Haldar, 1982) (Myxosporea: Myxobolidae), infecting the gills of the freshwater fish *Channa punctata* (Bloch) (Perciformes: Channidae) in India. Syst Parasitol. 94(3), 403–411. https://doi.org/10.1007/s11230-017-9705-9.

Chaudhary, A., Goswami, U., Gupta, A., Cech, G., Singh, H.S., Molnár, K., Székely, C., & Sharma, B. (2018). Morphological, histological, and molecular description of *Myxobolus ompok* n. sp. (Myxosporea: Myxobolidae), a kidney myxozoan from Pabdah catfish *Ompok pabda* (Hamilton, 1822) (Siluriformes: Siluridae) in India. Parasitol. Res. 117(6), 1899–1905. https://doi.org/10.1007/s00436-018-5882-y.

Chaudhary, A., Gupta, A., Goswami, U. Singh, H.S., & Székely, C. (2019). Molecular genetic studies on *Myxobolus cylindricus* and *Henneguya mystasi* (Myxosporea: Myxobolidae) infecting two Indian fish species, *Channa gachua* and *Mystus vittatus*, respectively. Acta Parasit. 64, 129–137. https://doi.org/10.2478/s11686-018-00014-8.

Chaudhary, A., Garg, A., Goswami, U., Chiary, H. R., Sharma, B., & Singh, H.S. (2024). Molecular Identification of Seven *Myxobolus* Species (Myxosporea: Myxobolidae) in Cyprinids from India. Int. J. Zool. Anim. Biol. 7(1), 1–18. https://doi.org/10.23880/izab-16000550.

Chen, Q.L., Ma, C.L., & Fauna, S. (1998). Myxozoa: Myxosporea. Science. Press, Beijing. (In Chinese).

Chen, W., Zhang, D., Whipps, C.M., Yang, C., & Zhao, Y. (2021). Description of *Myxidium pseudocuneiforme* n. sp. (Myxosporea: Myxidiidae) from *Cyprinus carpio* in China, with the resolution on a taxonomic dilemma of *Myxidium cuneiforme*. J. Eukaryot. Microbiol. 68(5), e12859. https://doi.org/10.1111/jeu.12859.

Cheng, P., Baran, E., & Touch, B.T. (2004). Synthesis of all published information on java barb *Barbonymus gonionotus* based on Fishbase 2004. Worldfish Center and Inland Fisheries Research and Development Institute, Cambodia.

Chinh, N.N., Ha, N.T.H., Doanh, P.N., Eiras, J.C., Whipps, C.M., & Shirakashi, S. (2023). Synopsis of myxosporean species (Cnidaria: Myxozoa) parasitizing fishes from Vietnam. Syst. Parasitol. 100(4), 325–344. https://doi.org/10.1007/s11230-023-10090-8.

Chong, V.C., Lee, P.K.Y., & Lau, C.M. (2010). Diversity, extinction risk and conservation of Malaysian fishes. J. Fish Biol. 76(9), 2009–2066.

Colquhoun, D.J., & Duodu, S. (2011). *Francisella* infections in farmed and wild aquatic organisms. Vet. Res. 42.

Colunga-Ramírez, G., Suhaimi, N.S., Cech, G., Molnár, K., Székely, C., & Sellyei, B. (2024). Morphological and molecular characterisation of two closely related species: *Myxobolus tihanyensis* n. sp. and *Myxobolus sandrae* Reuss, 1906. Int. J. Parasitol. Parasites Wildl. 23, 100909. https://doi.org/10.1016/j.ijppaw.2024.100909.

Cone, D.K., & Overstreet, R. (1997). *Myxobolus mississippiensis* n. sp. (Myxosporea) from gills of *Lepomis macrochirus* in Mississippi. J. Parasitol. 83, 122–124.

Cone, D.K., Yang, J., Sun, G., & Easy, R. (2005). Taxonomy and molecular phylogeny of *Myxobolus bilobus* n. sp. (Myxozoa) parasitizing *Notemigonus crysoleucas* (Cyprinidae) in Algonquin Park, Ontario, Canada. Dis. Aquat. Org. 66(3), 227–232. https://doi.org/10.3354/dao066227.

Darriba, D., Taboada, G.L., Doallo, R., & Posada, D. (2012). jModelTest 2: more models, new heuristics and parallel computing. Nat. Methods 9, 772. https://doi.org/10.1038/nmeth.2109.

da Silva, M.F., de Carvalho, A.E.F.B., Hamoy, I., & Matos, E.R. (2020). Coelozoic parasite of the family Ceratomyxidae (Myxozoa, Bivalvulida) described from motile vermiform plasmodia found in *Hemiodus unimaculatus* Bloch, 1794. Parasitol. Res. 119(3), 871–878. https://doi.org/10.1007/s00436-019-06505-5.

da Silva, M.F., da Silva, D.T., Giese, E., Furtado, A.P., Matos, P., Lima, A.M., Hamoy, I., & Matos, E. (2023). Phylogeny and ultrastructure of *Myxobolus rangeli* n. sp. (Myxozoa, Bivalvulida), a histozoic parasite in Siluriformes fish from the Amazon region. Braz. J. Vet. Parasitol. 32(2), e005923. https://doi.org/10.1590/S1984-29612023034.

Davis, H.S. (1917). The Myxosporidia of the Beaufort Region. A systematic and biological study. Bull. U.S. Bur.Fish. 35, 199–243.

Dayoub, A., Molnár, K., Salman, H., Al-Samman, A., & Székely, C. (2007). *Myxobolus* infections of common carp (Cyprinus carpio) in Syrian fish farms. Acta Vet. Hung. 55, 501–509. https://doi.org/10.1556/AVet.55.2007.4.9.

de Azevedo, R.K., Abdallah, V.D., Paes, J.V.K., da Silva, R.J., Matos, P., Velasco, M., & Matos, E. (2013). *Henneguya nagelii* n. sp. (Myxozoa: Myxobolidae) in *Cyphocharax nagelii* (Steindachner, 1881) (Teleostei: Characiformes: Curimatidae) from the Peixe's River, São Paulo State, Brazil. Parasitol. Res. 112(10), 3601–3605. https://doi.org/10.1007/s00436-013-3546-5.

de Carvalho, A.A., da Silva Ferreira, R.L., de Oliveira Nascimento, L.S., Morais, S.C., de Araujo, R.F., de Almeida Costa, M., Videira, M.N., & Giese, E.G. (2024). A gallbladder Ceratomyxidae (Myxozoa: Bivalvulida) parasite described in *Pimelodella cristata* (Müller & Troschel, 1848) from the Eastern Amazon. Acta Parasitol. 69(4), 2006–2015. https://doi.org/10.1007/s11686-024-00930-y.

Deli, A., Lekeufack-Folefack, G.B., Feudjio-Dongmo, B., Onana-Ateba, N.O., Tchoutezo-Tiwa, A.E., & Fomena, A. (2025). Diversity, ecological status and species associations of myxozoans (Cnidaria: Myxosporea) parasites of *Labeo senegalensis* Valenciennes, 1842 (Cyprinidae) from Lake Maga in Cameroon. Parasitol. Int. 103174. https://doi.org/10.1016/j.parint.2025.103174.

de Sena, N.M., Eduard, J., Pereira, C.M.B., Neto, J.L.S., & Velasco, M. (2025). *Myxobolus medusae* n. sp., a new species of Myxozoa with dendritic appendages. Parasitol. Int. 103106. https://doi.org/10.1016/j.parint.2025.103106.

Diamant, A. (1997). Fish-to-fish transmission of a marine myxosporean. Dis. Aquat. Org. 30(2), 99–105.

Diamant, A., Whipps, C.M., & Kent, M.L. (2004). A new species of *Sphaeromyxa* (Myxosporea: sphaeromyxina: Sphaeromyxidae) in devil firefish, *Pterois miles* (Scorpaenidae), from the northern Red Sea: Morphology, Ultrastructure, and Phylogeny. J. Parasitol. 90, 1434–1442. https://doi.org/10.1645/GE-336R.

Donec, Z. S. & Shulman, S.S. (1984). Cnidosporidia. In: Bauer, O.N (eds) *Key to the Parasites of Freshwater Fishes of the USSR*. 1, 88–251.

Dong, H.T. (2018). Emerging, re-emerging and new diseases of Tilapia. FAO. Sun Yat Sen University, China.

Dyková, I., & Lom, J. (1982). *Sphaerospora renicola* n. sp., a myxosporean from carp kidney, and its pathogenicity. Z. Parasitenkd. 68, 259–268.

Dyková, I., Lom, J., & Cirkovic, M. (1986). Brain myxoboliasis of common carp (*Cyprinus carpio*) due to *Myxobolus encephalicus*. Bull. Eur. Ass. Fish Pathol. 6, 10–12.

Dyková, I. & Lom J. (1988) Review of pathogenic myxosporeans in intensive culture of carp (*Cyprinus carpio*) in Europe. Folia Parasitol. 35, 289–307.

Dyková, I., Fiala, I., & Nie, P. (2002). *Myxobolus lentisuturalis* sp. n. (Myxozoa: Myxobolidae), a new muscle-infecting species from the Prussian carp, *Carassius gibelio* from China. Folia Parasitol. 49, 253–25.

Dyková, I., Tyml, T., Fiala, I., & Lom, J. (2007). New data on *Soricimyxum fegati* (Myxozoa) including analysis of its phylogenetic position inferred from the SSU rRNA gene sequence. Folia Parasitol. 54(4), 272.

Eiras, J.C. (2002). Synopsis of the species of the genus *Henneguya* Thélohan, 1892 (Myxozoa: Myxosporea: Myxobolidae. Syst. Parasitol. 52(1), 43–54.

Eiras, J.C., Malta, J.C., Varela, A., & Pavanelli, G.C. (2004). *Henneguya schizodon* n. sp. (Myxozoa, Myxobolidae), a parasite of the amazonian teleost fish *Schizodon fasciatus* (Characiformes, Anostomidae). Parasite 11, 169–173.

Eiras, J.C. (2005a). An overview on the myxosporean parasites in amphibians and reptiles. Acta Parasitol 50, 267–275.

Eiras, J.C., Molnár, K., & Lu, Y. (2005b). Synopsis of the species of *Myxobolus* bütschli, 1882 (Myxozoa: Myxosporea: Myxobolidae). Syst. Parasitol. 61(1), 1–46. https://doi.org/10.1007/s11230-004-6343-9.

Eiras, J.C. (2006). Synopsis of the species of *Ceratomyxa* Thélohan, 1892 (Myxozoa: Myxosporea: Ceratomyxidae). Syst. Parasitol. 65(1), 49–71.

Eiras, J.C., Takemoto, R.M., & Pavanelli, G.C. (2009). *Henneguya corruscans* n. sp. (Myxozoa, Myxosporea, Myxobolidae), a parasite of *Pseudoplatystoma corruscans* (Osteichthyes, Pimelodidae) from the Paraná River, Brazil: a morphological and morphometric study. Vet. Parasitol. 159:154–158. https://doi.org/10.1016/j.vetpar.2008.10.020.

Eiras, J.C., Saraiva, A., Cruz, C.F., Santos, M.J., & Fiala, I. (2011). Synopsis of the species of *Myxidium* Bütschli, 1882 (Myxozoa: Myxosporea: Bivalvulida). Syst. Parasitol. 80, 81–116. https://doi.org/10.1007/s11230-011-9315-x.

Eiras, J.C., Zhang, J., & Molnár, K. (2014). Synopsis of the species of *Myxobolus* Bütschli, 1882 (Myxozoa: Myxosporea, Myxobolidae) described between 2005 and 2013. Syst. Parasitol. 88(1), 11–36. https://doi.org/10.1007/s11230-014-9484-5.

Eiras, J.C., Cruz, C.F., Saraiva, A., & Adriano, E.A. (2021). Synopsis of the species of *Myxobolus* (Cnidaria, Myxozoa, Myxosporea) described between 2014 and 2020. Folia Parasitol. https://doi.org/10.14411/fp.2021.012.

El-Mansy, A., & Molnár, K. (1997a). Exrapiscine development of *Myxobolus drjagini* Akhmerov, 1954 (Myxosporea: Myxobolidae) in oligochaete alternate hosts. Acta Vet. Hung. 45(4), 427–438.

El-Mansy, A., & Molnár, K. (1997b). Development of *Myxobolus hungaricus* (Myxosporea: myxobolidae) in oligochaete alternate hosts. Dis. Aquat. Org. 31, 227–232. https://doi.org/10.3354/dao031227.

El-Mansy, A., Molnár, K., & Székely, C. (1998c). Development of *Myxobolus portucalensis* Saraiva & Molnár, 1990 (Myxosporea: Myxobolidae) in the oligochaete *Tubifex tubifex* (Müller). Syst. Parasitol. 41, 95–103.

El-Mansy, A., Székely, C., & Molnár, K. (1998a). Studies on the occurrence of actinosporean stages of fish myxosporeans in a fish farm of Hungary, with the description of triactinomyxon, raabeia, aurantiactinomyxon and neoactinomyxon types. Acta Vet. Hung. 46, 259–284.

El-Mansy, A., Székely, C., & Molnár, K. (1998b) Studies on the occurrence of actinosporean stages of myxosporeans in Lake Balaton, Hungary, with the description of triactinomyxon, raabeia and aurantiactinomyxon types. Acta Vet. Hung. 46, 437–450.

El-Matbouli, M., & Hoffmann, R. (1989). Experimental transmission of two *Myxobolus* spp. developing bisporogeny via tubificid worms. Parasitol. Res. 75(6), 461–464.

El-Matbouli, M., Fischer-Scherl, T., & Hoffmann, R.W. (1992). Transmission of *Hoferellus carassii* Achmerov, 1960 to goldfish *Carassius auratus* via an aquatic oligochaete. Bull. Eur. Assoc. Fish Pathol. 12, 54–56.

El-Matbouli, M., & Hoffmann, R.W. (1993). *Myxobolus carassii* Klokaceva, 1914 also requires an aquatic oligochaete, *Tubifex tubifex* as an intermediate host in its life cycle. Bull. Eur. Assoc. Fish Pathol. 13, 189–192.

El-Matbouli, M., Hoffmann, R.W., & Mandok, C. (1995). Light and electron microscopic observations on the route of the triactinomyxon-sporoplasm of *Myxobolus cerebralis* from epidermis into rainbow trout cartilage. J. Fish Biol. 46, 919–935.

Emery, C. (1909). I missosporidii sono Protozoi? Monitore Zoologico Italiano 22, 247.

Erséus, C., Envall, I., De Wit, P., Gustavsson, L.M. (2017). Molecular data reveal a tropical freshwater origin of Naidinae (Annelida, Clitellata, Naididae). Mol. Phylogenet. Evol. 115, 115–127. https://doi.org/10.1016/j.ympev.2017.07.016.

Estensoro, I., M., Redondo, J., Alvarez-Pellitero, P., & Sitjà-Bobadilla, A. (2010). Novel horizontal transmission route for *Enteromyxum leei* (Myxozoa) by anal intubation of gilthead sea bream *Sparus aurata*. Dis. Aquat. Org. 92(1), 51–58. http://doi.org/10.3354/dao02267.

Eszterbauer, E., Székely, C., Molnár, K., & Baska, F. (2000). Development of *Myxobolus bramae* (Myxosporea: myxobolidae) in an oligochaete alternate host, *Tubifex tubifex*. J. Fish. Dis. 23, 19–25. https://doi.org/10.1046/j.1365-2761.2000.00202.x.

Eszterbauer E., Benkó M., Dán Á., & Molnár K. (2001). Identification of fish-parasitic *Myxobolus* (Myxosporea) species using a combined PCR-RFLP method. Dis. Aquat. Org. 44, 35–39.

Eszterbauer, E. (2004). Genetic relationship among gill-infecting *Myxobolus* species (Myxosporea) of cyprinids: Molecular evidence of importance of tissue-specificity. Dis. Aquat. Org. 58, 35–40. https://doi.org/10.3354/dao05 8035.

Eszterbauer, E., & Székely, C. (2004). Molecular phylogeny of the kidney- parasitic *Sphaerospora renicola* from common carp (*Cyprinus carpio*) and *Sphaerospora* sp. from goldfish (*Carassius auratus auratus*). Acta Vet. Hung. 52, 469–478.

Eszterbauer, E., Marton, S., Rácz, O.Z., Letenyei, M., & Molnár, K. (2006). Morphological and genetic differences among actinosporean stages of fish-parasitic myxosporeans (Myxozoa): difficulties of species identification. Syst. Parasitol. 65, 97–114. https://doi.org/10.1007/s11230-006-9041-y.

Eszterbauer, E., Sipos, D., Forró, B., Holzer, A.S. (2013). Molecular characterization of *Sphaerospora molnari* (Myxozoa), the agent of gill sphaerosporosis in common carp *Cyprinus carpio carpio*. Dis. Aquat. Org. 104, 59–67. https://doi.org/10.3354/dao02584.

Eszterbauer, E., Atkinson, S., Diamant, A., Morris, D., El-Matbouli, M., & Hartikainen, H. (2015). Myxozoan life cycles: practical approaches and insights. In: *Myxozoan Evolution, Ecology and Development*. Springer, London, UK, pp. 175–198. https://doi.org/10.1007/978-3-319-14753-6_10.

FAO (2018). The state of world fisheries and aquaculture. Food and Agriculture Organization of the United Nations.

Feist, S.W., Longshaw, M., Canning, E.U., & Okamura, B. (2001). Induction of proliferative kidney disease (PKD) in rainbow trout *Oncorhynchus mykiss* via the bryozoan *Fredericella sultana* infected with *Tetracapsula bryosalmonae*. Dis. Aquat. Org. 45, 61–68.

Ferreira, R.L.D.S., Silva, D.T.D., Araújo, P.G.D., Hamoy, I., Matos, E., & Videira, M.N. (2020). *Henneguya sacacaensis* n. sp. (Myxozoa: Myxosporea) parasitizing gills of the acará bicudo *Satanoperca jurupari* (Osteichthyes: Cichlidae) in eastern Amazon. Rev. Bras. Parasitol. Vet. 29, e000620.

Fiala, I. (2006). The phylogeny of Myxosporea (Myxozoa) based on small subunit ribosomal RNA gene analysis. Int. J. Parasitol. 36, 1521–1534.

Fiala, I., & Bartošová, P. (2010). History of myxozoan character evolution on the basis of rDNA and EF-2 data. BMC Evol. Biol. 10, 228. https://doi.org/10.1186/1471-2148-10-228.

Fiala, I., Bartošová-Sojková, P., & Whipps, C.M. (2015a). Classification and phylogenetics of Myxozoa. Myxozoan Evol. Ecol. Dev. 85–110.

Fiala, I., Hlavničková, M., Kodádková, A., Freeman, M.A., Bartošová-Sojková, P., & Atkinson, S.D. (2015b). Evolutionary origin of *Ceratonova shasta* and phylogeny of the marine myxosporean lineage. Mol. Phylogenet. Evol. 86, 75–89. https://doi.org/10.1016/j.ympev.2015.03.004.

Fiala, I., Bartošová-Sojková, P., Okamura, B., & Hartikainen, H. (2015c). Adaptive radiation and evolution within the Myxozoa. Myxozoan evolution, ecology and development, 69–84.

Figueredo, R.T., Müller, M.I., Arana, S., Long, P.F., & Adriano, E.A. (2023). Phylogenetic and host-parasite relationship analyses of *Henneguya caquetaia* sp. nov (Myxosporea: Myxobolidae) infecting an Amazonian cichlid fish. Microbial Pathog. 179, 106116.

Fomena, A., Marqueś, A., Bouix, G., & Njine, T. (1994). *Myxobolus bilongi* n. sp., *Thelohanellus assambai* n. sp. et *T. sanagaensis* n. sp., myxosporidies parasites de *Labeo* sp. (Téléstéen: Cyprinidae) du bassin de la Sanaga au Cameroun (Afrique Centrale). Annales de la Faculte´ des Sciences, Chimie, Sciences Naturelles, 3, 131–142.

Fomena, A., Lekeufack Folefack, G.B., & Tang, C. (2007). II. New species of *Myxobolus* (Myxosporea: Myxobolidae) parasites of fresh water fishes in Cameroon (Central Africa). J. Biol. Sci. 7, 1171–1178.

Franzolin, G.N., Araújo, B.L., Zatti, S.A., Naldoni, J., & Adriano, E.A. (2022). Occurrence of the host-parasite system *Rhaphiodon vulpinus* and *Ceratomyxa barbata* n. sp. in the two largest watersheds in South America. Parasitol. Int. 91, 102651. https://doi.org/10.1016/j.parint.2022.102651.

Freeman, M.A., & Kristmundsson, Á. (2015). Histozoic myxosporeans infecting the stomach wall of elopiform fishes represent a novel lineage, the Gastromyxidae. Parasit Vectors. http://doi.org/10.1186/s13071-015-1140-7.

Freeman, M.A., & Kristmundsson, A. (2018). Studies of *Myxidium giardi* Cèpède, 1906 infections in Icelandic eels identifies a genetically diverse clade of myxosporeans that represents the *Paramyxidium* n. g. (Myxosporea: Myxidiidae). Parasit. Vectors 11, 551. https://doi.org/10.1186/s13071-018-3087-y.

Froese, R. & Pauly, D. (eds.), 2025. FishBase, World Wide Web electronic publication, search by country.
Available:https://www.fishbase.se/country/CountryChecklist.php?what=list&trpp=50&c_code=458&csub_code=&cpresence=present&sortby=alpha2&ext_pic=on&vhabitat=fresh. [Accessed 22.06.2025].

Garcia, L.M.B. (2020). Species composition and length-weight relationship of fishes in the Candaba Wetland on Luzon Island, Philippines. J. Appl. Ichthyol. 26, 946–948.

Georges, F., Timoléon, T., Minette, T. E., & Joseph, T. (2017). Two new species of *Myxobolus* (Myxozoa: Myxosporea) parasites of *Barbus callipterus* Boulenger, 1907 (Cyprinidae) and *Oreochromis niloticus* Linnaeus, 1758 (Cichlidae) in Cameroon. J. Res. Biol. 7(7), 2355–2360.

Ghosh, S., & Bandyopadhyay, P.K. (2017). Description of three new species of the genus *Myxobolus* infecting carp fishes of India. J. Parasit. Dis. 41, 155–166. https://doi.org/10.1007/s12639-016-0769-2.

Gonzalez-Lanza, M.C., & Alvarez-Pellitero, M.P. (1985). *Myxobolus* spp. of various cyprinids from the River Esla (León, NW Spain). Description and population dynamics. Angew. Parasitol. 26, 71–83.

Gorbunova, M. (1936). Changes in the parasitic fauna of pike and roach according to their age. Uchenye Zapiski Leningradskogo Ordena Lenina Gosudarstvennogo Universiteta, No. 7 (Biol. Ser.), Fasc. 3, Problems of Economical Parasitology, Leningrad, pp. 5–30. (In Russian).

Goswami, U. (2021). Comparative studies of myxozoan parasites of wild and cultured freshwater fishes in India and Hungary. The Hungarian University of Agriculture and Life Sciences, pp. 127.

Goswami, U., Molnár, K., Cech, G., Eiras, J.C., Bandyopadhyay, P.K., Ghosh, S., Czeglédi, I. & Székely, C. (2021). Evidence of the American *Myxobolus dechtiari* was introduced along with its host *Lepomis gibbosus* in Europe: molecular and histological data. Int. J. Parasitol. Parasites Wildl.15, 51–57.

Grabner, D.S., & El-Matbouli, M. (2008). Transmission of *Tetracapsuloides bryosalmonae* (Myxozoa: Malacosporea) to *Fredericella sultana* (Bryozoa: Phylactolaemata) by various fish species. Dis. Aquat. Org. 79, 133 –139.

Grabner, D.S., & El-Matbouli, M. (2010b) Experimental transmission of malacosporean parasites from bryozoans to common carp (*Cyprinus carpio*) and minnow (*Phoxinus phoxinus*). Parasitology 137, 629–639.

Grabner, D.S., & El-Matbouli, M. (2010a). *Tetracapsuloides bryosalmonae* (Myxozoa: Malacosporea) portal of entry into the fish host. Dis. Aquat. Org. 90, 197–206.

Grassé, P.P. (1970). Embranchement des Myxozoaires. In: *Prcis de zoologie 1, invertebrates*, *2nd ed.*, Grassé, P.P., Poisson, R.A. & Tuzet, O. (eds.). Masson et Cie, Paris, France, pp. 107–111.

Griffin, M.J., Pote, L.M., Wise, D.J., Greenway, T.E., Mauel, M.J., & Camus, A.C. (2008). A novel *Henneguya* species from channel catfish described by morphological, histological, and molecular characterization. J. Aquat. Anim. Healt. 20(3), 127–135.

Grossheider, G., & Körting, W. (1992). First evidence that *Hoferellus cyprini* (doflein, 1898) is transmitted by *Nais* sp. Bull. Eur. Ass. Fish Pathol. 12, 17–20.

Gunter, N.L., & Adlard, R.D. (2008). Bivalvulidan (Myxozoa: Myxosporea) parasites of damselfishes with description of twelve novel species from Australia's Great Barrier Reef. Parasitology 135(10), 1165–1178. http://doi.org/10.1017/S0031182008004733.

Gunter, N., & Adlard, R. (2010). The demise of *Leptotheca* Thelohan, 1895 (Myxozoa: Myxosporea: Ceratomyxidae) and assignment of its species to *Ceratomyxa* Thelohan, 1892 (Myxosporea: Ceratomyxidae), *Ellipsomyxa* Koie, 2003 (Myxosporea: Ceratomyxidae), *Myxobolus* Butschli, 1882 and *Sphaerospora* Thelohan, 1892 (Myxosporea: Sphaerosporidae). Syst. Parasitol. 75(2), 81–104.

Gupta, A., & Kaur, H. (2016). Morphological and histopathological description of *Myxobolus adlardi* n. sp. (Cnidaria: Myxosporea: Myxozoa) infecting an Indian major carp, *Labeo rohita* Hamilton, 1822 from a cold-water wetland in Punjab (India). Bull. Pure Appl. Sci. 35, 39–52. https://doi.org/10.5958/2320-3188.2016.00009.7.

Gupta, A., & Kaur, H. (2018). 18S and 28S rDNA identity and phylogeny of two novel myxosporeans infecting gills of cyprinid carps inhabiting a cold water wetland in northern India, Microb. Pathog. 120, 97–108.

Gurley, R.R. (1893). On the classification of Myxosporidia, a group of protozoan parasites infesting fishes. Bull. U. S. Fish. Comm. 11, 407–420.

Hallett, S.L., Erséus, C., & Lester, R.J.G. (1997). Actinosporea from Hong Kong marine oligochaeta. In Proceedings of the eight international marine biological workshop: the marine flora and fauna of Hong Kong and Southern China. Hong Kong University Press, Hong Kong. pp. 1–7.

Hallett, S.L., ÒDonoghue, P.J., & Lester, R.J.G. (1998). Structure and development of a marine actinosporean, *Sphaeractinomyxon ersei* n. sp. (Myxozoa). J. Eukaryot. Microbiol. 45, 142–150. https://doi.org/10.1111/j.1550-7408.1998.tb05082.x.

Hallett, S.L., & Lester, R.J.G. (1999). Actinosporeans (Myxozoa) with four developing spores within a pansporocyst: *Tetraspora discoidea* n. g. n. sp. and *Tetraspora rotundum* n. sp. Int. J. Parasitol. 29, 419–427.

Hallett, S.L., Erséus, C. & Lester, R.J.G. (1999). Actinosporeans (Myxozoa) from marine oligochaetes of the Great Barrier Reef. Syst. Parasitol. 44, 49–57.

Hallett, S. L., & Diamant, A. (2001). Ultrastructure and small-subunit ribosomal DNA sequence of *Henneguya lesteri* n. sp. (Myxosporea), a parasite of sand whiting *Sillago analis*

(Sillaginidae) from the coast of Queensland, Australia. Dis. Aquat. Org. 46, 197–212. https://doi.org/10.3354/dao046197.
Hallett, S.L., Erséus, C., ÓDonoghue, P.J., & Lester, R.J.G. (2001). Parasite fauna of Australian marine oligochaetes. Memoirs of the Queensland Museum 46, 555–576.
Hallett, S.L., Atkinson, S.D., & El-Matbouli, M. (2002). Molecular characterization of two aurantiactinomyxon (Myxozoa) phenotypes reveal one genotype. J. Fish. Dis. 25(10), 627–631.
Hallett, S.L., Atkinson, S.D., Erséus, C., & El-Matbouli, M. (2004). Molecular methods clarify morphometric variation in triactinomyxon spores (Myxozoa) released from different oligochaete hosts. Syst. Parasitol. 57, 1–14. https://doi.org/10.1023/B:SYPA.0000010682.90311.91.
Hallett, S.L., Atkinson, S.D., Erséus, C., & El-Matbouli, M. (2005). Dissemination of triactinomyxons (Myxozoa) via oligochaetes used as live food for aquarium fishes. Dis. Aquat. Org. 65, 137–152.
Hallett, S.L., Atkinson, S.D., Holt, R.A., Banner, C.R., & Bartholomew, J.L. (2006) A new myxozoan from feral goldfish (*Carassius auratus*). J. Parasitol. 92, 357–363.
Halliday, M.M. (1976). The biology of *Myxosoma cerebralis*: the causative organism of whirling disease of salmonids. J. Fish Biol. 9, 339–357.
Hartikainen, H., Gruhl, A., & Okamura, B. (2014). Diversification and repeated morphological transitions in endoparasitic cnidarians (Myxozoa: Malacosporea). Mol. Phylogenet. Evol. 76, 261–269. https://doi.org/10.1016/j.ympev.2014.03.010.
Hedrick, R.P., MacConnell, E., & De Kinkelin, P. (1993), Proliferative kidney disease of salmonid fish. Ann. Rev. Fish Dis. 3, 277–290. https:// doi.org/ 10. 1016/ 0959- 8030(93) 90039-E
Hedrick, R.P., McDowell, T.S., Mukkatira, K., Georgadis, M.P., & MacConnell, E. (2001). Susceptibility of three species of anadromous salmonids to experimentally induced infectious with *Myxobolus cerebralis*, the causative agent of whirling disease. J. Aquat. Anim. Health. 13, 43–50. https://doi.org/10.1577/1548-8667(2001)013<0043:SOTSOA>2.0.CO;2.
Heiniger, H., Gunter, N.L., & Adlard, R.D. (2011). Re-establishment of the family Coccomyxidae and description of five novel species of *Auerbachia* and *Coccomyxa* (Myxosporea: Bivalvulida) parasites from Australian fishes. Parasitology 138(4), 501–15. http://doi.org/10.1017/S0031182010001447.
Heiniger, H., & Adlard, R.D. (2013). Molecular identification of cryptic species of *Ceratomyxa* Thélohan, 1892 (Myxosporea: Bivalvulida) including the description of eight novel species from apogonid fishes (Perciformes: Apogonidae) from Australian waters. Acta Parasitol. 58(3), 342–60. http://doi.org/10.2478/s11686-013-0149-3.
Hensel, K. (1971). Some notes on the systematic status of *Carassius auratus gibelio* (Bloch, 1782) with further record of this fish from the Danube River in Czechoslovakia. Věstn. Československ. Spol. Zool. 3, 186–198.
Hepps Keeney, C.M., Waltzek, T.B., de Oliveira Viadanna, P.H., Frasca Jr, S., Reinhardt, E., Lovy, J., & Lewbart, G.A. (2023). *Myxobolus lentisuturalis* infection in a farmed population of goldfish *Carassius auratus* from the USA. Dis. Aquat. Org. 154, 7–14. https://doi.org/10.3354/dao.
Hillis, D.M., & Dixon, M.T. (1991). Ribosomal DNA: molecular evolution and phylogenetic inference. Q. Rev. Biol. 66, 411–453. https://doi.org/10.1086/417338.
Hoffman, G.L., Putz, R.E., & Dunbar, C.E. (1965). Studies on *Myxosoma cartilaginis* n. sp. (Protozoa: Myxosporidea) of centrarchid fish and a synopsis of the *Myxosoma* of North American freshwater fishes. J. Protozool. 12, 319–332.
Hoffman, G.L., & Putz, R. (1969). Host susceptinility and the effect of aging, freezing, heat, and chemicals on spores of *Myxosoma cerebralis*. Progr. Fish-Cult. 31, 35–37.
Hoffman, G.L. (1990). *Myxobolus cerebralis*, a worldwide cause of salmonid whirling disease. J. Aquat. Anim. Health 2(1), 30–37.

Holland, J.W., Okamura, B., Hartikainen, H., & Secombes, C.J. (2010). A novel minicollagen gene links cnidarians and myxozoans. Proc. Biol. Sci. 278(1705), 546.
Holzer, A.S., Sommerville, C., & Wootten, R. (2004). Molecular relationships and phylogeny in a community of myxosporeans and actinosporeans based on their 18S rDNA sequences. Int. J. Parasitol. 34(10), 1099–1111. https://doi.org/10.1016/j.ijpara.2004.06.002.
Holzer, A.S., Sommerville, C., & Wootten, R. (2006). Molecular identity, phylogeny and life cycle of *Chloromyxum schurovi* Shulman & leshko 2003. Parasitol. Res. 99, 90–96.
Holzer, A.S., Hartigan, A., Patra, S., Pecková, H., & Eszterbauer, E. (2014). Molecular fingerprinting of the myxozoan community in common carp suffering swim bladder inflammation (SBI) identifies multiple etiological agents. Parasit. Vectors 71–9. https:// doi. org/10. 1186/ 1756- 3305-7- 398.
Holzer, A.S., Sommerville, C., & Wootten, R. (2013). Tracing the route of *Sphaerospora truttae* from the entry locus to the target organ of the host, *Salmo salar* L., using an optimized and specific in situ hybridization technique. J. Fish Dis. 26, 647–655. https://doi.org/10.4060/cc0461en.
Huskanović, L. (2021). Utjecaj nametnika roda Myxobolus na zdravstveno stanje srebrnog karasa (*Carassius gibelio* Bloch, 1782) u otvorenim vodama [an impact of parasites from the genus *Myxobolus* on the health status of gibel carp (*Carassius gibelio* Bloch, 1782) in open waters] [Master thesis]. University of Zagreb (in Croatian).
Ikeda, I. (1912). Studies on some sporozoan parasites of sipunculoids. I. The life history of a new actinomyxidian Tetractinomyxon intermedium g. et sp. nov. Archiv für Protistenkunde 25, 240–272.
Imran, M., Sajid, M.S., Swar, S.O., Khan, M.K., Malik, M.A., & Ahmad, A. (2021). Parasitic diseases of fish. Vet. Pathobiol. Public Health 1, 203–214.
Ismail, M.Z. (1989). Systematics, zoogeography and conservation of the freshwater fishes of Peninsular Malaysia. Unpublished Ph.D. dissertation, Colorado State University, Fort Collins, Colorado, USA. 473 p.
Janiszewska, J. (1957). Actinomyxidia II. New systematics, sexual cycles, description of new genera and species. Zool. Pol. 8, 3–34.
Jeney, G. (1979). The occurrence of *Thelohanellus dogieli* Achmerov, 1955 (Myxosporidia) on carp (*Cyprinus carpio*) in fish ponds in Hungary. Parasit. Hung. 12, 19–20.
Jiménez-Guri, E., Philippe, H., Okamura, B., & Holland, P.W. (2007). *Buddenbrockia* is a cnidarian worm. Science 317, 116–118.
Jirků, M., Fiala, I., & Modrý, D. (2007). Tracing the genus *Sphaerospora*: rediscovery, redescription and phylogeny of the *Sphaerospora ranae* (Morelle, 1929) n. comb. (Myxosporea, Sphaerosporidae), with emendation of the genus *Sphaerospora*. Parasitology 134(12), 1727–1739. https://doi.org/10.1017/S0031182007003241.
Johnson, K.A. (1975). Host susceptibility, histopathologic, and transmission studies on Ceratomyxa shasta, a myxosporidan parasite of salmonid fish.
Johnson, K.A., Sanders, J.E., & Fryer, J.L. (1979). *Ceratomyxa shasta* in salmonids. US Fish and Wildlife Service.
Jorge, M., Vieira, D.H.M.D., Zago, A.C., Franceschini, L., & da Silva, R.J. (2022). *Henneguya polarislonga* n. sp. (Cnidaria: Myxosporea) parasitizing *Astyanax lacustris* (Lütken, 1875) with an insight on its life cycle. Parasitol. Int. 91, 102658. https://doi.org/10.1016/j.parint.2022.102658.
Jouiaei, M., Yanagihara, A.A., Madio, B., Nevalainen, T.J., Alewood, P.F., & Fry, B.G. (2015). Ancient Venom Systems: A Review on Cnidaria Toxins. Toxins, 7, 2251–2271. https://doi.org/10.3390/toxins7062251.
Kallert, D.M., El-Matbouli, M., & Haas, W. (2005a). Polar filament discharge of *Myxobolus cerebralis* actinospores is triggered by combined non-specific mechanical and chemical cues. Parasitology 131, 609–616.

Kallert, D.M., Eszterbauer, E., Erseus, C., El-Matbouli, M., & Haas, W. (2005b). Life cycle studies of *Myxobolus parviformis* sp. n. (Myxozoa: Myxobolidae) from bream. Dis. Aquat. Org. 66, 233–243. https://doi.org/10.3354/dao.

Kallert, D.M., Ponader, S., Adelt, S., Kaese, P., Geyer, R., Haas, W., & El-Matbouli, M. (2010). Analysis of rainbow trout *Oncorhynchus mykiss* epidermal mucus and evaluation of semiochemical activity for polar filament discharge in *Myxobolus cerebralis* actinospores. J. Fish Biol. 77, 1579–1598. https://doi.org/10.1111/j.1095-8649.2010.02785.x.

Källersjö, M., von Proschwitz, T., Lundberg, S., Eldenäs, P., & Erséus, C. (2005). Evaluation of ITS rDNA as a complement to mitochondrial gene sequences for phylogenetic studies in freshwater mussels: an example using Unionidae from north-western Europe. Zool. Scr. 34, 415–424. https://doi.org/10.1111/j.1463-6409.2005.00202.x.

Kalous, L., Bohlen, J., Rylková, K., & Petrtý, M. (2012). Hidden diversity within the Prussian carp and designation of a neotype for *Carassius gibelio* (Teleostei: Cyprinidae). Ichthyol. Explor. Freshw. 23, 11–18.

Karlsbakk, E., & Køie, M. (2012). The marine myxosporean *Sigmomyxa sphaerica* (Thelohan, 1895) gen. n., comb. n. (syn. *Myxidium sphaericum*) from garfish (*Belone belone* (L.)) uses the polychaete *Nereis pelagica* L. as invertebrate host. Parasitol. Res. 110, 211–218. https://doi.org/10.1007/s00436-011-2471-8.

Karlsbakk, E., Kristmundsson, Á., Albano, M., Brown, P., & Freeman, M.A. (2017). Redescription and phylogenetic position of *Myxobolus aeglefini* and *Myxobolus platessae* n. comb. (Myxosporea), parasites in the cartilage of some North Atlantic marine fishes, with notes on the phylogeny and classification of the Platysporina. Parasitol. Int. 66, 952–959. https://doi.org/10.1016/j.parint.2016.10.014.

Kato, E., Kasai, A., Tomochi, H., Li, Y. C., & Sato, H. (2017). Four *Myxobolus* spp. (Myxosporea: Bivalvulida) from the gill lamellae of common carp (*Cyprinus carpio*) and Japanese silver crucian carp (*Carassius langsdorfii*) in the western part of Japan, with the description of three new species (*M. tanakai* n. sp., *M. paratoyamai* n. sp., and *M. ginbuna* n. sp. Parasitol. Res. 116(9), 2427–2441. https://doi.org/10.1007/s00436-017-5545-4.

Kaur, H., & Singh, H.S. (2010). Two new species of *Myxobolus* (myxosporea, Bivalvulida) from the Indian major carp *Labeo rohita* Hamilton, 1822. Protistology 6, 264–270.

Kaur, H., & Gupta, A. (2017). Molecular and phylogenetic characterization of *Thelohanellus boggoti* Qadri, 1962 (Cnidaria, Myxosporea, Bivalvulida) infecting the fin of Indian minor carp *Labeo dero* (Hamilton, 1822). Mol. Biol. Res. Comm. 6(1), 13.

Kawai, T., Sekizuka, T., Yahata, Y., Kuroda, M., Kumeda, Y., Iijima, Y., Kamata, Y., Sugita-Konishi, Y., & Ohnishi, T. (2012). Identification of *Kudoa septempunctata* as the causative agent of novel food poisoning outbreaks in Japan by consumption of *Paralichthys olivaceus* in raw fish. Clin. Infect Dis. 54, 1046–1052. https://doi.org/10.1093/cid/cir1040.

Kawano, K.M., Sakurai, M., & Yanagida, T. (2025). Description of *Myxobolus iwagiensis* n. sp. (Myxosporea: Myxobolidae), infecting medaka *Oryzias latipes* (Temminck & Schlegel, 1846) (Beloniformes: Adrianichthyidae) in Japan. Parasitol. Int. 108, 103074. https://doi.org/10.1016/j.parint.2025.103074.

Kearse, M., Moir, R., Wilson, A., Stones-Havas, S., Cheung, M., Sturrock, S., Cheung, M., Sturrock, S., Buxton, S., Cooper, A., Markowitz, S., Duran, C., Thierer, T., Ashton, B., Meintjes, P., & Drummond, A. (2012). Geneious basic: an integrated and extendable desktop software platform for the organization and analysis of sequence data. Bioinformatics 28, 1647–1649. https://doi.org/10.1093/bioinformatics/bts199.

Kent, M.L., Whitaker, D.J., & Margolis, L. (1993). Transmission of *Myxobolus arcticus* Pugachev and Khokhlov, 1979, a myxosporean parasite of Pacific salmon, via a triactinomyxon from the aquatic oligochaete *Stylodrilus heringianus* (Lumbriculidae). Can. J. Zool. 71(6), 1207–1211.

Kent, M., & Lom, J. (1999). Can a new species of Myxozoa be described based solely on their actinosporean stage? Parasitol. Today 15(12), 472–473.

Kent, M.L., Andree, K.B., Bartholomew, J.L., El-Matbouli, M., Desser, S.S., Devlin, R.H., Feist, S.W., Hedrick, R.P., Hoffmann, R.W., Khattra, J., Hallett, S.L., Lester, R.J.G., Longshaw, M., Palenzeula, O., & Siddall, M.E. (2001). Recent advances in our knowledge of the Myxozoa. J. Eukaryot. Microbiol. 48, 395–413. https://doi.org/10.1111/j.1550-7408.2001.tb00173.x.

Kent, M.L., Margolis, L., & Corliss, J.O. (1994). The demise of a class of protists: taxonomic and nomenclatural revisions proposed for the protest phylum Myxozoa Grassé, 1970. Can. J. Zool. 72(5), 932–937.

Kenthao, A., & Jearranaiprepame, P. (2020). Ecomorphological diversification of some barbs and carps (Cyprininae, Cyprinidae) in the Lower Mekong Basin of Thailand. Zoology 143, 125830.

Køie, M. (2000). First record of an actinosporean (Myxozoa) in a marine polychaete annelid. J. Parasitol. 86(4), 871–872.

Køie, M., Whipps, C.M., & Kent, M.L. (2004). *Ellipsomyxa gobii* (Myxozoa: Ceratomyxidae) in the common goby *Pomatoschistus microps* (Teleostei: Gobiidae) uses *Nereis* spp. (Annelida: Polychaeta) as invertebrate hosts. Folia Parasitol. 51, 14–18.

Køie, M., Karlsbakk, E., & Nylund, A. (2007). A new genus *Gadimyxa* with three new species (Myxozoa, Parvicapsulidae) parasitic in marine fish (Gadidae) and the two-host life cycle of *Gadimyxa atlantica* n. sp. J. Parasitol. 93, 1459–1467. https://doi.org/10.1645/GE-1256.1.

Køie, M., Karlsbakk, E., & Nylund, A. (2008). The marine herring myxozoan *Ceratomyxa auerbachi* (Myxozoa: Ceratomyxidae) uses *Chone infundibuliformis* (Annelida: Polychaeta: Sabellidae) as invertebrate host. Folia Parasitol. 55, 100–104.

Køie, M., Karlsbakk, E., Einen, A.C.B., & Nylund, A. (2013). A parvicapsulid (Myxozoa) infecting *Sprattus sprattus* and *Clupea harengus* (Clupeidae) in the Northeast Atlantic uses Hydroides norvegicus (Serpulidae) as invertebrate host. Folia Parasitol. 60, 149–154. https://doi.org/10.14411/fp.2013.016.

Kottelat, M. (2001). Fishes of Laos. WHT Publications Ltd., Colombo.

Kovacs, G.E., & Molnár, K. (1983). Studies on the biology and pathology of the common carp parasite *Myxobolus basilamellaris* Lom et Molnár, 1983 (Myxozoa: Myxosporea). Acta Vet. Hung. 31, 91–102.

Ksepka, S.P., & Bullard, S.A. (2021). Two new species of *Myxobolus* Bütschli, 1882 (Cnidaria: Bivalvulida: Myxobolidae) infecting the gill of the black redhorse, *Moxostoma duquesnei* (Lesueur) (Cypriniformes: Catostomidae) in the Little Tennessee River Basin, North Carolina. Syst. Parasitol. 98, 713–730. https://doi.org/10.1007/s11230-021-10007-3.

Kudo, R. (1917). Contributions to the Study of Parasitic Protozoa. II. *Myxobolus toyamai* nov. spec., a new myxosporidian parasite in *Cyprinus Carpio* L. J. Parasitol. 3(4), 163–170.

Kudo, R. (1920). Studies on Myxosporidia. A synopsis of genera and species of Myxosporidia. Ill. Biol. Monogr. 5, 1–125.

Kudo, R. (1933). A taxonomic consideration of Myxosporidia. Trans. Am. Microsc. Soc. 52, 195–216.

Kumar, S., Stecher, G., Li, M., Knyaz, C., & Tamura, K. (2018). Mega X: molecular evolutionary genetics analysis across computing platforms. Mol. Biol. Evol. 35, 1547–1549.

Kurobe, T., Kurita, J., Haenen, O., Voorbergen-Laarman, M., & Ito, T. (2024). Mass mortality events associated with cyprinid herpesvirus 2 (CyHV-2) infection in wild Prussian carp *Carassius gibelio* in the Netherlands, and molecular biology of virus strains. J. Fish Dis. 47(1), e13868. https://doi.org/10.1111/jfd.13868.

Ky, H. (1971). Some myxosporidians of freshwater fishes of North Viet Nam. Acta Protozoologica 8, 283–298.

Ky, H., & Te, B.Q. (2007). Parasites on Freshwater fish in Viet Nam. Science and Technics Publishing House.

Leis, E.M., Rosser, T.G., Baumgartner, W.A., & Griffin, M.J. (2017). *Henneguya laseeae* n. sp. from flathead catfish (Pylodictis olivaris) in the upper Mississippi River. Parasitol. Res. 116, 81–89. https://doi.org/10.1007/s00436-016-5264-2.

Li, C., Suo, D., Yang, C.Z., & Zhao, Y. (2016). Redescription of *Myxidium cuneiforme* Fujita, 1924 (Myxosporea: Bivalvulida) and molecular phylogeny with its relative species. Sichuan J. Zool. 35, 384–390.

Li, Z.Y., Wang, J. T., Zhou, M., Sato, H., & Zhang, J.Y. (2023). Morphological and molecular characterization of a new freshwater *Ceratomyxa* species (Cnidaria: Myxozoa) from the yellow catfish, *Trachysurus fulvidraco* in China. Parasitol. Int. 97, 102778. https://doi.org/10.1016/j.parint.2023.102778.

Lin, D.J., Hanson, L.A., & Pote, L.M. (1999). Small subunit ribosomal RNA sequence of *Henneguya exilis* (Class Myxosporea) identifies the actinosporean stage from an oligochaete host. J. Eukaryot. Microbiol. 46, 66–68.

Liu, Y., Whipps, C.M., Gu, Z.M., & Zeng, L.B. (2010a). *Myxobolus turpisrotundus* (Myxosporea: Bivalvulida) spores with caudal appendages: investigating the validity of the genus *Henneguya* with morphological and molecular evidence. Parasitol. Res. 107, 699–706. https://doi.org/10.1007/s00436-010-1924-9.

Liu, Y., Gu, Z.M., & Luo, Y.L. (2010b). Some additional data to the occurrence, morphology and validity of *Myxobolus turpisrotundus* Zhang, 2009 (Myxozoa: Myxosporea). Parasitol. Res. 107, 67–73. https://doi.org/10.1007/s00436-010-1835-9.

Liu, Y., Whipps, C.M., Gu, Z.M., Huang, M.J., He, C., Yang, H.L., & Molnár, K. (2013). *Myxobolus musseliusae* (Myxozoa: Myxobolidae) from the gills of common carp *Cyprinus carpio* and revision of *Myxobolus dispar* recorded in China. Parasitol. Res. 112, 289–296. https://doi.org/10.1007/s00436-012-3136-y.

Liu, Y., Whipps, C.M., Nie, P. & Gu, Z. (2014a). *Myxobolus oralis* sp. n. (Myxosporea: Bivalvulida) infecting the palate in the mouth of gibel carp *Carassius auratus gibelio* (Cypriniformes: Cyprinidae). Folia Parasitol. 61, 505–511.

Liu, Y., Jia, L., Huang, M.J., Gu, Z.M. (2014b). *Thelohanellus testudineus* n. sp. (Myxosporea: Bivalvulida) infecting the skin of allogynogenetic gibel carp *C. arassius auratus gibelio* (Bloch) in China. J. Fish Dis. 37, 535–542. https://doi.org/10.1111/jfd.12141.

Liu, Y., Yuan, J., Jia, L., Huang, M., Zhou, Z., & Gu, Z. (2014c). Supplemental description of *Thelohanellus wuhanensis* Xiao & Chen, 1993 (Myxozoa: Myxosporea) infecting the skin of *Carassius auratus gibelio* (Bloch): ultrastructural and histological data. Parasitol. Int. 63, 489–491. https://doi.org/10.1016/j.parint.2014.01.003.

Liu, X.H., Zhang, J.Y., Batueva, M.D., & Voronin, V.N. (2015). Supplemental description and molecular characterization of *Myxobolus miyarii* Kudo, 1919 (Myxosporea: Myxobolidae) infecting intestine of Amur catfish (*Silurus asotus*). Parasitol. Res. 115, 1547–1556. https://doi.org/10.1007/s00436-015-4889-x.

Liu, X.H., Batueva, M.D., Zhao, Y.L., Zhang, J.Y., Zhang, Q.Q., Li, T.T., & Li, A.H. (2016a). Morphological and molecular characterisation of *Myxobolus pronini* n. sp. (Myxozoa: Myxobolidae) from the abdominal cavity and visceral serous membranes of the gibel carp *Carassius auratus gibelio* (Bloch) in Russia and China. Parasit. Vectors 9, 1–11.

Liu, X.H., Voronin, V.N., Dudin, A.S., & Zhang, J.Y. (2016b). Morphological and molecular characterization of *Myxobolus mucosus* sp. n. (Myxosporea: Myxobolidae) with basifilamental sporulation in two cyprinid fishes, *Rutilus rutilus* (L.) and Leuciscus leuciscus (L.) in Russia. Parasitology Research, 115(3), 1297–1304. https://doi.org/10.1007/s00436-015-4866-4.

Liu, Y., Zhai, Y., & Gu, Z. (2016c). Morphological and molecular characterization of *Thelohanellus macrovacuolaris* n. sp. (Myxosporea: Bivalvulida) infecting the palate in the mouth of common carp *Cyprinus carpio* L. in China. Parasitol. Int. 65(4), 303–307. https://doi.org/10.1016/j.parint.2016.02.013.

Liu, X.H., Zhang, J.Y., Batueva, M.D., & Voronin, V.N. (2016d). Supplemental description and molecular characterization of *Myxobolus miyarii* Kudo, 1919 (Myxosporea: Myxobolidae) infecting intestine of Amur catfish (*Silurus asotus*). Parasitol. Res. 115(4), 1547–1556.

Liu, X.H., Yuan, S., Zhao, Y.L., Fang, P., Chen, H., & Zhang, J.Y. (2016e). Morphological and molecular characterization of *Myxobolus sheyangensis* n. sp. (Myxosporea: Myxobolidae) with intralamellar sporulation in allogynogenetic gibel carp, *Carassius auratus gibelio* (Bloch) in China. Parasitol. Res. 115(9), 3567–3574. https://doi.org/10.1007/s00436-016-5122-2.

Lom, J., & Hoffman, G.L. (1972). Morphology of the spores of *Myxosoma cerebralis* (Hofer, 1903) and *M. cartilaginis* (Hoffman, Putz, and Dunbar, 1965). J. Parasitol. 57, 1302–1308.

Lom, J., Dyková, I., Pavlásková, M., & Grupcheva, G. (1983). *Sphaerospora molnari* sp. nov. (Myxozoa: Myxosporea), an agent of gill, skin and blood sphaerosporosis of common carp in Europe. Parasitology 86, 529–535.

Lom, J., & Molnár, K. (1983). *Myxobolus basilamellaris* sp. n. (Myxozoa, Myxosporea), a parasite of the gills of common carp (*Cyprinus carpio* L.). Folia Parasitol. 30, 1–3.

Lom, J., & Noble, E.R. (1984). Revised classification of the class Myxosporea Bütschli, 1881. Folia Parasitol. 31, 193–205.

Lom, J., & Arthur, J.R. (1989). A guideline for preparation of species descriptions in Myxosporea. J. Fish Dis. 12:151–156.

Lom, J., & Dyková, I. (1992). Myxosporidia (Phylum Myxozoa). In: *Protozoan parasites of fishes, Developments in Aquaculture and Fisheries Science*, Book 26. Elsevier.

Lom, J., & Dyková, I. (1993). Scanning electron microscopic revision of common species of the genus *Chloromyxum* (Myxozoa: Myxosporea) infecting European freshwater fishes. Folia Parasitol. 40, 161–174.

Lom, J., McGeorge, J., Feist, S. W., Morris, D., & Adams, A. (1997). Guidelines for the uniform characterisation of the actinosporean stages of parasites of the phylum Myxozoa. Dis. Aquat. Org. 30(1), 1–9.

Lom, J., & Dyková, I. (2006) Myxozoan genera: definition and notes on taxonomy, life-cycle terminology and pathogenic species. Folia Parasitol. 53, 1–36.

Longshaw, M., Frear, P. & Feist, S.W. (2003). *Myxobolus buckei* sp. n. (Myxozoa), a new pathogenic parasite from the spinal column of three cyprinid fishes from the United Kingdom. Folia Parasitol. 50, 251–262.

Low B.W., Tan H.H., & Britz, R. (2014). *Trichopodus poptae*, a new anabantoid fish from Borneo (Teleostei: Osphronemidae). Ichthyol. Explor. Freshwat. 25(1), 69–77.

Lowers, J.M., & Bartholomew, J.L. (2003). Detection of myxozoan parasites in oligochaetes imported as food for ornamental fish. J. Parasitol. 89, 84–91. https://doi.org/10.1645/0022-3395(2003)089[0084:DOMPIO]2.0.CO;2.

Lucký, Z. (1978). Occurrence of *Myxobolus pavlovskii* - the parasite of *Hypophthalmichthys molitrix* and *Aristichthys nobilis* in the Fish Ponds in Czechoslovakia. Acta Vet. Brno 47, 2039–208.

Majumder, S., Panda, S., Ghosh, S., & Bandyopadhyay, P.K. (2015). Description of a new species of *Myxobolus* Butschli, 1882 from the *Cirrhinus mrigala* Hamilton, 1822 an edible fish of India. J. Parasit. Dis. 39, 456–460. https://doi.org/10.1007/s12639-013-0369-3.

Mansour, O., Idris, M., Noor, N.M., & Das, S.K. (2017). Growth performance of tinfoil barb (*Barbonymus schwanenfeldii*) fry feeding with different protein content diets. AACL Bioflux. 10, 475–479.

Manrique, W.G., Figueiredo, M.A.P., de Andrade Belo, M.A. Martins, M.L., & Azevedo, C. (2016). Ultrastructural description of *Myxobolus cuneus* (Myxosporea) in the skeletal muscle and kidney of tropical farmed fish *Piaractus mesopotamicus* (Characiformes: Characidae). Parasitol. Res. 115, 2505–2510. https://doi.org/10.1007/s00436-016-5026-1.

Marcucci, C., Caffara, M., & Goretti, E. (2009). Occurrence of actinosporean stages (Myxozoa) in the Nera River system (Umbria, Central Italy). Parasitol. Res. 105, 1517–1530. https://doi.org/10.1007/s00436-009-1586-7.

Marquès, A. (1984). Contribution à la connaissance des Actinomyxidies: ultrastructure, cycle biologique, systématique. PhD Thesis, Université des Sciences et Techniques du Languedoc, Montpellier, France. Thèse d'État, 218 p.

Martinsen, E.S., Paperna, I., & Schall, J.J. (2006). Morphological versus molecular identification of avian Haemosporidia: an exploration of three species concepts. Parasitology 133, 279–288. https://doi.org/10.1017/S0031182006000424.

Marton, S., & Eszterbauer, E. (2011). The development of *Myxobolus pavlovskii* (Myxozoa: Myxobolidae) includes an echinactinomyxon-type actinospore. Folia Parasitol. 58, 157–163.

Marton, S., & Eszterbauer, E. (2012). The susceptibility of diverse species of cultured oligochaetes to the fish parasite *Myxobolus pseudodispar* Gorbunova (Myxozoa). J. Fish Dis. 35, 303–314. https://doi.org/10.1111/j.1365-2761.2012.01347.x.

Mathews, P.D., Naldoni, J., Maia, A.A., & Adriano, E.A. (2016). Morphology and small subunit rDNA-based phylogeny of *Ceratomyxa amazonensis* n. sp. parasite of *Symphysodon discus*, an ornamental freshwater fish from Amazon. Parasitol. Res. 115(10), 4021–4025. https://doi.org/10.1007/s00436-016-5173-4.

Mathews, P.D., Mertins, O., Espinoza, L.L., Milanin, T., Alama-Bermejo, G., Audebert, F., & Morandini, A.C. (2020). Taxonomy and 18S rDNA-based phylogeny of *Henneguya multiradiatus* n. sp. (Cnidaria: Myxobolidae) a parasite of *Brochis multiradiatus* from Peruvian Amazon. Microbial Pathog. 147, 104372.

Matsche, M.A., Yurakhno, V., Zhang, J., & Sato, H. (2021). Synopsis of the species of the genus *Zschokkella* Auerbach, 1910 (Myxozoa: Bivalvulida: Myxidiidae). Syst. Parasitol. 98, 25–55. https://doi.org/10.1007/s11230-020-09960-2.

McAllister, C.T., Cloutman, D.G., Leis, E.M., & Robinson, H.W. (2022). A new species of *Myxidium* (Cnidaria: Myxosporea: Myxidiidae) from the gallbladder of pickerels, *Esox* spp. (Esociformes: Esocidae), from southwestern Arkansas, USA. Syst. Parasitol. 99, 611–620. https://doi.org/10.1007/s11230-022-10050-8.

McAllister, C.T., Cloutman, D.G., Leis, E.M., Camus, A.C. & Robison, H.W. (2023). A new *Myxobolus* (Cnidaria: Myxosporea: Myxobolidae) from the gills of the southern striped shiner, *Luxilus chrysocephalus isolepis* (Cypriniformes: Leuciscidae), from southwestern Arkansas, USA. Syst. Parasitol. 100, 215–229. https://doi.org/10.1007/s11230-023-10082-8.

McAllister, C.T., Cloutman, D.G., Leis, E.M., & Robison, H.W. (2024). Myxozoans (Cnidaria: Myxosporea: Myxidiidae) Identified from the Gallbladder of Freckled Madtom, *Noturus nocturnus* (Siluriformes: Ictaluridae), from the Ouachita River Drainage of Southern Arkansas. J. Parasitol. 110(6), 642–648.

McAllister, C.T., Cloutman, D.G., Leis, E.M. Robinson, H.W. (2025). A new *Myxidium* (Cnidaria: Myxosporea: Myxidiidae) from the gallbladder of the yellow bullhead, *Ameiurus natalis* (Siluriformes: Ictaluridae), from Southwestern Arkansas, USA. Syst. Parasitol 102, 40. https://doi.org/10.1007/s11230-025-10234-y.

McGeorge, J., Sommerville, C., & Wootten, R. (1996). Transmission experiments to determine the relationship between *Sphaerospora* sp. from Atlantic salmon, *Salmo salar*, and *Sphaerospora truttae*: A revised species description for *S. truttae.* Folia Parasitol. 43(2), 107–116.

McGeorge, J., Sommerville, C., & Wootten, R. (1997). Studies of actinosporean myxozoan stages parasitic in oligochaetes from the sediments of a hatchery where Atlantic salmon harbour *Sphaerospora truttae* infection. Dis. Aquat. Org. 30(2), 107–119. https://doi:10.3354/dao030107.

McGurk, C., Morris, D.J., Auchinachie, N.A., & Adams, A. (2006a). Development of *Tetracapsuloides bryosalmonae* (Myxozoa: Malacosporea) in bryozoan hosts (as examined by light microscopy) and quantitation of infective dose to rainbow trout (*Oncorhynchus mykiss*). Vet Parasitol. 135, 249–257. https://doi.org/10.1016/j.vetpar.2005.07.022.

Milanin, T., Eiras, J.C., Arana, S., Maia, A.A., Alves, A.L., Silva, M.R., Carriero, M.M., Ceccarelli, P.S., & Adriano, E.A. (2010). Phylogeny, ultrastructure, histopathology and prevalence of *Myxobolus oliveirai* sp. nov., a parasite of *Brycon hilarii* (Characidae) in the Pantanal wetland, Brazil. Mem. Inst. Oswaldo Cruz 105, 762–769. https://doi.org/10.1590/S0074-02762010000600006.

Milanin, T., Atkinson, S.D., Silva, M.R., Alves, R.G., Maia, A.A., & Adriano, E.A. (2017). Occurrence of two novel actinospore types (Cnidaria: Mxosporea) in Brazilian fish farms, and the creation of a novel actinospore collective group, Seisactinomyxon. Acta Parasitol. 62, 121–128. https://doi.org/10.1515/ap-2017-0014.

Milanin, T., Atkinson, S.D., Silva, M.R.M., Alves, R.G., Tavares, L.E.R., Ribeiro, A.M. & Maia, A.A.M. (2018). Occurrence of two novel actinospore types (Cnidaria: Myxozoa) in fish farms in Mato Grosso do Sul state, Brazil. Parasitol. Res. 117, 1757–1764. https://doi.org/10.1007/s00436-018-5856-0.

Mitchell, L.G. (1967). *Myxidium macrocheili* n. sp. (Cnidospora: Myxidiidae) from the largescale sucker *Catostomus macrocheilus* Girard, and a synopsis of the *Myxidium* of North American freshwater vertebrates. J. Protozool. 14, 415–424.

Mitchell, C.W. (1977). Myxosporidia. In: *Kreier, J.P. (ed). Parasitic Protozoa*. Academic Press, Inc., New York. 115–154 p.

Mitchell, L.G. (1989). Myxobolid parasites (Myxozoa: Myxobolidae) infecting fishes of Western Montana, with notes on histopathology, seasonality, and intraspecific variation. Can. J. Zool. 67, 1915–1922. https://doi.org/10.1139/z89-274.

Mohsin A.K.M., & Ambak M.A. (1983). Freshwater fishes of Peninsular Malaysia. Universiti Putra Malaysia, Serdang.

Molnár, K. (1979). *Myxobolus pavlovskii* (Achmerov, 1954) (Myxosporidia) infection in the silver carp and bighead. Acta Vet. Acad. Sci. Hung. 27, 207–216.

Molnár, K. (1980). Renal sphaerosporosis in the common carp *Cyprinus carpio* L. J. Fish Dis. 3, 11–19.

Molnár, K., & Kovács-Gayer, É. (1982). Occurrence of two species of *Thelohanellus* (Myxosporea: Myxozoa) of Far-Eastern origin in common carp populations of the Hungarian fish farms. Parasit. Hung. 14.

Molnár, K., & Kovács-Gayer, É. (1986). Experimental induction of *Sphaerospora renicola* (Myxosporea) infection in common carp (*Cyprinus carpio*) by transmission of SB-protozoans. J. Appl. Ichthyol. 2(2), 86–94. http://doi.org/10.1111/j.1439-0426.1986.tb00433.x

Molnár, K. (1992). *Ceratomyxa hungarica* n. sp. and *Chloromyxum proterorhini* n. sp. (Myxozoa: Myxosporea) from the freshwater goby *Proterorhinus marmoratus* (Pallas). Syst. Parasitol. 22(1), 25–31.

Molnár, K. (1994). Comments on the host, organ and tissue specificity of fish myxosporeans and on the types of their intrapiscine development. Parasitol. Hung. 27, 5–20.

Molnár, K., & Székely, C. (1995). Parasitological survey of some important fish species of Lake Balaton. Parasit. Hung. 28, 63–82.

Molnár, K., Masoumian, M., & Abasi, S. (1996). Four new *Myxobolus* spp. (Myxosporea: Myxobolidae) from Iranian barboid fishes. Arch. Protistenkd. 147, 115–123. https://doi.org/10.1016/S0003-9365(96)80011-X.

Molnár, K., & Székely, C. (1999). *Myxobolus* infection of the gills of common bream (*Abramis brama* L.) in the Lake Balaton and Kis-Balaton Reservoir, Hungary. Acta Vet. Hung. 47(4), 419–432.

Molnár, K., El-Mansy, A., Székely, C., & Baska, F. (1999a). Development of *Myxobolus dispar* (Myxosporea: myxobolidae) in an oligochaete alternate host, *Tubifex tubifex*. Folia Parasitol. 46, 15–21.

Molnár, K., El-Mansy, A., Székely, C. & Baska, F. (1999b) Experimental identification of the actinosporean stage of *Sphaerospora renicola* Dykova and Lom, 1982 (Myxosporea: Sphaerosporidae) in oligochaete alternate hosts. J. Fish Dis. 22, 143–153.

Molnár, K. (2000). *Myxobolus intrachondrealis* sp. n. (Myxosporea: Myxobolidae), a parasite of the gill cartilage of the common carp, *Cyprinus carpio*. Folia Parasitol. 47, 167–171.

Molnár, K. (2002). Site preference of fish myxosporeans in the gill. Dis. Aquat. Org. 48, 197–207. https://doi.org/10.3354/dao048197.

Molnár, K., Eszterbauer, E., Székely, C., Dán, Á. & Harrach, B. (2002). Morphological and molecular biological studies on intramuscular *Myxobolus* spp. of cyprinid fish. J. Fish. Dis. 25, 643–652.

Molnár, K., & Székely, C. (2003). Infection in the fins of the goldfish *Carasius auratus* caused by *Myxobolus diversus* (Myxosporea). Folia Parasitol. 50, 31–36.

Molnár, K., Székely, C., Mohamed, K., & Shaharom-Harrison, F. (2006a), Myxozoan pathogens in cultured Malaysian fishes. I. Myxozoan infection of the sutchi catfish. Dis. Aquat. Organ. 68, 209–218. https://doi.org/10.3354/dao.

Molnár, K., Székely, C., Mohamed, K., & Shaharom-Harrison, F. (2006b). Myxozoan pathogens in cultured Malaysian fishes. II. Myxozoan infections of redtail catfish *Hemibagrus nemurus* in freshwater cage cultures. Dis. Aquat. Organ. 68, 219–226. https://doi.org/10.3354/dao.

Molnár, K., Marton, S., Eszterbauer, E., & Székely, C. (2006c). Comparative morphological and molecular studies on *Myxobolus* spp. infecting chub from the River Danube, Hungary, and description of *M. muellericus* sp. n. Dis. Aquat. Org. 73, 49–61. https://doi.org/10.3354/dao073049.

Molnár, K., Marton, S., Eszterbauer, E., & Székely, C. (2007). Description of *Myxobolus gayerae* sp. n. and re-description of *M. leuciscini* infecting European chub from the Hungarian stretch of the river Danube. Dis. Aquat. Org. 78, 147–153. https://doi.org/10.3354/dao.

Molnár, K., Székely, C., Hallett, S.L., & Atkinson, S.D. (2009a). Some remarks on the occurrence, host-specificity and validity of *Myxobolus rotundus* Nemeczek, 1911 (Myxozoa: Myxosporea). Syst. Parasitol. 72, 71–79. https://doi.org/10.1007/s11230-008-9161-7.

Molnár, K., Eszterbauer, E., Marton, S., Cech, G., & Székely, C. (2009b). *Myxobolus erythrophthalmi* sp. n. *and Myxobolus shaharomae* sp. n. (Myxozoa: Myxobolidae) from the internal organs of rudd, *Scardinius erythrophthalmus* (L.), and bleak, *Alburnus alburnus* (L.). J. Fish Dis. 32(3), 219–231.

Molnár, K., Marton, S., Székely, C., & Eszterbauer, E. (2010). Differentiation of *Myxobolus* spp. (myxozoa: myxobolidae) infecting roach (*Rutilus rutilus*) in Hungary. Parasitol. Res. 107, 1137–1150. https://doi.org/10.1007/s00436-010-1982-z.

Molnár, K., Cech, G., & Székely, C. (2011). Histological and molecular studies of species of *Myxobolus* Bütschli, 1882 (Myxozoa: Myxosporea) in the gills of Abramis, Blicca and Vimba spp.(Cyprinidae), with the redescription of *M. macrocapsularis* Reuss, 1906 and *M. bliccae* Donec & Tozyyakova, 1984. Syst. Parasitol. 79(2), 109–121.

Molnár, K., Eszterbauer, E., Marton, S., Székely, C., & Eiras, J.C. (2012). Comparison of the *Myxobolus* fauna of common barbel from Hungary and Iberian barbel from Portugal. Dis. Aquat. Org. 100, 231–248.

Molnár, K., Eszterbauer, E., Guti, C.F., & Székely, C. (2014). Two new *Myxobolus* spp. (Myxozoa: Myxobolidae) from white bream, *Blicca bjoerkna* (Linnaeus, 1758) developing in basifilamental location of gills. Acta Protozoologica 53(3).

Molnár, K., & Eszterbauer, E. (2015). Specificity of infection sites in vertebrate hosts. In: *Myxozoan Evolution, Ecology and Development*, 295–313.

Molnár, K., Nyeste, K., & Székely, C. (2018). Parasitology is a tool for identifying the original biotope of the gibel carp (*Carassius auratus gibelio* Berg, 1932) = Parazitológiai bizonyítékok az ezüstkárász (*Carassius auratus gibelio* Berg, 1932) eredetéről. Pisces. Hungarici 12, 87–94.

Molnár, K., Sellyei, B., & Székely, C. (2025). A Balaton halaiban kimutatott parazita fajok táblázatos Áttekintése. HALÁSZAT-Tudomány. 11, 10–40. (in Hungarian). https://doi.org/10.62397/HALTUD.2025.1.10.

Moran, J.D.W., Whitaker, D.J., & Kent, M.L. (1999). A review of the myxosporean genus *Kudoa* Meglitsch, 1947, and its impact on the international aquaculture industry and commercial fisheries. Aquaculture 172, 163–196.

Moreira, G.S.A., Adriano, E.A., Silva, M.R.M., Ceccarelli, P.S., & Maia, A.A.M. (2013). Morphology and 18S rDNA sequencing identifies *Henneguya visibilis* n. sp., a parasite of *Leporinus obtusidens* from Mogi Guacu River, Brazil. Parasitol. Res. 113, 81–90. https://doi.org/10.1007/s00436-013-3629-3.

Morris, D.J., & Freeman, M.A. (2010). Hyperparasitism has wide-ranging implications for studies on the invertebrate phase of myxosporean (Myxozoa) life cycles. Int. J. Parasitol. 40, 357–369. https://doi.org/10.1016/j.ijpara.2009.08.014.

Morris, D.J., & Adams, A. (2006), Transmission of freshwater myxozoans during the asexual propagation of invertebrate hosts. Int. J. Parasitol. 36, 371–377. https://doi.org/10.1016/j.ijpara.2005.10.009.

Müller, J. (1841). Über Psorospermien. Archiv für Anatomie, Physiologie und Wissenschaftliche Medicin 5, 477–496.

Müller, M.I., Figueredo, R.T., Atkinson, S.D., Bartholomew, J.L., & Adriano, E.A. (2023). *Henneguya correai* n. sp. (Cnidaria, Myxozoa) parasitizing the fins of the Amazonian fish *Semaprochilodus insignis*. Diversity 15(6), 702. https://doi.org/10.3390/d15060702.

Müller, M.I., Atkinson, S.D., Bartholomew, J.L., & Adriano, E.A. (2025). Novel Amazonian *Ceratomyxa* species (Cnidaria: Myxozoa) with amoeboid plasmodial motility. Microb. Pathog. 199, 107235. https://doi.org/10.1016/j.micpath.2024.107235.

Mulsow, K. (1911). Ein neuer Gehirnparasit des Karpfens. Allgemeine Fischerei-Zeitung. 36, 483–485.

Naldoni, J., Arana, S., Maia, A.A.M., Ceccarelli, P.S., Tavares, L.E.R., Borges, F.D.A., Pozo, C.F. & Adriano, E.A. (2009). *Henneguya pseudoplatystoma* n. sp. causing reduction in epithelial area of gills in the farmed pintado, a South American catfish: histopathology and ultrastructure. Vet. Parasitol. 166, 52–59. https://doi.org/10.1016/j.vetpar.2009.07.034.

Naldoni, J., Maia, A.A., da Silva, M.R., & Adriano, E.A. (2014). *Henneguya cuniculator* sp. nov., a parasite of spotted sorubim *Pseudoplatystoma corruscans* in the São Francisco Basin, Brazil. Dis. Aquat. Org. 107, 211–221. https://doi.org/10.3354/dao.

Naldoni, J., Zatti, S.A., Capodifoglio, K.R., Milanin, T., Maia, A.A., Silva, M.R., & Adriano, E.A. (2015). Host-parasite and phylogenetic relationships of *Myxobolus filamentum* sp. n. (Myxozoa: Myxosporea), a parasite of *Brycon orthotaenia* (Characiformes: Bryconidae) in Brazil. Folia Parasitologica, 62, 1.

Naldoni, J., Zatti, S.A., da Silva, M.R., Maia, A.A., & Adriano, E.A. (2019). Morphological, ultrastructural, and phylogenetic analysis of two novel *Myxobolus* species (Cnidaria: Myxosporea) parasitizing bryconid fish from São Francisco River, Brazil. Parasitol. Int. 71, 27–36. https://doi.org/10.1016/j.parint.2019.03.009.

Nolan, M.J., & Cribb, T.H. (2005). The use and implications of ribosomal DNA sequencing for the discrimination of digenean species. Adv. Parasitol 60, 101–162. https://doi.org/10.1016/S0065-308X(05)60002-4.

Ohnishi, T., Kikuchi, Y., Furusawa, H., Kamata, Y., & Sugita-Konishi, Y. (2013). *Kudoa septempunctata* invasion increases the permeability of human intestinal epithelial monolayer. Foodborne Pathog. Dis. 10 (2), 137–142. https://doi.org/10.1089/fpd.2012.129.

Okamura, B., & Canning, E.U. (2003). Orphan worms and homeless parasites enhance bilaterian diversity. Trends Ecol. Evol. 18, 633–639.
Okamura, B., Gruhl, A., & Bartholomew, J.L. (2015). An Introduction to Myxozoan Evolution, Ecology and Development. In: Okamura, B., Gruhl, A., Bartholomew, J. (eds) *Myxozoan Evolution, Ecology and Development.* Springer, Cham.
Oumouna, M., Hallett, S., Hoffmann, R., & El-Matbouli, M. (2003). Seasonal occurrence of actinosporeans (Myxozoa) and oligochaetes (Annelida) at a trout hatchery in Bavaria, Germany. Parasitol. Res. 89(3), 170–184.
Özer, A. & Wootten, R. (2000). The life cycle of *Sphaerospora truttae* (Myxozoa: Myxosporean) and some features of the biology of both the actinosporean and myxosporean stages. Dis. Aquat. Org. 40, 33–39.
Özer, A., Wootten, R., & Shinn, A.P. (2002). Survey of actinosporean types (Myxozoa) belonging to seven collective groups found in a freshwater salmon farm in Northern Scotland. Folia Parasitol. 49, 189–210.
Palumbi, S., Martin, A., Romano, S., McMillan, W.O., Stice, L., & Grabowski, G. (2002). The Simple Fools Guide to PCR. University of Hawaii, Honolulu. Available at: Version 2.0. http://palumbi.stanford.edu/SimpleFoolsMaster.
Paepke, H.J. (2009). The nomenclature of *Trichopodus pectoralis* Regan, 1910; *Trichopus cantoris* Sauvage, 1884 and *Osphronemus saigonensis* Borodin, 1930 (Teleostei: Perciformes: Osphronemidae). Vertebr. Zool. 59(1), 53–60.
Palikova, M., Balazova, A., Pojezdal, L., Papezikova, I., Mikulikova, I., Toulova, I., Motlova, J. & Pikula, J. (2025). Case report: Carp edema virus infection in overwintering fish. Front. Vet. Sci. 12:1532861. https://doi.org/10.3389/fvets.2025.1532861.
Patra, S., Hartigan, A., Morris, D.J., Kodádková, A., & Holzer, A.S. (2017). Description and experimental transmission of *Tetracapsuloides vermiformis* n. sp. (Cnidaria: Myxozoa) and guidelines for describing malacosporean species including reinstatement of *Buddenbrockia bryozoides* n. comb. (syn. Tetracapsula bryozoides). Parasitology 144, 497–511. https://doi.org/10.1017/S0031182016001931.
Patra, S.B. (2023). Observations on the abundance of Oligochaeta along with some environmental factors in an unmanaged freshwater wetland of West Bengal, India. Sustain. Agri. Food Envir. Res. 12(1). https://doi.org/10.7770/safer-V12N1-art2692.
Pavanelli, G.C., Eiras, J.D.C., & Saraiva, A. (1998). *Henneguya* spp. (Myxozoa, Myxosporea, Myxobolidae) parasitizing fishes from Paraná river, Brazil. Acta Sci. 20(2), 161–163.
Pérez-Ponce de León, G., & Nadler, S.A. (2010). What we don't recognize can hurt us: a plea for awareness about cryptic species. J. Parasitol. 96, 453–464.
Pfenninger, M., & Schwenk, K. (2007). Cryptic animal species are homogeneously distributed among taxa and biogeographical regions. BMC Evol. Biol. 7, 121. https://doi.org/10.1186/1471-2148-7-121.
Picon-camacho, S.M., Holzer, A.S., Freeman, M.A., Morris, D.J., & Shinn, A.P. (2009). *Myxobolus albi* n. sp. (Myxozoa) from the gills of the common goby *Pomatoschistus microps* Krøyer (Teleostei: Gobiidae). J. Eukaryot. Microbiol. 56(5), 421–427. https://doi.org/10.1111/j.1550-7408.2009.00419.x.
Pote, L.M., Hanson, L.A. & Shivaji, R. (2000). Small subunit ribosomal RNA sequences link the cause of poliferative gill disease in channel catfish to *Henneguya* n. sp. (Myxozoa: Myxosporea). J. Aquat. Anim. Health 12, 230–240.
Pote, L.M., Khoo, L., & Griffin, M. (2012). *Henneguya ictaluri*. In *Fish Parasites: Pathobiology and Protection*; Wallingford UK: CABI, 177–192 p.
Shpirer, E., Chang, E.S., Diamant, A. Rubinstein, N., Cartwright, P., & Huchon, D. (2014). Diversity and evolution of myxozoan minicollagens and nematogalectins. BMC Evol. Biol. 14, 205. https://doi.org/10.1186/s12862-014-0205-0.

Prunescu, C.C., Prunescu, P., Pucek, Z., & Lom, J. (2007). The first finding of myxosporean development from plasmodia to spores in terrestrial mammals: *Soricimyxum fegati* gen. et sp. n. (Myxozoa) from *Sorex Araneus* (Soricomorpha). Folia Parasitol. 54, 159–164.

Qadri, S.S. (1962). On a new myxosporidian, *Thelohaenellus boggoti* n. sp., from Indian fresh water fish *Labeo boggot*. Arch. Protistenkd. 106, 218–222.

Rácz, O.Z., & Timm, T. (2002). First report on the occurrence of actinosporean stages of fish myxosporeans (Myxozoa, Myxosporea) in Estonia. Acta Parasitol. 3, 47.

Rácz. O.Z., Székely, C., & Molnár, K. (2004). Intraoligochaete development of *Myxobolus intimus* (Myxosporea: Myxobolidae), a gill myxosporean of the roach (*Rutilus rutilus*). Folia Parasitol. 51, 199–207.

Racz, O.Z., Eszterbauer, E., & Molnár, K. (2005). Hungactinomyxon, a new actinosporean type and collective group (Myxozoa) from Branchiura sowerbyi Beddard (Oligochaeta). Syst. Parasitol. 61, 107–113. https://doi.org/10.1007/s11230-005-3136-8.

Radhi, A.M., Rohasliney, H., & Zarul, H. (2017). Fish composition and diversity in Perak, Galas and Kelantan rivers (Malaysia) after the major flood of 2014. Transylv. Rev. Syst. Ecol. Res. 19(3), 41–56.

Rainboth, W.J. (1996). Fishes of the Cambodian Mekong: FAO species identification field guide for fishery purposes. Food and Agriculture Organization of the United Nations, Rome.

Rangel, L.F., Santos, M.J., Cech, G., & Székely, C. (2009). Morphology, molecular data, and development of *Zschokkella mugilis* (Myxosporea, Bivalvulida) in a polychaete alternate host, *Nereis diversicolor*. J. Parasitol. 95, 561–569. https://doi.org/10.1645/GE-1777.1.

Rangel, L.F., Cech, G., Székely, C., & Santos, M.J. (2011). A new actinospore type Unicapsulactinomyxon (Myxozoa), infecting the marine polychaete, *Diopatra neapolitana* (Polychaeta: Onuphidae) in the Aveiro Estuary (Portugal). Parasitology 138, 698–712. https://doi.org/10.1017/S0031182011000163.

Rangel, L.F., Rocha, S., Castro, R., Severino, R., Casal, G., Azevedo, C., Cavaleiro, F., & Santos, M.J. (2015). The life cycle of *Ortholinea auratae* (Myxozoa: Ortholineidae) involves an actinospore of the triactinomyxon morphotype infecting a marine oligochaete. Parasitol. Res. 114, 2671–2678. https://doi.org/10.1007/s00436-015-4472-5.

Rangel, L.F., Castro, R., Rocha, S., Cech, G., Casal, G., Azevedo, C., Székely, C., Cavaleiro, F., & Santos, M.J. (2016b). Description of new types of sphaeractinomyxon actinospores (Myxozoa: Myxosporea) from marine tubificid oligochaetes, with a discussion on the validity of the tetraspora and the endocapsa as actinospore collective group names. Parasitol. Res. 115, 2341–2351. https://doi.org/10.1007/s00436-016-4983-8.

Rangel, L.F., Castro, R., Rocha, S., Severino, R., Casal, G., Azevedo, C., Cavaleiro, F., & Santos, M.J. (2016a). Tetractinomyxon stages genetically consistent with *Sphaerospora dicentrarchi* (Myxozoa: Sphaerosporidae) found in *Capitella* sp. (Polychaeta: Capitellidae) suggest potential role of marine polychaetes in parasite's life cycle. Parasitology 143(8), 1067–1073. https://doi.org/10.1017/S0031182016000512.

Rangel, L.F., Rocha, S., Casal, G., Castro, R., Severino, R., Azevedo, C., Cavaleiro, F., & Santos, M.J. (2017). Life cycle inference and phylogeny of *Ortholinea labracis* n. sp. (Myxosporea: Ortholineidae), a parasite of the European seabass *Dicentrarchus labrax* (Teleostei: Moronidae), in a Portuguese fish farm. J. Fish Dis. 40(2), 243–262. https://doi.org/10.1111/jfd.12508.

Rambaut, A. (2018). FigTree V. 1.4.4: Tree Figure Drawing Tool. http://tree.bio.ed.ac.uk/software/figtree/〉. (Accessed 10 August 2025).

Redondo, M.J., Palenzuela, O., & Alvarez-Pellitero, P. (2004). Studies on transmission and life cycle of *Enteromyxum scophthalmi* (Myxozoa), an enteric parasite of turbot *Scophthalmus maximus*. Folia Parasitol. 188–198.

Reed, C.C., Basson, L., & Van As, L.L. (2002). Myxobolus species (Myxozoa), parasites of fishes in the Okavango River and Delta, Botswana, including descriptions of two new species. Folia Parasitol. 49(2), 81–88.

Reed, C.C., Basson, L., & Van As, L.L. (2003). Myxozoans infecting the sharptooth catfish, *Clarias gariepinus* in the Okavango River and Delta, Botswana, including descriptions of two new species, *Henneguya samochimensis* sp. n. and *Myxobolus gariepinus* sp. n. Folia Parasitologica, 50(3), 183–189.

Roberts, T.R. (1989). The freshwater fishes of Western Borneo (Kalimantan Barat, Indonesia). Memoirs of the California Academy of Sciences, 14, 1–210.

Roberts, T.R. (1993). Systematic revision of the South Asian cyprinid fish genus *Labiobarbus* (Teleostei: Cyprinidae). Raffles Bull. Zool. 41(2), 315–329.

Rocha, E., Matos, E., & Azevedo, C. (1992). *Henneguya amazonica* n. sp. (Myxozoa, Myxobolidae), parasitizing the gills of *Crenicichla lepidota* Heckel, 1840 (Teleostei, Cichlidae) from Amazon River. Europ. J. Protistol. 28(3), 273–278.

Rocha, S., Alves, Â, Antunes, C., Azevedo, C., & Casal, G. (2019a). Molecular data infers the involvement of a marine aurantiactinomyxon in the life cycle of the myxosporean parasite *Paramyxidium giardi* (Cnidaria, Myxozoa). Parasitology 146 (12), 1555–1563. https://doi.org/10.1017/S0031182019000866.

Rocha, S., Rangel, L. F., Castro, R., Severino, R., Azevedo, C., Santos, M.J., & Casal, G. (2019b). The potential role of the sphaeractinomyxon collective group (Cnidaria, Myxozoa) in the life cycle of mugiliform-infecting myxobolids, with the morphological and molecular description of three new types from the oligochaete *Tubificoides insularis*. J. Invertebr. Pathol. 160, 33–42. https://doi.org/10.1016/j.jip.2018.12.001.

Rocha, S., Alves, Â., Fernandes, P., Antunes, C., Azevedo, C., & Casal, G. (2019c). New actinosporean description prompts union of the raabeia and echinactinomyxon collective groups (Cnidaria, Myxozoa). Dis. Aquat. Org. 135, 175–191. https://doi.org/10.3354/dao03389.

Rocha, S., Casal, G., Alves, Â. Antunes, C., Rodrigues, P., Azevedo, C. (2019d). Myxozoan biodiversity in mullets (Teleostei, Mugilidae) unravels hyperdiversification of *Myxobolus* (Cnidaria, Myxosporea). Parasitol. Res. 118, 3279–3305. https://doi.org/10.1007/s00436-019-06476-7.

Rocha, S., Rangel, L.F., Casal, G., Azevedo, C., Rodrigues, P., & Santos, M.J. (2020a). Involvement of sphaeractinomyxon in the life cycle of mugiliform-infecting *Myxobolus* (Cnidaria, Myxosporea) reveals high functionality of actinospore morphotype in promoting transmission. Parasitology 147(12), 1320–1329. https://doi.org/10.1017/S0031182020001043.

Rocha, S., Alves, Â., Antunes, C., Fernandes, P., Azevedo, C., & Casal, G. (2020b). Characterisation of sphaeractinomyxon types (Cnidaria: Myxozoa) from marine and freshwater oligochaetes in a Portuguese estuary, with the demise of the endocapsa collective group. Folia Parasitol. 67, 1–13.

Rocha, S. (2023). Synopsis of the aurantiactinomyxon collective group (Cnidaria, Myxozoa), with a discussion on the validity of morphotype definition and demise of guyenotia. Syst. Parasitol. 100, 307–323. https://doi.org/10.1007/s11230-023-10089-1.

Rocha, S., Alves, Â., Antunes, C., Rodrigues, P., & Casal, G. (2024). Characterization of novel aurantiactinomyxon types (Cnidaria, Myxosporea) from the oligochaete *Ilyodrilus templetoni* (Southern, 1909), with a comprehensive phylogeny of the collective group. J. Invertebr. Pathol. 203, 108043. https://doi.org/10.1016/j.jip.2023.108043.

Ronquist, F., Teslenko, M., van Der Mark, P., Ayres, D.L., Darling, A., Höhna, S., Larget, B., Liu, L., Suchard, M.A., & Huelsenbeck, J.P. (2012). MrBayes 3.2: efficient bayesian phylogenetic inference and model choice across large model space. Syst. Biol. 61, 539–542. https://doi.org/10.1093/sysbio/sys029.

Rosser, T.G., Griffin, M.J., Quiniou, S.M., Greenway, T.E., Khoo, L.H., Wise, D.J., & Pote, L. M. (2014). Molecular and morphological characterization of myxozoan actinospore types from a commercial catfish pond in the Mississippi Delta. J. Parasitol. 100, 828–839. https://doi.org/10.1645/13-446.1.

Rosser, T.G., Griffin, M.J., Quiniou, S.M.A., Khoo, L.H., Greenway, T.E., Wise. D.J., & Pote, L.M. (2015). Small subunit ribosomal RNA sequence links the myxospore stage of *Henneguya mississippiensis* n. sp. from channel catfish *Ictalurus punctatus* to an actinospore released by the benthic oligochaete *Dero digitata*. Parasitol. Res. 114, 1595–1602.

Rosser, T.G., Loch, T.P., Faisal, M., Baumgartner, W.A, & Griffin, M.J. (2021). *Henneguya michiganensis* n. sp. (Cnidaria: Myxosporea) from the gills of muskellunge *Esox masquinongy* Mitchill (Esociformes: Esocidae). Syst. Parasitol. 98, 119–130. https://doi.org/10.1007/s11230-021-09965-5.

Ruidisch, S., El-Matbouli, M., & Hoffmann, R.W. (1991). The role of tubificid worms as an intermediate host in the life cycle of *Myxobolus pavlovskii* (Akhmerov, 1954). Parasitol. Res. 77(8), 663–667.

Saha, M., & Bandyopadhyay, P.K. (2018a). Identification of a new myxosporean parasite *Thelohanellus indiana* n. sp. (Myxosporea: Myxobolidae) isolated from three major organs of goldfish, *Carassius auratus* L. highlighted with its morphological and SSU rDNA sequence based molecular description. Microbial Pathog. 122, 191–199. https://doi.org/10.1016/j.micpath.2018.05.038.

Saha, M., & Bandyopadhyay, P.K. (2018b). Morphological and ssrDNA sequence based molecular characterization of a novel *Thelohanellus* species (Myxosporea: Myxobolidae) infecting the fins of Goldfish, *Carassius auratus* L. with special reference to its histopathological alteration. Acta Tropica, 181, 25–34. https://doi.org/10.1016/j.actatropica.2018.01.019.

Saifullah, A.S.M., Abu Hena, M.K., Idris, M.H., Halima, A.R., & Johan, I. (2014). Seasonal variation of water characteristics in Sibuti river estuary in Sarawak, Malaysia. Malays. J. Sci. 33(1), 9–22.

Salim, K.Y., & Desser, S.S. (2000). Descriptions and phylogenetic systematics of *Myxobolus* spp. from cyprinids in Algonquin Park, Ontario. J. Eukaryot. Microbiol. 47(3), 309–318.

Salti, B., Atkinson, S.D., Brekhman, V., Smirnov, M., & Lotan, T. (2024). Exotic myxozoan parasites establish complex life cycles in farm pond aquaculture. J. Invertebr Pathol. 204, 108105. https://doi.org/10.1016/j.jip.2024.108105.

Samshuri, M.Á. (2018). Morphological and Molecular Characterisation of Parasitic Myxosporea (Cnidaria: Myxozoa) in Nemipterid Fishes from Terengganu Waters, Dissertation, Univerisiti Malaysia Terengganu, 2018.

Samshuri, M.Á., & Borkhanuddin, M.H. (2024). *Myxobolus acanthogobii* Hoshina, 1952 and *Myxobolus selari* n. sp. (Myxosporea: Myxobolidae) infecting brain of commercial fishes in Terengganu, Malaysia, Syst. Parasitol. 101, 39. https://doi.org/10.1007/s11230-024-10162-3.

Sarkar, N.K., Mazumder, S.K., & Pramanik, A. (1985). Observations on 4 new species of Myxosporidia (Myxozoa) from channid (ophicephalid) fishes of West Bengal, India. Archiv für Protistenkunde, 130(3), 289–296.

Sarkar, K.N. (2012) Three new species of Myxosporea (Bivalvulida), parasites of the gallbladder of scombrid fish, from the Bay of Bengal (Indian Ocean), West Bengal, India. Protistology 7, 172–177.

Schröder, O. (1910). Buddenbrockia plumatella, eine neue Mesozoenart aus Plumatella repens L. und Plumatella fungosa Pall. Z. Wiss. Zool. 96, 525–537.

Sekiya, M., Setsuda, A., Sato, H., Song, K., Han, J.K., Kim, G.J., & Yeo, I.K. (2016). *Enteromyxum leei* (Myxosporea: Bivalvulida) as the cause of myxosporean emaciation disease of farmed olive flounders (*Paralichthys olivaceus*) and a turbot (*Scophthalmus maximus*) on Jeju Island, Korea. Parasitol. Res. 115, 4229–4237. https://doi.org/10.1007/s00436-016-5200-5.

Sekiya, M., Sakai, H., Li, Y.C., Rosyadi, I., Yunus, M., & Sato, H. (2024). Morphological and molecular characterization of three myxosporean species of the genera *Myxobolus*,

Henneguya, and *Myxidium* (Cnidaria: Myxozoa) infecting freshwater fish, isolated for the first time in Japan. Life, 14(8), 974. https://doi.org/10.3390/life14080974.

Shahar, N.F., Shamsuri, M.A., Shaharom, F., & Borkhanuddin, M.H. (2017). First record of *Ceratomyxa* (thélohan, 1892) from the gall bladder of orange spotted grouper, *Epinephelus coioides* (Perciformes: Serranidae) from Setiu wetlands, Terengganu. J. Sustain. Sci. Manag. 12(2), 161–166.

Shariff, M. (1982). *Henneguya shaharini* sp. nov. (Protozoa: Myxozoa), a parasite of marble goby, *Oxyeleotris marmoratus* (Bleeker). J. Fish Dis. 5(1), 37–45.

Shpirer, E., Chang, E.S., Diamant, A., Rubinstein, N., Cartwright, P., & Huchon, D. (2014). Diversity and evolution of myxozoan minicollagens and nematogalectins. BMC Evol. Biol. 14(1), 205.

Shin, S.P., Jeong, J.M., Jun, J.W., Kim, J.H., Han, J.E., Baeck, G.W., & Park, S.C. (2014). The phylogenetic study on *Thelohanellus* species (Myxosporea) in relation to host specificity and infection site tropism. Mol. Phylogenet. Evol. 72, 31–34.

Shi, X.W., Wang, M., Chen, H.Z., Gao, L., Liu, X.C., Yang, C.Z., & Zhao, Y.J. (2022). Redescription and molecular phylogenetic analysis on *Myxobolus acutus* Wu and Chen, 1987 (Myxozoa: Myxobolidae). Acta Hydrobiol. Sin. 46, 555–562.

Singh, R., & Kaur, H. (2012a). Myxosporean species of the genus *Thelohanellus* Kudo, 1933 (Myxozoa: Myxosporea: Bivalvulida) from freshwater fishes of Punjab wetlands, India. Protistology 7(4), 209–217.

Singh, R., & Kaur, H. (2012b). *Thelohanellus* (Myxozoa: Myxosporea: Bivalvulida) infections in major carp fish from Punjab wetlands (India). Protistology 7, 178–188.

Singh, R., & Kaur, H. (2014). Two new and two already known species of genus *Thelohanellus* Kudo, 1933 (Myxozoa: Myxosporea: Bivalvulida) infecting Indian major carp fishes in Punjab wetlands (India). J. Parasit. Dis. 38(1), 49–60. https://doi.org/10.1007/s12639-012-0190-4.

Singh, R., & Kaur, H. (2015). Two new and one already known species of the genus *Thelohanellus* (Myxozoa: Myxosporea: Bivalvulida) parasitizing fresh water fishes in wetlands of Punjab, India. Biologia 70, 85–93.

Schulman, S.S. (1966) Myxosporidia of the USSR. Moscow-Leningrad: Izdatel'stvo Nauka AN SSSR, 508 p. (In Russian; English translation (1990), Rotterdam: A.A. Balkema, 631 p.

Sitjà-Bobadilla, A., Diamant, A., Palenzuela, O., & Alvarez-Pellitero, P. (2007). Effect of host factors and experimental conditions on the horizontal transmission of Enteromyxum leei (Myxozoa) to bass, *Dicentrarchus labrax* (L.). J. Fish Dis. 243–250.

Skovgaard, A., & Buchmann, K. (2012). *Tetracapsuloides bryosalmonae* and PKD in juvenile wild salmonids in Denmark. Dis. Aquat. Org. 101, 33–42. https://doi.org/10.3354/dao

Sokolov, S.G., & Frolova, S.E. (2015). Data of the Parasite Fauna of the Sakhalin Fishes. *Vestnik. Svnts. Dvo. Ran*. 90–97. (In Russian with English summary).

Sokolov, S.G., Lebedeva, D.I., Murzina, S.A., Parshukov, A.N., Bystrova, K.A., & Ieshko, E.P. (2019). Morphology and phylogeny of *Henneguya oviperda* infecting oocytes of *Esox lucius*, with description of parasite-induced histopathology. Dis. Aquat. Org. 133(2), 91–98. https://doi.org/10.3354/dao.

Stilwell, J.M., Stilwell, N.K., Camus, A. C., Griffin, M.J., & Rosser, T.G. (2019). A morphological, molecular, and histopathological redescription of *Henneguya nyongensis* Fomena & Bouix, 1996 (Cnidaria: Myxobolidae) infecting the gills of Peter's elephantnose fish, *Gnathonemus petersii* (Günther) (Osteoglossiformes: Mormyridae), imported from Nigeria. Syst. Parasitol. 96(9), 767–776.

Stilwell, J.M., Petty, B.D., Camus, A.C., Woodyard, E.T., Griffin, M.J., & Rosser, T.G. (2020). Characterisation of *Myxobolus stellatus* n. sp. (Cnidaria: Myxobolidae) infecting the cranial nerves and ganglia of the spotfin hatchetfish *Thoracocharax stellatus* (Kner) (Characiformes: Gasteropelecidae) from Colombia. Syst. Parasitol. 97(3), 305–314. https://doi.org/10.1007/s11230-020-09911-x.

Stilwell, J.M., Rosser, T.G., Woodyard, E.T., Richardson, B.M., López-Porras, A., Leary, J.H., Mischke, C.C. Camus, A.C., & Griffin, M.J. (2021). Characterisation of myxozoan fauna of western mosquitofish, *Gambusia affinis* (Baird and Gerard) (Cyprinodontiformes: Poeciliidae), inhabiting experimental catfish ponds in Mississippi, USA. Syst. Parasitol. 98(4), 423–441. https://doi.org/10.1007/s11230-021-09987-z.

Su, X.Q., & White, R.W.G. (1995). A new myxosporean, *Zschokkella leptatherinae* n. sp. (Myxozoa: Myxidiidae), from the hepatic ducts and gall-bladder of Australian marine fishes. Syst. Parasitol. 32, 125–129. https://doi.org/10.1007/BF00009511.

Székely, C., & Molnár, K. (1997). Preliminary survey of the parasite fauna of some important fish species in the Upper-Reservoir of the Kis Balaton System. Parasitol. Hung. 29–30.

Székely, C., El-Mansy, A., Molnár, K., & Baska, F. (1998). Development of *Thelohanellus hovorkai* and *Thelohanellus nikolskii* (Myxosporea: Myxozoa) in oligochaete alternate hosts. Fish Pathol. 33(3), 107–114. https://doi.org/10.3147/jsfp.33.107.

Székely, C., Molnár, K., Eszterbauer, E., & Baska, F. (1999). Experimental detection of the actinospores of *Myxobolus pseudodispar* (Myxosporea: Myxobolidae) in oligochaete alternate hosts. Dis. Aquat. Org. 38, 219–224. https://doi.org/10.3354/dao038219.

Székely, C., Molnár, K., & Rácz, O. (2001). Complete developmental cycle of *Myxobolus pseudodispar* (Gorbunova) (Myxosporea: Myxobolidae). J. Fish Dis. 24, 461–468. https://doi.org/10.1046/j.1365-2761.2001.00324.x.

Székely, C., Rácz, O., Molnár, K., & Eszterbauer, E. (2002). Development of *Myxobolus macrocapsularis* (Myxosporea: myxobolidae) in an oligochaete alternate host, *Tubifex tubifex*. Dis. Aquat. Org. 48, 117–123. https://doi.org/10.3354/dao048117.

Székely, C., Yokoyama, H., Urawa, S., Timm, T., & Ogawa, K. (2003). Description of two new actinosporean types from a brook of Fuji mountain, Honshu, and from Chitose River, Hokkaido, Japan. Dis. Aquat. Org. 53(2), 127–132. https://doi:10.3354/dao053127.

Székely, C., Avenant-Oldewage, A., & Molnár, K. (2004). Description of a new actinosporean type from South African freshwaters. Dis. Aquat. Org. 61, 95–102. https://doi.org/10.3354/dao061095.

Székely, C., Hallett, S.L., Al-Samman, A., & Dayoub, A. (2007). First description of myxozoans from Syria: novel records of hexactinomyxon, triactinomyxon and endocapsa actinospore types. Dis. Aquat. Org. 74, 127–137. https://doi.org/10.3354/dao074127.

Székely, C., Shaharom-Harrison, F., Cech, G., Ostoros, G., & Molnár, K. (2009a). Myxozoan infections in fishes of the Tasik Kenyir water reservoir, Terengganu, Malaysia. Dis. Aquat. Org. 83(1), 37–48. https://doi.org/10.3354/dao.

Székely, C., Shaharom-Harrison, F., Cech, G., Mohamed, K., & Molnár, K. (2009b). Myxozoan pathogens of Malaysian fishes cultured in ponds and net-cages. Dis. Aquat. Org. 83(1), 49–57. https://doi.org/10.3354/dao.

Székely, C., Hallett, S.L., Atkinson, S.D., & Molnár, K. (2009c). Complete life cycle of *Myxobolus rotundus* (Myxosporea: Myxobolidae), a gill myxozoan of common bream *Abramis brama*. Dis. Aquat. Org. 85(2), 147–155. http://dx.doi.org/10.3354/dao02068.

Székely, C., Shaharom, F., Cech, G., Mohamed, K., Zin, N.A.M., Borkhanuddin, M.H., Ostoros, G., & Molnár, K. (2012). Myxozoan infection of the Malaysian mahseer, *Tor tambroides*, of Tasik Kenyir Reservoir, Malaysia: description of a new species *Myxobolus tambroides* sp. n. Parasitol. Res. 111(4), 1749–1756. https://doi.org/10.1007/s00436-012-3020-9.

Székely, C., Borkhanuddin, M.H., Cech, G., Kelemen, O., & Molnár, K. (2014). Life cycles of three *Myxobolus* spp. from cyprinid fishes of Lake Balaton, Hungary involve triactinomyxon-type actinospores. Parasitol. Res. 113, 2817–2825. https://doi.org/10.1007/s00436-014-3942-5.

Székely, C., Cech, G., Atkinson, S.D., Molnár, K., Egyed, L., & Gubányi, A. (2015a). A novel myxozoan parasite of terrestrial mammals: description of *Soricimyxum minuti* sp. n. (Myxosporea) in pygmy shrew *Sorex minutus* from Hungary. Folia Parasitol. 62.

Székely, C., Cech, G., Chaudhary, A., Borzák, R., Singh, H.S., & Molnár, K. (2015b). Myxozoan infections of the three Indian major carps in fish ponds around Meerut, UP, India, with descriptions of three new species, *Myxobolus basuhaldari* sp. n., *M. kalavatiae* sp. n. and *M. meerutensis* sp. n., and the redescription of *M. catlae* and *M. bhadrensis*. Parasitol. Res. 114, 1301–1311.

Székely, C., Borzák, R., & Molnár, K. (2018). Description of *Henneguya jaczoi* sp. n. (Myxosporea, Myxobolidae) from *Perca fluviatilis* (l.) (Pisces, Percidae) with some remarks on the systematics of *Henneguya* spp. of European fishes. Acta Vet. Hung. 66(3), 426–443. https://doi.org/10.1556/004.2018.038.

Székely, C., Ghosh, S., Borzák, R., Goswami, U., Molnár, K., & Cech, G. (2021). The occurrence of known *Myxobolus* and *Thelohanellus* species (Myxozoa, Myxosporea) from Indian major carps with the description of *Myxobolus bandyopadhyayi* n. sp. in West Bengal. Int. J. Parasitol. Parasites Wildl. 16, 18–25. https://doi.org/10.1016/j.ijppaw.2021.07.008.

Talavera, G., & Castresana, J. (2007). Improvement of phylogenies after removing divergent and ambiguously aligned blocks from protein sequence alignments. Syst. Biol. 56(4), 564–577. https://doi.org/10.1080/10635 15070 1472164.

Tan, L. Q., Zhou, Y., Wang, M.M., Yang, C.Z., & Zhao, Y.J. (2022). Identification and phylogenetic analysis on *Myxobolus acinosu* Nie & Li, 1973, *Myxobolus pseudoacinosus* Guo, et al., 2018 and *Myxobolus toyamai* Kudo, 1917. Acta Hydro. Sin. 46, 545–554.

Thélohan, P. (1892). Observation sur les myxosporidies et éssai de classification de ces organismes. Bull. Soc. Philos. 4, 165–178.

Thu, M.M., Bawm, S., & Wilbur, N.D. (2023). Morphological and molecular detection of myxosporean parasites in freshwater fish in Myanmar. J. Parasit. Dis. 47(2), 429–435. https://doi.org/10.1007/s12639-023-01577-8.

Thumvittayakul, W., U-taynapun, K., & Wongsawad, C. (2018). Myxozoa parasites from some freshwater fishes in Chiang Mai Province. J. Agri. Res. Ext. 35, 445–454.

Tilley, M.F., Barry, D., Hanington, P.C., & Goater, C.P. (2024). Description, life cycle, and development of the myxozoan *Myxobolus rasmusseni* n. sp. in fathead minnows, *Pimephales promelas*: a possible emerging pathogen in southern Alberta, Canada. Int. J. Parasitol. Parasites Wildl. 24, 100944. https://doi.org/10.1016/j.ijppaw.2024.100944.

Timm, T. (1999) Naturalist Handbooks I: A Guide to the Estonian Annelida. Estonian Academic Publisher.

Thompson, J.D., Higgins, D.G., & Gibson, T.J. (1994). Clustal W: improving the sensitivity of progressive multiple sequence alignment through sequence weighting, position-specific gap penalties and weight matrix choice. Nucleic Acids Res. 22, 4673–4680. https://doi.org/10.1093/nar/22.22.4673.

Tops, S., Curry, A., & Okamura, B. (2005). Diversity and systematics of the Malacosporea (Myxozoa). Invertebr. Biol. 124(4), 285–295. http://doi.org/10.1111/j.1744-7410.2005.00026.x.

Tripathi, Y.R. (1948). Some new Myxosporidia from Plymouth with a proposed new classification of the order. Parasitology 39, 110–118.

Trouillier, A., El-Matbouli, M., & Hoffmann, R.W. (1996). A new look at the life-cycle of *Hoferellus carassii* in the goldfish (*Carassius auratus auratus*) and its relation to kidney. Folia Parasitol. 43, 173–187.

Tuzet, O., & Ormières, R. (1957). *Ceratomyxa anguillae* n. sp. myxosporidie parasite de la vesicule biliaire des anguilles de l'Etang de Thau. Ann. Parasitol. Hum. Comp, 32, 189–196.

Uma, A., Subash, P., & Praveenraj, J. (2025). Morphology and phylogenetic analysis of *Henneguya* sp. infecting the orange-spotted snakehead (*Channa aurantimaculata*) from Tamil Nadu, India. Acta Parasit. 70, 13. https://doi.org/10.1007/s11686-024-00961-5.

Úngari, L.P., Vieira, D.H.M.D., de Alcantara, E.P., Emmerich, E., Santos, A.L.Q., da Silva, R.J., & O'Dwyer, L.H. (2021). Description of a new species of myxobolid parasite, *Henneguya*

pindaibensis n. sp. (Cnidaria: Myxosporea), infecting the gills of *Boulengerella cuvieri* (Spix and Agassiz, 1829) from Brazil. Parasitol. Int. 83, 102319. https://doi.org/10.1016/j.parint.2021.102319.

U-taynapun, K., Penprapai, N., Bangrak, P., Mekata, T., Itami, T., & Tantikitti, C. (2011). *Myxobolus supamattayai* n. sp. (Myxosporea: Myxobolidae) from Thailand parasitizing the scale pellicle of wild mullet (*Valamugil seheli*). Parasitol. Res. 109(1), 81–91.

Urawa, S. (1994). Life cycle of *Myxobolus arcticus*, a myxosporean parasite of salmonid fishes. Int. Symp. Aquat. Anim. Health, Seattle, Book of Abstracts, P-W-10.3.

Urawa, S., Freeman, M.A., Johnson, S.C., Jones, S.R.M., & Yokoyama, H. (2011). Geographical variation in spore morphology, gene sequences, and host specificity of *Myxobolus arcticus* (Myxozoa) infecting salmonid nerve tissues. Dis. Aquat. Org. 96, 229–237. https://doi.org/10.3354/dao02398.

Uspenskaya, A.V. (1957). The ecology and spreading of the pathogen of *Myxosoma cerebralis* of trout in the fish ponds of the Soviet Union. In: *Parasites and diseases of fish*. Petrushevski, G.K. (ed). Bulletin of the Institute of Freshwater Fisheries, Leningrad.

Uspenskaya, A.V. (1995). Alternation of actinosporean and myxosporean phases in the life-cycle of *Zschokkela nova* (myxozoa). J. Eukaryot. Microbiol. 42, 665–668.

Velasco, M., Videira, M., Nascimento, L.D.C.S.D., Matos, P., Gonçalves, E.C., & Matos, E. (2016). *Henneguya paraensis* n. sp. (Myxozoa; Myxosporea), a new gill parasite of the Amazonian fish *Cichla temensis* (Teleostei: Cichlidae): morphological and molecular aspects. Parasitol. Res. 115(5), 1779–1787. https://doi.org/10.1007/s00436-016-4916-6.

Velasco, M., Neto, J.L.S., Eduard, J., Gonçalves, E.C., Videira, M., Oliveira, E., & Matos, E. (2024). New species of *Myxobolus* in potamodromous catfish from the eastern Amazon, Brazil. Parasitol. Int. 103, 102939. https://doi.org/10.1016/j.parint.2024.102939.

Velasco, M., Xavier, K.C., Furtado, A.M.M., Eduard, J., & Sindeaux-Neto, J.L. (2025). New *Henneguya* Species Cause Gill Disease of Commercial Amazonian Fish. Acta Parasit. 70(1), 36. https://doi.org/10.1007/s11686-024-00980-2.

Vidthayanon C., Karnasuta J., & Nabhitabhata J. (1997) Diversity of freshwater fishes in Thailand. Office of Environmental Policy and Planning, Bangkok.

Vieira, D.H.M.D., Alama-Bermejo, G., Bartholomew, J.L., Abdallah, V.D., & De Azevedo, R.K. (2017). Morphological and molecular description of *Myxobolus batalhensis* n. sp. (Myxozoa, Myxosporea), a liver and ovary parasite of *Salminus hilarii* in Brazil. Parasitol. Res. 116(12), 3303–3313. https://doi.org/10.1007/s00436-017-5644-2.

Vieira, D.H.M.D., Tagliavini, V.P., Abdallah, V.D., & de Azevedo, R.K. (2018). *Myxobolus imparfinis* n. sp. (Myxozoa: Myxosporea), a new gill parasite of *Imparfinis mirini* Haseman (Siluriformes: Heptapteridae) in Brazil. Syst. Parasitol. 95, 309–318. https://doi.org/10.1007/s11230-018-9776-2.

Vieira, D.H.M.D., Rangel, L.F., Tagliavini, V.P., Abdallah, V.D., Santos, M.J., & de Azevedo, R.K. (2020). A new species, *Henneguya lacustris* n. sp. (Cnidaria: Myxosporea), infecting the gills of *Astyanax lacustris* from Brazil. Parasitol. Res. 119, 4259–4265. https://doi.org/10.1007/s00436-020-06871-5.

Vieira, D.H.M.D., Rangel, L.F., Tagliavini, V.P., Abdallah, V.D., Santos, M.J., & de Azevedo, R.K. (2021). Morphological and molecular analysis of *Henneguya tietensis* n. sp. (Cnidaria: Myxosporea), parasitizing the gill filaments of *Prochilodus lineatus* (Valenciennes, 1837) from Brazil. Parasitol. Res. 120(1), 27–36. https://doi.org/10.1007/s00436-020-06918-7.

Vieira, D.H.M.D., Narciso, R.B., & da Silva, R.J. (2022). Morphological and molecular characterization of the cryptic species *Myxobolus cataractae* n. sp. (Cnidaria: Myxozoa: Myxobolidae) parasitizing *Imparfinis mirini* (Siluriformes: Heptapteridae). Parasitol. Int. 88, 102560. https://doi.org/10.1016/j.parint.2022.102560.

Wang, M., Zhao, Y., & Yang, C. (2019). The impacts of geographic and host species isolation on population divergence of *Myxobolus lentisuturalis*. Parasitol. Res. 118, 1061–1066. https://doi. org/10.1007/s0043 6-019-06234-9.

Wang, M.M., Zhang, J.Y., & Zhao, Y.J. (2021). New record for *Myxobolus basilamellaris* in China with histopathological insights into gill infestation. J. Fish. China, 45, 1555–1562.

Wang, M.M., Zhang, J.Y., & Zhao, Y.J. (2022). Morphological description and molecular identification of *Myxobolus dajiangensis* n. sp. (Myxozoa: Myxobolidae) from the gill of *Cyprinus carpio* in southwest China. PeerJ 10, e13023.

Weill, R. (1938). L'interprétation des Cnidosporidies et la valeur taxonomique de leur cnidome. Leur cycle comparé à la phase larvaire des Narcomeduses cuninides. Travaux. Stn. Zool. Wimereaux 13, 727–744.

Whipps, C.M., Adlard, R.D., Bryant, M.S., & Kent, M.L. (2003). Two unusual myxozoans, *Kudoa quadricornis* n. sp. (Multivalvulida) from the muscle of godspotted trevally (*Carangoides fulvoguttatus*) and *Kudoa permulticapsula* n. sp. (Multivalvulida) from the muscle of Spanish mackerel (*Scomberomorus commersoni*) from the Great Barrier Reef, Australia. J. Parasitol. 89, 168–173.

Whipps, C.M., & Kent, M.L. (2006). Phylogeography of the cosmopolitan marine parasite *Kudoa thyrsites* (Myxozoa: Myxosporea). J. Eukaryot. Microbiol. 53(5), 364–373. https://doi.org/10.1111/j.1550-7408.2006.00114.x.

Whipps, C.M., Grossel, G., Adlard, R.D., Yokoyama, H., Bryant, M.S., Munday, B.L., & Kent, M.L. (2004). Phylogeny of the Multivalvulidae (Myxozoa: Myxosporea) based on comparative ribosomal DNA sequence analysis. J. Parasitol. 90(3), 618–622.

Whipps, C.W., Atkinson, S.D., & Hoeksema, B.W. (2025a). World List of Myxozoa. Accessed at https://www.marinespecies.org/myxozoa on 2025-05-02.

Whipps, C.M., Ogburn, E.C., & Font, W.F. (2025b). A New *Myxidium* Species from the Least Killifish *Heterandria formosa* in Louisiana. J. Parasitol. 111(2), 163–171.

Whitaker, D.J., & Kent, M.L. (1991). Myxosporean *Kudoa thyrsites*: a cause of soft flesh in farm-reared Atlantic salmon. J. Aquat. Anim. Health 3(4), 291–294.

White, T.J., Bruns, T.D., Lee, S., & Taylor, J.W. (1990). Amplification and direct sequencing of fungal ribosomal RNA genes for phylogenetics. In: Innis, M.A., Gelfand, D.H., Sninsky, J.J., & White, T.J. (eds.) PCR Protocols: A Guide to Methods and Applications. Academic Press, London.

Wolf, K., & Markiw, M.E. (1984). Biology contravenes taxonomy in the Myxozoa: new discoveries show alternation of invertebrate and vertebrate hosts. Science 225, 1449–1452.

Woodyard, E.T., Rosser, T.G., Stilwell, J.M. Camus, A.C., Khoo, L.H., Waldbieser, G., Lorenz, W.W. & Griffin, M.J. (2022). New data on *Henneguya postexilis* Minchew, 1977, a parasite of channel catfish *Ictalurus punctatus*, with notes on resolution of molecular markers for myxozoan phylogeny. Syst. Parasitol. 99, 41–62. https://doi.org/10.1007/s11230-021-10015-3.

Xi, B.W., Zhang, J.Y., Xie, J., Pan, L.K., Xu, P., & Ge, X.P. (2013). Three actinosporean types (Myxozoa) from the oligochaete *Branchiura sowerbyi* in China. Parasitol. Res. 112, 1575–1582. https://doi.org/10.1007/s00436-013-3306-6.

Xi, B.W., Zhou, Z.G., Xie, J., Pan, L.K., Yang, Y.L., & Ge, X.P. (2015). Morphological and molecular characterization of actinosporeans infecting oligochaete *Branchiura sowerbyi* from Chinese carp ponds. Dis. Aquat. Org. 114, 217–228. https://doi.org/10.3354/dao02859.

Xi, B.W., Li, P., Liu, Q.C., Chen, K., Teng, T., & Xie, J. (2017). Description of a new Neoactinomyxum type actinosporean from the oligochaete *Branchiura sowerbyi* Beddard. Syst. Parasitol. 94, 73–80. https://doi.org/10.1007/s11230-016-9677-1.

Xi, B.W., Zhao, X., Li, P. & Xie, J. (2019). Morphological variation in *Myxobolus drjagini* (Akhmerov, 1954) from silver carp and description of *Myxobolus paratypicus* n. sp.

(Cnidaria: Myxozoa). Parasitol Res. 118, 2149–2157. https://doi.org/10.1007/s00436-019-06350-6.
Xu, L., Zhao, X., Huang, Y., Xin, Z., & Zhang, J. (2025). Morphological and molecular characterization of *Myxobolus aculeatus* n. sp. (Myxozoa: Myxosporea) from the ovary of *Macrognathus aculeatus*, Bloch, 1786 (Synbranchiformes: Mastacembelidae) in China. Parasitol. Int. 106, 103039. https://doi.org/10.1016/j.parint.2025.103039.
Xiao, C.X., & Chen, Q.L. (1993). Two new Myxosporidia (Protozoa) from freshwater fish in Hubei province. Trans. Res. Fish Dis. 1, 83–84 (In Chinese).
Xiao, C. & Desser, S.S. (1998a). The oligochaetes and their actinosporean parasites in Lake Sasajewun, Algonquin Park, Ontario. J. Parasitol. 84(5), 1020–1026.
Xiao, C., & Desser, S.S. (1998b). Actinosporean stages of myxozoan parasites of oligochaetes from Lake Sasajewun, Algonquin Park, Ontario: new forms of triactinomyxon and raabeia. J. Parasitol. 998–1009. https://doi.org/10.2307/3284634.
Xiao, C., & Desser, S.S. (1998c). Actinosporean stages of myxozoan parasites of oligochaetes from Lake Sasajewun, Algonquin Park, Ontario: new forms of echinactinomyxon, neoactinomyxum, aurantiactinomyxon, guyenotia, synactinomyxon and antonactinomyxon. J. Parasitol. 84, 1010–1019. https://doi.org/10.2307/3284635.
Xiang, Y., Zhang, J.Y., & Zhao, Y.J. (2021). New host record and molecular phylogeny of *Myxidium spinibarba* Chen et al., 2020. Acta Hydro. Sin. 45. https://doi.org/10.7541/2021.2020.186.
Yanagida, T., Sameshima, M., Nasu, H., Yokoyama, H., & Ogawa, K. (2006). Temperature effects on the development of *Enteromyxum* spp. (Myxozoa) in experimentally infected tiger puffer, *Takifugu rubripes* (Temminck & Schlegel). J. Fish Dis. 29(9), 561–567.
Yang, C., Zhou, Y., Zhao, Y., Huang, W., & Huang, C. (2017). Erection of *Unicapsulocaudum mugilum* gen. et sp. nov. (Myxozoa: Ceratomyxidae) based on its morphological and molecular data. J. Nat. Hist. 51, 457–467.
Yasuda, H., Ooyama, T., Iwata, K., Tun, T., Yokoyama, H., & Ogawa, K. (2002). Fish-to-fish transmission of *Myxidium* spp. (Myxozoa) in cultured tiger puffer suffering from emaciation disease. Fish Pathol. 37, 29–33. https://doi.org/10.3147/jsfp.37.29.
Ye, L.T., Li, W.X., Wang, W.W., Wu, S.G., & Wang, G.T. (2014). Updated morphology, histopathology and molecular phylogeny of *Myxobolus hearti*, cardiac myxosporea in gibel carp, *Carassius gibelio* (Bloch). J. Fish Dis. 37, 11–20. https://doi.org/10.1111/jfd.12026.
Yin, Q., Yang, Y., Liu, Y., Xiang, J., Li, D., Liu, X., & Yu, J. (2025) Morphological and molecular characteristic of *Myxidium chuatsi* n. sp. (Myxozoa: Myxidiidae) from the gallbladder of *Siniperca chuatsi* in China. 水生生物学报, 49(9), 9.
Yokoyama, H. (1997). Transmission of *Thelohanellus hovorkai* Achmerov, 1960 (Myxosporea: Myxozoa) to common carp *Cyprinus carpio* through the alternate oligochaete host. Syst. Parasitol. 36, 79–84. https://doi.org/10.1023/A:1005752913780.
Yokoyama, H. (2003). A review: gaps in our knowledge on myxozoan parasites of fishes. Fish Pathol. 38, 125–136.
Yokoyama, H., Ogawa, K., & Wakabayashi, H. (1993a). Involvement of *Branchiura sowerbyi* (Oligochaeta: Annelida) in the transmission of *Hoferellus carassii* (Myxosporea: Myxozoa), the causative agent of kidney enlargement disease (KED) of goldfish *Carassius auratus*. Fish Pathol. 28(3), 135–139.
Yokoyama, H., Ogawa, K., & Wakabayashi, H. (1993b). Some biological characteristics of actinosporeans form the oligochaetes *Branchiura sowerbyi*. Dis. Aquat. Org. 17, 223–228.
Yokoyama, H., Ogawa, K., & Wakabayashi, H. (1995). *Myxobolos cultus* n. sp. (Myxosporea, Myxobolidae) in the goldfish *Carassius auratus* transformed from the actinosporean stage in the oligochaete *Branchiura sowerbyi*. J. Parasitol. 81, 446–451. https://doi.org/10.2307/3283830.
Yuan, S., Xi, B.W., Wang, J.G., Xie, J., & Zhang, J.Y. (2015). *Thelohanellus wangi* n. sp. (Myxozoa, Myxosporea), a new gill parasite of allogynogenetic gibel carp (*Carassius*

auratus gibelio Bloch) in China, causing severe gill myxosporidiosis. Parasitol. Res. 114, 37–45. https://doi.org/10.1007/s00436-014-4157-5.

Zakaria, M.H., Amin, S.M.N., Romano, N., Arshad, A., Rahman, M.A., & Lee, S.G. (2018). Embryonic and larval development of lemon fin barb hybrid (♂ *Hypsibarbus wetmorei* x♀ *Barbonymus gonionotus*. J. Environ. Biol. 39(5), 732–740.

Zatti, S.A., Naldoni, J., Silva, M.R., Maia, A.A., & Adriano, E.A. (2015). Morphology, ultrastructure and phylogeny of *Myxobolus curimatae* n. sp. (Myxozoa: Myxosporea) a parasite of *Prochilodus costatus* (Teleostei: Prochilodontidae) from the São Francisco River, Brazil. Parasitol. Int. 64(5), 362–368. https://doi.org/10.1016/j.parint.2015.05.011.

Zatti, S.A., Atkinson, S.D., Bartholomew, J.L., Maia, A.A., & Adriano, E.A. (2017). Amazonian waters harbour an ancient freshwater *Ceratomyxa* lineage (Cnidaria: Myxosporea). Acta Tropica, 169, 100–106. https://doi.org/10.1016/j.actatropica.2017.02.006.

Zatti, S.A., Atkinson, S.D., Maia, A.A., Bartholomew, J.L., & Adriano, E.A. (2018a). *Ceratomyxa gracillima* n. sp. (Cnidaria: Myxosporea) provides evidence of panmixia and ceratomyxid radiation in the Amazon basin. Parasitol. 145(9), 1137–1146. https://doi.org/10.1017/S0031182017002323.

Zatti, S.A., Atkinson, S.D., Maia, A.A.M. Bartholomew, J.L, & Adriano, E.A. (2018b). Novel *Henneguya* spp. (Cnidaria: Myxozoa) from cichlid fish in the Amazon basin cluster by geographic origin. Parasitol. Res. 117(3), 849–859. https://doi.org/10.1007/s00436-018-5762-5.

Zatti, S.A., Araújo, B.L., Adriano, E.A., & Maia, A.A. (2023). A new freshwater *Ceratomyxa* species (Myxozoa: Ceratomyxidae) parasitizing a sciaenid fish from the Amazon Basin, Brazil. Parasitol. Int. 97, 102796. https://doi.org/10.1016/j.parint.2023.102796.

Zhang, B., Tu, X., & Gu, Z. (2023a). Morphological, histological and phylogenetic identification of three species of *Myxobolus* (Myxosporea: Myxobolidae) infecting different carp lineages in China. J. Fish Dis. 48(9), e13861.

Zhang, B., Shen, Y., Tu, X., & Gu, Z. (2023b). Identification and characterization of *Myxobilatus channi* n. sp. (Cnidaria: Myxosporea) infecting the alimentary tract of northern snakehead *Channa argus* cultivated in China. Aquaculture 575, 739723.

Zhang, B., Tu, X., & Gu, Z. (2023c). *Myxobolus shuifuensis* sp. n. (Myxozoa: Myxobolidae) infecting the exotic mrigal *Cirrhinus mrigala* feral in China. Parasitol. Int. 94, 102732. https://doi.org/10.1016/j.parint.2023.102732.

Zhang, J., Wang, Y., & Zhao, Y. (2023d). The description of *Myxobolus meijiangensis* n. sp. (Myxozoa: Myxobolidae) and its pathogenicity to the gills of goldfish. Parasitol. Int. 97, 102795. https://doi.org/10.1016/j.parint.2023.102795.

Zhang, J.Y., Gu, Z. M., Kalavati, C., Costa Eiras, J., Liu, Y., Guo, Q.Y., & Molnár, K. (2013). Synopsis of the species of *Thelohanellus* Kudo, 1933 (Myxozoa: Myxosporea: Bivalvulida). Syst. Parasitol. 86(3), 235–256.

Zhang, X.Y., Yao, X., Zhou, F., Yang, C.Z., & Liu, Y. (2022). Identification of *Thelohanellus pseudonikolskii* n. sp. and *Myxobolus koi* Kudo, 1920 from goldfish *Carassius auratus*. Aquac. Rep. 24, 101167. https://doi.org/10.1016/j.aqrep.2022.101167.

Zhao, Y.J., & Ma, Y.G. (1992). The *Thelohanellus* disease of carp from Sichuan Province. J. Southwest China Teachers University 17, 367371 (In Chinese).

Zhao, D.D., Borkhanuddin, M.H., Wang, W., Liu, Y., Cech, G., Zhai, Y., & Székely, C. (2016). The life cycle of *Thelohanellus kitauei* (Myxozoa: Myxosporea) infecting common carp (*Cyprinus carpio*) involves aurantiactinomyxon in *Branchiura sowerbyi*. Parasitol. Res. 115, 4317–4325. https://doi.org/10.1007/s00436-016-5215-y.

Zhao, D.D., Zhai, Y.H., Liu, Y., Wang, S.J., & Gu, Z.M. (2017). Involvement of aurantiactinomyxon in the life cycle of *Thelohanellus testudineus* (Cnidaria: Myxosporea) from allogynogenetic gibel carp *Carassius auratus gibelio*, with morphological, ultrastructural, and molecular analysis. Parasitol. Res. 116(9), 2449–2456. https://doi.org/10.1007/s00436-017-5547-2.

Appendix B: Supplementary Tables and Figures

Table S1 Primers used for amplification and sequencing of 18S rDNA and 28S rDNA regions in each myxosporean species and actinosporean types.

Parasite	PCR Primer and Sequencing	Application
Myxobolus lentisuturalis	ERIB-ERIB10 (1st round)	Nested PCR
	Myx1F-SphR (2nd round)	
	ACT1F, ACT1fr, ACT1R, ACT3R, CR1F, CR1R, Myxgen4F	Sequencing
Myxobolus pecsensis n. sp.	MyxospecR-18E and MyxospecF-18R	Direct PCR
	18E, MyxospecF, Myxgen4F, MyxospecR, SphR, 18R	Sequencing
Thelohanellus imrei n. sp.	MyxospecR-18E and MyxospecF-18R	Direct PCR
	18E, ACT1fr, ACT1F, MyxospecF, Myxgen4F, MyxospecR 18R	Sequencing
Zschokkella chezhachei n. sp.	MyxospecR-18E and MyxospecF-18R	Direct PCR
	18E, MyxospecF, Myxgen4R, 18R	Sequencing
Myxobolus diversus	MyxospecR-18E and MyxospecF-18R	Direct PCR
Myxobolus n. sp. 1	18E, MyxospecF, ACT1R, Myxgen4F, 18R	Sequencing
Sphaerospora molnari	ERIB-ERIB10 (1st round)	Nested PCR
	MC5-MC3 and MyxospecF-18R (2nd round)	
	ERIB1, ERIB10, MyxospecF, 18R, MC5, MC3, Smol1900R, Smol1220F, Smol2500R, Smol1800F, Sphaero10R, Sph9R	Sequencing
Thelhanellus serosae n. sp.	MyxospecF-18R and 18E-MyxospecR	Direct PCR
	MyxospecF, 18R, ACT1fr, ACT1F, ACT1R, SphR	Sequencing
Thelohanellus paranikolskii n. sp.; *Thelohanellus zahrahae;* *Henneguya* n. sp. 2; *Myxidium* n. sp. 2	ERIB1-ACT1R and MyxospecF-18R	Direct PCR
	ERIB1, ACT1R, MyxospecF, Myxgen4F, 18R	Sequencing
Thelohanellus nikolskii	MyxospecF-18R	Direct PCR
	ACT1F, MyxospecF, Myxgen4F, 18R	Sequencing
Thelohanellus hovorkai	MyxospecR-18E and MyxospecF-18R	Direct PCR
	18E, MyxospecF, MyxospecR, 18R	Sequencing
Myxobolus intrachondrealis Aurantiactinomyxon type 6	MyxospecR-18E and MyxospecF-18R	Direct PCR
	18E, ACT1fr, MyxospecF, Myxgen4F, MyxospecR, 18R	Sequencing
Myxobolus basilamellaris	MyxospecR-18E and MyxospecF-18R	Direct PCR
	ACT1fr, ACT1R, MyxospecF, Myxgen4F, 18R	Sequencing
Myxobolus n. sp. 2	MyxospecR-18E and MyxospecF-18R	Direct PCR
	18E, ACT1fr, ACT1F, MyxospecF, Myxgen4F, MyxospecR, SphR	Sequencing
Ceratomyxa schwanefeldii n. sp.	18E-18R (1st round)	Semi-nested PCR
	CerSAZ.1f-ACT1R; CerSAZ.1f-CerSAZ.3r; CerSAZ.4f-18R; MC5-18R (2nd round)	
	18E, 18R, CerSAZ.1f, MC5, ACT1R, CerSAZ.3r, CerSAZ.4f	Sequencing
	NLF184-NLR1270; NLF1050-NLR3284; Myxo28S1F-28S3R	Direct PCR
	NLF184, NLR1270, NLF1050, NLR1694, Myxo28S1F, My28SF	Sequencing
Myxobolus gonionoti n. sp.	ERIB1-ACT1R and MyxospecF-18R	Direct PCR
	ERIB1, MyxospecF, ACT1R, Myxgen4R, 18R	Sequencing
Myxobolus barbonymi n. sp. *Thelohanellus barbonymi* n. sp. Raabeia type 2	ERIB1-ACT1R and MyxospecF-18R	Direct PCR
	ERIB1, MyxospecF, Myxgen4F, ACT1R, Myxgen4R, 18R	Sequencing
Myxobolus faizahae n. sp.	ERIB1-ACT1R and MyxospecF-18R	Direct PCR
	ERIB1, ACT1F, ACT1R, Myxgen4R, 18R	Sequencing
Thelohanellus gonionoti n. sp.	Myx1F-ERIB10	Direct PCR
	Myx1F, ACT1fr, Myxgen4F, ACT1R, ERIB10	Sequencing
Myxobolus dykovae	MyxospecR-18E and MyxospecF-18R	Direct PCR
	18E, MyxospecF, Myxgen4F, ACT1R, Myxgen4R, 18R	Sequencing
Henneguya n. sp. 1	ERIB1-ACT1R and MyxospecF-18R	Direct PCR
	ERIB1, MyxospecF, ACT1R, MyxospecR, 18R	Sequencing

Henneguya n. sp. 3;	ERIB1-ACT1R and Myxgen4F-ERIB10	Direct PCR
Henneguya n. sp. 4	ERIB1, Myxgen4F, ACT1R, Myxgen4R, ERIB10	Sequencing
Henneguya n. sp. 5	ERIB1-ACT1R and Myxgen4F-ERIB10	Direct PCR
	ERIB1, ACT1fr, ACT1R, Myxgen4R, SphR, ERIB10	Sequencing
Henneguya n. sp. 6	ERIB1-ACT1R and Myxgen4F-ERIB10	Direct PCR
	ERIB1, ACT1fr, ACT1F, ACT1R, Myxgen4F, Myxgen4R, ERIB10	Sequencing
Henneguya n. sp. 7	ERIB1-ACT1R, Myxgen4F-ERIB10 and ACT1F-ACT1R	Direct PCR
Myxobolus n. sp. 3	ERIB1, ACT1R, ERIB10, Myxgen4F, ACT1F, ACT1fr	Sequencing
Henneguya n. sp. 6	Myxgen4F-ERIB10 and ACT1F-ACT1R	Direct PCR
Henneguya n. sp. 8	ERIB10, Myxgen4F, ACT1F, ACT1R	Sequencing
Henneguya n. sp. 9	Myx1F-ERIB10	Direct PCR
	ACT1fr, ACT1R, Myxgen4F, SphR	Sequencing
Henneguya n. sp. 10	Myx1F-ERIB10	Direct PCR
	ACT1fr, ACT1F, ACT1R, ACT3F, SphR	Sequencing
Henneguya n. sp. 11	Myxgen4R-ERIB10 and ERIB1-Myxgen4R	Direct PCR
	ERIB1, ACT1fr, Myxgen4F, Myxgen4R, ERIB10	Sequencing
Myxobolus n. sp. 4	Myxgen4F-ERIB10 and ACT1F-ACT1R	Direct PCR
	ERIB10, Myxgen4F, ACT1F, ACT1R, Myxgen4R	Sequencing
Myxobolus n. sp. 5	MyxospecF-18R and ERIB1-Myxgen4R	Direct PCR
	ERIB1, Myx1F, ACT1fr, MyxospecF, Myxgen4F, Myxgen4R, 18R	Sequencing
Myxobolus n. sp. 6	MyxospecF-18R and Myx1F-SphR	Direct PCR
	MyxospecF, 18R, MyxospecR, Myxgen4R, Myx1F	Sequencing
Myxobolus n. sp. 7	MyxospecF-18R and ERIB1-Myxgen4R	Direct PCR
	ERIB1, ACT1F, MyxospecF, Myxgen4F, SphR, 18R	Sequencing
Myxobolus n. sp. 8	MyxospecF-18R and ERIB1-Myxgen4R	Direct PCR
	ACT1F, MyxospecF, Myxgen4R, SphR, 18R	Sequencing
Myxobolus n. sp. 9	MyxospecF-18R and ERIB1-Myxgen4R	Direct PCR
	ACT1fr, MyxospecF, Myxgen4R, SphR, 18R	Sequencing
Myxobolus n. sp. 10;	MyxospecF-18R and ERIB1-Myxgen4R	Direct PCR
Thelohanellus n. sp. 2	ERIB1, ACT1fr, MyxospecF, Myxgen4R, SphR, 18R	Sequencing
Myxobolus n. sp. 11	ERIB1-Myxgen4R and Myxgen4F-ERIB10	Direct PCR
	ERIB1, Myxgen4F, Myxgen4R, ERIB10	Sequencing
Myxobolus n. sp. 12	MyxospecF-18R and ERIB1-Myxgen4R	Direct PCR
	MyxospecF, 18R, Myxgen4R, ERIB1	Sequencing
Myxobolus n. sp. 13	MyxospecF-18R and ERIB1-Myxgen4R	Direct PCR
	MyxospecF, 18R, Myxgen4R, ACT1F, ERIB1	Sequencing
Thelohanellus n. sp. 1	MyxospecF-18R and ERIB1-Myxgen4R	Direct PCR
	ERIB1, ACT1fr, ACT1F, MyxospecF, Myxgen4R, 18R	Sequencing
Myxidium n. sp. 1	MyxospecF-18R and Myx1F-SphR	Direct PCR
	MyxospecF, 18R, Myxgen4R, Myx1F	Sequencing
Myxidium n. sp. 3	ERIB1-ACT1R and Myxgen4F-ERIB10	Direct PCR
	ERIB1, ACT1R, ERIB10, Myxgen4F, Myxgen4R, ACT1fr	Sequencing
Triactinomyxon type 1	MyxospecF-ERIB10	Direct PCR
	MyxospecF, ERIB10, Myxgen4F, ACT1R	Sequencing
Raabeia type 1	Myx1F-ERIB10 and ERIB1-ACT1R	Direct PCR
	Myx1F, ERIB10, ERIB1, ACT1R, ACT1fr, 18R, Myxgen4F	Sequencing
Aurantiactinomyxon type 1	Myx1F-ERIB10 and ERIB1-ACT1R	Direct PCR
	Myx1F, ERIB10, ERIB1, ACT1R, ACT3F, Myxgen4F	Sequencing
Aurantiactinomyxon type 2	Myx1F-ERIB10 and ERIB1-ACT1R	Direct PCR
	Myx1F, ERIB10, ERIB1, ACT1R, SphR, ACT1fr, ACT3F	Sequencing
Aurantiactinomyxon type 3	MyxospecF-18R and 18E-MyxospecR	Direct PCR
	MyxospecF, 18R, 18E, MyxospecR, ACT1fr	Sequencing
Aurantiactinomyxon type 4	MyxospecF-18R and 18E-MyxospecR	Direct PCR
Aurantiactinomyxon type 5	MyxospecF-18R and 18E-MyxospecR	Direct PCR

	MyxospecF, 18E, MyxospecR, Myxgen4F	Sequencing
Neoactinomyxum type 1	Myx1F-ERIB10	Direct PCR
	Myx1F, ERIB10, 18R, ACT1R, Myxgen4F, ACT3F	Sequencing
Raabeia type 1 (Malaysia)	Myx1F-ERIB10	Direct PCR
	Myx1F, ACT3F, Myxgen4R, MyxospecR, ACT1R	Sequencing
Aurantiactinomyxon type 1 (Malaysia)	MyxospecF-18R and Myxgen4F-ERIB10	Direct PCR
	ERIB10, Myxgen4F, Myxgen4R, SphR	Sequencing
Aurantiactinomyxon type 2 (Malaysia)	MyxospecF-18R and ERIB1-Myxgen4R	Direct PCR
	MyxospecF, 18E, Myxgen4F, Myxgen4R, ERIB1, ACT1F	Sequencing
Aurantiactinomyxon type 3 (Malaysia)	MyxospecF-18R and ERIB1-Myxgen4R	Direct PCR
	MyxospecF, 18E, Myxgen4F, Myxgen4R, ACT1fr, SphR, ERIB1	Sequencing
Branchiodrilus hortensis *Ophidonais serpentina* *Limnodrilus hoffmeisteri* *Tubifex tubifex* *Branchiodrilus* sp. *Bothrioneurum* sp.	16sarL-16sbrH	Direct PCR & Sequencing
Aulodrilus acutus	ITS5-ITS4	Direct PCR
Aulophorus sp.	ITS5, ITS4, 5.8mussF, 5.8mussR	Sequencing

Table S2. Primers pairs and corresponding PCR protocols, including initial DNA denaturation, denaturation, annealing, synthesis across 35 cycles and final extension steps.

Primer pairs	Protocol	Reference
18E-MyxospecR MyxospecF-18R	95 °C (4 min) 95 °C (1 min) Annealing temperature: 48 °C (1 min) 72 °C (90 s) 72 °C (10 min)	Liu et al. (2016a)
ERIB1-ACT1R	95 °C (3 min) 95 °C (1 min) Annealing temperature: 55 °C (45 s) 72 °C (2 min) 72 °C (7 min)	Úngari et al. (2021)
ERIB1-ACT1R	95 °C (2 min) 94 °C (20 s) Annealing temperature: 55 °C (30 s) 72 °C (90 s) 72 °C (10 min)	Atkinston & Bartholomew (2009)
Myxgen4F-ERIB10 ACT1F-ACT1R Myx1F-SphR	94 °C (3 min) 94 °C (45 s) Annealing temperature: 55 °C (50 s) 72 °C (1 min) 72 °C (10 min)	Colunga et al. (2024)
18E-18R CerSAZ.4f-18R	95 °C (2 min) 94 °C (30 s) Annealing temperature: 60 °C (30 s) 72 °C (1 min) 72 °C (5 min)	Zatti et al. (2023)
CerSAZ.1f-ACT1R CerSAZ.1f-CerSAZ.3r	Annealing temperature: 62 °C (30 s)	
MC5-18R	Annealing temperature: 58 °C (30 s)	
Myx1F-ERIB10	95 °C (3 min) 95 °C (1 min) Annealing temperature: 55 °C (1 min) 72 °C (2 min) 72 °C (7 min)	This study
MyxospecF-ERIB10	95 °C (3 min) 95 °C (1 min) Annealing temperature: 50 °C (1 min) 72 °C (2 min) 72 °C (7 min)	This study
ERIB1-Myxgen4R	94 °C (3 min) 94 °C (45 s)	This study

	Annealing temperature: 50 ℃ (1 min) 72 ℃ (90 s) 72 ℃ (7 min)	
ERIB1-ERIB10	95 ℃ (5 min) 95 ℃ (50 s) Annealing temperature: 59 ℃ (50 s) 72 ℃ (2 min) 72 ℃ (7 min)	Eszterbauer et al. (2013)
MC5-MC3	95 ℃ (5 min) 95 ℃ (1 min) Annealing temperature: 52 ℃ (1 min) 72 ℃ (2 min) 72 ℃ (5 min)	Bittencourt et al. (2021)
ERIB1-ERIB10	95 ℃ (3 min) 94 ℃ (3 min) Annealing temperature: 52 ℃ (2 min) 72 ℃ (2 min) 72 ℃ (7 min)	Cech et al. (2015)
Myx1F-SphR	94 ℃ (3 min) 94 ℃ (45 s) Annealing temperature: 50 ℃ (50 s) 72 ℃ (1 min 40s) 72 ℃ (10 min)	
16sarL-16sbrH	95 ℃ (3 min) 94 ℃ (45 s) Annealing temperature: 53 ℃ (45 s) 72 ℃ (90 s) 72 ℃ (7 min)	Rocha et al. (2019a)
ITS5-ITS4	95 ℃ (5 min) 95 ℃ (30 s) Annealing temperature: 50 ℃ (30 s) 72 ℃ (90 s) 72 ℃ (8 min)	Erséus et al. (2017)
NLF184-NLR1270* NLF1050-NLR3284* Myxo28S1F-28S3R*	95 ℃ (3 min) 95 ℃ (1 min) Annealing temperature: 48 ℃ (1 min) 72 ℃ (1 min) 72 ℃ (10 min)	Bartošová et al. (2009)

*Amplification of DNA for 40 cycles

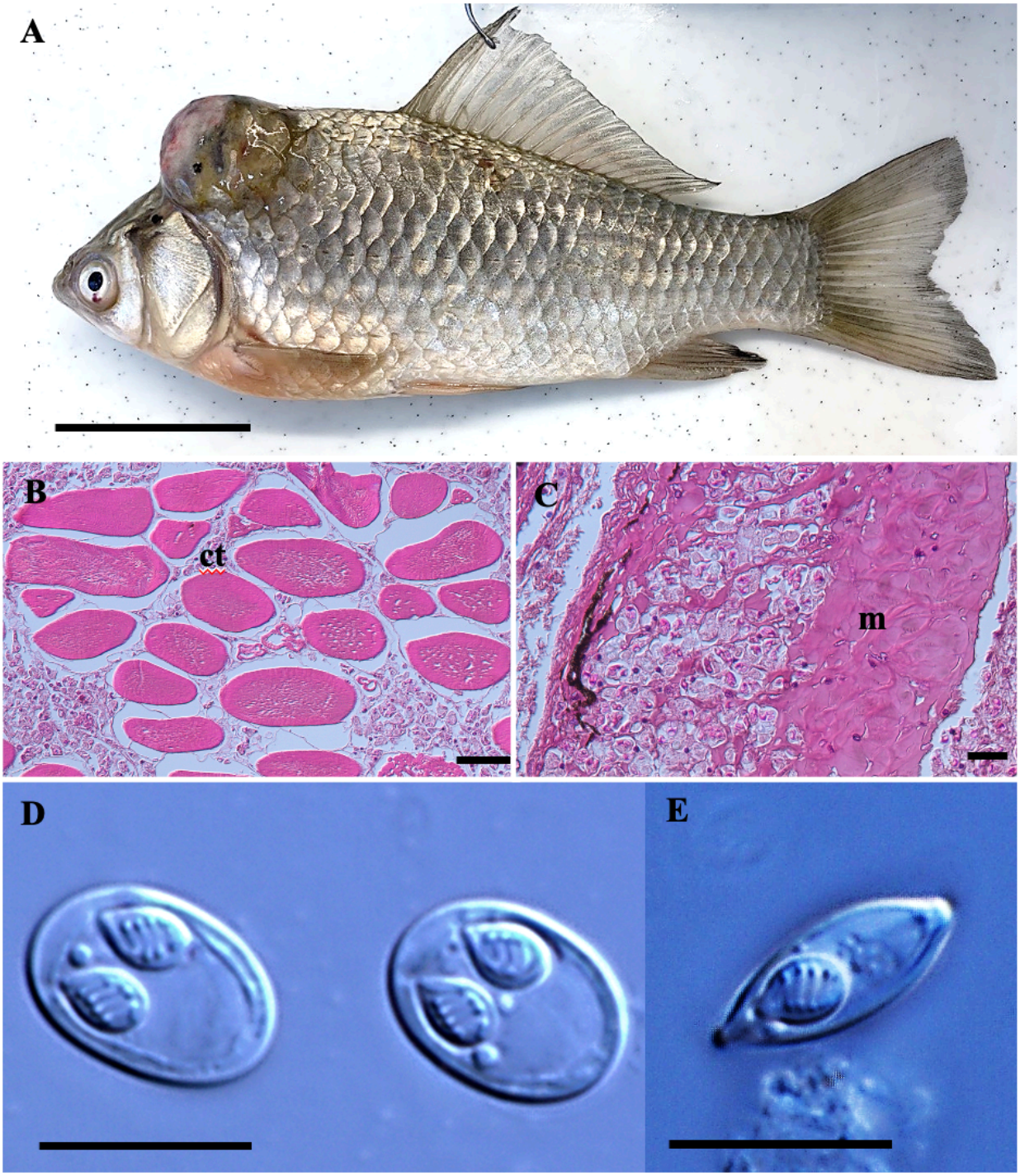

Figure S1. Infected *Carassius auratus gibelio* with *Myxobolus lentisuturalis*. A) Presence of dorsolateral hump between the head and dorsal fin of the gibel carp. B) Histological section of the dorsolateral hump showing spores and tissue debris within the intermuscular connective tissue (ct) observed in the peripheral part of the hump. C) Relatively intact muscle cells (m) partially invaded by *M. lentisuturalis* spores (sp) at the middle region of the hump. D) Mature spores of *M. lentisuturalis*. E) Spore in sutural view. Scale bars represent 10 µm except (A) 5 cm, (D) 50 µm and (E) 20 µm.

Table S3 Comparison of morphometric characteristics and measurements of *Myxobolus lentisuturalis* recorded from *C. auratus gibelio* and *C. auratus* according to previous studies and the present study. All measurements are provided in µm followed by the range in parentheses and unavailable data are indicated by a dash (–). Abbreviations: SL spore length, SW spore width, ST spore thickness, PCL polar capsule length, PCW polar capsule width, PFC polar filament coils.

	Dyková et al. (2002)	**Caffara et al. (2009)**	**Wang et al. (2019)**	**Huskanović (2021)**	**Hepps Keeney et al. (2023)**	**Present study**
Host	*Carassius auratus gibelio*	*Carassius auratus*	*Carassius auratus*	*Carassius auratus gibelio*	*Carassius auratus*	*Carassius auratus gibelio*
Predilection site	Muscle tissue	Muscle tissue	Gallbladder	Muscle tissue	Muscle tissue	Muscle tissue
Origin	Hubei, China	Bologna, Italy	Chongqing, China	Croatia	USA	Hungary
SL	11.8 (11.2–12.4)	10.5 (9.0–11.0)	11.9 (10.4–12.9)	11.9 (11.28–12.46)	11.4 (10.4–12.5)	11.8 (10.0–13.3)
SW	7.6 (7.2–8.4)	6.6 (6.0–7.0)	7.3 (6.4–7.9)	7.84 (7.43–8.34)	7.1 (6.4–8)	7.6 (6.6–8.6)
PCL	4.2 (4.0–4.4)	3.7 (3.0–4.5)	4.1 (3.4–5.0	4.22 (4.01–4.54)	4 (3.5–4.5)	4.3 (3.3–5.1)
PCW	2.5 (2.0–2.8)	2.2 (2.0–3.0)	2.4 (1.8–2.8)	2.45 (2.20–2.80)	2.6 (2.2–3)	2.7 (1.7–3.2)
ST	5.2	3.9 (3.0–5.0)	–	5.2 (5.03–5.35)	4.7 (3.9–5.5)	5.0 (4.1–5.6)*
Distance between anterior ends of polar capsules	2.4–2.8	1.5–2	–	2.53 (2.23–2.77)	–	3.0 (1.7–3.8)
PFC	4	4–5	4–5	4	4–5	4–5

* The thickness measurements are from 14 spores.

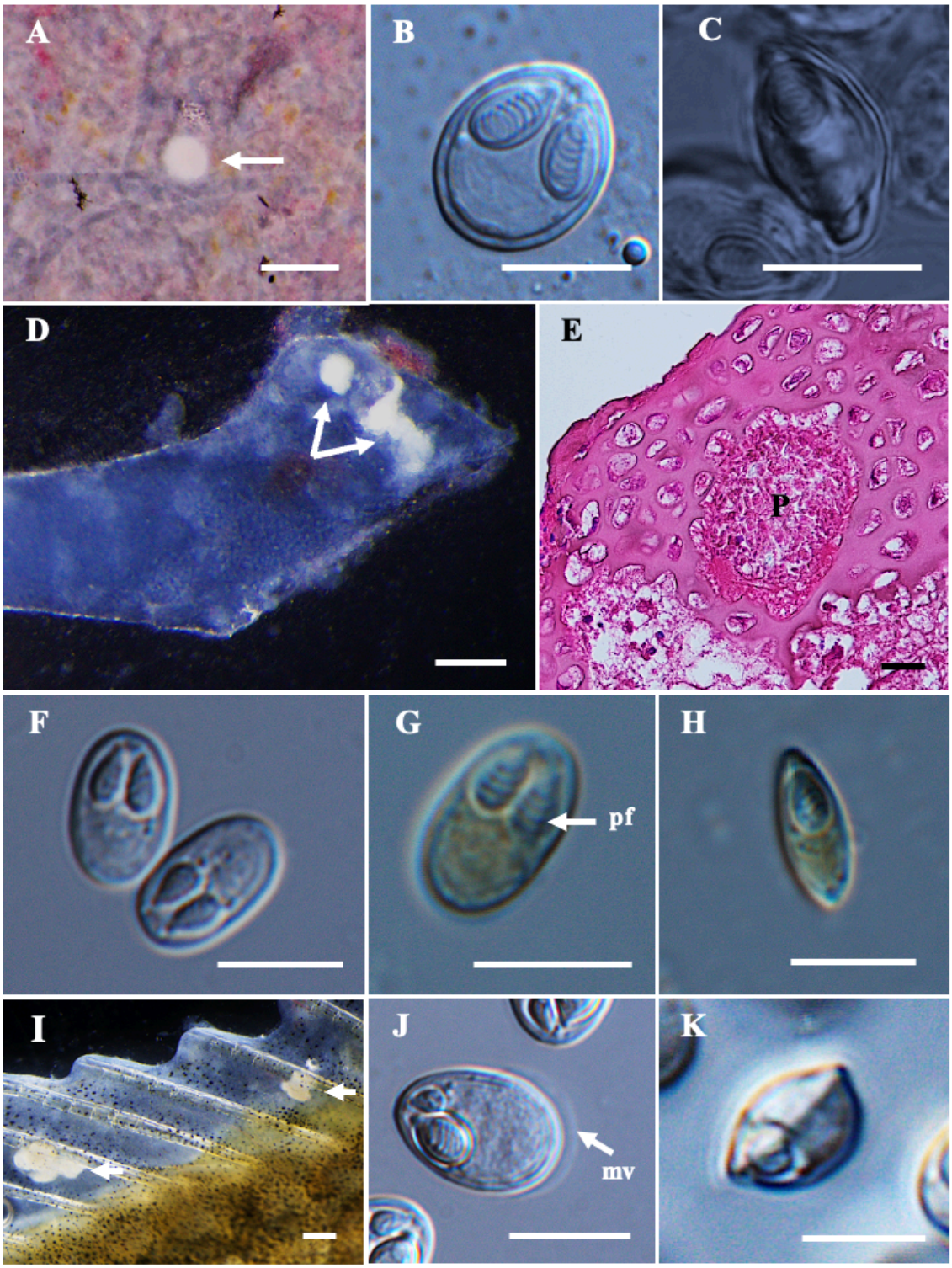

Figure S2. *Myxobolus* spp. infection in *Carassius auratus gibelio*. A) Plasmodium of *M. ocsardiensis* n. sp. in the kidney (white arrow). B) Mature spore of *M. ocsardiensis* n. sp. with two polar capsules containing seven coils and C) Spore in sutural view. D) Plasmodia of *M. pecsensis* n. sp. in the gill cartilage (white arrows). E) Histological section of the end of cartilaginous gill arch of gibel carp, showing plasmodium (P) within the hyaline cartilage. F) Mature spores of *M. pecsensis* n. sp. G) Ovoid spore with two polar capsules containing four coils (pf) and H) Spore in sutural view. I) Plasmodia of *M. diversus* in the fin rays at an intersegmental joint (white arrow). J) Mature spore of *M. diversus* with the presence of mucus envelopes (mv) and K) Spore in sutural view. Scale bars represent 10 µm except (A, I) 500 µm, (D) 200 µm and (E) 20 µm.

Table S4 Comparative data on spore measurements (mean ± standard deviation [SD], with ranges in parentheses) for Myxobolus *ocsardiensis* n. sp. from *C. auratus gibelio* and morphologically similar *Myxobolus* species. All measurements are in µm. Abbreviations: SL spore length, SW spore width, ST spore thickness, PCL polar capsule length, PCW polar capsule width, PFC polar filament coils, SM sutural markings, – no data.

Species	Host	Site infection	SL	SW	ST	PCL	PCW	PFC	SM	Reference
***M. ocsardiensis* n. sp.**	***Carassius auratus gibelio***	**Liver, kidney**	**14.6 ± 0.8 (12.8–16.4)**	**11.7 ± 0.6 (10.6–13.0)**	**7.3 ± 0.5 (6.2–8.6)**	**7.1 ± 0.5 (6.1–8.3)**	**3.9 ± 0.3 (3.2–4.7)**	**6–7**	**5–6**	**Present study**
M. carassii	*C. carassius*	Body cavity, liver, intestine	13–17	8–10	5–7	6–7	–	–	Visible	Kudo (1920)
M. pronini (Russia)	*C. auratus gibelio*	Abdominal cavity, visceral serous membranes	15.1 ± 0.3 (14.3–16.2)	10.1 ± 0.1 (9.6–10.8)	6.7 ± 0.15 (6.4–7.4)	5.4 ± 0.63 (4.3–6.7)	3.0 ± 0.16 (4.8–5.6)	5–6	3–5	Liu et al. (2016a)
M. pronini (China)	*C. auratus gibelio*	Abdominal cavity, visceral serous membranes	14.7 ± 0.24 (13.8–15.6)	9.6 ± 0.65 (9.0–13.3)	6.6 ± 0.16 (6.2–7.2)	5.3 ± 0.16 (4.8–5.6)	3.0 ± 0.12 (2.9–3.4)	5–6	3–5	Liu et al. (2016a)
M. qiankiangensis	*C. auratus*	Spleen, body cavity	17.3 (15.6–18.0)	11.4 (10.6–12.0)	8.3 (8.0–8.3)	8.6 (7.8–9.6)	3.8 (3.6–4.2)	6–7	–	Chen & Ma (1998)
M. hearti	*C. auratus gibelio*	Heart	14.1 ± 0.35 (13.6–15.0)	11.9 ± 0.34 (11.0– 12.0)	7.3 ± 0.36 (7.0– 8.0)	6.1 ± 0.29 (6.0– 7.0)	3.9 ± 0.31 (3.0– 4.0)	6–7	–	Ye et al. (2014)
M. oralis	*C. auratus gibelio*	Palate of the mouth	11.7 ± 0.4 (10.8–12.8)	8.9 ± 0.4 (8.2–9.9)	6.8 ± 0.3 (6.0–7.5)	4.8 ± 0.3 (4.0–5.5)	3.0 ± 0.2 (2.9–3.6)	5–6	2–5	Liu et al. (2014a)

Table S5 Comparative data on spore measurements (mean ± standard deviation [SD], with ranges in parentheses) for *Myxobolus pecsensis* n. sp., *Myxobolus intrachondrealis*, *Myxobolus* n. sp. 11 and others *Myxobolus* species found in the cartilage and retina. All measurements are in µm. Abbreviations: SL spore length, SW spore width, ST spore thickness, PCL polar capsule length, PCW polar capsule width, PFC polar filament coils, – no data.

Species	Host	Site infection	SL	SW	ST	PCL	PCW	PFC	Reference
***Myxobolus pecsensis* n. sp.**	***Carassius auratus gibelio***	**Gill cartilage**	**8.8 ± 0.5 (7.4–9.7)**	**5.5 ± 0.4 (4.9–6.4)**	**4.4 ± 0.4 (3.8–5.1)**	**3.3 ± 0.1 (2.4–4.1)**	**1.7 ± 0.1 (1.5–2.0)**	**4**	**Present study**
M. adlardi	*Labeo rohita*	Gill filaments	7.9 (7.8–8.1)	4.8 (4.7–4.9)	–	3.5 (3.4–3.6)	1.7 (1.6–1.8)	5	Gupta & Kaur (2016)
Myxobolus intrachondrealis	***Cyprinus carpio***	**Gill cartilage**	**10.1 ± 0.4 (9.4–11.0)**	**6.6 ± 0.2 (5.9–7.1)**	**4.6 ± 0.3 (4.1–5.4)**	**4.3 ± 0.3 (3.8–5.1)**	**2.4 ± 0.2 (2.1–2.8)**	**6–7**	**Present study**
M. intrachondrealis	*C. carpio*	Gill cartilage	10.2 (9.0–11.0)	6.5 (6.0–7.0)	4.0 (3.7–4.2)	4.5 (3.7–4.7)	2.2 (2.0–2.6)	9–11	Molnár (2000)
M. cultrati	*Pelecus cultratus*	Retina	9.8 ± 0.1 (9.2–10.4)	6.4 ± 0.5 (6.0–6.8)	–	4.5 ± 0.3 (4.4–4.8)	2.3 ± 0.8 (2.1–2.4)	–	Borzák et al. (2016)
M. cultus	*Carassius auratus gibelio*	Gill cartilage	11.9 (11.5–12.7)	8.6 (8.4–9.1)	6.3 (5.6–7.5)	5.0 (4.5–5.6)	3.0 (2.7–3.4)	4–5	Xi et al. (2013)
***Myxobolus* sp. 11**	***Osteochilus waandersii***	**Gill cartilage**	**7.9 ± 0.3 (7.2–8.4)**	**6.7 ± 0.3 (6.2–7.3)**	**–**	**3.7 ± 0.2 (3.4–4.1)**	**2.1 ± 0.2 (1.7–2.6)**	–	**Present study**
M. albi	*Pomatoschistus microps*	Cartilage of gill arch	9.4 (8.3–10.0)	9.1 (7.7–10.0)	6.6 (5.8–7.4)	3.9 (3.0–4.8)	2.8 (2.0–3.3)	4–5	Picon-camacho et al. (2009)
M. sharpeyi	*Barbus sharpeyi*	Gill cartilage	9.6 (9.2–9.8)	8.1 (7.5–8.6)	4.8 (4.4–5.3)	3.6 (3.3–4.0)	2.8 (2.2–2.4)	5	Molnár et al. (1996)
M. cartilaginis	*Lepomis macrochirus*	Head cartilage	10.2 (9.5–10.5)	8.9 (8.4–9.5)	6.4 (6.3–7.3)	5.3 (5.2–5.6)	3.3 (3.0–3.5)	5–7	Hoffman et al. (1965)

Table S6 Comparative data on spore measurements (mean ± standard deviation [SD], with ranges in parentheses) for *Myxobolus diversus*, *Myxobolus basilamellaris* and other *Myxobolus* species with unequal polar capsules. All measurements are in µm. Abbreviations: SL spore length, SW spore width, ST spore thickness, PCL polar capsule length, PCW polar capsule width, – no data.

Species	Host	Site infection	SL	SW	ST	Large		Short		Reference
						PCL	PCW	PCL	PCW	
Myxobolus diversus	***Carassius auratus gibelio***	**Fins**	**13.5 ± 0.5 (12.6–14.4)**	**9.3 ± 0.5 (8.4–10.6)**	**7.8 ± 0.5 (6.8–8.9)**	**5.3 ± 0.3 (4.5–5.9)**	**3.4 ± 0.2 (2.9–4.0)**	**3.0 ± 0.3 (2.1–3.6)**	**1.9 ± 0.2 (1.4–2.4)**	**Present study**
M. diversus	*C. auratus*	Fins	12.8 ± 0.8 (12.0–14.0)	8.7 ± 0.7 (8.0–9.5)	6.5 ± 0.5 (6.0–7.0)	4.5 ± 0.6 (4.0–5.5)	3.0 ± 0.5 (2.5–3.5)	2.7 ± 0.2 (2.5–3.0)	1.2 ± 0.2 (1.0–1.5)	Molnár & Székely (2003)
M. diversus	*C. auratus*	Fins	(12.0–13.9)	–	–	–	–	–	–	Chen & Ma (1998)
M. mapei	*Barbus callipterus, Oreochromis niloticus*	Kidney, liver	13.3 (10.5–16.5)	6.8 (6.0-9.0)	–	6.4 (6.0–8.2)	2.8 (2.2–4.5)	4.1 (3.0–5.2)	1.6 (1.5–2.2)	Georges et al. (2017)
M. absonus	*Pimelodus maculatus*	Opercular cavity	15.7 ± 1.5	10.2 ± 0.7	–	6.4 ± 0.7	3.6 ± 0.5	4.2 ± 0.6	2.5 ± 0.5	Cellere et al. (2002)
M. elliptoides	*C. carpio*	Fin rays	15.7 ± 0.6 (14.4–16.8)	10.4 ± 0.7 (9.2–12.0)	7.6 ± 0.4 (6.9–8.7)	5.9 ± 0.4 (4.8–6.5)	3.7 ± 0.2 (3.3–4.2)	4.8 ± 0.4 (4.1–5.6)	3.1 ± 0.2 (2.6–3.5)	Zhang et al. (2023a)
Myxobolus basilamellaris	***Cyprinus carpio***	**Base of gill filaments**	**10.2 ± 0.7 (9.0–12.2)**	**8.3 ± 0.4 (7.5–9.1)**	**6.2 ± 0.3 (5.7–6.7)**	**4.5 ± 0.4 (3.7–5.4)**	**2.9 ± 0.3 (2.4–3.5)**	**3.2 ± 0.3 (2.7–3.9)**	**2.1 ± 0.2 (1.8–2.5)**	**Present study**
M. basilamellaris	*C. carpio*	Base of gill filaments	10.5 ± 0.5 (9.3–11.8)	8.7 ± 0.4 (7.9–9.4)	6.4 ± 0.4 (5.8–7.1)	4.8 ± 0.3 (4.3–5.4)	3.2 ± 0.2 (2.8–3.8)	3.7 ± 0.3 (3.3–4.3)	2.6 ± 0.1 (2.3–3.8)	Zhang et al. (2023a)
M. basilamellaris	*C. carpio*	Base of gill filaments	(9.2–10.5)	(7.7–12.2)	4.5 (4.2–5.0)	(2.2–3.3)	(3.2–4.3)	(1.8–3.3)	(2.5–4.4)	Lom & Molnár (1983)

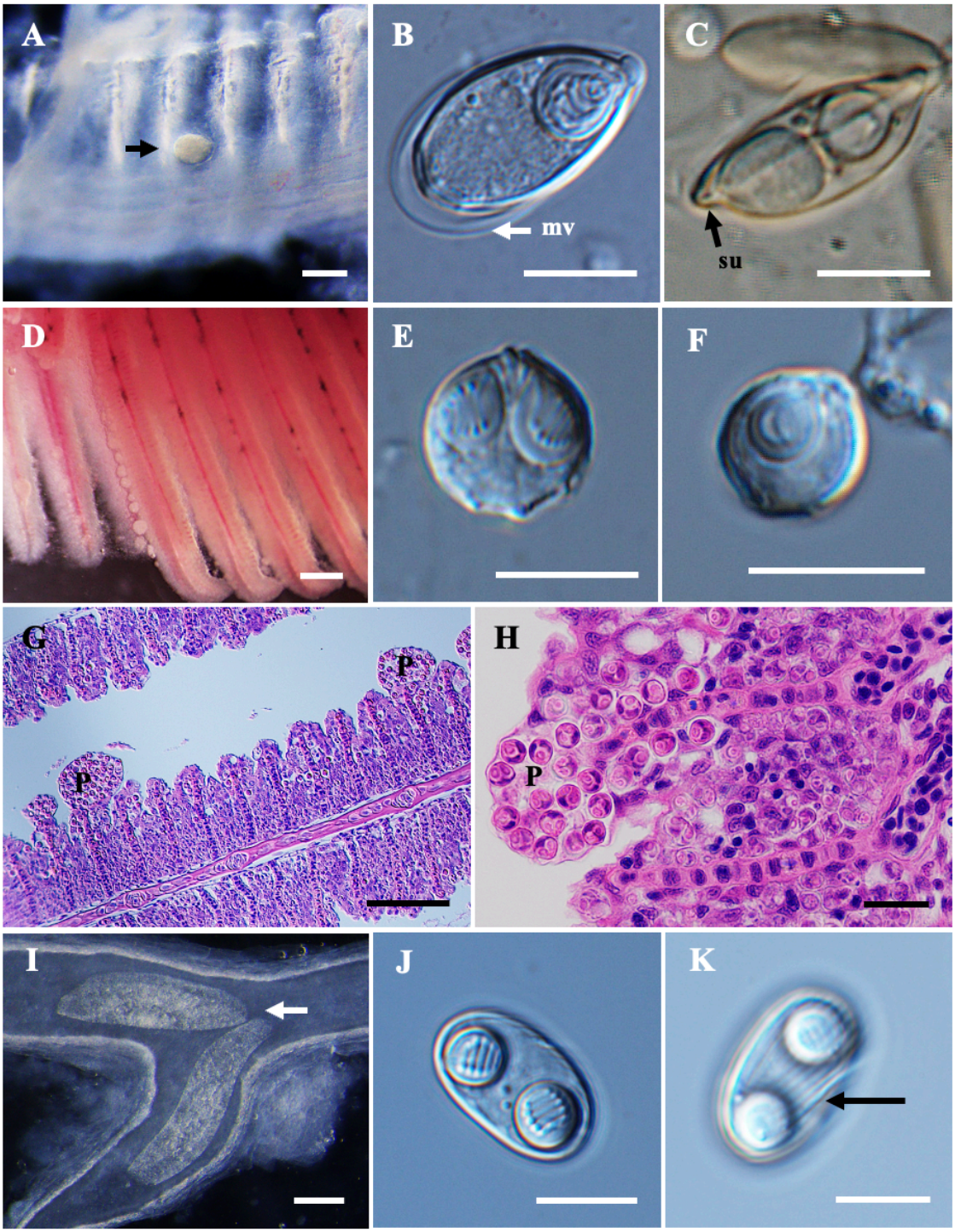

Figure S3. *Thelohanellus*, *Sphaerospora* and *Zschokkella* species in *Carassius auratus gibelio*. A) Plasmodium of *Thelohanellus imrei* n. sp. in between cartilaginous crests on the surface of gill arch. B) Mature spore of *T. imrei* n. sp. with the presence of a mucus envelope (mv) and C) Spore in sutural view showing the suture (su). D) Heavily infected gills with oval-shaped spore masses of *Sphaerospora molnari*. E) Mature spore of *S. molnari* showing subspherical shape with two polar capsules containing five coils and F) Spore in sutural view. G) Aggregated spores of *S. molnari* covered by a thin membrane developed in the epithelium of secondary lamellae, causing cellular proliferation (H&E) (P). H) Spores packaged together attached on the top of secondary lamellae (H&E) (P). I) Plasmodia of *Zschokkella chezhachei* n. sp. in the bile duct (white arrow). J) Mature spore of *Z. chezhachei* n. sp. and K) Spore in sutural view showing the sutural line (white arrow). Scale bars represent 10 µm except (A) 500 µm, (D, G) 100 µm, (H) 20 µm and (I) 200 µm.

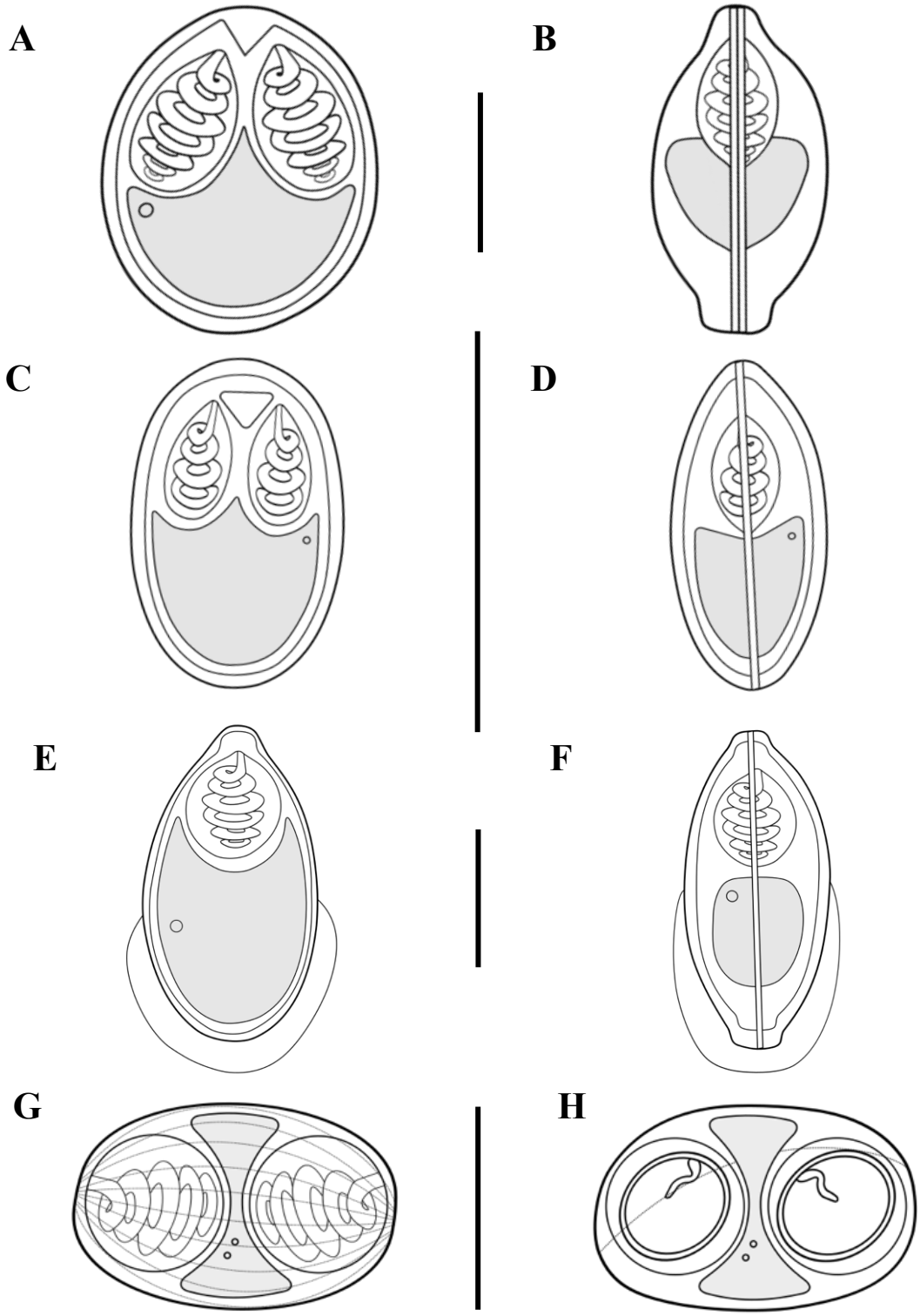

Figure S4. Schematic drawings of novel myxosporean parasites from *Carassius auratus gibelio*. A) *Myxobolus ocsardiensis* n. sp. in frontal view. B) *Myxobolus ocsardiensis* n. sp. in sutural view. C) *Myxobolus pecsensis* n. sp. in frontal view. D) *Myxobolus pecsensis* n. sp. in sutural view. E) *Thelohanellus imrei* n. sp. frontal view. F) *Thelohanellus imrei* n. sp. sutural view. G) *Zschokkella chezhachei* n. sp. in frontal view. H) *Zschokkella chezhachei* n. sp. in sutural view. Scale bars represent 10 μm.

Table S7. Comparative data on spore measurements (mean ± standard deviation [SD], with ranges in parentheses) for *Thelohanellus imrei* n. sp. from *Carassius auratus gibelio* and morphologically similar *Thelohanellus* species. All measurements are in μm. Abbreviations: SL spore length, SW spore width, ST spore thickness, PCL polar capsule length, PCW polar capsule width, PFC polar filament coils, – no data.

Species	Host	Site infection	SL	SW	ST	PCL	PCW	PFC	Reference
***Thelohanellus imrei* n. sp.**	***Carassius auratus gibelio***	**Gill cartilage, pharynx**	**20.9 ± 1.2 (18.2–22.9)**	**10.1 ± 0.7 (8.5–11.1)**	**9.0 ± 0.5 (8.4–9.9)**	**8.1 ± 0.5 (6.9–9.3)**	**6.4 ± 0.4 (5.2–7.1)**	**6**	**Present study**
T. wangi	*C. auratus gibelio*	Gill filaments	20.2 (16.5–22.3)	9.9 (9.1–10.8)	9.3 (8.2–10.4)	10.1 (8.4–11.2)	6.5 (6.1–7.0)	6–7	Yuan et al. (2015)
T. nanhaiensis	*C. auratus*	Gills	17.0 (15.6–18.0)	10.0 (9.6–10.8)	7.8 (7.4–8.2)	8.9 (8.2–9.6)	5.1 (4.6–5.8)	6–7	Chen & Ma (1998)
T. sagittarius	*Cyprinus carpio haematopterus*	Kidney, swim bladder, gills, intestine, etc.	20.0 (19.2–20.6)	9.6 (8.0–10.2)	8.0	10.6 (9.6–12.0)	7.2 (6.6–8.0)	8–9	Chen & Ma (1998)
T. parasagittarius	*C. carpio haematopterus, C. auratus*	Skin, gills, gallbladder	23.7 (22.8–24.6)	11.4 (10.2–12.0)	10.8	12.1 (11.8–13.2)	8.3 (8.2–8.4)	6–7	Chen & Ma (1998)
T. testudineus	*C. auratus gibelio*	Skin	19.7 ± 0.7 (18.6–20.8)	7.3 ± 0.5 (6.6–8.4)	–	11.1 ± 0.5 (10.0–11.9)	5.3 ± 0.3 (4.3–5.8)	7–8	Liu et al. (2014c)
T. hovorkai	*C. carpio haematopterus*	Mesenteries	20.4 (18.0–22.4)	9.8 (7.2–12.0)	8.5 (7.0–10.0)	10.8 (7.2–14.4)	8.9 (7.2–10.8)	6–7	Chen & Ma (1998)
T. macrovacuolaris	*C. carpio*	Palate	21.6 ± 0.9 (19.3–23.8)	12.5 ± 0.7 (10.3–13.6)	10.2 ± 0.4 (9.8–11.8)	9.1 ± 0.6 (8.0–10.0)	8.6 ± 0.5 (7.8–9.6)	7–8	Liu et al. (2016c)
T. wuhanensis	*C. auratus gibelio*	Skin	22.9 ± 0.6 (21.8–24.0)	13.3 ± 0.5 (12.2–14.3)	10.6 ± 0.5 (9.9–11.6)	10.8 ± 0.6 (9.6–11.9)	8.6 ± 0.5 (7.5–9.7)	8–10	Liu et al. (2014b)

Table S8 Comparative data on spore measurements (mean ± standard deviation [SD], with ranges in parentheses) for *Sphaerospora molnari* from *Carassius auratus gibelio* and morphologically similar *Sphaerospora* species. All measurements are in µm. Abbreviations: SL spore length, SW spore width, ST spore thickness, PCL polar capsule length, PCW polar capsule width, PFC polar filament coils, – no data.

Species	Host	Site infection	SL	SW	ST	PCL	PCW	PFC	Reference
Sphaerospora molnari	***Carassius auratus gibelio***	**Gill lamellae**	**9.9 ± 0.3 (9.1–10.4)**	**10.4 ± 0.4 (9.6–11.2)**	**8.6 ± 0.3 (8.1–8.4)**	**5.2 ± 0.4 (4.4–5.9)**	**4.1 ± 0.3 (3.5–4.7)**	**5**	**Present study**
S. molnari	*Cyprinus carpio*	Gill filaments	10.3 (9.5–11.0)	10.5 (10.0–11.0)	–	4.0–5.0	4.0–4.5	4 (3–5)	Lom et al. (1983)
S. molnari	*C. carpio*	Gill epithelium	9.9 ± 0.5 (8.7–11.1)	10.0 ± 0.5 (9.0–10.9)	–	4.6 ± 0.3 (3.9–5.8)	3.9 ± 0.2 (3.3–5.0)	4–5	Eszterbauer et al. (2013)
S. carassii	*C. auratus; C. gibelio; C. carpio carpio; Rutilus rutilus*	Gill filaments	(8.0–13.0)	(8.0–13.0)	–	(4.0–5.0)	(2.5–3.5)	5–6	Kudo (1920)
S. chinensis	*C. carpio carpio*	Gill epithelium	7.4	7.0	–	–	–	5	Lom et al. (1983)
S. dykovae	*C. carpio carpio*	Kidney tubules	7.3 (6.0–8.0)	7.2 (6.4–8.3)	–	1.7–2.3	1.3–1.6	4–5	Dyková & Lom (1982)

Table S9 Comparative data on spore measurements (mean ± standard deviation [SD], with ranges in parentheses) for *Zschokkella chezhachei* n. sp. from *Carassius auratus gibelio* and morphologically similar *Zschokkella* species. All measurements are in µm. Abbreviations: SL spore length, SW spore width, ST spore thickness, PCL polar capsule length, PCW polar capsule width, PFC polar filament coils, – no data.

Species	Host	Site infection	SL	SW	ST	PCL	PCW	PFC	Reference
***Zschokkella chezhachei* n. sp.**	***Carassius auratus gibelio***	**Bile duct**	**17.4 ± 0.3 (16.7–17.9)**	**10.1 ± 0.3 (9.5–10.6)**	**8.9 ± 0.4 (8.0–9.5)**	**6.4 ± 0.6 (5.4–7.3)**	**6.4 ± 0.6 (5.4–7.3)**	**5**	**Present study**
Z. scomberosis	*Scomberoides commersonnianus*	Gallbladder	17.8 ± 1.4 (16.5–19.5)	10.4 ± 1.4 (9.0–12.0)	–	4.9 ± 0.8 (3.7–5.2)	4.2 ± 0.5 (3.0–4.5)	–	Sarkar (2012)
Z. nilei	*Oreochromis niloticus*	Kidney tubules	10.6 ± 0.5 (9.0–11.2)	6.4 ± 0.4 (5.5–7.5)	6.3 ± 0.4 (6.0–6.8)	3.7 ± 0.3 (3.0–4.5)	3.7 ± 0.3 (3.0–4.5)	4–5	Abdel-Ghaffar et al. (2008)
Z. carassii	*Carassius auratus*; *Carassius cuvieri*	Gallbladder	13.2–15.6 (14.6)	8.4–9.0 (8.6)	7.8	6.0–7.6 (6.8)	6.0–7.6 (6.8)	5	Matsche et al. (2021)
Z. cyprini	*Cyprinus carpio*	Gallbladder	11.0–15.0	7.0–10.0	–	3.5–4.0	3.5–4.0	–	Matsche et al. (2021)
Z. linghuensis	*C. carpio*	Gallbladder	9.4–9.6 (9.5)	5.8–6.2 (6.0)	5.6–6.2 (5.8)	2.6–3.1 (2.9)	2.6–3.1 (2.9)	3–4	Matsche et al. (2021)
Z. nova	*Carassius carassius;* *C. auratus gibelio*	Gallbladder	8.0–12.0; 10.1–12.0 (10.6)	5.0–7.0; 5.8–6.2 (6.0)	5.0–6.5; 3.6–4.8 (4.5)	2.6–3.5; 3.0–3.6 (3.2)	2.6–3.0; 3.0–3.5 (3.2)	4–5; 3–4	Matsche et al. (2021)
Z. minuta	*C. carpio;* *C. auratus*	Gallbladder	8.0–9.0 (5.1)	4.8–5.8 (5.1)	5.2	2.3–3.1 (2.4)	2.3–3.1 (2.4)	4–5	Matsche et al. (2021)

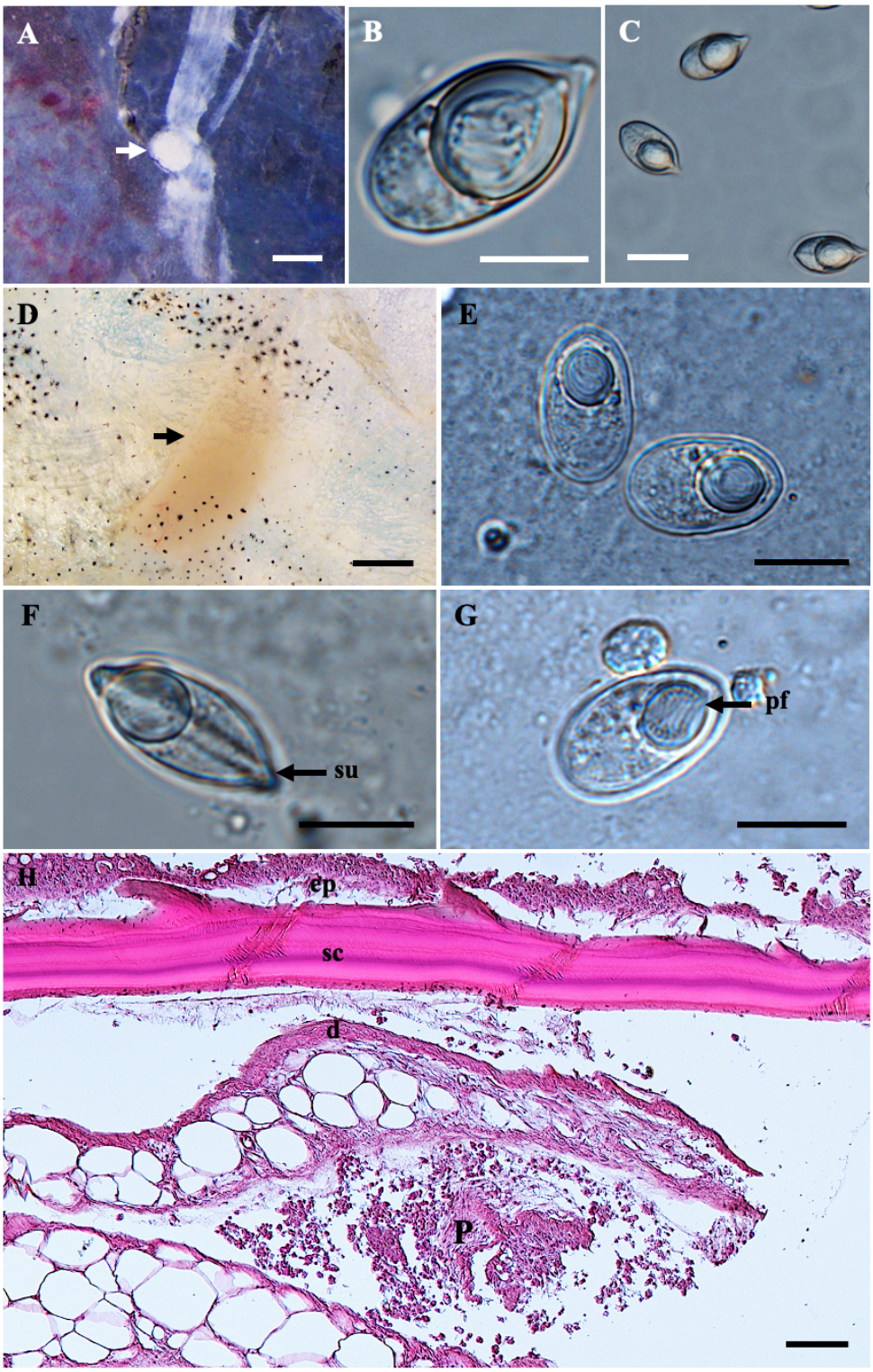

Figure S5. Novel *Thelohanellus* spp. from *Cyprinus carpio.* A) Plasmodium of *Thelohanellus serosae* n. sp. located on the external surface of the kidney, observed in a scraping of the serosal membrane (white arrow). B) Mature spores in frontal view and C) in sutural view. D). Plasmodium of *Thelohanellus paranikolskii* n. sp. in the skin (black arrow). (E) Mature spores in frontal view and (F) Mature spores in sutural view showing the suture (su). (G) Subspherical polar capsule showing seven to eight coils (pf). (H) Histological longitudinal section of common carp skin showing epidermis (ep), scales (sc), dermis (d) and stratum spongiosum (ss). A large plasmodium (P) is developing within the stratum spongiosum of the dermis, stained with hematoxylin and eosin (H&E). Scale bars represent 10 µm, except (A) 200 µm, (B) 20 µm, (D) 1 mm and (H) 100 µm.

Table S10 Comparative data on spore measurements (mean ± standard deviation [SD], with ranges in parentheses) for *Thelohanellus serosae* n. sp., *Thelohanellus hovorkai* from *Cyprinus carpio* and morphologically similar *Thelohanellus* species. All measurements are in μm. Abbreviations: SL spore length, SW spore width, ST spore thickness, PCL polar capsule length, PCW polar capsule width, PFC polar filament coils, – no data.

Species	Host	Site infection	SL	SW	ST	PCL	PCW	PFC	Reference
***Thelohanellus serosae* n. sp.**	***Cyprinus carpio***	**Serous membrane of kidney**	**22.6 ± 1.1 (20.0–25.1)**	**12.6 ± 0.6 (11.3–13.6)**	**12.1 ± 0.5 (10.8–12.9)**	**13.3 ± 0.8 (11.7–14.6)**	**10.5 ± 0.5 (9.5–11.5)**	**7**	**Present study**
Thelohanellus hovorkai	***C. carpio***	**Serous membrane of intestine**	**20.0 ± 0.8 (18.6–21.4)**	**9.9 ± 0.7 (8.9–11.6)**	**8.0 ± 0.5 (7.1–8.9)**	**10.4 ± 0.5 (9.5–11.9)**	**7.5 ± 0.4 (6.4–8.6)**	**8–10**	**Present study**
T. hovorkai	*C. carpio*	Mesenteries	(18.0–19.5)	(10.5–11.5)	(9.0–9.5)	12.0	9.0	–	Akhmerov (1960)
T. hovorkai	*C. carpio*	Swimbladder	19.0 (18.7–19.5)	8.5 (7.5–10.2)	8.4 (8.3–8.5)	10.2 (9.5–11.0)	7.5 (6.8–8.5)	–	Molnár & Kovács-Gayer (1982)
T. dogeili	*C. carpio haematopterus*	Skin	(20.0–21.0)	(8.5–9.0)	8.0	(13.5–15.0)	(5.5–6.0)	–	Akhmerov (1955)
T. dogeili	*C. carpio*	Fins	(17.2–18.6)	(10.2–12.4)	–	(8.4–8.6)	(6.4–6.6)	–	Jeney (1979)
T. dogeili	*C. carpio*	Fins	16.9 (15.7–20.0)	10.4 (9.3–11.8)	–	6.5 (6.2–7.4)	5.4 (4.4–6.4)	6–9 1–2	Dyková & Lom (1988)
T. hokiangensis	*C. carpio*	Intestine, nephric ducts	23.9 (22.1–25.5)	10.7 (9.4–11.1)	10.7 (9.4–11.9)	13.4 (11.9–15.3)	9.2 (8.5–9.4)	6–7	Zhang et al. (2013)
T. macrovacuolaris	*C. carpio*	Palate	21.6 ± 0.9 (19.3–23.8)	12.5 ± 0.7 (10.3–13.6)	10.2 ± 0.4 (9.8–11.8)	9.1 ± 0.6 (8.0–10.0)	8.6 ± 0.5 (7.8–9.6)	7–8	Liu et al. (2016c)
T. kitauei	*C. carpio*	Intestine wall	26.3 (23.0–29.0)	9.2 (8.0–11.0)	–	15.2 (10.4–21.5)	6.5 (6.3–7.9)	8–10	Zhang et al. (2013)

Table S11 Comparative data on spore measurements (mean ± standard deviation [SD], with ranges in parentheses) for *Thelohanellus paranikolskii* n. sp., *Thelohanellus nikolskii* from *Cyprinus carpio* and species with subspherical spore body. All measurements are in μm. Abbreviations: SL spore length, SW spore width, ST spore thickness, PCL polar capsule length, PCW polar capsule width, PFC polar filament coils, – no data.

Species	Host	Site infection	SL	SW	ST	PCL	PCW	PFC	Reference
***Thelohanellus paranikolskii* n. sp.**	***Cyprinus carpio***	**Skin**	**17.0 ± 0.7 (15.4–18.9)**	**9.9 ± 0.6 (8.5–10.8)**	**7.7 ± 0.4 (4.8–6.7)**	**6.8 ± 0.4 (5.8–7.6)**	**5.8 ± 0.3 (4.8–6.7)**	**7–8**	**Present study**
Thelohanellus nikolskii	***C. carpio***	**Caudal fin**	**17.3 ± 0.7 (15.9–18.6)**	**9.8 ± 0.5 (8.7–10.7)**	**8.4 ± 0.3 (8.0–8.9)**	**7.3 ± 0.3 (6.6–8.0)**	**6.0 ± 0.3 (5.5–6.5)**	**6–7**	**Present study**
T. nikolskii	*C. carpio*	Fin rays	17.2 ± 1.5 (15.6–19.0)	10.6 ± 1.0 (8.7–12.5)	8.6 ± 1.1 (7.5–10.0)	6.8 ± 0.6 (6.2–7.5)	5.3 ± 0.7 (4.7–5.2)	6–7	Borzák et al. (2021)
T. nikolskii	*C. carpio*	Scales	16.2 ± 1.8 (14.0–18.5)	9.0 ± 1.6 (7.5–11.2)	6.6 ± 0.6 (6.2–7.5)	6.3 ± 0.4 (5.8–6.6)	5.4 ± 0.8 (4.8–6.5)	6–7	Borzák et al. (2021)
T. leshanensis	*C. carpio haematopterus*	Skin, caudal fin	16.6 (14.8–18.4)	9.6 (8.8–10.3)	9.2 (8.8–9.6)	6.1 (5.6–7.2)	(4.2–4.5)	2–3	Zhao & Ma (1992)
T. wusihensis	*Ctenopharymgodon idellus*	Caudal fin	16.5 (15.6–17.0)	10.4 (9.6–12.0)	10.3 (9.6–12.0)	8.2 (7.8–8.4)	6.5 (6.2–7.2)	6	Chen & Ma (1998)
T. pseudonikolskii	*Carassius auratus*	Caudal and pectoral fins	19.0 ± 1.9 (16.3–23.6)	12.5 ± 0.7 (11.5–14.3)	–	7.8 ± 0.7 (6.1–9.2)	6.7 ± 0.5 (5.4–7.8)	5–6	Zhang et al. (2022)

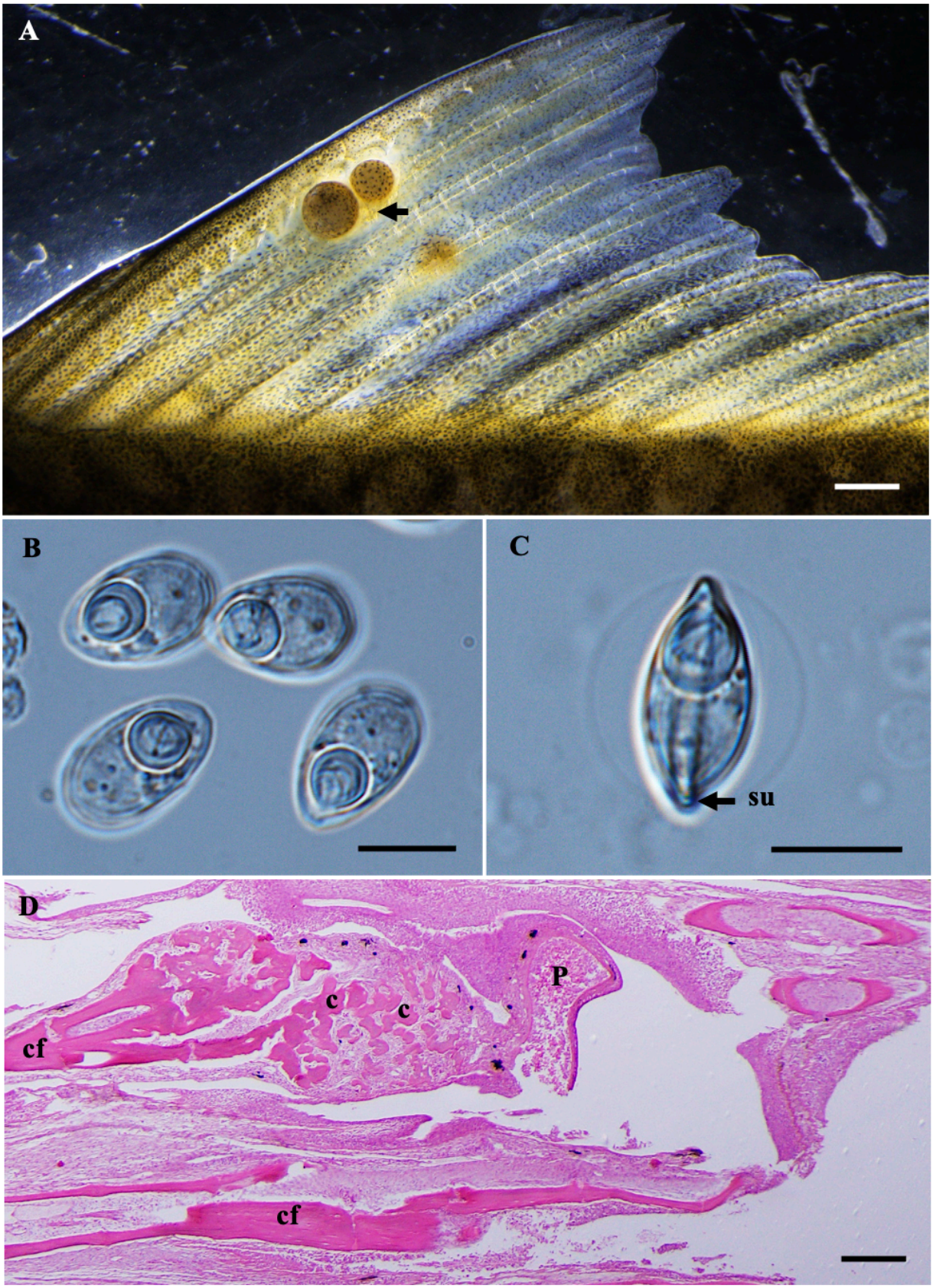

Figure S6. *Thelohanellus nikolskii* from common carp, *Cyprinus carpio*. A) Plasmodia on the fin (black arrow). B) Mature spores in frontal view. C) Mature spore in sutural view showing the suture (su). D) Histological longitudinal section of the fin showing a large plasmodium (P) developing within the cartilage of the fin ray (cf). The expansion of the plasmodium causes fragmentation of the cartilage into small pieces (c), stained with hematoxylin and eosin (H&E). Scale bars represent 10 µm, except (A) 1 mm and (D) 200 µm.

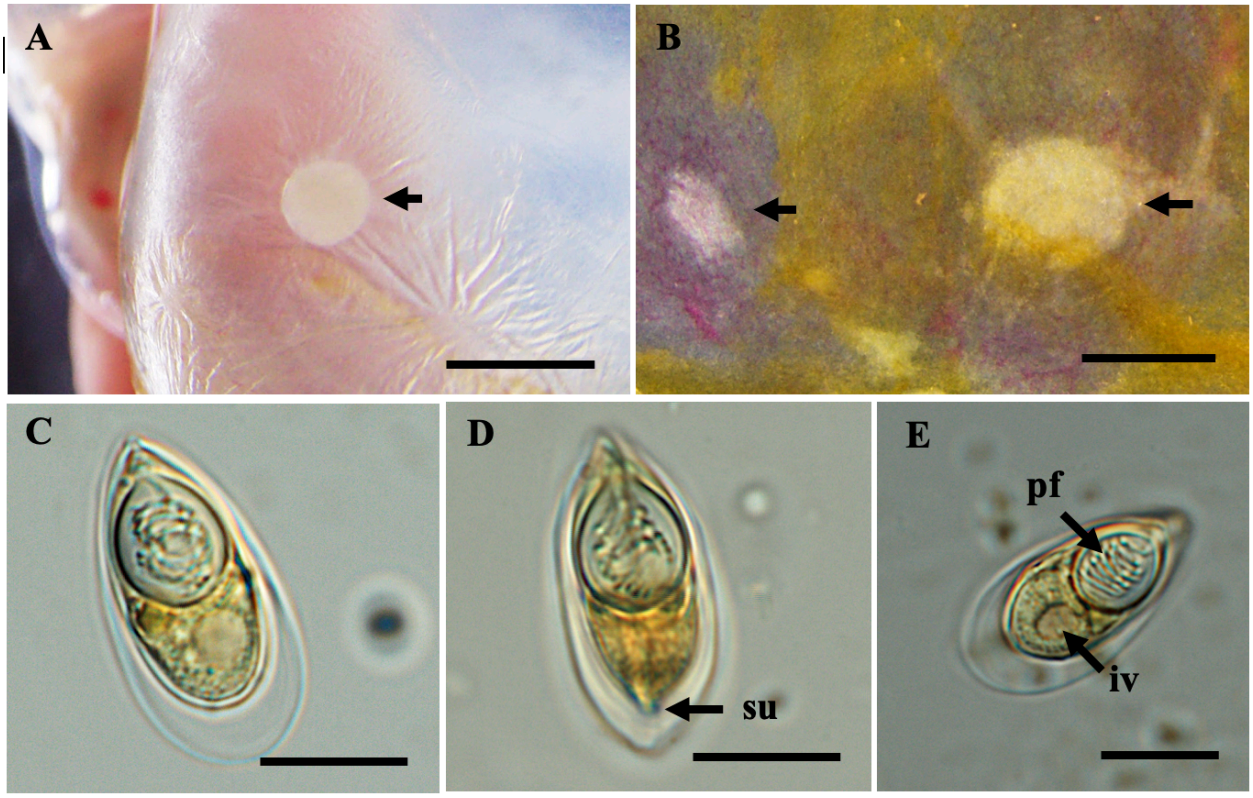

Figure S7. *Thelohanellus hovorkai* from common carp, *Cyprinus carpio*. A) Plasmodium on the swim bladder (black arrow). B) Plasmodia in the liver (black arrow). C) Mature spore in frontal view. D) Mature spore in sutural view showing the suture (su). E) Pyriform polar capsule showing eight to ten coils (pf) with the presence of iodinophilous vacuole (iv). Scale bars represent 10 µm, except (A) 2 mm and (B) 500 µm.

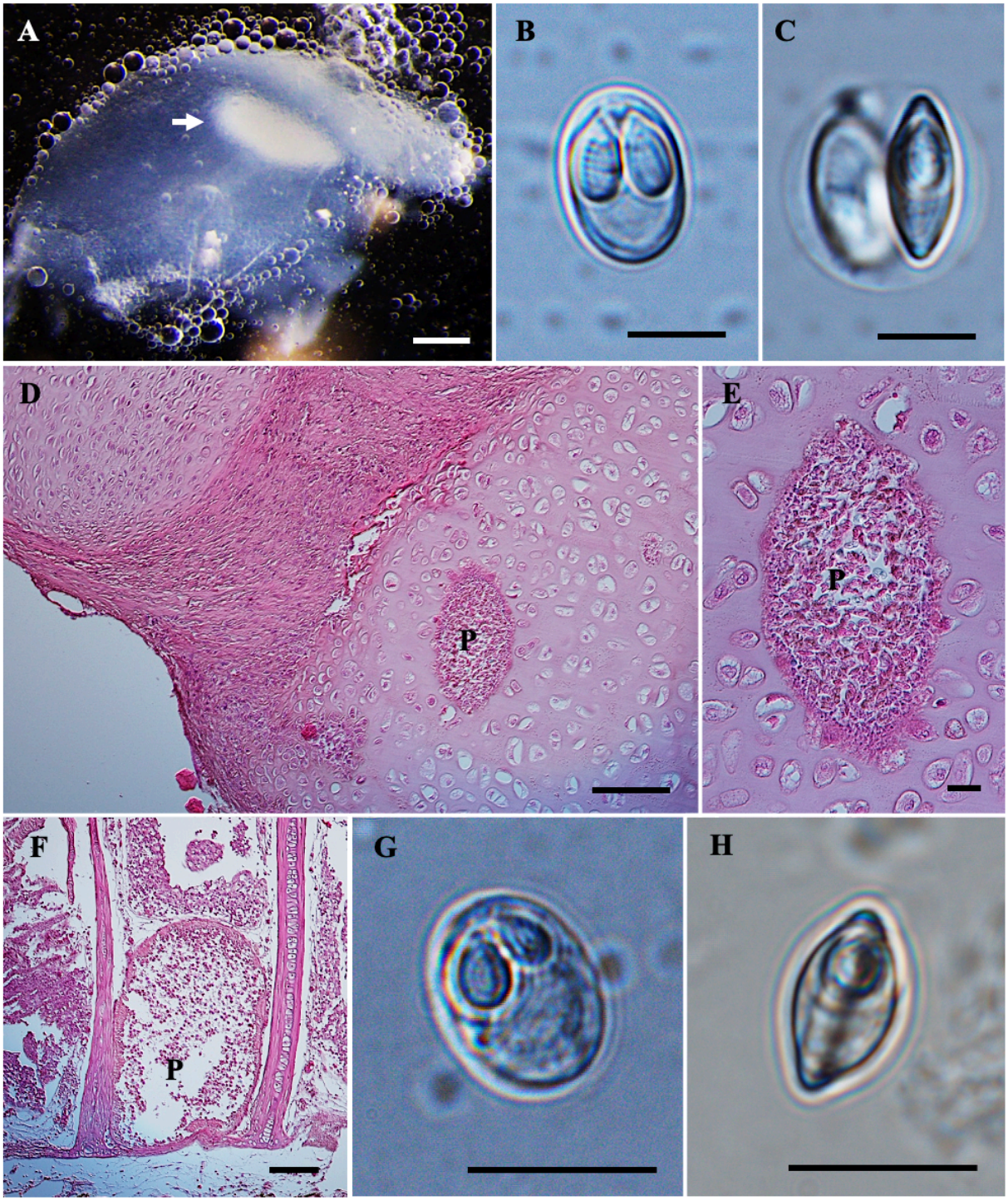

Figure S8. *Myxobolus* spp. from the gills of common carp, *Cyprinus carpio*. A) Plasmodium of *M. intrachondrealis* in the gill cartilage (white arrow). B) Mature spore of *M. intrachondrealis* with two polar capsules containing six coils and C) Spore in sutural view. D) Histological section of the cartilaginous gill arch, showing plasmodium (P) within the hyaline cartilage. E) Higher magnification of the plasmodium filled with spores, stained with hematoxylin and eosin (H&E). F) Histological section showing plasmodium (P) of *M. basilamellaris* located at the base of gill filaments, stained with hematoxylin and eosin (H&E). G) Mature spore of *M. basilamellaris* and H) Spore in sutural view. Scale bars represent 10 µm, except (A) 200 µm and (H) 100 µm.

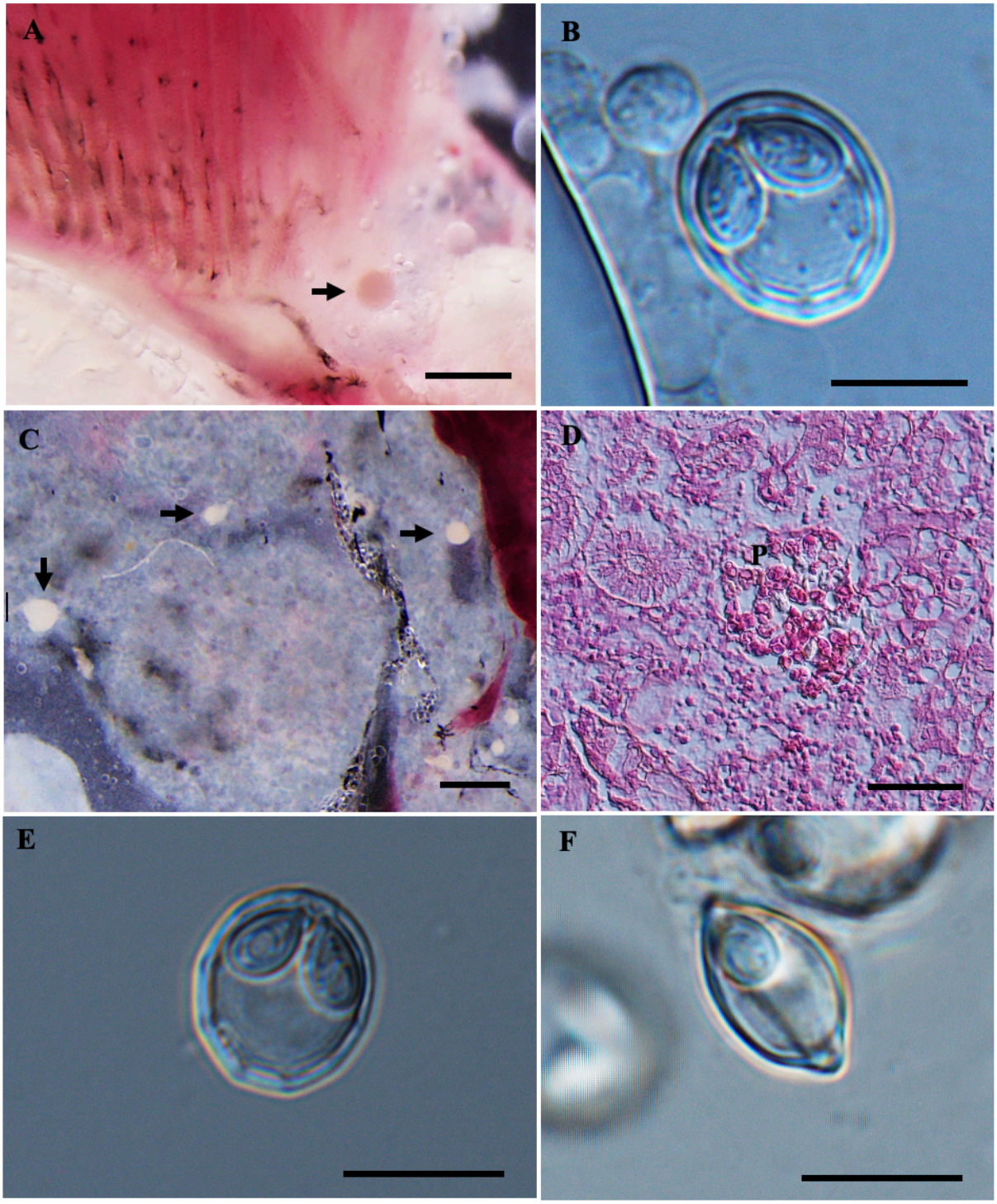

Figure S9. *Myxobolus* spp. from roach, *Rutilus rutilus*. A) Plasmodium of *Myxobolus* n . sp. 1 in the connective tissue of gill arch and B) Mature spore of *Myxobolus* n. sp. 1. C) Plasmodia of *Myxobolus* n. sp. 2 in the kidney. D) Histological section of kidney showing plasmodium (P) of the *Myxobolus* n. sp. 2 located in renal interstitium. E) Mature spore of *Myxobolus* n. sp. 2 and F) Spore in sutural view. Scale bars represent 10 µm, except (A, C) 500 µm and (D) 50 µm.

Table S12 Comparative data on spore measurements (mean ± standard deviation [SD], with ranges in parentheses) for *Myxobolus* spp. from *Rutilus rutilus* and morphologically similar *Myxobolus* species. All measurements are in µm. Abbreviations: SL spore length, SW spore width, ST spore thickness, PCL polar capsule length, PCW polar capsule width, PFC polar filament coils, SM sutural marking.

Species	Host	Site infection	SL	SW	ST	PCL	PCW	PFC	SM	Reference
***Myxobolus* n. sp. 1**	***Rutilus rutilus***	**Connective tissue of gill arch**	**13.0 ± 0.6 (11.9–14.4)**	**10.4 ± 0.5 (8.7–11.0)**	**7.5 ± 0.4 (7.0–8.1)**	**5.7 ± 0.4 (4.9–6.4)**	**3.4 ± 0.3 (2.8–4.0)**	**6**	**8–10**	**Present study**
M. rutili	*Rutilus rutilus*	Gill filaments	13.1 ± 1.2 (11.0–15.7)	9.9 ± 0.7 (8.0–10.8)	6.8 ± 1.1 (6.0–9.0)	5.9 ± 0.9 (4.0–7.2)	3.4 ± 0.6 (3.0–3.7)	6	4–6	Molnár et al. (2010)
M. feisti	*Rutilus rutilus*	Cartilaginous gill ray	11.7 ± 0.9 (11.5–13.2)	10.0 ± 0.7 (9.4–10.8)	6.7 ± 0.1 (6.6–7.0)	6.2 ± 0.1 (6.0–6.3)	3.7 ± 0.2 (3.3–4.0)	6	5–7	Molnár et al. (2010)
M. fundamentalis	*Rutilus rutilus*	Gill arch	15.5 ± 0.8 (14.4–17.0)	11.8 ± 0.5 (11.2–13.2	9.2 ± 0.3 (9.0–9.6)	6.7 ± 0.2 (6.5–7.2)	4.0 ± 0.2 (3.7–4.3)	6–7	8–9	Molnár et al. (2010)
M. gayarae	*Leucisscus cephalus*	Subepithelial in the intestinal lamina propria	15.1 ± 0.6 (13.7–16.5)	12.7 ± 0.7 (11.5–14.0)	7.9 ± 0.6 (7.3–8.7)	6.1 ± 0.6 (5.0–7.5)	4.0 ± 0.5 (3.2–4.5)	6	6–7	Molnár et al. (2007)
***Myxobolus* n. sp. 2**	***Rutilus rutilus***	**Kidney**	**12.6 ± 0.4 (11.7–13.2)**	**10.5 ± 0.4 (9.6–11.4)**	**7.4 ± 0.3 (6.7–8.1)**	**5.5 ± 0.3 (4.7–6.0)**	**3.3 ± 0.2 (2.9–3.9)**	**5–6**	**6–7**	**Present study**
M. zaikae	*R. rutilus*	Kidney	11.4 ± 0.1 (10.2–14.0)	10.3 ± 0.1 (9.6–11.0)	6.3 ± 0.1 (5.8–7.1)	4.5 ± 0.1 (3.4–5.2)	2.9 (2.6–3.3)	6	6–7	Batueva (2020)
M. erythrophthalmi	*Scardinius erythrophthalmus*	Renal interstitium	11.0 ± 0.5 (10.4–12.0)	9.5 ± 0.4 (8.3–10.2)	7.0 ± 0.4 (6.3–7.5)	5.7 ± 0.4 (5.0–6.3)	3.4 ± 0.2 (3.1–3.7)	5	7–9	Molnár et al. (2009b)
M. shaharomae	*Alburnus alburnus*	Renal interstitium, liver, testes	13.0 ± 0.8 (12.1–14.5)	10.4 ± 0.8 (9.0–11.3)	7.3 ± 0.2 (7.0–7.6)	6.1 ± 0.3 (5.6–7.0)	3.8 ± 0.1 (3.5–4.1)	5	5–7	Molnár et al. (2009b)

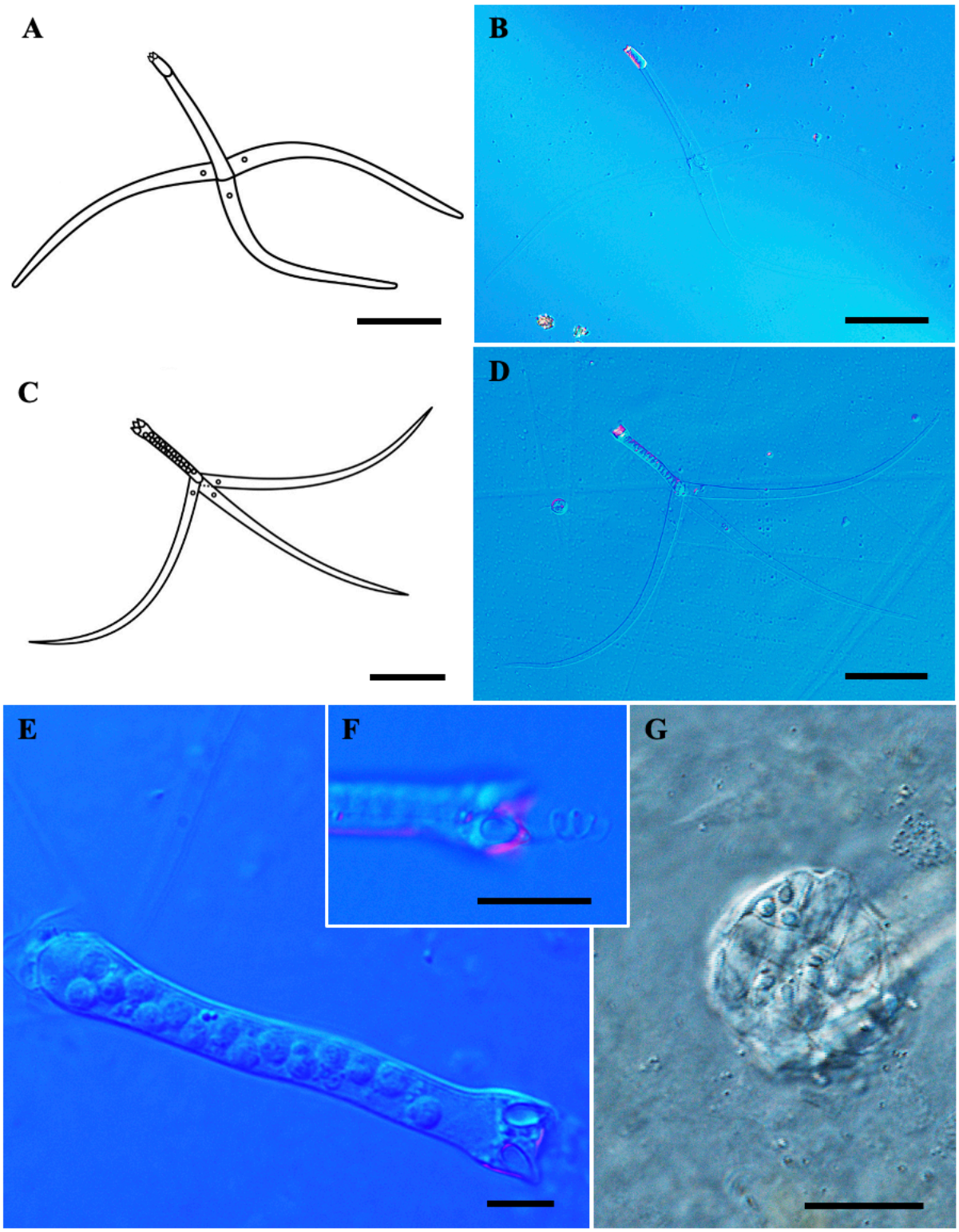

Figure S10. Triactinomyxon type 1 and raabeia type 1 from oligochaetes. A) Schematic drawing of mature triactinomyxon actinospore and B) Fresh unstained triactinomyxon type 1. C) Schematic drawing of mature raabeia type 1. D) Fresh unstained raabeia type 1. E) Higher magnification of spore body showing two of three polar capsules and secondary cells arranged in two columns. F) Polar capsule containing four coils. G) Pansporocyst of the raabeia type 1 in the intestinal epithelium of an infected oligochaete. Scale bars represent 10 µm, except (A, B) 100 µm, (C, D) 50 µm and (G) 20 µm.

Table S13 Comparison of morphometric measurements of triactinomyxon type 1 from Szigetbecse fish farm with data from previous studies. All measurements are in µm. Abbreviations: SBL spore body length, SBW spore body width, CPL caudal processes length, CPW caudal processes width, PCL polar capsule length, PCW polar capsule width, STL style length, STW style width, SC number of secondary cells, – no data.

Triactinomyxon type	Host	SBL	SBW	CPL	CPW	PCL	PCW	STL	STW	SC	Reference
Triactinomyxon type 1	***Limnodrilus hoffmeisteri***	**37.6 ± 4.9 (29.1–48.8)**	**13.6 ± 1.4 (11.5–5.8)**	**274.8 ± 15.3 (257.8–298.9)**	**21.2 ± 1.9 (17.2–24.4)**	**6.3 ± 0.7 (4.7–7.6)**	**4.0 ± 0.4 (3.4–5.0)**	**131.2 ± 13.9 (103.6–154.4)**	**16.4 ± 1.1 (14.7–19.6)**	**32**	**Present study**
Type 2	*Isochaetides michaelseni*	44.98 (39.0–49.94)	12.61 (10.4–15.6)	255.9 (176.8–286.0)	13.4 (10.4–16.9)	5.6	4.0	148.9 (124.8–171.6)	17.9 (15.6–20.8)	> 26	Székely et al. (2014)
Type 5	Actinospores collected from water	37.7	13.5	249	16.1	5.9	3.5	90.6	12.9/17.7	–	El-Mansy et al. (1998a)
Type 3	*Tubifex* sp.	36.0 (32.0–39.0)	12.0 (12.0–14.0)	270.0 (238.0–289.0)	–	6.0	5.0	192.0 (190.0–194.0)	16.0 (14.0–19.0)	8	Lowers & Bartholomew (2003)
Type 4	Actinospores collected from water	45	12.9	281.7	20.8	8.0	5.9	149	23.5/14.1	–	El-Mansy et al. (1998a)

Table S14 Comparison of morphometric measurements of raabeia type 1 and type 2 from Szigetbecse and Ócsárd fish farms with data from previous studies. All measurements are in µm. Abbreviations: SBL spore body length, SBW spore body width, CPL caudal processes length, CPW caudal processes width, PCL polar capsule length, PCW polar capsule width, SC number of secondary cells, – no data.

Raabeia type	Host	SBL	SBW	CPL	CPW	PCL	PCW	SC	Reference
Raabeia type 2	***Branchiura sowerbyi***	**22.6 (20.0–25.3)**	**9.5 (8.0–11.0)**	**204.1 (177.7–233.5)**	**6.4 (5.1–5.9)**	**2.7 (2.1–3.2)**	**2.8 (2.0–3.0)**	**16**	**Present study**
Raabeia of *Myxobolus cultus*	*B. sowerbyi*	24.8 (19.7–28.8)	8.2 (7.1–9.8)	250.8 (217.5–276.3)	6.7 (5.1–7.5)	4.1 (3.4–4.9)	1.8 (1.5–2.1)	16	Xi et al. (2013)
Raabeia of *M. cultus*	*B. sowerbyi*	23.0 (21.0–25.0)	10.0 (9.0–11.0)	191.0 (170–213)	7.0 (6.0–9.0)	4.0 (3.0–5.0)	2.5 (1.8–2.9)	16	Eszterbauer et al. (2006)
Raabeia of *M. cultus*	*B. sowerbyi*	21.0 (18.0–23.0)	8.0 (7.0–9.0)	204.0 (155.0–240.0)	–	–	–	11–16	Yokoyama et al. (1995)
Echinactinomyxon type CZ	*B. sowerbyi*	19.2 (18.5–20.0)	9.2 (8.5–10.2)	163.4 (158.5–167.2)	3.5 (3.0– 3.8)	5.8 (5.5–6.2)	3.0 (2.6–3.5)	–	Xi et al. (2015)
Type 2 & 4	*Tubifex* sp.	21.7	7.7	209.4	6.6	5.7	4.0		El-Mansy et al. (1998a, 1998b)
Raabeia type 1	***Limnodrilus hoffmeisteri***	**52.4 (50.1–53.8)**	**5.5 (4.7–7.0)**	**151.3 (141.3–157.6)**	**7.1 (5.4–9.3)**	**5.1 (4.9–5.3)**	**3.0 (2.4–3.6)**	**16**	**Present study**
Raabeia type 1	***L. hoffmeisteri***	**51.8 (47.7–50.2)**	**5.5 (4.1–6.0)**	**153.0 (123.9–136.0)**	**7.0 (5.5–8.7)**	**5.0 (3.9–4.7)**	**2.8 (1.9–2.7)**	**16**	**Present study**
Type 2	*Isochaetides michaelseni*	63.0 (60.0–67.0)	5.0 (5.0–6.0)	185.0 (136.0–209.0)	7.0 (6.0–8.0)	5.0	3.0	16	Borkhanuddin et al. (2014a)
"Triactinomyxon 'F'"	*L. hoffmeisteri*	50.0 (46.0–56.0)	6.4 (5.5–7.0)	180.0 (160.0–200.0)	(10.0–11.0)	5.0 (4.6–5.2)	3.0 (2.7–3.1)	16	Xiao & Desser (1998b)
Raabeia magna	*L. hoffmeisteri*	(51.0–58.0)	–	–	–	(6.0–7.0)	–	128	Janiszewska (1957)
Raabeia type	*Dero digitata*	28.2 (24.1–33.7)	6.44 (5.7–7.4)	150.65 (117.0–171.2)	7.3 (6.1–8.9)	–	–	–	Rosser et al. (2014)
Raabeia furciligera	*L. hoffmeisteri*	32.8	10.2	125	–	4.4	–	24	Marques (1984)

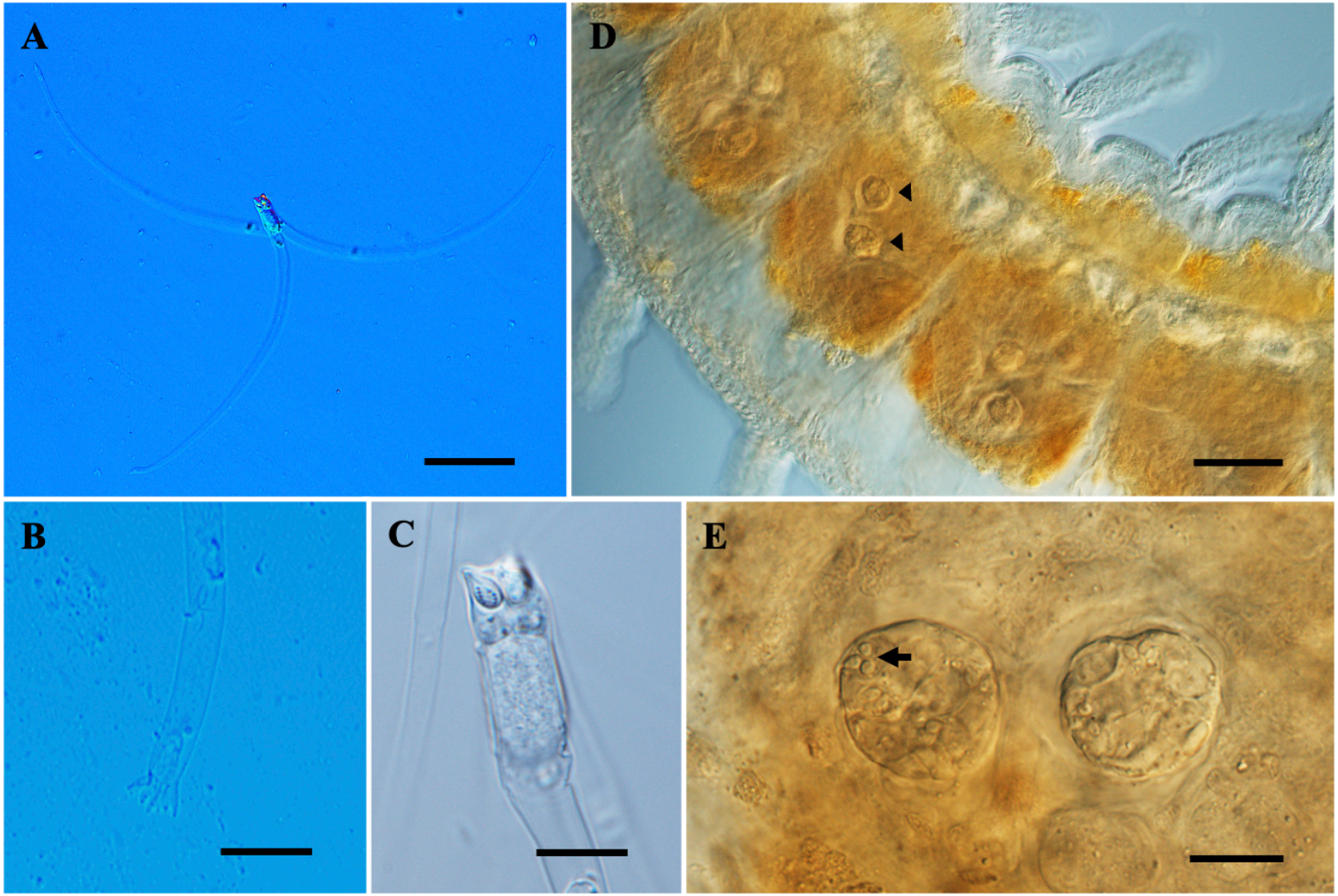

Figure S11. Raabeia type 2 of *Myxobolus cultus* released from *Branchiura sowerbyi*. A) Fresh raabeia type 2 in apical view. B) Branches end of the caudal process. C) Polar capsule with a polar tubule coiling five times. D) Numerous pansporocysts (arrowhead) visible in the intestinal epithelium of *B. sowerbyi* after treatment with lactic acid. E) Higher magnification of the pansporocysts, with polar capsules visible (arrow). Scale bars represent 50 µm (A), 100 µm (D), 20 µm (E), except 10 µm (B–C).

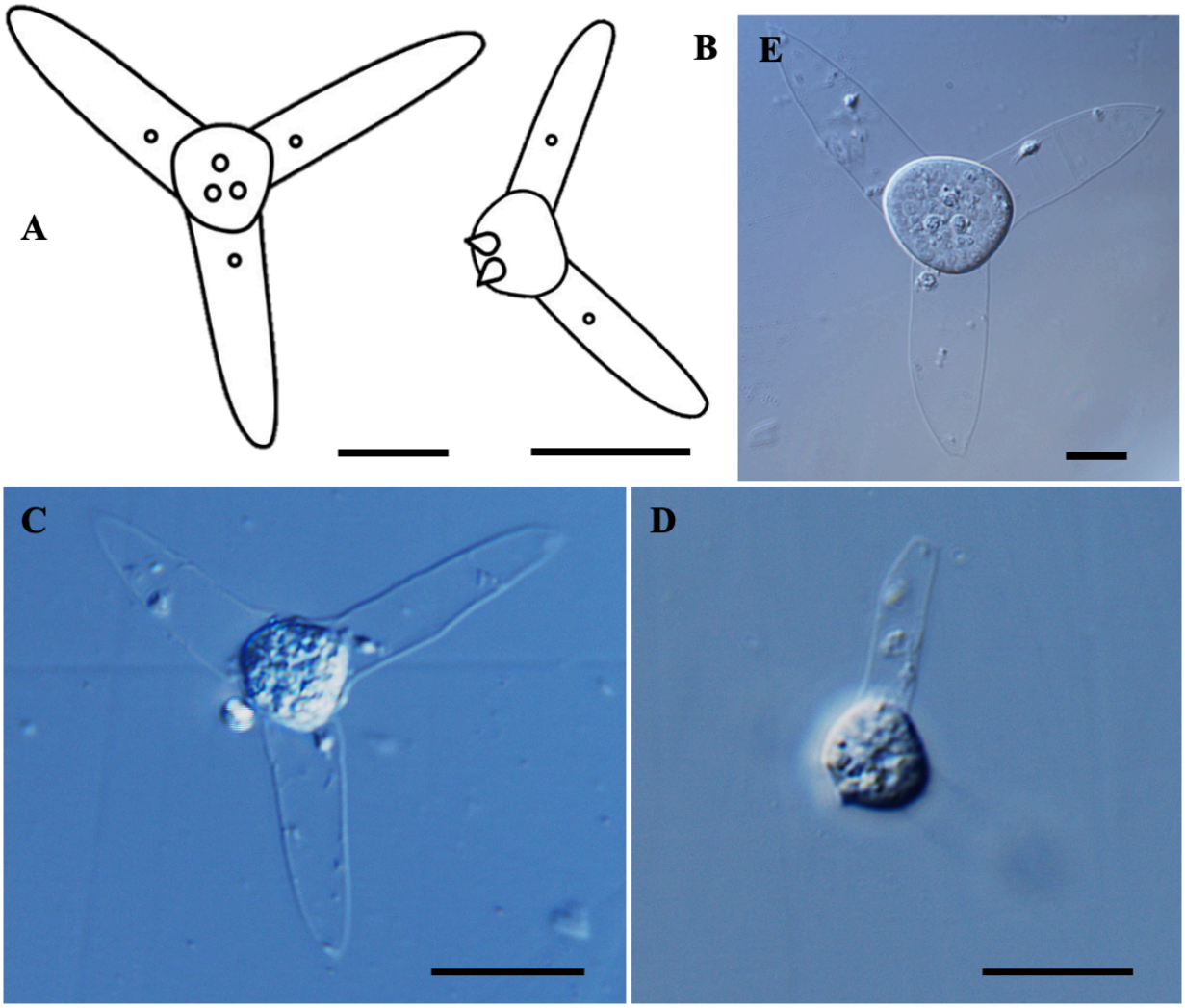

Figure S12. Aurantiactinomyxon type 1. A) Schematic drawing of mature aurantiactinomyxon type 1 in apical view. B) Schematic drawing of side view. Fresh unstained aurantiactinomyxon type 1 in C) apical view and D) side view. E) Higher magnification of mature spore showing the secondary cells in the spore body. Scale bars represent 20 µm, except (E) 10 µm.

Table S15 Comparison of morphometric measurements of aurantiactinomyxon type 1 from Mákád fish farm with data from previous studies. All measurements are in μm. Abbreviations: SBD spore body diameter, CPL caudal processes length, CPW caudal processes width, PCL polar capsule length, PCW polar capsule width, SC number of secondary cells, D diameter, – no data.

Aurantiactinomyxon type	Host	SBD	CPL	CPW	PCL	PCW	SC	Reference
Aurantiactinomyxon type 1	***Ophidonais serpentina***	**13.6 (8.2–17.3)**	**25.7 (21.3–31.6)**	**7.4 (4.2–10.1)**	**D: 2.4 (1.9–3.3)**	**D: 2.4 (1.9–3.3)**	**32**	**Present study**
Aurantiactinomyxon of *Thelohanellus testudineus*	*Branchuira sowerbyi*	15.5 (14.5–16.4)	13.2 (11.5–16.2)	7.4 (6.5–8.0)	2.5 (2.3–2.9)	2.0 (1.8–2.4)	32	Zhao et al. (2017)
Aurantiactinomyxon type	*Tubifex* sp.	13.7 (12.0–15.0)	25.6 (19.0–31.0)	12.0 (10.0–14.0)	D: 2.7 (2.0–3.0)	D: 2.7 (2.0–3.0)	–	McGeorge et al. (1997)
Type 1	*T. tubifex*	13.5 (13.0–14.0)	13.5 (13.0–14.0)	26.8 (25.0–30.0)	2.0	1.0	8	Székely et al. (2003)
Type 1 & Type 9	Actinospores collected from water	18.8	51.3	9.5	D: 2.3	D: 2.3	–	El-Mansy et al. (1998a, 1998b)
Type 4	*T. tubifex*	11.9 (11.2–14.0)	28.3 (23.4–31.2)	11.9 (10.9–14.0)	D: 2.5 (2.0–3.0)	D: 2.7 (2.0–3.0)	–	Özer et al. (2002)

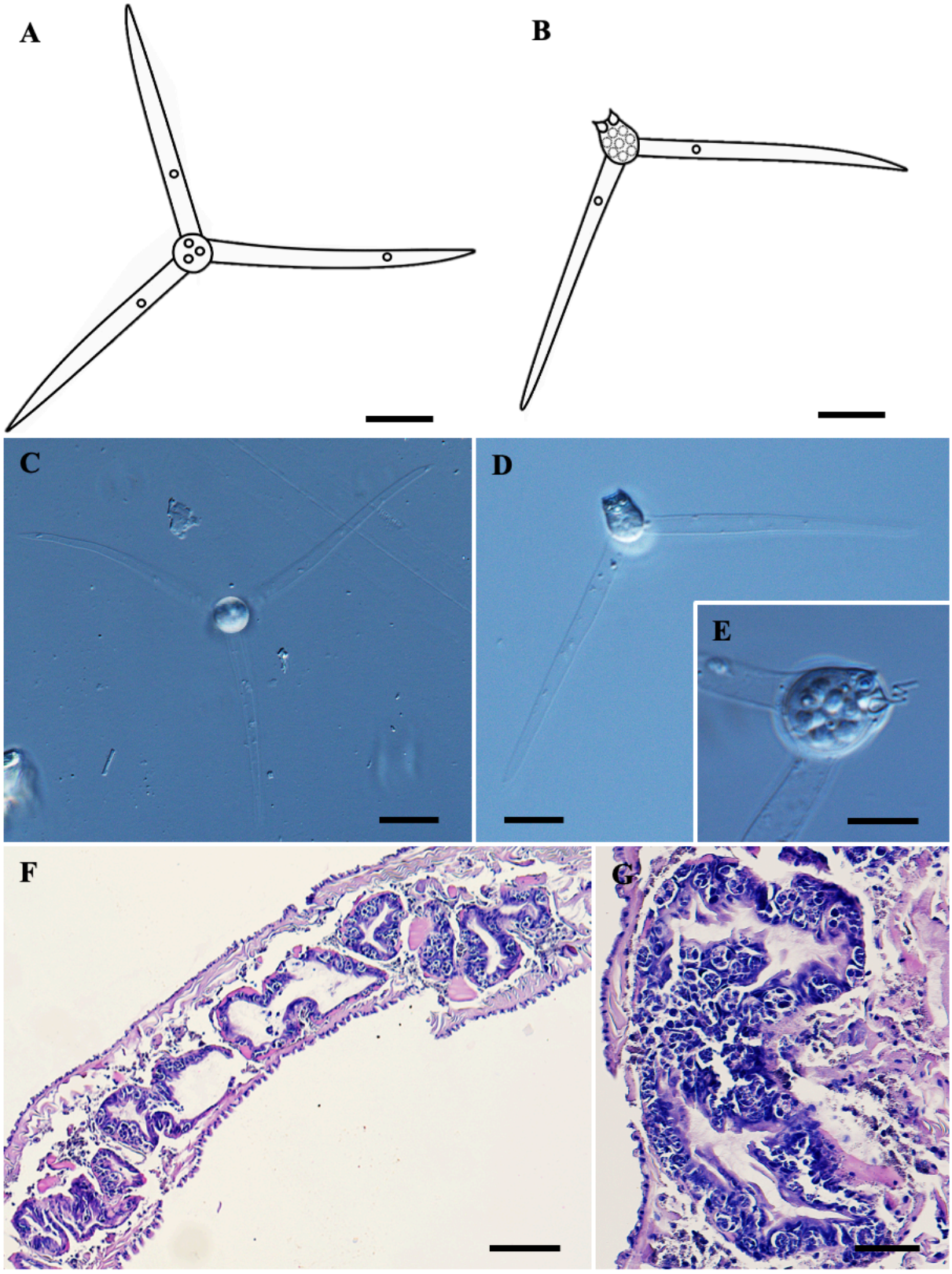

Figure S13. Aurantiactinomyxon type 2. A) Schematic drawing of mature aurantiactinomyxon type 2 in apical view. B) Schematic drawing of side view. Fresh unstained aurantiactinomyxon type 2 in C) apical view and D) side view. E) Higher magnification of the spore body showing eight secondary cells and polar tubules coils three times. F) Semithin sections showing heavily infected *Tubifex tubifex* with pansporocysts at various stages of development in the intestinal epithelium G) Higher magnification of the pansporocysts. Scale bars represent 20 µm, except (E) 10 µm, (F) 100 µm and (G) 50 µm.

Table S16 Comparison of morphometric measurements of aurantiactinomyxon type 2 from Szigetbecse and Ócsárd fish farms with data from previous studies. All measurements are in μm. Abbreviations: SBD spore body diameter, CPL caudal processes length, CPW caudal processes width, PCL polar capsule length, PCW polar capsule width, SC number of secondary cells, D diameter, L length, W width, – no data.

Aurantiactinomyxon type	Host	SBD	CPL	CPW	PCL	PCW	SC	Reference
Aurantiactinomyxon type 2	***Tubifex tubifex***	**10.5 (8.8–13.3)**	**64.5 (55.8–71.6)**	**4.7 (3.7–5.7)**	**D: 2.6 (2.0–3.2)**	**D: 2.6 (2.0–3.2)**	**16**	**Present study**
Aurantiactinomyxon type 2	***Tubifex tubifex***	**10.5 (9.5–11.9)**	**76.0 (72.6–80.1)**	**4.8 (4.1–5.7)**	**3.5 (2.6–4.6)**	**2.5 (2.1–2.9)**	**16**	**Present study**
Aurantiactinomyxon type	*Branchiura sowerbyi*	D: 19.7 L: 20.3 W: 19.6	170.8 (167.5 – 176.3)	12.9 (11.2 – 13.5)	3.1 (2.9–3.2)	1.7 (1.5–1.9)	64	Xi et al. (2013)
Type 2	*B. sowerbyi*	22.8	65.7	10.5	4.0	1.7	–	El-Mansy et al. (1998b)
Type 2	*Isochaetides michaelseni*	10.3 (8.0–13.4)	32.5 (29.4–38.6)	5.77 (4.6–7.1)	3.4	2.6	16	Borkhanuddin (2013)
Type 2	*Nais* sp.	10.3 (9.3–12.0)	14.6 (12.7–16.0)	6.5 (5.3–7.3)	3.3	2.6	8	Borzák et al. (2021)
Type 1	*T.tubifex*	14.4 (12.0–15.0)	32.0 (31.0–36.0)	14.8 (13.0–15.0)	2.7 (2.0–3.0)	2.7 (2.0–3.0)	64–128	Özer et al. (2002)
Type B2	*B. sowerbyi*	19.0 (18.0–21.0)	16.0 (14.0–20.0)	8.4 (7.0–10.6)	2.6 (2.0–4.1)	2.6 (2.0–4.1)	–	Eszterbauer et al. (2006)
Aurantiactinomyxon type	*Tubificoides pseudogaster*	L: 14.4 (13.6–15.9) W: 12.7 (11.3–13.3)	22.4 (18.1–27.6)	15.5 (13.3–17.0)	2.6 (1.9–3.5)	2.6 (1.9–3.5)	–	Rocha et al. (2019a)

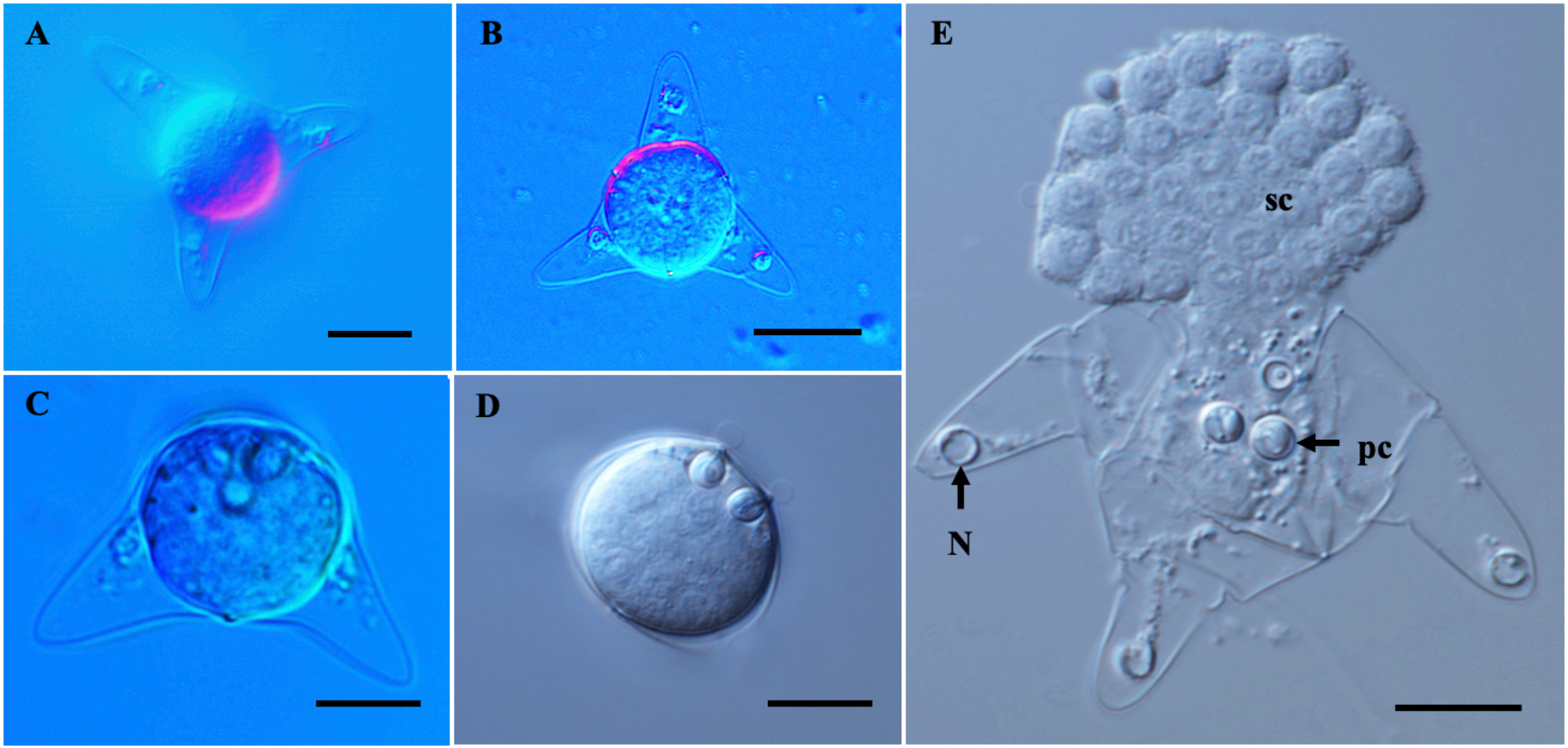

Figure S14. Aurantiactinomyxon type 3 released from *Branchiura sowerbyi*. (A, B) Fresh aurantiactinomyxon type 3 in apical view and (C, D) in side view. E) Rupture of the aurantiactinomyxon type 1 (under pressure), showing nuclei (N) at the end of each caudal processes, three polar capsules (pc), and 32 secondary cells (sc). Scale bars represent 10 µm, except (A, B) 20 µm.

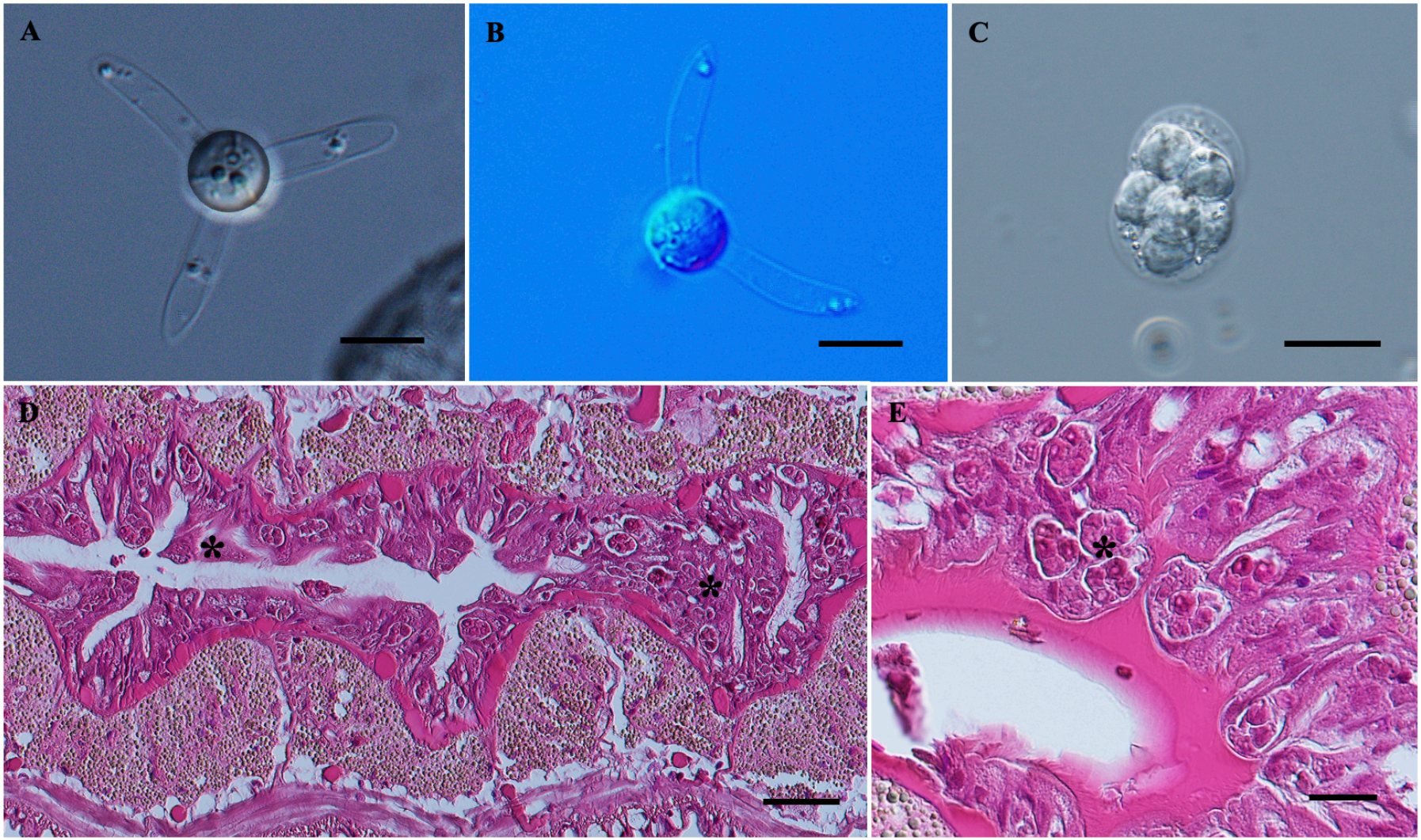

Figure S15. Aurantiactinomyxon type 4 of *Zschokkella chezhachei* released from *Branchiura sowerbyi*. A) Fresh aurantiactinomyxon type 4 in apical view and (B) in side view. C) Released pansporocyst of aurantiactinomyxon type 2, showing six of the eight actinospores from the intestinal epithelium of *B. sowerbyi*. D) Sections of heavily infected *B. sowerbyi*, with pansporocysts (*) visible in the intestinal epithelium. E) Enlarged section of a pansporocyst with mature spores (*). Stained with H&E. Scale bars represent 10 µm (A, B), 50 µm (D), and 20 µm (C, E).

Table S17 Comparison of morphometric measurements of aurantiactinomyxon type 3 and type 4 from Ócsárd fish farm with data from previous studies. All measurements are in µm. Abbreviations: SBD spore body diameter, CPL caudal processes length, CPW caudal processes width, PCL polar capsule length, PCW polar capsule width, SC number of secondary cells, D diameter, L length, W width, – no data.

Aurantiactinomyxon type	Host	SBD	CPL	CPW	PCL	PCW	SC	Reference
Aurantiactinomyxon type 3	***Branchiura sowerbyi***	**18.9 (16.5–20.8)**	**16.2 (14.0–19.1)**	**8.4 (6.7–10.5)**	**D: 3.4**	**D: 3.4**	**32**	**Present study**
Type 1	*T. tubifex*	18.3	17.5	9.9	D: 2.0	D: 2.0	–	El-Mansy et al. (1998b)
Type 7	Actinospores collected from water	18.9	24.4	9.5	2.8	2.5	–	El-Mansy et al. (1998b)
Type B1	*B. sowerbyi*	18.0 (17.0–20.0)	24.0 (20.0–30.0)	9.8 (9.0–10.0)	2.5 (2.0–3.0)	–	–	Eszterbauer et al. (2006)
Aurantiactinomyxon of *Thelohanellus testudineus*	*B. sowerbyi*	15.5 (14.5–16.4)	13.2 (11.5–16.2)	7.4 (6.5–8.0)	2.5 (2.3–2.9)	2.0 (1.8–2.4)	32	Zhao et al. (2017)
Aurantiactinomyxon of *Thelohanellus kitauei*	*B. sowerbyi*	19.7 (17.3–23.3)	20.4 (18.7–23.3)	8.9 (7.4–10.0)	3.4	2.8	> 28	Zhao et al. (2016)
Aurantiactinomyxon type 4	***Branchiura sowerbyi***	**10.9 (8.9–12.6)**	**18.9 (15.7–23.1)**	**4.5 (4.0–5.4)**	**D: 2.0 (1.7–2.5)**	**D: 2.0 (1.7–2.5)**	**–**	**Present study**
Type 3 and Type 5	*B. sowerbyi*	9.9	17.2	3.9	D: 1.4	D: 1.4	–	El-Mansy et al. (1998a, 1998b)
Guyenotia	*B. sowerbyi*	10 (9.5–11.0)	16 (15.0–19.5)	4.5 (4.0–5.5)	1.6 (1.3–2.0)	–	–	Eszterbauer et al. (2006)
Guyenotia	*B. sowerbyi*	10.3 (9.6–10.9)	18.5 (16.5–20.6)	6.0 (5.4–6.4)	D: 1.8 (1.6–2.1)	D: 1.8 (1.6–2.1)	–	Xi et al. (2013)
Guyenotia	*B. sowerbyi*	L: 9.5 W: 8.8	21.0 (16.0–25.0)	4.5–6.5	3.0 (2.8–3.3)	2.0 (1.8–2.2)	8–16	Xiao & Desser (1998c)

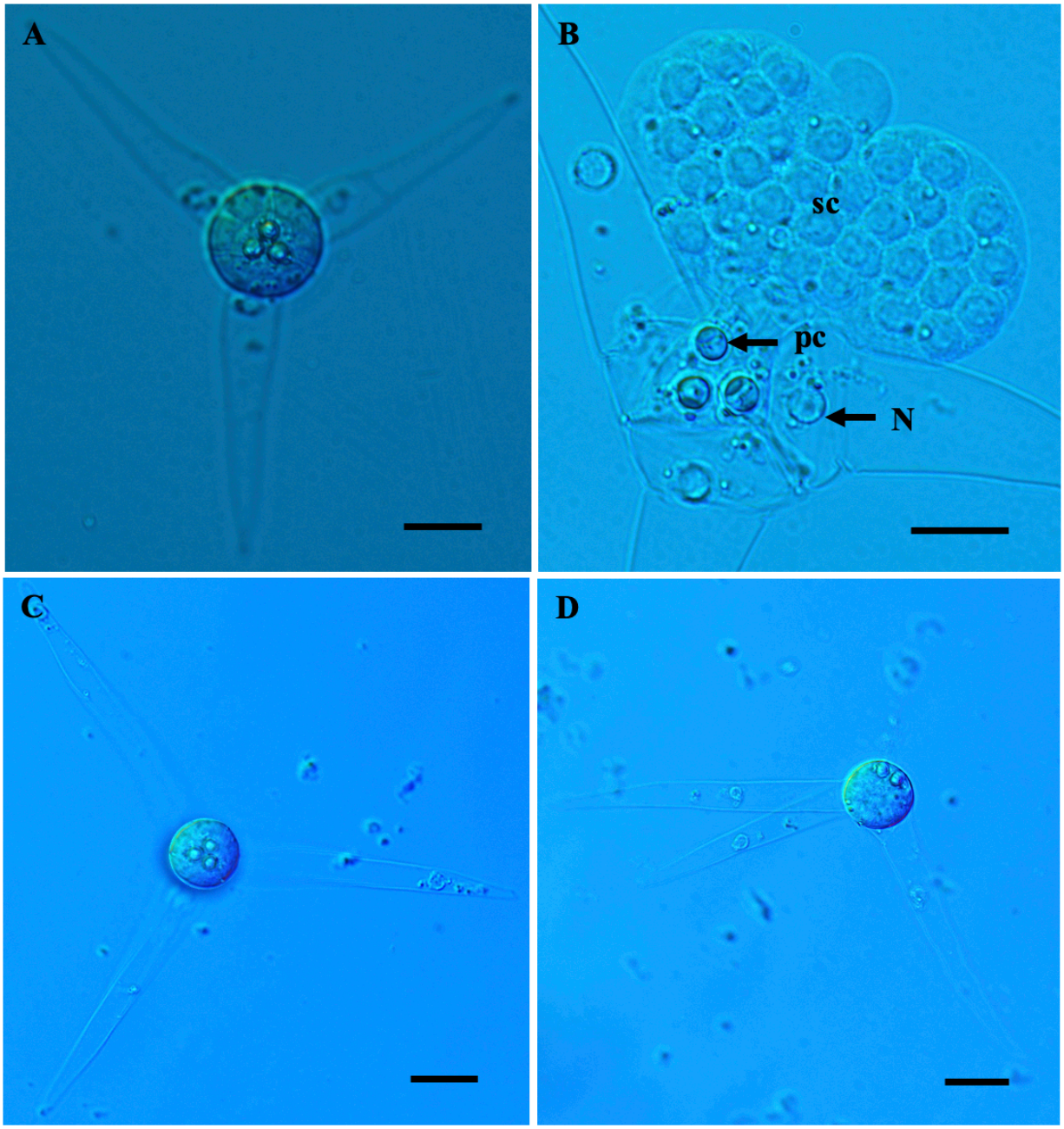

Figure S16. Actinospore stages of *Thelohanellus hovorkai*. (A) Fresh aurantiactinomyxon type 5 released from *Branchiura sowerbyi*. (B) Ruptured of the aurantiactinomyxon type 5 (under pressure), showing nuclei (N), three polar capsules (pc) and 32 secondary cells (sc). (C) Fresh aurantiactinomyxon type 6 released from *Branchiura sowerbyi* and (D) Aurantiactinomyxon type 6 in side view. Scale bars represent 20 µm, except (B) 10 µm.

Table S18 Comparison of morphometric measurements of aurantiactinomyxon type 5 and aurantiactinomyxon type 6 from Ócsárd fish farm with data from previous studies. All measurements are in µm. Abbreviations: SBD spore body diameter, CPL caudal processes length, CPW caudal processes width, PCL polar capsule length, PCW polar capsule width, SC number of secondary cells, – no data.

Aurantiactinomyxon type	Host	SBD	CPL	CPW	PCL	PCW	SC	Reference
Aurantiactinomyxon type 5	***Branchiura sowerbyi***	**20.7 ± 1.3 (18.7–24.1)**	**51.5 ± 4.0 (43.4–56.3)**	**9.9 ± 0.9 (8.3–11.3)**	**D: 3.5 ± 0.3 (3.1–4.1)**	**D: 3.5 ± 0.3 (3.1–4.1)**	**32**	**Present study**
Aurantiactinomyxon type 6	***Branchiura sowerbyi***	**19.7 ± 1.0 (17.4–21.6)**	**72.1 ± 6.1 (61.0–86.9)**	**9.0 ± 0.6 (7.8–10.1)**	**4.6 ± 0.4 (3.8–5.6)**	**3.3 ± 0.4 (2.7–3.9)**	**32**	**Present study**
Aurantiactinomyxon 'A' of *T. hovorkai*	*B. sowerbyi*	20.0 (18.0–22.0)	47.0 (37.0–58.0)	10.0 (8.0–12.0)	3.0 (2.0–3.3)	–	32	Eszterbauer et al. (2006)
Aurantiactinomyxon type of *T. hovorkai*	*B. sowerbyi*	18.6 (18.3–18.9)	29.0 (28.2–29.6)	9.2 (8.1–10.2)	3.42 (3.4–3.5)	3.36 (3.3–3.4)	32	Székely et al. (1998)
Aurantiactinomyxon type of *T. hovorkai*	*B. sowerbyi*	(18.0–22.0)	(25.0–33.0)	–	–	–	32	Yokoyama (1997)
Aurantiactinomyxon 'B1'	*B. sowerbyi*	18.0 (17.0–20.0)	24.0 (20.0–30.0)	9.8 (9.0–10.0)	2.5 (2.0–3.0)	–	–	Eszterbauer et al. (2006)
Aurantiactinomyxon 'B2'	*B. sowerbyi*	19.0 (18.0–21.0)	16.0 (14.0–20.0)	8.4 (7.0–10.6)	2.6 (2.0–4.1)	–	–	Eszterbauer et al. (2006)

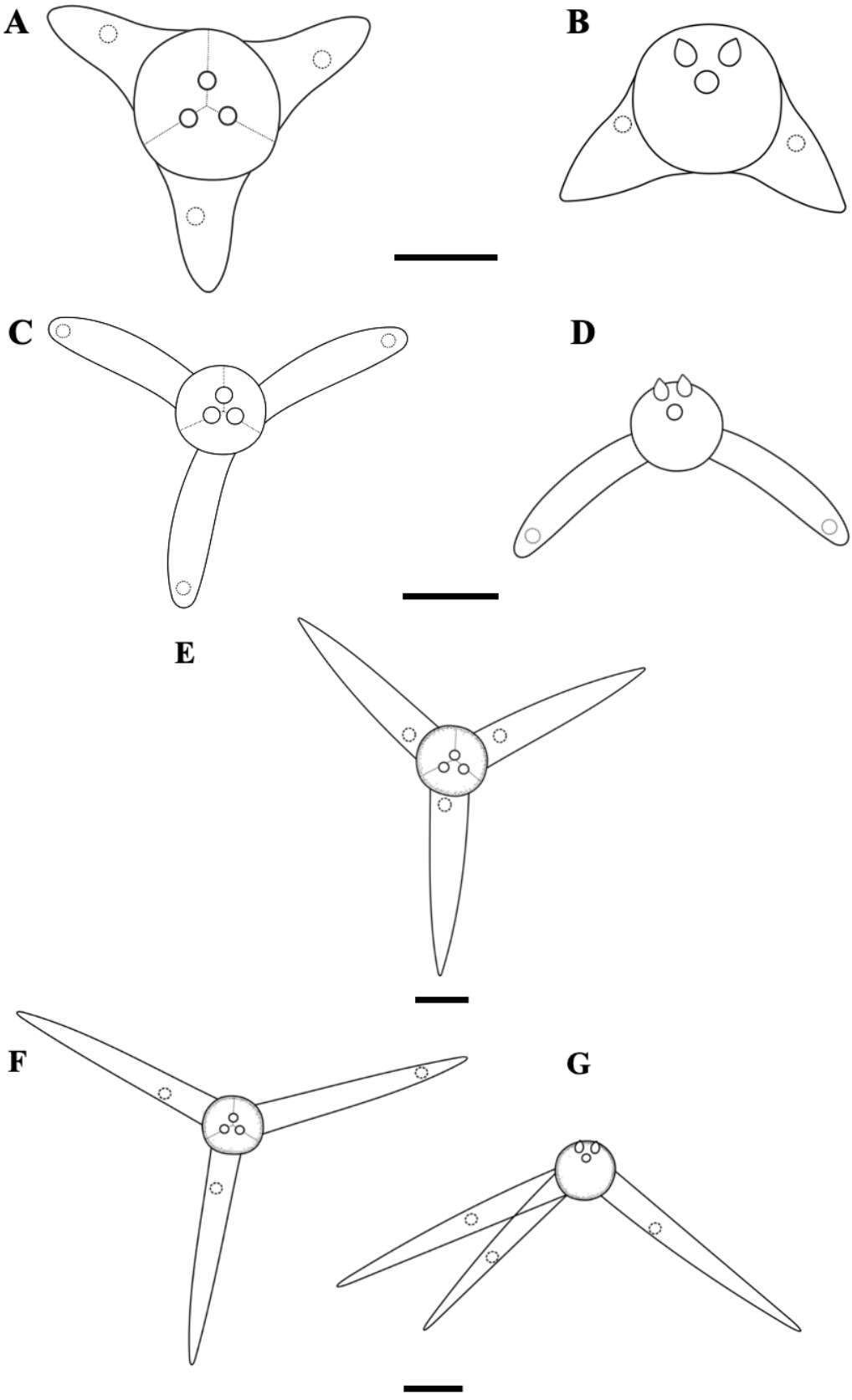

Figure S17. Schematic drawing of aurantiactinomyxon types. A) Aurantiactinomyxon type 3 in apical view and B) sutural view. C) Aurantiactinomyxon type 4 of *Zschokkella chezhachei* in apical view and D) sutural view. Schematic drawings of actinospore stages of *Thelohanellus hovorkai.* E) Aurantiactinomyxon type 5 in frontal view. F) Aurantiactinomyxon type 6 in frontal view and G) sutural view. Scale bars represent 10 µm.

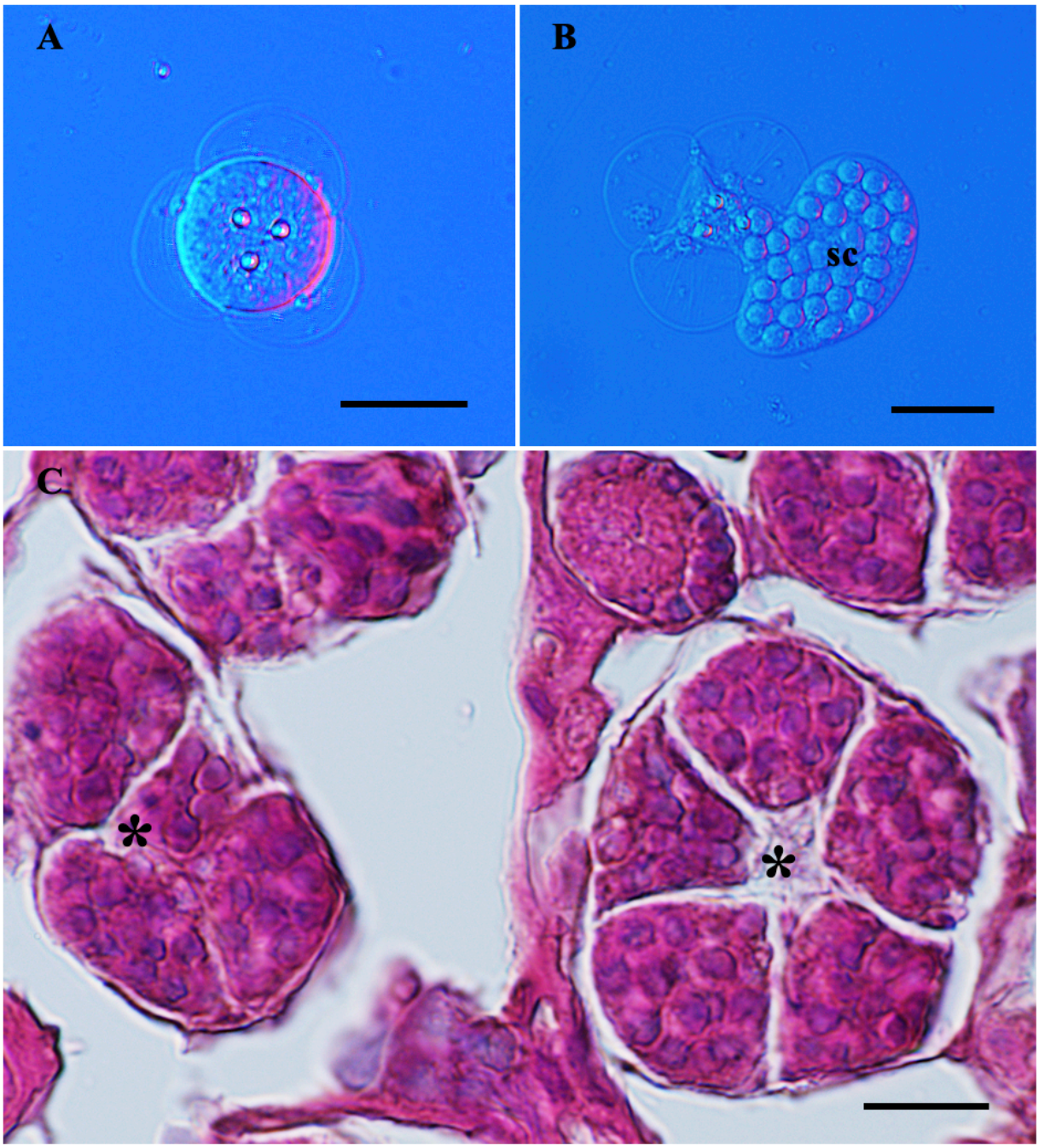

Figure S18. Neoactinomyxum type 1 of *Thelohanellus wangi* released from *Branchiura sowerbyi*. A) Fresh neoactinomyxum type in apical view. B) Rupture of the neoactinomyxum type 1 actinospore (under pressure), showing three polar capsules and 32 secondary cells (sc). C) Sections showing numerous pansporocysts (*) in the intestinal epithelium of *B. sowerbyi*, with mature spores containing secondary cells can be seen. Stained with H&E. Scale bars represent 20 µm (A–B), except 10 µm (C).

Table S19 Comparison of morphometric measurements of neoactinomyxum type 1 from Ócsárd fish farm with data from previous studies. All measurements are in μm. Abbreviations: SBD spore body diameter, CPL caudal processes length, CPW caudal processes width, PCL polar capsule length, PCW polar capsule width, SC number of secondary cells, – no data.

Neoactinomyxum type	Host	SBL	SBW	CPL	CPW	PCD	SC	Reference
Neoactinomyxum type 1	***Branchiura sowerbyi***	**21.6 ± 1.0 (20.2–23.8)**	**–**	**9.4 ± 0.7 (8.1–10.4)**	**22.0 ± 1.0 (20.2–24.0)**	**2.7 ± 0.3 (2.1–3.2)**	**32**	**Present study**
Neoactinomyxum type JD of *Thelohanellus wangi*	*B. sowerbyi*	20.7	22.4 (19.5 – 25.4)	9.3 (7.9– 0.3)	25.6 (23.2–29.7)	2.6 (2.0–3.2)	–	Xi et al. (2015)
Neoactinomyxum type CZ-2	*B. sowerbyi*	18.6 (17.8–19.5)	20.7 (19.8–22.0)	7.5 (6.6–8.4)	18.4 (16.8–21.5)	2.7 (2.4–2.8)	–	Xi et al. (2015)
Type A1	*B. sowerbyi*	21.0 (19.0–24.0)	–	8.0 (7.0–9.0)	19.0 (16.0–22.0)	2.6	16	Eszterbauer et al. (2006)
Type A2	*B. sowerbyi*	21.0 (19.0–22.0)	–	7.0 (5.0–8.0)	15.0 (14.0–18.0)	2.5 (2.0–3.2)	16	Eszterbauer et al. (2006)

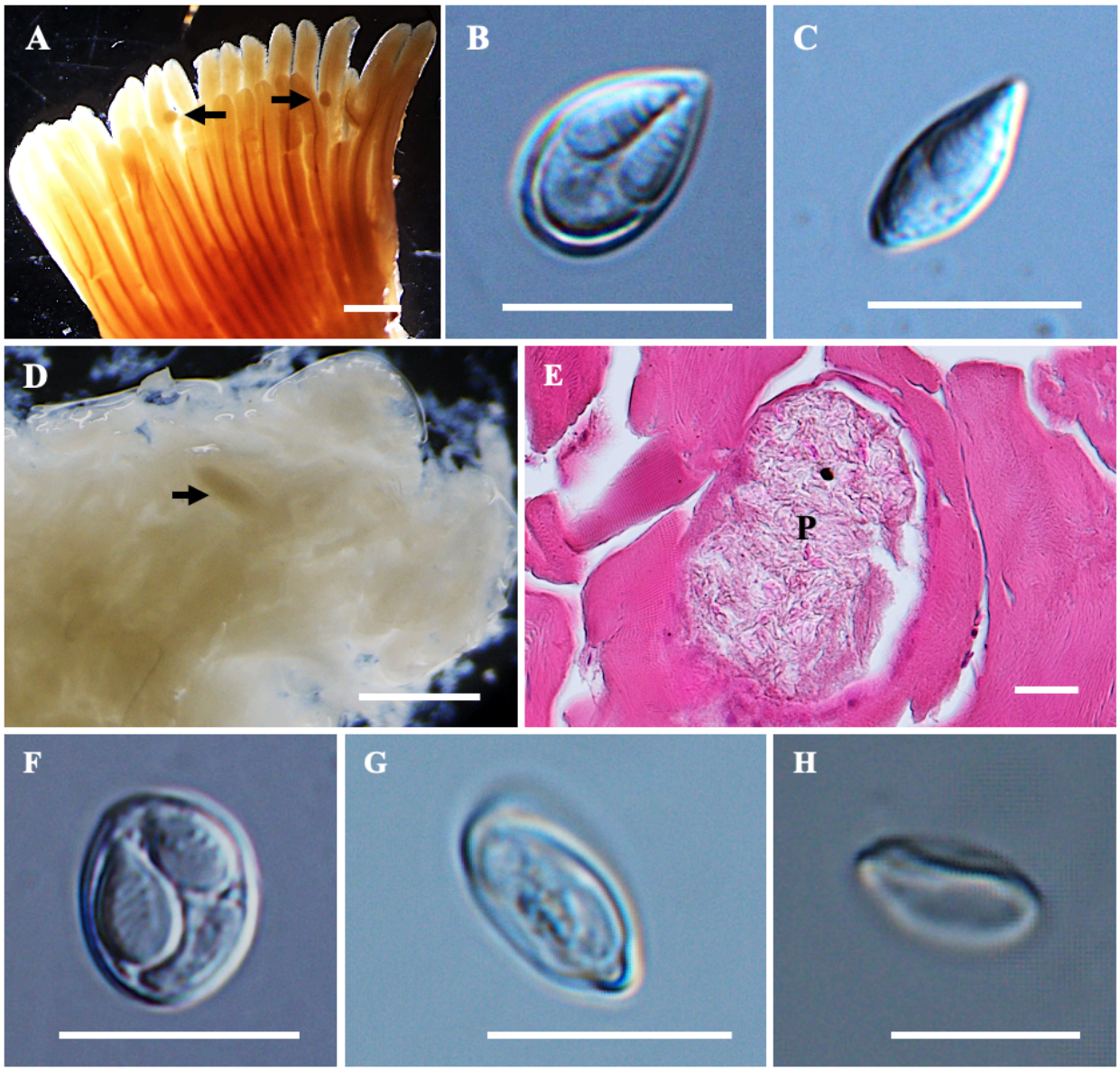

Figure S19. Myxosporean parasites from *Barbonymus gonionotus*. A) Plasmodia (black arrow) of *Myxobolus gonionoti* n. sp. in the formalin-fixed gill filaments. B) Spore in frontal view and C) Spore in sutural view. D) Plasmodium (black arrow) of *Myxobolus barbonymi* n. sp. in formalin-fixed muscle. E) Histological transverse section of muscle cells showing an intracellular plasmodium (P) of *M. barbonymi* n. sp. within a (skeletal) muscle cell, stained with hematoxylin and eosin (H&E). F) Spore in frontal view. G) Spore in sutural view and H) Sutural line of the spore. Scale bars represent 10 µm, except (A, D) 1 mm and (E) 20 µm.

Table S20 Comparative data on spore measurements (mean ± standard deviation [SD], with ranges in parentheses) for *Myxobolus gonionoti* n. sp., *Myxobolus dykovae* and species with tapered anterior ends. All measurements are in μm. Abbreviations: SL spore length, SW spore width, ST spore thickness, PCL polar capsule length, PCW polar capsule width, PFC polar filament coils, – no data.

						Large/ Equal			Small			
Species	Host	Site infection	SL	SW	ST	PCL	PCW	PFC	PCL	PCW	PFC	Reference
***Myxobolus gonionoti* n. sp.**	***Barbonymus gonionotus***	**Gill lamellae**	**9.3 ± 0.3 (8.2–9.8)**	**6.1 ± 0.3 (5.4–6.6)**	**4.7 ± 0.3 (4.4–5.1)**	**5.2 ± 0.3 (4.3–6.0)**	**2.1 ± 0.2 (1.6–2.4)**	**7**	**4.9 ± 0.3 (3.9–5.4)**	**1.9 ± 0.2 (1.6–2.3)**	**6**	**Present study**
M. sangei	*Brycinus macrolepidotus*	Gills, skin, kidneys	10.1 (9.0–10.5)	6.2 (6.0–6.8)	–	6.2 (5.7–7.0)	2.2 (2.0–3.0)	7–8	4.8 (4.0–5.5)	1.7 (1.5–2.0)	4–5	Fomena et al. (2007)
M. macrocapsularis	*Barbonymus gonionotus*	Gills	(10.9–11.6)	7.2	6.2	6.2	2.3	–	–	–	–	Ky & Te (2007)
M. dajiangensis	*Cyprinus carpio*	Gill lamellae	14.8 ± 0.4 (13.9–15.6)	8.0 ± 0.5 (7.3–9.1)	5.5	8.0 ± 0.4 (7.1–8.8)	2.5 ± 0.2 (2.0–3.2)	9–11	7.4 ± 0.4 (6.1–8.0)	2.5 ± 0.2 (2.0–3.2)	9–11	Wang et al. (2022)
M. carlhubbsi	*Luxilus chrysocephalus isolepis*	Gill filaments	12.7 ± 0.4 (12.0–13.4)	6.1 ± 0.3 (5.0–6.6)	5.4 ± 0.3 (5.1–6.0)	6.4 ± 0.3 (5.7–7.3)	2.1 ± 0.2 (1.8–2.3)	6–11	6.2 ± 0.3 (5.2–6.8)	2.2 ± 0.1 (1.8–2.5)	6–11	McAllister et al. (2023)
M. voremkhai	*Tachysurus fulvidraco*	Gill arch	14.3 ± 0.6 (10.4–12.6)	7.7 ± 0.4 (6.9–8.4)	5.7 ± 0.6 (4.9–6.8)	6.2 ± 0.4 (5.4–7.1)	2.7 ± 0.2 (2.5–3.0)	5–7	5.9 ± 0.3 (5.3–6.5)	2.5 ± 0.2 (2.2–2.8)	5–7	Zhang et al. (2023a)
M. dykovae	***Barbonymus schwanefeldii***	**Gill lamellae**	**11.7 ± 0.6 (10.3–12.8)**	**6.8 ± 0.4 (5.9–7.7)**	**5.4 ± 0.3 (5.1–5.7)**	**5.8 ± 0.5 (4.7–7.0)**	**2.2 ± 0.2 (1.8–2.6)**	**6–7**	**–**	**–**	**–**	**Present study**
M. dykovae	*Barbonymus schwanefeldii*	Gill lamellae	12.0 ± 0.5 (11.0–12.7)	6.2 ± 0.4 (5.6–6.7)	5.8 ± 0.16 (5.7–6.0)	6.0 ± 0.07 (5.9–6.1)	2.1 ± 0.14 (2.0–2.3)	6–7	–	–	–	Székely et al. (2009a)
M. alvarezae	*Leuciscus idus*	Gill filaments	11.7 ± 0.42 (11.3–12.6)	6.8 ± 0.31 (6.5–7.6)	6.4 ± 0.41 (6.1–6.9)	6.7 ± 0.32 (6.1–7.2)	2.3 ± 0.16 (2.0–2.5)	6	–	–	–	Cech et al. (2012)
M. koi	*Carassius auratus*	Gills	13.6 ± 0.6 (12.3–15.1)	8.3 ± 0.4 (7.6–9.1)	–	7.4 ± 0.5 (6.4–8.5)	2.8 ± 0.2 (2.4–3.4)	9–10	–	–	–	Zhang et al. (2022)

Table S21 Comparative data on spore measurements (mean ± standard deviation [SD], with ranges in parentheses) for *Myxobolus barbonymi* n. sp., *Myxobolus faizahae* n. sp., and species with unequal polar capsules. All measurements are in µm. Abbreviations: SL spore length, SW spore width, ST spore thickness, PCL polar capsule length, PCW polar capsule width, PFC polar filament coils, – no data.

Species	Host	Site infection	SL	SW	ST	Large			Small			Reference
						PCL	PCW	PFC	PCL	PCW	PFC	
***Myxobolus barbonymi* n. sp.**	***Barbonymus gonionotus***	**Muscle**	**8.4 ± 0.5 (7.4–9.9)**	**6.9 ± 0.5 (6.1–7.8)**	**5.2 ± 0.2 (4.9–5.4)**	**4.9 ± 0.3 (4.2–5.5)**	**2.9 ± 0.3 (2.4–3.4)**	**5–6**	**3.8 ± 0.4 (3.0–4.7)**	**2.4 ± 0.2 (2.0–2.8)**	**3–4**	**Present study**
***Myxobolus faizahae* n. sp.**	***Barbonymus altus***	**Muscle**	**9.3 ± 0.3 (8.7–9.9)**	**5.8 ± 0.2 (5.4–6.1)**	**4.4 ± 0.3 (3.5–4.8)**	**4.4 ± 0.3 (3.8–5.0)**	**2.8 ± 0.3 (2.3–3.3)**	**4–5**	**3.3 ± 0.2 (2.9–3.9)**	**1.9 ± 0.1 (1.6–2.2)**	**3–4**	**Present study**
M. bhadrensis	*Catla catla*	Muscle	10.0 ± 0.4 (9.2–10.4)	6.6 ± 0.3 (6.0–7.2)	4.5 ± 0.5 (4.0–5.3)	5.5 ± 0.3 (4.8–6.0)	2.0 ± 0.2 (1.6–2.6)	4	4.2 ± 0.4 (3.6–4.8)	2.0 ± 0.2 (1.6–2.6)	3	Székely et al. (2015b)
M. pseudodispar	*Rutilus rutilus, Blicca joerkna, Abramis brama*	Muscle	12.2 ± 0.8 (11.0–13.6)	7.0 ± 0.7 (5.8–8.3)	5.6 ± 0.3 (5.0–6.0)	5.9 ± 0.3 (5.6–6.6)	2.9 ± 0.3 (2.1–3.3)	4–6	3.8 ± 0.4 (3.5–5.0)	2.8 ± 0.1 (2.7–3.0)	3–4	Molnàr et al. (2002, 2010)
M. cyprini	*Cyprinus carpio*	Muscle	(10.0–16.0)	(8.0–12.0)	–	(5.2–7.0)	–	–	–	–	–	Eiras et al. (2005b)
M. musculi	*Barbus barbus*	Muscle	11.7 ± 0.6 (11.0–13.0)	9.4 ± 0.4 (8.7–9.8)	5.6 ± 0.4 (4.8–5.6)	6.7 ± 0.4 (6.2–7.3)	3.4 ± 0.4 (2.9–3.8)	4–5	5.9 ± 0.6 (5.3–6.6)	2.9 ± 0.5 (2.1–3.3)	3	Molnàr et al. (2012)

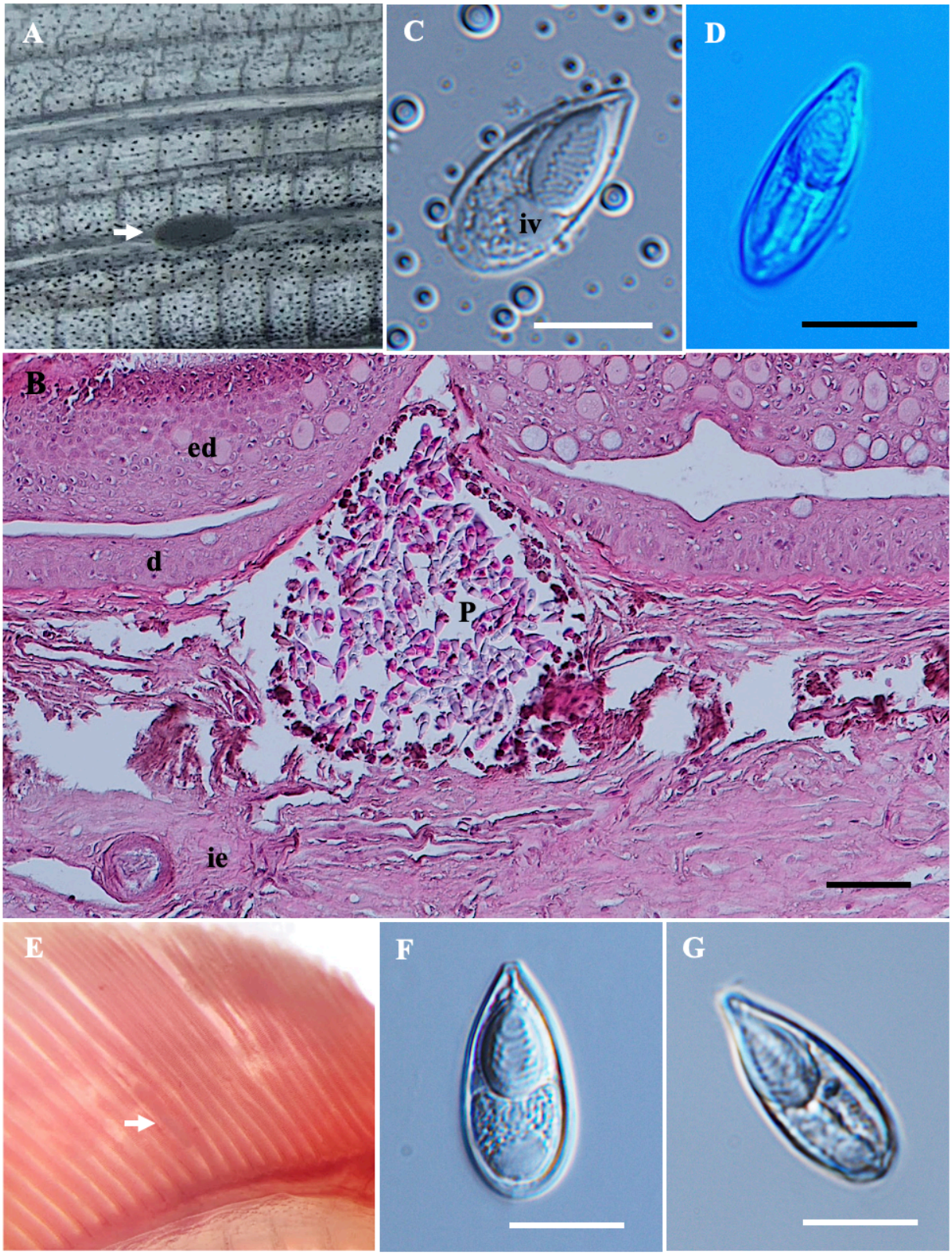

Figure S20. *Thelohanellus* spp. from *Barbonymus gonionotus*. A) Plasmodium (white arrow) of *Thelohanellus gonionoti* n. sp. under the dermis partially covering the fin ray and the interlepidotrichial ligament. B) Histological transverse section of the tail fin showing a plasmodium (P) located between the interlepidotrichial ligament (ie) and the dermis (d), and bulging toward the epidermis, stained with hematoxylin and eosin (H&E). C) Spore in frontal view with the presence of an iodinophilous vacuole (iv) within the sporoplasm. D) Spore in sutural view. E) Large elongated shape plasmodium (white arrow) of *Thelohanellus zahrahae* located inside a filament. F) Spore in frontal view and G) Spore in sutural view. Scale bars represent 10 µm, except (D) 50 µm.

Table S22 Comparative data on spore measurements (mean ± standard deviation [SD], with ranges in parentheses) for *Thelohanellus gonionoti* n. sp., *Thelohanellus barbonymi* n. sp., *Thelohanellus zahrahae* and species with truncate anterior ends. All measurements are in µm. Abbreviations: SL spore length, SW spore width, ST spore thickness, PCL polar capsule length, PCW polar capsule width, PFC polar filament coils, D diameter, – no data.

Species	Host	Site infection	SL	SW	ST	PCL	PCW	PFC	Reference
***Thelohanellus gonionoti* n. sp.**	*Barbonymus gonionotus*	**Fins**	**18.4 ± 1.0 (16.3–18.3)**	**8.9 ± 0.8 (7.2–9.2)**	**6.9 ± 0.4 (6.4–6.9)**	**9.2 ± 1.0 (7.3–10.3)**	**4.8 ± 0.5 (3.8–5.6)**	**8–9**	**Present study**
***Thelohanellus barbonymi* n. sp.**	*Barbonymus altus*	**Gill arch**	**22.0 ± 0.7 (20.3–23.2)**	**9.9 ± 0.6 (8.1–10.8)**	**7.7 ± 0.5 (6.7–8.3)**	**9.1 ± 0.5 (8.2–10.1)**	**5.4 ± 0.3 (4.9–5.9)**	**8**	**Present study**
Thelohanellus zahrahae	*Barbonymus gonionotus*	**Gill filaments**	**20.5 ± 0.5 (19.4–21.6)**	**9.1 ± 0.6 (8.1–10.6)**	**7.6 ± 0.2 (7.3–7.8)**	**8.8 ± 0.8 (6.6–10.2)**	**5.5 ± 0.5 (4.7–6.8)**	**7**	**Present study**
T. zahrahae	*Barbonymus gonionotus*	Gill filaments	23.8 ± 1.3 (21.7–26.3)	9.0 ± 0.3 (8.5–9.4)	7.6 ± 0.1 (7.5–7.9)	9.9 ± 1.0 (7.9–10.8)	6.3 ± 0.5 (5.3–6.6)	7	Székely et al. (2009b)
T. catlae	*Barbonymus gonionotus*	Gills, skin	19.8	9.9	8.2	D: 9.9	–	–	Ky & Te (2007)
T. boggoti	*Labeo boggut*	Gill lamellae	11.5 (11.0–12.0)	6.8 (6.0–7.5)	–	6.2 (5.5–7.0)	3.8 (3.6–4.0)	10–11	Qadri (1962)
T. assambai	*Labeo* sp.	Gills and fins	10.8 (9.0–12.0)	5.5 (5.0–7.0)	–	6.3 (5.0–7.6)	3.4 (3.0–4.0)	5–6	Zhang et al. (2013)
T. lamelliformis	*Catla catla*	Gill lamellae	10.27	4.9	0.5	3.8	2.6	6–7	Singh & Kaur (2015)

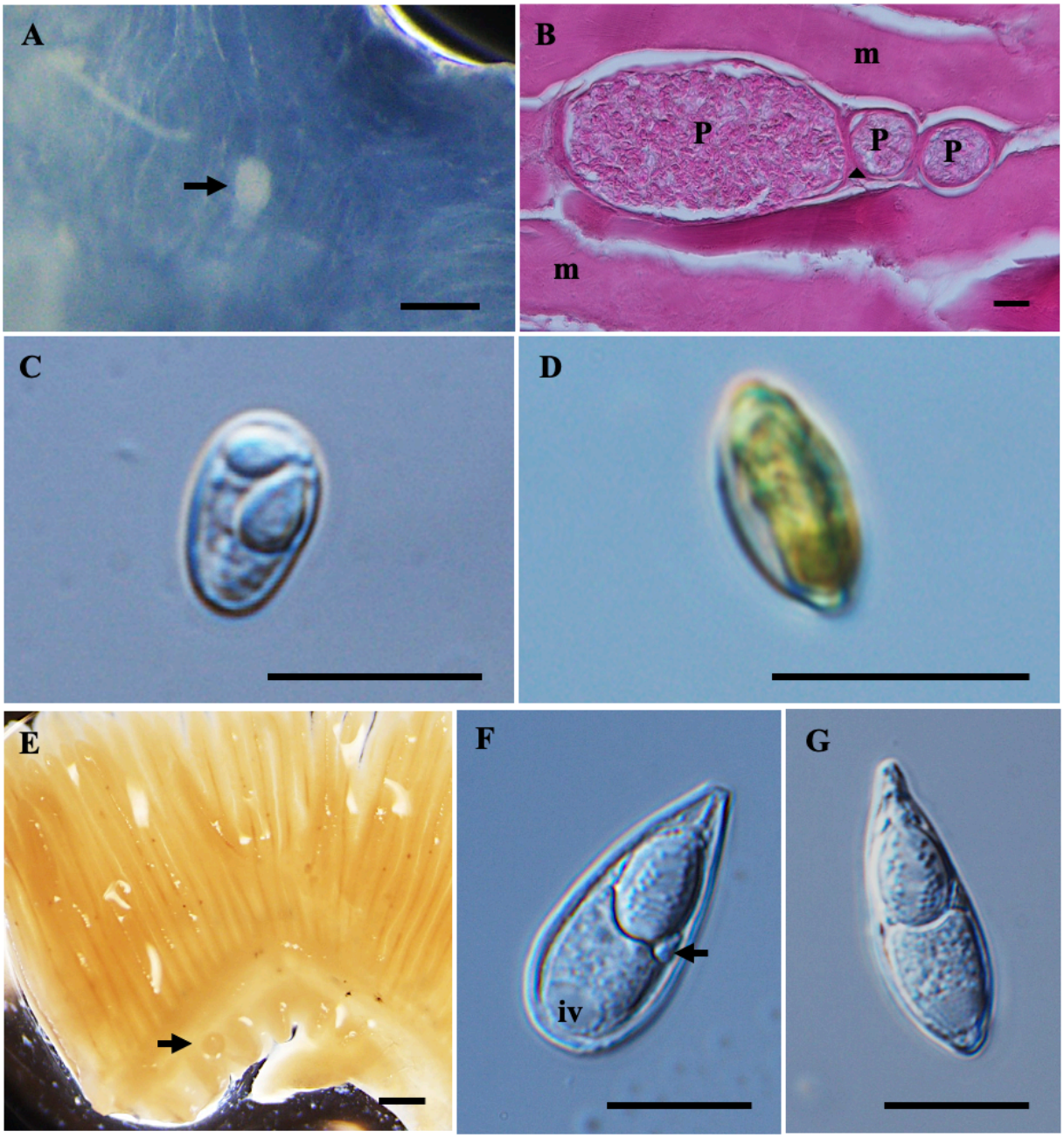

Figure S21. *Myxobolus* and *Thelohanellus* species from *Barbonymus altus*. A) Plasmodium (black arrow) of *Myxobolus faizahae* n. sp. in formalin-fixed muscle tissue. B) Histological longitudinal section of muscle cells showing plasmodia (P) located among (skeletal) muscle cells (m) of *B. altus*, surrounding connective tissue (arrowhead), stained with hematoxylin and eosin (H&E). C) Spore in frontal view and D) Spore in sutural view. E) Plasmodium (black arrow) of *Thelohanellus barbonymi* n. sp. in formalin-fixed gill arches. F) Spore in frontal view with the presence of single nucleus (black arrow) and an iodinophilous vacuole (iv) within the sporoplasm. (D) Spore in sutural view. Scale bars represent 10 µm, except (A) 100 µm, (B) 20 µm and (E) 500 µm.

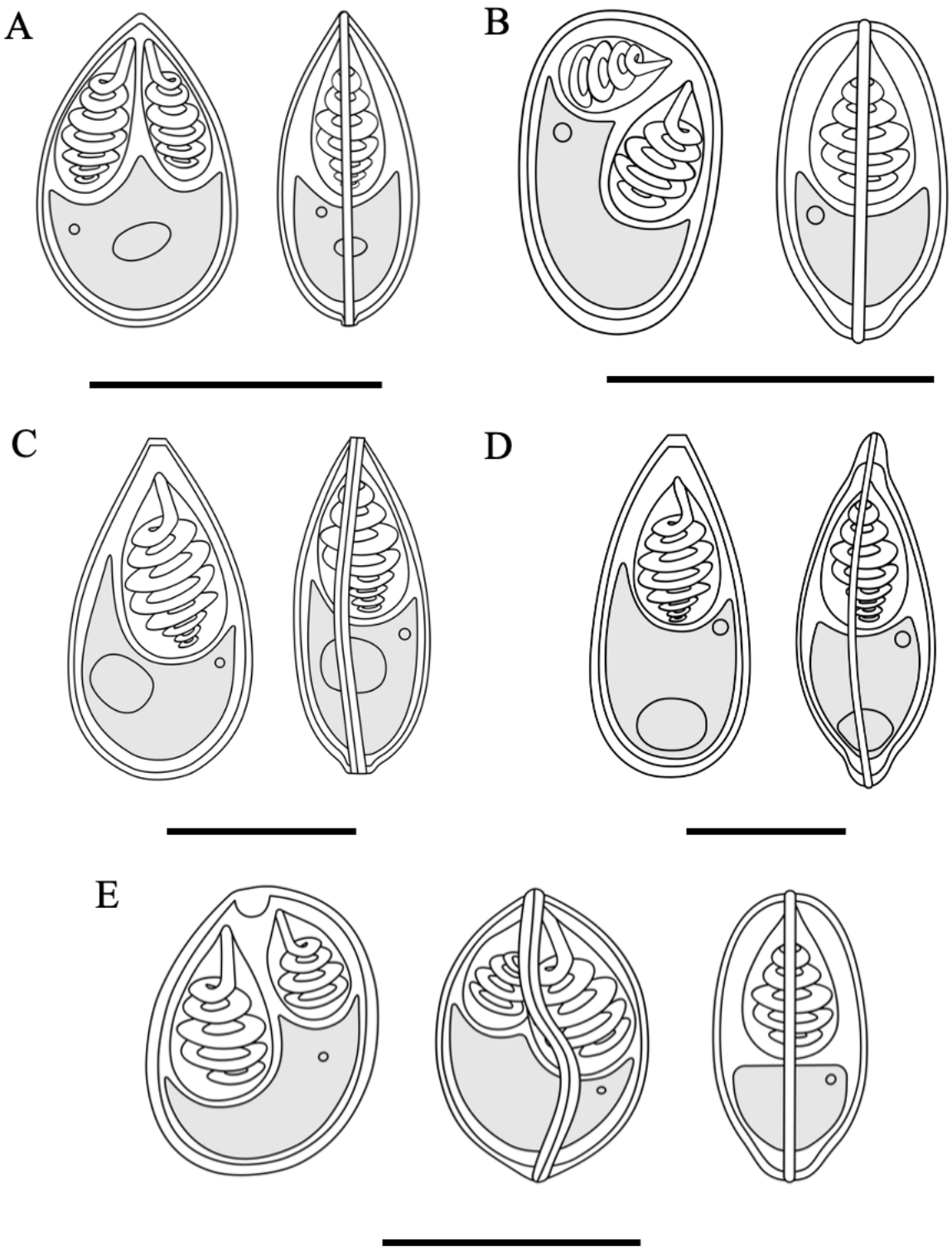

Figure S22. Schematic drawings of myxosporean parasites from *Barbonymus gonionoti* and *Barbonymus altus*. A) *Myxobolus gonionotus* n. sp. in frontal and sutural view. B) *Myxobolus faizahae* n. sp. in frontal and sutural view. (C) *Thelohanellus gonionoti* n. sp. in frontal and sutural view. (D) *Thelohanellus barbonymi* n. sp. in frontal and sutural view. (E) *Myxobolus barbonymi* n. sp. in frontal and sutural view Scale bars represent 10 µm.

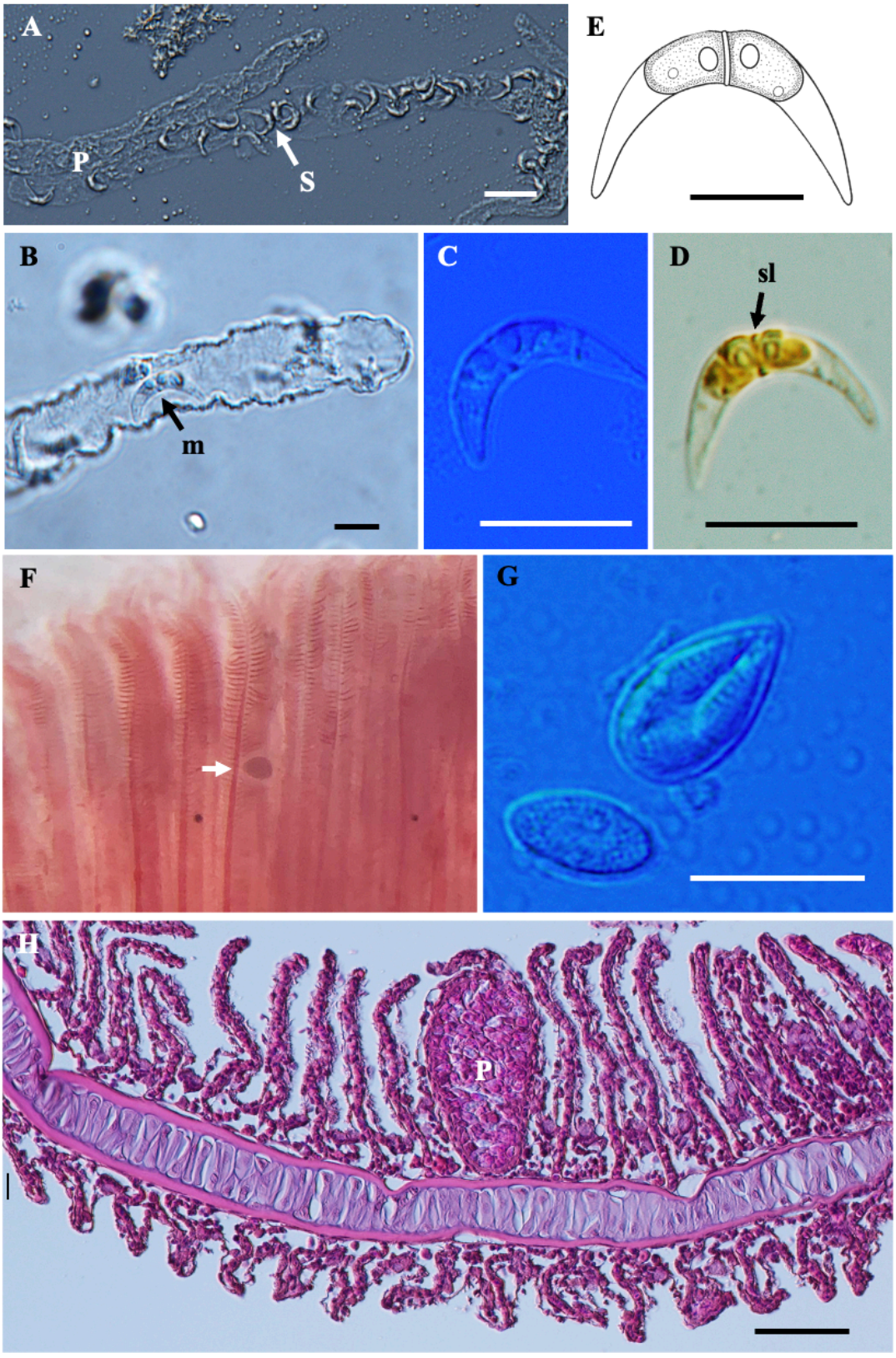

Figure S23. Myxosporean parasites from *Barbonymus schwanefeldii*. A) Formalin-fixed vermiform plasmodia (P) filled with *Ceratomyxa schwanefeldii* n. sp. in the gallbladder. B) Mature spore (m) within the plasmodium (P). C) Formalin-fixed *C. schwanefeldii* n. sp. D) Mature spore showing the sutural line (sl; black arrow), with the spore stained with Lugol solution. E) Schematic drawing of *C. schwanefeldii* n. sp. F) Plasmodium (white arrow) of *Myxobolus dykovae* located in the gills. G) Spore in frontal view. H) Histological transverse section of gill filament showing plasmodium (P) located between gill lamellae, stained with hematoxylin and eosin (H&E). Scale bars represent 10 µm, except (G) 50 µm.

Table S23 Comparative data on spore measurements (mean ± standard deviation [SD], with ranges in parentheses) for *Ceratomyxa schwanefeldii* n. sp. from *Barbonymus schwanefeldii* and other 17 freshwater *Ceratomyxa* spp. from Asia, South America and Europe. All measurements are in µm. Abbreviations: ST spore thickness, SL spore length, PA posterior angle, PCL polar capsule length, PCW polar capsule width, – no data.

Species	Host	Plasmodia shape	Spore shape	ST	SL	PA	PCL	PCW	Locality	Reference
***Ceratomyxa schwanefeldii* n. sp.**	***Barbonymus schwanefeldii***	**Vermiform**	**Crescent and strongly arched**	**12.6 ± 1.2 (10.8–15.4)**	**3.0 ± 0.4 (2.4–3.9)**	**104.8° (73.4–123.8)**	**1.5 ± 0.2 (1.2–1.8)**	**1.3 ± 0.2 (0.9–1.7)**	**Malaysia**	**Present study**
C. deformis	*Schyzodon vittatus*	Elongated	Lightly arched	35.7 ± 2.1	3.9 ± 0.3	167° (150–185)	1.8 ± 0.3	1.4 ± 0.2	Brazil	Müller et al. (2025)
C. anomala	*Schyzodon vittatus*	Elongated	Lightly arched	20.4 ± 4.1	3.5 ± 0.5	133° (109–160)	1.8 ± 0.3	1.3 ± 0.2	Brazil	Müller et al. (2025)
C. edilsonis	*Pimelodella cristata*	Elongated	Lightly arched	17.13 ± 2.6	1.64 ± 0.6	–	1.36 ± 0.17	0.9 ± 0.5	Brazil	de Carvalho et al. (2024)
C. ranunculiformis	*Plagioscion squamosissimus*	Rounded to oval	Elongated and crescent	37.6 (32.4–43.9)	4.9 (4–6.6)	165° (154–173)	2 (1.4–3.0)	1.9 (1.4–2.4)	Brazil	Zatti et al. (2023)
C. mandii	*Pimelodina flavipinnis*	Vermiform	Elongated/ lightly arched	31.2 ± 2.3 (26.2–36.3)	4.6 ± 0.5 (3.4–5.5)	162° (143–178)	1.8 ± 0.3 (1.0–2.5)	1.9 ± 0.3 (1.2–2.4)	Brazil	Araújo et al. (2022)
C. barbata	*Rhaphiodon vulpinus*	Vermiform	Elongated/ lightly arched	21.7 (17.5–29.9)	2.9 (2.1–3.8)	164° (139–178)	1.6 (1.1–2.3)	1.4 (1.1–1.5)	Brazil	Franzolin et al. (2022)
C. macapaensis	*Mesonauta festivus*	Vermiform	Elongated/ lightly arched	22.75 ± 0.3	4.2 ± 0.5	–	1.63 ± 0.1	1.86 ± 0.3	Brazil	Bittencourt et al. (2022)
C. fonsecai	*Hemiodus unimaculatus*	Vermiform	Elongated/ lightly arched	28.9 ± 2.7 (24.3–32.5)	2.6 ± 0.1 (2.3–2.8)	164.8°	1.9 ± 0.3 (1.5–2.3)	1.7 ± 0.2 (1.4–2.1)	Brazil	da Silva et al. (2020)
C. gracillima	*Brachyplatystoma rousseauxii*	Vermiform	Strongly arched	7.0 ± 0.5 (6.0–8.2)	4.4 ± 0.4 (3.0–5.7)	36.6° (35– 40)	1.9 ± 0.3 (1.5–2.5)	1.9 ± 0.3 (1.5–2.5)	Brazil	Zatti et al. (2018a)
C. brasiliensis	*Cichla monoculus*	Vermiform	Elongated/ lightly arched	41.2 ± 2.9 (37.1–47.6)	6.3 ± 0.6 (5.1–7.5)	147°	2.6 ± 0.3 (2–3.3)	2.5 ± 0.4 (1.8–3.7)	Brazil	Zatti et al. (2017)
C. vermiformis	*Colossoma macropomum*	Vermiform	Strongly arched	8.4 ± 0.4 (7.9–9.3)	4.5 ± 0.2 (4.8–4.2)	30.2° (22–43)	2.7 ± 0.1 (2.5–2.9)	2.7 ± 0.1 (2.5–2.9)	Brazil	Adriano & Okamura (2017)
C. amazonensis	*Symphysodon discus*	–	Arched	15.8 ± 0.4 (15.0–16.7)	7.0 ± 0.3 (6.2–7.6)	105° – 115°	3.2 ± 0.3 (2.4–3.6)	2.6 ± 0.17 (2.4–2.9)	Brazil	Mathews et al. (2016)
C. microlepis	*Hemiodus microlepis*	–	Elongated/ lightly arched	35.5 ± 0.9	5.2 ± 0.4	58° – 60°	2.2 ± 0.3	2.2 ± 0.3	Brazil	Azevedo et al. (2013)
C. mylei (syn. *Meglitschia mylei*)	*Myloplus rubripinnis*	–	Strongly arched	9.1	5	30°	2.1 ± 0.3	2.1 ± 0.3	Brazil	Azevedo et al. (2011)
C. huangheensis	*Trachysurus fulvidraco*	–	Crescent and arched	10.7 ± 1.3 (8.5–13.3)	4.7 ± 0.6 (3.3–5.5)	139.2° (137–156)	2.2 ± 0.4 (1.4–2.8)	2.0 ± 0.4 (1.0–2.5)	China	Li et al. (2023)
C. hongtzensis	*Pelterobagrus eupogon*	–	Arched	13.7 (9.8–17.5)	6.3 (4.4–9.0)	–	2.6 (2.4–3.2)	2.6 (2.4–3.2)	China	Chen & Ma (1998)
C. tienensis	*Pangasianodon hypophthalmus*	–	Elongated	4.5–5.0	8.4–9.0	–	2.2–2.5	2.2–2.5	Vietnam	Ky & Te (2007)
C. hungarica	*Proterorhinus marmoratus*	–	Elliptical	18.8 (18.5–19.5)	10.1 (10–10.5)	–	4.8 (4.5–5.0)	4.8 (4.5–5.0)	Hungary	Molnár (1992)
C. anguillae	*Anguilla anguilla*	–	Elongated	–	25–30	–	–	–	France	Tuzet & Ormiéres (1957)

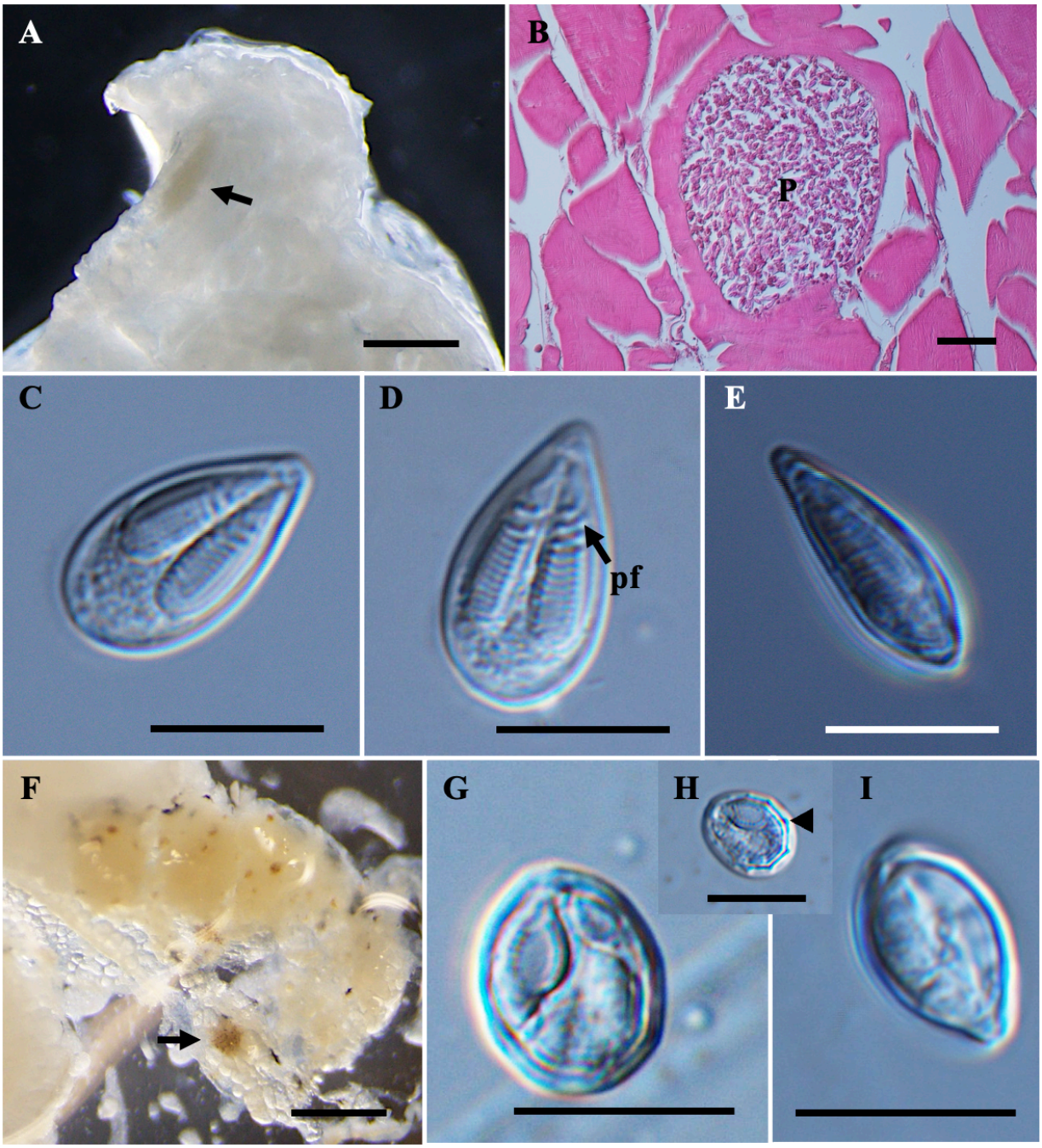

Figure S24. *Myxobolus* spp. from *Leptobarbus rubripinna* and *Barbodes binotatus*. A) Plasmodium (black arrow) of *Myxobolus* n. sp. 3 in formalin-fixed muscle tissue of *Leptobarbus rubripinna*. B) Histological transverse section of muscle cells showing an intracellular plasmodium (P) of *Myxobolus* n. sp. 3 within a (skeletal) muscle cell, stained with hematoxylin and eosin (H&E). C) Mature spore of *Myxobolus* n. sp. 3 in frontal view. D) Spore of *Myxobolus* n. sp. 3 showing two polar capsules with polar filaments (pf) and E) Spore in sutural view. F) Plasmodium (black arrow) of *Myxobolus* n. sp. 4 in ovary of *Barbodes binotatus*. G) Mature spore of *Myxobolus* n. sp. 4 in frontal view. H) Some spores exhibit six sutural markings (black triangle) and I) Spore in sutural view. Scale bars represent 10 µm, except (A, E) 500 µm and (B) 50 µm.

Table S24 Comparative data on spore measurements (mean ± standard deviation [SD], with ranges in parentheses) for *Myxobolus* n. sp. 3 from *Leptobarbus rubripinna* and species with blunt tapered anterior ends. All measurements are in µm. Abbreviations: SL spore length, SW spore width, ST spore thickness, PCL polar capsule length, PCW polar capsule width, PFC polar filament coils, – no data.

							Large		Small			
pecies	Host	Site infection	SL	SW	ST	PCL	PCW	PFC	PCL	PCW	PFC	Reference
***Myxobolus* n. sp. 3**	***Leptobarbus rubripinna***	**Muscle**	**16.2 ± 0.5 (15.1–17.2)**	**8.9 ± 0.3 (8.5–9.7)**	**5.5 ± 0.4 (5.0–5.9)**	**10.6 ± 0.4 (10.0–11.4)**	**3.0 ± 0.2 (2.7–3.6)**	**11–12**	**10.0 ± 0.4 (9.1–10.7)**	**2.9 ± 0.2 (2.4–3.4)**	**13–14**	**Present study**
M. leptobarbi	*Leptobarbus hoevenii*	Muscle	16.0 ± 0.7 (14.8–17.0)	8.9 ± 0.3 (8.4–9.6)	5.1 ± 0.32 (5.5–6.5)	5.9 ± 0.9 (4.0–7.2)	3.4 ± 0.6 (3.0–3.7)	13–15	9.9 ± 0.7 (8.8–10.6)	3.0 ± 0.4 (2.3–3.6)	13–15	Székely et al. (2009b)
M. catlae	*Cirrhinus cirrhosus*	Gill lamellae	17.1 ± 0.5 (16.6–17.6)	6.6 ± 0.05 (6.5–6.7)	5.4 ± 0.5 (4.8–6.0)	10.4 ± 0.5 (8.4–11.2)	2.5 ± 0.1 (2.5–2.6)	11–15	9.9 ± 0.6 (8.4–10.6)	2.4 ± 0.1 (2.3–2.4)	11–15	Székely et al. (2015b)
M. dajiangensis	*Cyprinus carpio*	Gill lamellae	14.8 ± 0.4 (13.9–15.6)	8.0 ± 0.5 (7.3–9.1)	5.5	8.0 ± 0.4 (7.1–8.8)	2.5 ± 0.2 (2.0–3.2)	9–11	7.4 ± 0.4 (6.1–8.0)	2.5 ± 0.2 (2.0–3.2)	9–11	Wang et al. (2022)
M. koi	*Leptobarbus rubripinna*	Gallbladder, kidney	14.6 (12.0–16.0)	7.5 (6.0–9.0)	5.9 (5.5–6.5)	10.2 (8.0–12.0)	2.6 (2.5–3.0)	–	–	–	13–15	Thumvittayakul et al. (2018)
M. koi	*C. carpio*	Gill lamellae	15.4 (14.5–16.5)	8.3 (7.1–9.0)	–	10.1 (9.0–10.9)	3.1 (2.5–3.5)	–	–	–	9–11	Camus & Griffin (2010)
M. tanakai	*C. carpio*	Gill filaments	17.2 (15.4–18.6)	6.8 (6.3–8.4)	6.3 (5.9–6.8)	8.7 (7.6–9.4)	2.4 (2.0–2.7)	–	–	–	8–10	Kato et al. (2017)
M. myleus	*Myleus rubripinnis*	Bile	19.3 ± 0.5 (19.0–20.0)	8.3 ± 0.5 (7.5–9.0)	4.0 ± 0.3 (3.5–4.5)	13.2 ± 0.4 (12.5–13.5)	3.0 ± 0.3 (2.5–3.5)	–	–	–	19–21	Azevedo et al. (2012)
M. maculatus	*Metynnis maculatus*	Kidney	21.0 (19.7–23.0)	8.9 (7.9–9.5)	7.5 (7.2–7.9)	12.7 (11.8–13.8)	3.2 (3.0–3.6)	–	–	–	14–15	Casal et al. (2002)

Table S25 Comparative data on spore measurements (mean ± standard deviation [SD], with ranges in parentheses) for *Myxobolus* n. sp. 4, *Myxobolus* n. sp. 12, and species with unequal polar capsules. All measurements are in µm. Abbreviations: SL spore length, SW spore width, ST spore thickness, PCL polar capsule length, PCW polar capsule width, PFC polar filament coils, SM sutural marking, – no data.

Species	Host	Site infection	SL	SW	ST	Large			Small			SM	Reference
						PCL	PCW	PFC	PCL	PCW	PFC		
***Myxobolus* n. sp. 4**	***Barbodes binotatus***	**Ovary**	**10.7 ± 0.4 (10.0–11.4)**	**8.3 ± 0.3 (7.8–8.9)**	**6.2 ± 0.3 (5.9–6.8)**	**4.8 ± 0.4 (4.0–5.8)**	**2.8 ± 0.2 (2.4–3.4)**	**6–7**	**2.7 ± 0.3 (2.1–3.1)**	**1.6 ± 0.2 (1.3–1.9)**	**4**	**8–10**	**Present study**
***Myxobolus* n. sp. 12**	***Osteochilus waandersii***	**Muscle**	**10.0 ± 0.3 (9.5–10.5)**	**7.7 ± 0.2 (7.2–8.3)**	**5.6 ± 0.2 (5.3–5.9)**	**4.5 ± 0.3 (3.7–5.2)**	**2.6 ± 0.2 (2.2–3.1)**	**6**	**2.5 ± 0.3 (1.8–3.0)**	**1.5 ± 0.1 (1.2–1.8)**	**3–4**	**6–8**	**Present study**
M. pavlovskii	*Hypophthalmichthys molitrix*	Gill filaments	(9.0–12.0)	(8.5–9.0)	(7.0–8.0)	(4.0–6.0)	(2.0–3.0)	–	(2.0–3.0)	(1.6–2.3)	3–4	–	Lucký (1978)
M. iwagiensis	*Oryzias latipes*	Brain tissue	12.1 ± 0.4 (11.3–12.8)	9.8 ± 0.3 (9.1–10.5)	7.9 ± 0.2 (7.5–8.2)	6.4 ± 0.2 (5.9–6.9)	4.0 ± 0.2 (3.4–4.4)	6–8	5.8 ± 0.3 (5.3–6.5)	3.5 ± 0.2 (3.1–4.0)	4–6	–	Kawano et al. (2025)
M. csabai	*Osteochilus hasselti*	Kidney	12.9 ± 0.5 (12.1–14.0)	8.6 ± 0.4 (8.2–9.6)	5.0 ± 0.4 (4.7–5.6)	6.1 ± 0.2 (6.4–6.8)	3.8 ± 0.1 (3.7–4.0)	6	3.6 ± 0.5 (3.3–4.8)	2.3 ± 0.3 (2.0–2.9)	6	–	Székely et al. (2009a)
M. acutus	*C. auratus auratus*	Gills, kidney	13.6 ± 0.9 (11.4–15.3)	10.2 ± 0.9 (7.5–12.8)	7.6 ± 0.6 (6.9–8.3)	6.2 ± 0.4 (5.1–7.5)	3.8 ± 0.4 (2.8–4.7)	5–8	2.7 ± 0.4 (1.7–3.7)	1.4 ± 0.4 (0.9–1.9)	2–3	–	Shi et al. (2022)
M. calbasui	*C. mrigala, C. reba*	Intestine, liver	13.8 ± 0.4 (13.0–14.6)	9.8 ± 0.6 (8.8–10.7)	7.3 ± 0.2 (6.7–7.8)	5.2 ± 0.3 (4.6–6.0)	3.4 ± 0.2 (3.1–3.9)	5–6	2.7 ± 0.2 (2.3–3.0)	1.8 ± 0.3 (1.3–2.3)	3–4	–	Chaudhary et al. (2024)
M. nekrasovae	*C. auratus gibelio*	Gill arch	13.8 ± 0.4 (12.2–15.0)	9.7 ± 0.2 (8.5–10.7)	6.7 ± 0.1 (6.0–7.6)	6.3 ± 0.1 (5.4–7.4)	3.4 ± 0.04 (3.1–4.0)	7	2.8 ± 0.1 (2.1–3.5)	1.4 ± 0.03 (1.0–1.6)	4	–	Batueva et al. (2023b)
M. paratypicus	*H. molitrix*	Gill filaments	13.8 (12.9–14.9)	9.9 (9.2–11.1)	7.0	7.5 (6.2–8.2)	5.0 (4.2–5.6)	7–8	2.7 (2.1–3.6)	1.4 (1.1–1.9)	–	–	Xi et al. (2019)
M. tauricus	*Barbus barbus, Luciobarbus bocagei*	Pin bones and fins	14.0 ± 0.5 (13.4–15.4)	10.2 ± 0.6 (8.8–11.0)	8.4 ± 0.1 (8.2–8.6)	7.2 ± 0.5 (6.6–7.8)	3.9 ± 0.4 (3.2–4.2)	6–7	5.3 ± 0.4 (5.0–5.9)	3.1 ± 0.3 (2.5–3.7)	5	–	Molnár et al. (2012)
M. shuifuensis	*Cirrhinus mrigala*	Kidney	15.6 ± 0.8 (13.9–17.1)	11.4 ± 0.5 (10.3–12.3)	7.9 ± 0.3 (7.5–8.5)	6.5 ± 0.3 (5.8–7.7)	4.0 ± 0.2 (3.5–4.6)	8–10	5.8 ± 0.3 (5.1–6.6)	3.5 ± 0.1 (3.1–3.8)	6–9	–	Zhang et al. (2023c)

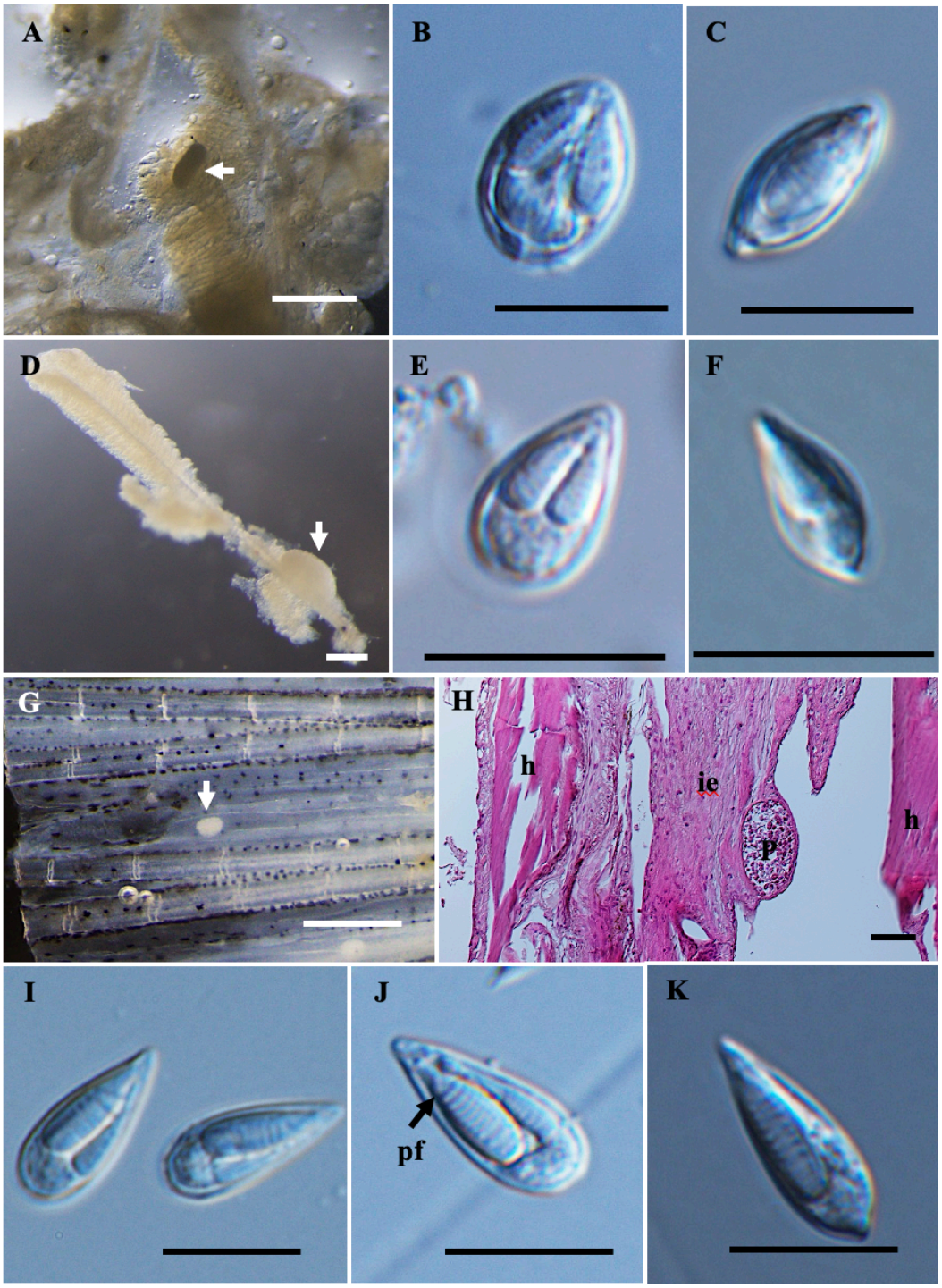

Figure S25. *Myxobolus* spp. from *Labiobarbus leptocheilus*. A) Plasodium (white arrow) of *Myxobolus* n. sp. 5 in a formalin-fixed gill arch membrane. B) Mature spore of *Myxobolus* n. sp. 5 in frontal view and C) Spore in sutural view. D) Plasmodium (white arrow) of *Myxobolus* n. sp. 6 attached to the gill filament. E) Mature spore of *Myxobolus* n. sp. 6 in frontal view and F) Spore in sutural view. G) Plasmodium (white arrow) of *Myxobolus* n. sp. 7 located in the loose connective tissue between bony rays. H) Histological longitudinal section showing the plasmodium (P) in the interlepidotrichial region (ie), adjacent to the hemisegments (h) of the fin rays, stained with hematoxylin and eosin (H&E). I) Mature spore of *Myxobolus* n. sp. 7 in frontal view. J) Spore of *Myxobolus* n. sp. 7 showing two polar capsules with polar filaments (pf) and K) Spore in sutural view. Scale bars represent 10 µm, except (A) 1 mm, (D) 200 µm, (G) 500 µm and (H) 50 µm.

Table S26 Comparative data on spore measurements (mean ± standard deviation [SD], with ranges in parentheses) for *Myxobolus* n. sp. 5 from *Labiobarbus leptocheilus* and morphologically similar species**.** All measurements are in µm. Abbreviations: SL spore length, SW spore width, ST spore thickness, PCL polar capsule length, PCW polar capsule width, PFC polar filament coils, – no data.

Species	Host	Site infection	SL	SW	ST	PCL	PCW	PFC	Reference
***Myxobolus* n. sp. 5**	***Labiobarbus leptocheilus***	**Connective tissue of gill arch**	**12.0 ± 0.3 (11.4–12.5)**	**7.8 ± 0.3 (7.4–8.4)**	**5.6 ± 0.3 (5.1–6.0)**	**6.0 ± 0.3 (5.3–6.7)**	**2.7 ± 0.2 (2.2–3.1)**	**7**	**Present study**
M. paludinosus	*Barbus paludinosus*	Gill lamellae	12.0 ± 0.87 (11.2–13.7)	8.6 ± 0.75 (7.5–10.0)	–	5.7 ± 0.88 (5.0–6.8)	2.4 ± 0.21 (2.0–2.5)	6–7	Reed et al. (2002)
M. aureus	*Salminus brasiliensis*	Liver	12.6 ± 0.5	8.3 ± 0.3	5.5 ± 0.3	5.7 ± 0.3	2.9 ± 0.2	7–8	Carriero et al. (2013)
M. iecoris	*Salminus franciscanus*	Liver	12.8 ± 0.8 (11.4–14.2)	8.7 ± 0.6 (7.7–9.9)	6.9 ± 0.4 (6.5–7.5)	5.9 ± 0.5 (4.9–7.4)	3.0 ± 0.2 (2.3–3.5)	8–9	Naldoni et al. (2019)
M. pyramidis	*Cyprinus langsdorfii*	Gill filaments	11.0 (9.9–11.7)	10.3 (9.4–11.1)	6.9 (6.5–7.4)	5.9 (5.3–6.9)	3.6 (2.9–4.0)	5–7	Kato et al. (2017)
M. curimatae	*Prochilodus costatus*	Gill filaments	13.2 ± 0.9 (12.0–14.7)	9.7 ± 1.0 (7.0–10.8)	–	5.2 ± 0.5 (4.1–5.8)	2.5 ± 0.5 (1.7–3.9)	9–10	Zatti et al. (2015)
M. tribolodonus	*Pseudaspius sachalinensis*	Gill filaments	9.2 (8.7–9.6)	7.0 (6.5–7.5)	–	5.1 (4.6–6.0)	1.9 (1.7–2.1)	4–5	Sekiya et al. (2024)
M. rangelli	*Pimelodus ornatus*	Heart	8.0 ± 0.2	5.8 ± 0.4	3.4 ± 0.3	3.6 ± 0.3	1.2 ± 0.2	6–7	da Silva et al. (2023)

Table S27 Comparative data on spore measurements (mean ± standard deviation [SD], with ranges in parentheses) for *Myxobolus* n. sp. 6 from *Labiobarbus leptocheilus* and morphologically similar species. All measurements are in µm. Abbreviations: SL spore length, SW spore width, ST spore thickness, PCL polar capsule length, PCW polar capsule width, PFC polar filament coils, – no data.

Species	Host	Site infection	SL	SW	ST	Large			Small			Reference
						PCL	PCW	PFC	PCL	PCW	PFC	
***Myxobolus* n. sp. 6**	***Labiobarbus leptocheilus***	**Gill filaments**	**8.8 ± 0.3 (8.3–9.5)**	**5.0 ± 0.3 (4.5–5.4)**	**3.9 ± 0.2 (3.6–4.2)**	**4.6 ± 0.2 (4.0–5.2)**	**1.7 ± 0.2 (1.3–2.0)**	**6–7**	**4.3 ± 0.3 (3.5–4.8)**	**1.5 ± 0.2 (1.1–1.9)**	**5–6**	**Present study**
M. imparfinis	*Imparfinis mirini*	Gill filaments	7.9 ± 0.3 (7.1–8.4)	5.5 ± 0.5 (4.5–6.2)	3.7 ± 0.3 (3.1–4.2)	3.9 ± 0.3 (3.4–4.5)	1.7 ± 0.1 (1.4–2.0)	6–7	3.4 ± 0.2 (3.1–3.8)	1.5 ± 0.2 (1.2–1.8)	6–7	Vieira et al. (2018)
M. filamentum	*Brycon orthotaenia*	Gill filaments	9.0 ± 0.3 (7.5–9.7)	6.2 ± 0.4 (5.2–7.3)	5.3 ± 0.3 (4.8–5.7)	6.3 ± 0.1 (5.4–7.4)	4.7 ± 0.3 (3.8–5.5)	10–11	–	–	–	Naldoni et al. (2015)
M. carlhubbsi	*Luxilus chrysocephalus isolepis*	Gill filaments	12.7 ± 0.4 (12.0–13.4)	6.1 ± 0.3 (5.0–6.6)	5.4 ± 0.3 (5.1–6.0)	6.4 ± 0.3 (5.7–7.3)	2.1 ± 0.2 (1.8–2.3)	6–11	6.2 ± 0.3 (5.2–6.8)	2.2 ± 0.1 (1.8–2.5)	6–11	McAllister et al. (2023)
M. tambroides	*Tor tambroides*	Gill lamellae	9.9 ± 0.4 (8.8–10.6)	7.4 ± 0.2 (6.8–7.9)	7.2 ± 0.3 (7.0–7.9)	5.7 ± 0.7 (5.0–7.0)	2.6 ± 0.1 (2.4–2.9)	5–6	–	–	–	Székely et al. (2012)
M. nyongana	*Barbus poechii*	Gill lamellae	11.2 ± 0.2 (11.0–11.2)	6.5 ± 0.3 (6.1–7.0)	–	4.4 ± 0.7 (3.0–5.5)	1.6 ± 0.4 (1.2–2.5)	7	–	–	–	Reed et al. (2002)
M. oliveirai	*B. hilarii*	Gill filaments	11.2 ± 0.4	7.4 ± 0.5	4.6 ± 0.6	5.6 ± 0.2	2.3 ± 0.2	6–8	–	–	–	Milanin et al. (2010)
M. dujardini	*Leuciscus cephalus*	Gill filaments	11.5 ± 0.4 (11.0–12.0)	7.4 ± 0.5 (6.5–8.0)	7.1 ± 0.4 (6.5–7.3)	5.5 ± 0.4 (5.0–6.0)	2.3 ± 0.4 (2.0–3.0)	6	–	–	–	Molnár et al. (2006c)
M. etsatsaensis	*Barbus thamalakanensis*	Gill filaments	13.0 ± 0.9 (12.8–15.0)	6.8 ± 0.6 (6.2–8.0)	–	7.5 ± 0.3 (7.0–8.0)	2.3 ± 0.4 (1.2–2.5)	7–8	–	–	–	Reed et al. (2002)
M. kalavatiae	*Labeo rohita*	Gills	12.1 ± 0.3 (11.4–12.7)	6.3 ± 0.2 (5.8–6.7)	5.2 ± 0.1 (4.9–5.4)	5.4 ± 0.2 (4.9–5.7)	1.6 ± 0.09 (1.5–1.8)	5	–	–	–	Chaudhary et al. (2024)
M. koi	*Cyprinus carpio*	Gills	15.4 (14.5–16.5)	8.3 (7.1–9.0)	–	10.1 (9.0–10.9)	3.1 (2.5–3.5)	9–811	–	–	–	Camus & Griffin (2010)
M. bilobus	*Notemigonus crysoleucas*	Gill filaments	21.0 ± 0.6 (20.0–22.1)	8.4 ± 0.5 (7.5–9.3)	6.0	10.8 ± 0.7 (9.2–12.0)	2.7 ± 0.2 (2.2–3.6)	7–9	10.1± 0.7 (9.1–11.0)	2.8 ± 0.2 (2.4–3.2)	7–9	Cone et al. (2005)

Table S28 Comparative data on spore measurements (mean ± standard deviation [SD], with ranges in parentheses) for *Myxobolus* n. sp. 7 from *Labiobarbus leptocheilus* and species with unequal polar capsules. All measurements are in µm. Abbreviations: SL spore length, SW spore width, ST spore thickness, PCL polar capsule length, PCW polar capsule width, PFC polar filament coils, – no data.

Species	Host	Site infection	SL	SW	ST	Large			Small			Reference
						PCL	PCW	PFC	PCL	PCW	PFC	
***Myxobolus* n. sp. 7**	***Labiobarbus leptocheilus***	**Fin rays**	**14.2 ± 0.4 (13.5–14.9)**	**5.8 ± 0.2 (5.5–6.4)**	**4.6 ± 0.4 (4.0–5.3)**	**9.1 ± 0.3 (8.6–9.9)**	**2.7 ± 0.2 (2.3–3.2)**	**8–10**	**8.0 ± 0.5 (7.1–9.0)**	**1.7 ± 0.1 (1.4–1.9)**	**6**	**Present study**
M. zoohuri	*C. mrigala*	Gill lamellae	14.9 ± 1.1 (13.2–17.3)	6.3 ± 0.5 (4.9–7.0)	–	11.1 ± 0.5 (10.4–12.0)	2.7 ± 0.2 (2.2–3.6)	17–18	10.6 ± 0.4 (10.1–11.2)	2.7 ± 0.3 (2.0–3.0)	15–16	Majumder et al. (2015)
M. pseudoacinosus	*Cyprinus carpio*	Gill filaments	15.9 ± 0.5 (15.1–17.0)	5.5 ± 0.5 (5.0–6.3)	–	7.7 ± 0.5 (6.7–8.7)	3.5 ± 0.3 (3.0–4.1)	7–8	3.2 ± 0.2 (2.5–3.5)	0.9 ± 0.1 (0.7–1.0)	2–3	Tan et al. (2022)
M. ginbuna	*Carassius langsdorfii*	Gill filaments	12.5 (11.7–13.9)	9.2 (8.5–9.8)	–	7.0 (6.6–7.6)	2.9 (2.7–3.2)	8–9	6.7 (6.1–7.1)	2.9 (2.4–3.4)	8–9	Kato et al. (2017)
M. sonarpurensis	*L. bata*	Gill lamellae	12.1 ± 0.9 (11.0–13.2)	6.7 (5.9–6.1)	–	8.8	3.0	–	7.7	3.1	–	Ghosh & Bandyopadhyay (2017)
M. elongatum	*Labeo bata*	Gill lamellae	16.2 ± 2.8 (13.0–17.6)	7.9 (7.0–9.0)	–	8.8 (7.0–10.0)	3.4 (3.0–4.0)	–	6.5 (6.0–7.0)	3.4 (3.0–4.0)	–	Ghosh & Bandyopadhyay (2017)
M. orissae	*C. mrigala*	Gill lamellae	17.3 ± 1.0 (15.6–19.7)	6.7 ± 0.7 (5.7–9.3)	–	8.8 ± 3.9 (6.8–13.5)	1.9 ± 0.9 (1.4–3.1)	–	7.4 ± 3.2 (6.9–11.5)	1.6 ± 0.7 (1.7–2.4)	–	Abraham et al. (2015)
M. carnaticus	*Cirrhinus mrigala*	Gill lamellae	9.4 ± 0.9 (8.1–12.9)	8.0 ± 0.62 (7.2–10.0)	–	3.0 (2.2–4.4)	2.0 (1.1–3.4)	9	2.7 (2.0–4.6)	1.9 (1.3–3.1)	8	Banerjee et al. (2015)
M. axelrodi	*Paracheirodon axelrodi*	Brain and retina	20.5 ± 0.7 (19.0–21.8)	6.6 ± 0.5 (5.7–7.9)	5.1 ± 0.4 (4.8–5.9)	9.9 ± 0.8 (8.0–11.2)	3.8 ± 0.3 (3.2–4.8)	15–17	4.1 ± 0.3 (3.5–4.5)	2.0 ± 0.1 (1.8–2.3)	5–6	Camus et al. (2017)

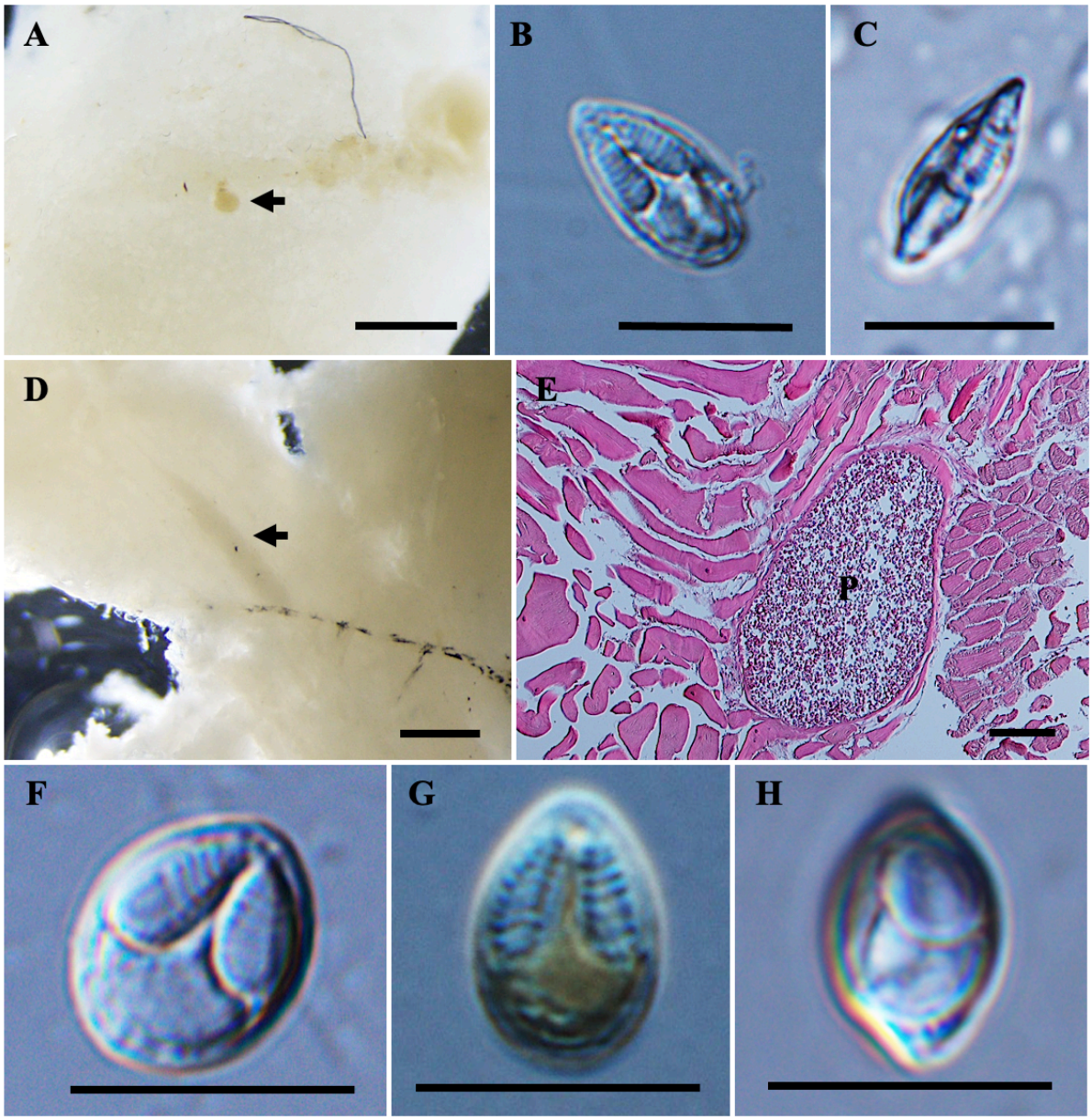

Figure S26. *Myxobolus* spp. from *Labiobarbus leptocheilus*. A) Plasmodium (black arrow) of *Myxobolus* n. sp. 8 in formalin-fixed ovary. B) Mature spore of *Myxobolus* n. sp. 8 in frontal view and C) Spore in sutural view. D) Plasmodium (black arrow) of *Myxobolus* n. sp. 9 in formalin-fixed muscle tissue. E) Histological transverse section of muscle cells showing an intracellular plasmodium (P) of *Myxobolus* n. sp. 9 within a (skeletal) muscle cell, stained with hematoxylin and eosin (H&E). F) Mature spore of *Myxobolus* n. sp. 9 in frontal view. G) Spore showing the two polar capsules with six coils and H) Spore in sutural view. Scale bars represent 10 µm, except (A) 1 mm, (D) 200 µm, (G) 500 µm and (H) 50 µm.

Table S29 Comparative data on spore measurements (mean ± standard deviation [SD], with ranges in parentheses) for *Myxobolus* n. sp. 8 from *Labiobarbus leptocheilus* and morphologically similar species**.** All measurements are in µm. Abbreviations: SL spore length, SW spore width, ST spore thickness, PCL polar capsule length, PCW polar capsule width, PFC polar filament coils, – no data.

Species	Host	Site infection	SL	SW	ST	PCL	PCW	PFC	Reference
***Myxobolus* n. sp. 8**	***Labiobarbus leptocheilus***	**Ovaries**	**11.3 ± 0.5 (10.4–12.5)**	**6.2 ± 0.5 (5.2–6.9)**	**4.7 ± 0.3 (4.1–5.2)**	**4.6 ± 0.4 (3.7–5.3)**	**1.6 ± 0.2 (1.4–2.1)**	**6**	**Present study**
M. marajoensis	*Rhamdia quelen*	Intestine	10.9 (10.0–11.6)	5.1 (4.2–5.4)	–	5.3 ± 0.6	1.6 ± 0.3	–	Abrunhosa et al. (2017)
M. paranensis	*Salminus maxillosus*	Testes, ovaries	(12.0–15.0)	(7.0–8.0)	–	(6.0–7.0)	2.5	8–11	Bonetto & Pignalberi (1965)
M. aculeatus	*Macrognathus aculeatus*	Ovaries	13.0 ± 0.4 (11.5–14.0)	6.4 ± 0.3 (6.0–7.2)	5.3 ± 0.2 (4.9–5.6)	4.5 ± 0.2 (3.5–4.7)	2.4 ± 0.1 (2.3–2.6)	5–6	Xu et al. (2025)
M. miyarii	*Silurus asotus*	Intestine	13.3 ± 0.4 (12.5–14.7)	6.6 ± 0.2 (6.2–7.4)	5.0 ± 0.2 (4.4–5.7)	6.5 ± 0.3 (6.2–7.5)	1.9 ± 0.1 (1.5–2.3)	8–9	Liu et al. (2016d)
M. ompok	*Ompok pabdah*	Kidney	14.4 ± 0.4 (13.6–14.4)	6.5 ± 0.3 (5.6–6.4)	5.9 ± 0.4 (5.2–6.4)	8.2 ± 0.2 (8.0–8.5)	1.8 ± 0.3 (1.5–2.4)	6	Chaudhary et al. (2018)
M. batalhensis	*Salminus hilarii*	Ovaries	15.2 ± 0.8 (14.0–15.4)	8.5 ± 0.5 (8.0–8.7)	5.2 ± 0.3 (5.0–5.2)	5.2 ± 0.3 (5.0–5.5)	2.8 ± 0.2 (2.6–3.0)	6–9	Vieira et al. (2017)
M. pharyngeus	*Gambusia affinis*	Branchial cavity epithelium	16.2 ± 0.7 (14.6–17.6)	6.8 ± 0.6 (5.4–7.6)	5.0 (4.9–5.0)	7.3 ± 0.4 (6.3–8.3)	2.1 ± 0.2 (1.4–2.6)	7–9	Stilwell et al. (2021)

Table S30 Comparative data on spore measurements (mean ± standard deviation [SD], with ranges in parentheses) for *Myxobolus* n. sp. 9, *Myxobolus* n. sp. 13, and morphologically similar species. All measurements are in µm. Abbreviations: SL spore length, SW spore width, ST spore thickness, PCL polar capsule length, PCW polar capsule width, PFC polar filament coils, – no data.

Species	Host	Site infection	SL	SW	ST	PCL	PCW	PFC	Reference
***Myxobolus* n. sp. 9**	***Labiobarbus leptocheilus***	**Muscle**	**10.1 ± 0.4 (9.4–10.8)**	**7.9 ± 0.5 (6.8–8.7)**	**5.7 ± 0.3 (6.0–6.3)**	**5.2 ± 0.3 (4.7–5.7)**	**2.6 ± 0.2 (2.1–3.1)**	**8**	**Present study**
M. talievi	*Cyphocottus eurystomus*	Muscle	10.9 ± 0.07 (10.2–11.9)	9.4 ± 0.07 (8.8–10.3)	7.3 ± 0.1 (6.9–7.6)	4.8 ± 0.1 (4.9–5.5)	2.9 ± 0.1 (2.6–3.3)	4	Batueva & Burdukovskaya (2022)
M. muscularis	*Chelon ramada*	Skeletal, heart muscle	9.1 ± 0.6 (8.0–10.0)	7.0 ± 0.6 (6.0–8.7)	5.2 ± 0.3 (4.7–6.0)	4.3 ± 0.3 (4.0–5.0)	2.7 ± 0.2 (2.0–3.3)	5–6	Rocha et al. (2019d)
M. cuneus	*Piaractus mesopotamicus*	Skeletal muscle, kidney	8.9 ± 0.3	5.7 ± 0.3	–	4.3 ± 0.3	1.9 ± 0.1	7–8	Manrique et al. (2016)
M. sheyangensis	*Carassius auratus gibelio*	Gill lamellae	11.0 ± 0.3 (10.5–11.9)	10.2 ± 0.2 (9.2–10.7)	6.3 ± 0.2 (5.9–6.9)	5.5 ± 0.3 (4.5–6.1)	3.4 ± 0.2 (2.9–4.0)	7–8	Liu et al. (2016e)
M. meijiangensis	*Carassius auratus*	Gill lamellae	11.0 ± 0.4 (10.4–11.6)	10.3 ± 0.3 (9.6–11.0)	–	5.6 ± 0.6 (4.5–6.4)	3.5 ± 0.5 (2.4–4.1)	8–9	Zhang et al. (2023d)
M. intimus	*Leuciscus idus*	Gill lamellae	11.5 ± 0.5 (10.8–12.6)	8.4 ± 0.6 (7.2–9.0)	7.0 ± 0.3 (6.5–7.6)	6.1 ± 0.5 (5.8–6.8)	3.3 ± 0.2 (3.0–3.6)	6	Cech et al. (2012)
M. tasikkenyirensis	*Osteochilus vittatus*	Muscle	12.8 ± 0.7 (11.8–13.8)	9.2 ± 0.5 (8.3–9.9)	6.0 (5.5–6.5)	6.4 ± 0.4 (5.9–7.2)	3.0 ± 0.2 (2.7–3.4)	5–6	Székely et al. (2009a)
***Myxobolus* n. sp. 13**	***Osteochilus waandersii***	**Muscle**	**12.9 ± 0.4 (12.1–13.8)**	**9.1 ± 0.4 (8.0–9.9)**	**6.4 ± 0.5 (5.8–6.6)**	**6.5 ± 0.5 (5.3–7.6)**	**3.0 ± 0.2 (2.5–3.5)**	**10**	**Present study**
M. osteochili	*Osteochilus hasselti*	Kidney	13.0 ± 0.6 (12.0–14.0)	8.7 ± 0.4 (8.0–9.0)	5.0 ± 0.4 (4.5–5.5)	6.6 ± 0.5 (6.0–7.0)	2.4 ± 0.4 (2.0–3.0)	8–10	Székely et al. (2009a)

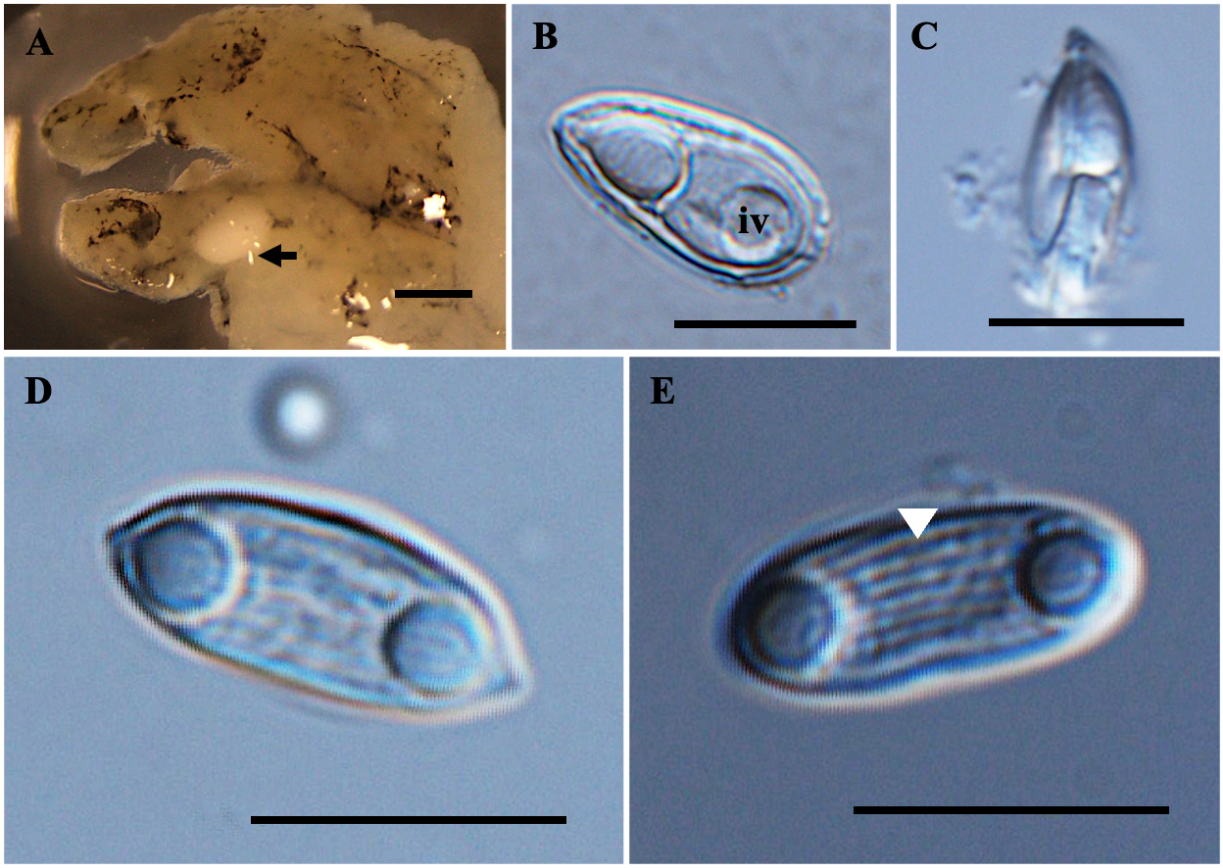

Figure S27. *Thelohanellus* and *Myxidium* species from *Labiobarbus leptocheilus*. A) Plasmodium (black arrow) of *Thelohanellus* n. sp. 1 in formalin-fixed skin. B) Mature spore of *Thelohanellus* n. sp. 1 in frontal view with the presence of an iodinophilous vacuole (iv) within the sporoplasm and C) Spore in sutural view. D) Dispersed mature spore of *Myxidium* n. sp. 1 observed in the gallbladder. E) *Myxidium* n. sp. 1 showing the six valvular striations (white triangle). Scale bars represent 10 µm, except (A) 1 mm.

Table S31 Comparative data on spore measurements (mean ± standard deviation [SD], with ranges in parentheses) for *Thelohanellus* n. sp. 1 from *Labiobarbus leptocheilus* and other *Thelohanellus* species infecting the skin. All measurements are in µm. Abbreviations: SL spore length, SW spore width, ST spore thickness, PCL polar capsule length, PCW polar capsule width, PFC polar filament coils, D diameter, – no data.

Species	Host	Site infection	SL	SW	ST	PCL	PCW	PFC	Reference
***Thelohanellus* n. sp. 1**	***Labiobarbus leptocheilus***	**Skin**	**16.0 ± 0.8 (14.1–17.8)**	**8.4 ± 0.5 (7.1–9.2)**	**6.7 ± 0.2 (6.4–7.0)**	**6.2 ± 0.6 (5.1–7.6)**	**4.1 ± 0.4 (3.3–4.6)**	**6**	**Present study**
T. leshanensis	*C. carpio haematopterus*	Skin, caudal fin	16.6 (14.8–18.4)	9.2 (8.8–9.6)	–	6.1 (5.6–7.2)	(4.2–4.5)	2–3	Zhao & Ma (1992)
T. indiana	*Carassius auratus*	Skin, gills, fins	13.8 (12.2–15.2)	8.0 (7.5–8.8)	–	6.8 (6.2–7.2)	4.0 (3.3–4.7)	–	Saha & Bandyopadhyay (2018a)
T. testudineus	*C. auratus gibelio*	Skin	19.7 ± 0.7 (18.6–20.8)	7.6 ± 0.4 (6.6–8.4)	7.3 ± 0.5 (6.6–8.8)	11.1 ± 0.5 (10.0–11.9)	5.3 ± 0.3 (4.3–5.8)	7–8	Liu et al. (2014b)
T. kanjalensis	*Catla catla*	Skin	11.67	6.6	–	7.5	3.3	–	Singh & Kaur (2012a)
T. pekingensis	*Cyprinus carpio haematopterus*	Skin, kidney	22.3 (20.4–24.0)	10.8 (9.5–11.8)	8.2 (7.2–8.4)	10.5 (8.4–13.2)	7.4 (6.6–8.4)	7–8	Chen & Ma (1998)
T. parasagittarius	*C. carpio haematopterus, C. auratus*	Skin, gills, gallbladder	23.7 (22.8–24.6)	11.4 (10.2–12.0)	–	12.1 (11.8–13.2)	8.3 (7.8–9.6)	6–7	Chen & Ma (1998)
T. wuhanensis	*Carassius auratus gibelio*	Skin	24.5 (21.9–26.9)	13.7 (11.4–15.5)	11.8 (10.8–14.1)	11.5 (9.6–12.8)	9.1 (8.1–10.3)	7–10	Xiao & Chen (1993)

Table S32 Comparative data for spore measurements (mean value ± standard deviation [SD] followed by the range in parentheses) of *Myxidium* n. sp. 1, *Myxidium* n. sp. 3, and species with similar morphologies. All measurements are in µm. Abbreviations: SL spore length, SW spore width, ST spore thickness, PCL polar capsule length, PCW polar capsule width, PFC polar filament coils, VS valvular striations, – no data.

Species	Host	Site infection	SL	SW	ST	PCL	PCW	PFC	VS	Reference
***Myxidium* n. sp. 1**	***Labiobarbus leptocheilus***	**Gallbladder**	**12.5 ± 0.6 (11.4–14.1)**	**5.1 ± 0.4 (4.4–5.8)**	**4.3 ± 0.4 (3.4–4.7)**	**3.3 ± 0.3 (2.6–3.7)**	**2.7 ± 0.2 (2.1–3.1)**	**4–5**	**6–7**	**Present study**
M. spinibarba	*Myxocyprinus asiaticus*	Gallbladder	12.6 ± 0.5 (11.6–13.4)	5.9 ± 0.5 (5.1–6.9)	–	3.5 ± 0.3 (2.6–4.2)	2.8 ± 0.2 (2.3–3.2)	4–5	8–10	Xiang et al. (2021)
M. horatioense	*Ameiurus natalis*	Gallbladder	12.2 ± 0.8 (10.8–12.6)	4.7 ± 0.4 (4.2–5.4)	–	3.0 ± 0.3 (2.4–3.6)	2.9 ± 0.3 (2.6–3.8)	3–4	6–7	McAllister et al. (2025)
M. hemiculteri	*Hemiculter leucisculus*	Gallbladder	12.1 (11.5–13.0)	6.9 (5.6–7.2)	–	3.1 (3.0–3.2)	3.4 (3.2–4.0)	–	4–5	Chen & Ma (1998)
M. chuatsi	*Siniperca chuatsi*	Gallbladder	10.7 ± 0.4 (10.0–11.4)	5.7 ± 0.3 (5.4–6.1)	5.8 ± 0.3 (5.4–6.1)	3.2 ± 0.2 (2.9–3.7)	2.8 ± 0.1 (2.6–3.2)	4–5	6–8	Yin et al. (2025)
M. whippsi	*Esox niger*	Gallbladder	8.7 (7.7–9.8)	5.1 (4.3–6.0)	–	2.5 (2.2–3.2)	2.4 (2.0–2.7)	3–5	5	McAllister et al. (2022)
***Myxidium* n. sp. 3**	***Channa gachua***	**Gallbladder**	**13.4 ± 0.4 (12.5–14.4)**	**6.5 ± 0.4 (5.7–7.3)**	**5.5 ± 0.3 (4.8–6.4)**	**4.1 ± 0.3 (3.5–4.8)**	**3.3 ± 0.2 (2.9–3.7)**	**4**	**7**	**Present study**
M. schilba	*Schilbe mystus*	Gallbladder	13.7 (12.7–14.9)	5.6 (4.9–6.1)	–	4.3 (3.0–4.9)	2.9 (2.0–3.4)	4	–	Eiras et al. (2011)
M. onyhosionmatis	*Varicorhinus simus*	Gallbladder	13.9 (13.6–14.4)	6.5 (6.0–7.2)	5.7 (5.0–6.0)	4.0 (3.9–4.0)	2.4 (2.3–2.4)	–	6–7	Chen & Ma (1998)
M. asiaticum	*M. asiaticus*	Gallbladder	14.4 ± 0.5 (13.4–15.5)	7.6 ± 0.5 (6.5–8.4)	6.7 ± 0.2 (6.3–7.0)	3.8 ± 0.2 (3.4–4.2)	3.0 ± 0.2 (2.7–3.4)	4–5	–	Lom & Dyková (2006)

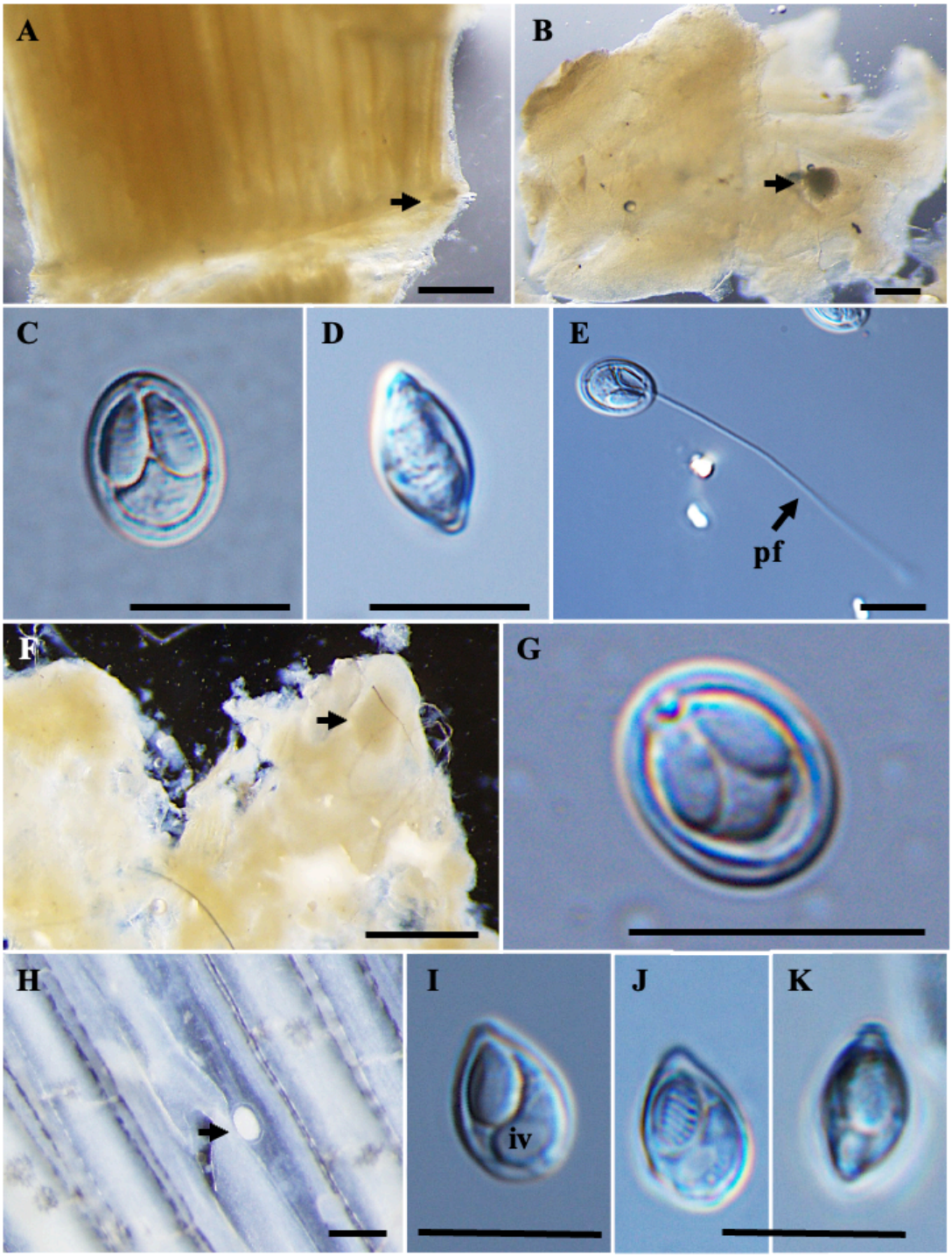

Figure S28. *Myxobolus* and *Thelohanellus* species from *Osteochilus waandersii*. A) Plasmodium (black arrow) of *Myxobolus* n. sp. 10 in formalin-fixed A) gill tissue and B) heart tissue. C) Mature spore of *Myxobolus* n. sp. 10 in frontal view. D) Spore in sutural view and E) Spores releasing the polar tubules (pf). F) Plasmodium (black arrow) of *Myxobolus* n. sp. 11 in formalin-fixed gill cartilage and G) Mature spore *Myxobolus* n. sp. 11. H) Plasmodium (black arrow) of *Thelohanellus* n. sp. 2 located in the loose connective tissue between bony rays. I) Mature spore of *Thelohanellus* n. sp. 2 in frontal view with the presence of an iodinophilous vacuole (iv) within the sporoplasm. J) Spore showing the polar capsule with seven coils and K) Spore in sutural view. Scale bars represent 10 µm, except (A, F) 500 µm and (B, H) 200 µm.

Table S33 Comparative data on spore measurements (mean ± standard deviation [SD], with ranges in parentheses) for *Myxobolus* n. sp. 10 from *Osteochilus waandersii* and other *Myxobolus* species infecting the gills**.** All measurements are in µm. Abbreviations: SL spore length, SW spore width, ST spore thickness, PCL polar capsule length, PCW polar capsule width, PFC polar filament coils.

Species	Host	Site infection	SL	SW	ST	PCL	PCW	PFC	Reference
***Myxobolus* n. sp. 10**	***Osteochilus waandersii***	**Cartilage of gill arch, bulbus arteriosus of heart**	**10.5 ± 0.6 (9.4–11.8)**	**8.3 ± 0.3 (7.4–8.9)**	**5.6 ± 0.4 (4.8–6.2)**	**5.3 ± 0.3 (4.6–5.8)**	**2.7 ± 0.2 (2.1–3.0)**	**7–8**	**Present study**
M. intrachondrealis	*Cyprinus carpio*	Gill cartilage	10.2 (9.0–11.0)	6.5 (6.0–7.0)	4.0 (3.7–4.2)	4.5 (3.7–4.7)	2.2 (2.0–2.6)	9–11	Molnár (2000)
M. lamellobasis	*Blicca bjoerkna*	Gill lamellae	10.1 ± 0.5 (9.1–10.8)	9.7 ± 0.5 (8.6–10.5)	5.5 ± 0.3 (5.2–6.1)	4.7 ± 0.2 (4.4–5.0)	3.3 ± 0.5 (2.7–4.8)	6	Molnár et al. (2014)
M. branchoipecten	*Moxostoma duquesnei*	Cartilage of gill raker	9.1 ± 0.7 (8.0–11.0)	7.6 ± 0.7 (6.0–9.0)	5.8 ± 0.4 (5.0–6.0)	4.4 ± 0.5 (4.0–6.0)	2.5 ± 0.5 (2.0–3.0)	6–8	Ksepka & Bullard (2021)
M. cataractae	*Imparfinis mirini*	Gill filaments	7.8 ± 0.4 (7.1–8.9)	5.9 ± 0.4 (5.1–6.6)	3.9 ± 0.3 (3.4–4.4)	3.5 ± 0.2 (3.0–3.9)	1.7 ± 0.2 (1.3–2.1)	6–7	Vieira et al. (2022)
M. xiaoi	*Notropis cornutus*	Cartilage of gill arch	11.0 (9.8–12.2)	8.5 (8.1–9.2)	6.0 (5.2–6.9)	4.8 (4.2–5.4)	2.8 (2.1–3.1)	5–7	Salim & Desser (2000)
M. branchiofilum	*Moxostoma duquesnei*	Gill lamellae	11.4 ± 0.5 (10.0–12.0)	10.2 ± 0.6 (9.0–11.0)	7.9 ± 0.6 (7.0–9.0)	5.1 ± 0.5 (4.0–6.0)	3.1 ± 0.4 (2.0–4.0)	5–7	Ksepka & Bullard (2021)
M. peleci	*Pelecus cultratus*	Cartilage of gill arch	12.1 ± 0.5 (11.6–13.2)	11.4 ± 1.0 (10.8–12.5)	5.8 ± 0.2 (5.6–6.0)	5.5 ± 0.2 (5.2–6.0)	3.2 ± 0.2 (2.8–3.4)	4–5	Borzák et al. (2016)
M. mucosus	*Leuciscus leuciscus*	Cartilage of gill arch	13.0 ± 0.8 (11.5–14.2)	10.8 ± 0.7 (10.2–11.5)	7.7 ± 0.5 (7.3–8.0)	5.6 ± 0.3 (5.1–6.2)	3.8 ± 0.2 (3.5–4.0)	5–6	Liu et al. (2016b)
M. bjoerknae	*Blicca bjoerkna*	Cartilage of gill arch	17.4 ± 0.8 (16.2–18.4)	13.1 ± 0.6 (11.9–13.9)	10.5 ± 0.5 (10.0–11.0)	6.7 ± 0.3 (6.3–7.4)	4.1 ± 0.2 (3.6–4.5)	6	Molnár et al. (2014)

Table S34 Comparative data on spore measurements (mean ± standard deviation [SD], with ranges in parentheses) for *Thelohanellus* n. sp. 2 from *Osteochilus waandersii* and other *Thelohanellus* species infecting the fins. All measurements are in µm. Abbreviations: SL spore length, SW spore width, ST spore thickness, PCL polar capsule length, PCW polar capsule width, PFC polar filament coils, D diameter, – no data.

Species	Host	Site infection	SL	SW	ST	PCL	PCW	PFC	Reference
***Thelohanellus* n. sp. 2**	***Osteochilus waandersii***	**Fin rays**	**9.4 ± 0.4 (8.8–10.4)**	**6.4 ± 0.3 (5.7–7.1)**	**5.3 ± 0.3 (4.5–5.8)**	**4.5 ± 0.2 (4.2–5.0)**	**2.8 ± 0.2 (2.5–3.2)**	**7**	**Present study**
T. goldi	*Carassius auratus*	Caudal fin	9.5 (8.7–10.2)	5.8 (4.1–7.8)	–	5.6 (4.9–7.6)	2.9 (2.3–3.1)	5–6	Saha & Bandyopadhyay (2018b)
T. boggoti	*Labeo dero*	Fins	8.3	4.7	–	4.7	3.9	7–9	Kaur & Gupta (2017)
T. assambai	*Labeo* sp.	Fins, gills	10.8 (9.0–12.0)	5.5 (5.0–7.0)	–	6.3 (5.0–7.6)	3.4 (3.0–4.0)	5–6	Fomena et al. (1994)
T. kalavatae	*Cirrhina reba*	Caudal fin	11.5	4.9	–	5.2	3.3	5–6	Singh & Kaur (2014)
T. globulosa	*C. reba*	Caudal fin	11.7 (11.1–12.3)	7.9 (7.6–8.2)	–	5.3 (4.8–5.8)	4.8 (4.3–5.3)	4–5	Singh & Kaur (2012b)
Thelohanellus sp. 3	*Labeo senegalensis*	Fins	13.0 (12.0–14.1)	9.3 (8.4–10.0)	–	6.3 (6.0–6.8)	3.5 (3.2–4.0)	–	Deli et al. (2025)
T. caudatus	*Labeo rohita*	Fins	13.7 ± 0.9 (12.3–14.6)	9.0 ± 0.8 (8.0–10.0)	6.8 ± 0.4 (6.2–7.3)	6.5 ± 0.4 (6.2–6.9)	4.7 ± 0.4 (4.2–5.0)	–	Székely et al. (2021)
T. habibpuri	*L. rohita*	Fins	13.8 ± 0.5 (13.0–14.3)	8.5 ± 0.0 (8.0–9.0)	–	6.0 ± 0.0 (6.0–6.5)	4.9 ± 0.0 (4.1–5.0)	3–4	Acharia & Dutta (2007)
T. gonionoti n. sp.	*Barbonymus gonionotus*	Fins	22.0 ± 0.7 (20.3–23.2)	9.9 ± 0.6 (8.1–10.8)	7.7 ± 0.5 (6.7–8.3)	9.1 ± 0.5 (8.2–10.1)	5.4 ± 0.3 (4.9–5.9)	8	Present study

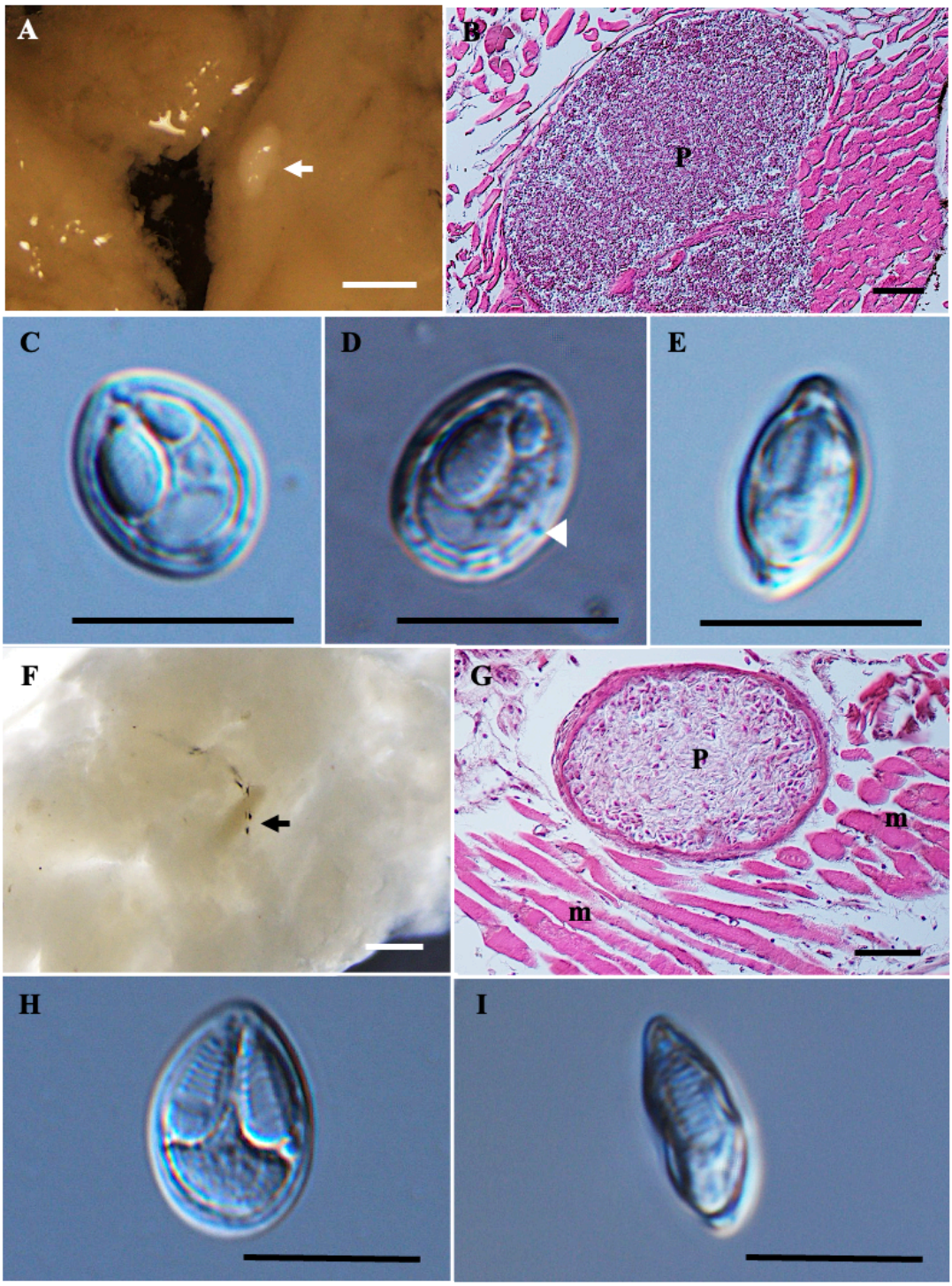

Figure S29. *Myxobolus* spp. from *Osteochilus waandersii*. A) Plasmodium (white arrow) of *Myxobolus* n. sp. 12 in formalin-fixed muscle tissue. B) Histological transverse section of muscle cells showing an intracellular plasmodium (P) of *Myxobolus* n. sp. 12 within a (skeletal) muscle cell, stained with hematoxylin and eosin (H&E). C) Mature spore of *Myxobolus* n. sp. 12 in frontal view. D) Spore exhibit eight sutural markings (white triangle) and E) Spore in sutural view. F) Plasmodium (black arrow) of *Myxobolus* n. sp. 13 in formalin-fixed muscle tissue. G) Histological longitudinal section of muscle cells showing plasmodia (P) located among (skeletal) muscle cells (m), stained with hematoxylin and eosin (H&E). H) Mature spore *Myxobolus* n. sp. 13 and I) Spore in sutural view. Scale bars represent 10 µm, except (A, F) 500 µm, (B) 100 µm and (G) 50 µm.

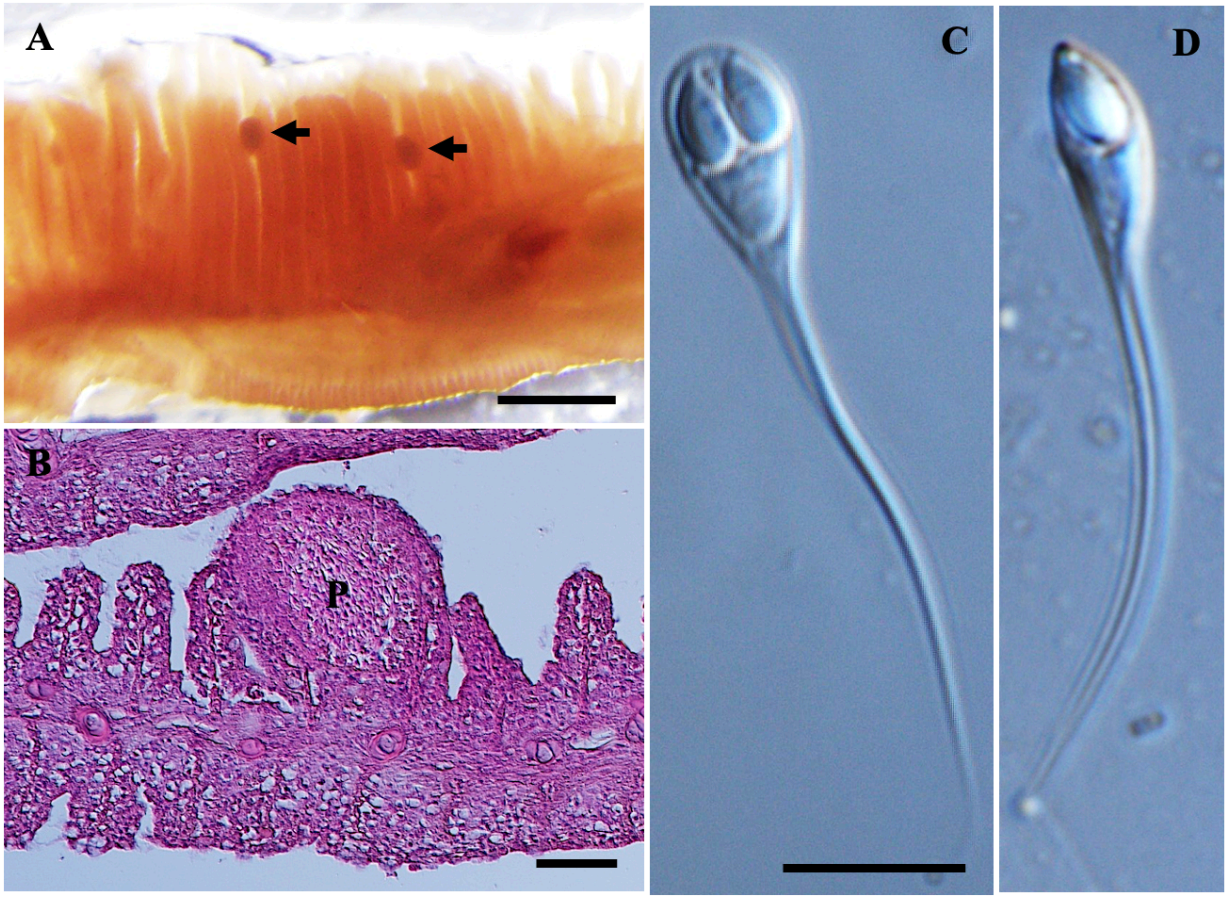

Figure S30. *Henneguya* species from the gills of *Trichopodus trichopterus*. A) Plasmodia (black arrow) of *Henneguya* n. sp. 1 observed in the formalin-fixed gill tissue. B) Histological transverse section of gill filament showing plasmodium (P) located between gill lamellae, stained with hematoxylin and eosin (H&E). C) Mature spore of *Henneguya* n. sp. 1 in frontal view. D) Spore in sutural view. Scale bars represent 10 µm, except (A) 1 mm and (B) 50 µm.

Table S35 Comparative data on spore measurements (mean ± standard deviation [SD], with ranges in parentheses) for *Henneguya* n. sp. 1 from *Trichopodus trichopterus* and other *Henneguya* species with blunt anterior ends**.** All measurements are in µm. Abbreviations: SL spore length, SW spore width, ST spore thickness, AL caudal appendage length, PCL polar capsule length, PCW polar capsule width, PFC polar filament coils, – no data.

Species	Host	Site infection	SL	SW	ST	AL	PCL	PCW	PFC	Reference
***Henneguya* n. sp. 1**	***Trichopodus trichopterus***	**Gill filaments**	**11.8 ± 0.5 (10.3–12.9)**	**6.8 ± 0.3 (6.3–7.5)**	**5.2 ± 0.2 (4.9–5.5)**	**36.7 ± 1.8 (33.1–39.5)**	**5.1 ± 0.3 (4.4–5.6)**	**2.6 ± 0.2 (2.2–3.1)**	**6–7**	**Present study**
Henneguya daoudi	*T. trichopterus*	Gills	12.3 ± 0.4 (11.4–12.8)	7.3 ± 0.3 (6.7–7.6)	5.3 ± 0.3 (4.7–5.7)	17.0 ± 2.0 (15.0–20.0)	5.9 ± 0.4 (5.2–6.2)	2.7 ± 0.3 (2.4–3.3)	6–7	Székely et al. (2009b)
H. schizura	*T. trichopterus*	Gills	(14.4–16.0)	8.0	–	40.0	(4.8–5.6)	1.6	4	Ky & Te (2007)
H. paraensis	*Cichla temensis*	Gill filaments	12.8 ± 0.4 (12.3–13.2)	8.6 ± 0.3 (8.1–8.9)	4.1 ± 0.1 (4.1–4.2)	29.5 ± 0.7 (28.7–30.2)	7.4 ± 0.1	2.6 ± 0.1	5–7	Velasco et al. (2016)
H. azevedoi	*Leporinus obtusidens*	Gill lamellae	10.0 ± 0.0 (9.9–10.2)	4.4 ± 0.4 (4.0–5.0)	–	35.6 ± 0.9 (34.9–36.5)	3.8 ± 0.3 (3.5–4.0)	1.0	6–7	Barassa et al. (2012)
H. ghaffari	*Lates niloticus*	Gill filaments, intestinal muscles	13.0 ± 0.6 (11.8–14.0)	7.5 ± 0.4 (6.9–7.9)	5.2 ± 0.5 (4.9–5.9)	43.2 (36.3–53.0)	5.2 ± 0.5 (4.8–5.9)	3.2 ± 0.3 (2.8–3.9)	4–5	Ali (1999)
H. jariensis	*Cichla monoculus*	Fins	13.4 ± 0.7 (11.9–14.6)	6.5 ± 0.5 (4.9–7.3)	–	33.1 ± 1.7 (30.2–37.0)	4.0 ± 0.3 (3.4–4.3)	2.0 ± 0.1 (1.7–2.4)	4	Zatti et al. (2018b)
H. voronini	*Lates calcarifer*	Base of the gill filaments	9.9 ± 0.3 (9.5–10.3)	6.8 ± 0.3 (6.3–7.3)	–	27.2 ± 1.4 (25.0–29.0)	3.7 ± 0.2 (3.5–4.0)	2.1 ± 0.1 (2.0–2.2)	6	Borkhanuddin et al. (2020b)
H. calcarifer	*L. calcarifer*	Skeletal muscles	9.4 ± 0.6 (8.3–10.0)	5.2 ± 0.3 (4.8–5.5)	3.8 ± 0.1 (3.7–4.0)	30.9 ± 3.0 (28.0–35.0)	3.4 ± 0.2 (3.1–3.7)	1.4 ± 0.2 (1.1–1.7)	6	Borkhanuddin et al. (2020b)
H. tapajoensis	*Cichla pinima*	Gill filaments	16.4 ± 1.2 (14.5–19.1)	7.0 ± 0.4 (5.7–9.3)	5.0 ± 0.1 (4.8–5.1)	39.0 ± 3.9 (31.7–46.5)	4.2 ± 0.5 (2.9–5.0)	2.1 ± 0.4 (1.5–2.8)	4–5	Zatti et al. (2018b)

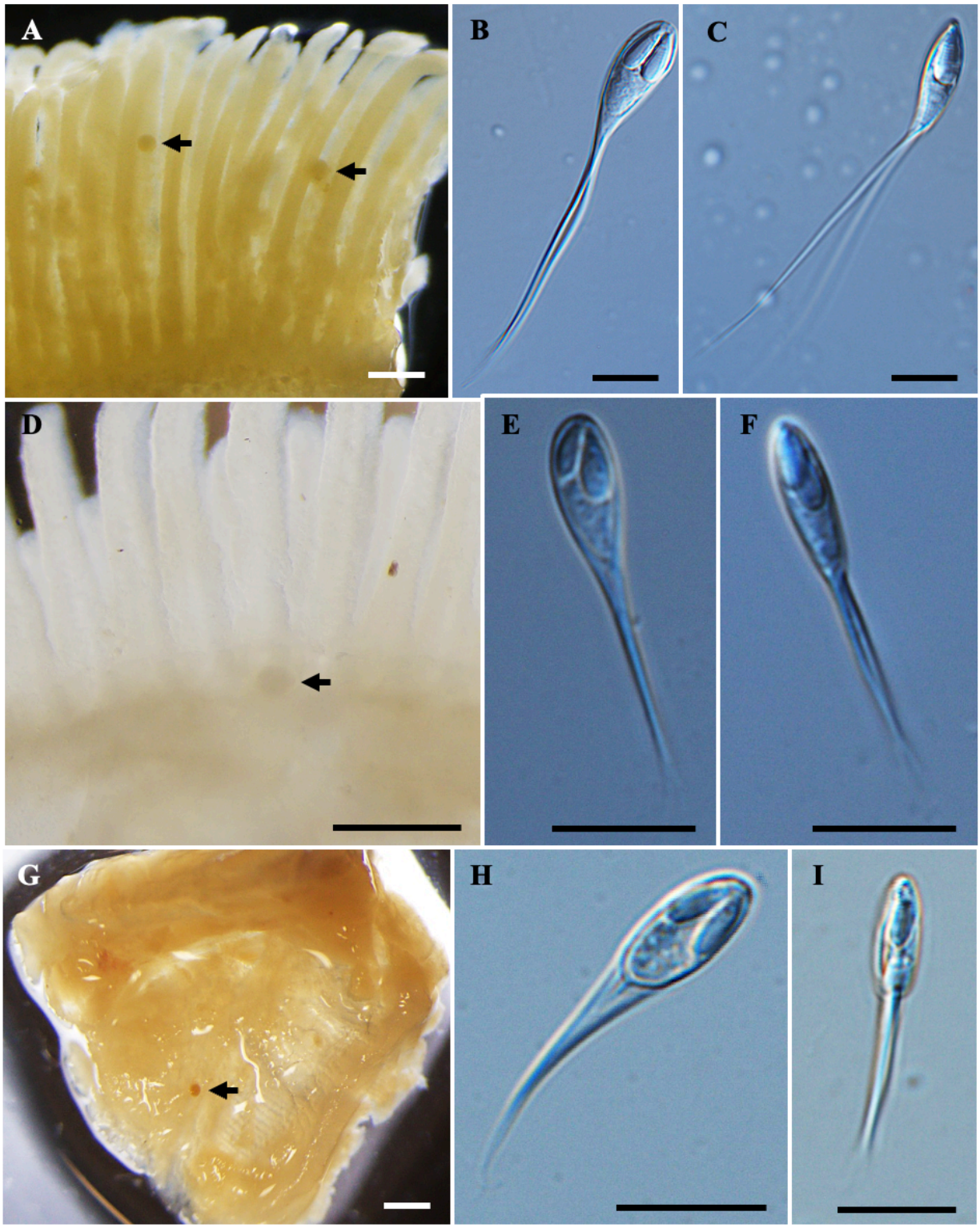

Figure S31. *Henneguya* spp. from the gills of *Trichopodus pectoralis*. A) Plasmodia (black arrow) of *Henneguya* n. sp. 2 developing within the gill lamellae of a formalin-fixed gill. B) Mature spore of *Henneguya* n. sp. 2 in frontal view and C) Spore in sutural view. D) Plasmodium (black arrow) of *Henneguya* n. sp. 3 embedded in the cartilaginous tissue of the gill arch. E) Mature spore of *Henneguya* n. sp. 3 in frontal view, showing unequal polar capsules and F) Spore of *Henneguya* n. sp. 3 in sutural view. G) Plasmodium (black arrow) of *Henneguya* n. sp. 4 located in the gill arch of a formalin-fixed specimen. H) Mature spore of *Henneguya* n. sp. 4 in frontal view and I) Spore of *Henneguya* n. sp. 4 in sutural view. Scale bars represent 10 µm, except (A, D, G) 500 µm.

Table S36 Comparative data on spore measurements (mean ± standard deviation [SD], with ranges in parentheses) for *Henneguya* n. sp. 2 from *Trichopodus pectoralis* and morphologically similar species. All measurements are in µm. Abbreviations: SL spore length, SW spore width, ST spore thickness, AL caudal appendage length, PCL polar capsule length, PCW polar capsule width, PFC polar filament coils, – no data.

Species	Host	Site infection	SL	SW	ST	AL	PCL	PCW	PFC	Reference
***Henneguya* n. sp. 2**	***Trichopodus pectoralis***	**Gill lamellae**	**19.4 ± 0.9 (17.5–20.9)**	**7.9 ± 0.5 (6.8–8.6)**	**5.3 ± 0.3 (4.7–5.8)**	**42.9 ± 2.2 (39.9–47.4)**	**7.7 ± 0.5 (6.5–8.6)**	**2.8 ± 0.2 (2.3–3.2)**	**10–12**	**Present study**
H. pungitii	*Pungitius tymensis*	Subcutis	18.4 (16.7–20.6)	5.2 (4.7–5.7)	–	39.8 (36.2–45.5)	8.2 (6.7–9.0)	2.3 (2.1–2.6)	–	Sokolov et al. (2015)
H. suprabranchiae	*Clarias gariepinus*	Gill cartilage	17.2 ± 0.5 (16.2–18.2)	6.0 ± 0.5 (5.0–6.3)	–	23.2 ± 1.4 (22.2–25.8)	7.5 ± 0.0 (7.5)	1.9 ± 0.0 (1.9)	9	Reed et al. (2003)
H. schulmani	*Anabas testudineus*	Gills	(16.8–20.4)	(4.8–6.0)	(3.6–4.2)	–	(8.0–10.2)	1.4–2.1	–	Ky (1971)
H. tietensis	*Prochilodus lineatus*	Gill filaments	16.2 ± 1.1 (15.0–16.9)	5.5 ± 0.1 (5.4–5.6)	3.8 ± 0.3 (3.7–4.2)	39.0 ± 2.0 (35.2–39.7)	7.3 ± 0.2 (7.1–7.5)	1.7 ± 0.2 (1.3–1.7)	11–13	Vieira et al. (2021)
Henneguya sp.	*Prochilodus lineatus*	Gill lamellae	12.5 (11.2–15.3)	4.8 (4.0–5.1)	3.6 (3.0–4.0)	37.1 (32.0–45.9)	5.8 (5.1–7.1)	2.0 (1.5–2.0)	–	Pavanelli et al. (1998)
H. nyongensis	*Marcusenius moori, Gnathonemus petersii*	Gill lamellae, skeletal muscle	11.2 ± 0.7 (9.6–12.3)	4.3 ± 0.2 (4.0–4.7)	3.3 ± 0.2 (3.0–3.6)	21.0 ± 1.5 (18.4–24.3)	4.7 ± 0.2 (4.2–5.2)	1.4 ± 0.1 (1.3–1.6)	5–6	Stilwell et al. (2019)
H. ganapatiae	*Notopterus notopterus*	Gills	9.7 ± 0.4 (9.3–10.0)	4.5 ± 0.5 (4.0–4.8)	–	30.9 ± 3.0 (28.0–35.0)	3.3 ± 0.2 (2.6–3.2)	1.6 ± 0.1 (1.4–1.8)	–	Borkhanuddin et al. (2020a)

Table S37 Comparative data on spore measurements (mean ± standard deviation [SD], with ranges in parentheses) for *Henneguya* n. sp. 3 from *Trichopodus pectoralis* and other *Henneguya* species with unequal polar capsules**.** All measurements are in µm. Abbreviations: SL spore length, SW spore width, ST spore thickness, AL caudal appendage length, PCL polar capsule length, PCW polar capsule width, PFC polar filament coils, – no data.

							Large		Small		
Species	Host	Site infection	SL	SW	ST	AL	PCL	PCW	PCL	PCW	References
***Henneguya* n. sp. 3**	***Trichopodus pectoralis***	**Cartilaginous tissue of gill arch**	**11.9 ± 0.6 (10.0–13.8)**	**4.7 ± 0.3 (4.0–5.2)**	**3.7 ± 0.2 (3.4–4.1)**	**19.1 ± 1.4 (16.9–22.3)**	**5.3 ± 0.4 (4.3–6.2)**	**2.0 ± 0.2 (1.6–2.2)**	**3.9 ± 0.4 (3.1–4.5)**	**1.6 ± 0.1 (1.3–1.8)**	**Present study**
H. gilbert	*Cyphocharax gilbert*	Gills	12.0 ± 0.7 (11.0–13.2)	5.3 ± 0.3 (4.9–5.5)	3.6 ± 0.2 (3.4–3.8)	16.8 ± 0.9 (15.6–18.5)	5.5 ± 0.3 (5.1–5.7)	1.3 ± 0.2 (1.1–1.5)	4.0 ± 0.5 (3.5–4.5)	1.3 ± 0.2 (1.1–1.5)	Casal et al. (2017)
Henneguya sp.	*Channa aurantimaculata*	Liver, spleen	12.1 ± 0.9 (10.1–14.7)	7.1 ± 0.6 (5.3–8.5)	4.4 ± 0.6	15.1 ± 1.2	6.1 ± 0.5 (5.1–7.4)	2.5 ± 0.4 (1.6–3.9)	6.0 ± 0.4 (5.2–6.4)	2.5 ± 0.3 (1.7–3.1)	Uma et al. (2025)
H. nagelii	*Cyphocharax nagelli*	Gills	12.1 ± 0.5 (11.2–11.9)	(4.9 ± 0.3 (4.4–5.5)	4.1 ± 0.2 (3.6–5.7)	22.4 ± 4.0 (14.7–27.3)	4.9 ± 0.4 (4.0–5.9)	1.8 ± 0.2 (1.5–2.2)	5.2 ± 0.4 (4.6–6.0)	1.8 ± 0.2 (1.5–2.2)	de Azevedo et al. (2013)
H. cyphocharax	*Cyphocharax gilbert*	Gills	11.3 (7.7–13.4)	4.4 (2.9–6.3)	–	23.7 (20.8–31.5)	5.2 (4.2–6.3)	1.9 (1.5–2.3)	4.5 (3.4–5.2)	1.7 (1.3–2.2)	Abdallah et al. (2007)
H. correai	*Semaprochilodus insignis*	Connective tissue in fins	14.4 ± 1.6 (12.4–20.5)	4.0 ± 0.6 (2.7–5.3)	3.1 ± 0.4 (2.7–3.6)	33.7 ± 4.5 (26.4–45.2)	7.2 ± 0.8 (5.2–8.3)	1.5 ± 0.3 (1.0–2.2)	5.6 ± 0.7 (4.0–6.3)	1.4 ± 0.2 (1.0–1.8)	Müller et al. (2023)
H. postexilis	*Ictalurus punctatus*	Gill lamellae	15.5 (12.1–17.2)	4.1 ± 0.3 (3.6–4.8)	3.5 (2.9–3.8)	31.2 ± 4.6 (25.7–38.1)	5.9 ± 0.6 (4.4–6.7)	1.4 ± 0.1 (1.1–1.6)	5.6 ± 0.5 (4.4–6.4)	1.4 ± 0.1 (1.1–1.6)	Woodyard et al. (2022)
H. sutherlandi	*Ictalurus punctatus*	Skin	15.4 ± 1.5 (12.2–19.3)	5.5 ± 0.6 (4.5–6.8)	4.7 ± 0.2 (4.2–5.0)	50.5 ± 8.3 (34.8–71.4)	6.1 ± 0.8 (4.0–7.9)	1.7 ± 0.3 (1.0–2.2)	–	–	Griffin et al. (2008)

Table S38 Comparative data on spore measurements (mean ± standard deviation [SD], with ranges in parentheses) for *Henneguya* n. sp. 4 and *Henneguya* n. sp. 5 from *Trichopodus pectoralis* and morphologically similar species. All measurements are in µm. Abbreviations: SL spore length, SW spore width, ST spore thickness, AL caudal appendage length, PCL polar capsule length, PCW polar capsule width, PFC polar filament coils, – no data.

Species	Host	Site infection	SL	SW	ST	AL	PCL	PCW	PFC	Reference
***Henneguya* n. sp. 4**	***Trichopodus trichopterus***	**Gill arch**	**10.9 ± 0.4 (10.3–11.7)**	**4.9 ± 0.3 (4.3–5.5)**	**4.0 ± 0.3 (3.7–4.7)**	**17.0 ± 1.1 (15.2–18.9)**	**5.0 ± 0.2 (4.6–5.4)**	**1.6 ± 0.1 (1.4–1.9)**	**–**	**Present study**
***Henneguya* n. sp. 5**	***Trichopodus trichopterus***	**Pharynx**	**11.8 ± 0.5 (10.9–12.7)**	**4.9 ± 0.3 (4.3–5.5)**	**4.0 ± 0.3 (3.6–4.5)**	**15.4 ± 0.9 (14.0–17.0)**	**5.9 ± 0.3 (5.5–6.5)**	**1.8 ± 0.2 (1.4–2.2)**	**4**	**Present study**
H. corruscans	*Pseudoplatystoma corruscans*	Gill lamellae	14.3 (13.0–15.0)	5.0	4.0	13.7 (12.0–15.0)	6.8 (6.0–7.0)	2.0	5–6	Eiras et al. (2009)
H. tchangi	*Schizotorax davidi*	Urinary bladder	10.9 (9.2–11.6)	7.6 (7.2–7.6)	7.7 (7.0–8.0)	16.2 (15.6–19.2)	4.9 (3.6–5.6)	3.2 (2.4–4.0)	–	Chen & Ma (1998)
H. hemibagri	*Mystus macropterus*	Gills	13.2 (12.8–14.0)	4.3 (4.0–6.0)	3.1 (2.8–3.7)	13.0 (12.0–14.4)	4.0 (2.8–4.8)	1.9 (1.6–2.4)	–	Chen & Ma (1998)
H. schizodon	*Schizodon fasciatum*	Kidney	(12.0–14.0)	(3.0–4.0)	–	(15.0–17.0)	(5.0–6.0)	(1.0–1.5)	8–10	Eiras et al. (2004)
H. cuniculator	*P. corruscans*	Gill filaments	12.1 ± 1.0 (10.0–14.7)	4.8 ± 0.4 (4.0–5.9)	4.2 ± 0.7 (3.9–4.9)	16.7 ± 2.0 (12.3–19.4)	6.2 ± 0.3 (5.2–6.2)	1.8 ± 0.1 (1.4–1.9)	10–11	Naldoni et al. (2014)
H. camerounensis	*Synodontis batesi*	Gills	10.2 (9.0–11.0)	4.4 (3.8–5.5)	–	–	5.3 (4.6–5.7)	1.3 (1.0–2.0)	–	Eiras (2002)
H. multiplasmodialis	*P. corruscans*	Gill arch	14.7 ± 0.5	5.2 ± 0.3	4.4 ± 0.1	15.4 ± 1.3	6.1 ± 0.1	1.4 ± 0.1	6–7	Adriano et al. (2012)
H. paramormyropsi	*Paramormyrops kingsleyae*	Gills, eyes, kidney	11.9 (10.7–12.8)	4.5 (3.9–5.9)	–	17.3 (14.0–20.3)	5.0 (4.2–5.0)	1.5 (1.2–1.9)	3–4	Benoît et al. (2020)

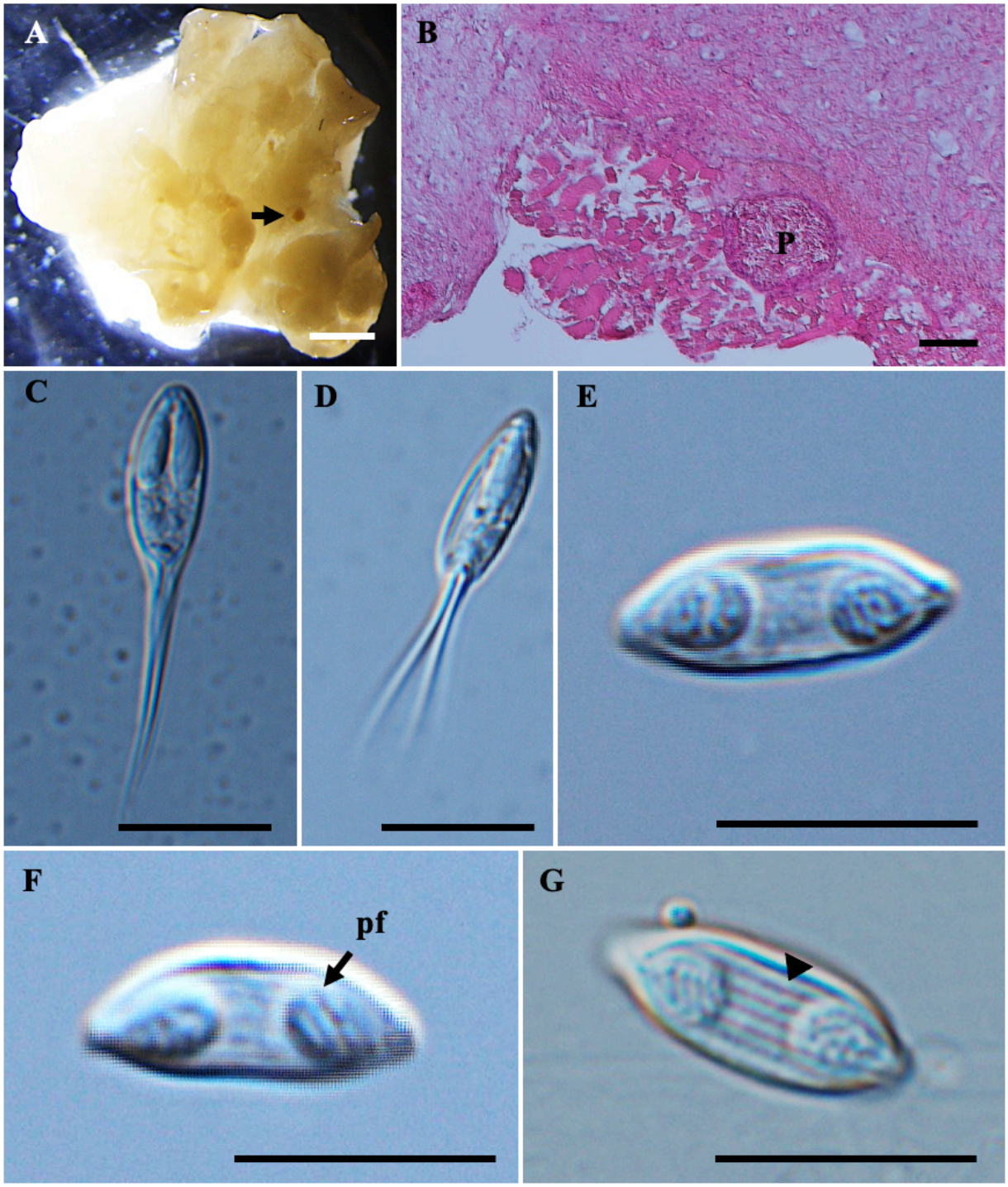

Figure S32. *Henneguya* and *Myxidium* species from *Trichopodus pectoralis*. A) Plasmodium (black arrow) of *Henneguya* n. sp. 5 located in the pharynx of a formalin-fixed specimen. B) Histological transverse section of the pharynx, showing the plasmodium (P) embedded within the stratified epithelial tissue, stained with hematoxylin and eosin (H&E). C) Mature spore of *Henneguya* n. sp. 5 in frontal view and (D) Spore of *Henneguya* n. sp. 5 in sutural view. E) Dispersed mature spore of *Myxidium* n. sp. 2 observed in the gallbladder. (F) Spore of *Myxidium* n. sp. 2 with polar capsules containing four polar filament coils and (G) Spore of *Myxidium* n. sp. 2 showing six valvular striations (black triangle). Scale bars represent 10 µm, except (A) 1 mm and (B) 50 µm.

Table S39 Comparative data for spore measurements (mean value ± standard deviation [SD] followed by the range in parentheses) of *Myxidium* n. sp. 2 from *Trichopterus pectoralis* and species with similar morphologies. All measurements are in µm. Abbreviations: SL spore length, SW spore width, ST spore thickness, PCL polar capsule length, PCW polar capsule width, PFC polar filament coils, VS valvular striations, – no data.

Species	Host	Site infection	SL	SW	ST	PCL	PCW	PFC	VS	Reference
***Myxidium* n. sp. 2**	***Trichopterus pectoralis***	**Gallbladder**	**11.7 ± 0.6 (10.8–12.5)**	**4.4 ± 0.3 (3.9–4.8)**	**3.8 ± 0.3 (3.1–4.3)**	**3.8 ± 0.3 (2.7–4.5)**	**2.7 ± 0.2 (2.3–3.0)**	**5–6**	**6**	**Present study**
M. macrocheili	*Catostomus macrocheilus*	Gallbladder	11.7 (10.0–14.4)	6.6 (5.5–8.0)	6.3 (5.5–8.0)	4.0 (3.0–5.5)	3.5 (2.0–4.5)	4–5	9–10	Mitchell (1967)
M. phyllium	*Gambusia affinis*	Gallbladder	11.0	8.0	–	3.0	3.0	–	–	Davis (1917)
M. cuneiforme	*Cyprinus carpio*	Gallbladder	12.5 ± 0.3 (12.0–13.1)	5.4 ± 0.3 (4.8–6.1)	–	4.3 ± 0.2 (4.0–4.6)	3.1 ± 0.2 (2.6–3.4)	5–6	6–8	Li et al. (2016)
M. pseudocuneiforme	*C. carpio*	Gallbladder	12.5 ± 0.3 (12.0–13.1)	5.4 ± 0.3 (4.8–6.1)	5.2 ± 0.4 (4.9–6.2)	3.9 ± 0.2 (3.5–4.2)	2.5 ± 0.1 (2.5–2.8)	5–6	6–8	Chen et al. (2021)
M. rhodei	*Barbatula barbatula*	Kidney	13.7 ± 0.6 (12.5–14.8)	5.4 ± 0.4 (4.6–5.9)	–	4.0 ± 0.4 (3.2–4.9)	3.1 ± 0.3 (2.6–3.6)	5	9–13	Baiko et al. (2024)
M. fonti	*Heterandria formosa*	Gallbladder	13.7 ± 0.1 (13.0–14.2)	6.5 ± 0.1 (5.4–7.2)	6.4 ± 0.1 (6.1–6.7)	4.3 (3.6–4.9)	3.6 (3.2–4.4)	4–6	9–12	Whipps et al. (2025b)
M. cf. notopterum	*Notopterus notopterus*	Gallbladder	14.7 ± 0.6 (13.8–16.0)	6.3 ± 0.6 (5.5–7.7)	–	5.7 ± 0.4 (4.6–6.4)	4.7 ± 0.4 (3.6–5.3)	3–4	8–10	Borkhanuddin et al. (2020a)
Myxidium sp.	*Noturus nocturus*	Gallbladder	14.8 ± 1.1 (13.8–16.2)	8.7 ± 1.1 (6.5–9.7)	–	4.9 ± 0.5 (4.3–5.7)	4.9 ± 0.5 (4.3–5.7)	4–6	7–8	McAllister et al. (2024)
M. djolonensis	*Paramormyrops kingsleyae*	Gallbladder, urinary bladder	16.3 (15.5–18.0)	6.1 (5.0–7.1)	–	4.9 (4.0–5.6)	3.5 (3.0–4.2)	5–7	7–9	Benoît et al. (2020)

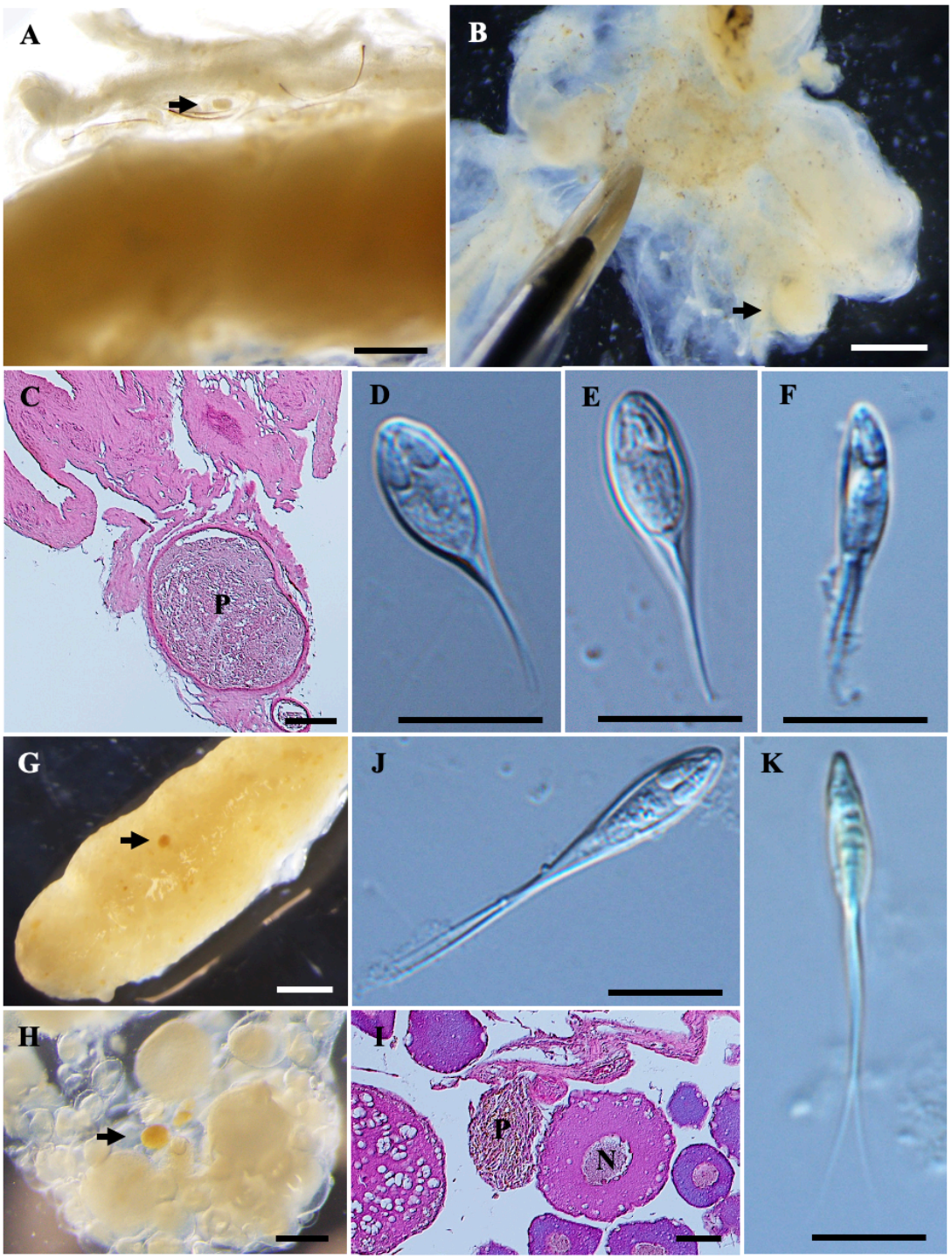

Figure S33. *Henneguya* spp. from *Channa gachua*. Plasmodium (black arrow) of *Henneguya* n. sp. 6 located at the A) serous membrane of a formalin-fixed intestine and B) kidney. C) Histological longitudinal section of the serosa membrane from the intestine, showing the plasmodium (P) embedded within the serosa membrane, stained with hematoxylin and eosin (H&E). D–E) Mature spore of *Henneguya* n. sp. 6 in frontal view and (F) Spore of *Henneguya* n. sp. 6 in sutural view. G–H) Plasmodium (black arrow) of *Henneguya* n. sp. 7 located in the formalin-fixed ovary. I) Histological longitudinal section of the ovary, showing the plasmodium (P) enclosed in the fibrous connective tissue surrounded by healthy oocytes with nucleus (N), stained with hematoxylin and eosin (H&E). J) Mature spore of *Henneguya* n. sp. 7 in frontal view and (K) Spore of *Henneguya* n. sp. 7 in sutural view. Scale bars represent 10 µm, except (A, B) 500 µm, (C) 100 µm, (G) 1 mm, (H) 200 µm and (I) 50 µm.

Table S40 Comparative data on spore measurements (mean ± standard deviation [SD], with ranges in parentheses) for *Henneguya* n. sp. 6 and *Henneguya* n. sp. 10 from *Channa gachua* and other *Henneguya* species with oval-shaped spore. All measurements are in µm. Abbreviations: SL spore length, SW spore width, ST spore thickness, AL caudal appendage length, PCL polar capsule length, PCW polar capsule width, PFC polar filament coils, – no data.

Species	Host	Site infection	SL	SW	ST	AL	PCL	PCW	PFC	Reference
***Henneguya* n. sp. 6**	***Channa gachua***	**Serous membrane of internal organs**	**10.6 ± 0.5 (9.6–11.4)**	**5.2 ± 0.3 (4.5–6.0)**	**4.0 ± 0.1 (3.9–4.1)**	**14.0 ± 1.6 (10.3–16.7)**	**3.4 ± 0.3 (2.6–3.9)**	**1.3 ± 0.1 (1.2–1.7)**	**–**	**Present study**
H. lacustris	*Astyanax lacustris*	Gill lamellae	10.4 ± 1.6 (9.2–12.1)	4.9 ± 0.9 (4.3–5.8)	–	7.2 ± 2.5 (6.2–9.9)	4.8 ± 0.3 (4.5–5.1)	1.5 ± 0.2 (1.4–1.5)	6–7	Vieira et al. (2020)
***Henneguya* n. sp. 10**	***Channa gachua***	**Muscle**	**11.1 ± 0.6 (10.2–12.9)**	**5.8 ± 0.5 (4.7–6.6)**	**4.1 ± 0.5 (3.2–5.4)**	**12.8 ± 2.0 (8.6–16.7)**	**4.0 ± 0.4 (3.3–4.6)**	**1.2 ± 0.2 (0.9–1.6)**	**–**	**Present study**
H. guanduensis	*Hoplosternum littorale*	Gills	14.6 (11.4–16.7)	6.5 (4.9–7.9)	4.0	19.0 (15.6–22.5)	4.4 (3.3–5.6) 4.1 (3.3–5.3)	2.0 (1.6–2.3) 2.2 (1.5–2.8)	3–6	Abdallah et al. (2007)
H. caquetaia	*Caquetaia spectabilis*	Opercula, fins, eyes	20.5 ± 3.9 (15.0–27.0)	7.9 ± 1.0 (6.2–10.8)	6.7 ± 2.5 (6.0–7.6)	20.5 (14.4–32.3)	4.3 ± 0.6 (3.3–5.4)	2.1 ± 0.3 (1.3–2.8)	–	Figueredo et al. (2023)

Table S41 Comparative data on spore measurements (mean ± standard deviation [SD], with ranges in parentheses) for *Henneguya* n. sp. 7 and *Henneguya* n. sp. 9 from *Channa gachua* and other *Henneguya* species with lanceolate-shaped spore. All measurements are in µm. Abbreviations: SL spore length, SW spore width, ST spore thickness, AL caudal appendage length, PCL polar capsule length, PCW polar capsule width, PFC polar filament coils, – no data.

Species	Host	Site infection	SL	SW	ST	AL	PCL	PCW	PFC	Reference
***Henneguya* n. sp. 9**	***Channa gachua***	**Gills**	**12.5 ± 0.5 (11.3–13.3)**	**4.6 ± 0.4 (3.6–5.3)**	**3.8 ± 0.1 (3.7–3.9)**	**25.3 ± 1.9 (22.1–28.8)**	**4.3 ± 0.5 (2.9–5.2)**	**1.4 ± 0.2 (1.0–1.7)**	**5–6**	**Present study**
***Henneguya* n. sp. 7**	***Channa gachua***	**Ovaries**	**12.7 ± 0.5 (11.4–13.3)**	**4.8 ± 0.5 (3.9–5.8)**	**3.6 ± 0.3 (3.0–4.2)**	**22.5 ± 2.2 (17.9–26.5)**	**4.7 ± 0.3 (4.1–5.3)**	**1.4 ± 0.2 (1.2–1.9)**	**5–6**	**Present study**
H. paraensis	*Cichla temensis*	Gill filaments	12.8 ± 0.4 (12.3–13.2)	8.6 ± 0.3 (8.1–8.9)	–	29.5 ± 0.7 (28.7–30.2)	7.4 ± 0.1 (6.6–7.5)	2.6 ± 0.1 (2.5–2.7)	5–7	Velasco et al. (2016)
H. pseudoplatystoma	Hybrid of *P. corruscans* and *P. fasciatum*	Gill filaments	10.4 ± 0.6	3.4 ± 0.4	4.5 ± 0.1	22.7 ± 1.7	3.3 ± 0.4	1.0 ± 0.1	6–7	Naldoni et al. (2009)
H. postexilis	*Ictalurus punctatus*	Gill lamellae	15.5 (12.1–17.2)	4.1 ± 0.3 (3.6–4.8)	3.5 (2.9–3.8)	31.2 ± 4.6 (25.7–38.1)	5.9 ± 0.6 (4.4–6.7) 5.6 ± 0.5 (4.4–6.4)	1.4 ± 0.1 (1.1–1.6)	6–8	Woodyard et al. (2022)
H. sacacaensis	*Satanoperca jurupari*	Gill filaments	16.5 ± 2.6	5.1 ± 0.9	–	30.0 ± 6.8	3.8 ± 0.3	1.6 ± 0.2	7–9	Ferreira et al. (2020)
H. laseeae	*Pylodictis olivaris*	Gill filaments	16.2 ± 0.5 (15.1–17.0)	6.0 ± 0.4 (5.1–6.6)	4.7 ± 0.2 (4.4–4.9)	54.3 ± 2.9 (49.1–61.7)	5.9 ± 0.3 (5.3–6.3)	1.8 ± 0.1 (1.6–2.1)	6–7	Leis et al. (2017)
H. michiganensis	*Esox masquinongy*	Gill lamellae	20.9 ± 1.0 (18.6–22.6)	6.3 ± 0.4 (5.4–6.9)	3.8 ± 0.3 (3.5–4.0)	58.3 ± 5.8 (47.3–75.6)	7.4 ± 0.6 (6.4–7.7)	2.0 ± 0.1 (1.8–2.1)	9–10	Rosser et al. (2021)

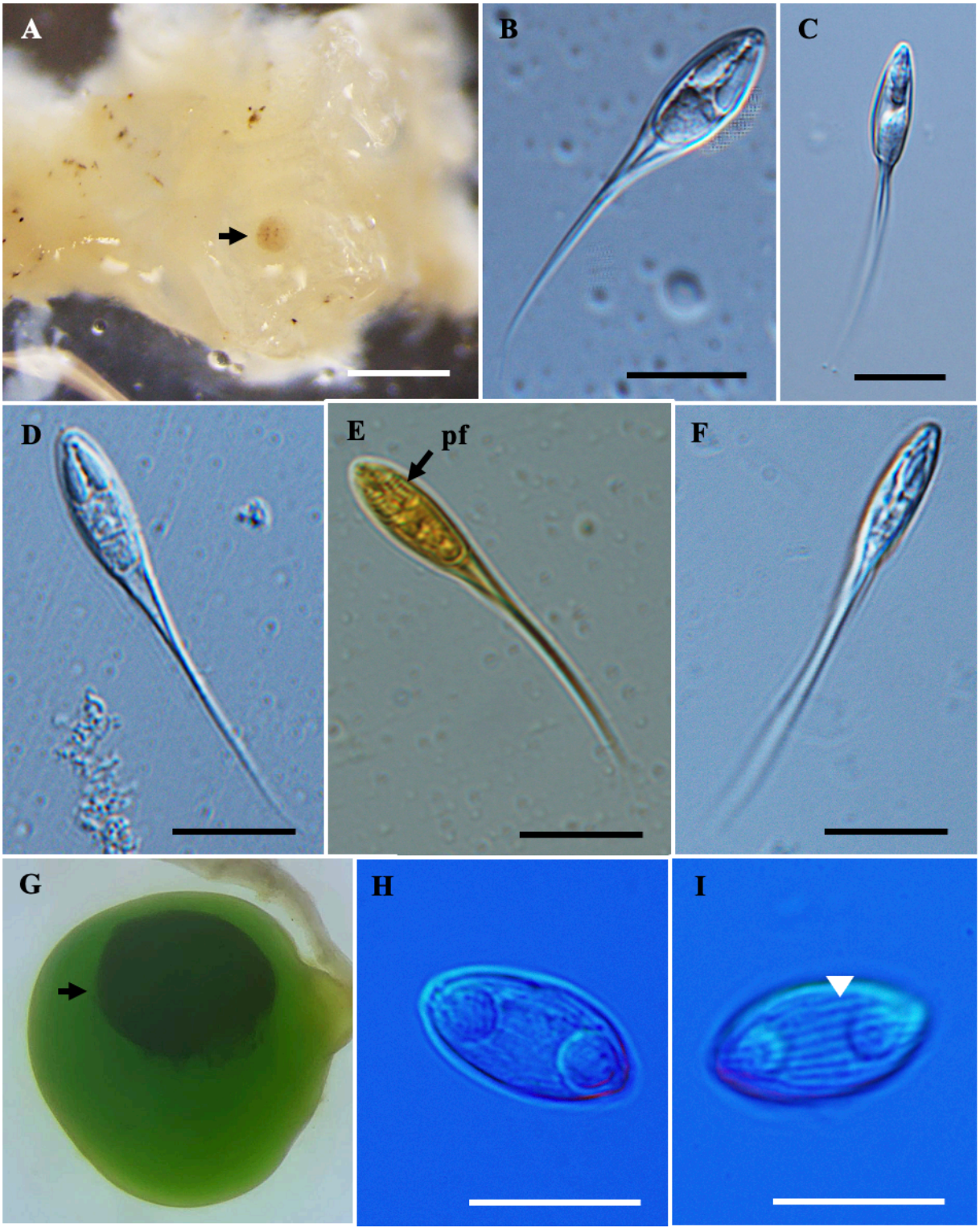

Figure S34. *Henneguya* and *Myxidium* species from *Channa gachua*. A) Plasmodium (black arrow) of *Henneguya* n. sp. 8 observed in formalin-fixed vertebral column. B) Mature spore of *Henneguya* n. sp. 8 in frontal view and C) Spore of *Henneguya* n. sp. 8 in sutural view. D) Mature spore of *Henneguya* n. sp. 9 in frontal view. E) Spore showing the polar capsule with six coils (pf) and F) Spore of *Henneguya* n. sp. 9 in sutural view. G) Large plasmodium (black arrow) in the gallbladder. H) Mature spore of *Myxidium* n. sp. 3 observed in the gallbladder and I) Spore of *Myxidium* n. sp. 3 showing seven valvular striations (white triangle). Scale bars represent 10 µm, except (A) 500 µm.

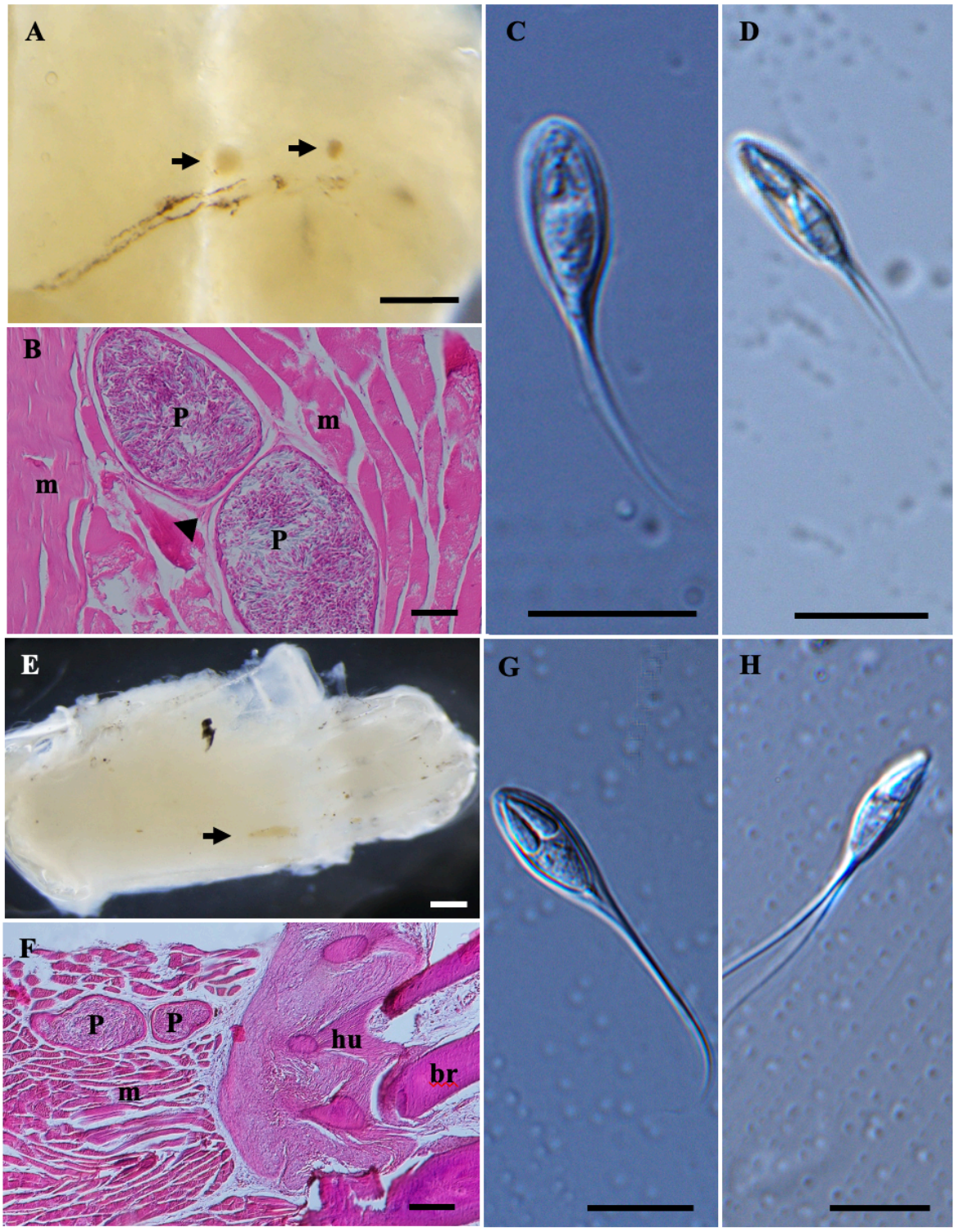

Figure S35. *Henneguya* spp. from *Channa gachua*. A) Plasmodium (black arrow) of *Henneguya* n. sp. 10 in formalin-fixed muscle tissue. B) Histological longitudinal section of muscle cells showing plasmodia (P) located among (skeletal) muscle cells (m), surrounding connective tissue (black triangle), stained with hematoxylin and eosin (H&E). C) Mature spore of *Henneguya* n. sp. 10 in frontal view and D) Spore of *Henneguya* n. sp. 10 in sutural view. E) Plasmodium (black arrow) of *Henneguya* n. sp. 11 in formalin-fixed caudal peduncle. F) Histological longitudinal section of the caudal fin showing the plasmodia (P) located among the skeletal muscle (m), along with the hypural (hu) and the bony rays (br), stained with hematoxylin and eosin (H&E). G) Mature spore of *Henneguya* n. sp. 11 in frontal view and H) Spore of *Henneguya* n. sp. 11 in sutural view. Scale bars represent 10 µm, except (A, E) 500 µm and (F) 100 µm.

Table S42 Comparative data on spore measurements (mean ± standard deviation [SD], with ranges in parentheses) for *Henneguya* n. sp. 8 and *Henneguya* n. sp. 11 from *Channa gachua* and other *Henneguya* species with ellipsoidal spore. All measurements are in μm. Abbreviations: SL spore length, SW spore width, ST spore thickness, AL caudal appendage length, PCL polar capsule length, PCW polar capsule width, PFC polar filament coils, – no data.

Species	Host	Site infection	SL	SW	ST	AL	PCL	PCW	PFC	Reference
***Henneguya* n. sp. 8**	***Channa gachua***	**Vertebral column**	**12.6 ± 0.4 (11.5–13.5)**	**5.2 ± 0.5 (4.3–6.7)**	**4.1 ± 0.4 (3.7–4.8)**	**23.8 ± 2.8 (17.7–28.9)**	**5.4 ± 0.5 (4.7–6.4)**	**1.5 ± 0.1 (1.2–1.8)**	**8–10**	**Present study**
H. mystasi	*Mystus vittatus*	Gill lamellae	12.6 ± 0.7 (12.0–14.0)	3.9 ± 0.1 (3.8–4.0)	3.1 ± 0.3 (2.4–3.6)	18.0 ± 1.0 (14.4–22.0)	6.0 ± 0.3 (5.6–6.4)	1.2 ± 0.3 (1.1–1.3)	–	Chaudhary et al. (2019)
H. psorospermica	*Esox lucius*	Gill filaments	12.4 ± 1.0 (9.6–14.4)	6.3 ± 0.6 (4.8–7.2)	7.7 ± 0.1 (7.6–7.8)	13.8 ± 1.0 (12.8–16.0)	6.3 ± 0.7 (5.0–7.2)	1.9 ± 0.2 (1.6–2.0)	12–13	Székely et al. (2018)
***Henneguya* n. sp. 11**	***Channa gachua***	**Muscle near caudal peduncle**	**13.0 ± 0.5 (11.9–14.1)**	**5.6 ± 0.4 (4.9–6.1)**	**4.3 ± 0.4 (4.0–4.6)**	**27.1 ± 1.6 (23.0–29.6)**	**5.5 ± 0.3 (4.9–6.1)**	**1.7 ± 0.2 (1.3–2.0)**	**8–9**	**Present study**
H. jaczoi	*Perca fluvialitis*	Buccal cavity, gill arch	14.1 ± 1.1 (13.2–15.2)	6.2 ± 0.6 (5.2–7.0)	5.1 ± 0.1 (4.8–5.2)	24.0 ± 2.4 (20.8–27.2)	6.4 ± 0.8 (4.8–7.2)	2.0 ± 0.2 (1.6–2.4)	12–13	Székely et al. (2018)
H. quelen	*Rhamdia quelen*	Kidney	15.6 ± 0.8 (14.3–16.4)	4.1 ± 0.3 (3.9–4.4)	–	24.3 ± 2.2 (21.0–26.5)	5.5 ± 0.5 (5.2–6.0)	1.6 ± 0.2 (1.4–1.8)	6	Abrunhosa et al. (2018)
H. oviperda	*E. lucius*	Ovaries	16.5 (13.9–19.9)	8.1 (7.8–8.6)	5.2 (5.2–5.4)	16.3 (6.5–7.8)	7.2 (6.5–7.8)	2.6 (2.1–3.1)	10–13	Sokolov et al. (2019)
H. multiradiatus	*Brochis multiradiatus*	Serosa of the visceral cavity	18.7 ± 0.9 (16.8–19.6)	7.1 ± 0.2 (6.6–7.4)	5.5 ± 0.3 (4.9–5.6)	25.8 ± 0.6 (24.7–26.5)	9.1 ± 0.1 (8.8–9.4)	1.7 ± 0.1 (1.6–1.8)	10–11	Mathews et al. (2020)
H. texta	*P. fluvialitis*	Gill lamellae	19.7 ± 1.8 (17.5–22.0)	8.3 ± 1.0 (7.2–9.6)	8.0 ± 0.9 (7.2–9.6)	15.0 ± 1.4 (11.0–12.0)	9.5 ± 1.4 (8.1–12.0)	2.9 ± 0.4 (2.4–3.2)	12–13	Székely et al. (2018)

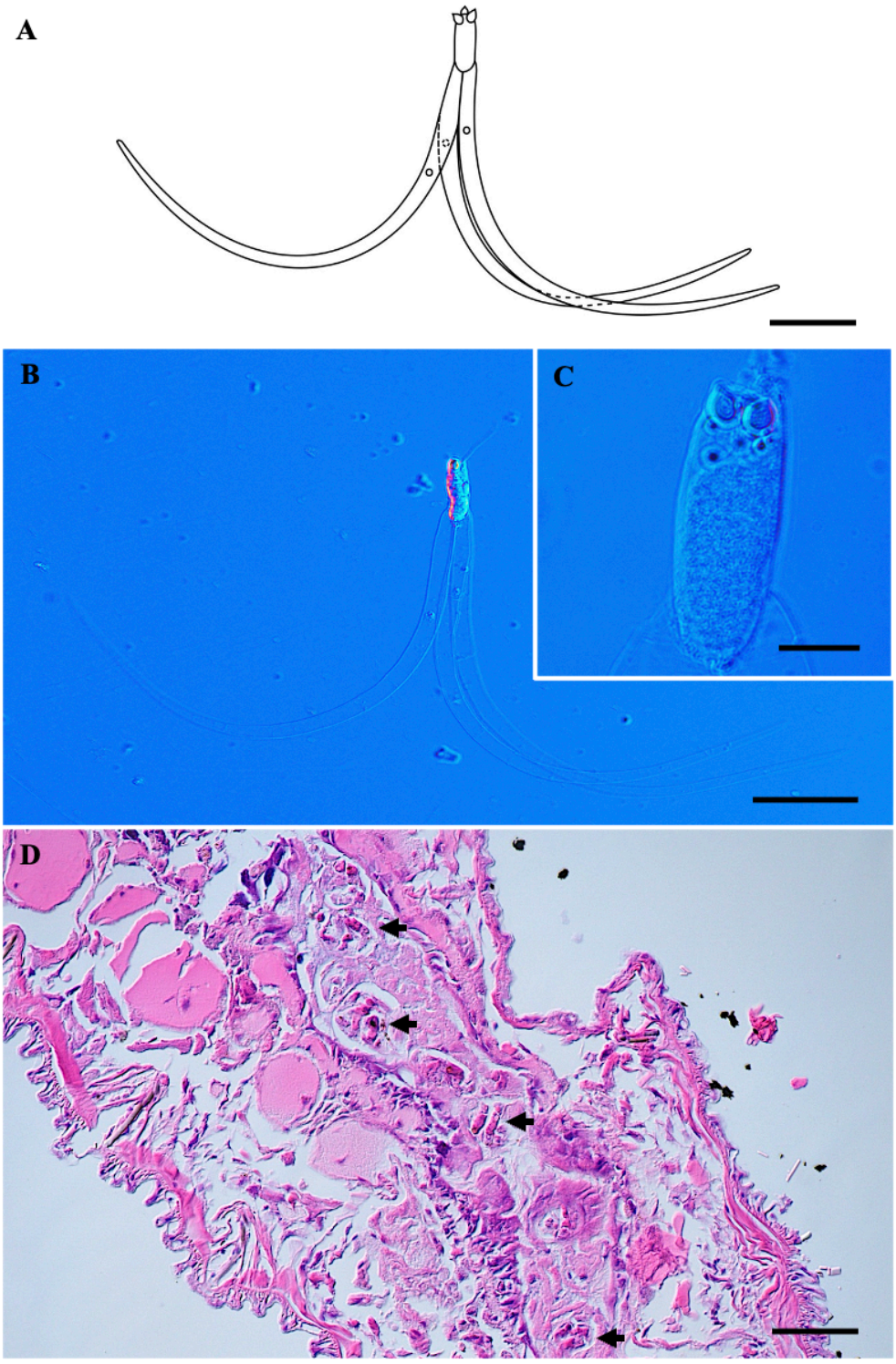

Figure S36. Raabeia type 1. A) Schematic drawing of mature actinospore. B) Fresh mount of raabeia type 1. C) Higher magnification of spore body showing two of three polar capsules with four coils of polar tubule. D) Semithin sections showing multiple pansporocysts (black arrow) of the raabeia type 1 in the intestinal epithelium of the freshwater oligochaete, *Aulodrilus acutus* from Tasik Telabak. Scale bars represent 50 µm, except (A) 10 µm.

Table S43 Comparison of morphometric measurements of raabeia type 1 from Tasik Telabak with data from previous studies. All measurements are in μm. Abbreviations: SBL spore body length, SBW spore body width, CPL caudal processes length, CPW caudal processes width, PCL polar capsule length, PCW polar capsule width, SC number of secondary cells, – no data.

Raabiea type/species	Host	SBL	SBW	CPL	CPW	PCL	PCW	SC	Reference
Raabeia type 1	***Aulodrilus acutus***	**29.7**	**11.1**	**271.2**	**9.7**	**5.3**	**3.6**	**–**	**Present study**
Raabeia noxubeensis	*Amphichaeta* sp.	27.5	11.8	53.9	9.1	–	–	12	Bellerud (1993)
Type E	*T. tubifex*	24.0	11.0	215	9.0–11.0	4.5	2.6	12	Xiao & Desser (1998b)
Type 3	*T. tubifex*	28.2	14.1	183.6	10.6	7.5	5.9	–	El-Mansy et al. (1998b)
Type 4	*T. tubifex*	29.6	16.5	142.7	–	8.0	5.0	32	Özer et al. (2002)
Type 6	*T. tubifex*	29.8	17.4	164.8	–	7.8	4.6	–	Özer et al. (2002)
Type 1	*Tubifex* sp.	35	12	245	–	5.0	3.0	20–28	Oumouna et al. (2003)
Type 2	Unidentified	18.0	15.0	80.0	–	4.0	3.0	–	Oumouna et al. (2003)
Type 1	Unidentified	27.2	16.8	213.2	11.2	3.9	3.2	12	Hallett et al. (2004)
Type 2	Unidentified	22.0	14.2	120.7	7.7	4.2	3.6	8	Hallett et al. (2004)
Raabeia of *M. cultus*	*Branchiura sowerbyi*	23	10	191	7	4	2.5	16	Eszterbauer et al. (2006)
Raabeia of *M. lentisuturalis*	*Branchiura sowerbyi*	22.1	10.8	196	–	4.7	2.9	–	Caffara et al. (2009)
Raabeia type	*Dero digitata*	28.2	6.44	150.65	7.3	–	–	–	Rosser et al. (2014)

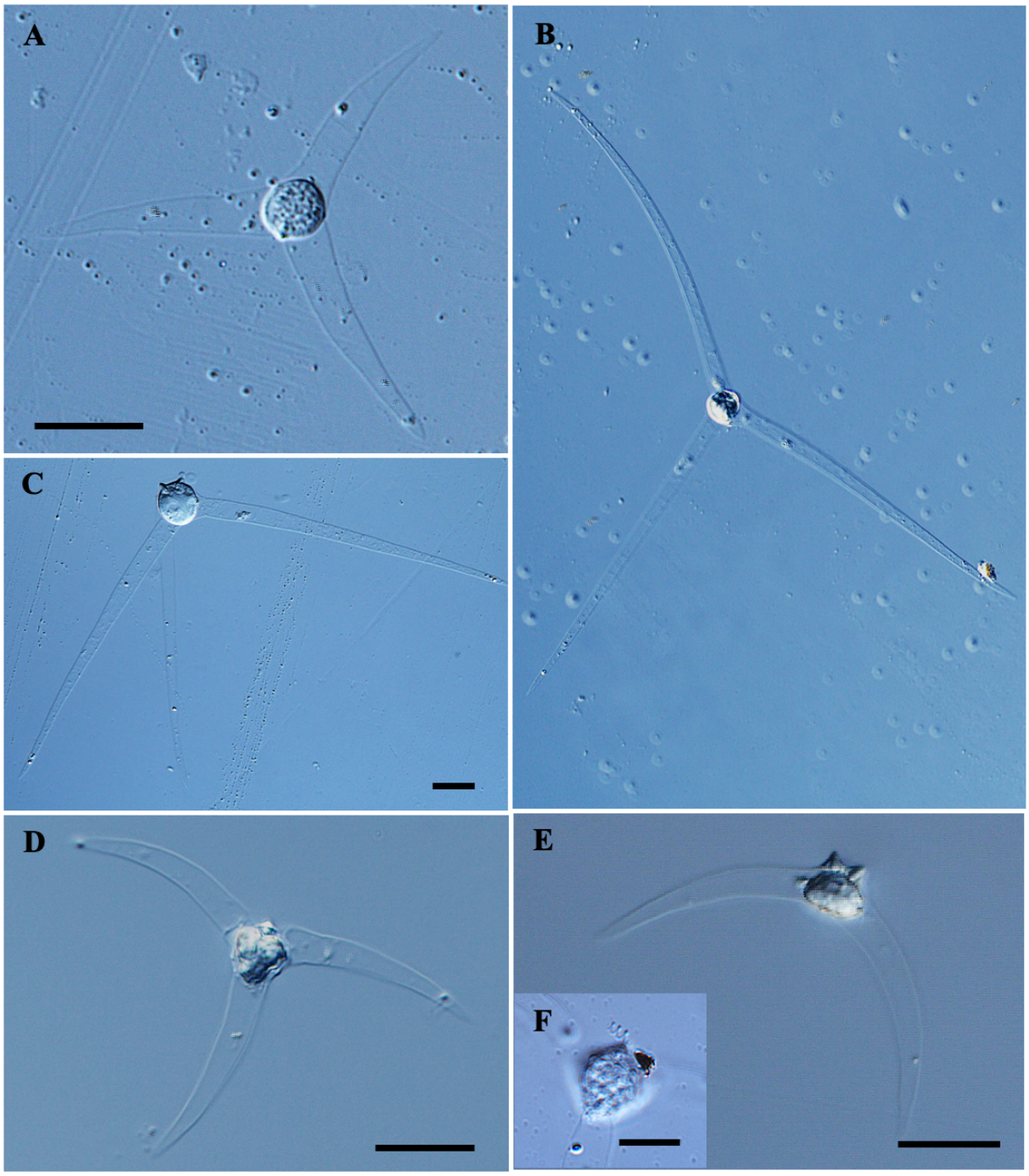

Figure S37. Aurantiactinomyxon types released from *Aulophorus* sp. A) Aurantiactinomyxon type 1 in apical view. B) Aurantiactinomyxon type 2 in apical view. C) Aurantiactinomyxon type 2 in sutural view. D) Aurantiactinomyxon type 3 in apical view. E) Aurantiactinomyxon type 3 in sutural view. F) Higher magnification of the spore body showing polar capsule with three coils of the polar tubule. Scale bars represent 20 µm, except (C) 50 µm and (G) 10 µm.

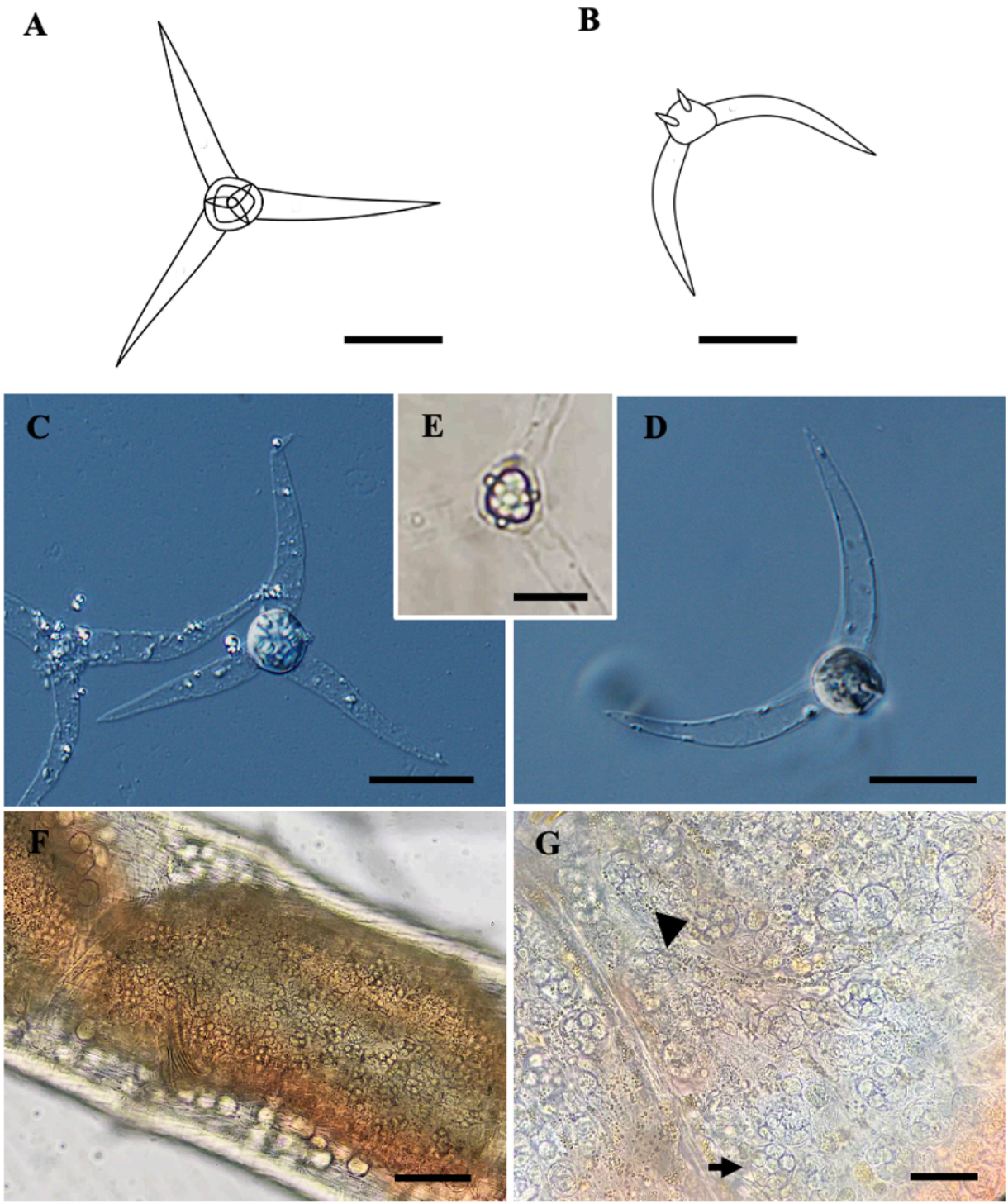

Figure S38. Aurantiactinomyxon type 4 released from *Bothrioneurum* sp. A) Schematic drawing of apical view and B) The side view of mature actinospores. C) Fixed (90% ethanol) aurantiactinomyxon spore in the apical view. D) Fixed (90% ethanol) aurantiactinomyxon spore in the side view. E) Higher magnification of fresh spore body showing three elongated polar capsules. F) Heavily infected *Bothrioneurum* sp. with pansporocysts at various stages of development in the intestinal epithelium. G) Pansporocyst showing six to seven of eight actinospores (arrowhead). In some spores, polar capsules can be seen (arrow). Scale bars represent 20 µm except E) 10 µm and F) 100 µm.

Table S44 Comparison of morphometric measurements of aurantiactinomyxon types from Tasik Telabak and morphologically similar types reported in previous literature. All measurements are in µm and '–' indicates no data. SBD spore body diameter, CPL caudal processes length, CPW caudal processes width, PCL polar capsule length, PCW polar capsule width, SC number of secondary cells, D diameter, L length, W width.

Aurantiactinomyxon type	Host	SBD	CPL	CPW	PCL	PCW	SC	Reference
Aurantiactinomyxon type 1	***Aulophorus* sp.**	**10.3 ± 0.5 (9.4–11.0)**	**39.7 ± 2.2 (34.4–43.4)**	**6.8 ± 0.4 (6.0–7.5)**	**2.6 (2.6–2.7)**	**1.6 ± 0.1 (1.5–1.8)**	**32**	**Present study**
Aurantiactinomyxon type 2	*Pristina synclites*	11.2 (10.2–11.9)	30.4 (25.0–33.3)	7.0 (5.4–7.7)	1.5 (1.3–1.8)	1.5 (1.3–1.8)	–	Milanin et al. (2018)
Aurantiactinomyxon type 2	***Aulophorus* sp.**	**16.4 ± 1.3 (14.3–19.7)**	**153.6 ± 7.2 (144.2–171.0)**	**8.4 ± 0.7 (7.1–9.9)**	**5.1 ± 0.3 (4.1–6.4)**	**2.6 ± 0.4 (2.0–3.3)**	–	**Present study**
Aurantiactinomyxon type	*B. sowerbyi*	19.7 (18.9–21.9)	170.8 (167.5–176.3)	12.9 (11.2–13.5)	3.1 (2.9–3.2)	1.7 (1.5–1.9)	64	Xi et al. (2013)
Aurantiactinomyxon type 3	*Tubifex tubifex*	L: 24 (23.4 – 24.9) W: 21.8 (20.3 – 23.4)	114.5 (101.4–124.8)	–	4.0	3.2	32	Özer et al. (2002)
Aurantiactinomyxon type 3	***Aulophorus* sp.**	**11.7 ± 0.7 (10.5–13.2)**	**44.3 ± 2.9 (40.4–49.3)**	**6.3 ± 0.5 (5.5–7.6)**	**3.2 ± 0.2 (2.7–3.5)**	**2.0 ± 0.2 (1.5–2.4)**	–	**Present study**
Aurantiactinomyxon type of *Henneguya exilis*	*Dero digitata*	11.7 ± 0.8 (10.2–13.3)	42.4 ± 2.4 (37.6–46.2)	6.5 ± 0.8 (5.2–8.5)	–	–	–	Rosser et al. (2014)
Aurantiactinomyxon type 4	***Bothrioneurum* sp.**	**8.8 ± 0.7 (7.6–10.1)**	**36.7 ± 2.7 (30.7–43.8)**	**4.9 ± 0.6 (3.9–6.2)**	**3.6 ± 0.3 (3.0–4.3)**	**1.3 ± 0.2 (1.1–1.9)**	–	**Present study**
Aurantiactinomyxon type 1	*Pacifidrilus vanus*	L: 10.1 W: 10.7	~3.0	~3.0	D: 1.9	D: 1.9	–	Hallett et al. (1997)
Aurantiactinomyxon type 11	Actinospores collected from water	8.5	31.9	3.7	3.4	2.0	–	El-Mansy et al. (1998b)
Aurantiactinomyxon type 1	*Pristina synclites*	8.7 (8.2–9.7)	14.6 (12.2–16.3)	6.9 (5.4–8.8)	D:1.3 (1.0–1.4)	D:1.3 (1.0–1.4)	–	Milanin et al. (2018)

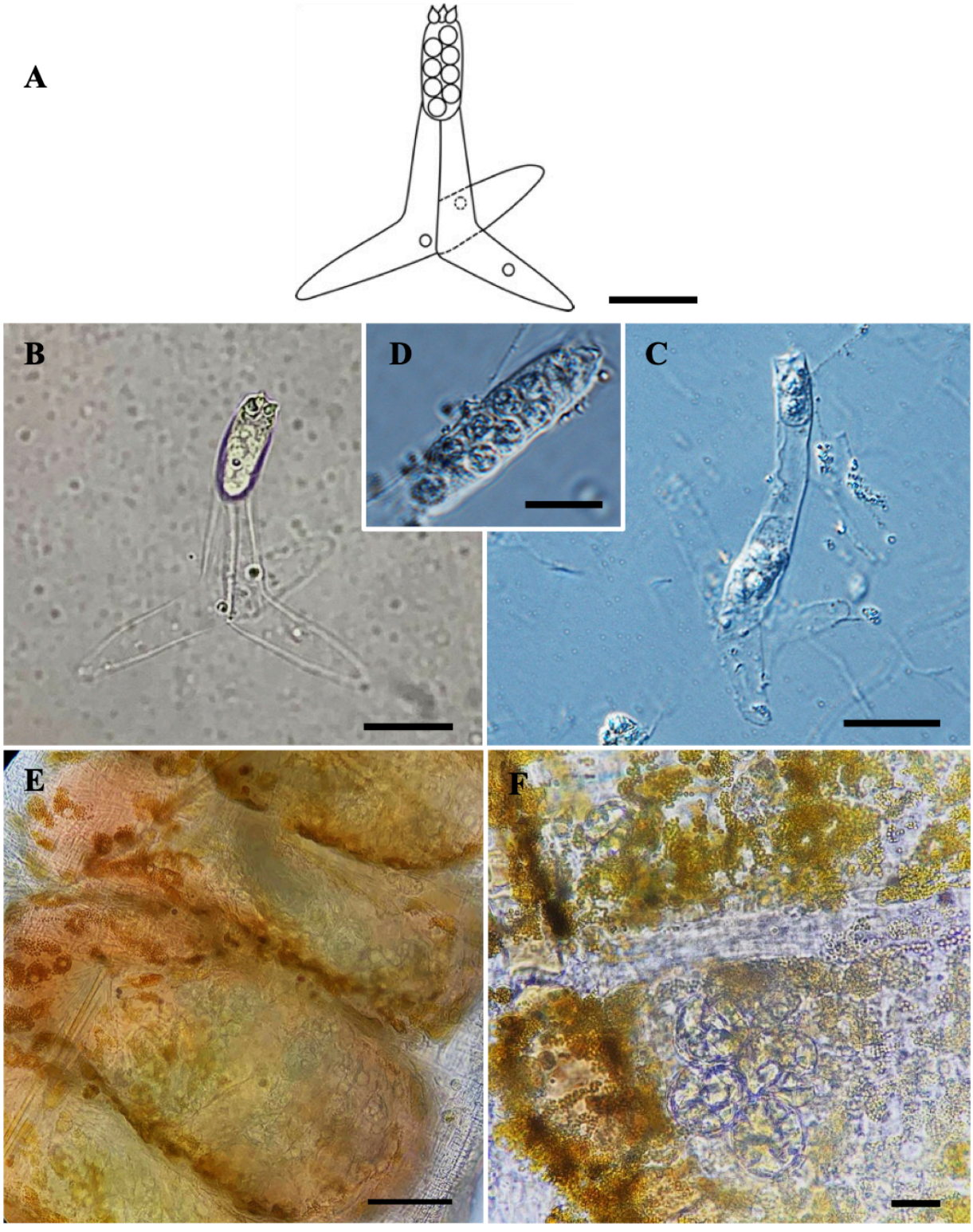

Figure S39. Triactinomyxon type 1. A) Schematic drawing of mature actinospore. B) Freshly released triactinomyxon from *Branchiodrilus* sp. C) Triactinomyxon spore fixed in 90% ethanol. D) Higher magnification of spore body showing eight secondary cells. E) Heavily infected *Branchiodrilus* sp. with pansporocysts at various stages of development in the intestinal epithelium. F) Higher magnification showing pansporocysts of triactinomyxon type 1 in the intestinal epithelium. Scale bars represent 20 µm, except D) 10 µm and E) 100 µm.

Table S45 Comparison of morphometric measurements of triactinomyxon type 1 with eight secondary cells from Tasik Telabak and previous literature. All measurements are in µm and '–' indicates no data. SBL spore body length, SBW spore body width, SL style length, SW style width, CPL caudal processes length, CPW caudal processes width, PCL polar capsule length, PCW polar capsule width, Lo long, Sh short.

Triactinomyxon type	Host	SBL	SBW	SL	SW	CPL	CPW	PCL	PCW	Reference
Triactinomyxon type 1	***Branchiodrilus* sp.**	**27.9**	**8.9**	**29.8**	**9.5**	**29.9**	**9.7**	**3.4**	**2.2**	**Present study**
Type 3	*Nais elinguis, T. Tubifex, L. hoffmeisteri*	47.1	10.6	102	9.4	128	10.6	7.0	3.5	El Mansy (1998a, 1998b)
Type C	*L. hoffmeisteri*	18	10–13	195	32	290	25	5	3	Xiao & Desser (1998b)
Triactinomyxon type	*T. tubifex*	–	–	170	–	160	–	4	3	Oumouna et al. (2003)
Triactinomyxon type	*T. tubifex*	37.6	12.2	134.3	16.5	Lo: 200.6 Sh: 154.4	Lo: 15 Sh: 14.9	5.3	3	Rácz &Timm (2002)
Type 4	Tubificid	–	–	103	–	221	–	5	5	Lowers & Bartholomew (2003)
Type 5	Tubificid	–	–	94	11	123	–	2	3	Lowers & Bartholomew (2003)
Triactinomyxon type	*T. tubifex*	25.6	10	112	19.2	Lo: 193.2 Sh: 115.4	Lo: 11.4 Sh: 12.7	4.3	2.5	Hallett et al. (2004)
Type A	*T. newaensis*	37	12	241	11	150	13	5.5	2.7	Eszterbauer et al. (2006)
Type B	*T. tubifex*	31	9	205	8	140	14	5	2.5	Eszterbauer et al. (2006)
Triactinomyxon type	*Psammoryctides albicola*	30	13	130	17	120	–	3	2	Székely et al. (2007)